

https://dspace.org/

Synthesis, reactions and multinuclear NMR spectroscopic studies of organo bimetallic and trimetallic compounds

Mampa, Richard Mokome

2012-10-01
http://hdl.handle.net/10539/11990

Downloaded from a DSpace repository. https://dspace.org/

SYNTHESIS, REACTIONS AND MULTINUCLEAR NMR SPECTROSCOPIC STUDIES OF ORGANO BIMETALLIC AND TRIMETALLIC COMPOUNDS

By

RM Mampa

A thesis submitted to the Faculty of Science, University of the Witwatersrand, Johannesburg, in fulfilment of the requirement for the degree of Doctor of Philosophy

Johannesburg, 2011

Dedicated

To my wife, Joyce

And

My daughter, Rijoy

DECLARATION

I hereby declare that the work presented in this thesis was carried exclusively by me under the supervision of Prof. L. Carlton. It has not been submitted before for any degree or examination in any other University. It is being submitted for the Degree of Doctor of Philosophy in the University of the Witwatersrand, Johannesburg.

…….

Richard Mokome Mampa

Date:

Abstract

The ^{207}Pb and ^{119}Sn NMR chemical shift were used to study the effect of temperature on Ph_3MCl (M= Pb and Sn) adducts in the presence of 10% excess pyridine. The ^{207}Pb and ^{119}Sn chemical shift indicate a slow exchange at low temperatures below -90 ^0C and a significant exchange at higher temperatures above 10 ^0C. A plot of temperature against ^{207}Pb or ^{119}Sn chemical shift showed a curve with gentle slope at lower and a steep slope at higher temperatures. A good linear correlation (coefficient. of 0.95) between Hammett substituent constant and ^{207}Pb or ^{119}Sn chemical shift of *para*-substituted derivatives of $Ph_3MCl.py^*$ ($py^* = NMe_2$, OMe, Me, Ph, H, Br, COPh and COMe; at -90 ^0C in CD_2Cl_2/CH_2Cl_2) was found. Both ^{207}Pb and ^{119}Sn chemical shift ranges are characteristic of five coordinate systems resolving into trigonal bipyramidal geometry as shown by X-ray crystal structures.

New complexes of the type $[CpFe(CO)(SnPh_3)L]$ (L = PPh_3, PBu_3, PCy_3, PMe_3, $P(NMe_2)_3$, $PMePh_2$, PMe_2Ph, $P(p\text{-}FC_6H_5)_3$, $P(p\text{-}OMeC_6H_4)_3$, $P(p\text{-tolyl})_3$, $P(OMe)_3$, and $P(OPh)_3$ were synthesized by ultraviolet irradiation of $[CpFe(CO)_2(SnPh_3)]$ and the appropriate phosphine or phosphite ligand. ^{57}Fe NMR studies of the complexes showed an increasing linear relationship with Tolman's steric parameter, whereas with Tolman's electronic parameter the ^{57}Fe chemical shift showed a decrease. The X-ray crystallographic profile of the selected new *piano stool* type complexes shows a significant correlation to the NMR data (solution state), i.e. Fe-Sn, Fe-P bond length and Sn-Fe-P bond angle against chemical shifts of ^{207}Pb and ^{119}Sn. Disubstituted complexes of the type $[CpFe(SnPh_3)L_2]$ (L = PMe_3, PMe_2Ph, $P(OMe)_3$ and $P(OPh)_3$ were synthesized under similar conditions as monosubstituted compounds. The correlation trends between the NMR data and X-ray crystallographic profiles are similar to those found for monocarbonylated complexes.

Tungsten phosphine complexes of the type $[W(CO)_5(PR_3)]$ (prepared from $[W(CO)_6]$ under thermal conditions) and $[W(CO)_4(NCMe)(PR_3)]$ (prepared from $[W(CO)_5(PR_3)]$ by use of Me_3NO-promoted decarbonylation) were synthesized and characterized by, among other methods X-ray diffraction techniques (R = Ph, *p*-tolyl, $p\text{-}OMeC_6H_4$, $p\text{-}FC_6H_4$, $p\text{-}CF_3C_6H_4$, and NMe_2). The tungsten complexes $[W(CO)_4(NCMe)(PR_3)]$ react with $[(dppp)Pt\{C{\equiv}C\text{-}C_5H_4N\}_2]$ at room temperature to form new complexes of the type $[(dppe)Pt\{C{\equiv}C\text{-}C_5H_4N\text{-}W(CO)_4(PR_3)\}_2]$

which were characterized unambiguously by NMR spectroscopy. There is a fair correlation between ^{195}Pt and ^{183}W NMR chemical shifts and Tolman's electronic parameter which indicates a fair influence by the substituents of the phosphorus atom on both metal centres.

Tungsten complexes of the type $[W(CO)_4(NCMe)(L)]$ (L= PPh_3, P(*p*-$FC_6H_4)_3$, P(*p*-$OMeC_6H_4)_3$, P(*p*-tolyl)$_3$, P(*p*-$CF_3C_6H_4)_3$, $PMePh_2$, and $PPh_2(C_6F_5)$ react with $[(PPh_3)_2Rh(H)_2(pytca)]$ (pytca = 2-(4-pyridyl)thiazole-4-carboxylate) to form new complexes of the type $[(PPh_3)_2Rh(H)_2(pytca)$-$W(CO)_4(L)]$ under mild conditions. These complexes were characterized principally by NMR spectroscopy and X-Ray crystallography (L = P(*p*-tolyl)$_3$). Crystallographic evidence was found for π-π-π interactions involving two phenyl rings, one of the two phosphines bonded to rhodium atom, one of the three phosphines bonded to tungsten and the pyridyl ring of the thiazole corboxylate group. A second π-π interaction is found between a thiazole and a phenyl ring of the phosphine ligand bonded to the rhodium atom. A fair correlation was found between the rhodium and tungsten chemical shift measured from this series of complexes as a result of varied *para*-phenyl substituent of phosphine ligand bonded to the tungsten atom. This therefore implies the possible existence of electronic communication between the two bridged metal centres.

Acknowledgements

I would like to thank my supervisor Prof. L Carlton for his assistance, guidance and support throughout the course of this project.

I also wish to thank the following people (in their own special way and in no order of importance):

Prof. J Darkwa and Prof. MJ Mphahlele for inspiration, encouragement, consistent interest in my studies and for all their helpful advice.

Dr MA Fernandes for patience, encouragement and for all the time he spent on mounting my crystals, recording, analysing and solving my crystal structures.

Dr MM Moutloali, Ms I Khumalo and Mr D Moloto for their support and encouragement over the years.

I wish to thank the School of Chemistry, under the guidance of Prof. J Michael and Prof. HM Marques for giving me the opportunity to study part-time and for the financial assistance towards my tuition fees and research material. I would also wish to thank National Research Foundation (NRF) for the financial support for research materials and conference attendances.

Lastly, special thanks go to Mom and Dad despite both being academically disadvantaged, found it worth it to support and encourage me throughout my entire educational career life.

To my wife, Joyce and my daughter, Rijoy for being the source of inspiration and pillar of support during many frustrating moments in my studies.

Table of Contents

Declaration iii

Abstract iv

Acknowledgments vi

Table of contents vii

List of figures xx

List of tables xxvi

List of schemes xxviii

Abbreviations xxx

Appendix

CHAPTER 1: Chemistry of the Selected Transition Metals …….....1

1.1 Historical perspective 2

1.2 Bimetallic complexes with direct metal-metal bonds.....3

1.2.1 Chemistry of metal-metal bonded complexes.....3

1.2.2 Synthesis of bimetallic complexes with direct metal-metal bonds.....5

1.2.3 Bimetallic complexes having transition and non-transition metals.....6

1.2.4 General synthetic routes to bimetallic complexes with a direct metal-tin bond.....6

1.3 Bridged bimetallic complexes.....7

1.3.1 Chemistry of bridged bimetallic complexes.....8

1.3.2 Synthetic routes to selected bridged heterobimetallic complexes.....10

1.4 Transition-metal clusters.....13

1.4.1 Chemistry of selected metal clusters.....15

1.4.2 Synthesis and derivatization of transition-metal clusters.....17

1.5 Decarbonylation of transition-metal carbonyl complexes.....18

1.6 Ligands of interest.....20

1.7 The *trans*-effect vs *trans*-influence in transition metal complexes.....21

1.8 Reaction mechanisms.....24

1.8.1 Oxidative addition reactions.....24

1.8.2 Reductive elimination reactions.....27

1.9. Conclusion.....28

1.10 References.....29

CHAPTER 2: NMR Spectroscopy with emphasis on the Transition Metals.....41

2.1. Brief historical perspective.....42

2.2. Principles of NMR spectroscopy.....43

2.2.1. Nuclear spin and magnetic moments.....43

2.2.2 Pulsed FT NMR spectroscopy.....46

2.2.3 Relaxation.....47

2.2.4 Chemical shift.....47

2.2.4.1 Influence of temperature on the Chemical shift.....49

2.2.4.2 Influence of solvent on the chemical shift.....50

2.2.4.3 Coordination effect.....50

2.2.5 Correlation of structural, chemical and spectroscopic parameters with metal chemical shifts.....51

2.2.6 Spin-Spin coupling.....53

2.4 Experimental Techniques for selected NMR nuclei.....54

2.4.1 Direct observation technique.....54
2.4.2 Polarisation Transfer method: INEPT pulse sequence.....55
2.4.3 The indirect detection method.....57
2.5 Calibration of spectra.....60
2.6 NMR spectroscopy of selected main group nuclei.....61
2.6.1 ^{15}N NMR spectroscopy.....61
2.6.1.1 Method of observation.....62
2.6.1.2 Calibration and Chemical shift 62
2.6.1.3 Factors affecting ^{15}N coupling constants.....63
2.6.2 ^{31}P NMR spectroscopy.....65
2.6.2.1 Factors influencing coupling constants. 66
2.6.3. ^{119}Sn NMR spectroscopy.....67
2.6.3.1 Spectral calibration.....68
2.6.3.2 ^{119}Sn chemical shift.....68
2.6.3.3 Patterns of ^{119}Sn coupling constants 69
2.6.3.4 Correlations of ^{119}Sn chemical shifts with ^{29}Si or ^{207}Pb Chemical shifts.....69
2.7 NMR spectroscopy of selected transition metals.....69
2.7.1 ^{57}Fe NMR Spectroscopy.....70
2.7.1.1 ^{57}Fe Chemical shift.....71
2.7.1.2 ^{57}Fe spin-spin coupling.....72
2.7.2 ^{103}Rh NMR spectroscopy.....72
2.7.2.1 ^{103}Rh Chemical shift 73
2.7.2.2 ^{103}Rh spin-spin coupling constants.....74
2.7.3 ^{183}W NMR spectroscopy.....74
2.7.3.1 ^{183}W Chemical shift and calibration.....74
2.7.3.2 ^{183}W spin-spin couplings.....75
2.7.4 ^{195}Pt NMR Spectroscopy.....75
2.7.4.1 ^{195}Pt spectrum calibration.....76
2.7.4.2 ^{195}Pt Chemical shift.....76

2.7.4.3 ^{195}Pt spin-spin coupling.....78
2.7 Conclusions.....78
2.8 References.....79

CHAPTER 3: Experimental Techniques 88

3.1 Materials and methods.....88
3.2 NMR spectroscopy.....89
3.2.1 Methods of observation…….92
3.3 X-ray crystallography.....94
3.4 Samples for elemental analysis.....96
3.5 Samples for IR analysis.....96
3.6 References.....97

CHAPTER 4: Triorganolead(IV) Halide and Triorganotin(IV) Halide Adducts ……98

4.1 Introduction.....41
4.2 Experimental.....100
4.2.1 Reagents and general reaction conditions.....100
4.2.2 Sample preparation for NMR Spectroscopy.....101
4.2.2.1 Calibration of spectra…….....101
4.2.2.2 Sample preparation for the study of the influence of concentration of pyridine on ^{119}Sn/^{207}Pb chemical shift of Ph_3MCl.py adducts…….....101
4.2.2.3 Sample preparation for the study of the influence of concentration of Ph_3MCl on the ^{119}Sn/^{207}Pb chemical shift of Ph_3MCl.py adducts…….....102
4.2.2.4 Sample preparation for the study of the influence of temperature..…….....102
4.2.2.5 Sample preparation for the investigation of possible existence of six-coordinate

Adducts.....102

4.2.3 X-ray diffraction data.....103

4.3 Results and discussion.....104

4.3.1 The influence of concentration on ^{207}Pb and ^{119}Sn chemical shifts of lead and tin adducts.....105

4.3.2 The influence of temperature on ^{207}Pb and ^{119}Sn chemical shift of lead and tin Adducts.....107

4.3.3 The NMR spectroscopic results of the five-coordinate adducts of the type $Ph_3MCl.py$*.....110

4.3.4 Correlation between Hammett substituent constants and ^{207}Pb or ^{119}Sn chemical shift in the five-coordinated systems.....110

4.4 X-ray Crystallographic study.....113

4.5 Conclusions.....116

4.6 References.....117

CHAPTER 5: Synthesis, NMR and X-Ray Crystallographic Study of Hetero-Bimetallic Complexes of the type [CpFe(CO)(PR_3)($SnPh_3$)].....120

5.1 Introduction.....120

5.2 Experimental.....122

5.2.1 Reagents and general techniques.....122

5.2.2 NMR spectroscopy.....122

5.2.3 X-ray Crystallography.....123

5.3 Synthesis.....125

5.3.1 Preparation of [Fe(Cp)$(CO)_2$($SnPh_3$)].....125

5.3.2 Preparation of [Fe(Cp)(CO)(PPh_3)($SnPh_3$)].....126

5.3.3 Preparation of [Fe(Cp)(CO){P(*p*-FC_6H_4)$_3$}($SnPh_3$)] 127

5.3.4 Preparation of [Fe(Cp)(CO){P(*p*-$OMeC_6H_4$)$_3$}($SnPh_3$)] 127

5.3.5 Preparation of [Fe(Cp)(CO){P(*p*-MeC_6H_4)$_3$}($SnPh_3$)] 128

5.3.6 Preparation of [Fe(Cp)(CO)P(Cy)$_3$($SnPh_3$)] 129

5.3.7 Preparation of [Fe(Cp)(CO)[P(NMe_2)$_3$]($SnPh_3$)] 130

5.3.8 Preparation of [Fe(Cp)(CO)($PMePh_2$)($SnPh_3$)] 131

5.3.9 Preparation of [Fe(CO)(Cp)(PBu_3)($SnPh_3$)].....132

5.3.10 Preparation of [Fe(CO)(Cp){P(OPh_3)}($SnPh_3$)] 132

5.3.11Preparation of [Fe(CO)(Cp)(P(OMe)$_3$($SnPh_3$)].....133

5.3.12 Preparation of [Fe(CO)Cp)(PMe_3)($SnPh_3$)] 134

5.3.13 reparation of [Fe(CO)(Cp)(PMe_2Ph)($SnPh_3$)] 135

5.4 Results and discussion.....136

5.4.1 NMR spectroscopy.....138

5.4.2 X-Ray crystallographic study 145

5.4.2.1 Molecular geometry around the Iron atom…….....145

5.4.2.2 The Iron-Tin bond interactions ……...147

5.4.2.3 The triphenyltin group ……152

5.5 Chemical and structural correlations of [CpFe(CO)(PR_3)($SnPh_3$) complexes……..152

5.5.1 Correlation of NMR parameters with Tolman's steric and IR parameters……..152

5.5.2 Correlation between of NMR parameters and X-ray structural properties…….156

5.6 Conclusions.....158

5.7 References.....159

CHAPTER 6: Synthesis, NMR and X-Ray crystallographic studies of Iron(II) Cyclopentadienyl *bis*-Phosphine and *bis*-Phosphite complexes.....163

6.1 Introduction.....163

6.2 Experimental: Preparation of disubstituted hetero-bimetallic complexes of Iron and Tin, $[Fe(Cp)(PR_3)_2(SnPh_3)]$.....164

6.2.1 Preparation of $[Fe(Cp)(PMe_3)_2(SnPh_3)]$ 164

6.2.2 Preparation of $[Fe(Cp)(PMe_2Ph)_2(SnPh_3)]$ 165

6.2.3 Preparation of $[Fe(Cp)\{P(OMe)_3\}_2(SnPh_3)]$.....166

6.2.4 Preparation of $[Fe(Cp)\{P(OPh_3)\}_2(SnPh_3)]$.....167

6.3 X-ray crystallography.....167

6.4 Results and discussions 169

6.4.1 NMR Spectroscopy 170

6.4.2 X-ray crystallographic study 172

6.4.2.1 The Iron-Tin interactions 178

6.4.2.2 The triphenyltin group 178

6.4.2.3 The Cyclopentadienyl ring.....179

6.5 Conclusions 179

6.6 References.....180

CHAPTER 7: Synthesis and Characterization of Tetracarbonyl Tungsten Complexes: $[W(CO)_4(NCMe)(PR_3)]$.....182

7.1 Introduction.....182

7.2 Experimental: Synthesis, NMR and characterization of $[W(CO)_5(PR_3)]$.....184

7.2.1 Preparation of $[W(CO)_5PPh_3]$.....184

7.2.2 Preparation of $[W(CO)_5P(p\text{-tolyl})_3]$.....185

7.2.3 Preparation of [$W(CO)_5P(p\text{-}OMeC_6H4)_3$].....185

7.2.4 Preparation of [$W(CO)_5P(p\text{-}FC_6H_4)_3$]…….....185

7.2.5Preparation of [$W(CO)_5P(p\text{-}CF_3C_6H_4)_3$].....186

7.2.6 Preparation of [$W(CO)_5P(NMe_2)_3$].....187

7.3 Experimental: Synthesis, NMR and X-ray characterization of

[$W(CO)_4(NCMe)(PR_3)$]……...187

7.3.1 Preparation of [$W(CO)_4(NCMe)(PPh_3)$].....187

7.3.2 Preparation of [$W(CO)_4(NCMe)P(p\text{-tolyl})_3$].....188

7.3.3 Preparation of [$W(CO)_4(NCMe)P(p\text{-}OMeC_6H_4)_3$].....189

7.3.4 Preparation of [$W(CO)_4(NCMe)P(p\text{-}FC_6H_4)_3$].....189

7.3.5 Preparation of [$W(CO)_4(NCMe)P(p\text{-}CF_3C_6H_4)_3$].....189

7.3.6 Preparation of [$W(CO)_4(NCMe)P(NMe_2)_3$].....191

7.4 X-ray Crystallography.....192

7.5 Results and discussion for Complexes of the type [$W(CO)_5(PR_3)$] 194

7.5.1 NMR spectroscopy 195

7.5.2 X-ray crystallographic studies.....196

7.6 Results and discussion for Complexes of the type [$W(CO)_4(PR_3)(NCMe)$].....198

7.6.1 NMR spectroscopic study of *cis*-[$W(CO)_4(NCMe)(PR_3)$] complexes.....198

7.6.2 X-Ray crystallographic studies.....200

7.7 Conclusions 205

7.8 References.....206

CHAPTER 8: Synthesis, X-Ray and NMR Spectroscopic Studies of Bridged Bimetallic Complexes of Rhodium and Tungsten ……208

8.1 Introduction …….....208

8.2 Experimental ….....211

8.2.1 Synthesis and characterization of [$RhH(PPh_3)_4$] …….....211

8.2.2 Synthesis and characterization of [$Rh(H)_2(O_2Cpyraz)(PPh_3)$] ..…..…..212

8.2.2.1 Reaction of [$(PPh_3)Rh(H)_2(O_2Cpyraz)$] with [$W(CO)_4(NCMe)(PPh_3)$] 212

8.2.3 Synthesis and characterization of [{$Rh(H)_2(PPh_3\}_2$(pyrazdca)] ….....212

8.2.4 Synthesis and characterization of [$Rh(H)_2$(pytca)$(PPh_3)_2$] ….....213

8.2.5 Synthesis and characterization of [$(PPh_3)_2Rh(H)_2$(pytca)$W(CO)_4(PPh_3)$] 213

8.2.6 Synthesis and characterization of [$(PPh_3)_2Rh(H)_2$(pytca)-$W(CO)_4P(tolyl)_3$] 214

8.2.7 Synthesis and characterization of [$(PPh_3)_2Rh(H)_2$(pytca)-$WCO)_4P(4\text{-}FC_6H_4)_3$].....214

8.2.8 Synthesis and characterization of [$(PPh_3)_2Rh(H)_2$(pytca)-$WCO)_4P(4\text{-}CF_3C_6H_4)_3$].....215

8.2.9 Synthesis and characterization of [$(PPh_3)_2Rh(H)_2$(pytca)-$WCO)_4P(4\text{-}OMeC_6H_4)_3$].....215

8.2.10 Synthesis and characterization of [$(PPh_3)_2Rh(H)_2$(pytca)-$WCO)_4(PMePh_2)$]……..216

8.2.11 Synthesis and characterization of [$(PPh_3)_2Rh(H)_2$(pytca)-$WCO)_4(PPh_2C_6F_5)$].……...216

8.3 X-ray crystallography …….....217

8.4 Results and discussion 218

8.4.1 Reaction of [$Rh(H)_2(O_2Cpyraz)(PPh_3$] with [$W(CO)_4(NCMe)(PPh_3)$] …….....218

8.4.2 Reaction of [$RhH(PPh_3)_4$] with pyrazinedicarboxylic (pyrazdca) ….....219

8.4.3 Reaction of [$RhH(PPh_3)_4$] with 2-(4-pyridyl)thiazole-4-carboxylate (pytca) ……....220

8.4.4 Reaction of [$Rh(H)_2(PPh_3)_2$(pytca)] with [$W(CO)_4(NCMe)PR_3$] complexes 220

8.5 NMR spectroscopy of the complexes of the type [$(PPh_3)_2Rh(H)_2$(pytca)-$W(CO)_4(PR_3)$]…224

8.6 NMR data correlations ...……..227

8.7 X-ray crystallography.....231

8.8 Conclusions.....235

8.9 References.....235

CHAPTER 9: Synthesis and Characterization of Bridged Trimetallic Complexes of Platinum and Tungsten..……..239

9.1 Introduction ……...239

9.2 Experimental ……241

9.2.1 Preparation of [(dppp)$PtCl_2$] ……....241

9.2.2 Preparation of [Pt(dppp)(4-ethynylpyridine)$_2$] …...……...242

9.3 Synthesis of trimetallic complexes of the type [(dppp)Pt{4-C≡CC_5H_4N-W$(CO)_4PR_3\}_2$]…243

9.3.1 Preparation of [(dppp)Pt{4-C≡CC_5H_4N-W$(CO)_4(PPh_3)\}_2$] ……...243

9.3.2 Preparation of [(dppp)Pt{4-C≡CC_5H_4N-W$(CO)_4$P(*p*-tolyl)$_3\}_2$] ……....243

9.3.3 Preparation of [(dppp)Pt{4-C≡CC_5H_4N-W$(CO)_4$P(*p*-OMe$C_6H_4)_3\}_2$] ……...244

9.3.4 Preparation [(dppp)Pt{4-C≡CC_5H_4N-W$(CO)_4$P(*p*-F$C_6H_4)_3\}_2$] …….....244

9.3.5 Preparation of [(dppp)Pt{4-C≡CC_5H_4N-W$(CO)_4$P(*p*-$CF_3C_6H_4)_3\}_2$] …….....245

9.3.6 Preparation [(dppp)Pt{4-C≡CC_5H_4N-W$(CO)_4$P($NMe_2)_3\}_2$] ……..245

9.4 Results and discussion: Alkynyl-bridged complexes of platinum and tungsten …….....246

9.4.1 Synthesis of ethynylplatinum(II) complex of the type [(dppp)Pt{4-C≡C$C_5H_4N\}_2$]…….....246

9.4.2 Synthesis of ethynylpyridineplatinum(II) complexes of the type [(dppp)Pt{4-C≡CC_5H_4N-W$(CO)_4PR_3\}_2$]……...249

9.4.3 NMR spectroscopic characterization of [(dppp)Pt{4-C≡CC_5H_4N-W$(CO)_4PPh_3\}_2$]……..249

9.5 Correlation between NMR data and with Tolman electronic parameter ……..255

9.6 Conclusions ……...259

9.7 References.....260

CHAPTER 10: Attempted Synthesis of Ethynyl and Diynyl Bridged Trimetallic Complexes ……..……..264

10.1 Introduction to trimetallic complexes linked by (-C≡C-)$_n$ chains ……...264

10.2 Experimental……...266

10.2.1 Preparation of [Hg(C≡CSiMe$_3$)]……...266

10.2.2 Preparation of [(dppe)PtCl$_2$]…….267

10.2.3 Preparation of *trans*- [(PPh$_3$)$_2$Pt(C≡CSiMe$_3$)$_2$]…….267

10.2.4 Preparation of [(dppe)Pt(C≡CC≡CH)$_2$]…….……...268

10.2.5 Preparation of [Rh(H)(CO)(PPh$_3$)$_3$]….……268

10.2.6 Preparation of [Rh(Cl)(CO)(PPh$_3$)$_2$]…….269

10.2.7 Attempted preparation of [Hg{C≡C-Rh(PPh$_3$)$_2$(XNC)$_2$}$_2$]….……..269

10.2.8 Attempted preparation of *trans*-[(PPh$_3$)$_2$Pt{C≡C-Rh(PPh$_3$)$_2$(XNC)$_2$}$_2$]..…..……..270

10.2.9.1 1st Attempted preparation of *trans*-[(PPh$_3$)$_2$Pt{C≡C-Rh(CO)(PPh$_3$)$_2$}$_2$].....……..270

10.2.9.2 2nd Attempted preparation of *trans*-[(PPh$_3$)$_2$Pt{C≡C-Rh(CO)(PPh$_3$)$_2$}$_2$]…….....…270

10.2.9.3 3rd Attempted preparation of *trans*-[(PPh$_3$)$_2$Pt{C≡C-Rh(CO)(PPh$_3$)$_2$}$_2$]…….....271

10.2.10.1 1st Attempted preparation of [Hg{C≡C-Rh(CO)(PPh$_3$)$_2$}$_2$]...…….……271

10.2.10.2 2nd Attempted Preparation of [Hg{(C≡C-Rh(CO)(PPh$_3$)$_2$}$_2$]..……271

10.2.11.1 1st Attempted preparation of [(dppe)Pt{C≡CC≡C-Rh(CO)(PPh$_3$)$_2$}$_2$]……272

10.2.11.2 2nd Attempted preparation of [(dppe)Pt{C≡CC≡C-Rh(CO)(PPh$_3$)$_2$}$_2$]…….....272

10.2.12 Attempted preparation of [(dppe)Pt{C≡CC≡C-Ir(CO)(PPh$_3$)$_2$}$_2$]…….....273

10.2.13a Attempted preparation of [(dppe)Pt{C≡CC≡C-Rh(XNC)(PPh$_3$)$_2$}$_2$] …….....273

10.2.13b Attempted preparation of [(dppe)Pt{C≡CC≡C-Rh(CO)(PPh$_3$)$_2$}$_2$].....273

10.3 Results and discussion…….....274

10.3.1 Synthesis of ethynyl compounds of platinum and mercury…….....275

10.3.2 Synthesis of rhodium(I) complexes…….....276

10.3.3 Attempted desilylation of ethynyl-bridged trimetallic complexes……....276

10.3.4 Attempted synthesis of butadiynyl-bridged complexes of platinum and rhodium or iridium……278

10.4 Conclusions……..279

10.5 References……280

CHAPTER 11: General conclusions……283

APPENDIX A……..…287

A.1 Crystal structure and refinement data for $[W(CO)_4(NCMe)\{P(Ph_2C_6F_5)\}]$ **31** 287

LIST OF FIGURES

Figure 1.1 Neutral molecular monomeric precursors; (A) diynyl bridge, and (B) N-donor ethynylpyridine bridge. ……..9

Figure 1.2 Assemblies of heteronuclear molecular squares of Pt^{II}, (M = Pd) where cyano- is the organic linker……..9

Figure 1.3 Squares of nanometer dimension (termed nanosquares) which could contain as many as twelve metal centres.…….....10

Figure 1.4 Catalytic cycle for the cluster-catalysed hydroformylation of ethylene…….....14

Figure 1.5 Multiple oxidation states in multimetallic clusters……..16

Figure 1.6 Heterosite reactivity of the heterometallic cluster $[Ru_2Co_2(CO)_{13}]$ …….....16

Figure 1.7 Illustration of the *trans*-influence in linear nitrosyl complexes with different types of *trans*-ligands. (a) σ-Donor NH_3/NR_3; (b) σ-donor – π-acceptor CN^- ligand; (c) σ-donor – π-donor Cl^- ligand. ……..23

Figure 2.1 Splitting of nuclear spin states in an external magnetic field. ……....44

Figure 2.2 An illustration of the precessional motion of a spinning nucleus having a magnetic moment, μ, in an applied field B_0……..45

Figure 2.3 The resultant precessional motion of a collection of nuclei producing a magnetic moment, μ…….....45

Figure 2.4 Precession of M about H_1 (B_o) in the rotating frame showing flip θ of 90^0 and $180^{0\cdots}$46

Figure 2.5 Correlation of $\delta(^{103}Rh)$ of substituted $(X)CpRh(CO)_2$ complexes with rate constants for the displacement of CO by PPh_3: (Δ) correlation points; (▲) $\delta(^{103}Rh)$ of complexes for which rates are unknown; $R^2 = 0.973$…….....52

Figure 2.6 A plot of $\delta(^{187}Os)$ vs. Tolman's electronic parameter χ (where $\chi \equiv \nu_{co}$ for complexes $[Os(p\text{-cymene})(Cl)_2(L)]$…….....52

Figure 2.7 Correlation of $\delta(^{57}Fe)$ with Tolman's cone angle θ of ligand L of $[CpFe(CO)(L)(COMe)]$ complexes (r = 0.941)……53

Fiqure 2.8 A representation of a simplified version of INEPT pulse sequence…….....56

Figure 2.9 Standard HMQC pulse sequence for inverse detection of (^{31}P,^{103}Rh){^{1}H}. (where Δ is equal to 1/2J and J = $J_{(Rh-P)}$) ……..……..…….....58

Figure 2.10 ^{1}H{^{119}Sn} (a); ^{1}H{^{31}P} (b), (f); ^{31}P{^{103}Rh} (c); ^{1}H{^{15}N} (d); and ^{31}P{^{15}N} (e) HMQC spectra recorded from [Rh(NCBPh_3)(H)($SnPh_3$)(py)(PPh_3)$_2$] (a-c) and [Rh(^{15}NCBPh_3)(H)($SnPh_3$)(PPh_3)$_2$] (d-f) in dichloromethane at 248 K using a Bruker DRX 400 spectrometer with the pulse sequence similar to the one shown in **Fig. 2.9....**59

Figure 2.11 Ranges of ^{15}N chemical shifts in metal complexes……..…….....64

Figure 2.12 ^{31}P chemical shift ranges for three coordinate phosphorus compounds……68

Figure 2.13 Schematic representation of ^{57}Fe chemical shift. ……71

Figure 2.14 A correlation chart between oxidation state and ^{103}Rh chemical shift in ppm relative to Ξ(^{103}Rh) = 3.16 MHz ……....73

Figure 2.15 Schematic diagram of ^{195}Pt chemical shift ranges for various oxidation states…...77

Figure 3.1 Three super conducting FT NMR instruments used during the research (300, 400 and 500 NMR instruments).....90

Figure 3.2 A picture of the upper probe interior and with NMR sample.....90

Figure 3.3 An image of a lower part of a 5 mm 400 MHz Bruker tripple resonance (TBI) probe…91

Figure 3.4 A Simplified representation of X-ray diffraction instrument.....95

Figure 3.5 Apex Bruker-Axs X-ray diffractometer.....……..95

Figure 4.1A A plot of temperature (K) vs. ^{207}Pb/^{119}Sn chemical shift (ppm)…….....109

Figure 4.2 A plot of Hammett substituent constant against ^{207}Pb chemical shifts (ppm) ….....112

Figure 4.3 A plot of Hammett substituent constants against ^{119}Sn chemical shifts (ppm). 113

Figure 4.4 ORTEP drawing (50% probability level) and labelling scheme for Ph_3SnCl.py (**A**) and Ph_3PbCl.py* (where py* is *para*-substituted pyridine) (**B**)…….....114

Figure 5.1 (a) ^{1}H spectrum of [CpFe(CO)P($OMe)_3$($SnPh_3$)] **11**; (b) ^{13}C{^{1}H} spectrum of [CpFe(CO)P($Cy)_3$($SnPh_3$)] (**6**); (c) ^{31}P{^{1}H} spectrum of [CpFe(CO)P(p-$C_6H_4)_3$ ($SnPh_3$)] **3**; (d) ^{119}Sn{^{1}H} spectrum of [CpFe(CO)P($NMe_2)_3$($SnPh_3$)] (**7**) all in $CDCl_3$ at 300 K…...43

Figure 5.2 ($^{57}Fe^{31}P$){^{1}H} spectrum of; (A) [CpFe(CO)P(OPh)$_3$(SnPh$_3$)] **10**; (B) [CpFe(CO)P(Cy)$_3$(SnPh$_3$)] **6**, in CDCl3 at 300 K (in A1 and B1 the ^{31}P shows axis the 1D $^{31}P\{^{1}H\}$ spectrum separately optimised and, in A2 and B2 the ^{31}P axis shows the internal projections)…….....144

Figures 5.3 (a) ORTEP diagrams of [CpFe(CO)P(*p*-FC$_6$H$_4$)$_3$(SnPh$_3$)] **3** and, (b) [CpFe(CO)P(p-tolyl)$_3$(SnPh$_3$)] **5** showing thermal ellipsoids at 50% probability level…….148

Figures 5.4 (a) ORTEP diagrams of [CpFe(CO)P(Cy)$_3$(SnPh$_3$)] **6** and, (b) [CpFe(CO)P(NMe$_2$)$_3$(SnPh$_3$)] (**7**) showing thermal ellipsoid at 50% probability level.…149

Figures 5.5 (a) ORTEP diagrams of [CpFe(CO)P(MePh$_2$)$_3$(SnPh$_3$)] **8** showing thermal ellipsoids at 50% probability level and, (b) SCHAKAL drawing [CpFe(CO)P(Bu)$_3$(SnPh$_3$)] **9** (SCHAKAl diagram chosen for clarity purpose). …...……..150

Figure 5.6 (a) SCHAKAL drawing of [CpFe(CO)P(OPh)$_3$(SnPh$_3$)] **10** and ORTEP diagram of [CpFe(CO)P(OMe)$_3$(SnPh$_3$)] **11** showing thermal ellipsoids at the 50% probability level…....151

Figure 5.7a A plot of δ(^{57}Fe) vs. δ(^{119}Sn); chemical shifts in ppm…….....153

Figure 5.7b A plot of δ(^{57}Fe) vs. δ(^{13}C) (CO); chemical shifts in ppm……...……...153

Figure 5.8a A plot of δ(^{57}Fe) (ppm) vs. IR (experimental *V*co) in cm^{-1}…….155

Figure 5.8b A plot of. δ(^{57}Fe) (ppm) vs Tolman's cone angle (θ)…….155

Figure 5.8c A plot of δ(^{119}Sn) (ppm) vs. IR (experimental *V*co)……156

Figure 5.9a A plot of Fe-P bond length (Å) vs. δ(^{57}Fe) (ppm)……...157

Figure 5.9b A plot of Fe-Sn bond length (Å) vs. δ(^{57}Fe) (ppm)……157

Figures 5.9c A plot Sn-Fe-P bond angle (°) against δ(^{57}Fe) (ppm) ……..158

Figure 6.1 ^{57}Fe NMR spectra of [CpFe(PMe$_2$Ph)$_2$(SnPh$_3$)] **15** in CDCl3 at 300 K……...171

Figure 6.2 ^{31}P NMR spectrum of [CpFe{P(OMe)$_3$}$_2$(SnPh$_3$)] **16** (top) and ^{119}Sn NMR spectrum of [CpFe{P(OPh)$_3$}$_2$(SnPh$_3$)] **17** (bottom)……..172

Fiqure 6.3 (A) ORTEP drawing of [CpFe(PMe$_3$)$_2$SnPh$_3$] **14** showing thermal ellipsoids at the

50% probability level and (B) SCHAKAL stereoview for clarity……..……..175

Fiqure 6.4 (A) ORTEP drawing of [CpFe(PMe_2Ph)$_2$$SnPh_3$] **15** showing thermal ellipsoids at the 50% probability level and (B) SCHAKAL stereoview for clarity…….……...176

Fiqure 6.5 (A) ORTEP drawing of [CpFe{$P(OMe)_3$}$_2$$SnPh_3$] **16** showing thermal ellipsoids at the 50% probability level and (B) SCHAKAL stereoview for clarity…...……...177

Figure 7.1 ORTEP diagram of [$W(CO)_5P(p\text{-}CH_3C_6H_4)_3$] **19** showing thermal ellipsoid drawing at 50% probability level. (Ball-and-stick view of isomeric forms of complex **19A** and **19B**).....196

Figure 7.2 ORTEP diagram of [$W(CO)_5P(p\text{-}CF_3C_6H_4)_3$] **22** showing thermal ellipsoids at 50% Probability level…..……..……197

Figure 7.3 ORTEP diagram of [$W(CO)_4(NCMe)(PPh_3)$] **24** showing thermal ellipsoid at 50% probability level. Hydrogen atoms have been omitted for clarity…….…….....202

Figure 7.4 ORTEP diagram of [$W(CO)_4(NCMe)P(p\text{-}MeC_6H_4)_3$] **25** showing thermal ellipsoid at 50% probability level. Hydrogen atoms have been omitted for clarity.....202

Figure 7.5 ORTEP diagram of [$W(CO)_4(NCMe)P(p\text{-}OMeC_6H_4)_3$] **26** showing thermal ellipsoids at 50% probability level. Hydrogen atoms have been omitted for clarity…….…..….203

Figure 7.6 ORTEP diagram of [$W(CO)_4(NCMe)P(p\text{-}FC_6H_4)_3$] **27** showing thermal ellipsoids at 50% probability level. Hydrogen atoms have been omitted for clarity…….……...203

Figure 7.7 ORTEP diagram of [$W(CO)_4(NCMe)P(p\text{-}CF_3C_6H_4)_3$] **28** showing thermal ellipsoids at 50% probability level. Hydrogen atoms have been omitted for clarity……..……..……204

Figure 7.8 ORTEP diagram of [$W(CO)_4(NCMe)P(NMe_2)_3$] **29** showing thermal ellipsoids at 50% probability level. Hydrogen atoms have been omitted for clarity…….…...…….204

Figure 8.1 Progress of reaction between compound [$(PPh_3)_2Rh(H)_2(pytca)$] **43** and tungsten [$W(CO)_4(NCMe)(PPh_3)$] **24**……...222

Figure 8.2 $^{31}P\{^1H\}$ NMR spectra of the reaction between [$Rh(H)_2(PPh_3)_2(pytac)$] **43** and

Tungsten [$W(CO)_4(NCMe)(PPh_3)$] **24**……..……223

Figure 8.3 ^{15}N-^{1}H NMR spectrum of [$(PPh_3)_2Rh(H)_2$(pytca)] **43** before coordination.....225

Figure 8.4 ^{15}N-^{1}H NMR spectrum of [$(PPh_3)_2Rh(H)_2$(pytca)-$W(CO)_4P(tolyl)_3$] **46**……..225

Figure 8.5 A representative NMR spectrum of ^{103}Rh-$^{31}P\{^{1}H\}$ of the complexes of the type [$(PPh_3)_2Rh(H)_2$(pytca)-$W(CO)_4PR_3$] (**45**, R = Ph) in (MeOD/THF at 300 K, f2 (Y-axis) projection represents ^{103}Rh and f1(X-axis) ^{31}P NMR scales 226

Figure 8.6 ^{183}W-$^{31}P\{^{1}H\}$ spectrum of [$(PPh_3)_2Rh(H)_2$(pytca)-$W(CO)_4P(4\text{-}FC_6H_4)_3$] **47** from a solution of MeOD/THF at 300 K 227

Figure 8.7 NMR data Correlation between $\delta(^{183}W)$ and $\delta(^{103}Rh)$ for complexes of the type [$(PPh_3)_2Rh(H)_2$(pytca)-$W(CO)_4P(R)_3$].....228

Figure 8.8A A plot $\delta(^{183}W)$ against Tolman electronic parameter for complexes of the type of [$(PPh_3)_2Rh(H)_2$(pytca)-$W(CO)_4P(R)_3$].....229

Figure 8.8B A plot $\delta(^{103}Rh)$ against Tolman electronic parameter for complexes of the type of [$(PPh_3)_2Rh(H)_2$(pytca)-$W(CO)_4P(R)_3$]……..…….230

Figure 8.9 ORTEP drawing of [$(PPh_3)_2Rh(H)_2$(pytca)-$W(CO)_4P(tolyl)_3$] **46** showing thermal ellipsoids at the 50% probability level ……..231

Figure 8.10 MERCURY capped generated stereo view with atom labeling for clarity for [$(PPh_3)_2Rh(H)_2$(pytca)-$W(CO)_4P(tolyl)_3$] **46**.....231

Figure 8.11 Simplified MERCURY generated capped sticks showing possible π-π stacking (between a phenyl and thiozole rings) and *π-π-π* stacking among three phenyl rings of [$(PPh_3)_2Rh(H)_2$(pytca)-$W(CO)_4P(tolyl)_3$] **46**……..233

Figure 9.1 Representation of a heterobimetallic complex bridged by unsaturated hydrocarbon link ……..240

Figures 9.2 The ^{15}N-^{1}H (top) and ^{195}Pt-$^{31}P\{^{1}H\}$ (bottom) correlation NMR spectra of compound

[(dppp)Pt{4-C≡CC$_5$H$_4$N}$_2$]……...247

Figure 9.3 NMR spectra of ^{195}Pt-^{31}P{^{1}H} (top) and ^{183}W-^{31}P{^{1}H} (bottom) for compound [(dppp)Pt{(4-C≡CC$_5$H$_4$N)W(CO)$_4$PPh$_3$}$_2$].....251

Figure 9.4 Long-range ^{15}N-^{1}H correlation NMR spectrum of *meta*-positioned proton of the pyridyl group for compound [(dppp)Pt{(4-C≡CC$_5$H$_4$N)W(CO)$_4$PPh$_3$}$_2$] .....……..253

Figure 9.5 ^{31}P-^{15}N{^{1}H} NMR spectrum of [(dppp)Pt{(4-C≡CC$_5$H$_4$N)W(CO)$_4$PPh$_3$}$_2$] **54**. Left; shows separately recorded spectrum of ^{31}P{^{1}H} and, right: shows internal ^{31}P spectrum projection…….....…...254

Figure 9.6 A plot δ(^{195}Pt) against δ(^{183}W) for complexes of the type [(dppp)Pt{(4-C≡CC$_5$H$_4$N)W(CO)$_4$PR$_3$}$_2$]..... 256

Figure 9.7 A plot ^{1}J$_{(Pt-P)}$ against ^{1}J$_{(W-P)}$ for complexes of the type [(dppp)Pt{(4-C≡CC$_5$H$_4$N)W(CO)$_4$PR$_3$}$_2$].....256

Figure 9.8 A plot δ(^{183}W) against the Tolman electronic parameter for PR$_3$ in complexes of the type [(dppp)Pt{(4-C≡CC$_5$H$_4$N)W(CO)$_4$PR$_3$}$_2$].....257

Figure 9.9 A plot δ(^{195}Pt) against IR$_{(C≡O)}$ electronic parameter for PR$_3$ in complexes of the type [(dppp)Pt{(4-C≡CC$_5$H$_4$N)W(CO)$_4$PR$_3$}$_2$].…….....……....257

Figure 9.10 A plot δ(^{183}W) against Hammett constants for PR$_3$ in complexes of the type [(dppp)Pt{(4-C≡CC$_5$H$_4$N)W(CO)$_4$PR$_3$}$_2$].……...258

Figure 9.11 A plot δ(^{195}Pt) against Hammett constants for PR$_3$ in complexes of the type [(dppp)Pt{(4-C≡CC$_5$H$_4$N)W(CO)$_4$PR$_3$}$_2$]...……...258

Figure 10.1 Typical neutral molecular squares composed of bis(phosphine)platinum (A) and (B) monodentate ligands as corner units with diynyl linkers……..……..265

List of tables

Table 1.1. Illustration of the comparative kinetic data derived from $MX(CO)(PR_3)_2$…….....26

Table 2.1 NMR Properties of tin isotopes…….67

Table 2.2 NMR parameters of selected transition metal nuclei……70

Table 3.1 Spin one-half nuclei of selected isotopes recorded in this thesis, NMR spectrometer frequencies and their respective standard reference materials.....92

Table 4.1 Crystal and structure refinement data for $Ph_3SnCl.py$ and $Ph_3PbCl.py$* (py* = 4-phenylpyridine)…….....103

Table 4.2 Results of the influence of concentration of pyridine (py) on $Ph_3MCl.py$ (M = Sn and Pb) adducts……..……..106

Table 4.3 ^{207}Pb and ^{119}Sn chemical shifts of $Ph_3PbCl.py$* and $Ph_3SnCl.py$*……..…….111

Table 4.4 Selected bond lengths (Å) and angles (°) of $Ph_3SnCl.py$* (**1a**) and $Ph_3SnCl.py$ (**1b**) adducts……..115

Table 5.1 Crystal and structure refinement data for the compounds **3**, **5**, **6**, **7**, **8**, **9**, **10** and **11**..124

Table 5.2 A list of Tolman's parameters, experimental yields and IR values in $CHCl_3$ solution of complexes of the type $[CpFe(CO)(PR_3)(SnPh_3)]$……....139

Table 5.3 NMR data for the hetero-bimetallic iron-tin complex, $[Fe(Cp)(CO)(PR_3)(SnPh_3)]$..140

Table 5.4 Coupling constants of the hetero-bimetallic Fe - Sn complexes of the type $[CpFe(CO)(PR_3)(SnPh_3)]$…….……142

Table 5.5 Selected bond lengths and angles for compounds **3**, **5**, **6**, **7**, **8**, **9**, **10** and **11**……..145

Table 5.6 Selected bond lengths of the Fe-C of the Cp ring for $[CpFe(CO)PR_3(SnPh_3)]$……..146

Table 6.1. Crystal Refinement Data for compound **14**, **15** and **16**…….….168

Table 6.2 NMR spectroscopic results of the complexes of the type $[CpFe(PR_3)_2SnPh_3]$……...170

Table 6.3 Selected Bond lengths (Å) and anlges (deg) for Compounds $[CpFe(PMe_3)_2SnPh_3]$

(**14**), [CpFe(PMe_2Ph)$_2SnPh_3$] (**15**) and [CpFe{$P(OMe)_3$}$_2SnPh_3$] (**16**)……..174

Table 7.1 Crystal Refinement Data for compound **19** and **22**……192

Table 7.2 Crystal refinement data for compound **24** – **29**……...193

Table 7.3 Selected NMR data for the complexes of the type [$W(CO)_5PR_3$] ……..195

Table 7.4 Selected bond lengths (Å) and angles (º) for compounds **19A**, **19B** and **22**……...197

Table 7.5 Selected NMR data for complexes **24**, **25**, **26**, **27**, **28** and **29**……199

Table 7.6 Selected bond lengths and angles for **24**, **25**, **26**, **27**, **28** and **29**. ……201

Table 8.1 Crystal and structure refinement data for the compound [$(PPh_3)_2Rh(H)_2$(pytca)$W(CO)_4P$(tolyl)$_3$]……217

Table 8.2 Selected chemical shifts of ^{15}N, ^{31}P, ^{103}Rh and ^{183}W, and the significant coupling constants for compounds **41** – **50**……...224

Table 8.3 Selected bond length (Å) and angles (deg) for compound [$(PPh_3)_2Rh(H)_2$(pytca)-$W(CO)_4P$(tolyl)$_3$] **46**……234

Table 9.1 Selected ^{31}P coupling constants for monometallic tungsten and ethynylpyridine-bridged trimetallic platinum-tungsten complexes……250

Table 9.2 Selected NMR data for monometallic tungsten and ethynylpyridine-bridged trimetallic platinum-tungsten complexes……..250

List of schemes

Scheme 1.1 Preparation of platinum metal complexes containing a –C≡C- bridge ...……..11

Scheme 1.2 CuI-catalysed preparation of heterobimetallic metal complexes containing -C≡C- bridge.....12

Scheme 1.3 Proposed reaction mechanism of CuI-catalysed reactions……..…….....13

Scheme 1.4 Proposed mechanism for Me_3NO decarbonylation. …….19

Scheme 1.5 A typical oxidative addition reaction process……....25

Scheme 1.6 Oxidative addition reaction of a polar A-B moiety to a five co-ordinate d^8 transition metal complex……...26

Scheme 1.7 A typical reductive elimination reaction process…….....27

Scheme 4.1 Schematic representation of the possible equilibrium in favour of the five coordinate $Ph_3MCl.py$ adducts (M= Pb, or Sn, and R = H)….....……..106

Scheme 5.1 General synthetic route to bimetallic complexes of iron and tin…….....137

Scheme 7.1 Reaction of [*fac*-$W(CO)_3(MeCN)(dppb)$] complex with C_{60}……..183

Scheme 7.2 Novel reaction of six coordinate tungsten(VI) compound with diphosphino complex.....183

Scheme 8.1 Examples of Bridging ligands containing a nitrogen atom……..209

Scheme 8.2 Coordination modes of pyrazca...……....210

Scheme 8.3 Schematic representation of different synthetic routes leading to carboxylate rhodium(III)dihydrido complexes……..218

Scheme 8.4 Reaction scheme for the synthesis of $[(PPh_3)_2Rh(H)_2(pytca)W(CO)_4P(tolyl)_3]$….221

Scheme 9.1 A simplified synthetic route towards the formation of trimetallic complex of the type $[(dppp)Pt\{4\text{-}C{\equiv}CC_5H_4N\text{-}W(CO)_4PR_3\}_2]$…….248

Scheme 9.2 Proposed molecular structure of $[(dppp)Pt\{4\text{-}C{\equiv}CC_5H_4N\text{-}W(CO)_4PPh_3\}_2]$……...252

Scheme 10.1 Reaction scheme for the synthesis of ethynyl-bridged heterotrimetallic complexes…….……274

Scheme 10.2 Syntheses of platinum and mercury ethynyl complexes…….**.....**275

Scheme 10.3 Preparation of rhodium(I)phosphine complexes…….**....**276

Scheme 10.4 Proposed reaction scheme for desilylation of mercury acetylide complexes ……..277

Scheme 10.5 Proposed reaction of platinum-diynyl complexes with rhodium(I) and iridium(I) phosphine complexes……..…….……279

Abriviations

Acac	acetylacetonate
BBI (probe)	Broadband Inverse
4,4-bipy	bipyridine
CCDC	Cambridge Crystallographic Data Centre
Cp	Cyclopentadienyl
DEPT	Distortionless Enhancement by Polarization Transfer
Diglyme	Diethyl glycol dimethyl ether
DNA	Deoxyribonucleic Acid
dppe	diphenylphosphinoethane
dppp	diphenylphosphinopropane
HMQC	Heteronuclear Multiple-Quantum Coherence
HOMO	Highest Occupied Molecular Orbital
HPLC	High Performance Liquid Chromatography
INEPT	Insensitive Nuclei Enhanced by Polarization Transfere
isoqca	isoquinoline-1-carboxylate
IUPAC	International Union of Pure and Applied Chemistry
LDA	Lithium Diisopropylamide
LUMO	Lowest Unoccupied Molecular Orbital
ORTEP	Oak Ridge Thermal Ellipsoid Plot
O_2Cpyraz	pyrazine-2-carboxylate

Ppca	4-(pyridine-4-yl)pyridine-2-carboxylate
py	pyridine
py*	*para*-substituted pyridine
pyca	pyridine-2-carboxylate
pyrazda	2,2-pyrazinedicarboxylate
pytca	2-(40pyridyl)thiazole-4-carboxylate
pyz	pyrazine
QNP	Quattro Nucleus Probe
TBAF	Tetrabutylammoniumflouride
TBI	Tripple-resonance Broadband Inverse probe
TMEDA	Tetramethylethylenediamine
Tolyl	*para*-methylphenyl
XCN	2,6-dimethylphenyl cyanide

CHAPTER 1

Chemistry of selected Transition Metals

Many important chemicals are produced commercially by reactions that are catalysed by organometallic compounds in either homogenous or heterogeneous medium and this fact provides one of the motivating forces for studying organometallic chemistry. Each type (homogenous or heterogenous medium) has its own advantages and disadvantages. However, homogenous catalysis is commonly used because of operating conditions, e.g. low temperatures and pressure, good selectivity and because solution reactions are generally better understood than are surface reactions of heterogeneous catalysis [1]. However, catalyst recovery in homogeneous phase remains the biggest disadvantage. Recently, catalysis in a liquid/liquid two-phase system has found industrial application wherein ligands such as tri(*m*-sulfonatophenyl)phosphine render the catalyst water-soluble allowing it to be recovered quantitatively from organic products [2]. Some of the important complexes that are active in homogeneous catalysis are those that contain the late transition metals.

Some of the homogeneously catalysed reactions are: hydroformylation by a cobalt complex ($[HCo(CO)_4]$, claimed to have been the first catalyst to be used industrially) or a rhodium complex $[Rh(H)(CO)(PPh_3)_3]$, the Wacker process by a palladium complex, the Heck reaction by a Pd^0 complex formed *in situ* from $Pd(OAc)_2$, Et_3N and PPh_3, Ziegler-Natta polymerisation from the combination of $TiCl_4$ and $AlEt_3$, hydrogenation of alkenes by Wilkinson's catalyst $[(Ph_3P)_3RhCl]$ and the Monsanto acetic acid process catalysed by a rhodium salt and a source of iodine to produce an active organometallic catalyst, $[Rh(CO)_2I_2]^-$ [2,3]. Chemists are now able to fine-tune the coordination sphere of a metal to obtain high selectivity in many reactions such as recent alkoxycarbonylation of propyne to give methyl methacrylate with 99% selectivity [4] and the perfectly alternating copolymerization of ethylene and carbon monoxide to give high-performance industrial polymers [5].

The activity of many transition metal catalysts is as a result of their ability to activate small molecules (e.g. H_2, O_2, N_2 and CO_2) or selectively activate bonds in larger molecules. In addition to the accessibility and the availability of a vacant coordination site, an appropriate oxidation state is important. The search for a catalyst for specific reactions (such as those relevant to organic synthesis under mild conditions) usually requires extensive exploratory studies in which the selectivity and effectiveness of the desired reaction is enhanced by tailoring the metal complex (the possible catalyst) in various ways. Small metal clusters have a potentially valuable role to play in catalysis since their chemistry is more varied and more versatile than that of mononuclear complexes [6]. Binuclear complexes of rhodium show outstanding catalytic activity in hydroformylation [7] and in methanol carbonylation [8].

1.1 Historical perspective

Compounds such as $[Pt(C_2H_4)(Cl)_3]^-$ (first synthesised by W.C. Zeise in 1827), $[PtCl_2(CO)_2]$ (reported by P. Schutzenberger in 1968) and $FeCp_2$ (discovered in 1951 and for which G. Wilkinson and E.O. Fischer shared a Nobel Prize in chemistry in 1973) clearly qualify as organometallic complexes whereas a complex such as $[Co(en)]^{3+}$, which contains carbon but has no M-C bond, does not. Cyano complexes such as $[Fe(CN)]^{2+}$ ions do have an M-C bond but they are generally not considered as organometallic, though by contrast complexes of the isoelectronic ligand carbon monoxide (CO) are considered as organometallic. This distinction is based on the fact some of these metal carbonyls are significantly different from coordination complexes both chemically and physically [3,9]. Likewise organoboron, organosilicon, organoarsenic, and organotellurium compounds are included in organometallic chemistry even though boron, silicon, arsenic, and tellurium are borderline metals.

An organometallic compound can therefore be defined as one that possesses at least one metal-carbon bond [10]. The bonding interaction as described by the journal *Organometallics* must be "ionic or covalent, localized or delocalized between one or more carbon atoms of an organic group molecule and a transition, lanthanide, actinide, or main group metal". The term *d*-block metal and transition metal are often used interchangeably even though they do not mean exactly the same thing. The IUPAC definition of a transition element is: "it is that element that has an

incomplete *d* sub-shell in either the neutral atom or its ions". Group 12 elements, Zn, Cd, and Hg are members of *d*-block but are not transition elements [9].

1.2 Bimetallic complexes with direct metal-metal bonds

Heterobimetallic complexes with direct metal-metal bonds continue to receive attention in view of their catalytic potential, e.g. in homogenous catalysis, and the possibility that a co-operative effect between different metal centres may enhance their reactivity [11]. As with mixed metal clusters, the current research into heterometallic complexes is stimulated by the belief that the more chemically active metal in the molecule may induce new and interesting reactivity owing to the co-operative effect between adjacent metal centres that are sufficiently polarised [12]. The metal-metal bond polarity in its extreme form involving transition elements is found in di- or polynuclear complexes in which molecular fragments containing metal atoms from the two ends of the *d* block in the periodic table are combined [13].

1.2.1 Chemistry of metal-metal bonded complexes

Complexes with a direct metal-metal bond have been of interest to chemists because of the nature of the bond between them i.e. the bonding order. As a consequence of the presence of two different metal centres this interaction becomes non-symmetrical. This chemical behaviour is realized in its extreme form in the chemistry of early to late heteronuclear complexes in which complex fragments in high oxidation states with no or few *d*-electrons are directly linked to those of the *d*-electron rich late transition metals in relatively low oxidation states [14].

Covalent metal-metal interactions involve electrons which would otherwise be unpaired on their respective metal centres whereas dative interaction involves the donation of nonbonding pairs of electrons from one centre to the other [15]. Covalent compounds of transition metals and the *p*-block elements have been extensively studied. However, there has been some controversy over their exact nature and, in particular, over the existence of multiple bonding between group IVa elements such as silicon, germanium, and tin and transition metals such as iron, cobalt, or manganese [16]. A number of structure determinations have been carried out, primarily on the

Mn-Sn, Fe-Sn, and Co-Si systems. In most cases, a metal-metal bond length significantly shorter than that of the sum of covalent radii has been found and from this information, multiple bond character has been inferred [17].

The first heteronuclear transition metal-metal carbonyl complexes appeared in the early 1960s. These included $[Cp(CO)_3Mo\text{-}W(CO)_3Cp]$ [18], $[Cp(CO)_3Mo\text{-}Fe(CO)_2Cp]$ [19], $[(CO)_5Mn\text{-}Fe(CO)_2Cp]$ [19] and $[Cp(CO)Ni\text{-}Fe(CO)_2Cp]$ [20]. The metal-metal bonds in these compounds can be viewed as covalent heteronuclear bonds derived from the 17 electron metal-containing fragment. To some extent, these results stimulated an overdue recognition of the widespread occurrence of covalent metal-metal bonding in inorganic chemistry. There are more than 30 metals that are capable of forming covalent bonds with each other and even more with binary bonding systems [21]. In 1985, Pomeroy et al. prepared the first example of mixed metal compounds containing heteropolar dative bonds, e.g. $(CO)_5W \leftarrow Os(CO)_4PMe_3$ [22] and $(CO)_5W \leftarrow Ir(CO)_2Cp$ [23], containing 16 electron and 18 electron metal-containing groups linked solely by the metal-metal bond.

Each of the metals in the bimetallic complex can be expected to influence the properties of the other especially if the distance between the two metal centres is significantly short [15]. A direct metal-metal bond may involve sharing of one or more pairs of electrons between the centres. Such a bond could either be covalent in nature or dative involving the donation of an otherwise nonbonding pair of electrons from one centre to the other. The properties of a donor atom in a bridging ligand e.g. CO may be modified by simultaneous coordination to the other metal centre. In a non-symmetrical system, the coordination sphere of the second metal centre might also be expected to have a significant steric effect on the first. Therefore structural information for a given complex should answer question such as: (a) How significant is the interaction between the metal centres? (b) How robust or strong is this interaction, and (c) What is the nature of this interaction (bond order)?

Among the numerous complexes with a direct metal – metal bond, those that are stable without bridging ligands are of special interest [24]. Direct homonuclear metal - metal complexes are known for metals in low and intermediate oxidation states. Examples of dinuclear complexes

with metal-metal single bonds include cyclopentadienyl metal compounds such as $[Cp(CO)_3M–M(CO)_3Cp]$, M = Cr [25a], Mo [25b] and W [25b]. Homonuclear complexes are generally symmetrical dimers with a non-polar metal-metal bond. Polarity can be introduced to a certain degree while maintaining the oxidation state of the metal by the one-sided exchange of a ligand in homoleptic complexes such as $[(CO)_5Re\text{-}Re(CO)_4L]$ [26], where L = C(Me)OMe, CNtBu and $[(Me_2N)_3W{\equiv}W(NMe_2)_2I]$ [27]. Strongly polar metal-metal bonds can be expected in heterobimetallic complexes in which the metal centres are present in significantly different oxidation states such as $[(CO)_5W\text{-}FeMe(CO)_4]$ [28].

1.2.2 Synthesis of bimetallic complexes with direct metal-metal bonds.

One of the earliest reports of a crystallographically characterised metal carbonyl dimer complex containing a non-bridged metal-metal bond was that of $Mn_2(CO)_{10}$ [29]. The synthesis of the first heterobimetallic carbonyl complex $[(Cp)(CO)_3MoW(CO)_3(Cp)]$ was reported in the early 1960's [30]. Many of the heterobimetallic complexes are prepared by metathesis of a halide ligand with an organometallic anion. The most common preparative method is the replacement of the halide ligand on a group 4 metal by an anionic complex such as $[CpM(CO)_2]^-$ (M = Fe, Ru [31] or $[M(CO)_4]^-$ (M = Co) [31b, 32]. A similar reaction has been used to prepare heterobimetallic lanthanide complexes [33]. However, group 6 metals can also form organometallic anions, the so called "metallo-ligand" $[CpM(CO)_3]^-$ (M = Cr, Mo, W) to displace halide ligands from complexes of group 10 metals to give products such as $[MNi(CO)_3(PPh_3)_2(\eta^5\text{-}C_5H_5)]$ (M = Mo or W) [34, 35]. One more example of group 6 metals is a nucleophilic molybdenum complex $[Cp_2Mo(CNEt)]$ which will displace chloride from $[(Ph_3P)AuCl$, forming the heterobimetallic complex $[Cp_2(EtNC)MoAu(PPh_3)]^+$ [36]. Similarly, the [tris(pyrazolyl)borate]molybdate anion $[\{HB(C_3HR_2N_2)_3\}Mo(CO)_3]^-$ (R = H, Me) will displace a halide ligand from a copper centre forming complexes such as $[(CO)_3TpMoCuL]$ (L = PPh_3, TMEDA) [37].

Other approaches to the synthesis of heterobimetallic complexes includes the protonolysis of a complex of an early metal by an acidic "hydride" complex of a late metal [31c, 31d] and the direct addition of $[FeMe(CO)_4]^-$ to $[W(CO)_5(thf)]$ resulting in the heterobimetallic anion $[(CO)_5WFeMe(CO)_4]^-$ having the methyl group *cis* to the tungsten-iron bond [38]. In 1982, two

comprehensive reports by Geoffrey and co-workers [39] on all heteronuclear bimetallic carbonyl complexes known at the time revealed that 111 publications had appeared in almost two decades since their first characterization. By 1995 more than 300 papers had already reported the chemistry of bimetallic compounds describing more than 700 structurally characterised mixed - metal complexes that contain iron [40]. Many more examples of non-bridged heterobimetallic carbonyl complexes of other transition metals have been reported and more complexes will undoubtedly continue to appear in the literature [15, 41, 42].

1.2.3 Bimetallic complexes having transition and non-transition metals.

Particular attention is hereby given to M-Sn complexes because of the diverse chemistry of tin. The ability of tin to complex with transition metals is made possible by the use of three of the *p* electrons in covalent bonding and the other electron can be used to form an adduct with another ionic ligand (listed on the next page). The low-lying empty *d*-orbitals are of suitable symmetry and orientation which when used in the hybridization of the orbitals of tin, create empty orbitals suitable for complex formation. There are several hybridization geometries [43] available for stannylenes and these are: *sp*, sp^2, sp^3, sp^3d and sp^3d^2. Some of the more recent articles dealing with transition-tin metal chemistry are listed [44].

1.2.4 General synthetic routes to bimetallic complexes with a direct metal-tin bond.

There are many synthetic routes to the transition metal–tin complexes which have been reported in the reviews [45, 46]. Some of those synthetic methods which lead to heterobimetallic complexes containing group *d* transition metal with tin are classified as follows (next page):

1. Salt elimination (nucleophilic attack)

$Ph_3SnCl + Na[(C_6H_5)Fe(CO)_2] \rightarrow (C_6H_5)Fe(CO)_2SnPh_3 + NaCl$ **(1.1)** [16,47]

$Me_3SnCl + Na[Mn(CO)_5] \rightarrow Me_3SnMn(CO)_5 + NaCl$ **(1.2)** [48]

$Ph_3SnLi + (C_6H_5)_2HfCl_2 \rightarrow Ph_3SnHf(C_6H_5)_2Cl + LiCl$ **(1.3)** [49]

2. Elimination of small molecules

$SnCl_4 + H_2Os(CO)_4 \rightarrow HOs(CO)_4SnCl_3 + HCl$ **(1.4)** [50]

$4Ph_3SnH + Ti(NEt_2)_4 \rightarrow Ti(SnPh_3)_4 + 4HNEt_2$ **(1.5)** [51]

3. Oxidative addition

$3Me_3SnH + Os_3(CO)_{12} \rightarrow 3HOs(SnMe_3)(CO)_4$ **(1.6)** [52]

$Me_3SnCl + Pt(PR_3)_2 \rightarrow Me_3SnPtCl(PR_3)_2$ **(1.7)** [53]

4. Oxidative elimination

$SnCl_4 + (C_6H_5)Co(CO)_2 \rightarrow (C_6H_5)(CO)CoCl(SnCl_3) + CO$ **(1.8)** [54]

$Me_6Sn_2 + Zr(C_6H_5Me)PMe_3 \rightarrow (Me_3Sn)_2Zr(C_6H_5Me) + PMe_3$ **(1.9)** [55]

5. Insertion of tin(II)

$SnCl_2 + [(C_6H_5)Fe(CO)_2]_2 \rightarrow [(C_6H_5)Fe(CO)_2]_2SnCl_2$ **(1.10)** [56]

$SnCl_2 + (C_6H_5)Fe(CO)_2Cl \rightarrow (C_6H_5)Fe(CO)_2SnCl_3$ **(1.11)** [57]

6. Activated tin addition

$Sn + 2Co_2(CO)_8 \rightarrow Sn[Co(CO)_4]_4$ **(1.12)** [58]

Oxidative addition reactions can be used to synthesize most of the tin complexes of transition metal families. This reaction is limited only by the availability of low-valent transition metal complexes. Tin nucleophiles are used predominantly to make complexes of the early transition metals, though these reagents are used to form complexes of the middle transition metals as well. The other major synthetic route is the "carbene" chemistry of tin(II) compounds [59]. Tin(II) compounds insert into metal – metal, metal – halogen, metal – hydride, and metal carbon bonds.

1.3 Bridged bimetallic complexes

Ligands capable of forming bimetallic complexes are usually differentiated by the number and type of the donor atoms they contain, and the length and the flexibility of the bridging unit. In a bimetallic complex, the structure of the bridging unit of the binucleating ligand is responsible for

keeping the donor atoms of the ligand at a specific distance and for determining the relative disposition of the unsaturated coordinative sites around the two metal centres and consequently the chemistry of the corresponding bimetallic complex [60].

1.3.1 Chemistry of bridged bimetallic complexes.

There has been a rapidly growing interest in the design and synthesis of organometallic complexes containing carbon-rich, yet rigid and π-conjugated chains due to their potential use as precursors for the syntheses of organometallic polymers and π-conjugated bi- or multi-metallic systems [61] of macromolecules of nanoscopic dimensions. This class of complexes also exhibits significantly altered physical properties compared with conjugated organic oligomers and polymers [62]. Nanostructure science and supramolecular chemistry are two fast evolving fields that are concerned with manipulation of materials that have important structural features of nanometer size. The self-assembly approach [63] to the design of metal-based supramolecules in which carbon-rich organometallic complexes plays a pivotal role as building blocks has contributed to the increased interest in the field.

The –C ≡ C- bonds of the alkynyl ligands, like those of the alkynes constitute a natural focal point for reactivity studies and have been shown to participate in a rich set of chemical reactions. Among the ligand-localised reactions of the metal-alkynyl complexes, are those that lead to the transformation of clusters in which the alkynyl ligand bridges multiple metal centres [64]. The linear geometry of the –C ≡ C- unit and its potential to act as a "molecular wire" that might enable electronic communication between its appended substituents has made synthesis and the study of polymers from metal-alkynyl building blocks an active area of research [65]. The one-dimensional units are exceptional linking ligands in that π-electron delocalization over all carbon atoms in the chain permits an intriguing metal-to-ligand-charge-transfer (MLCT) between two transition metals (**Figures 1.1, 1.2** and **1.3**). There has been a significant interest in past 20 years in the design of new monomeric models in order to evaluate the capability of communication between two metal centres M_1 and M_2 through conjugated organic bridges [63]. In addition, these conjugated oligomers and polymers have attracted considerable attention due to their potential application in materials science as one dimensional conductors or liquid crystal precursors, light

emitting diodes (LEDs), and their potential non-linear optical and photo-chemical (luminescence) properties [66].

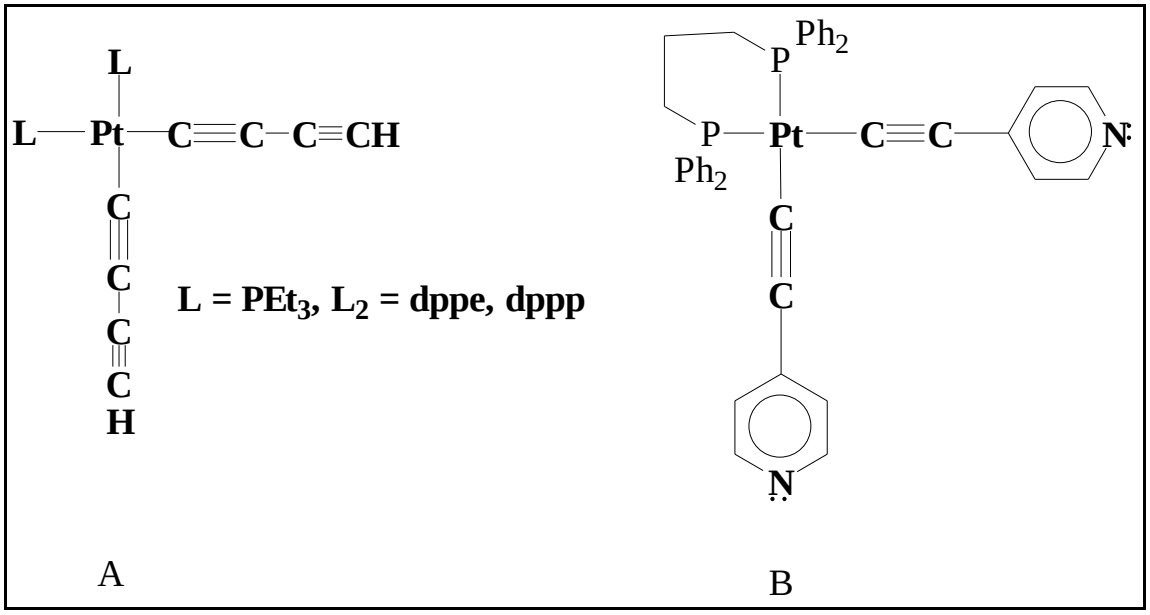


Figure 1.1. Neutral molecular monomeric precursors; (A) diynyl bridge [67], and (B) N-donor ethynylpyridine bridge [68].

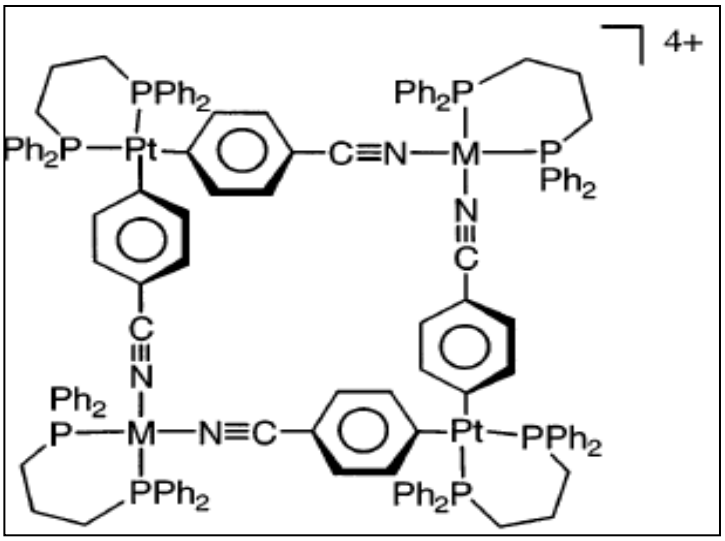


Figure 1.2. Assemblies of heteronuclear molecular squares of Pt^{II}, (M = Pd) where cyano- is the organic linker (Figure taken from ref. 69).

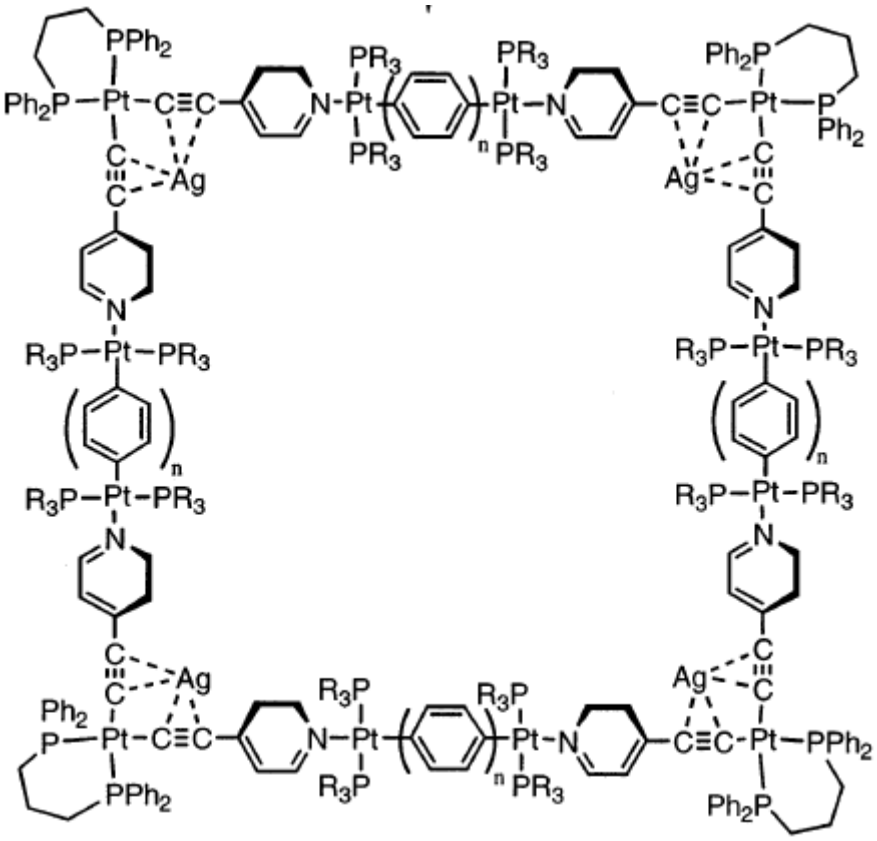


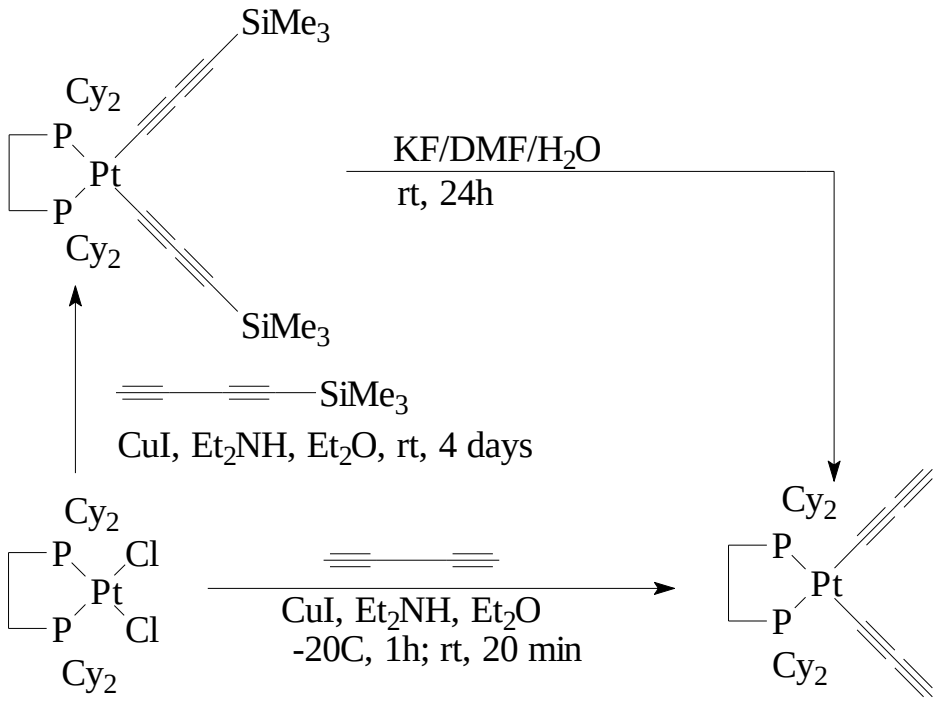
Figure 1.3. Squares of nanometer dimension (termed nanosquares) which could contain as many as twelve metal centres (Figure taken from ref. 70).

The self-assembly process therefore offers a valuable means of preparing coordination compounds whose structural complexity starts to approach that of biological dimensions. Self-assembly in coordination chemistry provides an important and powerful entry into supramolecular engineering and the associated fields of solid-state and crystal engineering [71]. It can potentially afford novel catalytic systems which may ultimately be induced to offer the selectivity and usefulness of biological catalysts [72].

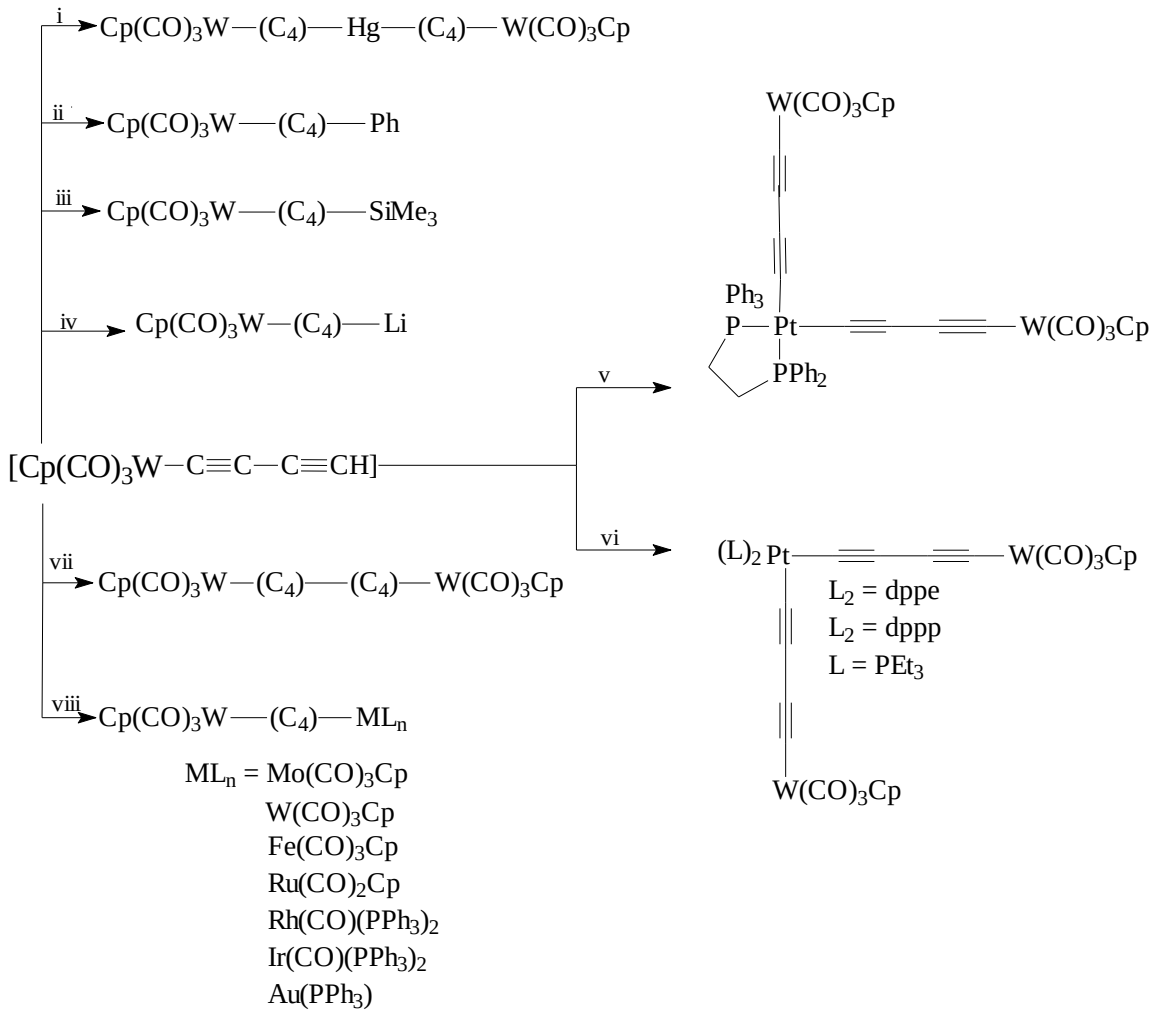
1.3.2 Synthetic routes to selected bridged heterobimetallic complexes.

Following the development of a generally applicable alkynyl coupling reaction by Sonogashira and co-workers [73], the synthesis of metal-diynyl and carbon chain bridged complexes have become commonly applied synthetic routes to a variety of homo- and hetero-metallic bridged compounds with the ultimate goal of a self assembly approach. CuI-catalysed reactions between

halide complexes of Fe, Mo, W, or Pt and an excess of buta-1,3-diyne in the presence of diethylamine lead to the formation of buta-1,3-diynyl compounds as convenient "metallo-ligands" shown in **scheme 1.1** and **1.2**.

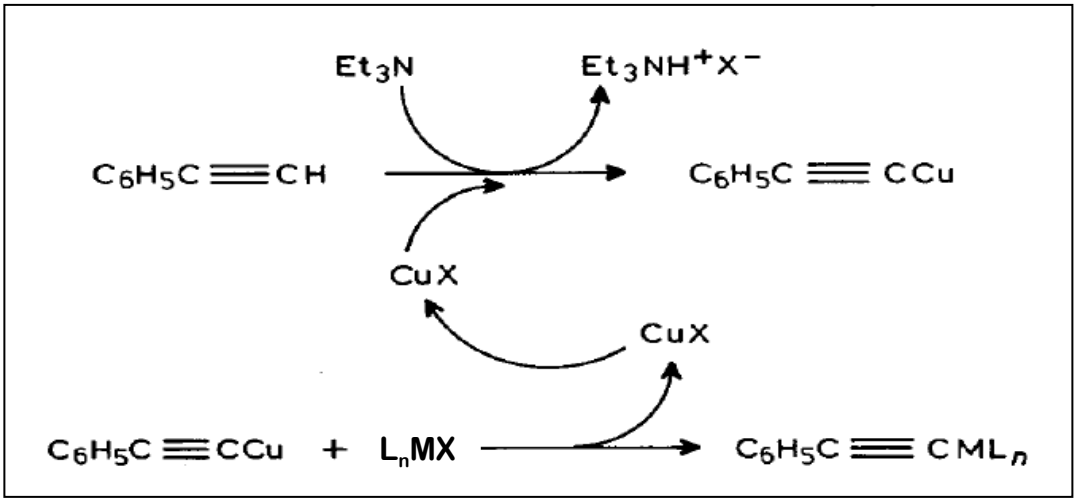


Scheme 1.1 Preparation of platinum metal complexes containing a –C≡C- bridge [74].



Scheme 1.2. CuI-catalysed preparation of heterobimetallic metal complexes containing -C≡C- bridge. Reagents: i, $Hg(OAc)_2$; ii, C_6H_5I, $[Pd(PPh_3)_4]$, CuI; iii, LDA, $SiClMe_3$; iv, $LiNPr^i_2$; v, $[PtCl_2(dppe)]$, CuI, Et_2NH; vi, $PtCl_2(L)_2$, CuI, Et_2NH; vii, [Cu(tmeda)]Cl, O_2; viii, Cl{ML_n} [66b, 75].

The reaction mechanism by which the CuI catalysed reaction proceeds has been proposed as illustrated [76] (**Scheme 1.3**).



Scheme 1.3. Proposed reaction mechanism of CuI catalysed reactions (ref. 76).

1.4 Transition-metal clusters

Metal atom cluster compounds can be formally defined as those in which a group of metal atoms (at least three) are held together entirely, mainly or at least to a significant extent by metal-metal bonds and surrounded by a shell of ligands [77]. A distinct characteristic feature of metal cluster compounds is that they contain a framework of metal atoms held together by metal-metal bonds. The popularity of clusters as a field of study is confirmed by the dedicated periodical *Journal of Cluster Science* in which transition metal clusters are the main focus. Metal cluster compounds of medium nuclearity (between 4 and 9) assume various skeletal frameworks which are discussed elsewhere [78]. A nano-dimensional mixed-metal cluster of the type, $[Pd_{145}(CO)_x(PtEt_3)_{30}]$ formed by reduction of $Pd(PEt_3)_2C_{l2}$ has been structurally rationalised to contain as many as sixty disordered CO ligands [79]. As with mononuclear metal complexes, there are clusters that are stabilised by ligands bonding via carbon, e.g. Fe_3CO_{12} and those that have no metal-carbon bonds, e.g. $[Pt_3(\mu_3\text{-dppp})(\mu_3\text{-Au})(PPh_3)]^+$ [80].

Although many clusters are active as homogeneous catalysts, these clusters can also serve as models for metal surfaces [81,82], as their chemistry approaches that occurring during

heterogeneous catalytic reactions. The role of transition metal clusters in catalysis can be either as direct catalysts or as catalyst precursors. The catalytic surface chemistry of the Fischer-Tropsch reaction has been studied using transition metal clusters as model precursors [83] (e.g hexanuclear ruthenium cluster, $[Ru_6C(CO)_{11}(\eta^6\text{-}C_6H_6)(\mu\text{-}\eta^2\text{:}\eta^2\text{-}C_6H_6)]$). Generally, transition metal clusters are used in the synthesis of heterogeneous catalysts for which they offer several advantages such as solubility in organic solvents [84]. Transition-metal clusters have been proven to be efficient homogeneous catalysts [85], for example, the homogeneously catalysed Fischer-Tropsch synthesis of ethylene glycol from CO and H_2 by $[Rh_{12}(CO)_{34}]^{2-}$ at 250 ^{0}C and 300 bar [86]. Another transition-metal cluster catalysed reaction is hydrofomylation of ethylene by $[HRu_3(CO)_{11}]^-$ [87] and its catalytic cycle has been established by isotopic labeling as shown in **figure 1.4**. There is however no general theory to treat all types of clusters for bonding and structure.

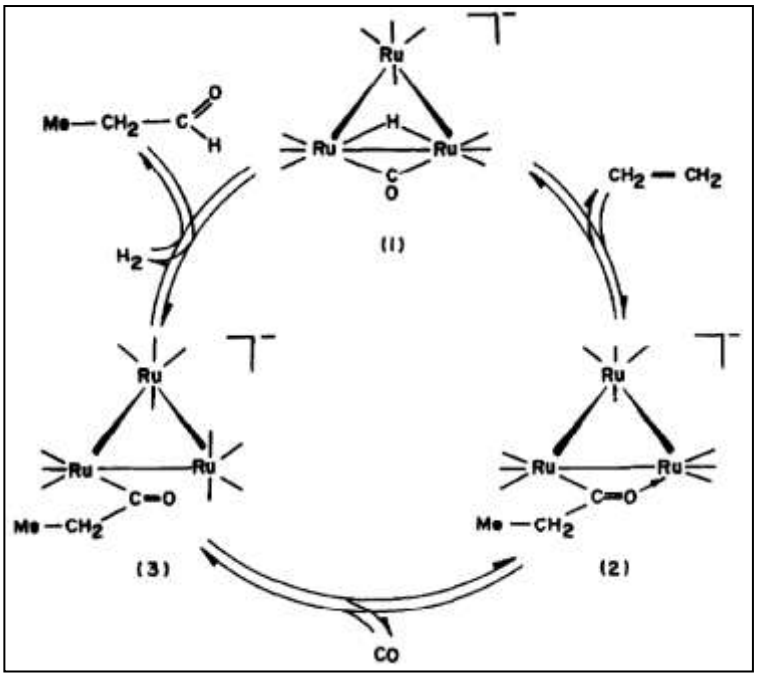


Figure 1.4. Catalytic cycle for the cluster-catalysed hydroformylation of ethylene (Figure taken from ref. 84)

1.4.1 Chemistry of selected metal clusters.

Transition metal clusters, particularly mixed-metal clusters exhibit almost similar opportunities in terms of their general chemistry as bimetallic systems, one being the cooperative effect due to multiple metal centres which offers the possibility of multicenter activation as well as multicenter reaction. A practical application of this ability is illustrated by the migration of a coordinated ligand from one metal atom to another (e.g. H or CO), also called scrambling, in clusters such as $[H_2FeRuOs_2(CO)_{13}$ [88]. The mobility of H and CO is important in catalytic reactions because as the substrates are brought closer together, the chance of a reaction increases. Transition metal clusters can act as an electron reservoir with both electron-donating and electron-accepting abilities. It has been established that some clusters that act as electron reservoirs have a lower ionisation energy and higher electron affinity than mononuclear transition metal complexes. The property of multiple oxidation states as shown by $[(\eta^5\text{-}C_5H_5)Fe(CO)]_4$ and $[Co_3Cp_3(\mu_3\text{-}S)_2]$, where four oxidation states are possible (+2, +1, 0 and -1) [89] (**Fig. 1.5**) can be biologically significant for a consistent supply of electrons to substrates. Heterosite reactivity is another chemical opportunity where transition mixed-metal clusters such as $[Ru_2Co_2(CO)_{13}]$ react with molecular H_2 under mild conditions at ruthenium atoms to form $[H_2Ru_2Co_2(CO)_{12}]$ and with acetylene at the cobalt atoms to give $[Ru_2Co_2(CO)_{11}(R_2C_2)]$ [90] (**Fig. 1.6**). The ability to activate more than one substrate offers a unique opportunity in designing site-specific catalysts for complicated reactions.

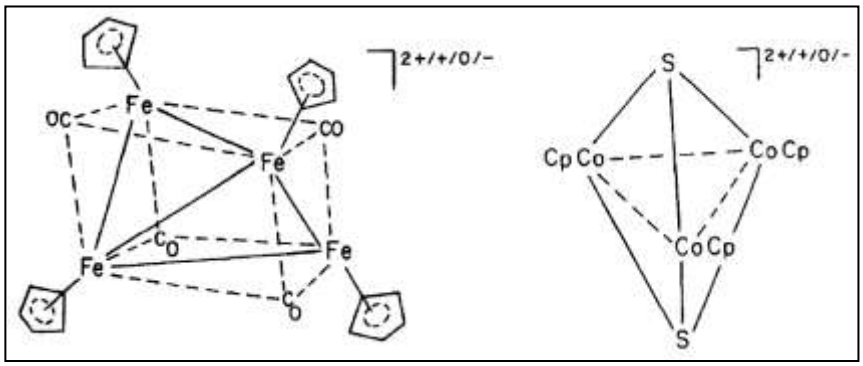


Figure 1.5. Multiple oxidation states in multimetallic clusters. (Figure taken from ref. 84)

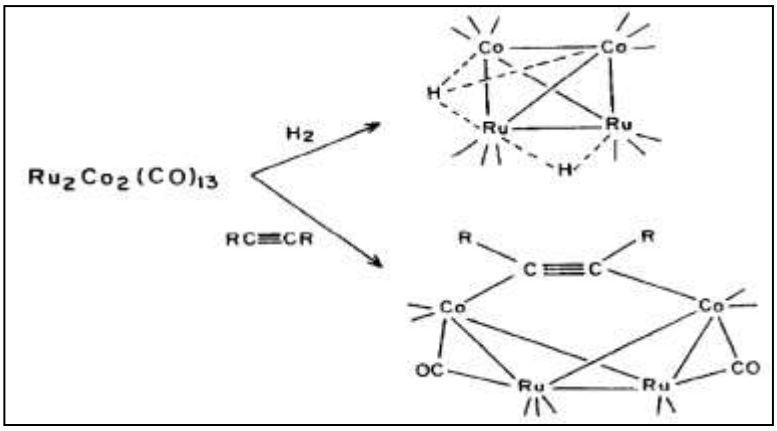


Figure 1.6. Heterosite reactivity of the heterometallic cluster $[Ru_2Co_2(CO)_{13}]$ (Figure taken from ref. 84)

Triiron dodecarbonyl $[Fe_3(CO)_{12}]$ was discoverd in 1906 [91], but its structure was not established until its solid state structure was elucidated by Dahl et al [92] and confirmed by Cotton [93]. However by 1995, there was still considerable confusion concerning the IR and the NMR spectra of this compound in solution. The IR data for $Fe_3(CO)_{12}$ in solution have been interpreted either to confirm to a bridged structure as found in the X-ray structure or a non-bridged structure similar to that found for $Ru_3(CO)_{12}$ and $Os_3(CO)_{12}$ [94]. Variable temperature ^{13}C NMR studies of $Fe_3(CO)_{12}$ in solution suggest a highly fluxional system exhibiting the "Cotton merry-go-round" mechanism (mechanism first observed by Cotton [95]) with the carbonyl groups being equivalent on the NMR time scale at -150^0C [96]. Earlier EXAFS [97] studies of $Fe_3(CO)_{12}$ in frozen solution revealed that in hexane, the compound possesses a non-

bridged D_3 structure, whereas in a frozen solution of a more polar solvent such as dichloromethane evidence suggests both bridged and non-bridged species are present similar to those observed by Mann [98] in $[Fe_3(CO)_9\{P(OR)_3\}_3]$ (R = Me and Pr^i). Substitution reactivity of $Fe_3(CO)_{12}$ has been a focus of investigation [99] in an effort to come up with a more acceptable solution structure of $Fe_3(CO)_{12}$ and to formulate a clear descriptive chemistry of this compound.

The substitution reactivity of $Fe_3(CO)_{12}$ has been studied using derivatives containing mono dentate phosphines, phosphites and isocyanide ligands [100]. It has been demonstrated that reactions of $Fe_3(CO)_{12}$ with group 15 ligands give a mixture of complexes of the general formula $[Fe_3(CO)_{12-n}(L)_n]$ [99] which decompose rapidly in solution. Phosphite derivatives are more stable than those of phosphines, arsines and stibines respectively. More often, substitution of the triiron cluster is accompanied by fragmentation of the cluster to give well known $[Fe(CO)_4(L)]$, $[Fe(CO)_3(L)_2]$ and more stable $Fe_3(CO)_{9-n}(L)_n$ derivatives. In 1996, Stein and Fujiwar [101] succeeded in reacting $Fe_3(CO)_{12}$ with tertiary phosphines, i.e.1,2-bis(diphenylphosphino)ethane (dppe), 1,4-bis(diphenylphosphino) butane (dppb), 1,4-bis(diphenylphosphino)benzene (dppbz) and 1,1'-bis(diphosphino)ferrocene (dppf), though in low yields. Structural and fluxional studies of $[Fe_3(CO)_{10}(dppe)]$ displayed the so-called "merry-go-round" mechanism [102]. As demonstrated before, the challenge is to restrict fluxionality, thus improving the chances of derivatising the compound by substituting carbonyl atoms with limited decomposition and fragmentation.

1.4.2 Synthesis and derivatization of transition-metal clusters.

A number of trimetallic clusters in which the tridentate phosphine ligand tris(diphenylphophine)methane (tppm), chelates to three metal atoms at a time have been successfully characterised, e.g. $[Au_3(\mu\text{-tppm})I_3]$ [103], double capped $[Au_3(\mu\text{-tppm})_2Cl]^{2+}$ [104] and $[Au_3(\mu\text{-tppm})Cl_3]$ [105]. The successful synthesis of $[Fe_2Ru(CO)_{12}]$ and $[FeRu_2(CO)_{12}]$ by Giordano and Sappa [106] provides a motivation to attempt the synthesis of hetero-trimetallic clusters of the type $[Fe_2W(CO)_n]$, $[Fe_2Rh(CO)_n]$, etc. The so-called 'linear cluster' compounds of osmium have also been synthesised by oxidative addition reaction of $(PPh_3)AuCl$ with $Os_3(CO)_{12}$

to a give the complex $[Os_3(CO)_{12}(AuPPh_3)(Cl)]$ for which the IR spectrum suggest a linear arrangement of metal atoms [107]. Another significant milestone in the synthesis of 'linear cluster' compounds was the reaction of the triangular $Os_3(CO)_{12}$ cluster with $SnCl_4$, hydrides and alkyl substituents, first reported by Moss and Graham [108]. These compounds were confirmed as linear on the basis of spectroscopic properties [109] and chemical reactivities [110]. Phosphine substituted metal carbonyl clusters have been extensively studied [99, 100, 101].

1.5 Decarbonylation of transition-metal carbonyl complexes

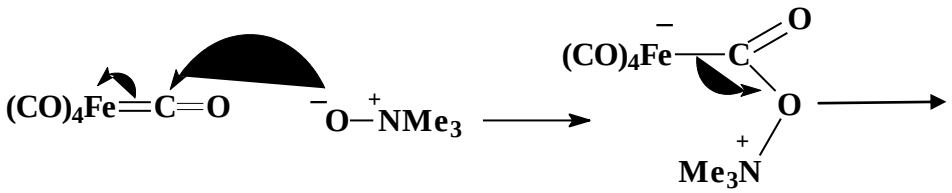
An important aspect of the chemical reactivity of both bi- and poly-metallic CO-containing complexes is catalytic decarbonylation. Transition metal carbonyl complexes have been a significant source of low oxidation state metals for synthetic organometallic chemistry, as catalysts and reagents in organic synthesis and industrial processes [111]. Photochemical and thermal conditions have been traditionally prominent methods of choice for decarbonylation despite numerous difficulties in some reactions to achieve the simple transformation (**Eq. 13**) [112].

$$\mathbf{M(CO)_n + L \rightarrow M(CO)_{n-1}L + CO} \qquad \mathbf{(13)}$$

A very useful decarbonylation method (see below) makes use of trimethylamine oxide. Other methods that are applicable for successful decarbonylation of metal carbonyl complexes, though utilised to a lesser extent are: (a) electrochemically induced substitution reactions [113], (b) catalytically induced substitution reactions [114], (c) photochemically-induced reactions [115] with an often high probability of product distribution, (d) organic reagents as catalysts e.g. sodium diphenylketyl in THF as reducing agent [116] which offers some advantages such as mild conditions, easy handling, probability of stepwise characterisation, and lastly (e) phase-transfer catalysis [117]. An interesting use of transition metal compounds (e.g. $RhCl(PPh_3)_3$ [118]) as catalysts for decarbonylation of other transition metal complexes have been noted, a

reaction which presumably involves the labilisation of a CO ligand by a change in oxidation state of the metal carbonyl complex substrate [119]. Therefore a choice of decarbonylation agent is very important especially if specific potential complications or consequences are to be avoided such as decomposition, fragmentation and product distribution. Certain desirable conditions in decarbonylations which are often not achieved through traditional methods are (a) mild reaction conditions, (b) multiple, stepwise replacement of CO ligands, (c) high product yields and (d) short reactions times. Trimethylamine N-oxide satisfies most of the desirable conditions.

The earliest report of the reaction of trimethylamine N-oxide (Me_3NO) with a transition metal carbonyl complex was made by Hieber and Lipp in 1959 [120]. Subsequent work by Alper and Edward [121] demonstrated the generality of the decarbonylation process. The mechanism proposed for trimethylamine oxide-induced decarbonylation reactions involves a nucleophillic attack of the amine oxide at a carbonyl carbon atom, followed by release of CO_2 and (in the absence of a coordinating solvent) complexation of Me_3N as illustrated by the decarbonylation of $Fe(CO)_5$ (**Scheme 1.5**).



$$(CO)_4Fe{-}NMe_3 + L \longrightarrow (CO)_4Fe(L) + Me_3N$$

L = ligand/Solvent

Scheme 1.5. Proposed reaction mechanism for Me_3NO decarbonylation [119, 122].

Gladysz and co-workers [123] have successfully demonstrated the utility of this route for decarbonylation of arylmanganese compounds, which were not amenable to decarbonylation by either thermal or photochemical methods. Since its successful application to iron carbonyls, the

use of the Me_3NO method for decarbonylation purposes, has been extended to include many other metal carbonyl complexes. Some of the notable advantages of using Me_3NO are:

(a) Me_3NO is an inexpensive, white crystalline material readily available commercially in anhydrous form or as the dihydrate, $Me_3NO.2H_2O$.

(b) Me_3NO has been used in a variety of solvents, e.g. THF [124], acetonitrile [125], benzene [126], toluene [127], dichloromethane [128], chloroform [129], acetone [130], 2-methoxymethanol [131] and methanol [132]. In many instances MeCN is added as a labile donor co-solvent [133]. The high volatility of trimethylamine produced in the reaction leads to its facile removal from the reaction mixtures [119].

(c) Both substituted and unsubstituted metal carbonyl complexes will undergo a CO replacement step.

(d) Me_3NO is widely applicable to a variety of metal carbonyl clusters [134].

(e) Relatively mild conditions are utilised (25-70^{O}C).

(f) The use of acetonitrile as a labile donor solvent in the reactions of M(CO)n and Me_3NO allows for the isolation of $M(CO)_{n-1}(NCMe)$ complexes from which the acetonitrile can be displaced under mild conditions.

1.6 Ligands of interest

A ligand can be defined as any molecule or ion that has at least one or more electron pairs to donate and can therefore be regarded as a Lewis base. Some of the ways in which ligands can be classified are: (a) as simple σ-donor or π-bonding molecules, (b) electronically according to the number of electrons donated to the central metal atom and, (c) structurally according to the number of connections they make with the central metal atom. A π-bonding ligand interaction with the metal atom is made possible by properties such as the availability of low lying empty *d*-orbitals on the metal and that the ligand has not only donor ability but also acceptor orbitals.

Phosphorus and nitrogen as donor atoms are of interest to us (as a replacement for CO) because of a number of factors. Interesting P, N-ligands capable of establishing binucleating or bridging interactions for bimetallic complexes have been reviewed elsewhere [135]. As already noted in **figure 1.2 and 1.3**, N-donor bridged complexes can also result in the formation of complexes

with different binding modes [136]. Of particular interest are phosphines (PR_3) and phoshites {$P(OR)_3$} because their electronic and steric properties can be altered in systematic and predictable ways depending on the nature of the R group. They are commonly employed to stabilize an exceptionally wide variety of organometallic complexes. This feature, although not limited to phosphines and phosphites, has been quantified successfully by Tolman [137] who also compared the frequencies $\nu_{(CO)}$ with the cone angle (θ) of a series of complexes of the type $LNi(CO)_3$, containing different PR_3 ligands on the so called 'steric – electronic map'. Because of the size of the PR_3 ligands which in relation to CO are bulkier, only a certain number of phosphines can fit around the metal. This feature comes as an advantage in that by using the bulky PR_3 ligands, low-coordinate metal complexes are accessible thus leaving room for smaller weakly binding ligands to coordinate to the central metal.

1.7 The *trans*-effect vs *trans*-influence in transition metal complexes.

The *trans* effect, which is defined as 'the ability of a ligand in a transition metal complex to labilize the ligand in the *trans* position towards substitution [138] has been well illustrated using square planar complexes with a d^8 electronic configuration because of their stability, relative ease to synthesise and the occurrence of ligand exchange at rates that are easy to monitor. The *trans* effect is a kinetic phenomenon which depends upon transition state factors and is distinct from purely ground state properties such as bond length. The phenomenon of *trans*-effect has long been recognised (over 100 years) in complexes in which certain ligands are observed to influence the rate of reactions involving ligand positions *trans* to themselves – the effect originally called '*trans*-elimination' [139]. A theoretical understanding of the *trans*-effect as a kinetic phenomenon is of benefit to synthetic coordination chemistry and synthetic organic chemistry.

The *trans* influence on the other hand, is a ground state effect observed in both square planar and octahedral complexes and has been described by Pidcock et al [140] as the extent to which a ligand weakens the bond *trans* to itself in the ground state of the complex. Therefore the *trans*-influence can be regarded as thermodynamic phenomenon. It can be assessed by looking at

ground state properties such as bond lengths, NMR spin coupling constants, and IR stretching frequencies. A comprehensive review of the *trans*-influence by Appleton et al provides experimental observations in the form of structural determinations and spectroscopic data [141].

Many theories have been advanced to account for both the *trans* effect and *trans* influence. Since the factors influencing the processes are largely the same (the interaction of the orbitals on the metal and the ligand, electron-donating and electron-withdrawing effects), these must be rationalised from the transition state of the substitution process in the *trans* effect and for the ground state in the *trans* influence. The following theories have been advanced as providing the best explanation of the *trans*-influence including, (i) polarization theory which suggested that an easily polarisable donor group induces charge in the *trans* ligand, thereby weakening the trans bond, (ii) hybridization of the metal orbitals in such a way that the opposing metal-ligand bonds will compete for the available *s* and *d* orbitals with a strength proportional to their covalent bond character, (iii) metal-ligand π-back-bonding, especially in the case of ligands such as phosphines which contain the orbitals of appropriate symmetry for overlap with filled metal d_{π}–orbitals [141] and, (iv) molecular-orbital (MO) theory which requires consideration of the σ- and π-bonding properties of both the metal centre and the ligand [142] (**Figure 1.7**).

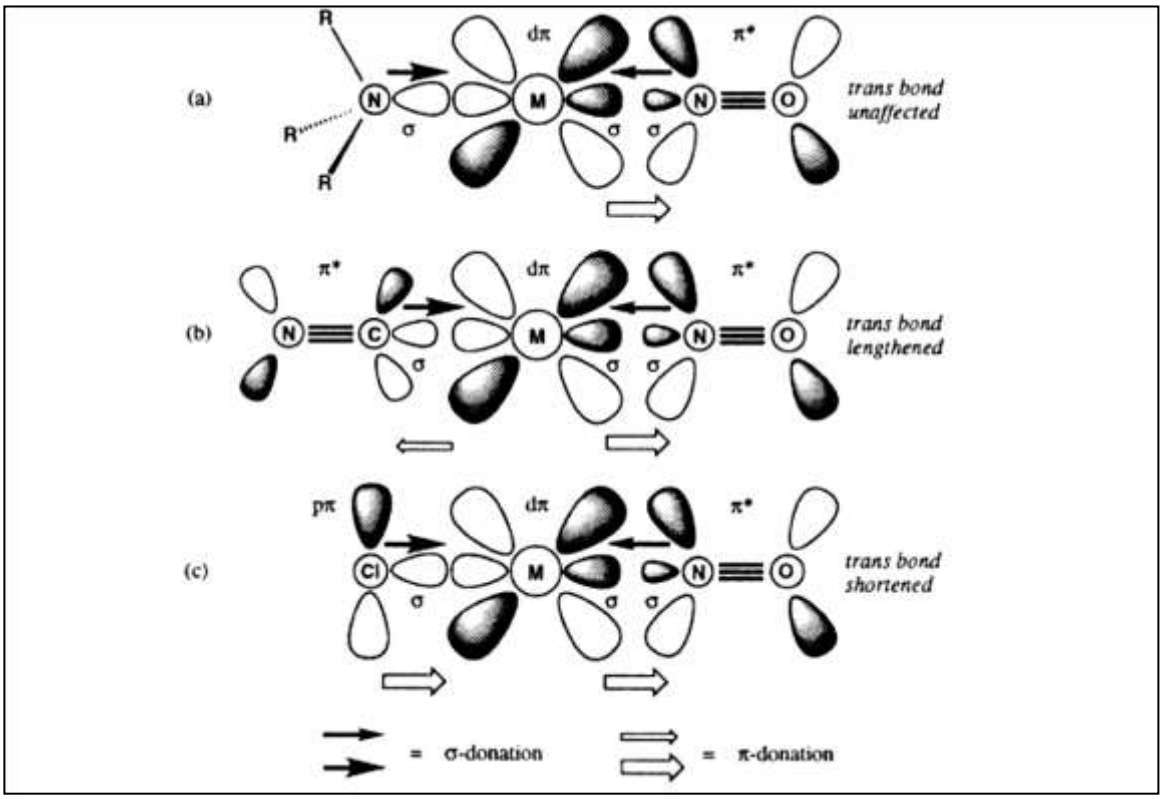


Figure 1.7 Simplified orbital representation of the bonding in linear metal nitrosyl complexes with different types of *trans*-ligands showing changes in the M-L bond *trans* to NO. (a) σ-Donor NH_3/NR_3; (b) σ-donor – π-acceptor CN^- ligand; (c) σ-donor – π-donor Cl^- ligand (Figure taken from ref. 139)

The high trans effect of ligands such as ethylene and CO can be accounted for in terms of metal to ligand π-back bonding. In the case of ethylene, the mechanism involves the transfer of electrons from the filled *π*-orbitals to the vacant *σ*-type metal orbitals whilst at the same time the π-back bonding results in the flow of electrons from the filled d_{xz} or other *dπ-pπ* hybrid orbitals into antibonding orbitals of the ligand.

An explanation for high enthalpies of *cis*-$PtX_2(PR_3)_2$ (X = halogen) isomerisation to the *trans*-isomer [143] and smaller $^1J(^{195}Pt\text{-}^{31}P)$ [144] for *cis*- than *trans*- has been given in terms of competition by the phosphine ligands for available *d*-electrons where in *trans* complexes the two phosphine ligands have to share the same metal d_π-orbitals so that the Pt-P bonds are weakened. The *trans*-effect, therefore involves a lowering of the energy barrier of the transition state in

favour of ligand substitution or transformation. A *trans*-directing ligand series for a typical Pt(II) system is given below even though the order can change for different metals and oxidation states [3c, 12c]:

$$\mathbf{H_2O < OH^- < NH_3 < Cl^- < Br^- < CN^- < CO, C_2H_4, CH_3^- < I^- < SCN^- < PR_3 < H^-}$$

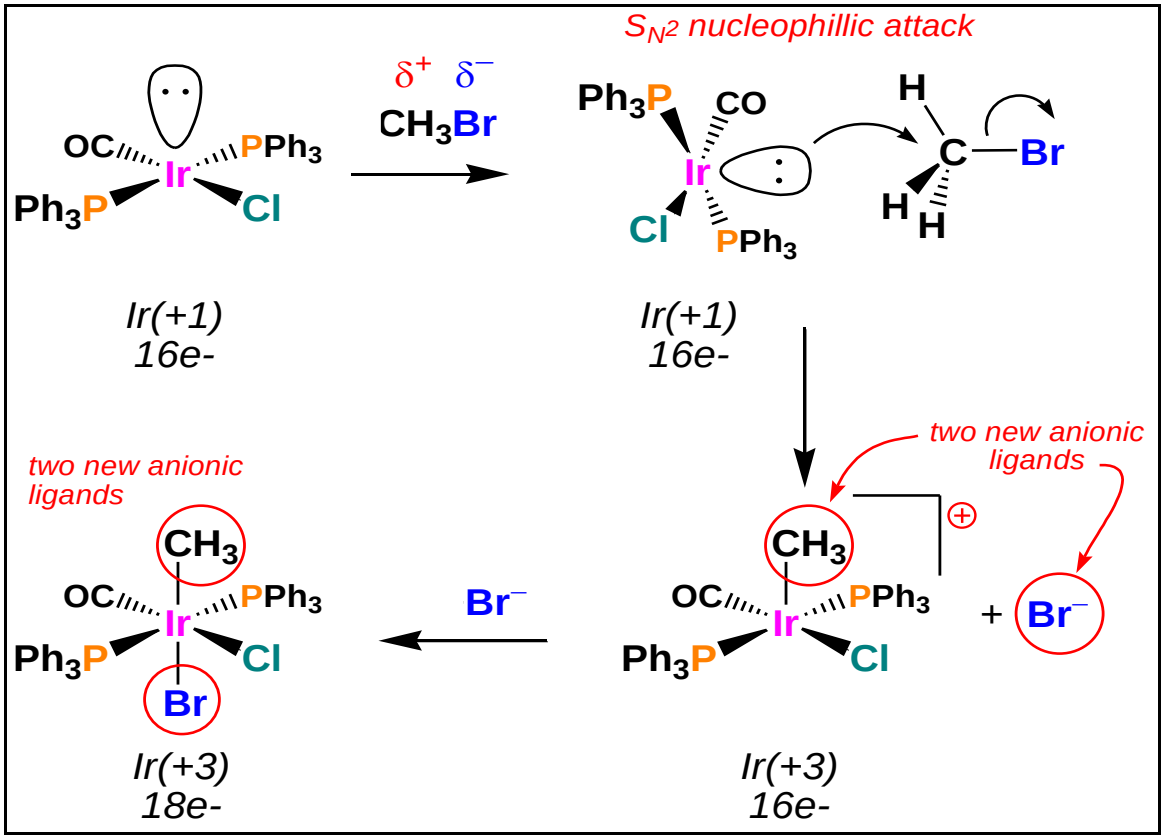
← low *trans* effect high *trans* effect →

1.8 Reaction mechanisms

There are several pathways by which one ligand can replace another in complexes with varied coordination geometries, i.e. square planar, octahedral, tetrahedral, etc. Some of these pathways are nucleophilic substitution, electrophilic substitution and oxidative addition followed by reductive elimination [145]. A special focus on oxidative addition and reductive eliminations reactions is hereby given because of its relevance to the work to be discussed in later chapters.

1.8.1 Oxidative addition reactions.

The oxidation addition reaction is one in which a neutral molecule combines with a metal centre so as to occupy two coordination sites and in doing so oxidises the metal, typically by 2 electrons. Because oxidative addition involves oxidation (removal of electrons) from the metal centre, the more electron-rich the metal is the easier the oxidative addition to the metal centre will be. The transfer of the two electrons from the metal to the incoming ligand breaks a bond in that ligand, thus forming two new anionic ligands (or a single dianionic ligand e.g. O_2^{2-}) as illustrated in the reaction **scheme 1.5**. The above assertion does not always result in oxidative-addition reactions as is the case of complexes of the type $[Rh(H)\{(\mu\text{-}H)SnR_3\}_2]$, (R = ^{n}Bu, Ph) and $M(O_2)$ where a 'three-centre' bond system result [146]. Some of the most common substrates which often do require the presence of an empty orbital on the metal to perform the oxidative addition reaction are: X_2 (X = Cl, Br, I), R-X, Ar-X, H-X, O_2, etc. An example of the oxidative addition of CH_3Br to $[IrCl(CO)(PPh_3)_2]$ is shown in **scheme 1.6**.

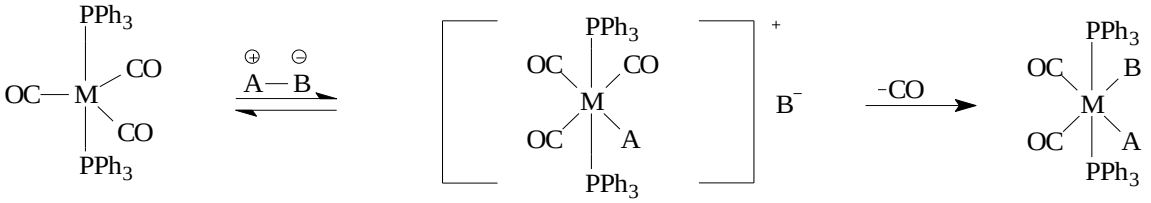


Scheme 1.6. A typical oxidative addition reaction process. (Figure taken from ref. 147)

Many rhodium(I) and iridium(I) complexes, readily undergo oxidative addition reactions which are accompanied by a change in coordination geometry from square planar to an octahedral system. One of the best studied cases is the addition of H_2 to 16 electron square planar d^8 [$IrCl(CO)(PPh_3)_2$], Vaska's complex, to give an 18 electron d^6 octahedral dihydride complex [148]. Oxidative addition reactions are not limited to square planar complexes only, but also five coordinate complexes where reagent addition has been to be found to occur in the *cis* mode [149]. The oxidative addition reactions are governed by the principle "the more electron-rich the metal is, the easier the oxidative addition to the metal will be".

When a polar or electrophilic reagent such as hydrogen halide or alkyl halide is added to a five coordinate complex, an oxidative addition reaction can occur in two ways, one shown in **scheme 1.7**. The alternative pathway involves the five co-ordinate complex losing a ligand in order to form a more reactive four co-ordinate complex before undergoing oxidative addition. Heating or

irradiation of a five co-ordinate complex may result in a loss of a ligand as in this case. **Table 1.1** illustrates the fact that the more electron rich the metal centre is (through the better donating ligands), the faster the oxidative addition reactions. The only exception is the oxidative addition reaction of CH_3I with the Ir-Cl, I because of steric factors.



M = Os, Ru

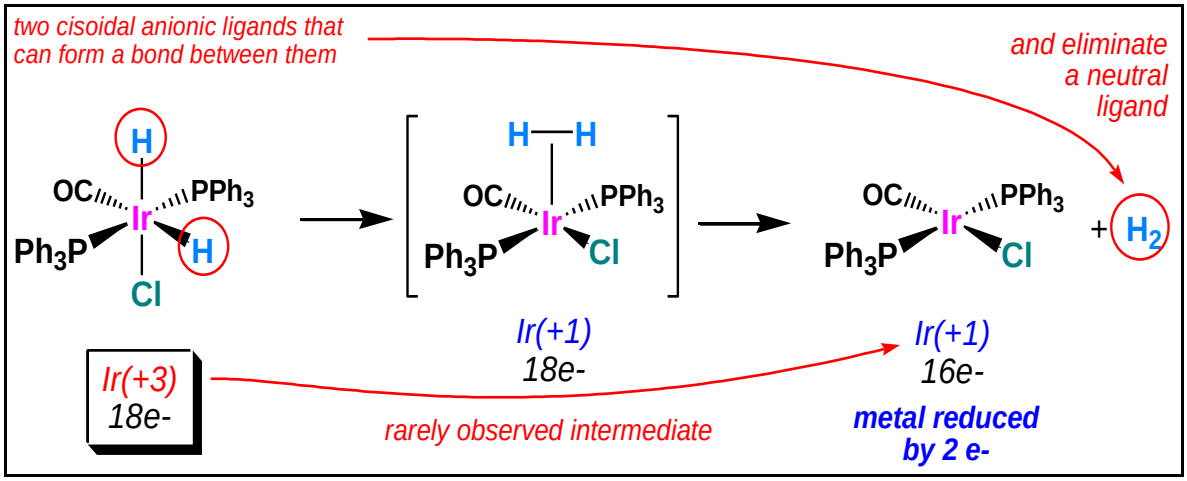
Scheme 1.7. Oxidative addition reaction of a polar A-B moiety to a five co-ordinate d^8 transition metal complex.

Table 1.1. Illustration of the comparative kinetic data derived from $MX(CO)(PR_3)_2$ [150].

M	X	PR_3	Reactant	Rate Const M^{-1} Sec^{-1}	$\Delta H^{\ddagger}$ (kcal/mol)	$\Delta S^{\ddagger}$ (J/mol K)
Ir	Cl	PPh_3	H_2	0.67	10.8	-23
	Br			10.5	12.0	-14
	I			> 100		
Ir	Cl	PPh_3	O_2	3.4×10^{-2}	13.1	-21
	Br			7.4×10^{-2}	11.8	-24
	I			30×10^{-2}	10.9	-24
Ir	Cl	PPh_3	CH_3I	3.5×10^{-3}	5.6	-51
	Br			1.6×10^{-3}	7.6	-46
	I			0.9×10^{-3}	8.8	-43
Ir	Cl	P(*p*- $OMeC_6H_4)_3$	CH_3I	3.5×10^{-2}	8.8	-35
		P(*p*- $ClC_6H_4)_3$		3.7×10^{-5}	14.9	-28
Rh	Cl	PPh_3	CH_3I	12.7×10^{-4}	9.1	-44
		P(*p*- $OMeC_6H_4)_3$		51.5×10^{-4}	10.2	-43

1.8.2 Reductive elimination reactions.

A reductive elimination reaction is the reverse of an oxidative addition and is a very important step in catalytic cycles as terminating step. It is a reaction in which two cisoidal anionic ligands on a metal centre couple together. It is the most often seen in higher oxidation states because the formal oxidation state of the metal is reduced by two units in the reaction **scheme 1.8**. The reaction is especially efficient for intermediate oxidation states, such as the d^8 metals Ni(II), Pd(II), and Au(III) and the d^6 metals Pt(IV), Pd(IV), Ir(III), and Rh(III).



Scheme 1.8 A typical reductive elimination reaction process. (Figure taken from ref. 147)

Reductive elimination can be stimulated by a change in the oxidation state or photolysis [151] in which a reduction in the electron density of the metal is induced by the dissociation of a neutral ligand.

1.9. Conclusion

In this introduction, an attempt was made to highlight the rich history of transition metal chemistry and its profound industrial impact. The somewhat artificial distinctive difference between coordination and organometallic chemistry has arguably inhibited research in the borderline areas. The versatile chemistry of the heterobimetallic complexes derived from metals in the *p* block elements bonded to *d* block still poses some interesting challenges to this day especially the nature of metal-metal bond and this very fact informs one of the aims for this thesis. The well established variety of decarbonylation agents provide opportunities to synthesise derivatives of a wide range of transition metal complexes including heterobimetallic complexes, bridged metal complexes, transition metal clusters and hopefully new interesting monometallic complexes.

The scope and current activity of the bridged mixed-metal self-assemblies provide a new window of opportunities in the field of supramolecular chemistry. Their diverse application in the field of catalysis, as sensors and sieves, molecular electronics and as motifs in coordination chemistry is well documented [63,152]. CuI-catalysed coupling reactions offer a promising route to the synthesis of mixed metal complexes with new organic linkers.

References

1. Iwao Omae, *Application of Organometallic Compounds*, John Wiley and Sons, Chichester, (1999) 1.

2. C.H. Elschenbroich and A. Salzer, *Organometallics, A Concise Introduction*, 2nd Ed. VCH, Weinheim, (1992) 411.

3. (a) J.P. Collman, L.S. Hegedus and R.G. Finke, *Principles and Applications of Organotransition Metal Chemistry*, 2nd Ed., University Science books, Mill Valley (1987) 523; (b) F.A. Cotton and G. Wilkinson, *Advanced Inorganic Chemistry, Comprehensive Text*, 4th Ed., John Wiley and Sons, New York (1980) 67, 1266; (c) J.E. Huheey, E.A. Keiter, and R.L. Keiter, *Inorganic. Chemistry, Principles of Structure and Reactivity*, 4th Ed., Harper-Collins, New York (1993) 705.

4. E. Drent, P. Arnoldy and P.H.M. Budzelaar, *J. Organomet. Chem*., 475 (1994) 57.

5. E. Drent, P.H.M. Budzelaar, *Chem. Rev*., 96 (1996) 663.

6. A. Sevin, Y. Hengtai and P. Chaquin, *J. Organomet. Chem*. 262 (1984) 391

7. (a) P. Kalck, J. -M. Frances, P.-M. Pfister, T.M. Southern and A. Thores, *J. Chem. Soc. Chem. Commun*., (1983) 510; (b) P. Kalck, *Polyhedron*, **7** (1988) 2441.

8. J.R. Dilworth, J.R. Miller, N. Wheatley, M.J. Baker and J.G. Sunley, *J. Chem. Soc. Chem. Commun*., (1995) 1579.

9. G. H. Lutz, *Angew. Chem. Int. Ed*., 39 (2000) 2658.

10. (a) D.W. Stephen, *Coord. Chem. Rev*., 95 (1989) 41; (b) N. Wheatley and P. Kalck, *Chem. Rev*., 99 (1999) 3379.

11. P. Aktins and D.F. Shriver, *Inorganic Chemistry*, Oxford University Press, 4th Ed., Oxford, (2006) 525.

12. (a.) F. A. Cotton and G. Wilkinson, in *Advanced Inorganic Chemistry, A comprehensive Text*, John Wiley, 4th Ed., New York, (1980) 48; (b) C. Elschenbroich; in *Organometallics*, Wiley- VCH, 3rd Ed, Weinheim, (2006) 11, 451, 579; (c) R.H. Crabtree, in *The Organometallic Chemistry of the Transition Metals*, John Wiley, New York, (2005) 1, 102, 159; (d) G. Wilkinson; F.G.A. Stone and E.A. Abel, (eds.) in *Comprehensive Organometallic Chemistry*, Pergamon, Oxford, Vol 9 (1982) 431; (e) R.H. Crabtree and D.M.P. Mingos, in *Comprehensive Organometallic Chemistry III*, Elsevier, Amsterdam, vol **1** (2007) 1; (f) A.F. Hollenman and E. Wiberg, in *Inorganic Chemistry*, Academic Press, New York, (2001) 1140; (g) G. Wilkinson, R. D. Gillard and J.A. McCleverty, in *Comprehensive Coordination Chemistry*, Pergamon Press, Oxford, Vol. **1**, (1987) 1.

13. (a) P. Braunstein and J. Durand, et al., *J. Chem. Soc. Dalton Trans*., (1999) 4175, (b) M. Cano, P. Ovejero and J.V. Heras, *J. Organomet. Chem*., 438 (1992) 329.

14. J. Lewis and R.S. Nyholm, *Science Progress*, 52 (1964) 208, 557.

15. N. Wheatley and P. Kalck, *Chem. Rev*. 99 (1999) 3379.

16. (a) R.D. Gorsich, *J. Chem. Soc*., 84 (1961) 2486; (b) W.R. Cullen, J. R. Sams, and J. A. Thompson, *Inorg. Chem*., 10 (1971) 843.

17. (a) H. Braunschweig, H. Bera, B. Geibel, R. Dörfler, D. Götz, F. Seeler, T. Kupfer and K. Radacki, *Eur. J. Inorg. Chem*. (2007) 3416; (b) J. Beckmann, K. Jurkschat, U. Kaltenbrunner, S. Rabe and M. Schürmann, *Organometallics*, 19 (2000) 4887; (c) P. McArdle, L. O'Neill and D. Cunningham, *Inorg. Chim. Acta*, 291 (1999) 252.

18. E.W. Abel, A. Singh and G. Wilkinson, *J. Chem. Soc*. (1960) 1321.

19. R.B. King, P.M. Treichel and F.G.A. Stone, *Chem. Ind*. (London) (1961) 747.

20. J.F. Tilney-Bassett, *Proc. Chem. Soc*. (1960) 419.

21. H.R.H. Patil and W.A.G Graham, J. *Am. Chem. Soc*., 87 (1965) 673.

22. F.W.B. Einstein, T. Jones, R.K. Pomeroy and P. Rushman, *J. Am. Chem. Soc*., 106 (1984) 2707.

23. F.W.B. Einstein, R.K. Pomeroy, P. Rushman and A.C. Willis, *Organometallics*, 4 (1985) 250.

24. M.H. Chisholm. *Acc. Chem. Res*., 23 (1990) 419.

25. (a) R.D. Adams, D.M. Collins and F. A. Cotton, *J. Am. Chem. Soc*., 96 (1974) 965; (b) R.D. Adams, D.M. Collins and F.A. Cotton, *Inorg. Chem*., 13 (1974) 1086.

26. (a) L = carbine: E.O. Fischer, E. Offhaus, J. Müller and D. Nöthe, *Chem. Ber*., 105 (1972) 3027; (b) L = isonitrile: M.O. Albers, J.C. Boeyens, N.J. Coville and G.W. Harries, *J. Organomet. Chem*., 260 (1984) 99.

27. H. Schulz, K. Folting, J.C. Huffman, W.E. Streib and M.H. Chisholm. *Inorg, Chem*., 32 (1993) 6056.

28. L.W. Arndt, B.T. Bancroft, M.Y. Darensbourg and C.P. Jansen, C.M. Kim, J. Reibenspies, K.E. Varner and K.A. Youngdahl, *Organometallics*, **7** (1988) 1302.

29. L.F. Dahl and R.E. Rundle, *Acta Crystallogr*., 16 (1963) 419.

30. R.B. King, P.M. Treichel and F.G.A. Stone, *Chem. Industr*, (1961) 747.

31. (a) B. Findeis, M. Schubart, C. Platzek, L.H. Gade, I. Scowen and M. McPartlin, *Chem. Commun.* (1996) 219; (b) S. Friedrich, L.H. Gade, I.J. Scowen and M. McPartlin, *Angew. Chem., Int. ed. Engl*. 35 (1996) 1338; (c) S. Friedrich, H. Memmler, L.H. Gade, W.–S,I. J. Scowen, M. McPartlin and C.E. Housecroft, *Inorg. Chem*., 35 (1996) 2433; (d) J. Sundermeyer and D.

Runge, *Angew. Chem., Int. Ed. Engl*., 33 (1994) 1255; (e) J. Sundermeyer, D. Runge and J.S. Field, *Angew. Chem., Int. Ed. Engl*., 33 (1994) 678; (f) D. Selent, M. Ramm and C. Janiak, *J. Organomet. Chem*., 501 (1995) 235.

32. (a) D. Selent, R. Beckhaus and J. Pickardt, *Organometallics*, 12 (1993) 2857; (b) D. Selent, R. Beckhaus and T. Bartik, *J. Organomet. Chem*., 405 (1991) C15; (c) T. Bartik, B. Happ, A. Sorkau, K.-H. Thiele and G. Pályi, *Organometallics*, 8 (1989) 558.

33. I.P. Beletskaya, A.Z. Voskoboynikov, E.B. Kirillova, A.K. Shestakova, A.I. Parshina, A.I. Gusev and G.K. -I Magomedov, *J. Am. Chem. Soc*., 115 (1993) 3156.

34. (a) F.-E. Hong, I.-R. Lue, S.-C. Lo and Y.-C. Yang, C. -C. Lin, *Polyhedron*, 15 (1996) 2793; (b) I.-R. Lue, S.-C. Lo, C.-C. Lin and F. -E. Hong, *Polyhydron*, 14 (1995) 1419.

35. (a) L. Carlton, W.E Lindsell, K.J. McCullough and P.N. Preston, *J. Chem. Soc. Dalton Trans*. 8 (1984) 1693; (b) *J. Chem. Soc. Dalton Trans*., 11 (1987) 2741.

36. A.M. Martins, M.J. Calhorda, C.C. Romão, C. Vökel, P. Kiprof and A. C. Filipou, J. *Organomet. Chem*., 423 (1992) 367.

37. Y.-Y. Liu, A. Mar, S.J. Rettig, A. Storr and J. Trotter, *Can. J. Chem*., 66 (1988) 1997.

38. (a) M. Galakhov, A. Martin, M. Mena and C. Yélamos, *J.Organomet. Chem*., 496 (1995) 217; (b) W.J. Sartain and J.P. Selegue, *Organometallics*, 8 (1989) 2153.

39. (a) W.L. Gladfelter and G.L. Geoffrey, *Adv. Organomet. Chem*., 18 (1980) 207; (b) D.A. Roberts and G.L. Geoffrey in G. Wilkinson, E.W. Abel and F.G.A. Stone (Eds.), *Comprehensive Organometallic Chemistry*, Pergamon, Oxford, 6 (1982) 763

40. W.-T. Wong, in R.H. Crabtree and D.M.P. Mingos, *Comprehensive Organometallic Chemistry* III, Elsevier, Amsterdam, vol.6 (2007) 319.

41. N.S. Vyazankin, G.A. Razuvaev and O.A. Krugkaya, *Organomet. Chem Rev*., 3A (1968) 323.

42. (a) E.H. Brooks and R.J.Cross, *Organomet. Chem. Rev*., 6A (1970) 227; L.H. Gade, Angew. Chem. Int. Ed., 39 (2000) 2658.

43. J.D. Donaldson, *Prog. Inorg. Chem*., 8 (1968) 287

44. (a) J. Beckmann, K. Jurkschat, U. Kaltenbrunner, S. Rabe and M. Schürmann, *Organometallics*, 19 (2000) 4887; (b) P. McArdle, L. O'Neill and D. Cunningham, *Inorg. Chim. Acta*, 291 (1999) 252; (c) H. Braunschwieg, H. Bera, B. Geibel, R. Dörler, D. Götz, F. Seeler, T. Kupfer and K. Radacki, *Eur. J. Inorg. Chem*., (2007) 3416

45. E.H. Brooks and R.J. Cross, *Organomet. Chem. Rev*., 6A (1970) 227.

46. N.S. Vyazankin, G.A. Razuvaev and O.A. Krugkaya, *Organomet. Chem. Rev*., 3A (1968) 323.

47. Cenini, R. Ugo, and F. Bonati, *Inorg. Chimi. Acta*, 1 (1967) 541.

48. W. Jetz, P.B. Simons, J.A. Thompson and W.A. Graham, *Inorg. Chem*., 5 (1966) 2217.

49. B.F. Kingston and M.F. Lappert, *J. Chem. Soc. Dalton Trans*., (1972) 69.

50. J.R. Moss and W.A.G. Graham, *J. Organomet. Chem*., 18 (1969) 24.

51. H.M. Creemers, J.C. Verbeek and H.G. Noltes, *J. Organomet. Chem*., 15 (1968) 125.

52. S.R.A. Knox, C.M. Mitchell and F.G.A. Stone, *J. Organomet. Chem*., 16 (1967) 67.

53. H.C. Clark and K. Itoh, *Inorg. Chem*., 10 (1971) 1707.

54. M. Elder and D. Hall, *Inorg. Chem*., 8 (1969) 1268.

55. F.G.N. Cloke, K.P. Cox, M.L. Green, J. Bashkin and K. Prout, *J. Chem. Soc. Chem. Commun*., (1981) 117.

56. F. Bonati and G. Wilkinson. *J. Chem. Soc*., *A* (1964) 179.

57. P. Mazerolles, J. Dubac and M. Lesbre, *J. Organomet. Chem*., 12 (1968) 143.

58. G. Schmid and G. Etzrot, *J. Organomet. Chem*., 131 (1977) 477.

59. M.S. Holt, W.L. Wilson and J.H. Nelson, *Chem. Rev*., 89 (1989) 11.

60. M. Maggini, *Coord. Chem. Rev*., 253 (2009) 1793.

61. V.W.W. Yam, K.M.C. Wong and N. Zhu, *J. Am. Chem. Soc*., 124 (2002) 6506.

62. K.M.C. Wong, C.K. Hui, K.L. Yu and V.W.W. Yam, *Coord. Chem. Rev*., 229 (2002) 123.

63. (a) S.L. Leninger, B. Olenyuk and P.T. Stang, *Chem Rev*., 100 (2000) 853; (b) G.F. Swiegers and T.J. Malefetse, Chem. Rev. 100 (2000) 3483; (c) G.F. Swiegers and T.J. Malefetse, *Coord. Chem. Rev*., 225 (2002) 91.

64. (a) S. Lots, P.H. van Rooyen and R. Meyer, *Adv Organomet. Chem*., 37 (1995) 219S; (b) S. –J. Chiang, Y. Chi, P.-C. Su, S.-M. Peng and G.-H. Lee, *J. Am. Chem. Soc*. 116 (1994) 11181; (c) M. Akita, S. Sugimoto, A. Takabuchi, M. Tanaka and Y. Moro-oka, *Organometallics* 12 (1993) 2925; (d) J. R. Berenguer, L.R. Falvello, J. Fornies, E. Lalinda and M. Tomas, *Organometallics* 12 (1993) 6.

65. (a) H. Lang, *Angew. Chem. Int. Ed. Engl*. 33 (1994) 547; (b) M.H. Chisholm, *Angew. Chem. Int. Ed. Engl*. 30 (1991) 673; (c) J.R. Berenger, E. Lalinde and M.T. Moreno, *Coord. Chem. Rev*., 254 (2010) 832.

66. (a) V.W. Yam et al, *J. Organomet. Chem*., 670 (2003) 205; (b) M.I. Bruce, B.C. Hall, P.J. Low, M.E. Smith, B.W. Skelton and A.H. White, *Inorg. Chim. Acta*, 3002-302 (2000) 633; (c) N.L. Narvor, L. Toupet and C. Lapinte, *J. Am. Chem. Soc*. 117 (1995) 7129; (d) O. Lavastre, J. Plass, P. Bachmann, S. Guesmi, C. Moinet and P.H. Dixneuf, *Organometallics* 16 (1997) 184; (d).

67. M.I. Bruce, K. Costuas, J.-F. Halet, B.C. Hall, P.J. Low, B.K. Nicholson, B.W. Skelton and A.H. White, *J. Chem. Soc. Dalton Trans*., (2002) 383.

68. M. Janka, G.K. Anderson and N.P. Rath, *Organometallics* 23 (2004) 4382.

69. (a) J. A. Whiteford, C.V. Lu and P.J. Stang , *J. Am. Chem. Soc*., 119 (1997) 2524; (b) P.J. Stang and J.A. Whiteford, *Organometallics* 113 (1994) 3776.

70. J. Manna, C.J. Kuehl, J. A. Whiteford, P.J.Stang, D.C. Muddiman, C.D. Hofstadler and R. D. Smith, *J. Am. Chem. Soc*., 119 (1997) 11611.

71. (a) R. Dagai, *Chem. Eng. News* 76 (23) (1998) 35; (b) A.E. Rowen and R.J.M. Nolte, *Angew. Chem. Int. Ed. Engl*. 37 (1998) 63.

72. C. L. Hill and X. Zhang, *Nature* 373 (1995) 324.

73. K. Sonogashira, T. Yataki, Y. Tohda, S. Takahashi and N. Hagihara, *J. Chem. Soc., Chem. Commun.* (1971) 291.

74. S.M. Al Qaaisi, K.J. Galat, M. Chai, D.G. Ray, P.L. Rinaldi, C.A. Tessier and W.J. Young, *J. Am. Chem. Soc*., 120 (1998) 12149.

75. M.I. Bruce, M. Ke and P.J. Low, *J. Chem. Soc. Chem. Commun*., (1996) 2405.

76. D. Villemin and E. Schigeko, *J. Organomet. Chem*. 346 (1988) C24-C26.

77. (a) F.A. Cotton, *J. Am. Chem. Soc*., 88 (1966) 4371; (b) F.A. Cotton, *Chem. Soc. Rev*., 3 (1966) 389.

78. D.M.P. Mingos and A.S. May, in D.F. Shriver, H.D. Kaez and R.D. Adams (eds.), *The Chemistry of Metal Cluster Complexes*, VCH, Weinheim, (1990) 11

79. L.F. Dahl, *Angew.Chem. Int. Ed. Engl*., 39 (2000) 4121

80. R.J. Puddephatt, *Polyhedron*, 9 (1990) 2767

81. (a) R.D. Adams and B. Captain, *J. Organomet. Chem*., 689 (2004) 4521; (b) B.C. Gates, *Chem. Rev*., 95 (1995) 511.

82. E.L. Muetterties, T.N. Rhodin, E. Band, C.F. Bruker and W.R. Pretzer, Chem. Rev., 79 (1979) 91.

83. (a) A.W. Olsen and K.J. Klabunde, *Encyl. Phys.Sci. Technol*., 8 (1987) 110; (b) M.P. Gomez-Sal, B.F.G. Johnson, J. Lewis, P.R. Raithby and A.H. Wright, J. Chem. Soc., Chem. Commun., (1985) 1682.

84. B.H.S. Thimmappa, *Coord. Chem. Rev*., 143 (1995).

85. (a) T. Madach and H. Vehrenkamp *Chem. Ber*,., 114 (1981) 505; (b) P. kalck, Y. Peres and J. Jenk, *Adv. Organomet. Chem*., 32 (1991) 121.

86. R.L. Pruett, *U.S. Patent* 3,957,857 (1976).

87. G. Süss-Fink and G. Herrmann, *J. Chem. Soc., Chem. Commun*., (1985) 735.

88. D. Braga and B.T. Heaton, *J. Chem. Soc., Chem. Commun*., (1987) 608.

89. (a) P. Lemoine, *Coord. Chem. Rev*., 83 (1988) 169; (b) P. Lemoine, *Coord. Chem. Rev*., 47 (1982) 56.

90. E. Roland and H. Vehrenkamp, *Organometallics*, 2 (1983) 183.

91. J. Dewer and H.O. Jones, *Proc. R. Soc. London, Ser. A*., 76 (1906) 66.

92. (a) C.H. Wei and L.F. Dahl, *J. Am. Chem. Soc*., 88 (1966) 1821; (b) L. F. Dahl and J.F Blount, *Inorg. Chem*., 4 (1965) 1373.

93. F.A. Cotton and J.M. Troup, *J. Am. Chem. Soc*., 96 (1974) 4155.

94. (a) M.R. Churchill, F.J. Hollander and J.P. Hutchison, *Inorg. Chem*., 16 (1977) 2655; (b) L.F. Dahl and E.R. Corey, *Inorg. Chem*. 1 (1962) 521.

95. F.A. Cotton and D.L. Hunter, *Inorg. Chim. Acta*., 11 (1974) L9

96. (a) H. Adams, N.A. Baily, G.W. Bently and A.E. Mann, *J. Chem. Soc. Dalton Trans*., (1989) 1831; (b) B.E. Mann, *J. Chem. Soc. Dalton Trans*., (1997) 1457

97. N. Binstedt, J. Evans, N. Greaves and R.J. Price, *J. Chem. Soc. Chem. Comm*., (1987) 1330.

98. H. Adams, X. Chen and B.E. Mann, *J. Chem. Soc. Dalton Trans*., (1996) 2159

99. (a) A. Shojale and J.D. Atwood, *Organomet*., 4 (1985) 187; (b) W.S. MacDonald, J. R. Moss, G. Raper and B.L. Shaw, *J. Am. Chem. Soc. Chem. Comm*., (1969) 1295; (c) P. J. Pollick and A. Wojcicki, *J. Organomet. Chem*., 14 (1968) 469.

100. S.M. Grant and A.R. Manning, *Inorg. Chimi. Acta*, 31 (1978) 41.

101. E. Stein, and F.Y. Fujiwara, *J. Organomet. Chem*. 525 (1996) 31.

102. H. Adams, and S.C. M. Agustinho, B.E. Mann, and S. Smith, *J.Organomet.Chem*., 607 (2000) 175.

103. A. Stutzer, P. Bissinger, and H. Schmidbuar, *Chem. Ber*., 125 (1992) 367.

104. Ching- Ming Che and Hong-Kay Yip, *J. Chem. Soc. Dalton Trans*., (1992) 427.

105. Hong Xiao and Yu-Xiang Weng, *J. Chem. Soc. Dalton Trans*., (1997) 221.

106. R. Giordano and E. Sappa, *J. Organomet. Chem*., 448 (1993) 157.

107. C.W. Bradford and R.S. Nyholm, *J. Chem. Soc. Chem. Commun*., (1968) 867.

108. (a) J.R. Moss and W.A.G. Graham, *J. Organomet. Chem*., 18 (1968) 24; (b) *Inorg. Chem*., 16 (1977) 75.

109. M. Gochin and J.R. Moss, *J. Organomet. Chem*., 192 (1980) 409.

110. J.R. Moss and W.A.G. Graham, *J. Chem. Soc. Dalton Trans*., (1977) 89

111. M. Beller and C. Bolm, (Editors), in *Transition metals for Organic Synthesis, Building blocks and Fine chemicals*, Vol.1, 2nd Ed., John Wiley, Weinheim, (2004) 601, 619.

112. (a) R.B. King, C.C. Frazier, R.M. Hanes and A.D. King, *J. Am. Chem. Soc*., 100 (1979) 479; (b) E.L. Meutterties and J. Stein, *Chem. Rev*., 79 (1979) 479; (c) P. Chini, G. Longoni and V.G. Albano, *Adv. Organomet. Chem*., 14 (1976) 285,

113. (a) J.M. Savéant, *Acc. Chem. Res*., 13 (1980) 323; (b) G.A. Tedoradze, *J. Organomet. Chem*., 88 (1975) 1.

114. A.N. Webb and J.J. Mitchell, *J. Phys. Chem*., 63 (1959) 1878.

115. (a) W.R. Cullen, J.R. Sams, and J.A.J. Thompson, *Inorg. Chem*., 10, 4 (1974) 843; (b) L. Carlton, W.E. Lindsell, and P.N. Preston, *J. Chem. Soc. Dalton Trans*., (1982) 1483.

116. J.W. Bruce, D.C. Kehoe, J.G. Matisons, B.K. Nicholson, P.H. Rieger and M.L. Williams, *J. Chem. Soc., Chem. Commun*. (1982) 442.

117. H. Alpers, *Adv. Organomet. Chem*., 19 (1981) 183.

118. M.O. Albers, N.J. Coville, C.P. Nicolaides, R.A. Webber, T.V. Ashworth and E. Singleton, *J. Organomet. Chem*., 217 (1981) 247.

119. M.O. Albers and N.J. Coville, *Coord. Chem. Rev*., 53 (1984) 227.

120. W. Hieber and A. Lipp, *Chem. Ber*., 92 (1959) 2085.

121. H. Alpers and J.T. Edwad, *Can. J. Chem*., 48 (1970) 1543.

122. Tien-Yau Luh, *Coord. Chem. Rev*., 60 (1984) 255.

123. J.A. Gladysz and J.C. Steiburg, *J. Chem. Soc. Dalton Trans*., (1997) 2309.

124. G.F. Stung, J.R. Shapley and C.G. Pierpont, *Inorg. Chem*., 17 (1978) 2596.

125. U. Koelle, *J. Organomet. Chem*., 155 (1978) 53.

126. Y. Shvo and E. Hazum, *J. Chem. Soc., Chem. Commun*. (1974) 336.

127. U. Koelle, *J. Organomet. Chem*., 133 (1977) 53.

128. J.R. Moss and B.J. Smith, *S. Afr. J. Chem*. 35 (1982) 126.

129. J.A. Gladysz, J.C. Selover and C.E. Strouse, *J. Am. Chem. Soc*., 100 (1978) 6766.

130. W.A. Hermann, J. Plank, Ch. Bauer, M.L. Ziegler, E. Guggolz and R. Alt, Z. *Anorg. Allg. Chem*., 487 (1982) 85.

131. D.St.C. Black, G.B. Deacon and N.C. Thomas, *Inorg. Chim. Acta*, 65 (1982) L75.

132. G. Sub-Fink, *Z. Naturforsch., Teil B*, 35 (1980) 454.

133. B.F.G. Johnson, J. Lewis and D. Pippard, *J. Chem. Soc. Dalton Trans*. (1981) 407.

134. (a) G.F. Stunz and J.R. Shapley, *J. Organomet. Chem*. 213 (1981) 389; (b) B.F.G. Johnson, J. Lewis and D. Pippard, *J. Organomet. Chem*., 160 (1978) 263.

135. S. Maggini, *Coord. Chem. Rev*., 253 (2009) 1793.

136. I. Dance et al., *Angew. Chem. Int. Ed. Engl*., 34 (1995) 314.

137. C.A. Tolman, *Chem. Soc. Rev*., 1 (1972) 337.

138. F. Basolo and R.G. Pearson, Prog. *Inorg. Chem*., 4 (1962) 381.

139. B.J. Coe and S.J. Glenwright, *Coord. Chem. Rev*. 203 (2000) 5

140. A. Pidcock, R.E. Richards and L.M. Venanzi, *J. Chem. Soc. A*, (1966) 1707.

141. T.G. Appleton, H.C. Clark and L.E. Manzer, *Coord. Chem. Rev*., 10 (1973) 335.

142. (a) J.K. Burdett and T.A. Albright, *Inorg. Chem*., 18 (1979) 2112, (b) E.M. Shustorovich, M.A. Porai-Koshits, Yu.A. Buslaev, *Coord. Chem. Rev*., 17 (1975) 1.

143. J.Chatt and R.G.Wilkins, *J. Chem. Soc*., London, (1952) 4300; (1956) 525.

144. S.O. Grim, R.L. Keiter and W. McFarlane, *Inorg. Chem*. 6 (1967) 1133.

145. R. Cross, *J. Chem. Soc. Rev*., 14 (1985) 197.

146. (a) L. Carlton and R. Weber, *Inorg. Chem*., 35 (1996) 5843; (b) L. Calrton and R. Weber, *Inorg. Chem*., 32 (1993) 4169

147. G.O. Spessard and G.L. Miessler, *Organometallic Chemistry*, Prentice-Hall, New Jersey, (1997) 138

148. L. Vaska, *Acc. Chem. Res*., 1 (1968) 335.

149 J.P. Collman and W.R. Roper, *Adv. Organomet. Chem*., 7 (1968) 53.

150. (a) R. Ugo, A. Pasini, A. Fusi, S. Cenini, *J. Am. Chem. Soc.*, 94 (1972**)** 7364; (b) P.B. Chock and J. Halpern, *J. Am. Chem. Soc.*, 88 (1966**)** 3511; (c) I.C. Douek and G. Wilkenson, *J. Chem. Soc. (A)*, (1964**)** 2604.

151. G.L. Hillhouse, *Organometallics*, 14 (1995) 4421.

152. B.J. Holliday and C.A. Mirkin, *Angew. Chem. Int. Ed*., 40 (2001) 2022.

CHAPTER 2

NMR Spectroscopy with emphasis on Transition Metal Complexes

Nuclear magnetic resonance of metal nuclei in complexes has been successfully used as an investigative tool in the study of both structural and bonding features in many transition and post-transition metal systems. Transition metal NMR chemical shifts are readily measured by modern two-dimensional pulse techniques and serve as a probe into electronic and steric effects of ligands and substituents in metal complexes [1]. The metal chemical shift and line width (for nuclei with $I > ½$) are remarkably sensitive to the nature of the ligand and the geometric structure of the complex, and spin-spin coupling is often observed between metal and ligand nuclei. These structural and ligand dependencies of the metal chemical shift of complexes have their origin in the electron distribution and orbital utilization resulting from the nature and the geometric placement of the ligand. The differences from one ligand system to another, affect both the nuclear shielding and the coupling mechanism [2]. Quantitative correlations of metal chemical shift with reaction rates and catalytic activities provide insight into mechanistic information as well as reactivity predictions and screening of some of homogeneous catalysts [1a].

Transition metal NMR has an advantage over proton NMR for several reasons. Firstly, hydrogen is a peripheral atom in most organometallic complexes except for metal hydrides whilst the reactivity is associated with the metal centre, and secondly, transition metal nuclei offer very large chemical shift ranges, hence sensitivity to subtle structural changes [1]. Transition metal NMR spectroscopy is one of the few non-destructive principal techniques used to obtain physical, chemical, electronic and structural information about molecules mainly in solution state. It can also provide detailed information on the topology, molecular dynamics and three-dimensional structure of molecules in solution and the solid state. NMR has wrought a revolution in biological sciences and in medicine through magnetic resonance imaging, and will continue to do so as a result of its non-invasive and selective NMR spectroscopic analysis of biological systems, including human biology. NMR spectroscopy and X-ray crystal-structure analysis

remain the two most important complementary techniques in the study of organometallic compounds.

2.1. Brief historical perspective

In the early 1920s Stern and Gerlach had shown that a beam of atoms passed through an inhomogeneous magnetic field is split into two discrete beams because of the magnetic effects arising from the quantized orbital angular momentum of the electron spin [3]. Later, in 1938, I.I. Rabi and his colleagues made a major improvement by employing a homogeneous magnet and applying a radio frequency (rf) electromagnetic field to measure nuclear magnetic moment and this achievement earned Rabi a Nobel Prize in 1944 [4]. Up to this point, the discoveries were concentrated on the elucidation of the NMR phenomenon. It was not until 1945-46 that the NMR phenomenon was demonstrated in bulk materials by two independent groups, one directed by Professor F. Bloch, W.W. Hansen (the electronics expert) and graduate student M. Packard, at Stanford University [5], and another at Massachusetts Institute of Technology (MIT), directed by Dr. E.M. Purcell, H.C. Torrey and R.V. Pound (experiments conducted at Harvard University) [6]. Bloch and Purcell shared the 1952 Nobel Prize in Physics because the two discoveries at MIT-Harvard and at Stanford were deemed independent and essentially concurrent.

The introduction of superconducting magnets, Fourier-transform methods and multiple-pulse excitation made NMR the currently only known method for determining the structure and conformation of complex molecules in solution. Advances in both radiofrequency generation and data handling technology in the 1970's and 1980's gave rise to the rapid development of a wide range of one- and two-dimensional techniques [7]. Even though most of the two-dimensional pulse sequences were not originally designed for the study of transition metal NMR spectroscopy, the techniques were soon applied fruitfully for recording the spectra of low-γ metal nuclei.

The concept of 2D was first proposed by the Belgian scientist Jean Jeener and later developed by Richard Ernst who won a Nobel Prize in Chemistry in 1991 for his contributions to FT NMR in

both one and two frequency dimension [8]. The introduction in the 1970's of Fourier-transform NMR spectroscopic methods and broad-band decoupling techniques accompanied by a dramatic increase in NMR sensitivity, represented the biggest quantum leap in the application of NMR. This development let to an upsurge in interest in the less sensitive nuclei such as ^{15}N, ^{13}C and many more. The pulsed Fourier-transform technique has been widely used at the expense of continuous-wave method for practical reasons such as sensitivity.

2.2. Principles of NMR spectroscopy

A brief discussion on the subject of principles and fundamentals of NMR spectroscopy will be outlined in the thesis. A more detailed discussion on the subject can be found elsewhere [3, 9]

2.2.1. Nuclear spin and magnetic moments.

Nuclear magnetic resonance (NMR) is a physical phenomenon based upon the quantum mechanical magnetic properties of an atom's nucleus i.e. nuclear spin quantum number *I*. When a nucleus with a non-zero *I* is placed in a strong magnetic field B_o, the orientation of its spin axis becomes quantised, with possible orientations having different energies. A radio frequency electromagnetic field of suitable energy will cause nuclear energy transitions which, when detected and amplified, result in signal that forms the basis NMR spectroscopy. The elementary particles, neutrons and protons, comprising an atomic nucleus have an intrinsic quantum mechanical property of spin giving rise to the overall spin of the nucleus which can have zero or non-zero value and is determined by the spin quantum number *I*. In most cases the overall spin is non-zero i.e. *I* can take a value of 1/2, 1, 3/2, 5/2 or 7/2, corresponding to orientations of the nucleus in magnetic field numbering 2, 3, 4, 6 or 8 respectively. A spinning charged particle having spherical symmetry behaves as a magnetic dipole and has a magnetic moment μ which is collinear with the angular momentum *P* (**Eq 2.1**)

$$\mu = \gamma P \qquad (2.1)$$

where the proportionality constant γ is called the gyromagnetic ratio. It is this magnetic moment that is exploited in NMR spectroscopy. The magnetic moment of a spin ½ nucleus, in a magnetic

field can take up two possible positions; either aligned with the field (magnetic quantum number m = +1/2) or against the field (m = -1/2) as shown in **Figure 2.1**, where the energy levels are given by **Eq. 2.2** and energy difference by **Eq. 2.3**

$$E = \hbar B_0 m\gamma \qquad \textbf{(2.2)}$$

$$\Delta E = \hbar B_0 \gamma = h\nu \qquad \textbf{(2.3)}$$

where $\hbar$ (i.e. $\hbar = h/2\pi$) is Planck's constant, B_0 is the magnetic field and $h\nu$ is the energy of a photon, hence

$$\nu = \Delta E/h = \gamma B_0/2\pi \qquad \textbf{(2.4)}$$ (the *Larmor* equation)

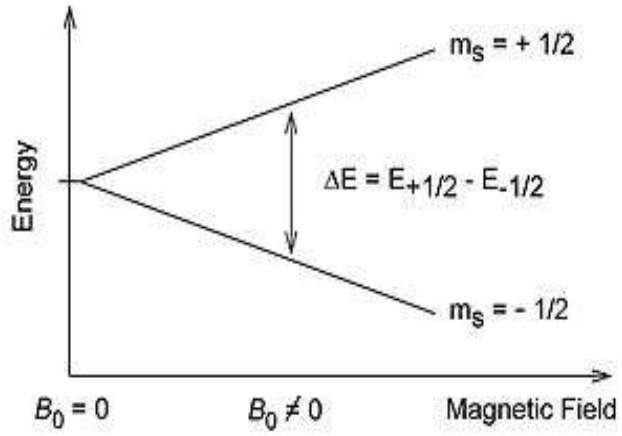


Figure 2.1 Splitting of nuclear spin states in an external magnetic field (ref. [3]).

A spinning nucleus will experience a precessional motion the moment it is placed in a magnetic field, without absorption of energy (illustrated in **Figure 2.2)**.

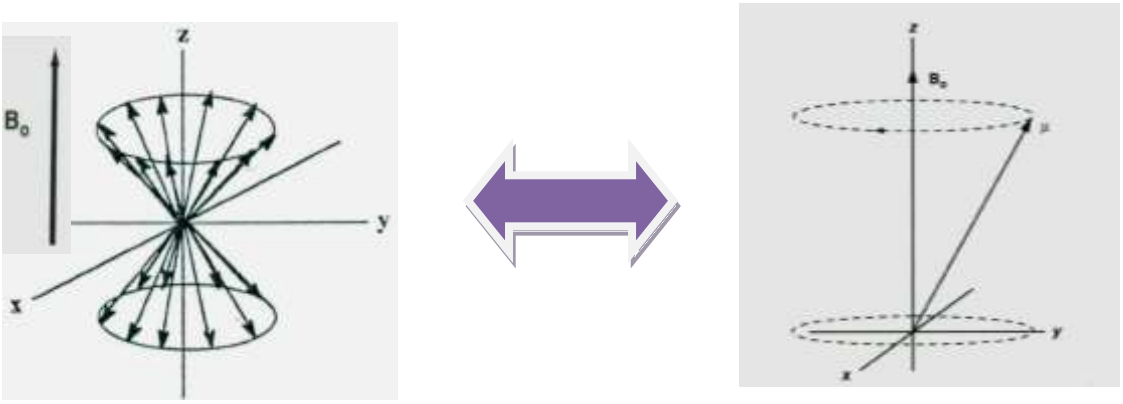


Figure 2.2 An illustration of the precessional motion of a spinning nucleus having a magnetic moment, μ, in an applied field B_0 (ref. [3]).

Therefore, when a collection of nuclei of spin ½ absorb energy and start precessing in a magnetic field, their resultant collective magnetism can be represented by **Figure 2.3.**

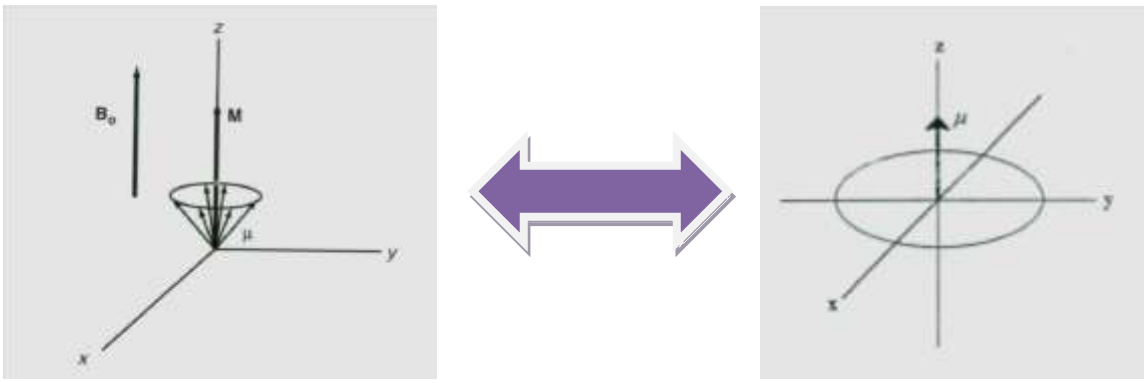


Figure 2.3. The resultant precessional motion of a collection of nuclei producing a magnetic moment, μ (ref. [3]).

The spin ½ magnetic moments in a magnetic field each take up one of two levels, aligned with the field (M = +1/2, n_α) or against the field (M = -1/2, n_β). An expression for the population difference of the two levels can be obtained using the Boltzmann **Equation 2.5** where k is the Boltzmann constant**.**

$$\frac{n_\beta}{n_\alpha} = e^{-\Delta E/kT} = e^{-\gamma \hbar Bo/kT} \qquad (2.5)$$

The fractional excess of nuclei in the level of lower energy can now be given by **Equation 2.6** below assuming the high temperature approximation $e^{-x} \approx 1 - x$, where x is negligible.

$$\frac{n_\alpha - n_\beta}{n_\alpha} = \frac{\gamma \hbar B_0}{kT} \qquad (2.6)$$

2.2.2 Pulsed FT NMR spectroscopy

Pulsed Fourier Transform Nuclear Magnetic Resonance (FT NMR) spectroscopy became a convenient alternative to the continuous wave method mainly because of a great saving on instrument time and the development of accurate radio frequency generators, timing circuits and data handling technology. A simplified description of pulsed FT NMR is represented by **Figure 2.4**. A linearly polarised electromagnetic field (RF pulse) can be regarded as consisting of two counter-rotating components, one component rotating so as to match the precessional motion of the nuclei and the other against. However, when radio frequency of correct energy *hv*, of the

electromagnetic radiation that matches this energy difference is applied in the presence of a magnetic field B_0, a precessional motion occurs around the axis of the applied field B_1 (the *Larmor frequency* and is defined by the *Larmor* Equation **2.7**) where θ is the angle between the direction of the applied field and the axis of nuclear rotation.

$$\nu = \Delta E/h = \gamma B_1/2\pi \qquad \textbf{(2.7)}$$

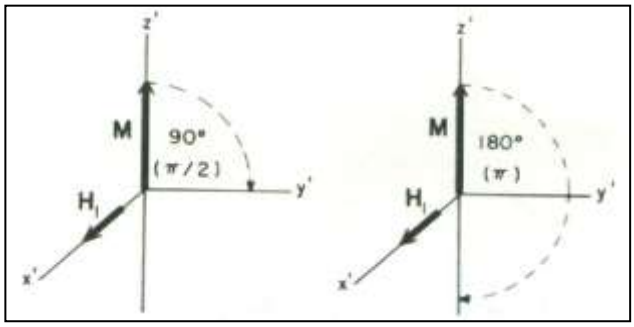


Figure 2.4 Precession of M about H_1 (B_o) in the rotating frame showing flip θ of 90^0 and 180^0 (ref. [3]).

If a short intense rf pulse of duration t_1 (which makes θ to flip by 90^0) is applied to perturb the macroscopic magnetization M from its equilibrium position, M will precess and rotate so as to lie along the y´ axis (see the rotating frame of reference, **Figure 2.4**).

At resonance, during application of the radiofrequency pulse field, B_1 the magnetic moment vector precesses (at the Larmor frequency) in the yz plane. At the end of the 90^0 pulse precession about B_0 resumes. The generation of magnetisation in the xy plane by the precessing nucei induces a voltage (in microvolts) in the receiver coil, which is aligned so as to detect magnetisation in the xy plane. The maximum magnetisation in the xy plane (from a properly adjusted t_1, called the *pulse width*) is obtained from 90^0 flip θ, resulting in the maximum signal intensity, called a 90^0 pulse. Following the pulse, the vector continues to precess about the static field B_0 and returns to alignment with the z axis as a result of relaxation processes. As a result of precession motion and decay process (in the xy plane) free induction decay (FID) of the magnetisation follows, from which, after Fourier transformation (FT), the spectrum is obtained.

2.2.3 Relaxation

Relaxation is a non-spontaneous process by which the nuclei return to the position of alignment with the applied field. Two relaxation mechanisms can occur as a result of an absorption of energy and the return to the thermodynamic state before being perturbed again, i.e. spin-lattice T_1 (or longitudinal) relaxation in which the vector moments realign themselves with the z axis and spin-spin T_2 (or transverse) relaxation in which the vector moments fan out in the x, y plane. These are two independent, first order decay processes [9]. In the absence of paramagnetic additives, nuclei with I = ½ tend to have relatively long relaxation times whereas T_1 and T_2 for nuclei I > ½ tend to be short. This is because if I > ½, the nucleus possesses an electric quadrupole moment and the presence of an electric field gradient at the nucleus leads to efficient relaxation [10]. Relaxation of a spin ½ nucleus can also occur by spin-rotation, dipole-dipole interaction which is a major contributor, shielding anisotropy and scalar coupling mechanisms [11]. Dipole-dipole interaction occurs as a result of the tumbling of all molecules in solution which gives rise to a flutuating magnetic field which influences the relaxation processes.

2.2.4 Chemical shift

Chemical shift is a measure of effective shielding of a magnetic nucleus by the surrounding electrons. The transition metal nuclei exhibit very large chemical shift ranges that may extend to more than ten thousand parts per million (ppm) and therefore this parameter becomes pertinent in the study of electronic and stereo-chemical environments.

$$B_{eff} = (1 - \sigma)B_0 \qquad \textbf{(2.8)}$$

Equation 2.8, describes the relationship between the effective magnetic field (B_{eff}) experienced by the nucleus and the external magnetic field (B_0), and σ is the shielding tensor. However, for liquids or solutions where molecules undergo rapid random motion, only the average value of the tensor needs consideration. Chemical shifts are governed by *diamagnetic* and *paramagnetic* shielding terms (**Eq. 2.9**).

$$\sigma_i = \sigma_i^{dia} + \sigma_i^{para} + \sigma_{ij} \qquad \textbf{(2.9)}$$

where σ_i is the overall shielding, σ_i^{dia} is the diamagnetic shielding of the nucleus being considered, σ_i^{para} is the paramagnetic shielding, and σ_{ij} is the shielding from other atoms and is usually insignificant. The diamagnetic shielding term σ_i^{dia} describes the local electronic density around the nucleus and it accounts for the unperturbed spherical motion of the electrons and plays a dominant role in proton NMR spectroscopy. Changes in chemical shift for a given transition metal are largely determined the *paramagnetic* shielding term σ_i^{para}, which not only depends on the electron density at the nucleus but is also related to an electronic excitation energy ΔE^{-1} and a non-*s*-orbital expansion terms ‹ r^{-3} › shown in the Ramsey equation [12] as revised by Juranic [13] (**Eq. 2.10**)

$$\sigma^{para} = -\frac{8\mu_0\mu_B^2}{\pi} \langle r_d^{-3} \rangle_F \frac{\beta}{\Delta E} \qquad (\mathbf{2.10})$$

The terms μ_0 refers to the permeability of vacuum, μ_B is the Bohr magneton and $\langle r_d^{-3} \rangle_F$ refers to the *d* orbital radius of the free ion and is constant for a given oxidation state. A deduction from equation **2.10** is that σ^{para} is proportional to $\frac{1}{\Delta E}$ i.e. a decrease in ΔE leads to an increase in the paramagnetic shielding value. A value of ΔE can be obtained from electronic spectra and similarly β, the *nephelauxetic* ratio (*Nephelauxetic* means "cloud expanding") can be determined from the measureable *d-d* electronic interactions in a metal atom. The quantity β is defined as the ratio (B_c/B_f) of the Racah parameters B_c for the complex and B_f for the free ion [14] and it provides a good measure of *d-d* electronic transitions in the metal. The ordering of ligands according to their influence on β is known as *nephelauxetic* series [15]. As a consequence of forces of repulsion between the *d* electrons, the orbitals expand as a result of the reduction of the effective nuclear charge on the metal through the ligand electron donation. Ligands that are most effective in delocalising the metal electrons display the largest values of the *nephelauxetic* series parameter β.

The parameter ΔE, which represents the energy difference between the ground state and a low lying excited state, is highly influenced by the σ donor/π accepter properties of the ligand. In a complex with σ donor (or $\sigma + \pi$ donor) non-π acceptor ligands, the build up of electron density on the metal centre increases the repulsive forces between the valence orbitals, with the result

that their energy rises and the ΔE decreases. In a complex with strong π acceptor ligands much of the electron density on the metal brought by σ donation is returned to the ligand through a process of π-back bonding with the result that ΔE is increased. Based on a wide variety of complexes, the relative influence of a ligand upon ΔE is given in order of increasing field strength in the *spectrochemical* series [16] (in part):

$I^- < Br^- < Cl^- < F^- < OH^- < H_2O < NCS- < Py < NH_3 < NR_3 < PR_3 < CN^-$, CO, ~ PF_3

According to the spectrochemical series strong σ donors and poor π acceptors ('weak' ligands) will give rise (via low ΔE) to a high δ_{metal} and strong π-acceptors to a low δ_{metal}. From the *nephelauxetic* series ligands of low polarisability will favour a high δ_{metal} (via low r) and ligands of high polarisability will favour a low δ_{metal} [15].

Transition metal chemical shifts are influenced by a number of factors and only few are dealt with here in detail. Many of the influences on the metal chemical shifts are also significant for all NMR active nuclei including the main group elements. Among those not included in the discussion are (discussed elsewhere, 17,18,19): change in coordination geometry, diastereomeric dispersion, change in the oxidation state of the central metal atom, pressure, etc. Experimentally, chemical shifts in transition metal complexes are found to correlate with the symmetry of the complex [20], with *trans*-influences [21], and with properties of the metal centre such as *d* electron configuration [22], the oxidation number and periodicity. It was noted by Goodfellow [11] that generally lower oxidation states give lower frequency shifts despite a considerable overlap between different oxidation states and that complexes of strong field donors resonate at low frequencies. In most cases, ligand donor atom shielding, seems to increase across a row and down a group for transition metals [23].

2.2.4.1 Influence of temperature on the Chemical shift

Temperature dependence of the order of 0.5 – 1.5 ppm/K is commonly encountered for the transition metal chemical shift. These temperature dependent changes in the metal chemical shift have their origin in the vibration of metal-ligand bonds [17]. This effect known as vibrational shielding is well documented [24] and theoretically accounted for [25]. The temperature

dependent change in the population of vibrational levels gives rise to a change in ΔE (see section 2.2.1), hence the chemical shift.

As noted earlier, the influence of temperature in the chemical shifts is not limited to transition metals, but is also found for NMR active nuclei of the main group elements as well. It has been found that the shielding of ^{119}Sn increases roughly linearly with increasing temperature [26], although the slope of this relationship can be expected to depend critically on the type of the compound and also upon the solvent medium.

2.2.4.2 Influence of solvent on the chemical shift.

The chemical shift of a metal in a metal complex in solution can be influenced by non-bonded interactions with solvent arising from the bulk susceptibility, electric field effects, van der Waals interactions and non-random averaging orientation of magnetically anisotropic solvent molecules relative to solute molecules [27], and by other interactions such as hydrogen bonding. In dilute solutions collisions and repulsive interactions between solute and solvent molecules can distort the electronic environment of a given nucleus, hence alter its chemical shielding. As noted by Carlton [28], temperature-dependent hydrogen bonding effects are likely to involve direct interaction with the metal rather than a ligand (for complexes in which the metal has a vacant coordination site). The temperature-dependence of the ^{103}Rh chemical shifts in the complexes $[Rh(X)(PPH_3)_3]$ show dependence on both solvent and ligand X. Therefore, the influence on the chemical shift of temperature and solvent are best studied together in the presence of varied ligand X.

2.2.4.3 Coordination effect

In the study of organometallic complexes, changes in NMR chemical shift provide valuable information about the changes in the coordination sphere of the metal. A change in coordination system occurs as a result of oxidative addition or coordination reactions (transformations which are not accompanied by a change in oxidation state). Chemical shift changes that occur as result of a change in a coordination system accompanied by a change in oxidation state can be as large

as several thousand ppm for complexes of ^{195}Pt [29] and ^{103}Rh [30]. The change in the chemical shifts is attributed to the reduction in ΔE, (a phenomenon already discussed in detail earlier) as a result of transformation from a square to a square pyramidal or octahedral geometry. The properties of the ligands in terms of type or class are equally important in the study of coordination effects. Four-coordinate complexes of platinum and rhodium generally have a lower chemical shift than five- or six-coordinate compounds in cases where similar ligands are involved.

Bucher and co-workers [31] have reported significant ^{103}Rh chemical shift changes as a results of equilibria between four and five coordinate complexes with several boron-substituted tris-pyrazolylborate ligands that coordinate as bidentate or tridentate in [Rh(Tpz)$(L)_2$]. Lindner and co-workers [32] have demonstrated that the [Rh(Cl)$(Cy_2PCH_2CH_2OCH_3)_2$] complex can bind to SO_2 to form either five-coordinate or a four-coordinate products depending on the solvent. In acetone solution, the complex behaves as a Lewis base, by donating an electron pair to sulphur whereas in hexane it behaves as Lewis acid by accepting an electron pair from sulphur.

2.2.5 Correlation of structural, chemical and spectroscopic parameters with metal chemical shifts.

Transition metal chemical shifts have been found to correlate with a number of chemical, physical and structural parameters, which include:

(a) Rate constant [33] (**Figure 2.5**) and catalytic activity [34],
(b) Stability constants [35],
(c) Tolman's [36] electronic parameter, ν_{CO} [37] (**Figure 2.6**),
(d) Tolman's steric parameter θ [37,38] (**Figure 2.7**) and Taft's steric parameter E [37, 38],
(e) Structural parameters from crystallographic data [39],
(f) Hammett function, σ [40], (which σ is a measure of the electron donating/withdrawing properties of a functional group [41]).

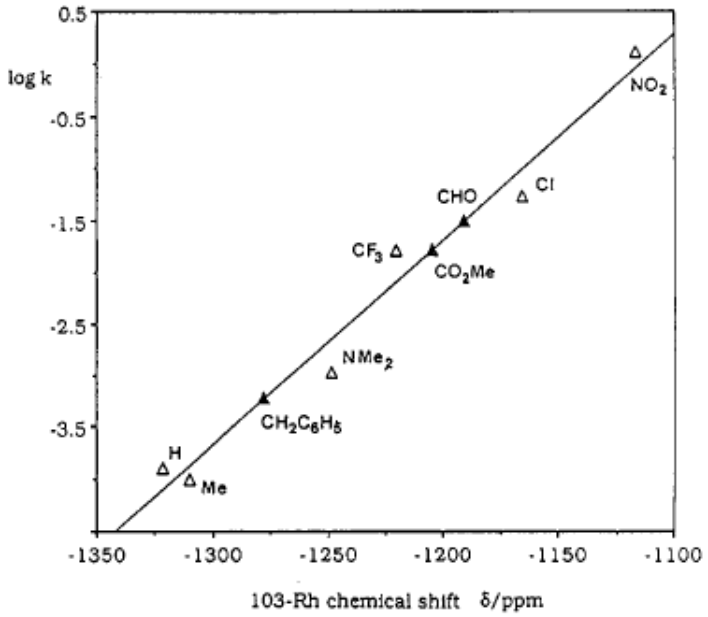


Figure 2.5 Correlation of δ(^{103}Rh) of substituted (X)CpRh(CO)$_2$ complexes with rate constants for the displacement of CO by PPh_3: (Δ) correlation points; (▲) δ(^{103}Rh) of complexes for which rates are unknown; $R^2 = 0.973$ (Fig. taken from ref [33b])

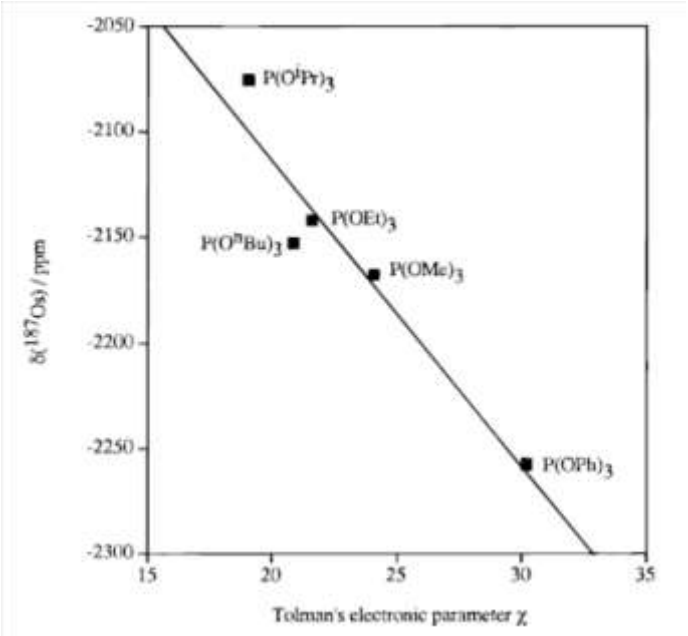


Figure 2.6 A plot of δ(^{187}Os) vs. Tolman's electronic parameter χ (where $\chi \equiv \nu_{co}$ for complexes [Os(p-cymene)(Cl)$_2$(L)] (Fig. taken from ref. [37]).

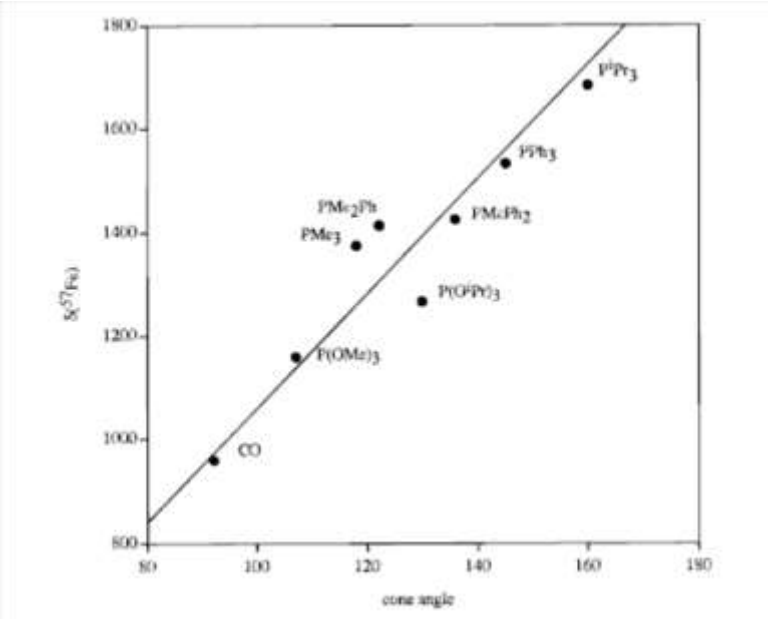


Figure 2.7 Correlation of δ(^{57}Fe) with Tolman's cone angle θ [36] of ligand L of CpFe(CO)(L)(COMe) complexes (r = 0.941) (Fig. taken from ref. [38]).

2.2.6 Spin-Spin coupling

Nuclear spin coupling has been formulated in a molecular orbital framework by Pople and Santry [42]. In a fluid solution, by virtue of thermal molecular motion, through-space (dipole-dipole) interactions are averaged to zero and only the scalar coupling interactions $^{n}J_{(A,X)}$, which are transmitted by electrons mainly through bonds are observed (*n* is the number of bonds between atoms A and X , and *J* is expressed in frequency units of Hz). These scalar couplings are independent of the external magnetic field strength. The sign of the coupling constant between the nuclei is positive if an antiparallel configuration of the nuclear spin is favoured and the negative if a parallel configuration is favoured. The relative signs of coupling constants can be measured by double resonance methods or by spectral analysis [10]. However, when quoted, absolute signs of the coupling constant, |J| are usually given without the modulus symbol.

Coupling constants are subject to the influence of several molecular factors such as: (i) magnetogyric ratios, (ii) the *s* character of the bond, i.e. hybridization effects; (iii) low lying empty *d* orbitals; (iv); energy difference (ΔE) between the ground state and a low lying excited state; (v) the molecular geometry of the coupling nuclei; (vi) electronegativity of substituents, and to a lesser extent, (vi) electron density in the bond [10,17,43]. For two spin ½ nuclei in atoms connected by a σ bond, the interaction of an electron in the bond with one of the two nuclei has consequences at the second nucleus. The magnitude of this effect is inversely proportional to the energy separation ΔE between electronic ground and excited state as found for the chemical shift (already discussed section 2.2.4) [42]. Therefore major influences on *J* are, therefore, the s character of the bond and ΔE, with the electron density in the bond exerting a lesser influence.

2.4 Experimental Techniques for selected NMR nuclei

Sections 2.4.1 and 2.4.2 are discussed in this thesis for historical and practical reasons because of the wealth of data that has been collected through the use of direct observe and INEPT methods. The use of the INEPT method in particular has been superseded by HMQC and other related 2D methods which give much better signal enhancement. It is however, interesting to note that as recently as 2006 both direct observe and INEPT were still in use for nuclei such as ^{57}Fe and ^{183}W [44].

2.4.1 Direct observation technique

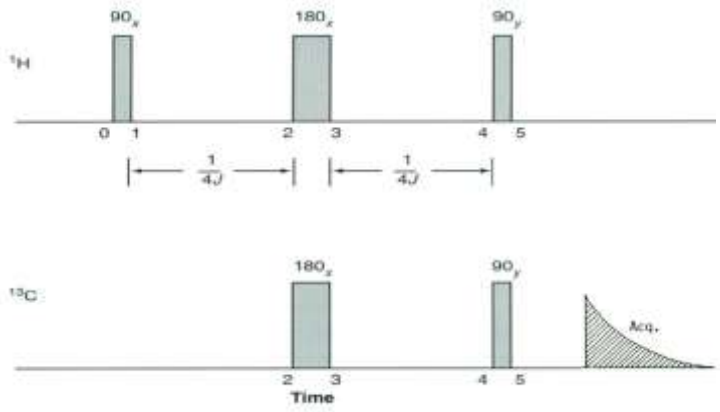
The success of direct observation depends on a number of factors such as high natural abundance, high-γ values, and relatively high sensitivity. The direct observe method which involves broad-band (noise) decoupling is applied mainly in the study of nuclei (Y) that show spin coupling to protons. The spectrum of Y{^{1}H} (where Y could be ^{13}C, ^{15}N, ^{19}F, ^{29}Si ^{31}P, etc) is simplified by effective loss of spin-spin coupling during acquisition. There is a large body of data collected over the years of the use of this method (only few reviews are quoted) for many spin 1/2 nuclei such as the following selected main group and transition metals: ^{119}Sn and ^{205}Pb [45, 46], ^{107,109}Ag, ^{57}Fe, ^{103}Rh, ^{111}Cd, ^{187}Os, ^{195}Pt and ^{199}Hg [44, 47,48]. However, the relatively

high chemical shift ranges of many of the transition metal nuclei often make it impossible to cover the entire range in a single measurement involving irradiation at a fixed frequency. The technique will require several measurements to avoid 'folding-back' of a signal into the spectral range especially if the expected chemical shift position is not known.

^{1}H NMR spectra on other hand, as with ^{31}P, provide invaluable information with regard to coupling constants and are in many cases a valuable probe into molecular environments of organometallic compounds such as metal hydrides. The proton chemical shift range of 25 > $\delta(^{1}H)$ > -40 ppm for diamagnetic organotransition-metal compounds is common. The range is widened with paramagnetic organometallic complexes where chemical shifts of several hundred ppm has been recorded e.g. [$(C_6H_6)_2V^{\cdot}$, δ (^{1}H) = 290 ppm] [43]. The high field resonance of metal hydrides can be accounted for by the characteristic feature of the transition-metal complexes of having low-lying, orbitals which create a shielding effect on the hydride ligand due to the induced magnetic moment at the central metal.

2.4.2 Polarisation Transfer method: the INEPT pulse sequence

Insensitive Nuclei Enhanced by Polarization Transfer (INEPT) [49] as with Distortionless Enhancement by Polarisation Transfer (DEPT) [50] uses polarization transfer to enhance the sensitivity of the insensitive nucleus by a factor of $\eta = \gamma_H/\gamma_X$. The method is based on the application of non-selective pulses on a scalar-coupled heteronuclear spin system ($^{1}J_{(X\text{-}H)}$) which leads to spin polarization transfer from the more sensitive nuclei to the low-γ spin-1/2 nuclei. The simplest version of the INEPT pulse sequence is shown in **figure 2.8**. The optimum success of this method depends on the accuracy and the magnitude of $^{1}J_{(X\text{-}Y)}$ where X is the low-γ spin-1/2 nucleus and Y is the sensitive nucleus, and that the sensitive nuclei should not be further spin-coupled to other similar nuclei.



Fiqure 2.8 A representation of a simplified version of INEPT pulse sequence (ref. 3).

The one dimensional INEPT method has been applied successfully to enhance the sensitivity of less sensitive nuclei of low magnetic moment such as ^{13}C, ^{15}N, ^{119}Sn, ^{103}Rh and ^{57}Fe [44b,51] by the more sensitive nuclei such as ^{1}H, ^{31}P and ^{19}F. As already indicated, there is a substantial amount of data collected with the use of INEPT method for nuclei such as ^{15}N [52,53], ^{119}Sn [54] and for transition metals such as ^{57}Fe, ^{103}Rh, ^{109}Ag, and ^{183}W [55]. Some successes were achieved with the use of ^{31}P as the source for polarization transfer because of a number of advantages: (a) it has a high-γ spin-1/2 nucleus in 100% natural abundance, (ii) a sizeable $^{1}J_{(X-P)}$ value ranging from 10 to more than 1000 Hz, (iii) shorter T_1 values of phosphorus-containing metal complexes and (iv) many transition metal complexes are stabilized by phosphorus ligands. A major drawback for the INEPT method is the potential loss of magnetisation due to relatively long evolution periods, artefacts due to signal modulation from additional couplings especially where ^{1}H is the sensitive nucleus [56] and significant loss of signal due to the wide chemical shift range of many of transition metal nuclei [57]. The INEPT method was an improvement on double-resonance methods which also relied heavily on the value of $J_{(X-Y)}$, required the use isotopically enriched nuclei and long measuring time. The double resonance method was also applied successfully to determine ^{57}Fe chemical shifts by the group of Koridze [58] and in determining the ^{57}Fe shift of iron porphyrins [59].

2.4.3 The indirect detection method

The indirect detection method, as with polarisation transfer method (i.e. INEPT method), requires a non-zero scalar $J_{(M-S)}$ coupling with $J_{(M-S)} > 1/T_2$ (where M is an insensitive, low-γ spin-1/2 transition metal nucleus and S is a sensitive, high-γ spin-1/2 nucleus). The first widely used HMQC (*Heteronuclear Multiple-Quantum Coherence*) pulse-sequence by Bax et al [60] (originally intended for $^{1}H\{^{15}N\}$ detection) has been adopted for indirect detection of nuclei such as ^{103}Rh *via* ^{31}P with concomitant ^{1}H decoupling as shown in a modified pulse sequence by von Philipsborn [1] **figure 2.9**. HMQC is a two dimensional method which can be applied for proton-detected experiments such as $^{1}H\{M\}$ (M = ^{183}W, ^{103}Rh, ^{57}Fe, etc), where M is a low-γ nucleus and has been applied successfully to measure ^{183}W chemical shifts with correlations of up to six [61] and seven bonds [62] i.e. $^{6}J_{(W-H)}$ and $^{7}J_{(W-H)}$ respectively. The above mentioned method of indirect detection is convenient for metal hydrides and other transition metal complexes where the hydrogen is suitably positioned. In the absence of a suitable hydrogen for indirect detection the use of ^{31}P or ^{19}F may be a valuable alternative.

The indirect detection method for $^{1}H\{M\}$ can be implemented on a routine spectrometer equipped with a two-channel ^{1}H-broadband probe-head, while $(^{31}P,M)\{^{1}H\}$ is a triple-resonance experiment which requires a third radiofrequency channel and a suitable probehead. The notation of the indirect detection pulse sequence is $(^{31}P,M)\{^{1}H\}$- HMQC correlation spectroscopy (shown in **figure 2.9).** This shorthand is intended to convey the information that ^{31}P is the observe nucleus, M is the nucleus from which chemical shift information (as a frequency) is encoded, by means of the pulse sequence, in the magnetization of the observed nucleus (e.g. ^{31}P). This procedure is accompanied throughout by broadband proton decoupling (the nucleus in {}). The encoded frequency is extracted from the raw data by a two dimensional Fourier transform. A signal enhancement of $(\gamma_S/\gamma_M)^{5/2}$ and (γ_S/γ_M) is achieved with respect to the direct observation and INEPT polarisation transfer methods respectively [63].

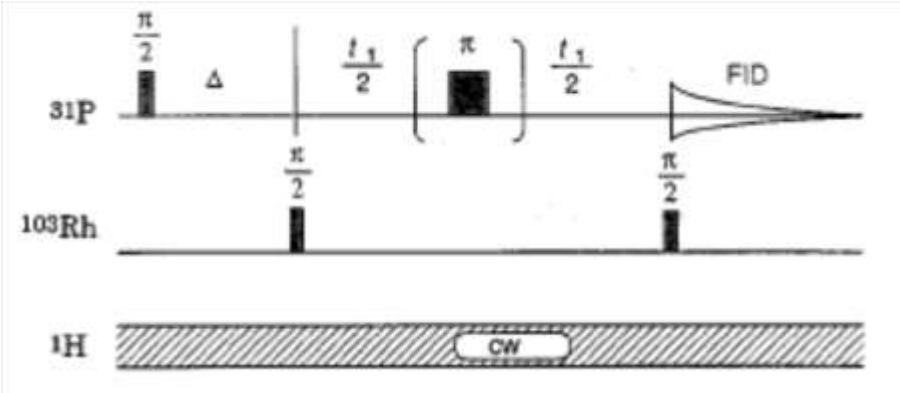


Figure 2.9 Standard HMQC pulse sequence for inverse detection of (^{31}P,^{103}Rh){^{1}H}. (Figure taken from reference [1], Δ is equal to 1/2J, where J = $J_{(Rh-P)}$)

Among the many advantages of the indirect detection method is that an error margin of 10-20 % of $J_{(X-M)}$ is in most cases good-enough to yield reasonable results. Some of the major advantages of the indirectly detected method include: (i) ability to cover large metal chemical ranges with one experiment, (ii) flexibility to focus on a specific chemical shift range, (iii) possibility of determining the number of attached protons or phosphorus ligands to the metal through spin interaction and lastly, (iv) determination of the magnitude of couplings of the magnetically active nuclei attached to the metal centre. These advantages are demonstrated very well in **figure 2.10**. There is large body of NMR data that has been acquired through the extensive use of the indirect detection method and only a few cases are noted here for ^{57}Fe, ^{103}Rh and ^{183}W [17,28,63].

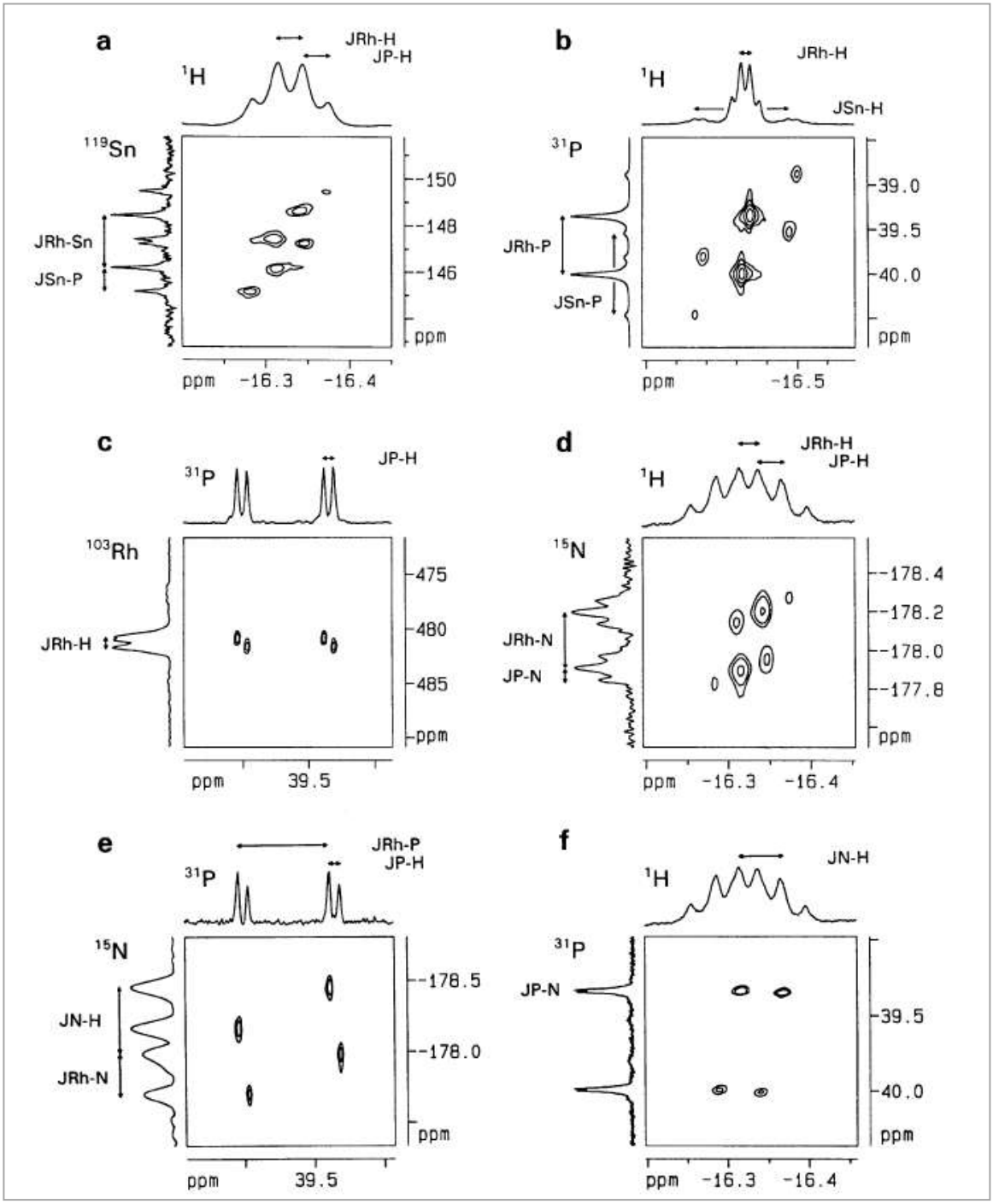


Figure 2.10 $^{1}H\{^{119}Sn\}$ (a); $^{1}H\{^{31}P\}$ (b), (f); $^{31}P\{^{103}Rh\}$ (c); $^{1}H\{^{15}N\}$ (d); and $^{31}P\{^{15}N\}$ (e) HMQC spectra recorded from $[Rh(NCBPh_3)(H)(SnPh_3)(py)(PPh_3)_2]$ (a-c) and $[Rh(^{15}NCBPh_3)(H)(SnPh_3)(py)(PPh_3)_2]$ (d-f) in dichloromethane at 248 K using a Bruker DRX 400 spectrometer with the pulse sequence similar to the one shown in **Fig. 2.9**. (ref.[17])

2.5 Calibration of spectra

The chemical shift as a measure of effective nuclear shielding of the surrounding electrons on a magnetic nucleus is the main focus of NMR spectroscopy. Therefore a correct measurement of the chemical shift is an absolute necessity at all times. In the interest of uniformity, it is important therefore to adhere to set rules with respect to referencing of spectra. There are three accepted method of referencing the chemical shift and each applies to a specific situation because of factors such as the influence of the solvent and temperature [17] (which are particularly large for the shielding of the heavier nuclei), complexation, and bulk susceptibility or concentration [10]. These are: (i) the use of an internal reference standard, (ii) the use of an external reference standard, and (iii) the use of absolute frequency. Whilst the use an internal standard as a reference may be a preferred method, often the reference is not inert and this presents the problem of finding the best internal standard. The chemical shifts of many metal nuclei are never measured with a reference sample in the same tube but separately where the field is assumed to the same and consistent for both measurements. The best internal standard reference material by far is tetramethylsilane (TMS) which also serves as a point of reference for an absolute frequency. Absolute frequencies on this scale are denoted by Ξ with the presumption that the nuclei of interest resonate in a field in which the protons of TMS resonate at exactly 100 MHz and are defined by **Eq. 2.11** [10]**.**

$$\Xi_{\mathrm{x}} = \frac{100\gamma_x(1-\sigma_x)}{\gamma(1_H)[1-\sigma^{TMS}(1_H)]} \qquad \textbf{(2.11)}$$

From **Eq. 2.11**, a variety of chemical shift values can be corrected using the following equation **2.12** [10]:

$$\delta = \delta' \frac{\Xi \text{ ref}'}{\Xi \text{ ref}} + \frac{\Xi \text{ ref}' - \Xi \text{ ref}}{\Xi \text{ ref}} \text{ x } 10^6 \qquad \textbf{(2.12)}$$

where δ is the corrected chemical shift, δ' the chemical shift with respect to the reported reference, Ξ ref the frequency of the required reference, and Ξ ref′ the frequency of the reported reference. The generally accepted ^{103}Rh reference frequency is 3.16 MHz in a field in which the protons of TMS resonate at exactly 100 MHz. Therefore, for a spectrometer in which the protons of TMS resonate at exactly 400.13001 MHz, the Ξ (^{103}Rh) frequency at the point defined as zero

on the ^{103}Rh scale is 3.16 x 400.13001/100 = 12.644108 MHz and that of ^{195}Pt is 21.4 x 400.13001/100 = 85.62782214 MHz [10], assuming that variations in $\delta(^{1}H)_{TMS}$ arising from changes is solvent and temperature are insignificant. Specific reference standards for other NMR active transition metals of interest will be dealt with in the next section.

2.6 NMR spectroscopy of selected main group nuclei

Transition metal complexes form a base of this thesis and many of the complexes under study are stabilised by ligands that have hydrogen (e.g. metal hydrides), carbon (e.g. CO), nitrogen (pyridine), phosphorus (phosphites and phosphines), tin (e.g. Ph_3Sn^-) and lead (e.g. Ph_3Pb^-) as coordinating ligands. It is on the basis of these metal-ligand interactions that a brief discussion of selected NMR active elements of the main group becomes necessary because of their extensive interaction with the metal centres in our quest to synthesize and study the transition metal complexes of interest. However, only a limited number of these nuclei will be discussed, i.e. ^{15}N, ^{31}P and ^{119}Sn are discussed whereas the other nuclei are discussed elsewhere [3,10,64].

2.6.1 ^{15}N NMR spectroscopy

Nitrogen NMR spectroscopy has been a subject of several literatures reviews [15,51,52, 65,66]. Nitrogen occurs naturally in two isotopic forms, ^{14}N and ^{15}N. ^{15}N has a low natural abundance of only 0.365%, spin quantum number of ½ and γ value with relative sensitivity (equal number of nuclei) to ^{1}H of 1.04 x 10^{-3} and absolute sensitivity (taking account of natural abundance) of 3.85 x 10^{-6}. The observable spin-coupling interaction of ^{15}N to transition metal nuclei can provides structural information much more readily than ^{14}N. Magnetic properties of the two isotopes are significantly different in that ^{14}N has a quadrupolar nucleus which contributes to broad lines of approximately 100 - 1000 Hz whereas the ^{15}N nucleus yields lines of 1 Hz or less [65]. ^{15}N is considerable lower in sensitivity, 280 times smaller than the ^{14}N nucleus. There has been steady increase in the use of ^{15}N NMR in transition metal chemistry [53,66,67,68]. The interest in ^{15}N is informed by the variety of transition metal complexes that are stabilised by nitrogen containing ligands where nitrogen is a donor atom [69]. Nitrogen is a common element in many biological

systems such as DNA and proteins. Nitrogen is also an important element in anti-cancer drugs from which important structural information can be accessible through a combination of NMR experiments including ^{15}N observation [70].

2.6.1.1 Method of observation

The double resonance method of spin polarisation transfer (INEPT) from the high-γ spin ½ ^{1}H to the low-γ spin ½ ^{15}N with signal enhancement factor of $\gamma H/\gamma N = 9.86$ was used by a number researchers [52a,b] in the years before 1986. As already mentioned before (section 2.4.2) the success of the polarisation transfer method depends heavily on the magnitude of scalar coupling between the two nuclei i.e. $J_{(N-H)}$ and the value differs from compound to compound. The correct $J_{(N-H)}$ is important to calculate the delay time for optimising the INEPT pulse sequence. In the last 20 years or so, the inverse detection method $^{1}H\{^{15}N\}$ by means of the HMQC pulse sequence [60] with gradient suppression of the signal from protons in the ^{14}N-containing molecules is currently the most widely used method. This is a heteronuclear experiment in which the magnetization of the less sensitive is detected through the use of a more sensitive nucleus which is in this case ^{1}H. The $^{1}H\{^{15}N\}$ by means of the HMQC requires a non-zero scalar $J_{(N-H)}$ coupling with $J_{(N-H)} > 1/T_2$.

2.6.1.2 Calibration and Chemical shift

Nitrogen-15 is a nucleus that has been referenced to number of substances, as internal or external standard and these include NH_4NO_3, HNO_3, NH_3, CH_3NO_2 and TMS [52b]. Nitromethane (CH_3NO_2) is the most commonly used of these substances due to its good solvent properties in organic substances and relatively sharp signals. However, there are challenges in using CH_3NO_2 as internal reference, including the fact that the chemical shift of $CH_3{}^{15}NO_2$ is notoriously solvent- and concentration- dependent [52] varying by as much as 7 ppm. Therefore it would be preferable to have one reference such as TMS with respect to a neat CH_3NO_2 as external reference where Ξ (^{15}N) is 10.136783 MHz [10]. The ^{15}N chemical shifts span a range of 1000 ppm which in many respects parallels that of ^{13}C and is significantly affected by different oxidation states and hybridization (sp^3, sp^2, sp). The introduction of electronegative substituents

leads to deshielding as shown in **Figure 2.11** (Chemical shifts relative to $MeNO_2$ at 0.00 ppm). Mason [66], interpreted changes in ^{15}N chemical shift as variations in effective excitation energy (ΔE, equation 2.9) which tends to decrease as the asymmetry increases. Therefore, ^{15}N chemical shift patterns can be attributed to three shielding factors: the larger the radial term $\langle r^{-3} \rangle_{2p}$ for nitrogen, the larger asymmetries in the valence shell when the nitrogen carries a lone pair and very low-lying $n_N \rightarrow \pi^*$ states, as in the nitrosyl group. The highest shielding is found in the amines, for which the radial factor is small, the symmetry fairly high and the ΔE large [66].

2.6.1.3 Factors affecting ^{15}N coupling constants

Nitrogen-15 spin-coupling interactions, as with ^{15}N chemical shift, are also sensitive to hybridisation and electronegativity influences. The largest coupling constants in ^{15}N spectroscopy are observed for N-H bonds where the influence of *s* character of the hybrid orbitals is evident. An important trend was observed for one bond coupling of ^{15}N to nuclei such as ^{13}C, ^{15}N and ^{31}P where the coupling constant decreases with the decreasing gyromagnetic ratio of the X nucleus [71]. The lone pair on the nitrogen influences both the ^{15}N chemical shift and the coupling constants [72]. This has been demonstrated by von Philipsborn who showed that such interaction can lead to configurational and conformational information [73]. Nitrogen *J* couplings are peculiarly sensitive to the presence and orientation of the lone pair on the nitrogen, a factor which is diagnostic of coordination, chelation, protonation and also can reflect departures from planarity, conformational relationships, stereochemistry, solvent effects and solution equilibria [15]. Of particular interest are the values of $J_{(^{15}N\text{-}^{1}H)}$ which are commonly found in the following range [9]: $^{1}J_{(^{15}N\text{-}^{1}H)}$ = 70 – 100 Hz, $^{2}J_{(^{15}N\text{-}^{1}H)}$ = 1–15 Hz and $^{3}J_{(^{15}N\text{-}^{1}H)}$ = 1 – 3 Hz.

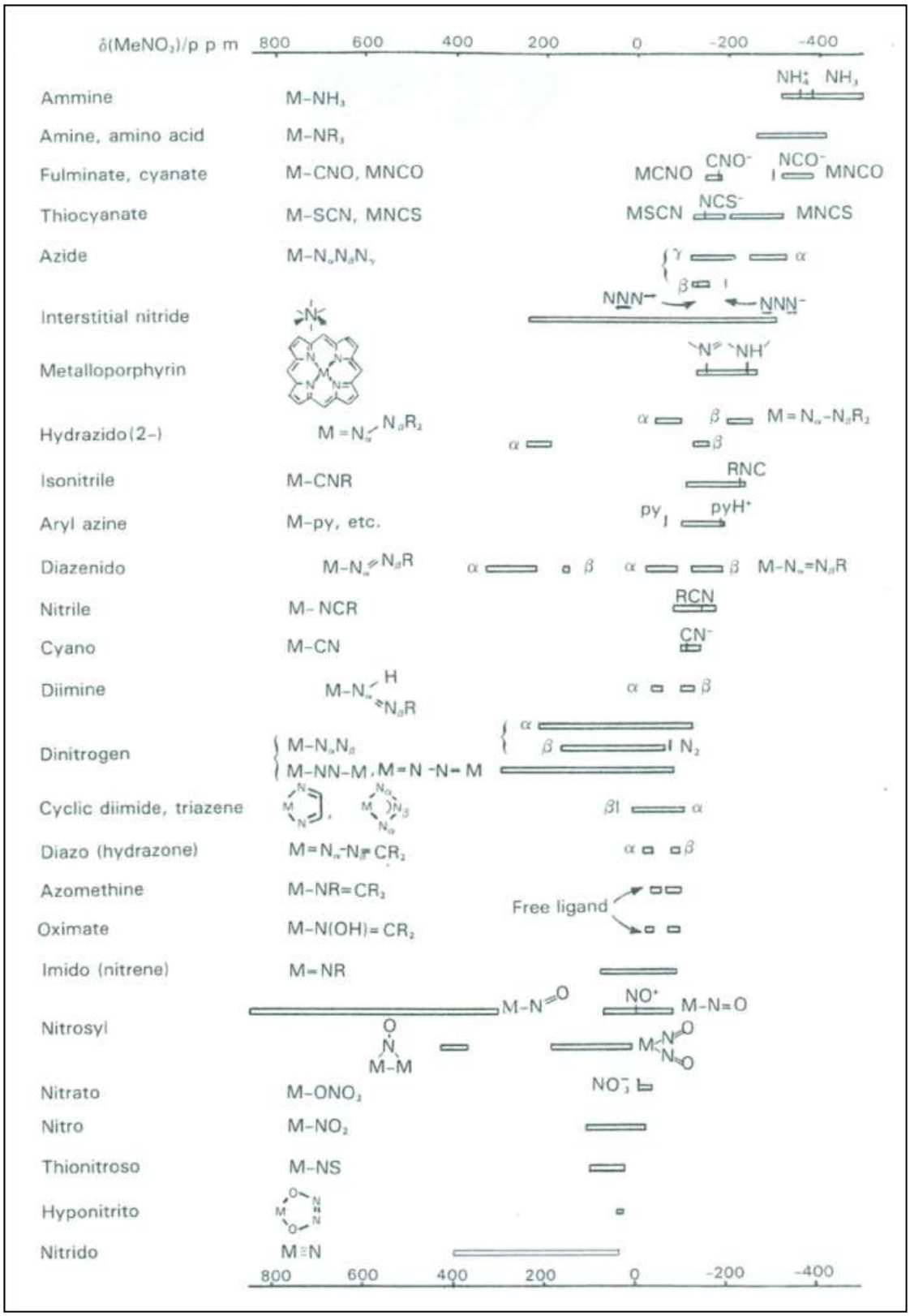


Figure 2.11 Ranges of ^{15}N chemical shift in metal complexes (Ref. [15]).

2.6.2 ^{31}P NMR spectroscopy

A truly comprehensive compilation on ^{31}P NMR spectroscopic data may now be almost impossible due to the routine nature of the technique. A wide application of phosphorus in coordination chemistry, organometallic chemistry, organophosphorus chemistry and biochemistry has effectively deterred such efforts. Recently, dedicated reviews such as *Topics in Phosphorus Chemistry* [74] and Specialist Periodical Reports by the Royal Society of Chemistry (RSC) on phosphorus NMR [75], provide the more recent developments. One of the first prominent reviews on ^{31}P NMR appeared in 1969 by Verkade [76].

Phosphorus-31 has a spin ½ nucleus and natural abundance of 100% making it one of the relatively easy NMR nuclei to record even at levels as low as 5 ppm [77], hence the amount of data in the literature. The first measurement of ^{31}P was reported in 1951 [78]. Since phosphorus compounds are generally reactive, the use of an internal reference is not an option. Whilst P_4O_6 seems to give sharper signals than H_3PO_4, its extremely hazardous nature serves as a deterrent to many would-be users. It has become a common practice to reference the ^{31}P NMR spectra to the ^{2}H internal lock signal referenced to TMS. There is unfortunately little agreement between Ξ (^{31}P) for 85% H_3PO_4 with different values quoted in the literature [10]. The only method of observation employed for ^{31}P is direct observe NMR spectroscopy with an option of broad band proton decoupling i.e. the ^{31}P{^{1}H}-technique.

^{31}P NMR chemical shifts span a range of just over 700 ppm, (i.e. from as low field as 245 ppm for PF_2Me to as high field as -461 ppm for P^{III} compounds) depending on the oxidation state of the phosphorus. **Figure 2.12** shows the ^{31}P chemical shift range for three-coordinate phosphorus compounds. The ^{31}P chemical shift range for two-coordinate compounds (where the RP group is bridging two metal atoms with no M-M bond) has been noted to resonate as low as 1362 ppm [79].

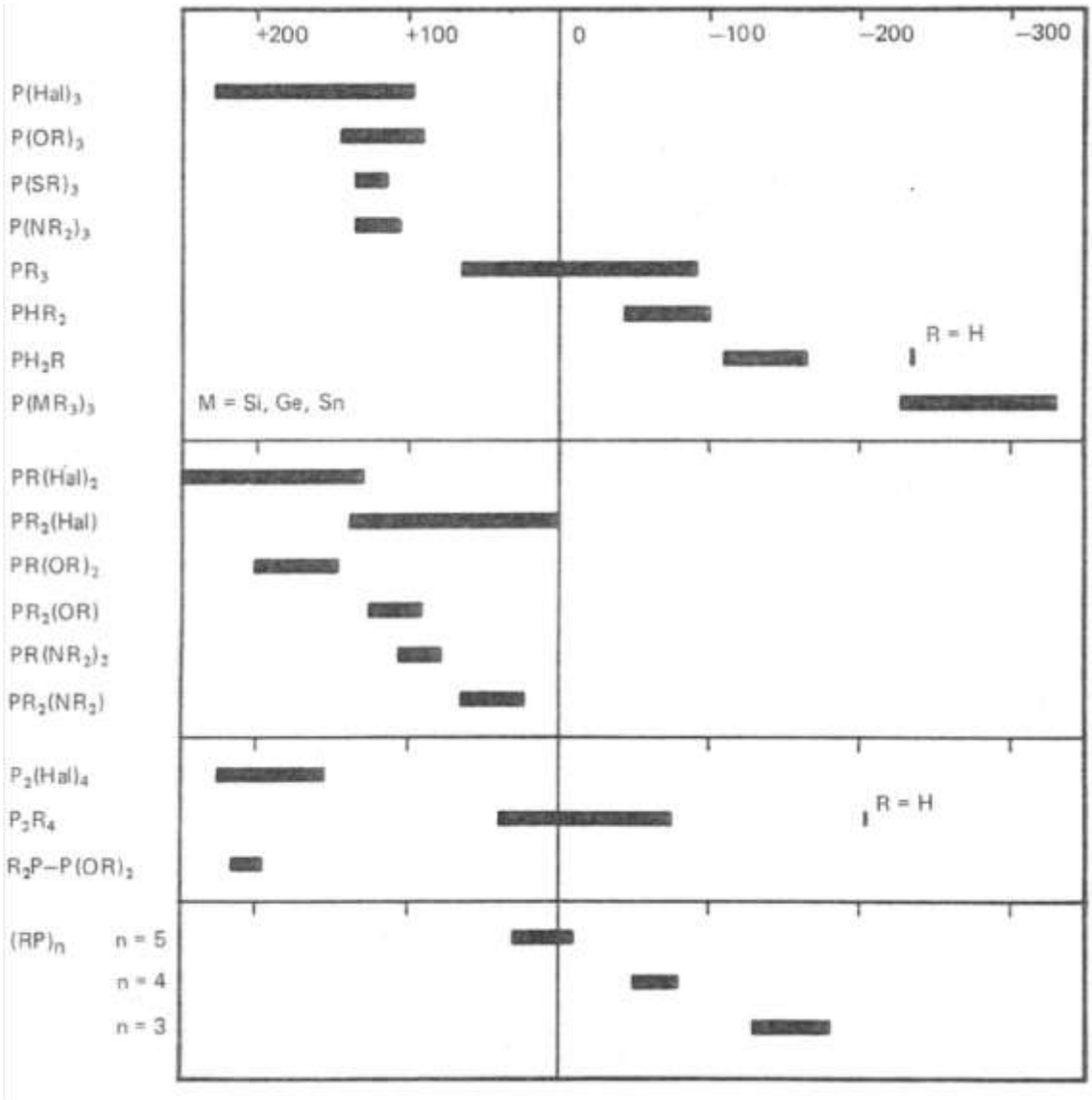


Figure 2.12 ^{31}P chemical shift ranges for three-coordinate phosphorus compounds. (Ref. [11])

2.6.2.1 Factors influencing coupling constants.

Almost all observable spin ½ nuclei do spin couple to ^{31}P nucleus with measurable coupling constants. Factors such as oxidation state, formal hybridization, coordination number and electronegativity of the substituents on the phosphorus, all contribute significantly towards the magnitude of coupling constant [10]. Phosphorus-31 coupling to transition metals such as ^{195}Pt gives some of the largest coupling constants among the elements of the periodic table. Spin

coupling to transition metals provides valuable information in relation to structure and the geometry of the complex.

2.6.3. ^{119}Sn NMR spectroscopy

Several major reviews have appeared in the literature on Sn NMR spectroscopy in the past [45, 46, 80]. The element tin has ten (10) known isotopes and only three have non-zero nuclear magnetic moment i.e. ^{115}Sn, ^{117}Sn and ^{119}Sn. The higher natural abundance, higher γ and sensitivity of ^{119}Sn make it the more favourable for detection of a tin NMR spectrum (**Table 2.1**).

Table 2.1 NMR Properties of tin isotopes [81].

Isotope	Natural abundance (%)	Magnetic moment (μ/μ_N)	Magnetogyric ratio γ (10^7 rad T^{-1} sec^{-1}	Resonance frequency[a] (MHz)[e]	Relative sensitivity[b]
^{115}Sn	0.35	-1.582	-8.7475	32.718780	$3.56x10^{-2}$
^{117}Sn	7.61	-1.723	-9.530	35.632295	$4.60x10^{-2}$
^{119}Sn	8.58	-1.803	-9.971	37.290665	$5.27x10^{-2}$

[a] Neat $(CH_3)_4Sn$ for various solvents

[b] Relative to ^{1}H (equal number of nuclei)

[e] Scaled at the ^{1}H resonance of TMS at exactly 100 MHz

The first tin measurement was performed in the 60's by Burke and Lauterbur [82] long after its magnetic moment was measured in 1949 [9] and long before the advent of Pulsed Fourier-Transform (PFT) NMR spectroscopy. Tin measurements are commonly performed by use of the one-dimensional broad-band decoupling method i.e. ^{119}Sn{^{1}H}. Alternatively, tin isotopes can be observed by proton-detected HMQC [54] with an enhancement of about 4.16 and by spin polarisation transfer techniques such as INEPT [45a] with a signal enhancement factor of about 2.8. It has been noted that the greatest enhancement is dependent on the number of identical protons coupled to the tin isotope. The use of these methods has a substantial impact on time

saving because each of the pulse sequence programs benefits from the shorter relaxation time (T_1) of the protons. Despite the lower natural abundance and relatively smaller γ of ^{117}Sn, this nucleus is readily detected by direct observation [45,80].

2.6.3.1 Spectral calibration

Tetramethyltin (Me_4Sn) is used as the most common reference standard by many researchers even though its resonance occurs in the middle of the chemical shift range. The extreme toxicity of tetramethyltin is minimised by the preparation of the standard in a sealed capillary tube.

2.6.3.2 ^{119}Sn chemical shift

The known ^{119}Sn chemical shifts ranges are ca. 3000 ppm compared to ca. 9000 ppm for ^{207}Pb compounds [11]. In addition to the factors affecting chemical shifts already discussed in section 2.2.4 (temperature dependence, solvent effects and isotope effects), pertinent to ^{119}Sn are:

(i) Coordination number. There is an increase in ^{119}Sn nuclear shielding for compounds in which the coordination number increases from 2 to 6 [45]. The accompanying ^{119}Sn chemical shift change from low to high frequencies in going from lower to higher coordination number is convenient in the study the donor-acceptor interactions in solutions.

(ii) Effective electronegativity of the substituents on the tin. An increase in the electron-withdrawing ability of the groups bound to tin leads to a decrease in the tin shielding. Also, the steric and electronic properties of these substituents affect the ^{119}Sn chemical shift.

(iii) Effects brought about by variations of interbond angles at tin. Steric constraints such as ring closure have a direct effect on bond angles and as a consequence these changes are reflected in the ^{119}Sn resonance [45].

(iv) Bulky substituent effect. As more bulky subsituents are added on the tin atom, so is the possibility of deshielding as been noted for ^{195}Pt and ^{205}Pb [83]. However, this relationship is not always applicable.

(v) And lastly, as discussed in section 2.2.4, variations in ΔE (the energy difference between highest occupied and lowest unoccupied orbitals in tin).

2.6.3.3 Patterns of ^{119}Sn coupling constants

There are a great number of $J(^{119}Sn\text{-}X)$ values available for X nuclei throughout almost the entire periodic table. Of particular importance to us is the ^{119}Sn spin-spin coupling to spin ½ transition metals isotopes like ^{57}Fe, ^{103}Rh and ^{195}Pt [45]. The presence of $^{1}J_{(Sn\text{-}M)}$ demonstrates the kinetic stability of the M-Sn bond and this fact is illustrated by oxidative addition reactions of organotin compounds to Platinum(0) complexes [84]. The magnitude of $^{1}J(^{195}Pt\text{-}^{119}Sn)$ has been established to be strongly dependent on the polarisability of ^{195}Pt nucleus, which is partly a function of the ligands *trans* to tin. Thus $^{1}J(^{195}Pt\text{-}^{119}Sn)$ increases with a decreasing "trans influence".

2.6.3.4 Correlations of ^{119}Sn chemical shifts with ^{29}Si or ^{207}Pb Chemical shifts

There are broad parallels between the shielding of ^{29}Si/^{119}Sn [85] or ^{119}Sn/^{207}Pb [86], indicating that the structures in solution are analogous and that the influences of various ligands can be compared with respect to bond polarity and excitation energies.

2.7 NMR spectroscopy of selected transition metals

NMR spectroscopy of metal nuclei is playing an increasingly important role in the chemistry of transition metal complexes. The distinctive aspects of transition metal NMR spectroscopy include mainly the large range of chemical shifts (which reflect small structural changes at the metal centre), and the dominance of the paramagnetic shielding term (see **Eq. 2.9**). The sensitivity of many of the transition metal nuclei is low and hence, Mann [51], called them

"Cinderella nuclei". The nuclei of interest to us are, ^{57}Fe, ^{103}Rh, ^{183}W and ^{195}Pt (which admittedly, has been observed with relative ease).

A number of general reviews and monographs are listed in **Table 2.2** which provides the pertinent magnetic properties of these nuclei relative to resonance frequency in a 9.4 T field.

Table 2.2 NMR parameters of selected transition metal nuclei

Isotope	Natural abundance (%)	Magnetic moment (μ/μ_N)	Magnetogyric ratio γ (10^7 rad T^{-1} sec^{-1}	Resonance frequency[a] (MHz)	Major Reviews
^{57}Fe	2.19	0.1563	0.8644	12.955	[10,11]
^{103}Rh	100	-0.1522	-0.8420	12.750	[10,11,17, 63a, 87]
^{183}W	14.4	0.2013	1.1131	16.671	[10,63b, 88, 89, 90]
^{195}Pt	33.8	1.0398	5.7505	86.015	[10,11,18,19,44,47,91 , 92,]

[a] Scaled at the ^{1}H resonance of TMS at exactly 400 MHz in a 9.4 field.

2.7.1 ^{57}Fe NMR Spectroscopy

The advent of indirect detection FT NMR spectroscopic methods saw a sudden focus of attention on ^{57}Fe NMR despite the nucleus having one of the lowest sensitivities in the periodic table, long relaxation times and a low resonance frequency. The percentage natural abundance of ^{57}Fe is a mere 2.2 which makes it one most difficult nuclei to observe by direct methods without isotopic enrichment (see **Table 2.2**).

2.7.1.1 ^{57}Fe Chemical shift

The first direct measurement of ^{57}Fe from $Fe(CO)_5$ (neat liquid) requiring over 20 hrs of recording time was done by Schwenk *et al* in the 1970's [93]. Iron-57 chemical shifts are conveniently expressed relative to neat $Fe(CO)_5$ as an external reference, which is unfortunately known to respond to temperature and the solvent medium. The total chemical shift range of the ^{57}Fe nucleus is known to amount 12,000 ppm corresponding to 150 KHz at a frequency of 12.9 MHz as shown in **Figure 2.13**. It is apparent from **Figure 2.13** that the formal oxidation state of the iron in the organometallic and inorganic complexes determines the position on the shift scale. Iron-57 is known to have the highest oxidation state dependence of any nucleus with as big a gap as 500 ppm separating the states [94]. The benefit of the triple resonance method of indirect 2D HMQC (^{31}P,^{57}Fe){^{1}H} NMR spectroscopy makes it possible to observe a ^{57}Fe chemical shift with 5-mg samples in recording time of about 2hrs. It is however, interesting to note that recently, the use of direct observe (the only available method in the absence of donor atoms such as proton in metal-hydrides or phosphine complexes) and INEPT are still preferable methods [44] for some researchers.

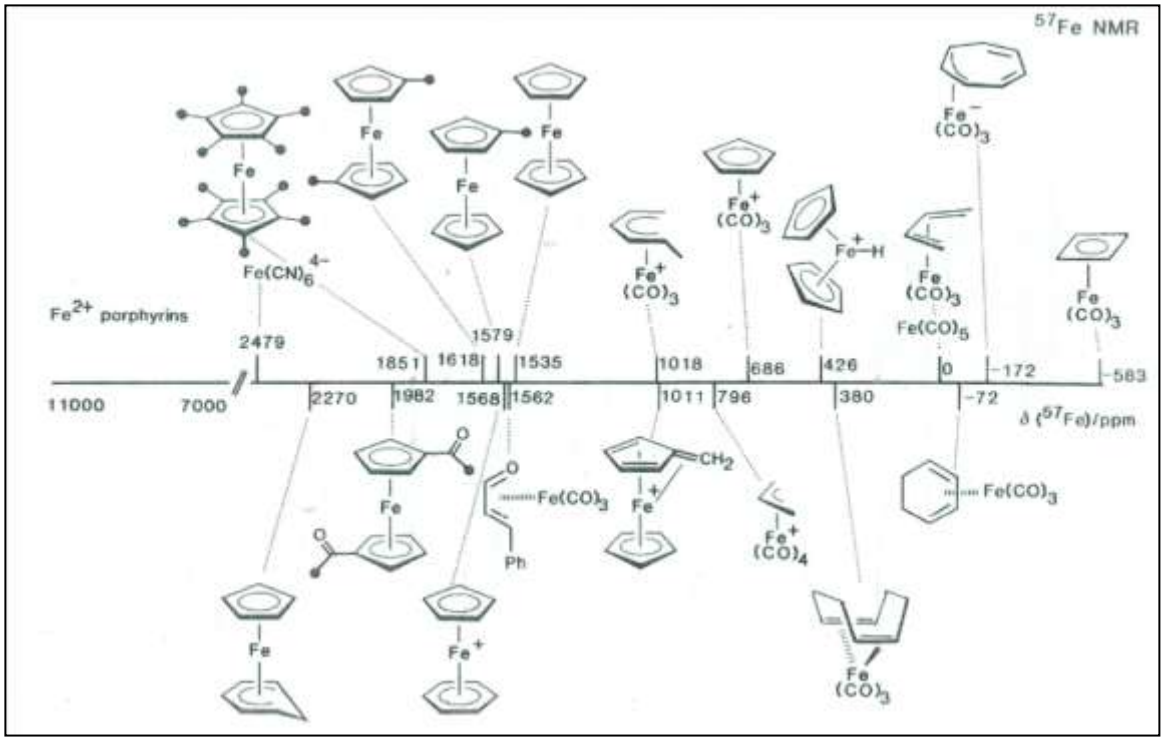


Figure 2.13 Schematic representation of ^{57}Fe chemical shift (Fig. taken from ref. [43]).

2.7.1.2 ^{57}Fe spin-spin coupling

^{57}Fe is known to spin-couple to number of nuclei such as ^{1}H, ^{13}C, ^{15}N, ^{19}F and ^{31}P. The presently known $J_{(Fe-X)}$ values span the range of 0.5 to 150 Hz with the largest recorded for X = ^{31}P. The sign of $^{1}J_{(^{57}Fe-^{31}P)}$ has been determined experimentally by two-dimensional indirect (^{1}H,^{57}Fe) and (^{31}P,^{57}Fe){^{1}H} spectroscopy to be positive [95]. From a sizeable series of measurements of $J_{(Fe-P)}$ on 18-electron complexes, it was established that $J_{(Fe-P)}$ depends on the coordination geometry around the iron atom and that the value of $J_{(Fe-P)}$ decreases on going from trigonal to five-coordinate iron complexes. The largest $^{1}J_{(Fe-P)}$ values are found when phosphines with the highest π-acceptor power are employed. This trend can be rationalised by the Fermi contact term because the electron-withdrawing substituents produce an increase in the s character of the metal-phosphorus bond, thereby increasing $^{1}J_{(Fe-P)}$ [63].

2.7.2 ^{103}Rh NMR spectroscopy

^{103}Rh is one of the few spin ½ nuclei with 100% abundance. This advantage is however, limited by a very small magnetic moment, long relaxation times and low resonance frequencies, but nevertheless the sensitivity of ^{103}Rh exceeds that of ^{57}Fe by a factor of 42. The first direct observation of a ^{103}Rh signal was reported in 1979 [51]. The popularity of ^{103}Rh NMR spectroscopy is evidenced by the number reviews on the subject (see **Table 2.2**). The sensitivity of the ^{103}Rh nucleus was enhanced by the use of the INEPT technique [96] until the advent of the indirect detection method. Spin polarisation transfer from ^{1}H using INEPT leads to a signal enhancement by a factor 31.5 and spin polarisation transfer from ^{31}P leads to an enhancement by a factor of 12.86. The best current methods for observation of ^{103}Rh are by two-dimensional indirect detection methods (^{1}H,^{103}Rh) and (^{31}P,^{103}Rh){^{1}H}. These methods provide a maximum possible enhancement of $(\gamma_H/\gamma_{Rh})^{5/2}$ = 5635 times over simple ^{103}Rh{^{1}H} observation and 590 times for (^{31}P,^{103}Rh){^{1}H} observation, using the method of Bax *et al* [60].

2.7.2.1 ^{103}Rh Chemical shift

The ^{103}Rh chemical shifts are commonly referenced to the absolute frequency Ξ(^{103}Rh) = 3.16 MHz in a field in which the protons of TMS resonate at exactly 100 MHz [10]. The factors affecting the ^{103}Rh chemical shift are in principle similar to those influencing ^{57}Fe NMR chemical shift and these were discussed under section 2.2.4. ^{103}Rh chemical shifts span a range of approximately 12 000 ppm as shown in **Figure 2.14** below.

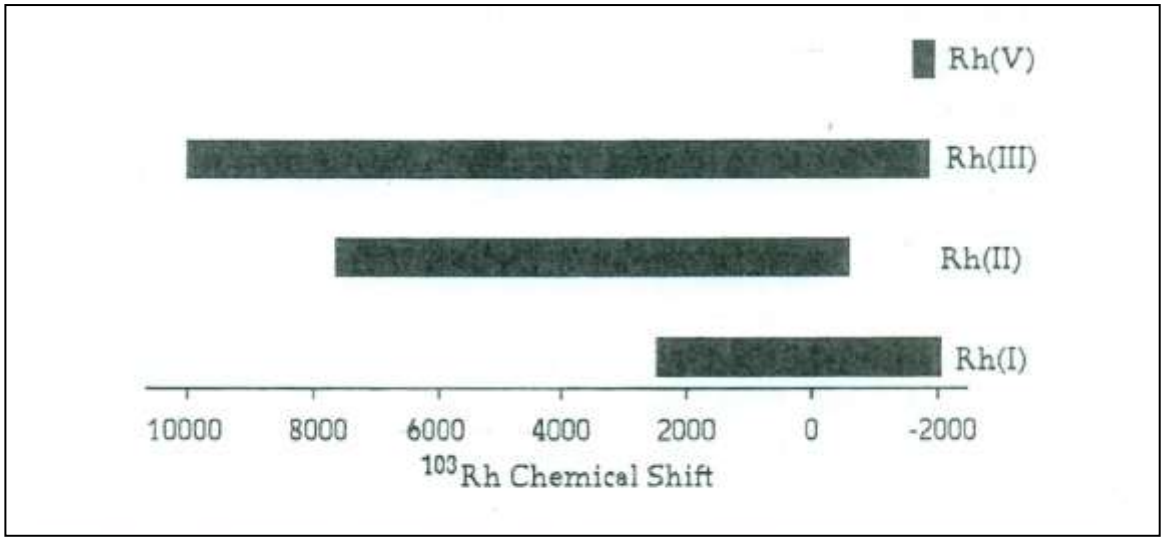


Figure 2.14 A correlation chart showing oxidation state and ^{103}Rh chemical shift in ppm relative to Ξ(^{103}Rh) = 3.16 MHz (Fig. taken from ref. [97])

It is evident from the chart that there is no clear relationship between ^{103}Rh chemical shift and the oxidation state of rhodium. However, there exists a linear correlation between the ^{103}Rh chemical shift and the wavelength of the lowest-energy absorption band in the UV/Vis spectrum of the ligand substituted complex of (acetylacetonato)rhodiumbis(ethylene) [43]. This confirms the δ(^{103}Rh) dependence on ΔE^{-1}, as suggested by Ramsey the equation **2.10**.

2.7.2.2 ^{103}Rh spin-spin coupling constants.

The data on ^{103}Rh spin-spin coupling to spin ½ nuclei is extensive. ^{103}Rh is known to couple to ^{1}H, ^{13}C, ^{15}N, ^{19}F, ^{29}Si, ^{31}P, ^{77}Se, ^{119}Sn, ^{125}Te, ^{183}W, ^{195}Pt, ^{199}Hg and ^{207}Tl [17] (and articles cited there in),63,87]. The experimentally determined signs of coupling constants involving rhodium are $^{1}J_{(Rh-P)}$ [98], $^{1}J_{(Rh-F)}$ [98a], $^{2}J_{(Rh-F)}$ [98b] and $^{1}J_{(Rh-H)}$ [98a] negative and $^{1}J_{(Rh-N)}$ [98b], $^{1}J_{(Sn-Rh)}$ [99], $^{1}J_{(Te-Rh)}$ [100] and $^{1}J_{(Rh-Rh)}$ [101] as positive. The $J_{(Rh-P)}$ span a range of between 80 and 200 Hz [102].

2.7.3 ^{183}W NMR spectroscopy

The ^{183}W nuclide is the only NMR-active isotope in natural tungsten and has spin ½ with natural abundance of 14.3%. However due to its low resonance frequency of 8.325 MHz at 4.7 T, relatively low natural abundance and low sensitivity of 0.059 relative to ^{13}C (see T**able 2.2**), it is one of the more difficult nuclides to observe (several reviews are cited in **Table 2.2**). The magnetic properties of the ^{183}W nucleus makes the observation of this nuclide by indirect detection spectroscopy, i.e. (^{1}H,^{183}W) or (^{31}P,^{183}W){^{1}H} a very favourable option. As noted elsewhere [44], there are researchers still using direct and INEPT methods to observe ^{183}W chemical shifts. The expected increase in sensitivity over a direct detection experiment would be a factor of $(\gamma_X/\gamma_M)^{5/2}$ (X = ^{1}H or ^{19}F or ^{31}P; M = ^{183}W) which correspond to gains of 2830, 2430 and 295 using ^{1}H, ^{19}F and ^{31}P respectively

2.7.3.1 ^{183}W Chemical shift and calibration

The first observation of a ^{183}W spectrum was by Klein and Happe [103] in 1961 when the spectrum of WF_6 was observed indirectly using a double resonance technique. From this observation, WF_6 was proposed as a chemical shift reference in the work of McFarlane et al [104], but a proposal later by Kidd and Goodfellow [10,105] suggested the use of absolute frequency, Ξ (^{183}W) of 4.161733 MHz for WF_6 in the field where protons of the TMS resonate at 100.000 MHz. Later, it was McFarlane et al [106] who suggested the use of $W(CO)_6$ as a standard reference. Depending on the scope of ^{183}W research, the choice of reference could be

anything from (i) absolute frequency, Ξ (^{183}W) at the field in which the ^{1}H of TMS resonate at exactly 100 MHz, or external reference solution of (ii) $W(CO)_6$ and (iii) Na_2WO_4 (used for poloxytungstates) [90]. It could be seem from these historical events that the lack of uniform approach to ^{183}W chemical shift is source of confusion among researchers. A new reference approach has since been proposed for ^{183}W NMR [107] (as for ^{103}Rh) rather than a reference material.

The ^{183}W chemical shifts span the range of about 11000 ppm with an accompanying marginal pattern based on the oxidation state [108]. It is worth noting that the highest oxidation state compounds have high chemical shifts and lower oxidation state compound are found at low chemical shift [109]. The study of the compounds of the type $[CpW(CO)_3X]$ demonstrated the influence of halogen on the ^{183}W chemical shift [110]. The downfield shift for the ^{183}W upon replacement of CO by PR_3 can be explained in terms of the poorer π-acceptor ability of the phosphines.

2.7.3.2 ^{183}W spin-spin couplings

^{183}W has been observed to couple to a number of nuclei as 14.4 % satellite peaks to nuclei having close to 100% natural abundance (e.g. ^{31}P, ^{19}F, ^{1}H). The coupling of ^{183}W to low natural abundance nuclei such as ^{15}N and ^{13}C has been reported elsewhere [90]. Coupling to these nuclei has provided information on stereochemistry. Coupling constants of $^{2}J_{W\text{-}O\text{-}W}$ in polyoxytungstate species have been used to rationalise the structures of some of these species in solution [90]. The coupling range of $^{1}J_{(M\text{-}X)}$ has been observed to be 28-80 Hz for X = ^{1}H and 140-500 Hz for ^{31}P [90, 111, 112].

2.7.4 ^{195}Pt NMR Spectroscopy

There are six naturally occurring platinum isotopes and of these, only ^{195}Pt with natural abundance of 33.8%, relatively high sensitivity and spin = ½ is important to NMR spectroscopy.

There is a wealth of literature on ^{195}Pt which has been observed through the use of direct, double-resonance and triple-resonance methods (**Table 2.2**).

2.7.4.1 ^{195}Pt spectrum calibration

There is controversy with regard to the δ(^{195}Pt) standard reference material as for ^{183}W. Kidd and Goodfellow [10] and Kidd [105] have recommended the use of an absolute frequency, Ξ(^{195}Pt) = 21.4 MHz at a field where protons of TMS resonate at exactly 100 MHz as the primary shift reference and $Pt(CN)_6^{2-}$ as a secondary reference. Kerrison and Sadler [113] and Pregosin [44] have recommended using $PtCl_6^{2-}$ as the primary shift reference. It soon becomes obvious that the chemical shift of $PtCl_6^{2-}$ comes near the high end of the observed chemical shift range which means nearly every chemical shift for ^{195}Pt will have a negative value, whereas the scale of Goodfellow and Kidd [10] leads to a positive value of the chemical shift for the majority of Pt complexes. According to Goodfellow and Kidd's scale, the chemical shift of $PtCl_6^{2-}$ occurs at 4522 ppm with respect to the absolute frequency, Ξ(^{195}Pt) = 21.4 MHz, providing a convenient correction factor for the other reference scales. It must noted that the chemical shift of the proposed reference material, $PtCl_6^{2-}$ is highly solvent-dependent with a possible error margin as large as 400 ppm [114] and for $PtCl_4^{2-}$ of about 200 ppm [115]. These δ(^{195}Pt) variations are not only limited to solvent effects but temperature effects as well [114]. There is a need among researchers to apply a single form of ^{195}Pt chemical shift reference given the amount of data available for this nuclide.

2.7.4.2 ^{195}Pt Chemical shift.

^{195}Pt chemical shifts span a range of about 15 000 ppm. ^{195}Pt chemical shift sensitivity is the same as for iron, rhodium and tungsten (discussed in 2.2.4). The first reports of ^{195}Pt chemical shift was by McFarlane [116] and by Dean and Green [117] in 1968. There is a wealth of literature data for three different types of platinum complexes: octahedral Pt(IV), square-planar Pt(II), and Pt(0) (**Table 2.2**). The regions of ^{195}Pt chemical shift for the different oxidation states are shown in **Figure 2.15**. The range illustrated is not a true reflection of the entire 15 000 ppm ^{195}Pt chemical shift range.

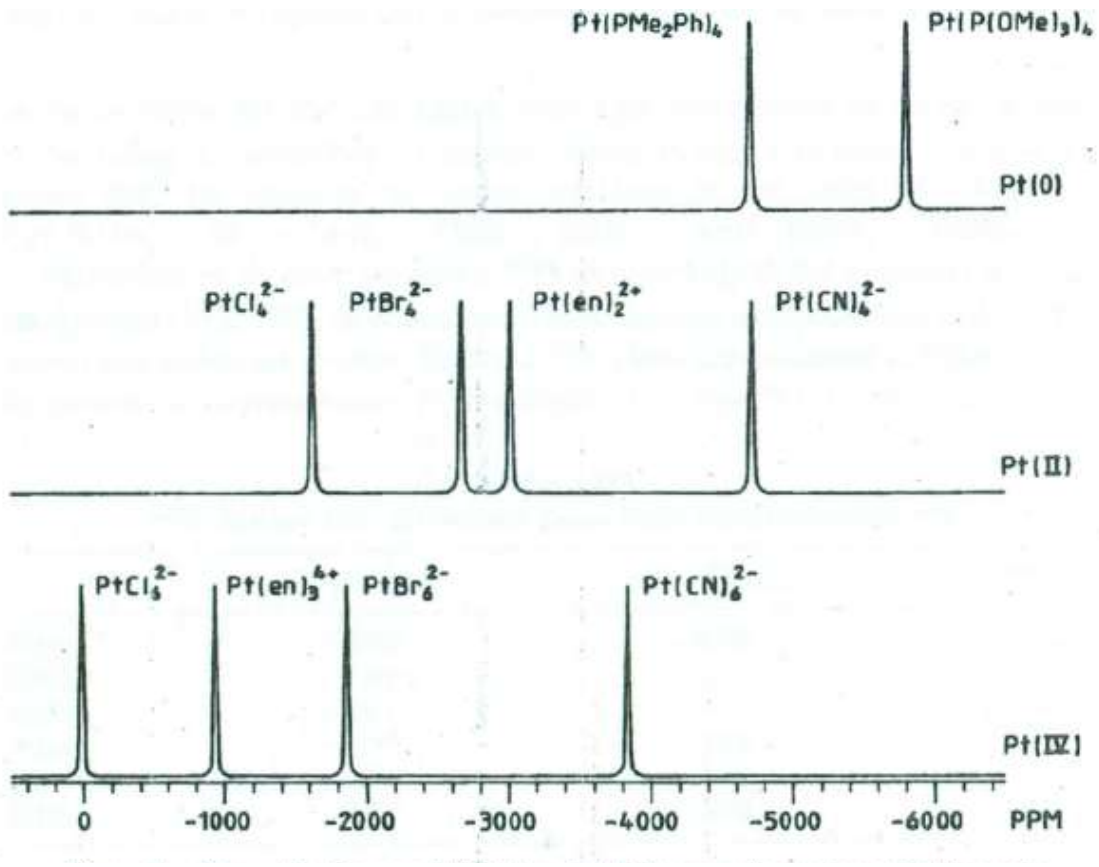


Figure 2.15 Schematic diagram of ^{195}Pt chemical shift ranges for various oxidation states (Fig. taken from ref. [47c]).

Notable influences on δ(^{195}Pt) include: (i) coordination to the Pt nucleus by relatively hard ligands which induce a large change of about 500-1000 ppm or even more, (ii) the δ(^{195}Pt) in halide complexes is a function of halogen, with low frequency shift associated with increasing atomic number, (ii) there is a slight dependence on the oxidation state, because the nature of the ligand is as important as the oxidation state, (iii) δ(^{195}Pt) is a function of complex geometry, a fact that is clearly evident in the square planar complexes of *cis*- and *trans*- orientation [44a]. In general, for square-planar Pt(II) complexes PtL_2X_2, the *trans* isomer is found downfield of the *cis* isomer by as much as 100-400 ppm [118]. It is interesting to note that there seems to be insensitivity of δ(^{195}Pt) to the substituents on the donor atoms. The sensitivity of δ(^{195}Pt)

becomes apparent when the signal for $PtCl_6^{2-}$ is observed at 9.4T and the splitting arising from the isotopomers is resolved [119].

2.7.4.3 ^{195}Pt spin-spin coupling

^{195}Pt is a very desirable coupling partner for a number of reasons, one of those being its large gyromagnetic ratio of 5.7505. The isotope is known to couple to almost all spin ½ nuclei in the periodic table. The $J_{(Pt-X)}$ coupling range varies greatly with the coupling partner, from as low $^3J_{(Pt-H)}$ = 15-50 Hz to as high as $^1J_{(Pt-Sn)}$ = 28 954 Hz for a cis[$PtCl(SnCl_3)PEt_3)_2$] [120] (reports of J_{Pt-Sn} of 50000 Hz have recently been noted). Changes in $^1J_{(Pt-L)}$ with *trans* ligands have been used to provide information relating to *trans* influence and form the basis of widely used structural tools. The $^1J_{(Pt-N)}$ is particularly important in the chemistry and spectroscopy of Platinum(II), and in the bioinorganic field of study for nitrogen chemistry of Pt(II) and Pt(IV) complexes. The $^1J_{(Pt-N)}$ coupling range currently spans from 88-755 Hz [121].

2.7 Conclusions

A tremendous development in the field of NMR spectroscopy has been outlined in line with the objectives of this thesis. The wealth of information that has been documented to date as a result of advances in the field of NMR spectroscopy, from chemical structure analysis of micro-scale to nano-scale dimension and to biological environment is overwhelming and impossible to summarise into one manuscript.

The application of NMR spectroscopy in the field of synthesis, catalysis and structure determination serves as a great influence in this thesis. A series of complexes with varying ligands will be closely followed with the help of NMR spectroscopy. However, the lack of agreement about the reference materials for some of the nuclei to be investigated remains a serious inconvenience.

Reference

1. (a) W. von Philipsborn, *Chem. Soc. Rev*., 28 (1999) 95; (b) R.J. Carbajo, L. Zhang and F. López-Ortiz, *Magn. Reson. Chem*., 36 (1998) 807;

2. J.J. Pesek and W.R. Mason, *J. Magn. Reson*., 25 (1977) 519.

3. E.D. Becker in *High Resolution NMR; Theory and Chemical Applications*, Academic Press, New York, 3rd Ed., (2000) 2.

4. I.I. Rabi, J.R. Zacharias, S. Millman and P. Kusch, *Phys. Rev*., 53 (1938) 318.

5. F. Bloch, W.W. Hansen and M. Packard, *Phys. Rev*., 69 (1946) 127.

6. E.M. Purcell, H.C. Torrey and R.V. Pound, *Phys. Rev*., 69 (1946) 37.

7. (a) H. Kessler, M. Gerke and C. Griesinger, *Angew. Chem. Int. Ed. Engl*., 27 (1988) 500; (b) G.A. Morris, *Magn. Reson. Chem*., 24 (1986) 371; (c) R. Benn and H. Günther, *Angew. Chem. Int. Ed. Engl*. 22 (1983) 350; (d) R. Freeman and G.A. Morris, *Bull. Magn. Reson*., 1 (1979) 5.

8. R. Ernst, Angew. *Chem. Int. Ed. Engl*., 31 (1992) 805.

9. W. Kemp, in *NMR in Chemistry, A Multinuclear In troduction*, Macmillan, London, (1986) 25.

10. R.G. Kidd and R.J. Goodfellow, in: *NMR and the Periodic Table*, R.K. Harris and B.E. Mann, eds., Academic Press, London, (1978).

11. J. Mason, *Multinuclear NMR*., Plenum Press, London, (1987), 335

12. N.R. Ramsey, *Phys. Rev*., 78 (1950) 699.

13. N. Juranic, *Coord. Chem. Rev*., 96 (1989) 253.

14. C.K. Jørgensen, *Prog. Inorg. Chem*., 4 (1962) 73.

15. J. Mason, *Chem. Rev*., 87 (1987) 1299.

16. J.E. Huheey, E.A. Keiter and R.L. Keiter, in *Inorganic Chemistry Principles of Structure and Reactivity*, 4th Ed, Harper Collins College, (1993) 405.

17. L. Carlton, *Ann. Rep. NMR Spectrosc*., 63 (2008) 49.

18. J.R.L. Prequeler, I.S. Butler and F.D. Rochon, *Applied Spectroscopic Rev*., 41 (2006) 185.

19. J.J. Dechter, in *Progress in Inorganic Chemistry*, ed S.J. Lippard, 33 (1986) 393.

20. R. Freeman, G.R. Murray and R.E. Richards, *Proc. R. Soc*. (Lond), A242 (1957) 455.

21. (a) L.G. Marzilli, Y. Hayden and M.D. Reily, *Inorg. Chem*. 25 (1986) 974; (b) F.D. Rochon and V. Buculei, *Inorg. Chim. Acta*, 358 (2005) 2040.

22. G.P. Betteridge and R.M. Golding, *J. Chem. Phys*., 51 (1969) 2497.

23. J. Mason, *Chem. Rev*. 81 (1981) 205.

24. (a) G.B. Benedek, R. Engleman and J.A. Amstrong, *J. Chem. Phys*., 39 (1963) 3349, (b) T.H. Brown and S.M. Cohen, *J. Chem . Phys*., 58 (1973) 395.

25. (a) C.J. Jameson, *J. Am. Chem. Soc*., 109 (1981) 2586, (b) C.J. Jameson, D. Rehder and M. Hoch, *J. Am. Chem. Soc*., 109 (1981) 2589.

26. T. Gasparis-Ebeling, H. Nöth and B. Wrackeyer, *J. Chem. Soc., Dalton Trans*., (1983) 97.

27. (a) A.D. Buckingham, T. Schaefer and W.C. Schneider, *J. Chem. Phys*., 32 (1960) 1227, (b) I. Ando and G.A. Webb, *Org. Magn. Reson*., 15 (1981) 111.

28. L. Carlton, *Magn. Reson. Chem*., 42 (2004) 760.

29. C. Carr, P.L. Goggin and R.J. Goodfellow, *Inorg. Chim. Acta*, 81 (1984) L25.

30. (a) J.M. Ernsting, S. Gaemers and C.J. Elsevier, *Magn. Reson. Chem*., 42 (2004) 721; (b) B.E. Mann and C.M. Spencer, *Inorg. Chim. Acta*, 76 (1983) L65.

31. U.E. Bucher, T.F. Currao, R. Nesper, H. Rueegger, L.M. Venanzi and E. Younger, *Inorg. Chem*., 34 (1995) 66.

32. E. Lindner, B. Keppeler, R. Fawzi and M. Steimann, *Chem. Ber*., 129 (1996) 1103.

33. (a) M. Koller and W. von Philipsborn, *Organometallics*, 11 (1992) 467, (b) V. Tedesco and W. von Philipsborn, *Organometallics*, 14 (1995) 3600.

34. R. Fornika, H. Görls, B. Seemann and W. Leitner, *J. chem. Soc., Chem. Commun*., (1995) 1479

35. M.C. Read, J. Glaser, I. Pesson and M. Sandström, *J. Chem. Soc. Dalton Trans*., 1994 (3243).

36. C.A. Tolman, *Chem. Soc. Rev*., **1** (1972) 337.

37. A. G. Bell, W. Koźmiński, A. Linden and W. von Philipsborn, *Organometallics*, 15 (1996) 3124.

38. E.J.M. Meier, W. Koźmiński, A. Linden, P. Lustenberger and W. von Philipsborn, *Organometallics*, 15 (1996) 2469.

39. W. Leitner, M. Bühl, R. Formika, C. Six, W. Baumann, E. Dinjus, M. Kessler, C. Krüger and A. Rufińska, *Organometallics*, 18 (1999) 1196.

40. P.B. Graham, M.D. Rausch, K. Täschler and W. von Philipsborn, *Organometallics*, 10 (1991) 3049.

41. C. Hansch, A. Leo and R.W. Taft, *Chem. Rev*., 91 (1991) 165.

42. J.A. Pople and D.P Santry, *Mol. Phys*., 8 (1964) 1.

43. C.H. Elschenbroich and A. Salzer, *Organometallics, A Concise Introduction*, 2nd Ed. VCH, Weinheim, (1992) 411.

44. (a) C. López, R. Bosque, S. Pérez, A. Roig, E. Molins, X. Salons and M. Font-Bardía, *J. Organomet. Chem*., 691 (2006) 475; (b) B. Wrackmeyer, O.L. Tok and M. Herberhold, *Organometallics*, 20 (2001) 5774; (c) B. Wrackmeyer, A. Ayazi, H.E. Maisel and M.

Herberhold, *J. Organomet. Chem*., 630 (2001) 263; (d) W. Levason and D. Pletcher, *Platinum Metal Rev*., 37 (1993) 17.

45. (a) B. Wrackmeyer, *Annual Reports on NMR Spetroscopy*, 16 (1985) 73; (b) P.J. Smith and A.P. Tupčiauskas, *Annul Reports on NMR Spectroscopy*, 8 (1978) 291.

46. B. Wrackmeyer and K. Horchler, *Annual Reports on NMR Spectroscopy*, 22 (1990) 249.

47. (a) P.S. Pregosin, *Annual Reports on NMR Spectroscopy*, 17 (1986) 285; (b) D. Rehder, *Coord. Chem. Rev*., 110 (1991) 161; (c) J.J. Dechter, in: *Progress in Inorganic Chemistry*, S.J. Lippard , (Ed.), 33 (1985) 393

48. T. Jenny, W. Von Philipsborn, J. Kronbitter and A. Schwenk, *J. Organomet. Chem*., 205 (1981) 211.

49. G.A. Morris and R.J. Freeman, *J.Am.Chem. Soc*., 101 (1979) 760.

50. (i) D.M. Doddrel, D.T. Pegg and M.R. Bendall, *J. Magn, Reson*., 48 (1982); D.T. Pegg, D.T. Doddrel and M.R. Bendall, *J. Chem. Phys*., 77 (1982) 2745.

51. B.E. Mann,(ed G.A. Webb), *Annual Reports on NMR Spectroscopy*, 23 (1991) 141.

52. (a) M. Witanowski, L. Stefaniak and G.A. Webb, *Annual Reports in NMR spectroscopy*, 7 (1977) 117; (b) 11b (1981) 136; (c) 18 (1986) 43,

53. L.Carlton and M.P. Belcuig, *J. Organomet. Chem*. 378 (1989) 469

54. B. Wreckmeyer, E. Kupce and J. Kummerlen, *Magn. Reson. Chem*., 30 (1992) 403

55. (a) C. Brevard and R. Schimpf, *J. Magn. Reson*., 47 (1982) 528; (b) S.J. Berners Price, C. Brevard, A. Pagelot and P.J. Sadler, *Inorg. Chem*., 24 (1985) 4278

56. K.v. Schenker, W.v. Philipsborn, *J. Magn. Reson*., 66 (1986) 219.

57. R. Benn, H. Brenneke, J. Heck, and A. Rufińska, *Inorg. Chem*., 26 (1987) 2826

58. A.A. Koridze, P.V. Petroskii, S.P. Gubin and E.I. Fedin, *J. Organomet. Chem*., 93 (1975) C26.

59. G.N. La Mar, C.M. Dellinger and S.S. Sanker, *Biochem. Biophys. Res. Commun*., 128 (1985) 628.

60. A. Bax, R.H. Griffey and B.L. Hawkins, *J. Magn. Reson*., 55 (1983) 301.

61. A. Macchioni, P.S. Pregosin, H. Rüegger, G. van Koten, P.A. van der Schaaf and R.A.T.M. Abbenhuis, *Magn. Reson. Chem*., 32 (1994) 235.

62. A. Macchioni, P.S. Pregosin, P.F. Engel, S. Mecking, M. Pfeffer, J.-C. Daran and J. Vaissermann, *Organometallics*, 14 (1995) 1637.

63. (a) R. Benn, in: *Transition Metal Nuclear Magnetic Resonance*, P.S. Pregosin ed., Elsevier, Amsterdam, (1991) 10; (b) R.J. Carbajo, L. Zhang and F. López-Ortiz, *Magn. Reson. Chem*., (1998) 1.

64. Atta-ur-Rahman, in *One and Two Dimensional NMR spectroscopy*, Elsevier, Amsterdam, (1989) 77.

65. E.W. Randall and D.G. Gillies, *Progress in NMR Spectroscopy*, 6 (1970) 119

66. J. Mason, *Chem. Rev*., 81 (1981) 205

67. R.C. Duthaler and J.D. Roberts, *J. Am. Chem. Soc*., 100 (1978) 4969.

68. W.v. Philipsborn and R. Muller, *Angew. Chem. Int. Ed. Engl*., 25 (1986) 383

69. S. Maggini, *Coord. Chem. Rev*., 253 (2009) 1793

70. (a) S.J. Berners-Price and P.J. Sadler, *Coord. Chem. Rev*., 151 (1996) 1; (b) L. Ronconi and P.J. Sadler, *Coord. Chem. Rev*., 252 (2008) 2239.

71. J. Muller, *Z. Naturforsh. B*., 34B (1979) 437.

72. W. Holzer and W.v. Philipsborn, *Magn. Reson. Chem*., 27 (1989) 511.

73. V.M.S. Gil and W.v. Philipsborn, *Magn. Reson. Chem*., 27 (1989) 409.

74. M. Grayson and E.J. Griffith, Eds., *Top. Phosphorus Chem*., Interscience, New York, Vols- .

75. (a) *Spec. Per. Rep*., NMR, RSC., London, series of Vols-.; (b) *Spec. Per. Rep.*, *Organophosphorus Chemistry*, RSC., London, series of Vols-.; (c) *Spec. Per. Rep. Prop. Inorg. Organomet. Compounds*, RSC., London, series of Vols-.

76. J.G. Verkade, *Coord. Chem. Rev*. 9 (1972) 1.

77. D.J. Craik, *Annual Reports on NMR Spectrocopy*, 15 (1983) 1.

78. W.C. Dickenson, *Phys. Rev*., 91 (1951) 717.

79. (a) G. Hutter, J. Borm and L. Zsolnai, *J. Organomet. Chem*., 263 (1984) C33; (b) H. Lang, O. Orama and G. Hutter, *J. Organomet. Chem*., 291 (1985) 293.

80. P.J. Smith and A.P. Tupciauskas, *Annual Reports on NMR Spectroscopy*, 8 (1978) 292.

81. F. Kayser, M. Biesemans, M. Gielen and R. Willem, in: *Advanced Application of NMR to Organometallic Chemistry*, M. Gielen, R. Willem and B. Wrackmeyer, eds., John Wiley and Sons, New York, (1996) 45.

82. J.J. Burke and P.C. Lauerbur, *J.Am.Chem. Soc*., 83 (1961) 326

83. (a) J.D. Kennedy, W. McFarlane, G.S. Pyne and B. Wrackmeyer, *J. Chem. Soc. Dalton Trans*., (1975) 386; (b) J.D. Kenndy, W. McFarlane and B. Wrackmeyer, *Inorg. Chem*., 15 (1976) 1299.

84. S. Carr, R. Colton and D. Dakternieks, *J. Oganomet. Chem*., 249 (1983) 327.

85. T.N. Mitchell, *J. Organomet. Chem*., 255 (1983) 279

86. J.D Kennedy, W. McFarlane and G.S. Pyne, *J. Chem. Soc., Dalton Trans*., (1977) 2332

87. J.M. Enrsting, S. Gaemers and C.J. Elsevier, *Magn. Reson. Chem*., 42 (2004) 721

88. Ya-Guang Chen, J. Gong and Lun-Yu Qu, *Coord. Chem. Rev*., 248 (2004) 245.

89. M.A. Fedotov and R.I. Maksimovskaya, *J. Struct. Chem*., 47 (2006) 952.

90. M. Minelli and J.H. Enemark, *Coord. Chem. Rev*., 68 (1985) 169.

91. B.M. Still, P.G. A. Kumar, J.R. Aldrich-Wright and W.S. Price, *Chem. Soc. Rev*., 36 (2007) 665.

92. P.S. Pregosin, *Coord. Chem. Rev*., 44 (1982) 247.

93. (a) A. Schwenk, *J. Magn. Reson*., 5 (1971) 376; (b) A. Schwenk, *J. Magn. Reson*., 37 (1980) 551.

94. R.G. Kidd, in *Annual Report on NMR Spectroscopy*, 23 (ed G.A. Webb), (1991) 85

95. R. Benn, H. Brenneke, A. Frings, H. Luhmkuhl, G. Mehler, A. Rufińska and T. Wildt, *J. Am. Chem. Soc*., 110 (1988) 5661.

96. (a) G.A. Morris and R. Freeman, *J. Am. Chem. Soc*., 101 (1979) 760; (b) D.M. Doddrel, D.T. Pegg, W. Brooks and M.R. Bendall, *J. Am. Chem. Soc*., 103 (1981) 727.

97. B.E. Mann, in *Studies in Inorganic Chemistry*, *Vol 13 Transition Metal Nuclear Magnetic Resonance*, P.S. Pregosin, Ed. Elsevier, (1991) 177.

98. (a) E.M. Hyde, J.D. Kennedy, B.L. Shaw and McFarlane, *J. Chem. Soc. Dalton Trans*., (1977) 1571; (b) I.J. Coluhoun and W. McFarlane, *J. Magn. Reson*., 46 (1982) 525; (c) P.L. Goggin, R.J. Goodfellow, J.R. Knight, M.G. Norton and B.F. Taylor, *J. Chem. Soc. Dalton Trans*., (1973) 2220; (d) J. Browning, P.L. Goggin, R.J. Goodfellow, M.G. Norton, A.J.M. Rattray, B.F. Taylor and J. Mink, *J. Chem. Soc. Dalton Trans*., (1977) 2061.

99. L. Carlton, *Inorg. Chem*., 39 (2000) 4510.

100. S.J. Anderson, J.R. Barnes, P.L. Goggin and R.J. Goodfellow, *J. Chem. Res*., (1978) 286.

101. A.L. Davis and R.J. Goodfellow, *J. Chem. Soc. Dalton Trans*., (1993) 2273

102. T.G. Appleton, H.C. Clark and L.E. Manzer, *Coord. Chem. Rev*., 10 (1973) 335

103. M.P. Klein and J. Happe, *Bull. Am. Phys*. Soc., 6 (1961) 104

104. W. McFarlane, A.M. Noble and J.M. Winfield, *J. Chem. Soc*. (A), (1971) 948.

105. R.G. Kidd, *Annual Report on NMR Spectroscopy*, 10A (1980) 1

106. G.T. Andrews, I.J. Colquhoun, W. McFarlane and S.O. Grim, *J. Chem. Soc., Dalton Trans*., (1982) 2353.

107. L.Carlton, A. Emdin, A. Lemmerer and M.A. Fernandes, *Magn. Reson. Chem*., 46 (2008) s56.

108. Ya-Guang Chen, J. Gong and Lun-Yu Qu, *Coord. Chem. Rev*., 248 (2004) 245

109. (a) C.J. Jameson and J. Mason, in: J. Mason (Ed), *Multinuclear NMR*, Plenum Press, New York, (1987); (b) J.J. Detcher, *Prog. Inorg. Chem*., 33 (1985) 429.

110. H.C.E. McFarlane, W. McFarlane and D.S. Rycroft, *J. Chem. Soc., Dalton Trans*., (1976) 1616.

111. F.A. Cotton and G.N. Mott, *J. Am. Chem. Soc*., 47 (1982) 528.

112. (a) R.J. Carbajo, L. Zhang and F. López-Ortiz, *Magn. Reson. Chem*., 36 (1998) 807; (b) F.A Cotton and G.N. Mott, *J. Am. Chem. Soc*., 47 (1982) 528.

113. S.J.S. Kerrison and P.J. Sadler, *J. Magn. Reson*., 31 (1978) 321.

114. W. Freeman, P.S. Pregosin, S.N. Szen and L.M. Venazi, *J. Magn. Reson*., 22 (1976) 473.

115. J.J. Pesek and W.R. Mason, *J. Magn. Reson*., 25 (1977) 519.

116. W. McFarlane, *J. Chem. Soc., Chem. Commun*., (1968) 393.

117. R.D. Dean and J.C. Green, *J. Chem. Soc. (A)*, (1968) 3047.

118. W. McFarlane, *J. Chem. Soc., Dalton Trans*., (1974) 324.

119. I.M. Ismail, S.J.S. Kerrison and P.J. Sadler, *J. Chem. Soc., Chem. Commun*., (1980) 1175.

120. M.A. Sens, N.K. Wilson, P.D. Ellis and J.D. Odom, *J. Magn. Reson*., 19 (1975) 323

121. (a) F.E. Wood and A.L. Balch, *Inorg. Chim. Acta*, 76 (1983) L63; (c) S.J.S. Kerrison and P.J. Sadler, *J. Chem. Soc., Dalton Trans*., (1982) 2363.

CHAPTER 3

Analytical Techniques

In this chapter, the three main analytical techniques used during the course of this thesis will be described as methods for molecular and structural identification, namely: Nuclear Magnetic Resonance (NMR), Infra-Red (IR) spectroscopy and single crystal X-ray diffraction crystallography. In addition to the three mentioned techniques Elemental Analysis (EA) was also used.

3.1 Materials and methods

Unless specifically mentioned all operations, reactions and manipulations were performed under an atmosphere of either high purity nitrogen or argon using standard Schlenk techniques. Starting materials and ligands (preserved under an inert atmosphere of either high purity nitrogen or argon) were used as purchased (from mainly Sigma Aldrich, Merck or Strem Chemicals for Research) without purification. High purity solvents were used without purification (absolute EtOH and MeOH) or distilled before use, i.e. tetrahydrofuran (THF) from Na/benzophenone, toluene from sodium wire, n-hexane, acetonitrile, benzene and diethyl-ether from CaH_2, and dichloromethane from P_2O_5. All solvents without exception were deoxygenated before use. Methods for purification of other starting materials and solvents were as described in Errington's [1] manual.

Specialised custom-designed and modified glassware apparatuses were made with high-precision through our departmental glassblowing facility and the raw materials were procured from commercial suppliers. All the glassware was thoroughly cleaned (with dilute or fuming nitric acid when necessary) and finally rinsed with absolute ethanol, dried (in an oven) and flushed with nitrogen or argon before use. All reactions requiring preparation in the dark were carried out in foil – wrapped Schlenk tubes in a darkened fume-hood. Column chromatography was

performed on neutral Silica gel 60 (Merck, particle size 0.063 – 0.216) or celite (545) using typically 5 mm x 30 cm column length.

Low temperature experiments were performed in a dewer containing variable mixture of crushed-ice or ice-blocks with water only, ice-water and sodium chloride (NaCl), xylene and liquid nitrogen or acetone and liquid nitrogen depending on the required temperature.

3.2 NMR spectroscopy

A detailed discussion of the principles and different techniques of NMR spectroscopy was presented in chapter 2. NMR experiments were recorded on a Bruker Avance 300 spectrometer (using a 5 mm BBI or QNP probe) operating at the proton frequency of 300 MHz, a Bruker DRX 400 spectrometer (using a 5 mm triple resonance inverse (TBI) probe with a dedicated ^{31}P channel and extended decoupler range) operating at the proton frequency of 400.13 MHz (later upgraded to Bruker Avance *III 400* using a TBI probe also with dedicated ^{31}P channel) or Bruker Avance *III* 500 MHz spectrometer operating at a proton frequency of 500.133 MHz (less than 5% of the work). All the triple resonance and variable temperature experiments were recorded on the Bruker DXR 400 spectrometer (65% of thesis work).

Samples for NMR measurements were prepared under an inert atmosphere of nitrogen or argon unless otherwise stated. Deuterated solvents were deoxygenated before use when possible. In some specific cases, samples were prepared in a sealed NMR tube under vacuum following a freeze-thaw method. The vacuum-sealed NMR tube experiments were particularly important for highly air sensitive compounds and for samples that required continuous monitoring over an extended period i.e. a week or more. The amount of sample for NMR measurements differed according to the minimum practical amount and where possible multiple measurements were done on the same sample. The amount of sample for NMR measurement ranged on average from 10 to as much as 50 mg in 0.6 ml of deuterated solvent in the case of studies of bulk or concentration effects. Only in exceptional cases was the amount more than 90 mg in 0.7 ml solution of benzene. The volume of deuterated solvent or solvent mixtures was approximately 0.6 – 0.7 ml (in some cases concentrated by evaporation under argon in the NMR tube to maintain the required volume). **Figure 3.1** shows pictures of three superconducting FT-NMR

magnets housed in the School of Chemistry which contains the probes in which the sample sits (console unit and an interactive workstation are not shown on the pictures).



Figure 3.1 Three superconducting FT-NMR instruments used in the research (300, 400 and 500 NMR spectrometers)

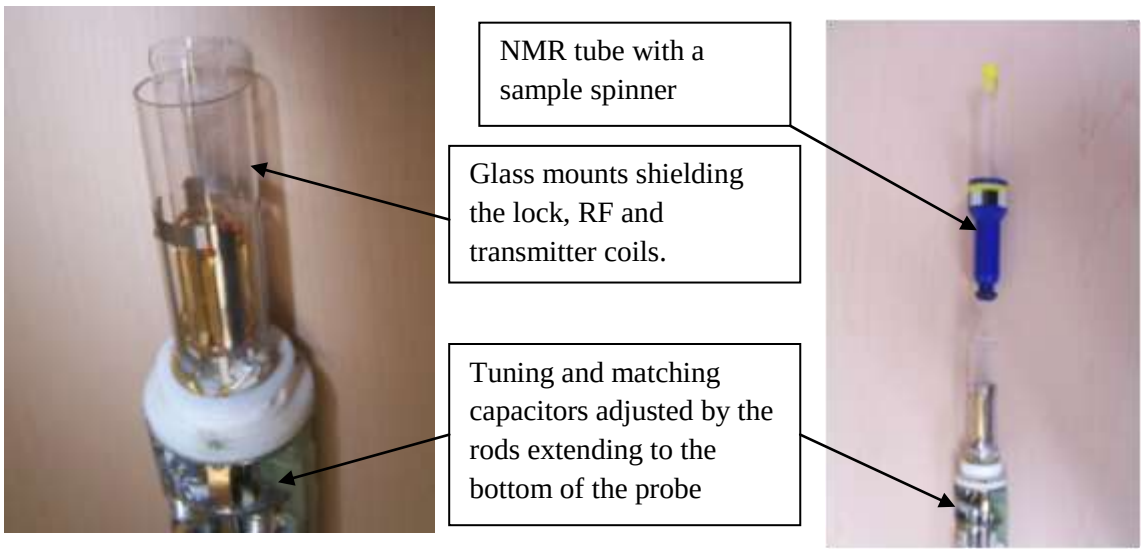


Figure 3.2 A picture of the upper probe interior (right) and with NMR sample tube (left).

Figure 3.2 shows the upper region of a typical 5 mm probe (casing removed) with an NMR sample tube sitting closest to the RF coils for optimum sensitivity (NMR instruments are inherently insensitive compared to for example FT-IR, hence the presence of powerful amplifiers

to increase the intensity of the signal). **Figure 3.3** shows the lower regions of a triple resonance (TBI) probe which was used extensively during the research. The top picture shows connections for the RF (^{31}P label not clearly visible) and gradient channels and, the bottom showing the tuning capacitor adjustment knobs/slide controls.



Figure 3.3 An image of a lower part of a 5 mm 400 MHz Bruker tripple resonance (TBI) probe

Table 3.1 Spin one-half nuclei of selected isotopes recorded in this thesis, NMR spectrometer frequencies and their respective standard reference materials.

Isotope	300 MHz Spectrometer frequency	400 MHz Spectrometer frequency	500 MHz Spectrometer frequency	Standard Reference Sample[a]
^{1}H	300 MHz	400.132 MHz	500.133 MHz	Me_4Si (TMS)
^{13}C	75.468 MHz	100.623 MHz	125.770 MHz	Me_4Si (TMS)
^{15}N		40.460 MHz	50.685 MHz	$MeNO_2$, neat
^{31}P	121.495 MHz	161.982 MHz	202.446 MHz	85% H_3PO_4
^{57}Fe		12.955 MHz		$Fe(CO)_5$, neat
^{103}Rh[b]		12.642 MHz		Mer-$[RhCl_3(SMe_2)_3]$
^{119}Sn	111.920 MHz	149.09 MHz		Me_4Sn, neat
^{183}W[c]		16.671 MHz		$W(CO)_6$
^{195}Pt		86.015 MHz		$Na_2Pt(Cl)_6$[d]
^{205}Pb	62.789 MHz	83.710 MHz		$Pb(NO_2)_3$[e]

[a] Most of the reference standards (with the exception of TMS) are used externally in a capillary. [b] The ^{103}Rh chemical shifts are commonly referenced to the absolute frequency $\Xi(^{103}Rh)$ = 3.16 MHz in a field in which the protons of TMS resonate at exactly 100 MHz [2]. [c] Chemical shift in ppm relative to $W(CO)_6$ $\Xi(^{183}W)$ = 4.15 MHz in which the protons of TMS resonate at exactly 100 MHz. To convert to a scale relative to $W(CO)_6$ {$\Xi(^{183}W$ = 4.151888 MHz [3] subtract 455 ppm, to convert to a scale relative WF_6 $\Xi(^{183}W$ = 4.161780 MHz [4] subtract 2831 ppm; to convert to a scale relative to WO_4^{2-} [3] subtract 3939 ppm. [d] Chemical shift relative to $\delta(^{195}Pt)$ = 0.00 ppm from a solution Na_2PtC_6 (0.220 M) in D2O at 300 K in the field in which the protons of TMS resonate at 400 MHz. [e] 1 M sample in 99.9% D_2O at pH 3.3 which gives a reference position of -2960 ppm relative to $Pb(CH_3)_4$) was used as secondary external reference sample corresponding to a frequency of 83.7120440 MHz in a field in which the protons of TMS (in CD_2Cl_2 at 300 K) resonate at 400.1328000 MHz.

3.2.1 Methods of observation.

Direct observe: The direct observe method which involves broad-band (noise) decoupling is applied mainly in the study of nuclei (Y) with sufficiently high γ and natural abundance to permit acquisition of a spectrum in a reasonably short period of time and also show spin coupling

to protons. The spectrum of Y{^{1}H} (where Y could be ^{13}C, ^{19}F, ^{29}Si ^{31}P, etc) is simplified by effective loss of spin-spin coupling during acquisition.

Indirect detection method: M – ^{31}P (where M = ^{57}Fe, ^{103}Rh, ^{183}W or ^{195}Pt) spectra were obtained by indirect detection using the pulse sequence of Bax, Griffey and Hawkins [5]:

$$\pi/2(^{31}P)\text{-}1/[2J(M,^{31}P)]\text{-}\pi/2(M)\text{-}\tau\text{-}\pi(^{31}P)\text{-}\tau\text{-}\pi/2(M)\text{-}1/2[2J(M),(^{31}P)]\text{-}Acq(^{31}P)$$

with broadband ^{1}H decoupling throughout and M decoupling omitted during acquisition. A spectral width in f2 (^{31}P) varied according to the specific circumstance between 10 – 30 ppm and acquisition time of 0.0526 s give a digital resolution of 0.7 Hz per point. In f1 (M), a final spectral width varied accordingly between 40 - 100 ppm and time domain varied (64, 128 or 256) to achieve a digital resolution of about 1.9 Hz per point. In order to eliminate possible folding of signals, the spectra were first recorded with a spectral width in the f1 dimension of 2000 ppm (occasionally as high as 4000 ppm) progressively reduced to between 40 and 80 ppm.

Nitrogen- 15 spectra were recorded on a Bruker 400 spectrometer operating at 400.13 MHz (^{1}H) and 40.55 MHz (^{15}N). ^{15}N-^{1}H spectra were obtained by indirect detection using in principle the same pulse sequence as for the phosphine/phosphite transition metals above but with refocusing pulses and gradients [5]:

$$\pi/2(^{1}H)\text{-}1[4J(^{15}N,^{1}H)]\text{-}\pi(^{1}H)\pi(^{15}N)\text{-}1/[4J(^{15}N,^{1}H)]\text{-}\pi/2(^{15}N)\text{-}\tau\text{-}\pi/2(^{1}H)\pi/2(^{15}N)\text{-}grad\text{-}\pi/2(^{1}H)\pi/2(^{15}N)\text{-}1/[4J(^{15}N,^{1}H)]\text{-}(^{15}N)\text{-}grad\text{-}1/[4J(^{15}N,^{1}H)]\text{-}\pi(^{1}H)\pi/2(^{15}N)\text{-}grad\text{-}1/[2J(^{15}N,^{1}H)\text{-}Acq(^{1}H)$$

with delay times optimized for a coupling of about 8 Hz and omitting ^{15}N decoupling during acquisition. A spectral width in f2 of between 3 and 6 ppm, an acquisition time of 0.320 s and 1k data points giving a resolution of ~ 1.5 Hz per point; in f1 (^{15}N), a spectral width of between 40 and 60 ppm, and 20 – 80 increments in the time domain were used depending on the concentration of the material. In order to eliminate signal folding, spectra were first measured with a spectral width of 400 ppm which was reduced accordingly. The relaxation delay was set at 2.5 s with 64 scans per increment (in some cases as high as 4000 depending on the sample concentration), and the time for data collection varied from 3 hrs to 3 days. Nitrogen chemical shifts were referenced to external neat nitromethane in $CDCl_3$ at 300 K, corresponding to a

frequency of 40.560302 MHz in a field in which the protons of TMS in $CDCl_3$ resonate at 400.129996 MHz. The following abbreviations are used for NMR spectrum interpretation: singlet (s), doublet (d), doublet of doublet (dd), triplet (t), quartet (q), multiplet (m) and; *o* (ortho), *m* (meta) and *p* (para).

3.3 X-ray crystallography

The principal stages of X-ray crystallography involve:

- Crystal growth: Crystals were grown from different solvent such as n-hexane, CH_2Cl_2, MeOH or mixtures of different solvents such as CH_2Cl_2/n-hexane, $CDCl_3$/n-hexane, THF/n-hexane at low or room temperatures. Different methods of crystallisation were employed including slow evaporation, solvent diffusion, seeding and precipitation. X-ray diffraction quality crystals were identified using a polarising microscope.
- Specimen collection and preparation.
- Crystal mounting and collection: Intensity data were collected on a Bruker SMART 1K CCD area detector diffractometer with graphite monochromated Mo K_α radiation (50 kV, 30 mA). The collection method involved ω-scans of width 0.3°.
- Data collection: Data reduction was carried out using the program *SAINT+* [6] and face indexed absorption corrections were made using the program *XPREP* [6] or SADABS [7].
- The crystal structure was solved by direct methods using *SHELXTL* [8].
- Structure refinement: Non-hydrogen atoms were first refined isotropically followed by anisotropic refinement by full matrix least-squares calculations based on F^2 using *SHELXTL*.
- Calculation of geometrical parameters: Hydrogen atoms were first located in the difference map then positioned geometrically and allowed to ride on their respective parent atoms.
- Graphical representation of the structure: Diagrams and publication material were generated using CCDC software platforms such as SHELXTL and PLATON [9] and MERCURY.

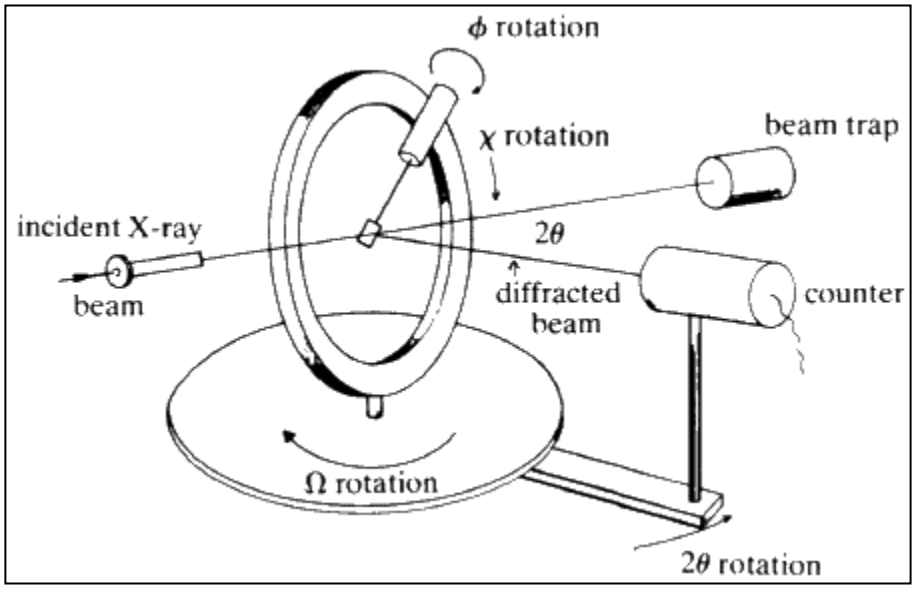


Figure 3.2 A Simplified representation of X-ray diffraction instrument

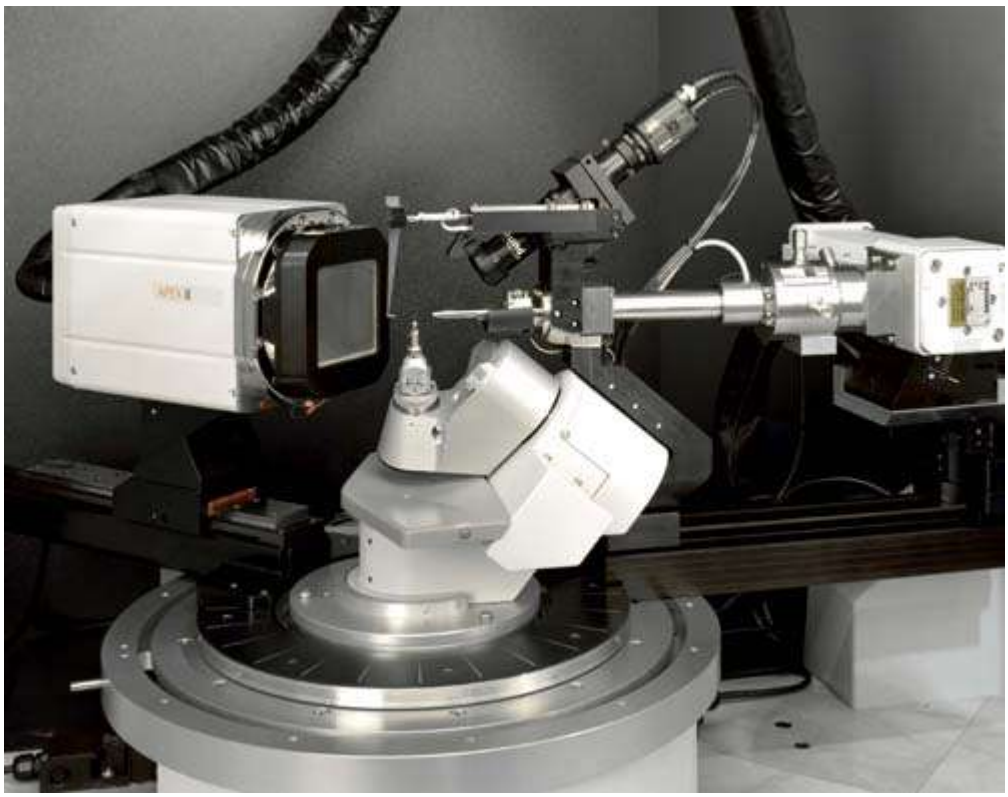


Figure 3.3 Apex Bruker-Axs X-ray diffractometer

3.4 Samples for elemental analysis

Samples were sent for elemental analysis to confirm atomic percentage compositions of carbon and hydrogen, nitrogen and sulphur in some cases. Sample for elemental analyses were vacuum dried for overnight. Sample masses ranged from as little as 2 mg to as much as 8 mg depending on the abundance of the material. Elemental analyses were performed by the Soil, Climate and Water institute in Pretoria.

3.5 Samples for IR analysis

Infra-Red (IR) spectroscopy was used to confirm the molecular structure of synthesized compounds by the presence or absence of stretching frequencies of functional groups such as C=O, C≡O, CN, -C≡C-, Rh-H, etc. IR measurements were recorded following different methods of preparation depending on the sophistication of the instrument and the nature of the sample, i.e. liquid or solid. In some cases samples were recorded from a solution in chloroform in a NaCl cell on a Bruker Vector 22 FT-IR machine on which duplicate runs were recorded. Solid samples were also recorded as compact material between two diamond stages on Bruker FT-Tensor spectrometer.

References

1. R.J. Errington, *Advanced Practical Inorganic and Metalorganic Chemistry*, Blackie Academic and Professional, London, (1997) 92

2. R.G. Kidd and R.J. Goodfellow, in: *NMR and the Periodic Table*, R.K. Harris and B.E. Mann, eds., Academic Press, London, (1978).

3. R. Benn, C. Brevard, A. Rufińska, G. Schroth, *Organometallics*, 6 (1987) 838.

4. H.C.E. McFarlane, W. McFarlane, D.S. Rycroft, *J. Chem. Soc., Dalton Trans*., (1976) 1616.

5. A. Bax, R.H. Griffey and B.L. Hawkins, *J. Magn. Reson*., 55 (1983) 301.

6. Bruker, *SAINT+*. Version 6.02 (includes XPREP and SADABS). Bruker AXS Inc., Madison, Wisconsin, USA (1999).

7. G.M. Sheldrich, *SADABS*, University of Göttingen: Göttingen, Germany, 1996

8. Bruker, *SHELXTL. Version 5.1. (includes XS, XL, XP, XSHELL)* Bruker AXS Inc., Madison, Wisconsin, USA, *(1999)*.

9. (a) Spek, A. L. (2003). *J. Appl. Cryst.* **36**, 7-13; (b) A.L. Spek, *J. Appl. Crystallogr*., 36 (2003) 7.

CHAPTER 4

Triorganolead(IV) and triorganotin(IV) halide adducts

4.1 Introduction

Reference to the chemistry of organo-lead and tin adducts dates back to the years 1916 and 1960 respectively [1]. The use of NMR spectroscopy in the study of organotin and organolead compounds has been a subject of interest especially with respect to the understanding of the coordination chemistry and geometry of many of these complexes [2]. The properties of the NMR active nuclei ^{119}Sn and ^{207}Pb (discussed in Chapter 2, section 2.6.3) are important in the study of complexes of tin and lead adducts where their chemical shifts are sensitive to the changes in the electronic environment within their coordination sphere. There are direct correlations between ^{119}Sn and ^{207}Pb NMR chemical shifts in terms of coordination number, effective electronegativity of the substituents on the lead or tin compounds, concentration effects, steric constraints and variations in ΔE [2b,2c, 3]. The interaction of tin and lead compounds with solvents causes a considerable change in chemicals shifts. The possibility of distinguishing between various types of coordination geometries of triphenyltin(IV) complexes in coordinating and non-coordinating solvents using ^{13}C and ^{119}Sn NMR chemical shifts has been well documented by Holeček and co-workers [4] who found that upon coordination, chemical shifts decrease dramatically.

A change from lower to higher coordination number in triorganotin complexes is accompanied by a significant increase in shielding by as much as several hundred ppm depending largely on the position of dynamic equilibrium [2c]. The first report of ^{207}Pb NMR chemical shifts in studies of the Lewis acidities of triorganolead halide adducts in the presence of monodendate

bases in CH_2Cl_2 and CH_3CN medium was reported in 2003 [2i]. In this study the ^{207}Pb chemical shift was observed to increase upon moving from lower to higher coordination numbers [2h]. Previous attempts to coordinate triorganolead halide compounds by bidendate bases such as diphenyphosphinomethane (DPPM), diphenylphosphinoethane (DPPE) and diphenylphosphinopropane (DPPP) to form six-coordinate adducts were unsuccessful and only the formation of five-coordinate adducts was evident from the ^{207}Pb NMR chemical shift data [2h,i]. However, six-coordinate systems of diphenyltin(IV)dihalides {$[Ph_2SnCl_2(OPBu_3)_2]$ and $[Ph_2SnBr_2(OPBu_3)_2]$} have been observed and rationalised by NMR analysis at low temperatures (i.e < -85 ºC) [5]. Only two isomers of each of the two compounds are observed at low temperatures from five possible structures. These compounds are rationalised to be fluxional between the possible octahedral isomers. A series of six-coordinate complexes of the type Bu_2SnX_2, where X is a chelating ligand, ranging from OCOR (R = Me, Ph, CH_2OPh) [6], acac (acetyl acetonate), Etdc (N,N-diethyldithiocarbamate), oxin (8-hydroxychinolate) [7], dbzm (dibenzoylmethanoate), bzac (benzoylacetonate), pic (1-picolinate), Me.oxin (2-methyl-8-hydroxychinolinate) and Bu_2SnCl_2.bipy (2,2´-bipyridine) and Bu_2SnCl_2.phen (1.10-phenonthroline) [8] have been synthesized and characterized.

Tin and lead compounds share common applications such as heat stabilizers for polyvinyl chloride (PVC) plastics, glass coatings, electronics/electrical, solder alloys, etc [9]. Tin and lead compounds find even more application as catalysts in organic synthesis [10] and reticulation of silicones, synthesis of polyesters, preparation of polyurethanes, wood preservation and as pesticides in agriculture [11]. Potential applications of organotin compounds as agents for cancer chemotherapy [12], where the coordination number and the nature of groups bonded to the central atom determines the binding ability towards DNA [13], are being pursued. Lead and lead compounds are known generally as hazardous (e.g. as potent neurotoxin and carcinogenic humans), but nevertheless find application in, for example, batteries and radiation shielding.

The purpose of the present study is to examine the reactivity of organotin and organlead adducts with *p*-substituted pyridine derivatives and as potential metallo-ligands in the synthesis of

bimetallic complexes (Chapter 5). We therefore report here the formation of five-coordinate tin and lead complexes and the correlations between ^{119}Sn or ^{207}Pb NMR chemical shifts with the corresponding Hammett substituent constants of *p*-substituted pyridines. A representative crystal structure of each of the five coordinate triorganotin(IV) and triorganolead(IV) complexes is presented and discussed to provide comparative geometric information.

4.2 Experimental

4.2.1 Reagents and general reactions conditions

All reactions were carried under dry and high purity nitrogen or argon atmosphere. Solvents were dried, distilled and deoxygenated before use. The solvent dichloromethane was distilled from P_2O_5 and preserved over CaH_2 as for the highest possible purity (HPLC grade) n-hexane. Solutions for NMR spectroscopy were prepared under an atmosphere of argon in 5 mm NMR tubes and NMR grade deuterated dichloromethane was used (as a mixture of CD_2Cl_2/CH_2Cl_2 in 1:8 ratio) without further purification. Organolead and organotin halides were obtained commercially and were used without further purification. All reagents including pyridine and its derivatives (4-acetylpyridine, 4-phenylpyridine, 4-dimethylaminopyridine, 4-benzoylpyridine, 4-methylpyridine, 4-methoxypyridine, methyl-isonicotinate, 4-benzylpyridine and pyridine-4-carboxaldehyde) were obtained commercially and used without further purification. 4-Bromopyridine was prepared before use as outlined in the procedure below.

Preparation of 4-bromopyridine from 4-bromopyridine hydrochloride was done as follows: solid 4-bromopyridine hydrochloride (210 mg, 1.183 mmol) was dissolved in an aqueous solution of Na_2CO_3 (250 mg, 3.108 mmol). Yellow droplets formed and settled at the bottom of the aqueous solution. Excess aqueous solution was removed before the organic layer was extracted with Et_2O (4 ml) and dried with Mg_2SO_4 (400 mg) and filtered. The solvent ether was removed by means of a steady flow of nitrogen to give a yield of 130 mg (69%).

4.2.2 Sample preparations for NMR Spectroscopy

4.2.2.1 Calibration of spectra

Spectra were recorded on a Bruker, DRX 400 spectrometer equipped with a 5-mm triple-resonance inverse probe with a dedicated ^{31}P channel and extended decoupler range, operating at 400.13 MHz (^{1}H), 149.21 MHz (^{119}Sn) and 83.71 MHz (^{207}Pb). The ^{1}H chemical shift (δ) data in ppm are referenced to tetramethylsilane (TMS), with negative values indicating stronger shielding. The chemical shift of $SnMe_4$ (neat liquid, 248 K) with CD_2Cl_2 external lock corresponding to δ(^{119}Sn) of 0.0 ppm at the frequency of 149.210995 MHz (9.398 T) in a field in which the protons of TMS (in CD_2Cl_2 at 300 K) resonate at 400.1328000 MHz was used as external reference for ^{119}Sn. Ideally, the chemical shift of ^{207}Pb NMR resonances would be best referenced to $Pb(CH_3)_4$ [2f] because the standard is relatively insensitive to sample conditions such as concentration, solvent interaction and temperature, whereas the chemical shift exhibited by $Pb(NO_3)_2$ is highly sensitive to sample concentration, temperature and pH [14]. However, in order to avoid difficulties arising from the established hazardous recorded properties of $Pb(CH_3)_4$, $Pb(NO_3)_2$ (1 M sample in 99.9% D_2O at pH 3.3 which gives a reference position of -2960 ppm relative to $Pb(CH_3)_2$) was used as secondary external reference sample corresponding to a frequency of 83.7120440 MHz in a field in which the protons of TMS (in CD_2Cl_2 at 300 K) resonate at 400.1328000 MHz. The influence of temperature on the NMR chemical shift of ^{119}Sn and ^{207}Pb using a solution of the five-coordinate adduct of $Ph_3MCl.py$ was monitored in the temperatures ranging from 183 K to 333 K, whilst the influence of concentration was monitored by varying the concentration of pyridine in the formation of $Ph_3MCl.py$ where M is Pb or Sn. The preparation time for the NMR sample was restricted to just under five (5) minutes for uniformity.

4.2.2.2 Sample preparation for the study of the influence of concentration of pyridine on $^{119}Sn/^{207}Pb$ chemical shift of $Ph_3MCl.py$ adducts.

Preparation of $Ph_3MCl.py$ complexes (M = Sn and Pb) for concentration effect studies was as follows: solutions of Ph_3MCl (M = Sn and Pb, 0.026 M and 0.021 M respectively) in

CD_2Cl_2/CH_2Cl_2 (0.6 ml) were prepared in an NMR tube and pyridine concentration was increased from 5 to 30% of total volume in 5% increments i.e. to 5, 10, 15 and 20%. Consequently, each time the concentration of pyridine was increased, the concentration of Sn or Pb decreased accordingly. The NMR spectra were recorded at 183 K.

4.2.2.4 Sample preparation for the study of the influence of temperature

The $Ph_3MCl.py$ complexes (M = Sn and Pb) for temperature studies were prepared as follows: Solutions of Ph_3MCl (10 mg) (M = Sn and Pb, 0.026 mol and 0.021 mol respectively) in CD_2Cl_2/CH_2Cl_2 (0.6 ml) were prepared in an NMR tube and a 10% excess of pyridine by volume was added. The temperature was increased from 183 to 313 K at 10 K intervals.

4.2.3 X-ray diffraction study

Intensity data were collected on a Bruker SMART 1K CCD area detector diffractometer with graphite monochromated Mo K_α radiation (50 kV, 30 mA). The collection method involved ω-scans of width 0.3º. Data reduction was carried using the program *SAINT+* [15] and face indexed absorption corrections were made using the program SADABS [16]. The crystal structures were solved by direct methods using *SHELXTL* [17]. Non-hydrogen atoms were first refined isotropically followed by anisotropic refinement by full matrix least-squares calculation based on F^2 using *SHELXTL*. Hydrogen atoms were located from the difference map and then positioned geometrically and allowed to ride on their respective parent atom. Diagrams and publication material were generated using SHELTXL, PLATON [18] and ORTEP-3 [19]. Crystal and structure refinement data are given in **Table 4.1**; selected bond lengths and angles for $Ph_3SnCl_3.py$ and $Ph_3PbCl.py$* (py* = 4-phenylpyridine) are given in **Table 4.2**.

Table 4.1. Crystal and structure refinement data for $Ph_3SnCl.py$ and $Ph_3PbCl.py$* (py* = 4-phenylpyridine)

Parameter	**1a**: $Ph_3PbCl.py$*	**1b**: $Ph_3SnCl.py$
Molecular formula	$C_{29}H_{24}ClNPb$	$C_{23}H_{20}ClNSn$
Formula weight	629.13	464.54
Temperature (K)	173(2)	173(2)
Wavelength (Å)	0.71073	0.71073
Crystal system	Monoclinic	Monoclinic
Space group	P2(1)/c	P2(1)/n
Unit cell dimensions: a (Å)	9.3903(2)	9.7376(12)
b (Å)	18.4329(4)	14.3851(18)
c (Å)	14.1860(3)	14.7927(19)
α (^{0})	90	90
β (^{0})	98.1850(10)	90.322(2)
γ (^{0})	90	90
Volume (Å^3)	2430.45(9)	2072.1(5)
Z	4	4
Density (Calculated) (Mg/m^3)	1.719	1.489
Absorption coefficient (mm^{-1})	7.068	1.368
F(000)	1216	928
Crystal size (mm^3)	0.59 x 0.18 x 0.10	0.50 x 0.36 x 0.18
Theta range for data collection (^{0})	1.82 t0 28.00	1.97 to 28.00
Index ranges	-11<=h<=12,	-12<=H<=12
	-24<=k<=24	-17<=K<=19
	-18<=l<=18	-19<=l<=19
Reflections collected	31172	12684
Independent reflections	5873[R(int) = 0.0712]	4994[R(int) = 0.0279]

Completeness to θ_{MAX} (%)	100	99.9
Absorption correction	Integration	Integration
Max. and min. transmissions	0.5383 and 0.1029	0.7909 and 0.5480
Data / restraints / parameters	5873 / 0 / 289	4994 / 0 / 235
Goodness-of-fit on F^2	0.939	1.026
Final R indices [I>2sigma(I)]	R1 = 0.0257, wR2 = 0.0540	R1 = 0.0211, wR2 = 0.0500
R indices (all data)	R1 =0.0379, wR2 = 0.0563	R1 = 0.0282, wR2 = 0.0526
Largest diff. peak and hole (e.Å^{-3})	1.091 and -1.007	0.309 and -0.438

4.3 Results and discussion

A number of organolead and organtin adducts of the type $Ph_3MCl.py^*$ (py* = 4-substituted pyridine) were prepared by the use of a generally simple and straightforward method whereby the lone pair of electrons on the nitrogen of the pyridine and its derivatives was used to coordinate to the metal centre accompanied by a change in the coordination system. All the tin and lead adducts were characterised in solution by NMR spectroscopy. All the five-coordinate organolead and organotin adducts were isolated as white to off-white crystalline solids. The isolated tin and lead adducts were sealed and stored under a nitrogen atmosphere at -10 ºC for several months without any signs of decomposition. The quality of the crystals deteriorated upon isolation due to loss of the solvent (a general challenge in securing good crystals of adducts for X-ray diffraction). The solubility of starting materials in dichloromethane was enhanced by the addition of pyridine or its derivatives. Both organotin and organolead adducts showed increased solubilities at higher temperatures with the increased formation of precipitates at lower temperatures. Crystals of X-ray quality were isolated for $Ph_3SnCl.py$ and $Ph_3PbCl.py^*$ (where py* is 4-phenylpyridine) and their molecular structures are reported later in this Chapter.

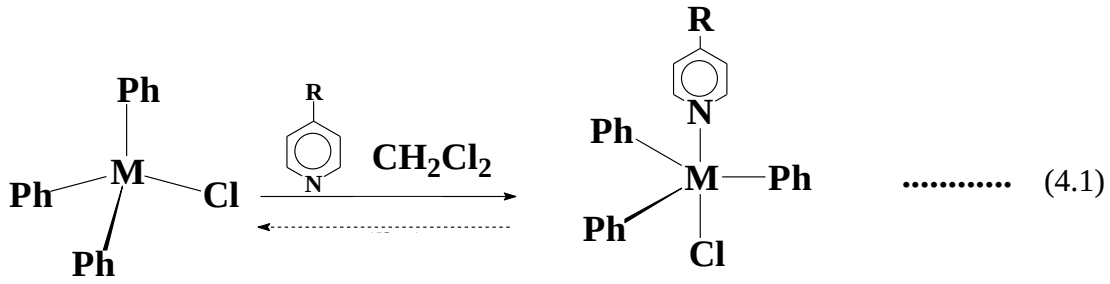
4.3.1 The influence of concentration on ^{207}Pb and ^{119}Sn chemical shifts in the five-coordinate adducts.

Studies of the influence of concentration of pyridine on the chemical shift of ^{207}Pb and ^{119}Sn was demonstrated by the reaction of Ph_3PbCl or Ph_3SnCl with varying percentage concentration by volume of pyridine in a CH_2Cl_2/CD_2Cl_2 medium in an NMR tube i.e. the amount of Ph_3MCl was kept constant. The results of this investigation, which show a very small if any significant change in the ^{207}Pb or ^{119}Sn chemical shift of $Ph_3PbCl.py$ (**1a**) and $Ph_3SnCl.py$ (**1b**) complexes when the concentration of pyridine is increased by percentage volume from 5% to 20%, are presented **Table 4.2**. A slight broadening of signals (ca. 20%) was noticed upon increasing the concentration of pyridine. The slight changes in the chemical shifts of ^{207}Pb and ^{119}Sn can be assumed to be as a result of magnetic susceptibility and line broadening due to bulk solvent effects. The net result of the above investigations suggests therefore that the equilibrium (Eq. 1) shifts to right immediately upon introduction of pyridine. Samples for NMR analysis were prepared under similar conditions such as room temperature, deuterated solvent volume (i.e. 0.6 ml), argon environment and NMR parameters. All the NMR spectra were recorded at 183 K and the reason for the choice of this temperature will be discussed in **Section 4.4.**

Table 4.2 Results of the influence of concentration of pyridine (py) on $Ph_3MCl.py$ (M = Sn and Pb) adducts.

Concentration of pyridine (% volume)	$\delta(^{207}Pb)$[a] (ppm)	$\delta(^{119}Sn)$[a] (ppm)
0	23.87	-44.50
5	-220.91	-230.31
10	-220.47	-230.15
15	-220.25	-230.10
20	-219.63	-229.84

[a] NMR spectra recorded at 183 K



..... (4.1)

Scheme 4.1 Schematic representation of the possible equilibrium in favour of the five coordinate $Ph_3MCl.py$ adducts (M= Sn, **1a** or Pb, **1b** and R = H)

The distinct chemical shift change of ^{207}Pb and ^{119}Sn upon introduction of pyridine can be rationalised in terms of base coordination to the central atom which is accompanied by a change in the geometry from quasitetrahedral or distorted tetrahedral Ph_3MCl (M = Sn or Pb) to bipyramidal geometry $Ph_3MCl.py$ as shown by the crystal structure of $Me_3SnCl.py$ [20] and also confirmed by the representative crystal structures reported in this thesis (**Section 4.3.4**). The formation of the five-coordinate adducts can be further explained in terms of dynamic stabilization of pyridine coordination to the metal centre represented by a shift in equilibrium in

favour of complex formation in the presence of excess pyridine as shown in reaction **Scheme 4.1.** The net effect of this dynamic equilibrium on the NMR timescale is supported by the consistent ^{119}Sn and ^{207}Pb chemical shift positions, a confirmation of five-coordinate species probably in the presence of slight excess of ligand. These results are in agreement with previous observations by Epply e*t al* [2h] who found a similar trend with diorganotin dihalide adducts. During our study no six coordinate adducts were either observed or isolated despite the presence of an excess of pyridine or its derivatives in the solution. It is worth mentioning however, that six-coordinate adducts of diorganolead complexes of the type Ph_2PbCl_2 have been reported [2i]. The trend observed in this study is in part consistent with that observed by Margolis *et al* [2i] for the triorganolead(IV) chloride adduct ($Ph_3/Me_3PbCl.X$, X = Cl).

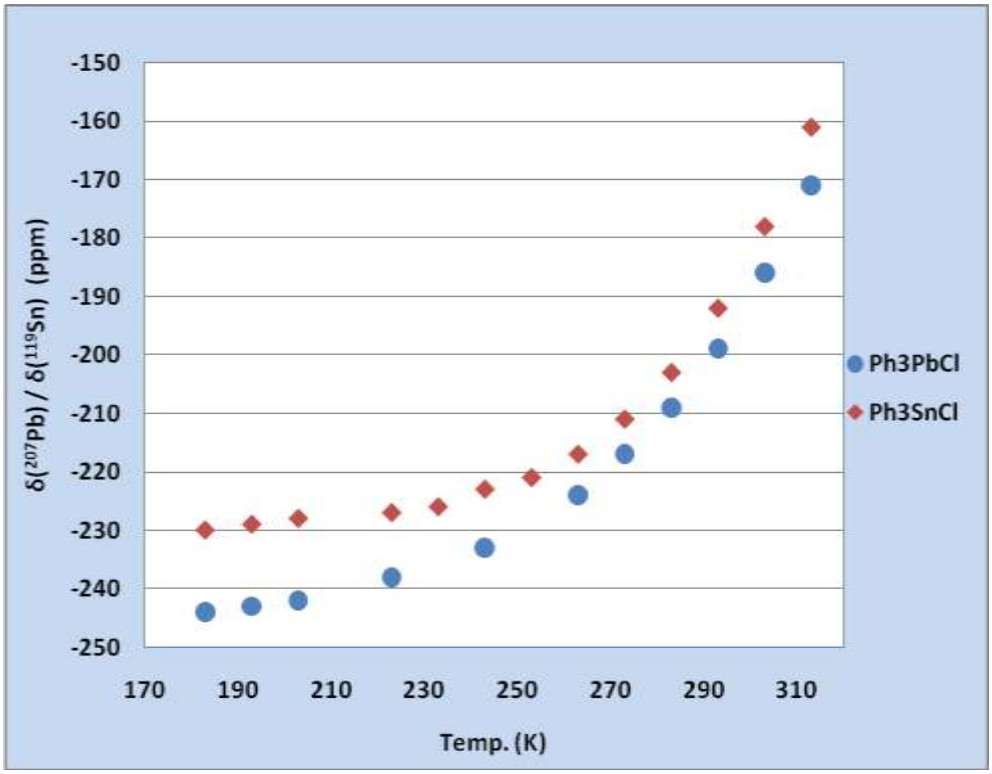
4.3.2. The influence of temperature on the ^{207}Pb and ^{119}Sn chemical shift of tin and lead adducts formed with pyridine.

A systematic study of the influence of temperature on the stability of five-coordinate adducts of $Ph_3PbCl.py$ (**1a**) and $Ph_3SnCl.py$ (**1b**), as reflected by the change in ^{207}Pb and ^{119}Sn NMR chemical shift, was undertaken during this research. The change in the concentration of pyridine or metal (Pb or Sn) species led to insignificant changes (at least within the range of 5 to 20%) in the NMR chemical shift of ^{119}Sn and ^{207}Pb for adduct solutions of **1a** and **1b** containing 10% excess of pyridine by volume. The NMR samples of **1a** and **1b** containing 10% excess of pyridine by volume were monitored over a range of 130 K starting from a low temperature (183 K) and increasing to a high temperature (313 K). The ^{207}Pb and ^{119}Sn NMR chemical shifts seem to show signs of dynamic equilibrium which favours the formation of the five-coordinate complexes from the starting materials (Ph_3MCl, M = Pb or Sn) and pyridine. As observed for concentration effects, the equilibrium can be thought of as in favour of the five-coordinate systems even at low temperatures (183 K), hence the predominance of only one singlet NMR signal indicative of one type of adduct. At temperatures below 183 K, a significant amount of precipitates, presumably of the five-coordinate adduct start to form as reflected by the loss of NMR signal intensity (upon warming the sample to room temperature, only one signal consistent

with a five-coordinate complex was observed). The results of the influence of temperature as reflected by the change in ^{119}Sn and ^{207}Pb chemical shifts are shown in **Figure 4.1.**

Figure 4.1 show clearly that temperature has a profound influence on ^{207}Pb and ^{119}Sn chemical shifts of these metallorganic compounds. **Figure 4.1** shows a smooth curve with gentle to steep slopes as the temperature increase. In the region of gentle slope, a relatively smaller change is observed at the temperatures in the range 183 - 243 K where a chemical shift difference of about 11 ppm is noticed for **1a** and about 7 ppm difference for **1b** which represent a chemical shift change of 0.18 ppm/K and 0.12 ppm/K respectively. It can be assumed that at these temperatures the equilibrium is highly shifted to the right in favour of the formation of the five-coordinate adducts. The significance of this temperature region in terms of NMR measurements is the accuracy or reproducibility of NMR chemical shifts data owing to relatively sharper signals. In the region of steep slope, at temperatures between 243 - 313 K, significant chemical shift change in ^{119}Sn of about 61 ppm for **1b** and a change of about 62 ppm in ^{207}Pb for **1a** is noticed. The average change of 0.88 ppm/K for **1a** and 0.87 ppm/K for **1b** observed.

The NMR chemical shift sensitivity due to the change in temperature can be explained by the rate of ligand exchange in the dynamic equilibrium that is favouring a higher concentration of the coordinated product. It therefore means that at higher temperatures, reversible dissociation of pyridine is rather fast i.e. spending less time coordinated to the metal centre, hence an average chemical shift change towards the higher chemical shift values of the starting material. It can therefore confidently be assumed that throughout the entire temperature range examined, the ^{207}Pb and ^{119}Sn chemical shifts show predominance of the five-coordinate adducts over the uncoordinated starting materials as indicated by single signals and that both the δ^{119}Sn and δ^{207}Pb chemical shifts are distinctly different from their respective four-coordinate tetrahedral starting materials i.e. 23.87 ppm for Ph_3PbCl and -44.50 ppm for Ph_3SnCl. Therefore a choice of a temperature such as 183 K is crucial for reproducibility of results where the equilibrium position seems to favour the almost complete formation of five-coordinate adducts.



Ph_3SnCl (0.026 mol) + py (10% excess) + CD_2Cl_2/CH_2Cl_2 and Ph_3PbCl (0.021 mol) + py (10% excess) + CD_2Cl_2/CH_2Cl_2

Figure 4.1 A plot of temperature (K) vs. $^{207}Pb/^{119}Sn$ chemical shift (ppm) for Ph_3MCl/pyridine mixtures

The ^{1}H NMR spectra for both $Ph_3PbCl.py$ **1a** and $Ph_3SnCl.py$ **1b** were not influenced in the same way as ^{207}Pb and ^{119}Sn chemical shifts of the adducts in response to the change in the coordination system from distorted-tetrahedral to bipyramidal at the metal atom. There were no significant changes in terms of line width of ^{1}H NMR signals or $\delta(^{1}H)$.

4.3.3. NMR spectroscopic results for the five-coordinate adducts of the type $Ph_3MCl.py^*$

The effect of NMR nuclear shielding on the metal centres has been studied by use of ^{119}Sn and ^{207}Pb NMR on coordination complexes of the type $Ph_3MCl.py^*$ where M = Sn or Pb and py* = monodendate pyridine derivatives as indicated in **Table 4.4.** As a consequence of the sensitivity of ^{119}Sn and ^{207}Pb NMR chemical shifts of the five-coordinated adducts (**1a** and **1b)** at different temperatures, it was logical to choose a temperature which offers an opportunity for reproducible results (i.e. a temperature at which the chemical shift change per Kelvin is smallest). Samples for NMR analysis in CD_2Cl_2/CH_2Cl_2 solution in the presence of average 10% excess of pyridine derivatives were recorded at 183 K within an average preparation time of 30 minutes and the results are shown in **Table 4.4**.

A significantly larger change in ^{207}Pb chemical shift of 267 ppm is observed between the four coordinate triphenyleadchloride and the five-coordinate $Ph_3PbCl.py$ compared to $\delta(^{119}Sn)$ variation of 185 ppm between triphenyltinchloride and $Ph_3SnCl.py$ (**Table 4.2**).

4.3.4 Correlation between Hammett substituent constants and ^{207}Pb or ^{119}Sn chemical shift in the five-coordinated systems.

A plot ^{119}Sn and ^{207}Pb NMR chemical shift against Hammett substituent constants [21] as a measure of electron donating or withdrawing properties of pyridine derivatives on the metal centres are shown in **Figure 4.2** and **4.3**. The NMR spectroscopic results given in **Table 4.3** clearly show the effect of the electron withdrawing ability of the *para*-substituent of the pyridine derivatives coordinated to the metal centre which is in good agreement with electron donating or withdrawing abilities of the substituted pyridines. A decrease in the metal shielding for both tin and lead was made more evident with the *para*-dimethylaminopyridine complexes which showed the highest chemical shift change of 23 ppm for ^{119}Sn and 48 ppm for ^{207}Pb relative to pyridine. The variations in the chemical shift position can be rationalised by the energy difference between

the highest occupied and the lowest unoccupied orbitals in each of metal centres (refer to Chapter 2, **Section 2.2.4**).

Table 4.3. ^{207}Pb and ^{119}Sn chemical shifts of $Ph_3PbCl.py^*$ and $Ph_3SnCl.py^*$

***para*-substituent on the pyridine (py*)**	**δ(^{119}Sn)[a] (ppm)**	**δ(^{207}Pb)[a] (ppm)**	**Hammett substituent Constant (σ)**
1. Dimethylamino	-253	-268	-0.600
2. Methoxy	-239	-244	-0.268
3. Methyl	-235	-231	-0.170
4. Phenyl	-232	-223	0.009
5. H (py)	-230	-220	(0.00)
6. Carboxaldehyde	-216	-195	0.216
7. Bromo	-220	-202	0.232
8. Methyl isonicotinate	-217	-178	0.450
9. Benzoyl	-218	-199	0.459
10.Acetyl	-219	-200	0.516

[a] NMR spectra recorded at 183 K.

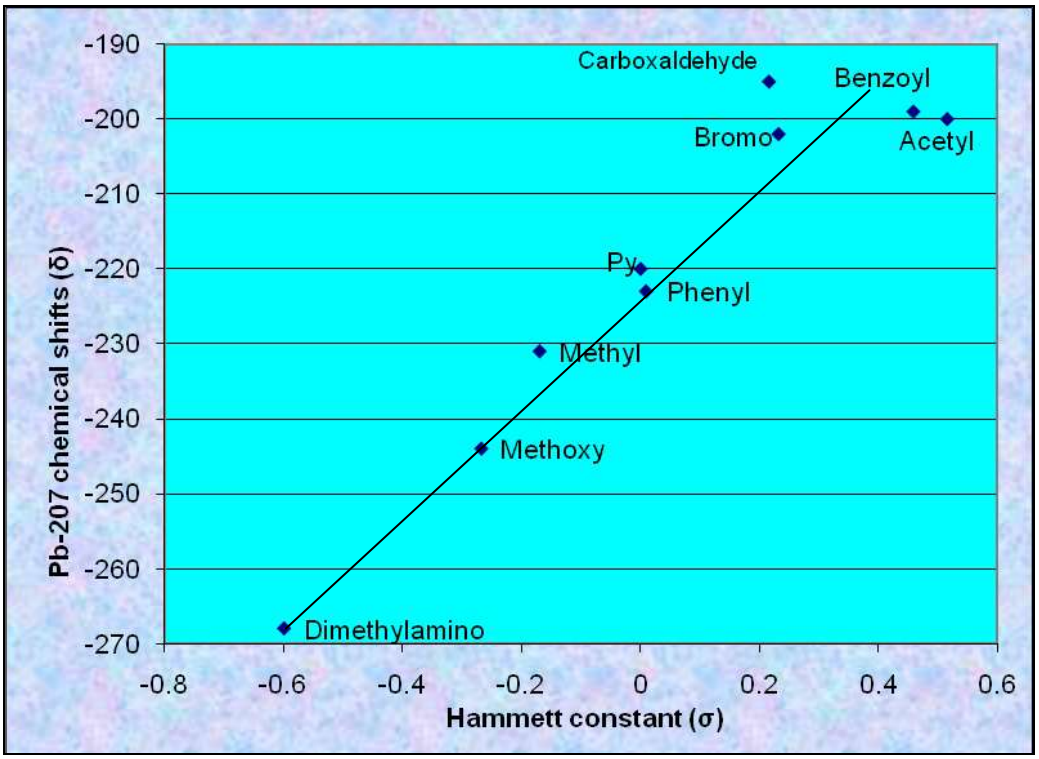


Figure 4.2 A plot of Hammett substituent constant against ^{207}Pb chemical shifts (ppm) (r^2 = 0.95, *p*-value = 0.0000718).

For the plots shown in **Figures 4.2** and **4.3** a good correlation coefficient, r^2 of 0.95 for both organo-lead and organo-tin adducts is observed. A similar correlation between Hammett constant and metal chemical shift has been found for different types of complex and for different metals e.g $[(C_5H_4Y)Fe(CO)(Ph_3)Me]$ [22] where Y is a substituent on the cyclopentadiene ring. The Hammett σ for Y was found to correlate with the ^{57}Fe chemical shift. The similarities in the electronic properties of organo-lead and organo-tin adducts as reflected by the changes in the NMR chemical shift of the metal nuclei do not necessarily translate into similar chemical properties such as degree of biological toxicity of lead and tin compounds in animals including people. The electron withdrawing ability of the *para*-substituted pyridine derivatives as reflected by the Hammett substituent constant increases accordingly with respect to δ(^{207}Pb) and δ(^{119}Sn) (data for the 4-acetyl- and 4-carboxaldehyde-pyridines are not in complete agreement with the trend, **Table 4.2 and 4.3**). According to Suresh [23], the total electronic effect of the substituent

R is a cumulative addition of all the constituents of R group which therefore places the Hammett constants, Σσ as the best measure reflecting total effect of py* on lead and tin. It can therefore be concluded that Hammett substituent constant represent the best parameter that quantifies the electronic influence of a substituent R which also reflect a linear relationship between steric and electronic effects.

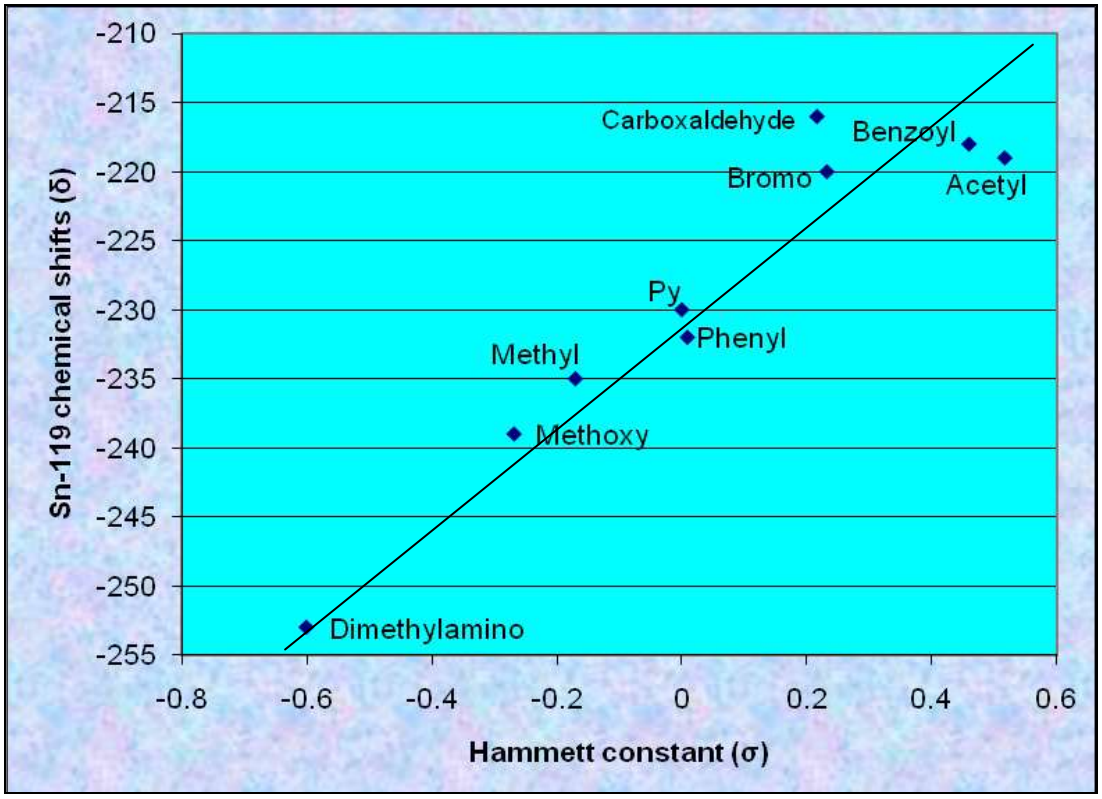


Figure 4.3 A plot of Hammett substituent constant against ^{119}Sn chemical shifts (ppm). (r^2 = 0.95, *p*-value = 0.0000763)

4.4 X-ray Crystallographic study

Triorgatinhalide compounds are known to exist in solution as simple tetrahedral (four hybrid sp^3 orbitals) molecules and as complexes with trigonal bipyramidal geometry (*cis* or *trans*) at the five-coordinate central tin atom which can be confirmed by their $^1J_{(^{119}Sn-^{13}C)}$ [4a]. The solid state

structure analysis as determined by single crystal X-ray diffraction confirmed the formation of five-coordinate trigonal bipyramidal compounds for both $Ph_3SnCl.py$ and $Ph_3PbCl.py^*$ (py* = 4-phenylpyridine) adducts (illustrated by the representative crystal structure models shown in **Figure 4.4)**. The relevant bond angles and distances are reported in **Table 4.4**. The isomorphous compounds show the three phenyl groups occupying the equatorial positions. The substituent py* and Cl are in axial positions i.e. resulting in *trans*-trigonal bipyramidal geometry. The phenyl groups are positioned in a staggered orientation, presumably to minimize steric hindrance. The structural arrangement of the five-coordinate system can be interpreted in terms of the so called "three-centre orbital" model [24]. According to this model and assuming the participation of 5*s* and 5*p* (contribution of 5*d* orbitals to the bonding being very low [25]) orbitals in the five-coordinate system, the three Sn/Pb-C bonds are formed by sp^3 hybrid orbitals, whereas the remaining 5*p* orbital participates in bonding with the substituent X (Cl) and the ligand L (where L is monodentate, py) using the low lying 5d orbital.

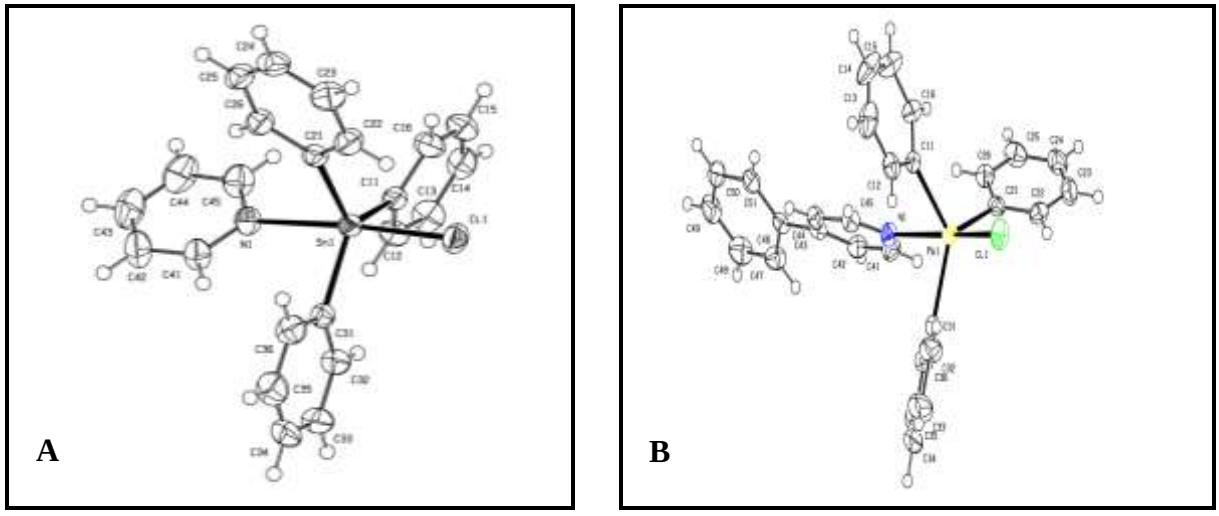


Figure 4.4 ORTEP drawing (50% probability level) and labelling scheme for $Ph_3SnCl.py$ (**A**) and $Ph_3PbCl.py^*$ (where py* is 4-phenylpyridine) (**B**).

Table 4.4 Selected bond lengths (Å) and angles (°) of organo-lead (**1a**) and organo-tin (**1b**) adducts.

Parameter	**1a**: $Ph_3PbCl.py$* M = Pb	**1b**: $Ph_3SnCl.py$ M = Sn
M – Cl	2.6085(9)	2.4960(5)
M – N	2.700(3)	2.5071(15)
M – C(11)[a]	2.207(3)	2.1495(18)
M – C(21)[a]	2.197(3)	2.1310(18)
M – C(31)[a]	2.199(4)	2.1327(18)
Cl – M – C(11)[a]	92.09(9)	92.03(5)
Cl – M – C(21)[a]	96.39(9)	96.32(5)
Cl – M – C(31)[a]	94.26(10)	92.37(5)
N – M – Cl	171.61(6)	174.12(4)
N – M – C(11)[a]	82.25(10)	84.53(6)
N- M – C(21)[a]	91.47(11)	89.55(6)
N – M – C(31)[a]	83.97(11)	85.49(6)
C(11)[a] – M – C(21)[a]	111.88(12)	117.63(7)
C(11)[a] – M – C(31)[a]	124.42(13)	122.91(7)
C(21)[a] – M – C(31)[a]	122.07(13)	118.33(7)

[a] Carbons of the phenyl rings are arbitrarily labelled.

Figure 4.4 shows representative geometrical structures of both the organolead and organotin adducts. They both crystallise in the monoclinic crystal systems and in very similar space

groups; triogano-lead adduct crystallises in the P2(1)/c space group, whilst triorgano-tin adducts crystallised in P2(1)n. Confirmation of the five coordinate molecular structure of $Me_2SnCl.py$ by single crystal X-ray diffraction showed organo-groups to be occupying the equatorial positions [26] and reports of ^{119}Sn NMR spectroscopic data for Ph_3SnX adducts (where X = Cl) [4a] provided more insight into their possible coordination geometry where the ^{207}Pb and ^{119}Sn chemical shifts seem to decrease with an increasing coordination number. In a manner similar to $Me_3SnCl.py$ [27], $Ph_3SnCl(TPPO)$ and $Ph_3PbBr(TPPO)$ (TPPO = triphenylphosphine oxide) [2h] the five coordinate $Ph_3SnCl.py$ and $Ph_3PbCl.py^*$ adducts show *trans*-triorganobipyramidal geometry with organo-groups occupying the equatorial positions, pyridine or py* and chlorine occupying the axial positions. The M–Cl and M–N bonds for $Ph_3PbCl.py^*$ are slightly longer than that of $Ph_3SnCl.py$. The departure from linearity of the N–M–Cl bond angle is slightly larger for $Ph_3SnCl.py$ than for $Ph_3PbCl.py^*$ analogue. A possible *cis*-trigonal five-coordinate bipyramidal geometry for $Ph_3MX.L$ adducts (where X = halide and L = ligand) has not been observed in the present study nor is there any report of their existence in the literature.

4.4 Conclusions

NMR spectroscopy has been successfully applied in the study of the formation of five-coordinates adducts of triorgano-lead and triorgano-tin halides in the presence of a variety of *para*-substituted pyridine derivatives. At 183 K, the ^{207}Pb and ^{119}Sn chemical shifts were found not to be sensitive to the influence of changes in the concentration of pyridine (at least within the range of interest). Interesting results were observed when the temperature was varied between 183 K and 313 K. The sensitivity of ^{207}Pb and ^{119}Sn chemical shifts to the changing conditions was unambiguously demonstrated, a factor which is crucial when chemical shift of these types of compounds is quoted. Solid state structure geometries are consistent with literature reports. As far as we are aware the study of the correlation (corr. coeff. = 0.95) between ^{207}Pb or ^{119}Sn chemical shifts of five coordinate compounds of the type $Ph_3MCl.py^*$ with the Hammett substituent constant is the first to be reported.

References

1. (a) P. Pfeiffer, P. Truskier and P. Disselkamp, *Chem. Ber*., 49 (1916) 2445; (b) J.J. Burke and P.C. Lauterbur, *J. Am. Chem. Soc*., 83 (1961) 326.

2. (a) A.G Davis and P.G. Harrison, *J. Chem. Soc*., (1969)1136; (b) P.J. Smith and A.P. Tupčiauskas, *Annul Reports on NMR Spectroscopy*, 8 (1978) 291; (c) B. Wrackmeyer, *Annual Reports on NMR Spetroscopy*, 16 (1985) 73; (d) J.N. Spencer, S.W. Barton, B.M. Cader, C.D. Corsico, L.E. Harrison, M.N. Mankuta and C.H. Yoder, *J. Organomet. Chem*., 3 (1985) 394; (e) J.N. Spencer, B.G. Enders, A. Grushow, S.P. Kneizys, W.L. Nachlis, D. Mokrynka, S.M. Coley, J.C. Otter and C.H. Yoder, *J. Organomet. Chem*., 362 (1989) 53; (f) B. Wrackmeyer and K. Horchler, *Annual Reports on NMR Spectroscopy*, 22 (1990) 249 ; (g) C.H. Yoder, J.C.Otter, A. Grushow, T.F. Ganunis, B.G. Enders, A.L. Zafar and J.N. Spencer, *J. Organomet. Chem*., 385 (1990) 33; (h) H.J. Eppley, J.L. Ealy, C.H. Yoder and J.N. Spencer, *J. Organomet. Chem*., 431 (1992) 133; (i) L.A. Margolis, C.D. Schaeffer Jr and C.H. Yoder, *Appl. Organomet. Chem*., 17 (2003) 236.

3. J.D Kennedy, W. McFarlane and G.S. Pyne, *J. Chem. Soc., Dalton Trans*., (1977) 2332.

4. (a) J. Holeček, M. Nádvorník, K. Handlíř and A. Lyčka, *J. Organomet. Chem*., 241 (1983) 177; (b) *J. Organomet. Chem*., 275 (1984) 43 ; (c) *J. Organomet. Chem*., 315 (1986) 299.

5. R. Colton, *Inorg. Chim. Acta*, 148 (1988) 31.

6. J. Holeček, K. Handlíř, A. Lyčka, T.K. Chattopadyay, B. Majee and A.K. Kumar. Chem. Commun., 51 (1986)1100.

7. M. Nádvorník, J. Holecék and K. Handlír, *J. Organomet. Chem*., 275 (1984) 43.

8. W.F. Howard, R.W. Crecely and W.H. Nelson, *Inorg. Chem*., 24 (1985) 2204.

9. B. Jousseaume, *Mikrochim. Acta*, 109 (1992) 5.

10. M. Pereyre, J.P. Quintard and A. Rahm, *Tin in Organic Synthesis*, Butterworths, 1986.

11. C.J. Evans and S. Karpel, *J. Organomet. Chem*., 285 (1985) 16.

12. (a) S. Tabassum and C. Pettinari, *J. Organomet. Chem*., 691 (2006) 1761; (b) A.K. Saxena and F. Huber, *Coord. Chem. Rev*., 95 (1989) 109.

13. (a) F. Cima, L. Ballarin, *Appl. Organomet. Chem*., 13 (1999); (b) 697C. Pellerito, P.D. Agati, T. Fiore, C. Mansueto, V. Mansueto, G. Stocco, L. Nagy, L Pellerito, *J. Inorg. Biochem*. 99 (2005) 1294.

14. G. Neue, C. Dybowski, M. Smith and A.H. Mark, *Nucl. Magn. Reson*., 6 (1996) 241.

15. Bruker, *SAINT+* Version 6.02 (includes XPREP and SADABS), Bruker AXS: Madison, WI, (1999).

16. G.M. Sheldrick, *SADABS*, University of Göttingen: Göttingen, Germany, (1996).

17. Bruker, *SHELXTL* Version 5.1 (includes XS, XL, XP, XSHELL), Bruker AXS: Madison, WI, (1999).

18. A.L. Spek, *J. Appl. Crystallogr*., 36 (2003) 7.

19. L.J. Farrugia, *J. Appl. Crystallogr*., 30 (1997) 565.

20 R. Hulme, *J. Chem. Soc*., (1963) 1524.

21. C. Hansch, A. Leo and R.W. Taft, *Chem. Review*., 91 (1991) 165.

22. E.J.M. Meier, W. Koźmiński, A. Linden, P. Lustenburger and W. von Philipsborn, *Organometallics*, 15 (1996) 2477.

23. C.H. Suresh, *Inorg. Chem*., 45 (2006) 4982.

24. R. Okawara and M. Wada, in F.G.A Stone and R. West (Eds.). *Advances in Organometallic Chemistry*, Academic Press, New York, London, Vol. 5, (1967) 144.

25. M.M. McGrady and R.S. Tobias, *J. Am. Chem. Soc*., 87 (1965) 1909.

26. R. Hulme, *J. Chem. Soc*., (1963) 1524.

27. R. Colton, *Inorg. Chim. Acta*, 148 (1988) 31.

CHAPTER 5

Synthesis, NMR and X-Ray Crystallographic Study of Hetero-Bimetallic Complexes of the type [$CpFe(CO)(PR_3)(SnPh_3)$]

5.1 Introduction

The chemistry of metal-metal bonded complexes and their potential applications have been discussed in chapter 1 (section 1.2.1). Reviews of the coordination chemistry of the element tin to a variety of transition metals have appeared in the literature from as early as the 1960's [1]. Metal-metal interactions in heterobimetallic complexes where tin is coordinated to cyclopentadienylmetal have been of interest to researchers for many years [2]. The coordination of Sn to the transition metal centre is influenced by the presence of phosphine or phosphite ligands which are well known to stabilize transition metals in low to higher oxidation states as well as to metals with a d^0 electronic configuration [3]. Coordination of phosphine and phosphite ligands to metal carbonyls is influenced by their steric effect (measured by the size of cone angle in the case of monodentate ligands or a bite angle in the case of polydentate ligands) and their electronic properties. The electronegativity of substituents on the phosphorus atom and the angles between them have been found to be the most important factors in the determination of ^{31}P chemical shift and spin coupling interactions [4].

Quantitative evidence for steric effects in reactions of metal carbonyls and other organometallic compounds was first reported in 1966 [5]. An increase in Tolman's steric parameter for a coordinated phosphine or phosphite, quantified by a measure of a cone angle is generally accompanied by an increase in ^{31}P chemical shift. Tolman [6] was successful in correlating the properties of complexes such as the reactivity (given by the rate constant), infrared stretching frequency (as a measure of the net electron donating ability of the ligand), metal-phosphorus coupling constant, etc., to steric effects of phosphine and phosphite ligands (as a measure of the size of the ligand provided by the size of cone angle). Tolman defined the cone angle as the apex

angle of a cylindrical cone centered 2.28 Å from the center of a phosphorus atom that touches the van der Waals radii of the outermost atoms. Tolman's cone angles have since been used as predictive measure of steric effects as they allow a quantitative description of the dependence of many physicochemical properties on the ligands involved in the coordination sphere. Alternative methods have also been employed to refine steric parameters for phosphine ligands and these includes molecular mechanics models and X-ray structural data [7]

Complexes of iron and tin of the type: (dicarbonyl-η^5-cyclopentadienyliron(II))triphenyltin, [$CpFe(CO)_2(SnPh_3)$] [8]; (carbonyl-η^5-cyclopentadienyliron(II))triphenyltin phosphine, [$CpFe(CO)(PPh_3)(SnPh_3)$] [9]; (η^5-cyclopentadienyliron(II))trimethyltin diphosphine, [$CpFe(PMe_3)_2(SnPh_3)$] [9c] and bis(dicarbonyl-η^5-cyclopentadienyliron(II)) diphenyltin, $Ph_2Sn[CpFe(CO)_2]_2$ [10] have been known for many years but have not been fully studied by NMR. As part of our aims, we decided to investigate complexes of the type [$CpFe(CO)(PR_3)(SnPh_3)$] in particular to correlate solution state NMR spectroscopic parameters and structural properties such as bond length and angles of monocarbonylated iron-tin complexes in particular to steric effects of phosphine and phosphite ligands. As a result of our investigation, a series of monocarbonylated phosphine complexes of iron-tin were synthesized and characterized by NMR spectroscopy, infrared (IR) spectroscopy, elemental analysis and X-ray crystallography. Particular attention is given to the structural features around iron with respect to tin and phosphorus atoms, their influence on the Cp-Fe bond distances and how they correlate to NMR data and Tolman's parameters.

5.2 Experimental

5.2.1 Reagents and general techniques.

Hetero-bimetallic complexes of the general formula [CpFe(CO)(PR_3)($SnPh_3$)], where PR_3 is: triphenylphosphine, (PPh_3) **2**; tris(*para*-fluorophenyl)phosphine, {P(*p*-FC_6H_4)$_3$} **3**, tris-(para-methoxyphenyl)phosphine, {P(*p*-$OMeC_6H_4$)$_3$} **4**; {tris(para-tolyl)phosphine}, {P(*p*-tolyl)$_3$} **5**; tricyclohexylphosphine, {P(Cy)$_3$} **5**; tris(dimethylamino)phosphine, {P(NMe_2)$_3$} **7**; methyldiphenylphosphine, {P($MePhe_2$)} **8**; tributylphosphine, {P(Bu)$_3$} **9**; triphenylphosphite, {P(OPh)$_3$} **10**; trimethylphosphite, {P(OMe)$_3$} **11**; trimethylphosphine, {P(Me)$_3$} **12** and dimethyphenylphosphine, {P(Me_2Ph)} **13** were synthesized from [CpFe($CO)_2SnPh_3$] **1** for the purposes of NMR spectroscopic and X-ray crystallographic studies. Unless specifically mentioned all operations, reactions and manipulations were performed under inert atmosphere of high purity nitrogen or argon using standard Schlenk techniques.

Starting materials and ligands (preserved under an inert atmosphere of either high purity nitrogen or argon) were used as purchased (from Aldrich or Merck) without further purification. All solvents except methanol and ethanol were distilled before use, i.e. tetrahydrofuran (THF) from Na/benzophenone, toluene, n-hexane, acetonitrile and diethyl-ether from CaH_2, and dichloromethane from P_2O_5. All solvents including high purity methanol and ethanol were deoxygenated before use. All the glassware was dried and flushed with nitrogen or argon before use. A 400 W medium pressure mercury UV lamp was positioned at most 20 mm away from the sample for all the reactions requiring the UV source. All the IR spectra were recorded in chloroform solution on a Bruker Vector 22 FT-IR machine. Elemental analyses were performed by the Institute for Soil, Climate and Water in Pretoria.

5.2.2 NMR spectroscopy

Unless otherwise stated all NMR spectra were recorded on a Bruker Avance DRX 400 spectrometer operating at 400.13 (^{1}H), 100.60 (^{13}C), 161.98 (^{31}P), 12.97 (^{57}Fe) or 149.21 (^{119}Sn)

MHz and referenced to TMS (^{1}H and ^{13}C), 85% H_3PO_4, neat $Fe(CO)_5$ (primary external reference at 0.00 ppm) and neat Me_4Sn respectively. The ^{57}Fe {^{31}P} spectra were obtained by indirect detection using the pulse sequence of Bax, Griffey and Hawkins [11]:

$$\pi/2(^{31}P)\text{-}1/[2J(^{57}Fe,^{31}P)]\text{-}\pi/2(^{57}Fe)\text{-}\tau\text{-}\pi(^{31}P)\text{-}\tau\text{-}\pi/2(^{57}Fe)\text{-}1/2[2J(^{57}Fe),^{31}P)]\text{-}Acq(^{31}P)$$

with broadband ^{1}H decoupling throughout and ^{57}Fe decoupling omitted during acquisition. A spectral width in f2 (^{31}P) was varied according to the specific circumstance from 5 - 10 ppm with the acquisition time varying accordingly. In the f1 dimension (^{57}Fe), the spectral width was varied between 40 and 80 ppm and the time domain varied from 64 to 128, 256 and 512 (in very rare cases). In order to eliminate possible folding of signals, the spectra were first recorded with a spectral width in the f1 dimension of 1000 ppm before reducing the width to between 40 and 80 ppm. The concentration of solutions for NMR analysis varied from 0.01 to 0.02 M; all spectra were recorded from a solution in $CDCl_3$ at 300 K. Only ^{1}H and ^{13}C data are included in the characterisation of the synthesised compounds and ^{31}P, ^{57}Fe and ^{119}Sn data are given in **Table 5.3**. The following abbreviations are used for NMR spectrum interpretation: singlet (s), doublet (d), doublet of doublet (dd), triplet (t), quartet (q) and multiplet (m); *o* (ortho), *m* (meta) and *p* (para).

5.2.3 X-ray Crystallography

Intensity data were collected on a Bruker SMART 1 K CCD area detector diffractometer with graphite monochromated Mo K_α radiation (50 kV, 30 mA). The collection method involved ω-scans of width 0.3°. Data reduction was carried out using the program *SAINT+* [12] and face indexed absorption corrections were made using the program *XPREP* [12] or SADABS [13].The crystal structure was solved by direct methods using *SHELXTL* [14]. Non-hydrogen atoms were first refined isotropically followed by anisotropic refinement by full matrix least-squares calculations based on F^2 using *SHELXTL*. Hydrogen atoms were first located in the difference map then positioned geometrically and allowed to ride on their respective parent atoms. Diagrams and publication material were generated using SHELXTL and PLATON [15].

Table 5.1 Crystal and structure refinement data for the compounds **3**, **5**, **6**, **7**, **8**, **9**, **10** and **11**

Parameter	**3**	**5**	**6**	**7**	**8**	**9**	**10**	**11**
Molecular formula	$C_{42}H_{32}F_3$ FeOPSn	$C_{45}H_{41}$ FeOPSn	$C_{42}H_{53}$ FeOSn	$C_{30}H_{38}$ FeN_3OPSn	$C_{37}H_{33}$ FeOPSn	$C_{36}H_{47}$ FeOPSn	$C_{42}H_{35}Fe$ O_4PSn	$C_{27}H_{29}$ FeO_4PSn
Formula weight	815.19	803.29	779.35	662.14	699.14	700.92	808.99	623.01
Temperature (K)	293(2)	293(2)	293(2)	293(2)	293(2)	173(2)	293(2)	173(2)
Wavelength (Å)	0.71073	0.71073	0.71073	0.71073	0.71073	0.71073	0.71073	0.71073
Crystal system	Monoclinic	Monoclinic	Triclinic	Triclinic	Triclinic	Orthorhombic	Triclinic	Monoclinic
Space group	P2(1)/n	P2(1)/c	P-1	P-1	P-1	Pbca	P-1	P2(1)/c
Unit cell dimensions								
a (Å)	11.6044(10)	9.0331(14)	10.434(3)	8.652(5)	10.1908(15)	17.874(2)	9.9203(13)	9.4349(2)
b (Å)	18.8906 (14)	19.981(3)	11.587(3)	10.780(5)	12.2765(18)	18.164(2)	10.1167(13)	30.0110(4)
c (Å)	16.4893(12)	21.111(3)	17.538(5)	15.899(5)	14.472(2)	21.060(3)	20.665(3)	9.8551(8)
α (^{0})	90	90	88.728(5)	85.457(5)	87.082(3)	90	102.302(2)	90
β (^{0})	101.753(3)	92.744(3)	89.563(5)	86.610(5)	71.182(2)	90	103.441(3)	109.710(10)
γ (^{0})	90	90	63.888(4)	82.198(5)	68.380(3)	90	93.486(2)	90
Volume (Å^3)	3538(5)	3805(10)	1903.3(9)	1462.8(12)	1588.5(4)	6837.5(16)	1957.5(5)	2626.99(8)
Z	4	4	2	2	2	8	2	4
Density (Calculated) (Mg/m^3)	1.530	1.402	1.360	1.503	1.462	1.411	1.451	1.575
Absorption coefficient (mm^{-1})	1.209	1.113	1.110	1.432	1.321	0.977	1.092	1.594
F(000)	1640	1640	808	676	708	3024	870	1256
Crystal size (mm^3)	0.34 x 0.26 x 0.19	0.46 x 0.42 x 0.24	0.16 x 0.16 x 0.11	0.39 x 0.25 x 0.15	0.40 x 0.32 x 0.32	0.46 x 0.37 x 0.23	0.20 x 0.12 x 0.10	0.20 x 0.13 x 0.07
Theta range for data collection (^{0})	1.66 to 60.00	1.93 to 27.00	1.16 to 26.00	1.29 to 28.38	1.49 to 26.00	1.87 to 28.42	1.04 to 26.00	2.29 to 26.00
Index ranges	-12<=h<=14 -23<=k<=19 -20<=l<=20	-11<=h<=11 -25<=k<=25 -19<=l<=26	-12<=h<=10 -14<=k<=11 -20<=l<=21	-11<=h<=11 -14<=k<=14 -21<=l<=21	-12<=h<=12 -15<=k<=8 -17<=l<=17	-22<=h<=23 -24<=k<=22 -27<=l<=25	-9<=h<=12 -12<=k<=12 -25<=l<=21	-11<=h<=11 -37<=k<=37 -12<=l<=9
Reflections collected	15539	23785	9896	39462	9246	44480	11642	23940
Independent reflections	6941[R(int)= 0.047]	8286 [R(int) = 0.0303]	7341[R(int) = 0.0400]	7263 [R(int) =0.0218]	6152 [R(int) = 0.0227]	8403[R(int) = 0.0591]	7610[R(int) = 0.023]	5159[R(int) = 0.0235]
Completeness to θ_{MAX} (%)	99.6	99.7	98.1	98.7	98.6	97.8	99.0	99.9
Absorption correction	Integration	Integration	Integration	Multirun	Integration	Integration	Integration	Integration
Max. and min.	0.8186 and	0.7737 and	0.8833 and	0.8139 and	0.7317 and		0.9198 and	0.8966 and

transmissions	0.6936	0.6401	0.8069	0.6052	0.6080		0.8332	0.7410
Data / restraints / parameters	6941/0/442	8286/0/445	7341/0/415	7263/0/340	6152/0/371	8403/0/347	7610/63/494	5159/0/307
Goodness-of-fit on F^2	0.930	1.061	1.035	1.031	1.038	1.014	1.016	1.115
Final R indices [I>2sigma(I)]	R1 =0.0334, wR2=0.0699	R1 =0.0326, wR2=0.0662	R1=0.0471, wR2=0.0886	R1=0.0173, wR2=0.0435	R1=0.0252, wR2=0.623	R1=0.0643, wR2=0.1548	R1=0.0313, wR2=0.0684	R1=0.0280, wR2=0.0612
R indices (all data)	R1 = 0.0571 wR2=0.0761	R1 =0.0481, wR2=0.0721	R1=0.0882, wR2=0.1007	R1 =0.0196, wR2=0.0447	R1=0.0305, wR2=0.0653	R1=0.0942, wR2=0.1824	R1=0.0430, wR2=0.0742	R1=0.0333, wR2=0.0630
Largest diff. peak and hole (e.Å^{-3})	0.651 and -0.434	0.441 and -0.408	0.579 and -0.677	0.434 and -0.307	0.737 and -0.442	3.008 and -1.866	0.538 and -0.285	0.691 and -0.378

Crystals suitable for X-ray diffraction analysis for **9** and **10** were grown from saturated solution in n-hexane (at room temperature) and toluene/n-hexane solution (< - 5ºC) respectively, whereas **3**, **5**, **6**, **7**, **8** and **11** were grown from saturated solutions in CH_2Cl_2/n-hexane at low temperature (-10 to 10 ºC, i.e. in a freezer or fridge).

5.3 Synthesis

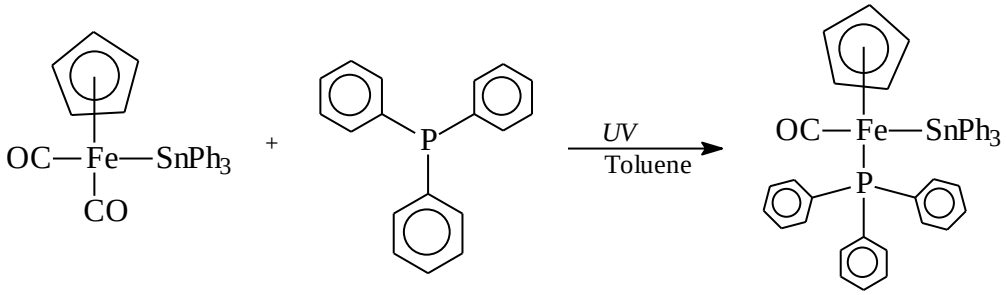
5.3.1 Preparation of $[Fe(Cp)(CO)_2(SnPh_3)]$ …….. (**1**)

The synthesis and characterization of compound (**1**) have been described by Gorsich **[8]**. A slightly modified approach was used in our investigation. A dark red solution of $[Fe(Cp)(CO)_2]_2$ (500 mg ~ 1.413 mmol) and THF (35 ml) was added dropwise (within 2 minutes) to a stirred sodium amalgam (100 mg Na and 2 ml Hg). The initial dark red solution changed to reddish-brown within five minutes of vigorous stirring after which the solution was left stirring gently overnight at room temperature. The reddish-brown solution of $Na[Fe(Cp)(CO)_2]$ (32 ml) was transferred into a new schlenk tube (as quickly as possible) before a solution of Ph_3SnCl (992 mg ~ 2.573 mmol) in THF (12 ml) was added dropwise within a period of approximately five minutes. An immediate colour change from reddish-brown to dark-brown was noticed. After 24 hrs of constant stirring at room temperature, the solvent (THF) was removed *in vacuo* and the product extracted with CH_2Cl_2 (2 x 2 ml). Precipitates were separated by centrifuge and the solution concentrated to approximately 2 ml after which n-hexane (~ 30 drops) was added to induce crystallisation. The resulting bright yellow needle crystals were then washed with n-

hexane (3 x 3 ml) and ethanol (2 x 2 ml) to give a yield of 801 mg (88%). NMR spectra were recorded from a solution in $CDCl_3$ at 300 K. ^1H NMR ($\delta_{(ppm)}$): 7.5 – 7.24 (m, 15H, Sn<u>Ph</u>$_3$); 4.80 (s, 5H, Cp). ^{13}C NMR ($\delta_{(ppm)}$): 214.42 (s, C, <u>C</u>O); 143.90 (s, *ipso*, 3C, Sn<u>Ph</u>$_3$); 136.60 (s, *m*, 6C, $SnPh_3$, d, satellite, $^3J_{(Sn\text{-}C)}$ = 36.3 Hz); 128.22 (s, *o*, 6C, $SnPh_3$, d, satellite, $^2J_{(Sn\text{-}C)}$ = 43.7 Hz); 128.12 (s, 3C, $SnPh_3$); 82.27 (s, 5C, Cp).

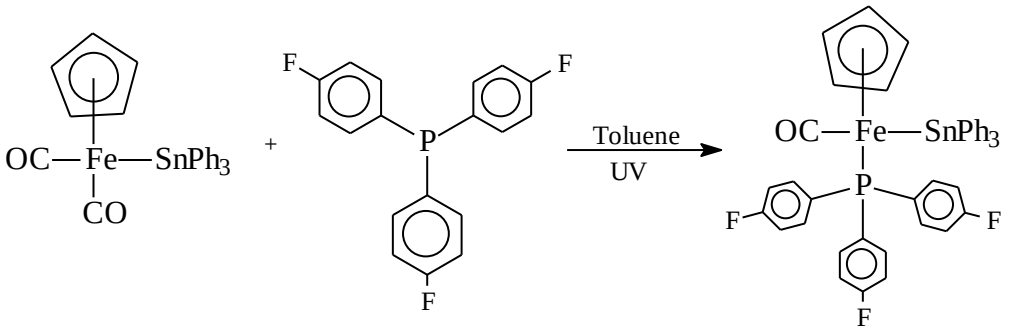
5.3.2 Preparation of $[Fe(Cp)(CO)(PPh_3)(SnPh_3)]$…… (**<u>2</u>**)

Compound (**<u>2</u>**) was prepared according to the method of Cullen *et al* [9b,e]. A clear pale yellow



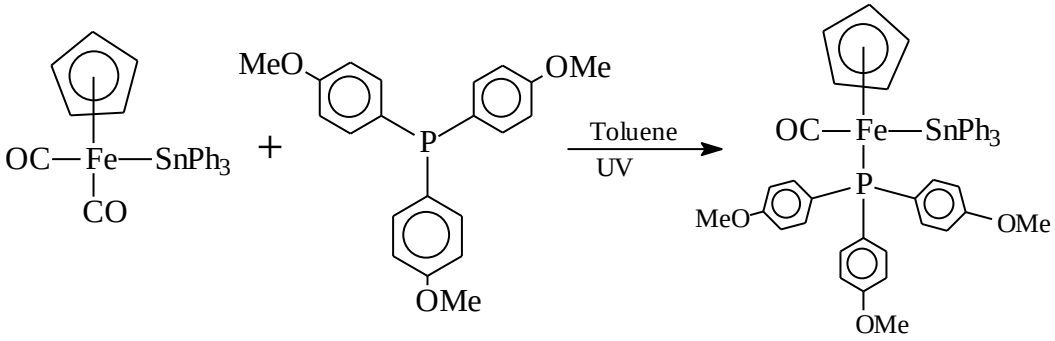
solution of $[Fe(Cp)(CO)_2(SnPh_3)]$ (**<u>1</u>**) (50 mg ~ 0.095 mmol) and a 50% excess of PPh_3 in toluene (10 ml) was sealed in a Schlenk tube and irradiated using a UV light source for approximately 24 hrs. An IR analysis (ν_{CO} = 1908.2) of the resulting red-orange solution confirmed a complete conversion of the (**<u>1</u>**) to a monocarbonylated product. The solvent was removed *in vacuo* and the product extracted with CH_2Cl_2 (2 ml). The resulting precipitates were separated by centrifuge before the solution was concentrated to approximately 1 ml after which n-hexane (~ 30 drops) was added dropwise to effect crystallisation. The dark-orange crystals were then washed with methanol (2 x 2 ml) to give a yield of 38 mg (50%). The product was initially extracted with diethyl-ether which gave a very low yield compared to dichloromethane. NMR spectra were recorded from a solution in $CDCl_3$ at 300 K. ^1H NMR ($\delta_{(ppm)}$): 7.28 – 7.04 (m, 30H, P<u>Ph</u>$_3$ and Sn<u>Ph</u>$_3$); 4.26 (d, 5H, Cp, $^3J_{(P\text{-}H)}$ = 1.4 Hz). 13C NMR ($\delta_{(ppm)}$): 220.50 (d, 1C, CO, $^2J_{(P\text{-}C)}$ = 28.6 Hz); 147.90 (s, *ipso*, 3C, Sn<u>Ph</u>$_3$); 137.55 (s, ipso, 3C, P<u>Ph</u>$_3$); 137.15 (s, *m*, 6C, $SnPh_3$, d, satellite, $^3J_{(Sn\text{-}C)}$ = 31.8 Hz); 133.12 (d, *m*, 3C, PPh_3, $^3J_{(P\text{-}C)}$ = 10.0 Hz); 129.44 (d, *p*, 3C, PPh_3, $^4J_{(P\text{-}C)}$ = 1.9 Hz); 127.69 (d, *o*, 6C, PPh_3, $^2J_{(P\text{-}C)}$ = 9.6 Hz); 127.54 (s, *o*, 6C, $SnPh_3$, d, satellite, $^2J_{(Sn\text{-}C)}$ = 35.8 Hz); 126.81 (s, *p*, 3C, $SnPh_3$); 81.72 (s, 5C, Cp).

5.3.3 Preparation of [Fe(Cp)(CO){P(*p*-FC$_6$H$_4$)$_3$}(SnPh$_3$)]…….... (3)



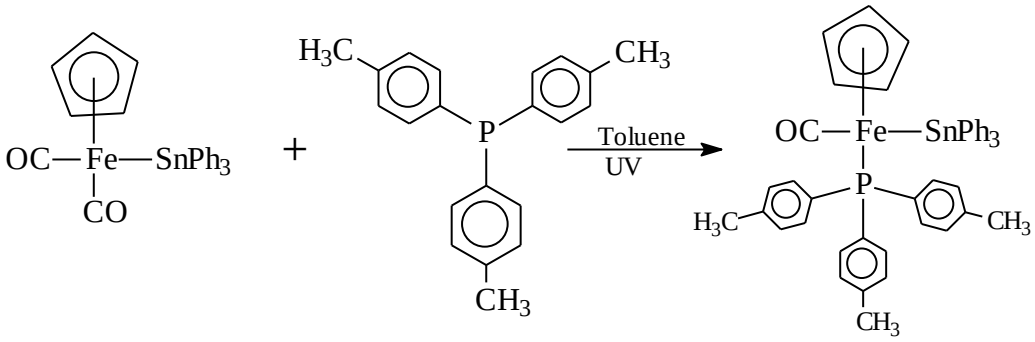
Compound (**3**) was prepared using the same procedure as for (**2**). A pale yellow solution of [Fe(Cp)(CO)$_2$(SnPh$_3$)] (**1**) (50 mg ~ 0.095 mmol) and tris(4-fluorophenyl)phosphine (50% excess) in toluene (10 ml) was sealed in a Schlenk tube and irradiated using a UV light source for 24 hrs. An accompanying colour change from pale-yellow to red-orange was noticed. An IR analysis (ν_{CO} = 1908.7) was recorded to determine the progress of reaction before the solvent was removed *in vacuo* and the product extracted with dichloromethane (3 ml) and the precipitates were separated by centrifuge. The solution was then concentrated to approximately 1 ml before n-hexane (~ 10 drops) was added dropwise to effect crystallisation. The resulting red-brown crystals were then washed with n-hexane (2 x 2 ml) to provide a yield of 44 mg (57%). NMR spectra were recorded from a solution in $CDCl_3$ at 300 K. ^{1}H NMR ($\delta_{(ppm)}$): 7.33 (m, 6H, Sn<u>Ph</u>/*p*-C$_6$H$_4$F); 7.12 (m, 16H, Sn<u>Ph</u>/*p*-C$_6$H$_4$F); 6.72 (m, 6H, Sn<u>Ph</u>/*p*-C$_6$H$_4$F); 4.27 (s, 5H, Cp). ^{13}C NMR ($\delta_{(ppm)}$): 220.23 (d, 1C, <u>C</u>O, $^2J_{(C\text{-}P)}$ = 29 Hz); 163.41 (d, *p*, 3C, P(*p*-FC$_6$H$_4$)$_3$, $^1J_{(C\text{-}F)}$ = 249.8 Hz); 147.23 (s, *ipso*, 3C, Sn<u>Ph</u>$_3$); 136.99 (s, *o*, 6C, Sn<u>Ph</u>$_3$, d, satellite, $^2J_{(Sn\text{-}C)}$ = 31.6 Hz); 134.91 (m, *o*, 6C, *p*-C$_6$H$_4$F); 133.04 (d, *ipso*, 3C, *p*-C$_6$H$_4$F), $^1J_{(C\text{-}P)}$ = 47.5 Hz); 127.73 (s, *m*, 6C, Sn<u>Ph</u>$_3$, d, satellite, $^3J_{(Sn\text{-}C)}$ = 36 Hz); 127.08 (s, *p*, 3C, Sn<u>Ph</u>$_3$); 115.25 (m, *p*, 3C, *p*-FC$_6$H$_4$), 81.68 (s, 5C, Cp). Elemental analysis: calculated for C$_{42}$H$_{32}$OF$_3$PFeSn: C, 61.87; H, 3.96%. Found: C, 61.64; H, 3.94%. IR ($CHCl_3$ solution): ν_{CO} 1908.7 cm^{-1}.

5.3.4 Preparation of [Fe(Cp)(CO){P(*p*-OMeC$_6$H$_4$)$_3$}(SnPh$_3$)]……. (4)



Compound (**4**) was prepared using the same procedure as for (**2**). A pale yellow solution of $[Fe(Cp)(CO)_2(SnPh_3)]$ (**1**) (50 mg ~ 0.095 mmol) and tris(4-methoxyphenyl)phosphine (50% excess) in a toluene (10 ml) was irradiated using a UV light source for approximately 19 hrs in a sealed Schlenk tube. An IR analysis (ν_{CO} = 1902.7) of the resulting red-orange solution was recorded to determine the progress of reaction before the solvent was removed in *vacuo*. The product was extracted with dichloromethane (3 ml) and the precipitates separated by centrifuge. The resulting solution was concentrated to approximately 1 ml before drop-wise addition of n-hexane (15 drops) to effect crystallisation. The orange crystals were washed with n-hexane (3 x 2 ml) to give a yield of 74 mg (87%). NMR spectra were recorded from a solution in $CDCl_3$ at 300 K. ^{1}H NMR ($\delta_{(ppm)}$): 7.38(m, 6H, Sn<u>Ph</u>$_3$); 7.16 (m, 15H, Sn<u>Ph</u>/ *p*-C_6H_4OMe); 6.61(m, 6H, <u>SnPh</u>/ *p*-C_6H_4OMe); 4.33 (d, 5H, Cp, $^3J_{(P-H)}$ = 1.3 Hz); 3.75 (s, 9H, O<u>Me</u>). ^{13}C NMR ($\delta_{(ppm)}$): 220.79 (d, 1C, <u>C</u>O, $^2J_{(P-C)}$ = 41.5 Hz); 160.18 (s, *p*, 3C, *p*-C_6H_4OMe); 148.12 (s, *ipso* , 3C, Sn<u>Ph</u>$_3$); 137.11 (s, *o*, 6C, Sn<u>Ph</u>$_3$); 134.47 (s, 6C, *o*, *p*-C_6H_4OMe); 130.38 (s, *ipso*, 3C, *p*-C_6H_4OMe); 127.40 (s, *m*, 6C, Sn<u>Ph</u>$_3$); 126.63 (s, *p*, 3C, Sn<u>Ph</u>$_3$); 113.47 (s, *m*, 6C, *p*-C_6H_4OMe); 129.06, 113.30 (18C,);, 137.11, 127.40, 126.63 (18C, Sn<u>Ph</u>$_3$); 81.52 (s, 5C, Cp); 58.36, 55.04 (s, 3C, O<u>Me</u>). Elemental analysis: Calculated for $C_{45}H_{41}O_4PFeSn$: C, 63.51; H, 4.82%. Found: C, 63.35; H, 4.86%. IR ($CHCl_3$ solution): ν_{CO} 1902.7 cm^{-1}.

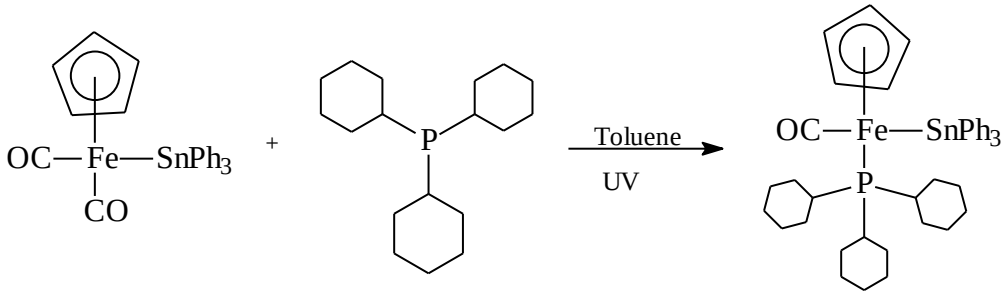
5.3.5 Preparation of [Fe(Cp)(CO){P(*p*-MeC$_6$H$_4$)$_3$}(SnPh$_3$)]…. …….. (<u>5</u>)



Compound (**5**) was prepared using the same procedure as for (**2**). A pale yellow solution of $[Fe(Cp)(CO)_2(SnPh_3)]$ (**1**) (50 mg ~ 0.095 mmol) with tris(*p*-tolyl)phosphine (50% excess) in toluene (10 ml) was irradiated using a UV light source for approximately 19 hrs in a sealed Schlenk tube. An IR analysis (ν_{CO} = 1904.3) of the resulting red-orange solution was recorded to determine the progress of the reaction before the solvent (toluene) was removed *in vacuo*. The

product was extracted with dichloromethane (3 ml) and the precipitates separated before the solution was concentrated to approximately 1 ml before n-hexane (10 drops) to induce crystallisation. The resulting orange crystals were washed with n-hexane (2 x 2 ml) to provide a yield of 51 mg (63%). NMR spectra were recorded from a solution in $CDCl_3$ at 300 K. ^{1}H NMR ($\delta_{(ppm)}$): 7.39 (m, 6H, Sn<u>Ph</u>$_3$); 7.14 (m, 15H, Sn<u>Ph</u>$_3$/*p*-C_6H_4Me); 6.90 (m, 6H, Sn<u>Ph</u>$_3$/*p*-C_6H_4Me); 4.31 (d, 5H, Cp, $J_{(P,H)}$ = 1.4 Hz); 2.28 (s, 9H, Me). ^{13}C NMR ($\delta_{(ppm)}$): 220.98 (d, <u>C</u>O, $^2J_{(P-C)}$ = 28.8 Hz); 147.98 (s, *ipso*, 3C, Sn<u>Ph</u>$_3$); 139.32 (s, *p*, 3C, *p*-C_6H_4Me); 137.18 (s, *o*, 6C, Sn<u>Ph</u>$_3$, d, satellite, $^2J_{(P-C)}$ = 31.8 Hz); 134.40 (d, *ipso*, 3C, *p*-C_6H_4Me, $^1J_{(P-C)}$ = 44.4 Hz); 132.99 (d, *m*, 6C, *p*-C_6H_4Me, $^3J_{(P-C)}$ = 10.3 Hz); 128.57 (d, *o*, 6C, *p*-C_6H_4Me, $^2J_{(P-C)}$ = 9.9 Hz); 127.23 (s, *m*, 6C, Sn<u>Ph</u>$_3$, d, satellite, $^3J_{(Sn-C)}$ = 35.4 Hz); 126.61 (s, *p*, 3C, Sn<u>Ph</u>$_3$); 81.62 (s, 5C, Cp); 21.24 (s, 3C, *p*-C_6H_4<u>Me</u>). Elemental analysis: Calculated for $C_{45}H_{41}OPFeSn$: C, 67.30; H, 5.11%. Found: C, 67.38; H, 5.09%. IR ($CHCl_3$ solution): ν_{CO} 1904.3 cm^{-1}.

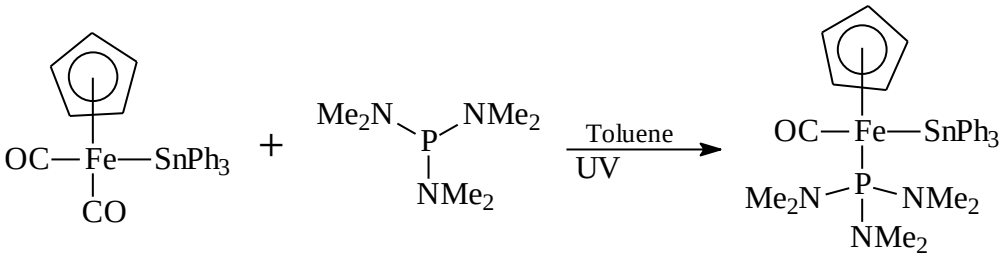
5.3.6 Preparation of [Fe(Cp)(CO){P(Cy)$_3$}(SnPh$_3$)]…… (<u>6</u>)



Compound (**<u>6</u>**) was prepared using the same procedure as for (**<u>2</u>**). A pale yellow solution of [Fe(Cp)(CO)$_2$(SnPh$_3$)] (**<u>1</u>**) (50 mg = 0.095 mmol) and 50% excess of tricyclohexylphosphine in toluene (10 ml) was irradiated using a UV light in a sealed Schlenk tube overnight. An IR analysis (ν_{CO} = 1893.6) of the resulting red-orange solution (ν_{CO} = 1894 cm^{-1}) was recorded to determine the progress of reaction after approximately 18 hrs of constant stirring before the solvent was removed *in vacuo*. The product was extracted with dichloromethane (2 ml) and the precipitates separated by centrifuge before the solution was concentrated to approximately 1 ml. n-Hexane (15 drops) was added to induce crystallisation and the resulting red-orange crystals were then washed with n-hexane (2 x 2 ml) to give yield of 47 mg (60%). NMR spectra were recorded from a solution in $CDCl_3$ at 300 K. 1H NMR ($\delta_{(ppm)}$): 7.64 (m, 6H, Sn<u>Ph</u>$_3$); 7.21 (m, 9H, Sn<u>Ph</u>$_3$); 4.62 (d, 5H, Cp, $^3J_{(P-H)}$ = 1.0 Hz); 1,7-0.9 (m, 33H, Cy). ^{13}C NMR ($\delta_{(ppm)}$): 221.90 (d,

1C,CO, $^{2}J_{(P-C)}$ = 27.0 Hz); 148.86 (s, *ipso*, 3C, Sn**Ph**$_3$); 137.39 (s, *o*, 6C, Sn**Ph**$_3$,d, satellite, $^{2}J_{(Sn-C)}$ = 30.1 Hz); 127.53 (s, *m*, 6C, Sn**Ph**$_3$, d, satellite, $^{3}J_{(Sn-C)}$ = 33.5 Hz); 126.80 (s, *p*, 3C, Sn**Ph**$_3$); 39.04 (d, 3C, Cy); 30.78 (s, 3C, Cy); 29.47 (s, 3C, Cy); 27.34 (d, 3C, Cy, $J_{(P-C)}$ = 9.0); 27.00 (d, 3C, Cy); 26.42 (s, 3C, Cy). Elemental analysis: Calculated for $C_{45}H_{53}OPFeSn$: C, 63.37; H, 6.74%. Found: C, 63.03; H, 6.87%. IR ($CHCl_3$ solution): ν_{CO} 1893.6 cm^{-1}.

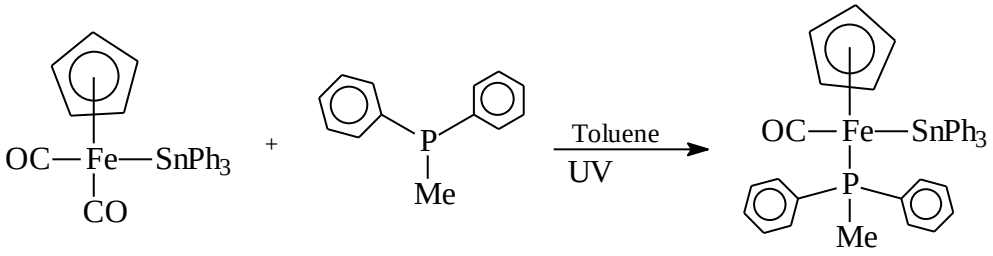
5.3.7 Preparation of [Fe(Cp)(CO){P(NMe$_2$)$_3$}(SnPh$_3$)]…… (**7**)



Compound (**7**) was prepared using the same procedure as for (**2**). A pale yellow solution of [Fe(CO)$_2$(Cp)(SnPh$_3$)] (**1**) (50 mg = 0.095 mmol) and an excess of tris(dimethylamino)phosphine (10 drops) in toluene (10 ml) was charged into a Schlenk tube and irradiated using a UV light accompanied by constant stirring overnight. An IR measurement (ν_{CO} = 1899.9) was recorded to determine the progress of reaction. After ca. 20 hrs the solvent was removed *in vacuo* from the resulting orange solution and the product extracted with dichloromethane (3 ml) from which the precipitates were separated by centrifuge. The orange solution was concentrated to ca. 1 ml before drop-wise addition of *n*-hexane (20 drops) to effect crystallisation. The light orange powder was washed with hexane (2 x 2ml) to give a yield of 65 mg (95%). Good quality crystals for X-ray work were obtained from CH_2Cl_2/n-hexane solution at temperatures below 5 ºC. NMR spectra were recorded from a solution in $CDCl_3$ at 300 K. ^{1}H NMR ($\delta_{(ppm)}$): 7.60 (m, 6H, Sn**Ph**$_3$); 7.24(m, 9H, Sn**Ph**$_3$); 4.6 (s, 5H, Cp); 2.41 (d, Me, 18H, $^{1}J_{(P-H)}$ = 9.2 Hz). ^{13}C NMR ($\delta_{(ppm)}$): 222.09 (s, 1C, CO, $^{2}J_{(P-C)}$); 148 (s, 3C, *ipso*, Sn**Ph**$_3$); 137.39 (s, *o*, 6C, Sn**Ph**$_3$, d, satellite, $^{2}J_{(Sn-C)}$) = 31.3 Hz); 127.30 (s, *m*, 6C, Sn**Ph**$_3$), d, satellite, $^{3}J_{(Sn-C)}$ = 34.0 Hz); 126.74 (s, 3C, *p*, Sn**Ph**$_3$) 79.22 (s, 5C, Cp); 39.00 (d, 6C, Me, $^{2}J_{(P-C)}$ = 4.2 Hz). Elemental analysis: Calculated for $C_{30}H_{38}ON_3PFeSn$: C, 54.40; H, 5.79%. Found: C, 54.44; H, 5.89%. IR ($CHCl_3$ solution): ν_{CO} 1899.9 cm^{-1}.

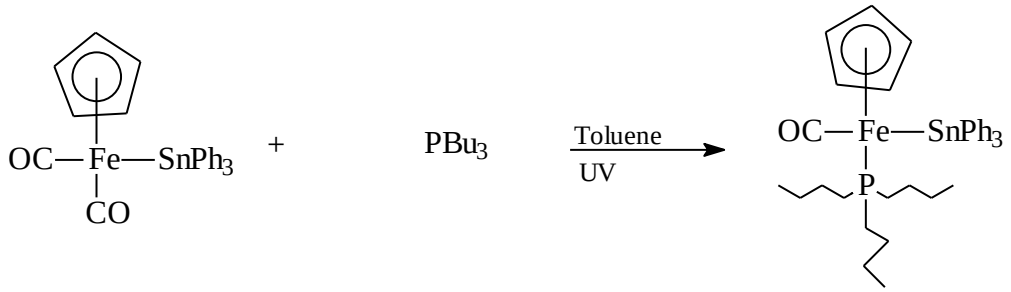
5.3.8 Preparation of [Fe(Cp)(CO)($PMePh_2$)($SnPh_3$)]……. (**8**)

Compound (**8**) was prepared using the same procedure as for (**2**). A pale yellow solution of



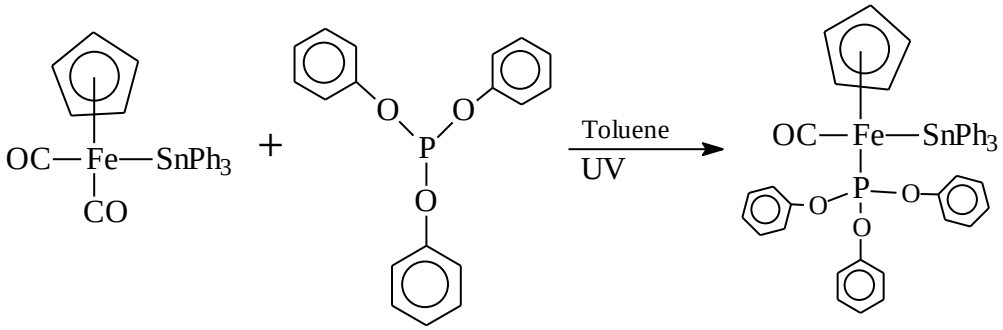
[Fe(Cp)$(CO)_2$($SnPh_3$)] (**1**) 50 mg ~ 0.095 mmol) and an excess of diphenylmethylphosphine (4 drops) in toluene (10 ml) was irradiated using a UV light overnight in a sealed Schlenk tube with constant stirring. After ca. 19 hrs, the solvent was removed *in vacuo* from the resulting orange coloured solution and the product extracted with dichloromethane (3 ml). The precipitates were separated and the solution was concentrated to ca. 1 ml before n-hexane (~20 drops) was added drop-wise to effect crystallisation. The solution was left to crystallise at low temperature (ca. –5 ^{0}C) to give red and orange crystals (which gave identical NMR data) with the combined yield of 54 mg (70%). NMR spectra were recorded from a solution in $CDCl_3$ at 300 K. ^{1}H NMR ($\delta_{(ppm)}$): 7.24 (m, 25H, Sn<u>Ph</u>$_3$/PMe<u>Ph</u>$_2$); 4.36 (s, 5H, Cp); 1.40 (d, Me, 3H, $^1J_{(P-H)}$ = 8.4 Hz). ^{13}C NMR ($\delta_{(ppm)}$): 219.29 (d, 1C, <u>C</u>O, $^1J_{(C-P)}$ = 29.1 Hz); 147.32 (s, ipso, 3C, $SnPh_3$); 141.97 (d, *ipso*, 2C, PMe<u>Ph</u>$_2$, $^1J_{(P-C)}$ = 40.0 Hz); 138,58 (d, 2C, *ipso*, PMe<u>Ph</u>$_2$, $^1J_{(C-P)}$ = 40.9 Hz); 137.24 (s, *o*, 6C, Sn<u>Ph</u>$_3$, d, satellite, $^2J_{(Sn-C)}$ = 33.0 Hz); 131.69 (d, *o*, 2C, PMe<u>Ph</u>, $^2J_{(P-C)}$ = 9.9 Hz); 131.09 (d, *m*, 2C, PMe<u>Ph</u>, $^3J_{(P-C)}$ = 9.9 Hz); 129.8 (s, *p*, 1C, PMe<u>Ph</u>); 129.15 (s, *p*, 1C, PMe<u>Ph</u>); 128.8 (d, *m*, 2C, PMe<u>Ph</u>, $J_{(P-C)}$ = 9.3 Hz); 128.15 (d, *m*, 2C, PMe<u>Ph</u>, $^3J_{(P-C)}$ = 9.3 Hz); 127.56 (s, *m*, 6C, $SnPh_3$, d, satellite, $^3J_{(Sn-C)}$ = 36 Hz); 127.06 (s, *p*, 3C, Sn<u>Ph</u>$_3$); 80.91 (s, 5C, Cp); 19.60 (d, 1C, Me, $J_{(P-C)}$ = 34.1 Hz). Elemental analysis: Calculated for $C_{37}H_{33}OPFeSn$: C, 63.55; H, 4.84%. Found: C, 63.20; H, 4.84%. IR ($CHCl_3$ solution): ν_{CO} = 1906.9 cm-1.

5.3.9 Preparation of [Fe(CO)(Cp)(PBu$_3$)(SnPh$_3$)]…… (**9**)



Compound (**9**) was prepared using the same procedure as for (**2**). A pale yellow solution of [Fe(CO)$_2$(SnPh$_3$)] (**1**) (53 mg = 0.101 mmol) and an excess (~ 50%) of tris-n-butylphosphine (two drops) in toluene (10 ml) was prepared in a Schlenk tube and irradiated using UV light overnight under constant stirring. After ca. 19 hrs, the solvent was removed *in vacuo* from the resulting orange solution and the product extracted with dichloromethane (2 ml). The dark orange solution was concentrated to ca. 1 ml before addition of hexane (1 ml) to effect crystallisation. However, no crystals formed and the hexane/dichloromethane mixture was evaporated using a gentle flow of nitrogen and the supernatant solution redissolved in hexane (2 ml). The solution was concentrated until orange crystals started forming to give a yield of 61 mg (87%). NMR spectra were recorded from a solution in C_6D_6 at 300 K. ^{1}H NMR ($\delta_{(ppm)}$): 7.91(m, 6H, Sn<u>Ph</u>$_3$); 7.23(m, 9H, Sn<u>Ph</u>$_3$); 4.31 (s, 5H, Cp); 0.75.1-1.41 (m, 18H, Bu); ^{13}C NMR ($\delta_{(ppm)}$): 219.81 (d, 1C, <u>C</u>O); 148. 21 (s, *ipso*, 3C, Sn<u>Ph</u>$_3$); 137.26 (s, *o*, 6C, Sn<u>Ph</u>$_3$, d, satellite, $^2J_{(Sn-C)}$ = 32.1 Hz); 127.62 (s, *m*, 6C, Sn<u>Ph</u>$_3$, d, satellite, $J_{(Sn-C)}$ = 34.6 Hz); 127.02 (s, *p*, 3C, Sn<u>Ph</u>$_3$); 79.15 (s, 5C, Cp); 30.40 (d, α, 3C, Bu, $^1J_{(P-C)}$ = 25.4 Hz); 26.02 (s, 3C, Bu); 24.19 (d, β, Bu, $^2J_{(P-C)}$ = 12.4 Hz); 13.71 (s, 3C, Bu). Elemental analysis: Calculated for $C_{36}H_{47}OPFeSn$: C, 61.65; H, 6.75%. Found: C, 60.83; H, 6.91%. IR ($CHCl_3$ solution): ν_{CO} = 1905.3 cm^{-1}.

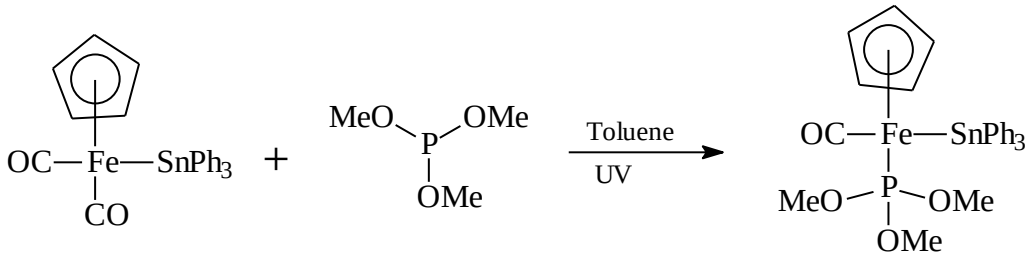
5.3.10 Preparation of [Fe(CO)(Cp){P(OPh$_3$)}(SnPh$_3$)]…….….. (**10**)



Compound (**10**) was prepared using the same procedure as for (**2**). A pale yellow solution of [Fe(CO)$_2$Cp)(SnPh$_3$)] (**1**) (53 mg, 0.106 mmol) and triphenylphosphite (3 drops from pipette) in toluene (10 ml) was charged into a Schlenk tube and irradiated using a UV light overnight with constant stirring. After 16 hrs the solvent toluene was removed *in vacuo* from the resulting light orange solution and the product extracted with dichloromethane (2 ml). The solution was concentrated to ca. 1 ml before drop-wise addition of hexane (1 ml) to effect crystallisation. However no crystals formed and the hexane/dichloromethane mixture was evaporated under a stream of nitrogen before re-dissolving and concentrating in toluene (1 ml) to give yellow crystals overnight at room temperature (56 mg, 62%). NMR spectra were recorded from a solution in $CDCl_3$ at 300 K. ^{1}H NMR ($\delta_{(ppm)}$): ^{1}H NMR ($\delta_{(ppm)}$): 7.66(m, 6H, Sn<u>Ph</u>$_3$); 7.25-7.07 (m, 18H, Sn<u>Ph</u>$_3$/P(O<u>Ph</u>)$_3$); 6.79-6.77 (m, 6H, Sn<u>Ph</u>$_3$/P(O<u>Ph</u>)$_3$); 4.25 (s, 5H, Cp). ^{13}C NMR ($\delta_{(ppm)}$): 216.86 (d, 1C, <u>C</u>O, $^2J_{C\text{-}P}$= 40.6 Hz); 151.74 (d, *ipso*, 3C, P(O<u>Ph</u>)$_3$, $^1J_{C\text{-}P}$ = 10.56 Hz); 146.65 (s, *ipso*, 3C, Sn<u>Ph</u>$_3$); 137.29 (s, *o*, 6C, Sn<u>Ph</u>$_3$, d, satellite, $^2J_{(Sn\text{-}C)}$ = 33.9 Hz); 129.34 (s, *o*, 6C, P(O<u>Ph</u>)$_3$); 127.74 (s, *m*, 6C, Sn<u>Ph</u>$_3$, d, satellite, $^3J_{(Sn\text{-}C)}$ = 39 Hz), 127.27 (s, *p*, 3C, Sn<u>Ph</u>$_3$); 124.44 (s, *p*, 3C, P(O<u>Ph</u>)$_3$); 121.40 (d, *m*, 6C, P(O<u>Ph</u>)$_3$, $^3J_{(P\text{-}C)}$ = 6.9 Hz); 80.166 (s, 5C, Cp). Elemental analysis: Calculated for $C_{42}H_{35}O_4PFeSn$: C, 62.33; H, 4.36%. Found: C, 62.38; H, 4.47%. IR ($CHCl_3$ solution): ν_{CO} 1935.7 cm^{-1}.

5.3.11 Preparation of [Fe(CO)(Cp)(P(OMe)$_3$(SnPh$_3$)] …… (<u>11</u>)

Compound (**11**) was prepared using the same procedure as for (**2**). A pale yellow solution of

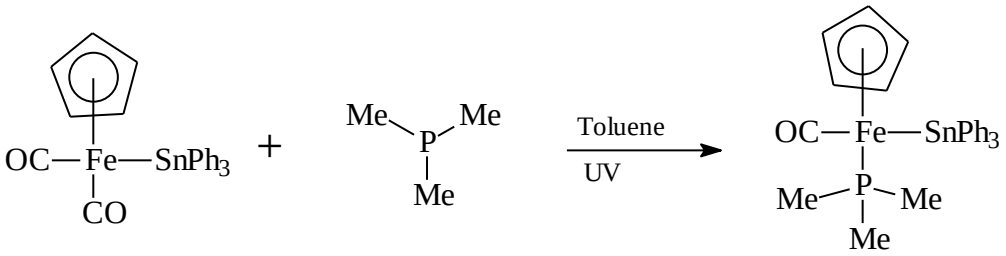


[Fe(Cp)(CO)$_2$(SnPh$_3$)] (**1**) (53 mg, ca. 0.106 mmol) and trimethyl phophite (1 drop ~10 mg) in toluene (10 ml) in a sealed Schlenk tube was irradiated using a UV light overnight (ca. 19 hrs) with constant stirring. The solvent was removed *in vacuo* from the resulting light orange solution and the product extracted with approximately 2 ml of dichloromethane and concentrated to ca. 1 ml before addition of hexane (1 ml) to effect crystallisation at –5 ^{0}C overnight. A bright yellow

microcrystallline powder was obtained and was washed with hexane (2 x 2 ml) and dried under a steady flow of nitrogen to give yield of 19 mg (30.5%). NMR spectra were recorded from a solution in $CDCl_3$ at 300 K. ^1H NMR ($\delta_{(ppm)}$): 7.59(m, 6H, $SnPh_3$); 7.25(m, 9H, $Sn\underline{Ph}_3$); 4.56 (d, 5H, Cp, $J_{(P-H)}$ = 0.6 Hz); 3.39 (d, 9H, O$\underline{Me}$, $J_{(P-H)}$ = 11.37 Hz). ^{13}C NMR ($\delta_{(ppm)}$): 217.47 (d, 1C, $\underline{C}O$, $^2J_{(P-C)}$ = 41.55 Hz); 147.52 (s, *ipso*, 3C, $Sn\underline{Ph}_3$); 137.14 (s, *o*, 6C, $Sn\underline{Ph}_3$, d, satellite, $^2J_{(Sn-C,)}$ = 33.7 Hz); 127.48 (s, *m*, 6C, $Sn\underline{Ph}_3$, d, satellite, $^3J_{(Sn-C,)}$ = 38.1 Hz); 127.02 (s, *p*, 3C, $Sn\underline{Ph}_3$); 79.79 (s, 5C,Cp); 52.10 (d, 3C, POMe, $^2J_{(P-C)}$ = 6.1 Hz). Elemental analysis: Calculated for $C_{27}H_{29}O_4PFeSn$: C, 52.21; H, 4.70%. Found: C, 51.94; H, 5.03%. IR ($CHCl_3$ solution), ν_{CO} = 1922.2 cm^{-1}.

5.3.12 Preparation of $[Fe(CO)Cp)(PMe_3)(SnPh_3)]$ …….…… (**12**)

Compound (**12**) was prepared using the same procedure as for (**2**). A pale yellow solution of

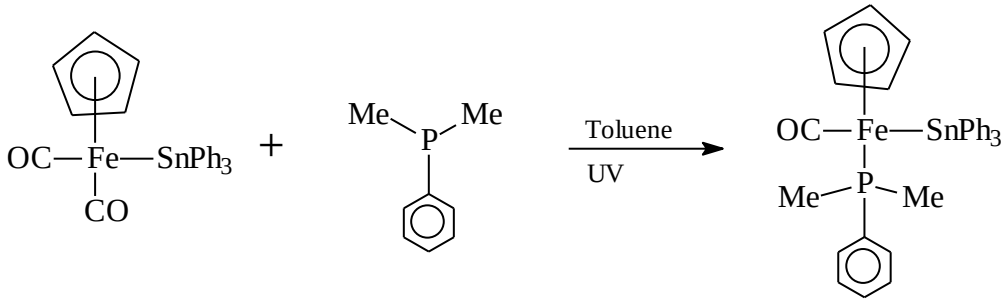


$[Fe(Cp)(CO)_2(SnPh_3)]$ (**1**) (67 mg ~ 0.127 mmol) and triemethyl phosphine (7,6 mg ~ 0.127 mmol) in toluene (10 ml) was prepared in a Schlenk tube and irradiated using a UV light overnight (15 hrs) constant stirring. A solution IR spectrum (ν_{CO} = 1903.3) was recorded to determine the progress of the reaction. The solvent was then removed *in vacuo* from the resulting orange solution and the product crystallized from toluene after separating the precipitates by centrifuge. After washing with hexane, the small micro-crystals lost crystallinity by forming lumps which were dried under a steady flow of nitrogen gas. The yellow lumps gave a yield of 34 mg (59%). NMR spectra were recorded from a solution in $CDCl_3$ at 300 K. ^1H NMR ($\delta_{(ppm)}$): 7.59 (m, 6H, $Sn\underline{Ph}_3$); 7.25(m, 9H, $Sn\underline{Ph}_3$); 4.47 9 (s, 5H, Cp); 1.24 (d, 9H, Me_3, $^2J_{(P-H)}$ = 9.00 Hz). ^{13}C NMR ($\delta_{(ppm)}$): 218.91 (d, 1C, $\underline{C}O$, $^2J_{(P-C)}$ = 30.08 Hz); 147.68 (s, *ipso*, 3C, $Sn\underline{Ph}_3$); 137.22 (d, *o*, 6C, $^2J_{(Sn-C)}$ = 33.00 Hz); 127.74 (s, *m*, 6C, $Sn\underline{Ph}_3$); 127.13 (s, *p*, 3C, $Sn\underline{Ph}_3$); 79.49 (s, 5C, Cp); 23.21 (d, 3C, Me_3, $^1J_{C-P}$ = 29.68 Hz). Elemental analysis: Calculated for

$C_{27}H_{29}OPFeSn$: C, 56.39; H, 5.08%. Found: C, 56.39; H, 5.09%. IR ($CHCl_3$ solution): ν_{CO} = 1903.3 cm^{-1}.

5.3.13 Preparation of [Fe(CO)(Cp)(PMe_2Ph)($SnPh_3$)]…… (**13**)

Compound (**13**) was prepared using the same procedure as for (**2**). A pale yellow solution of

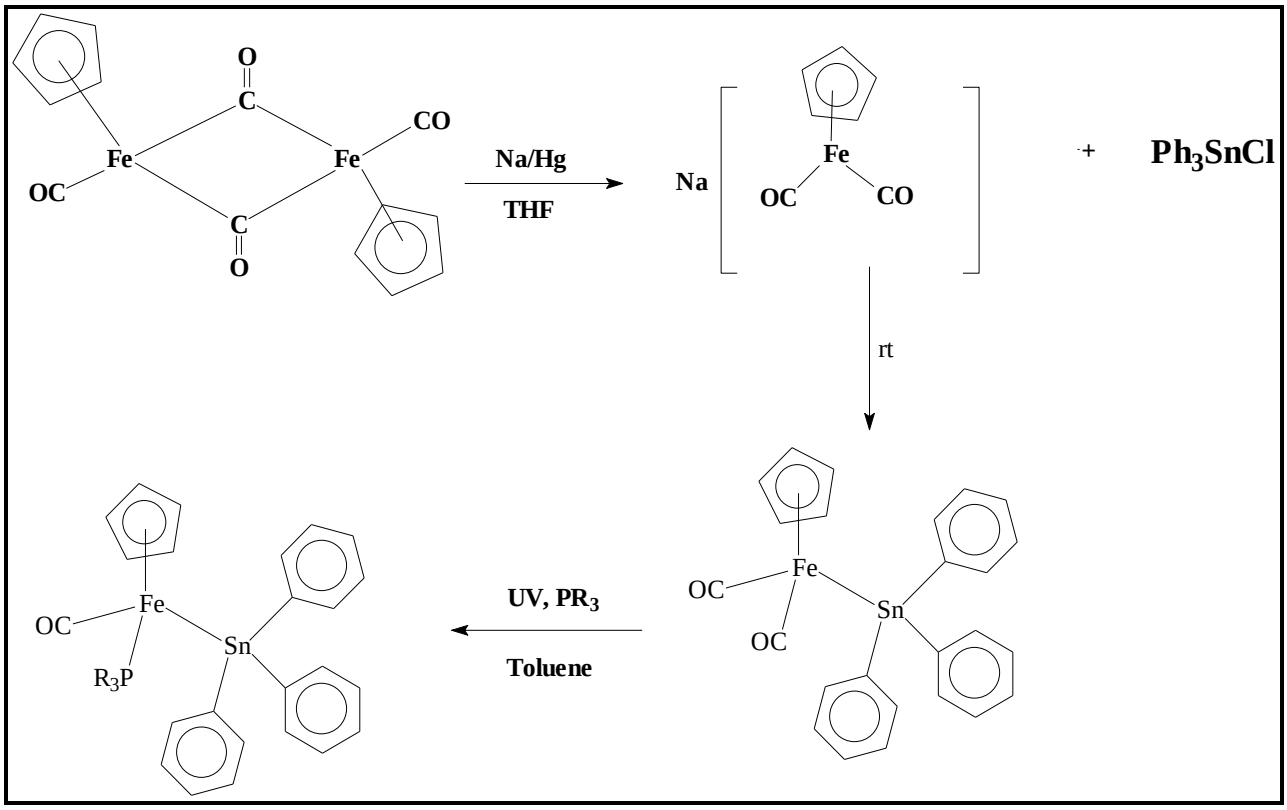


[Fe(Cp)$(CO)_2$($SnPh_3$)] (**1**) (60 mg ~ 0.114 mmol) and dimethylphenyl phosphine (15.7 mg ~ 0.114 mmol) in toluene (10 ml) was prepared in a Schlenk tube and irradiated using a UV light overnight (ca. 16 hrs) with constant stirring. A solution IR measurement (ν_{CO} = 1903.2) was recorded to determine the progress of reaction before the solvent was removed. The solvent was removed *in vacuo* from the resulting orange solution to give a sticky red-orange product which showed some signs of decomposition in dichloromethane. NMR spectra were recorded from a solution in $CDCl_3$ at 300 K. ^{1}H NMR ($\delta_{(ppm)}$): 7.50-7.07 (m, 20H, Ph_3); 4.19 (s, 5H, Cp); 1.50 (d, 3H, Me, $^2J_{(P-H)}$ = 8.7 Hz); 1.20 (d, 3H, Me, $^2J_{(P-H)}$ = 8.8 Hz). ^{13}C NMR ($\delta_{(ppm)}$): 219.25 (d, CO, $^2J_{(C-P)}$ = 29.08 Hz); 147.54 (s, *ipso*, 3C, Sn<u>Ph</u>$_3$, d, satellite, $^1J_{(Sn-C)}$ = 252.9 Hz); 143.62 (d, *ipso*, 1C, PMe_2<u>Ph</u>, $^1J_{(P-C)}$ = 39.1 Hz); 137.08 (s, *o*, 6C, Sn<u>Ph</u>$_3$, satellite, $^2J_{(Sn-C)}$ = 32.9 Hz); 129.25(d, *o*, 2C, PMe_2<u>Ph</u>, $^2J_{(P-C)}$ = 9.2 Hz); 128.88 (d, *m*, 2C, PMe_2<u>Ph</u>, $^3J_{(P-C)}$ = 8.4 Hz); 128.20 (s, *m*, 6C, Sn<u>Ph</u>$_3$, d, satellite, $^3J_{(Sn-C)}$ = 35.3 Hz); 127.63 (s, *p*, 3C, Sn<u>Ph</u>$_3$); 125.74 (s, *p*, 1C, PMe_2<u>Ph</u>); 80.25 (s, 5C, Cp); 21.30 (d, 2C, PMe_2Ph, $J_{(P-C)}$ = 22.1 Hz). IR ($CHCl_3$ solution): ν_{CO} 1903.2 cm^{-1}.

5.4 Results and discussion

The direct metal-metal bonded complex [η^5-$C_5H_5Fe(CO)_2(SnPh_3)$] (**1**) [9f] is obtained by ionic reaction between Na[η^5-$C_5H_5Fe(CO)_2$] [16] and Ph_3SnCl in THF as stable (in air) bright yellow needles in good yield. Heterobimetallic complexes of the general formula [η^5-$C_5H_5Fe(CO)(PR_3)$-$SnPh_3$] (R_3 = Me_3, Ph_3, $MePh_2$, Me_2Ph, Bu_3, Cy_3, {*p*-$OMeC_6H_4$}$_3$, {*p*-tolyl}$_3$, {*p*-FC_6H_4}$_3$, {NMe_2}$_3$, {OMe}$_3$ and {OPh}$_3$) (**2**-**13**) were obtained in moderate to good yield as yellow to orange-red crystals by UV irradiation of [η^5-$C_5H_5Fe(CO)_2(SnPh_3)$] and the corresponding phosphine or phosphite in toluene. Irradiation period ranged from 14 – 19 hrs at room temperatures [9a] (**Scheme 5.1**). With respect to product isolation the exceptions in this series of complexes are the tributylphosphine substituted complex (**9**) which crystallized from n-hexane solution and the triphenylphosphite complex (**10**) from toluene/n-hexane solution.

It must be noted that another feasible method of obtaining these monocarbonylated Fe-Sn complexes could make use of decarbonylating agents such as Me_3NO [17]. However the use of other decarbonylating agents was not attempted due to the success of the simpler and (in this case) cleaner photochemical reaction. We have isolated only the expected heterobimetallic complexes of the type [$CpFe(CO)(PR_3)(SnPh_3)$] (**2** – **13**) in yields ranging from 30 – 95% under stoichiometric conditions despite to the generally accepted potential problem of product distribution from photochemical reactions [18]. The isolated compounds were invariably stored under the atmosphere of nitrogen at ca. -10 ºC. There were no signs of decomposition under these storage conditions for several months. However in chloroform solution after three days at 300 K, the complexes showed signs of decomposition (possibly as a result of reaction with the solvent induced by traces of oxygen), visible in the ^{31}P NMR spectrum. No comprehensive study on the stability of these iron-tin complexes in solution was carried as part of the present study. All complexes were characterised in solution by IR and multinuclear (^{1}H, ^{13}C, ^{31}P, ^{57}Fe and ^{119}Sn) NMR spectroscopy (**Table 5.3 and 5.4**).



Scheme 5.1 General synthetic route to bimetallic complexes of iron and tin.

The importance of using stoichiometric quantities of the phosphine or phosphite ligands was demonstrated by the isolation of mixtures of the monosubstituted (**10**, **11**, **12** and **13**) and disubstituted (decarbonylated) bimetallic iron-tin complexes, to be discussed in Chapter 6. An interesting phenomenon occurs with synthesis of compound **12** (PR_3 = PMe_3) which seems to defy the stoichiometric conditions by favouring the formation of a disubstituted phosphine complex accompanied by complete loss of carbonyls in the presence of excess starting material **1**, which suggests a lower energy barrier towards disubstitution upon monosubstitution. The duration of exposure of the reagents to the UV light seems to determine the extent of substitution wherein the disubstituted decarbonylated Fe - Sn complex is isolated after 6 hrs of exposure in the presence of excess complex **1**. X-ray quality crystals of **12** proved difficult to obtain because very often only the disubstituted complex was isolated (as orange crystals) instead of the yellow-orange micro-crystals or solid lumps of compound **12**. The experimental details and discussion of the disubstituted complexes of the type [$CpFe(PR_3)_2$-$SnPh_3$] will be discussed in Chapter 6.

5.4.1 NMR spectroscopy

NMR spectroscopic results for the hetero-bimetallic complexes of the general type [$CpFe(PR_3)_2$-$SnPh_3$] are given in **Table 5.2** together with Tolman's electronic and steric parameters and IR (ν_{CO}) values. The chemical shift of the hydrogens of the Cp for all complexes **2** - **13** appear between 4.1 – 4.6 ppm and their corresponding $^3J_{(P-H)}$ ranges between 0.7 – 2 Hz. Chemical shifts of the hydrogens of the Cp ring are indicated in **Table 5.3** and $^3J_{(P-H)}$ for the Cp hydrogens of some the complexes is indicated in **Table 5.4**. However the coupling range of 0.7 – 1.9 Hz is rather too small to be able to make any predictive conclusions. The chemical shift positions of -OMe (**4** and **11**, δ = 3.75 and 3.39 ppm respectively) are expectedly higher than those of the -Me groups (**5**, **7**, **8**, **12** and **13**, δ = 2.28, 2.41, 1.40, 1.24 and 1.35 ppm respectively) with the corresponding J_{P-H} ranging between 8.4 – 11.4 Hz.

The NMR ^{13}C chemical shift trend of the carbonyl group seems to be insensitive with respect to the type of phosphine/phosphite ligand but rather increases as the cone angle increases (**Table 5.2** and **5.3**). A rather interesting observation to note is a very pronounced $^3J_{(P-H)}$ of 11.3 Hz for (**11**) larger than $^2J_{P-H}$, observed in the series and that the spin coupling is through an oxygen atom (**Figure 5.1 a**). The values of $^3J_{(P-H)}$ which shows angular dihedral dependence (Karplus relationship), have been noted for systems containing P-C-C-H [19], P-O-C-H [20], P-N-C-H [21] and P-S-C-H [22]. Thus, in the tricovalent phosphorus compounds such as phosphines and phosphites the value of $^3J_{(P-H)}$ can be dependent on the orientation of the lone pair or the position of the metal in the event of ligation, in which case higher coupling interactions are a results of hydrogens that are positioned *syn* to the metal complex [23]. Based on these literature findings and the molecular structure determination from the X-ray diffraction analysis (see **Figure 5.6**) we can confidently assign the position of iron as syn to the hydrogens of the $P(OCH_3)_3$ ligand in solution on the NMR time scale.

Table 5.2 A list of Tolman's parameters, experimental yields and IR values in $CHCl_3$ solution of complexes of the type $[CpFe(CO)(PR_3)(SnPh_3)]$.

Compound	Ligand $P(R)_3$	Tolman's steric parameter $(\theta)^a$	Tolman's Electronic Parameter $(cm^{-1})^a$	Solution IR ν_{CO} $(cm^{-1})^b$	Yield (%)
2	$P(Ph)_3$	145	2068.9	1908.2	75
3	$P(p\text{-}FC_6H_4)_3$	145	2071.3	1908.7	57
4	$P(p\text{-}OMeC_6H_4)_3$	145	2066.1	1902.7	87
5	$P(p\text{-tolyl})_3$	145	2066.7	1904.3	63
6	$P(Cy)_3$	170	2056.4	1893.6	60
7	$P(NMe_2)_3$	159	2061.9	1899.9	95
8	$P(MePh_2)$	136	2067.0	1906.9	70
9	$P(Bu)_3$	132	2060.3	1905.3	87
10	$P(OPh)_3$	128	2085.3	1935.7	62
11	$P(OMe)_3$	107	2079.5	1922.2	31
12	$P(Me)_3$	118	2064.1	1903.3	59
13	$P(Me_2Ph)$	122	2065.3	1903.2	57

[a] Values obtained from ref. [6]. [b] All IR (ν_{co}) spectra were recorded in $CHCl_3$ solution.

Table 5.3 shows NMR chemical shift data of the significant groups in addition to the data provided in the experimental section. Results of different spin-coupling interactions within the system $[CpFe(CO)(PR_3)(SnPh_3)]$ are given in **Table 5.4**.

Table 5.3. NMR data for the heterobimetallic iron-tin complex, [Fe(Cp)(CO)(PR_3)($SnPh_3$)].

Compound[a]	Ligand (PR_3)	$\delta(^1H)$ (Cp) (ppm)	$\delta(^{13}CO)$ (ppm)	$\delta(^{31}P)$ (ppm)	$\delta(^{57}Fe)$ (ppm)	$\delta(^{119}Sn)$ (ppm)
2	$P(Ph)_3$	4.34 (d)	220.5	75.3	637.3	9.3
3	$P(p\text{-}FC_6H_4)_3$	4.27 (s)	220.6	74.6	599.2	10.3
4	$P(p\text{-}OMeC_6H_4)_3$	4.33 (d)	220.8	70.1	658.7	9.8
5	$P(p\text{-tolyl})_3$	4.31 (d)	220.7	72.6	646.4	10.4
6	$P(Cy)_3$	4.62 (d)	222.0	74.2	843.6	6.0
7	$P(NMe_2)_3$	4.60 (s)	222.1	171.6	692.4	17.8
8	$PMePh_2$	4.36 (d)	219.3	56.8	499.3	32.8
9	$P(Bu)_3$[b]	4.31 (s)	219.8	50.5	520.5	34.2
10	$P(OPh)_3$	4.25 (s)	216.8	171.1	439.7	46.6
11	$P(OMe)_3$	4.56 (d)	217.5	185.4	302.0	47.7
12	$P(Me)_3$	4.47 (s)	218.9	29.1	432.9	46.7
13	PMe_2Ph	4.19 (s)	219.2	40.2	477.6	44.1

S = singulet, d = doublet, dd = doublet-of-doublet and m = multiplet. All spectra were recorded in $CDCl_3$ solution at 300 K. [b] Recorded in C_6D_6 solution at 300 K.

The values of $\delta(^{31}P)$ of all the Fe – Sn complexes under study were characteristic of phosphine and phosphite ligands within the coordination sphere of transition metals i.e. the phosphorus of phosphites resonating at higher frequencies than phosphines [24]. The ^{31}P chemical shift of **7** {$PR_3 = P(NMe_2)_3$} as with $^1J_{(Fe\text{-}P)}$ and $^2J_{(P\text{-}CO)}$ compares very well with the phosphites (**10** and **11**) due to the deshielding effect of the electron withdrawing oxygen and nitrogen atoms. The ^{31}P NMR signal of [CpFe(CO)$P(p\text{-}FC_6H_4)_3$($SnPh_3$)] (**3**) shows $^5J_{(31P\text{-}19F)}$ (= 1.7 Hz) and a significant $^2J_{(^{31}P\text{-}^{119/117}Sn)}$ = 366 / 350 Hz (**Figure 5.1C)**. The ^{31}P signals for all complexes studied showed coupling to both ^{119}Sn and ^{117}Sn isotopes ranging from 534.6 - 330 and 510.5 - 315 Hz respectively (**Table 5.4**). An average value of 18 Hz is calculated for $^2J_{(^{119}Sn\text{-}^{31}P)}$ - $^2J_{(^{117}Sn\text{-}^{31}P)}$ which can be regarded as being within the limits of numerical accuracy for higher values of J. Therefore, the difference in this case can be rationalised by their different values of γ for ^{117}Sn and ^{119}Sn nuclei (see Chapter **2**, section **2.6.3**). The magnitude of $\delta(^{57}Fe)$ reflects both the electron-donating and electron-withdrawing capacities of the substituent on the phosphorus

atom. The trend by which ligands influence the chemical shift of the transition metals has been discussed in Chapter **2** (section 2.2.4) whereby the hard/soft or weak/strong properties of the ligands exert a profound influence on the *d* orbital radius (nephelauxetic effect) and the electronic excitation energy ΔE (HOMO-LUMO gap) of the metal [25].

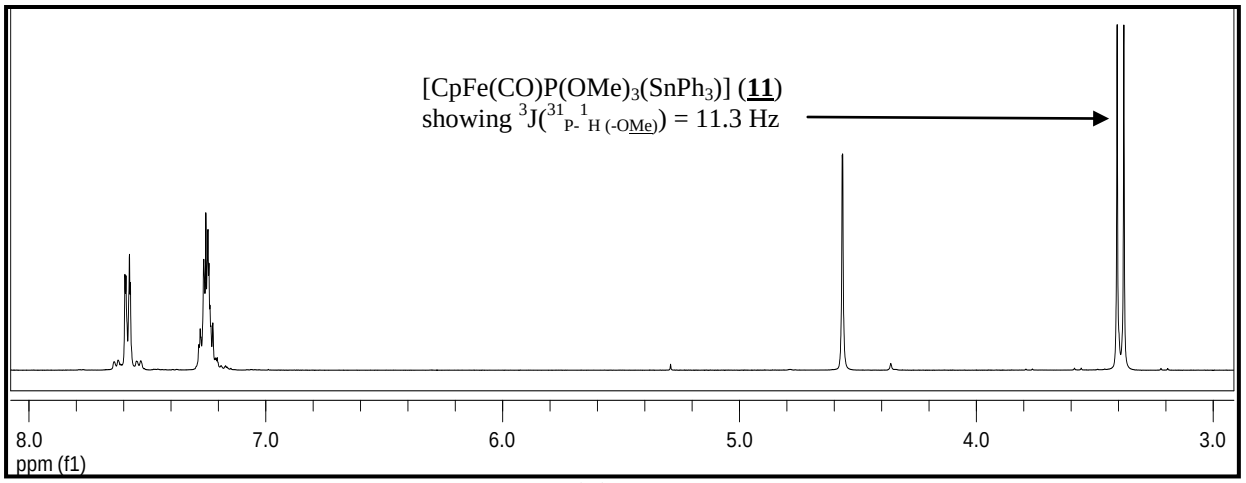
The ^{57}Fe chemical shifts of the phosphite complexes, **10** and **11** are relatively low compared to the corresponding phosphine complexes. Differences in the ^{57}Fe chemical shift between phosphine and phosphite complexes can be generally rationalised in terms of the weak or strong ligand field property whereby phosphites provide a stronger ligand field than phosphines leading to larger ΔE in the absence of steric influences, hence lower metal chemical shifts as was found in a ^{183}W NMR study of phosphine and phosphite of tungsten [26]. Therefore the trend towards lower $\delta(^{57}\text{Fe})$ of the phosphite complexes can be explained by the electron withdrawing capacity of the phosphorus's substituents which in the case of the phosphorus atom becoming a poorer σ donor, results in the reduction of electron density on the metal which leads to smaller repulsion between the *d* orbitals and a larger ΔE, therefore a decrease in the chemical shift. However the $\delta(^{57}\text{Fe})$ for complex **12** which falls in the same range as the phosphite complexes can be explained by the steric property, defined by cone angle θ as having a major influence. The $\delta(^{57}\text{Fe})$ range of about 542 ppm has been observed as testimony to the subtle NMR sensitivity to the changes in the coordination sphere of the transition metal centres. The influence of the electronic properties of the substituent groups on the phosphorus atom as reflected by the NMR chemical shifts of ^{13}C, ^{31}P, ^{57}Fe and ^{119}Sn show interesting trends which suggest the steric parameter has a major influence particularly on ^{57}Fe rather than on ^{13}C and ^{119}Sn (to be discussed detail in **section 5.5**).

Table 5.4 Coupling constants of the hetero-bimetallic Fe - Sn complexes of the type [CpFe(CO)(PR_3)($SnPh_3$)]

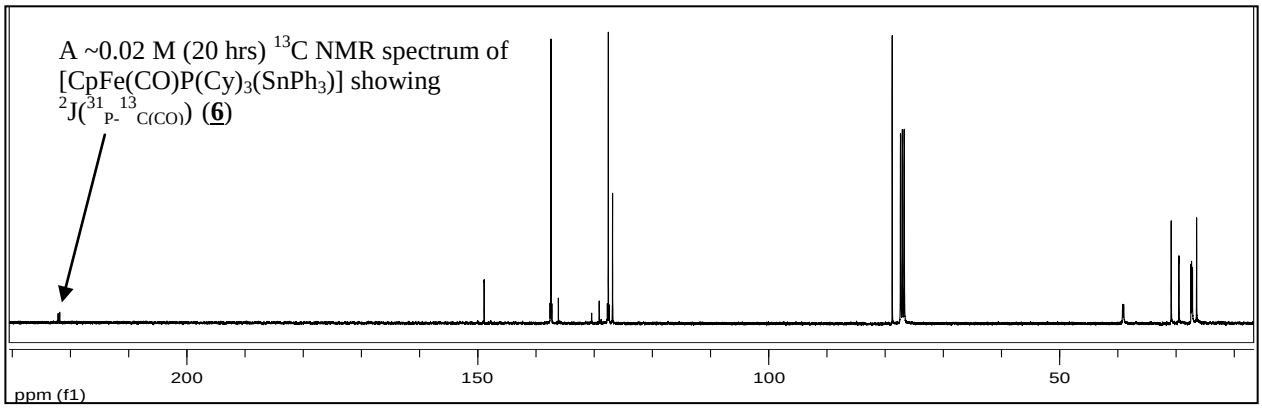
Compound	Ligand (PR_3)	$^1J_{(Fe-P)}$	$^2J_{(^{119}Sn-P)}$	$^2J_{(^{117}Sn-P)}$	$^2J_{(P-\underline{C}O)}$	$J_{(P-H, -Me)}$	$^3J_{(P-H,Cp)}$
2	$P(Ph)_3$	56.5	369	352	28.6		1.34
3	$P(p\text{-}FC_6H_4)_3$	55.9	366	350	29.1		
4	$P(p\text{-}OMeC_6H_4)_3$	55.9	378	361	29.3		1.43
5	$P(p\text{-tolyl})_3$	56.9	372	356	28.8		1.42
6	$P(Cy)_3$	55.0	330	316	27.0		0.95
7	$P(NMe_2)_3$	55.0	460	440	27.0	9.2[a]	
8	$P(MePh_2)$	55.0	387	369	29.1	8.4[a]	1.90
9	$P(Bu)_3$	53.7	391	373	28.8		
10	$P(OPh)_3$	102.7	496	474	40.6		
11	$P(OMe)_3$	92.1	535	510	41.5	11.3[b]	0.68
12	$P(Me)_3$	52.6	427	408	30.1	9.0[a]	
13	$P(Me_2Ph)$	53.7	506	484	29.1	8.7[a]	

[a] Refers to ^2J and [b] refers to ^3J in Hz.

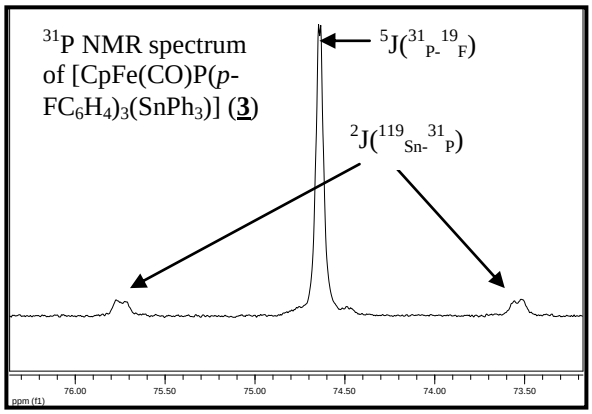
The highest $\delta(^{57}Fe)$ which reflects low shielding (i.e. a high frequency resonance) is found for compound **6** which has the highest cone angle size of 170 degrees and the lowest ν_{co}. Similarly the opposite applies to compound **11** which has the smallest cone angle size of 107 degrees and the lowest $\delta(^{57}Fe)$. This ligand effect in cyclopentadienyliron(II) complexes has been noticed for complexes of the type [CpFe(CO)(L)COMe] (where L is a phosphine ligand) [27], $[CpFe(CO)_2R]$ [28] and for other transition metal complexes where a series of such ligands were studied [29]. **Figure 5.2** shows two-dimensional spectra of $(^{57}Fe\text{-}^{31}P)\{^1H\}$ of selected complexes of the type [CpFe(CO)(PR_3)($SnPh_3$)] where the f2 dimension refers to the ^{31}P chemical shift scale and f1 refers to the ^{57}Fe chemical shift scale. The steric influence is discussed in greater details in section 5.5.1.



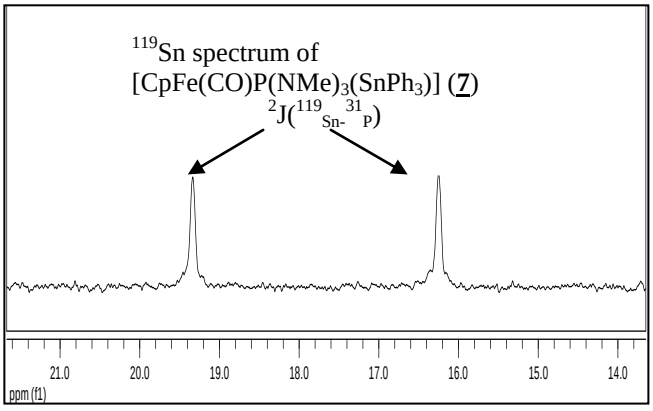
(A)



(B)



(C)



(D)

Figure 5.1 (a) ^{1}H spectrum of [CpFe(CO)P(OMe)$_3$(SnPh$_3$)] (**11**); (b) $^{13}C\{^{1}H\}$ spectrum of [CpFe(CO)P(Cy$_3$)(SnPh$_3$)] (**6**); (c) $^{31}P\{^{1}H\}$ spectrum of [CpFe(CO)P(p-FC$_6$H$_4$)$_3$(SnPh3)] (**3**); (d) $^{119}Sn\{^{1}H\}$ spectrum of [CpFe(CO)P(NMe$_2$)$_3$(SnPh$_3$)] (**7**) all in CDCl$_3$ at 300 K

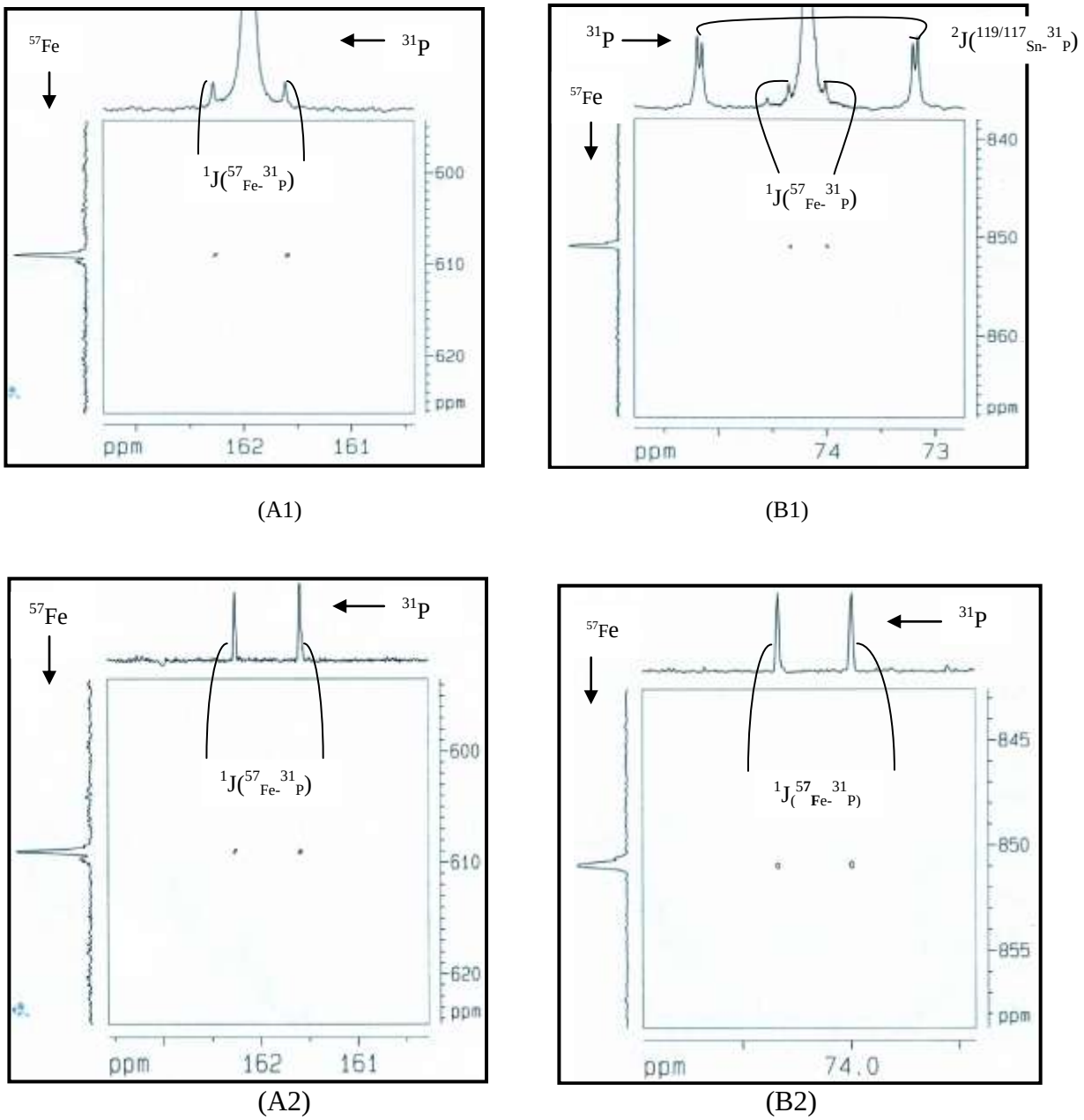


Figure 5.2 (^{57}Fe-^{31}P){^{1}H} spectrum of; (A) [CpFe(CO)P(OPh)$_3$(SnPh$_3$)] (**10**); (B) [CpFe(CO)P(Cy$_3$)(SnPh$_3$)] (**6**), in CDCl$_3$ at 300 K (in A1 and B1 the ^{31}P axis shows the 1D ^{31}P{1H} spectrum separately optimised and, in A2 and B2 the ^{31}P axis shows the internal projections).

5.4.2 X-Ray crystallographic study

The crystal structures of **3**, **5**, **6**, **7**, **8**, **9**, **10** and **11** are described and discussed here. The averaged selected inter-atomic distances and inter-bond angles are listed in **Table 5.5**. The ORTEP [30] and SCHAKAL [31] diagrams of complexes **3**, **5**, **6**, **7**, **8**, **9**, **10** and **11** showing the atomic numbering scheme and the overall stereochemistry of the selected hetero-bimetallic complexes of the monocarbonylated [CpFe(CO)(PR_3)($SnPh_3$)] are shown in **Figures 5.3 – 5.10.** The change from ORTEP to SCHAKAL diagrams has been done for clarity purposes only. Reviews on the structural aspects of transition metal – tin complexes have appeared in the literature [32]. The choice of complexes for structure analysis was guided by the potential influence of steric size (cone angle θ) on the structural properties of these compounds. Molecular structures of **9** and **11** complexes were analyzed and confirmed by X-ray at 173 K because of the loss of crystal lattice at room temperatures due to probable loss of solvent from cavities.

Table 5.5 Selected bond lengths and angles for compounds **3**, **5**, **6**, **7**, **8**, **9**, **10** and **11**[a].

Compound	Ligand (PR_3)	Crystal System	Fe-Sn (Å)	Fe-P (Å)	Fe-CO (Å)	Fe-C(Cp) (Å)	P-Fe-CO (θ)	P-Fe-Sn (θ)	Sn-Fe-CO (θ)
3	P(*p*-FC_6H_4)$_3$	Monoclinic	**2.5518(5)**	**2.198(9)**	**1.727(3)**	**2.105(3)**	**95.50(10)**	**98.56(3)**	**87.48(11)**
5	P(*p*-tolyl)$_3$	Monoclinic	**2.5532(5)**	**2.2032(8)**	**1.730(3)**	**2.104(3)**	**94.79(9)**	**98.67(2)**	**86.90(9)**
6	P(Cy)$_3$	Triclinic	**2.5569(9)**	**2.2681(14)**	**1.729(6)**	**2.100(9)**	**93.15(16)**	**99.80(4)**	**86.87(16)**
7	P(NMe_2)$_3$	Triclinic	**2.530(10)**	**2.2031(8)**	**1.720(9)**	**2.098(1)**	**96.09(6)**	**98.47(4)**	**85.71(5)**
8	P($MePh_2$)	Triclinic	**2.545(8)**	**2.195(7)**	**1.738(3)**	**2.099(4)**	**91.73(9)**	**94.13(2)**	**89.63(9)**
9	P(Bu)$_3$	Orthorhombic	**2.5196(9)**	**2.164(2)**	**1.752(7)**	**2.113(1)**	**91.1(3)**	**98.84(8)**	**89.0(2)**
10	P(OPh)$_3$	Triclinic	**2.5487(5)**	**2.107(8)**	**1.741(4)**	**2.091(3)**	**96.12(11)**	**91.70(3)**	**86.08(11)**
11	P(OMe)$_3$	Monoclinic	**2.523(6)**	**2.120(5)**	**1.745(3)**	**2.092(3)**	**91.07(10)**	**89.55(2)**	**88.12(11)**

[a] All phenyl rings were refined as rigid six-membered rings with average inter-atomic distance, d(C-C)=390 Å.

5.4.2.1 *Molecular geometry around the Iron atom.*

All the complexes assume a three legged "piano stool" geometry with the cyclopentadiene ring lying above the Fe atom, and P, CO and Sn atoms forming the legs. The geometry of these complexes can in simple terms be regarded as distorted octahedral (or tetrahedral) depending on the description of the π-bonding linkage to the cyclopentadienyl ring. The compounds studied in

the series exhibit three types of crystal systems, monoclinic (**11**, **5** and **3**), triclinic (**10**, **8**, **7** and **6**) and orthorhombic (**9**). There seems to be no relationship between the crystal system and the size of the cone angle among phosphine and phosphite complexes.

The following trend by the angles subtended at the iron atom is observed for all phosphine complexes: Sn-Fe-CO < P-Fe-CO < P-Fe-Sn. However the phosphite complexes (**10** and **11**) show a different trend whereby the same bond angles as in the phosphine complexes increase progressively on average as follows: Sn-Fe-CO < P-Fe-Sn < P-Fe-CO. There is perhaps a trend with regard to the bond lengths between Fe and the carbons of the Cp ring (Cp carbons have been arbitrarily labeled following a progressive trend of bond lengths) between phosphine and phosphite compounds which can be divided into possibly four averages (bond lengths which are closer within significant numerical accuracy limits of measurement). Phosphine complexes **3**, **5**, **6**, and **7** show at most three bond averages (see **Table 5.6**).

Table 5.6 Selected bond lengths of the Fe-C of the Cp ring for [CpFe(CO)PR_3($SnPh_3$)]

Compound	Ligand (PR_3)	Fe-C(Cp) (Å)	Fe-C1 [a] (Cp)	Fe-C2 [a] (Cp)	Fe-C3 [a] (Cp)	Fe-C4 [a] (Cp)	Fe-C5 [a] (Cp)
3	P(*p*-FC_6H_4)$_3$	**2.105(3)**	**2.096(3)**	**2.103(3)**	**2.106(3)**	**2.106(3)**	**2.114(3)**
5	P(*p*-tolyl)$_3$	**2.104(3)**	**2.097(3)**	**2.101(3)**	**2.105(3)**	**2.106(3)**	**2.111(3)**
6	P(Cy)$_3$	**2.100(9)**	**2.083(5)**	**2.092(5)**	**2.105(6)**	**2.108(5)**	**2.114(6)**
7	P(NMe_2)$_3$	**2.098(1)**	**2.081(3)**	**2.082(19)**	**2.103(7)**	**2.104(8)**	**2.118(7)**
8	P($MePh_2$)	**2.099(4)**	**2.089(3)**	**2.095(3)**	**2.100(3)**	**2.106(3)**	**2.107(3)**
9	P(Bu)$_3$	**2.113(1)**	**2.103(6)**	**2.112(7)**	**2.114(6)**	**2.114(7)**	**2.119(7)**
10	P(OPh)$_3$	**2.091(3)**	**2.079(3)**	**2.080(4)**	**2.094(3)**	**2.095(4)**	**2.107(3)**
11	P(OMe)$_3$	**2.092(3)**	**2.086(3)**	**2.090(3)**	**2.092(3)**	**2.096(3)**	**2.096(3)**

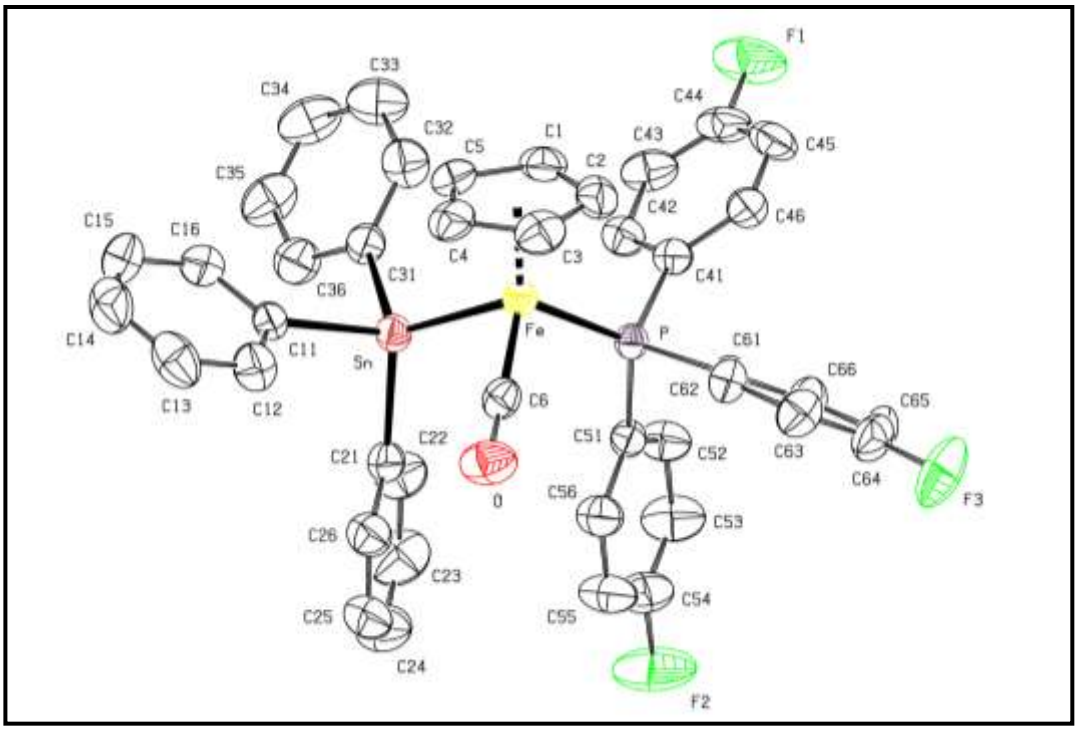
[a] Carbon labeling has been assigned arbitrarily following the trend in increasing value.

However, the Fe-C bond averages of the Cp ring for phosphite can at most be classified as having two distinct averages. This assertion does not necessarily suggests the tridentate coordination system of the Cp ring to the metal centre. If a single line is drawn from the iron atom to the centroid of the ring as may be the case for complexes **10** and **11** which have Fe-Cp bond average of 2.091(8) Å, an approximate tetrahedral arrangement results. Figures **5.3 – 5.10** show the overall structure representation and atomic numbering scheme for eight of the twelve

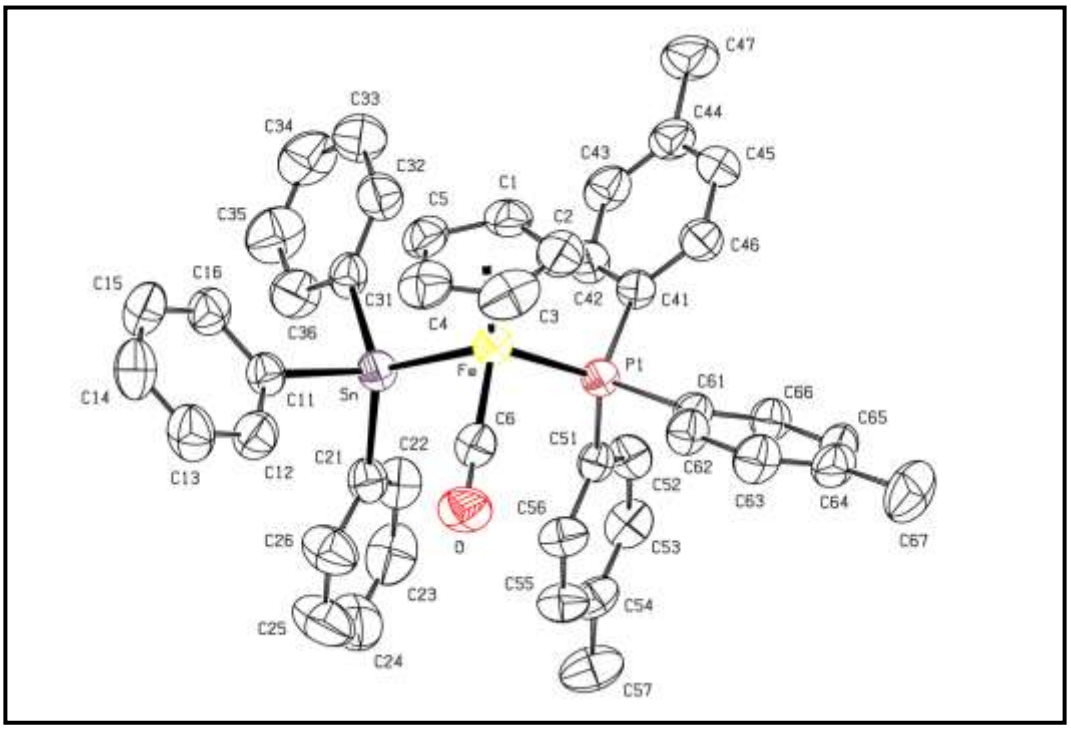
complexes synthesized. The C-C bond lengths in the Cp ring average 1.40(9) Å for both phosphine and phosphite complexes of [CpFe(CO)(PR_3)($SnPh_3$)], which is slightly larger than the corresponding mean value of 1.396(14)Å for [CpFe($CO)_2$($SnPh_3$)] **1** [34].

5.4.2.2 *The Iron-Tin interactions*.

The M-Sn bond interactions (where M is transition metal) have been rationalized as consisting of both σ and π components [1]. Differences in the π bonding character can arise as a result of changes in the substituent groups on the tin and this can influence the length of the transition metal-tin bond. The presence of highly electronegative substituents such as chlorides ($[SnCl_3]^-$) cause the loss of electron density from the tin atom, lowering the energy of its empty orbitals and thus enhancing iron's π-back bonding to the tin. As noted by Graham and co-workers [33], it has been customary to interpret bond shortening relative to single bond radii as indicative of multiple bond character. The Fe-Sn bond distances range from 2.5196(9) Å for [CpFe(CO)P($Bu)_3$($SnPh_3$)] (**9**) to 2.5569(9) Å for [CpFe(CO)P($Cy)_3$($SnPh_3$)] (**6**) and are similar to the dicarbonylated complex [CpFe($CO)_2SnPh_3$] (2.537 Å) [34]. The Fe-Sn bond distance seems to be shortened with [CpFe($CO)_2SnCl_3$] where a value of 2.466(2) Å is found [35]. This bond shortening is attributed to Sn in $[SnCl_3]^-$ group as being poor σ donor and good π acceptor. It has also been noted that a change from $[SnMe_3]^-$ to $[SnPh_3]^-$ does not yield any significant change in Fe-Sn bond distance due to the similarities of these Sn atoms as σ donors and π acceptors with these substituents. In the case of our study of the influence of phosphine and phosphite ligands on the Fe-Sn bond lengths there is no noticeable trend in response to the different groups on the phosphorus atom. The Fe – Sn bond length, where the substituent on the Sn is constant, will be influenced by the amount of electron density on the iron atom that is available for bonding with Sn which consequently varies according to PR_3.

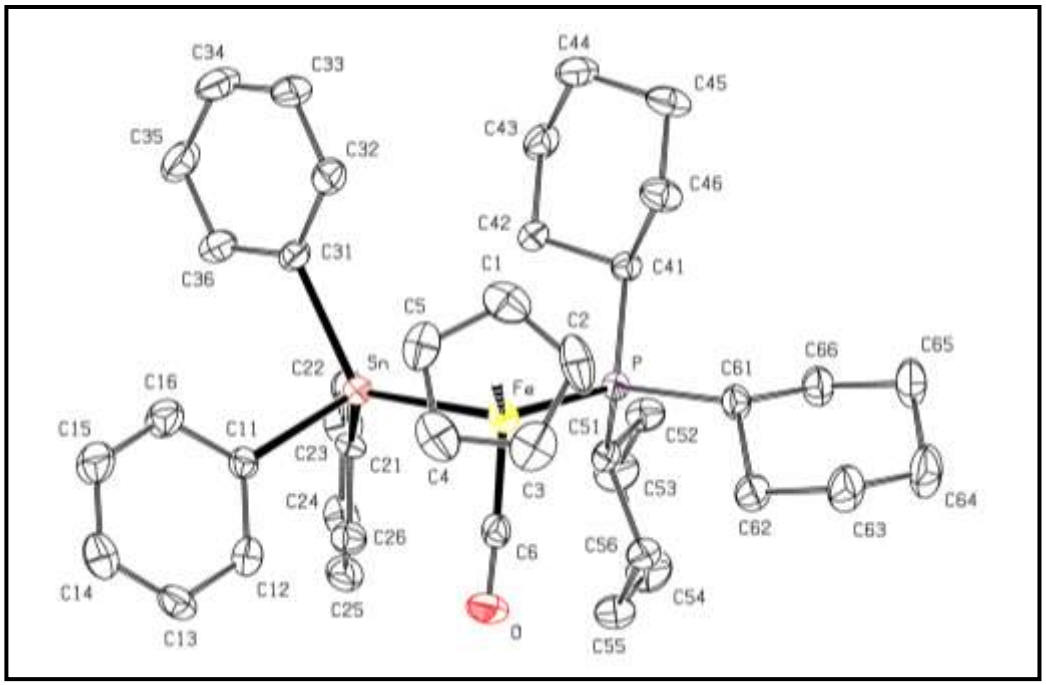


(a) **<u>3</u>**

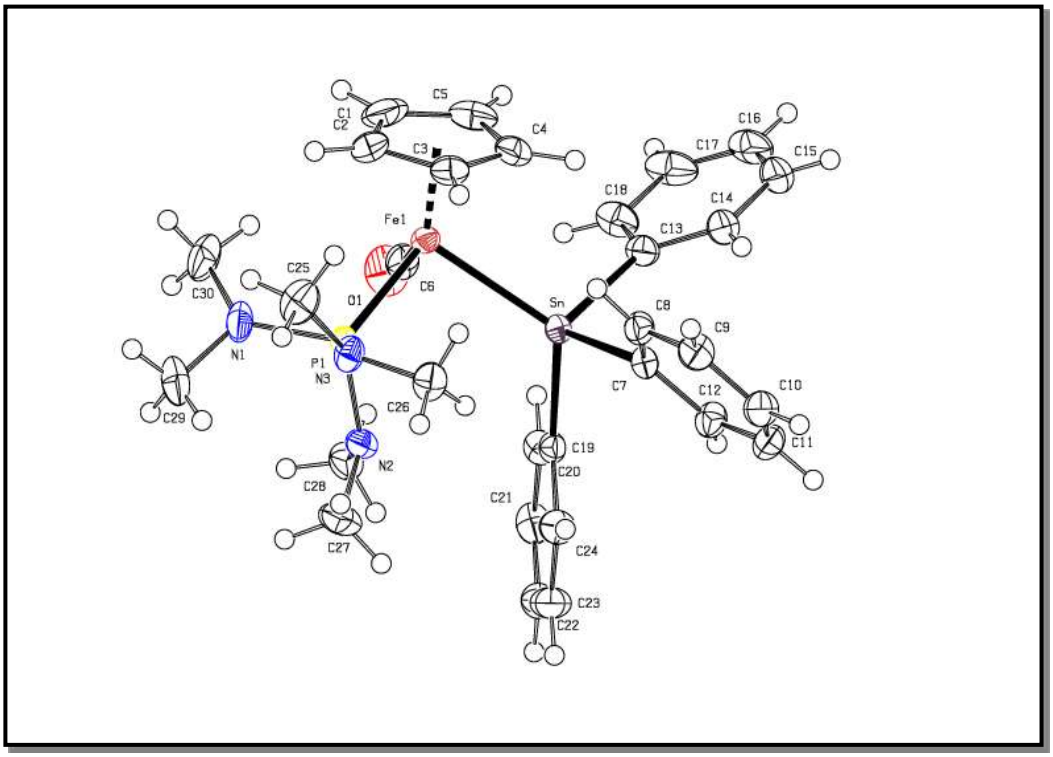


(b) **<u>5</u>**

Figures 5.3 (a) ORTEP diagrams of [CpFe(CO)P(*p*-$FC_6H_4)_3(SnPh_3)$] (**<u>3</u>**) and, (b) [CpFe(CO)P(*p*-tolyl)$_3(SnPh_3)$] (**<u>5</u>**) showing thermal ellipsoids at the 50% probability level.

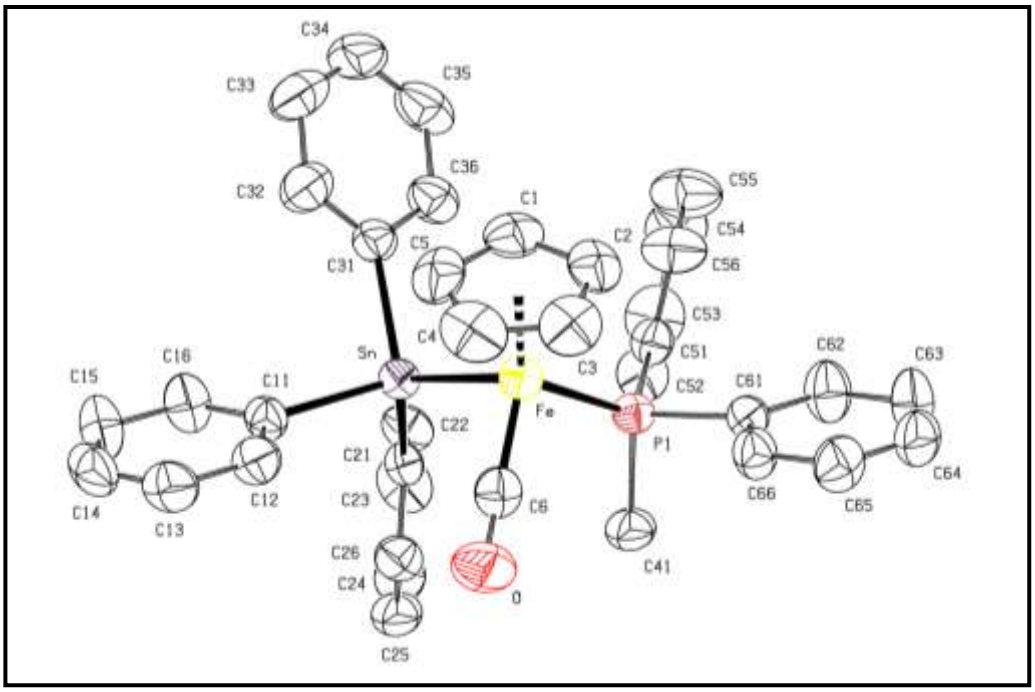


(a) **6**

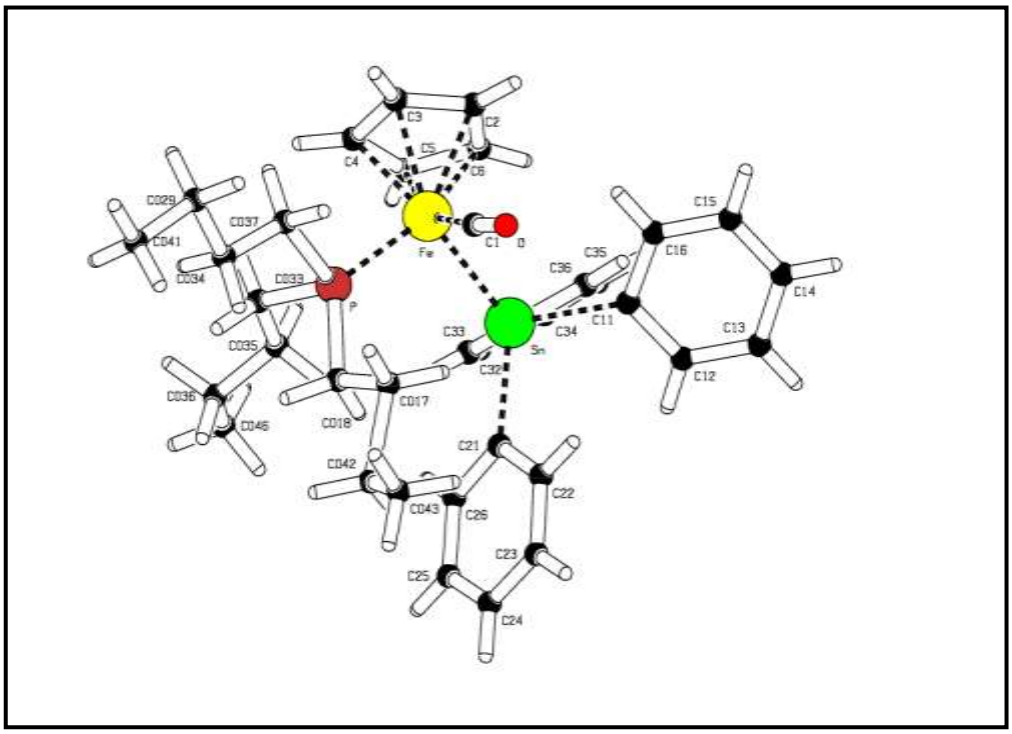


(b) **7**

Figures 5.4 (a) ORTEP diagrams of [CpFe(CO)P(Cy)$_3$(SnPh$_3$)] (**6**) and, (b) [CpFe(CO)P(NMe$_2$)$_3$(SnPh$_3$)] (**7**) showing thermal ellipsoids at the 50% probability level.

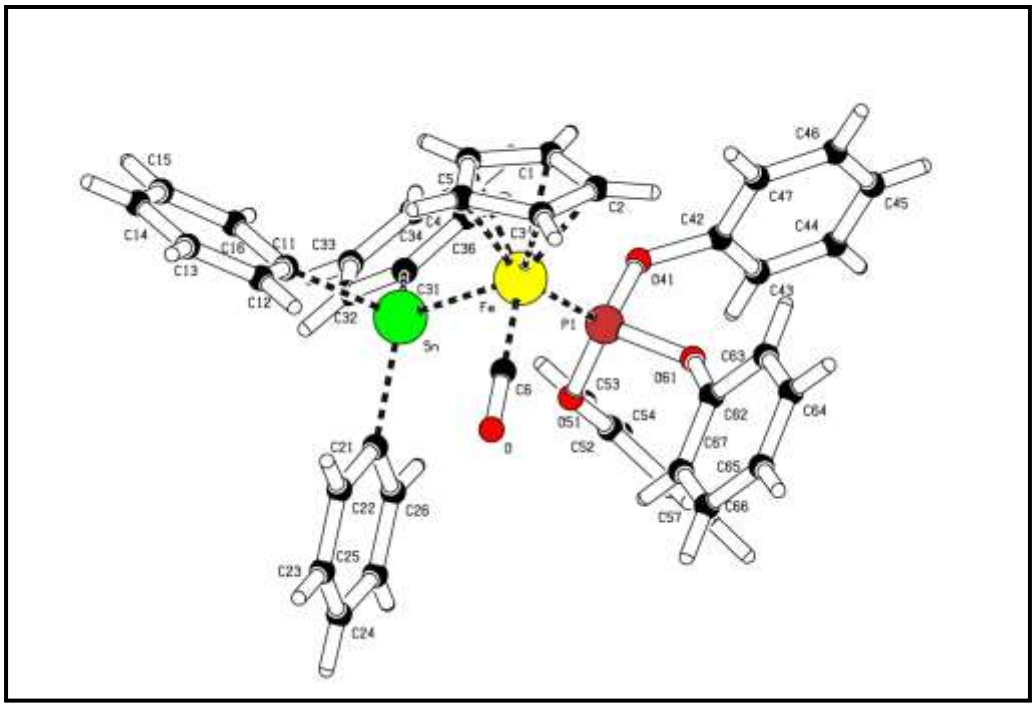


(a) **8**

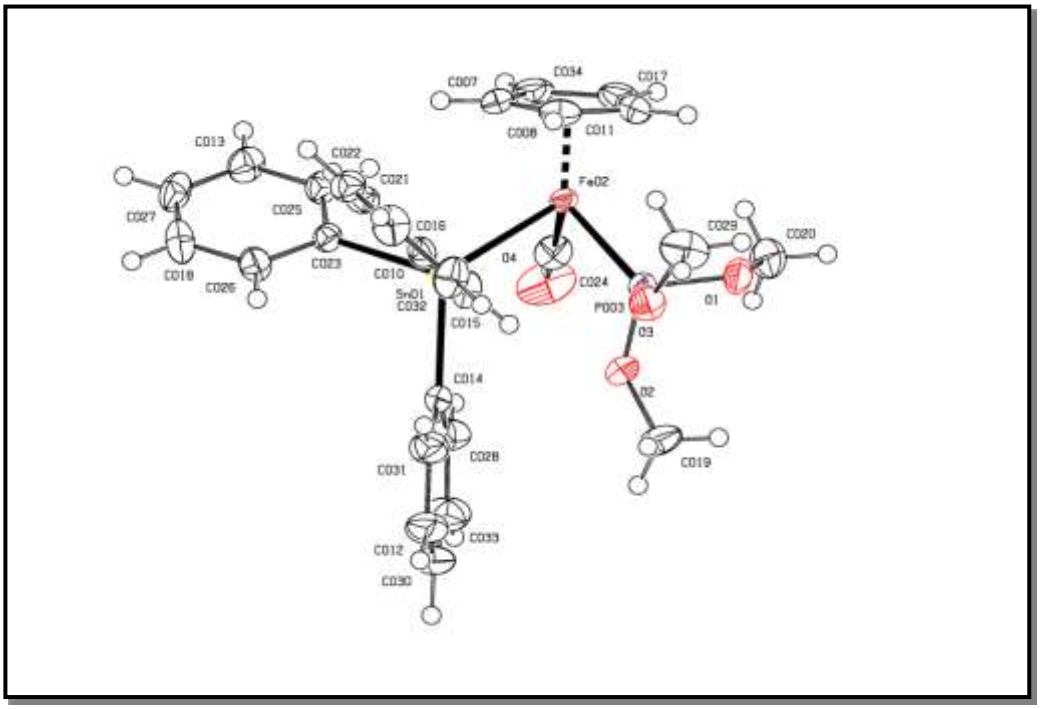


(b) **9**

Figures 5.5 (a) ORTEP diagrams of [CpFe(CO)P(MePh$_2$)$_3$(SnPh$_3$)] (**8**) showing thermal ellipsoids at the 50% probability level and, (b) SCHAKAL drawing [CpFe(CO)P(Bu)$_3$(SnPh$_3$)] (**9**) (SCHAKAl diagram chosen for clarity purpose).



(a) **10**



(b) **11**

Figure 5.6 (a) SCHAKAL drawing of [CpFe(CO)P(OPh)$_3$(SnPh$_3$)] **10** and ORTEP diagram of [CpFe(CO)P(OMe)$_3$(SnPh$_3$)] **11** showing thermal ellipsoids at the 50% probability level (SCHAKAL diagram chosen for clarity purpose).

5.4.2.3 *The triphenyltin group*.

The Sn-C (phenyl carbon) bond lengths for phosphine and phosphite complexes of the type [CpFe(CO)(PR_3)($SnPh_3$)] average 2.19(8) Å which is higher than the average 2.114(3) Å for the Sn-C (methyl carbon) of the type [CpFe$(CO)_2$($SnMe_3$)] and slightly larger than the average 2.18 Å observed for the tetramethyltin and trimethyltin halides [8], but falls within the average lengths found in other M–tin (M is a transition metal) compounds as summarized by Schempler [36]. The tin atom has an approximate tetrahedral geometry consisting of three-triphenyl groups and a fourth position occupied by the iron atom.

5.5 Chemical and structural correlations of [CpFe(CO)(PR_3)($SnPh_3$)] complexes.

Several correlations have been established among NMR, Tolman's steric and electronic, and structural parameters and only few of these correlations are shown in **Figures 5.7 to 5.9**. **Figures 5.7** deal with the best correlations among NMR parameters whilst **Figures 5.8** deal mainly with NMR solution properties, Tolman steric and experimental electronic properties.

5.5.1 Correlation of NMR parameters with Tolman's steric and IR parameters.

The NMR parameters of transition metals such as chemical shift and coupling constants have been previously correlated with structural features including steric properties [26,27,29,37] and chemical factors such as electronic properties [26,27,29,38], stability constants [39], reaction rates and catalytic performance [29,40]**.** Based on this background, we have established fair to good correlations between ^{13}CO and ^{119}Sn chemical shifts with ^{57}Fe chemical shifts (**Figures 5.7 a,b**). The correlation between the chemical shifts of ^{57}Fe and ^{13}CO is positive whilst that of ^{57}Fe and ^{119}Sn is negative (**Figures 5.7 a,b**). Definite trends exist in which as increasingly electronegative substituent groups are introduced on the phosphorus, the ^{57}Fe and ^{13}C(CO) nuclei become progressively deshielded. Correlation coefficient (r^2) and the *p*-value (which is a measure of the probability that the observed correlation between the two variables is fortuitous, i.e. the smaller the *p*-value the less likely it is that the observed correlation is fortuitous) are listed where a good correlation agreement seems to exists.

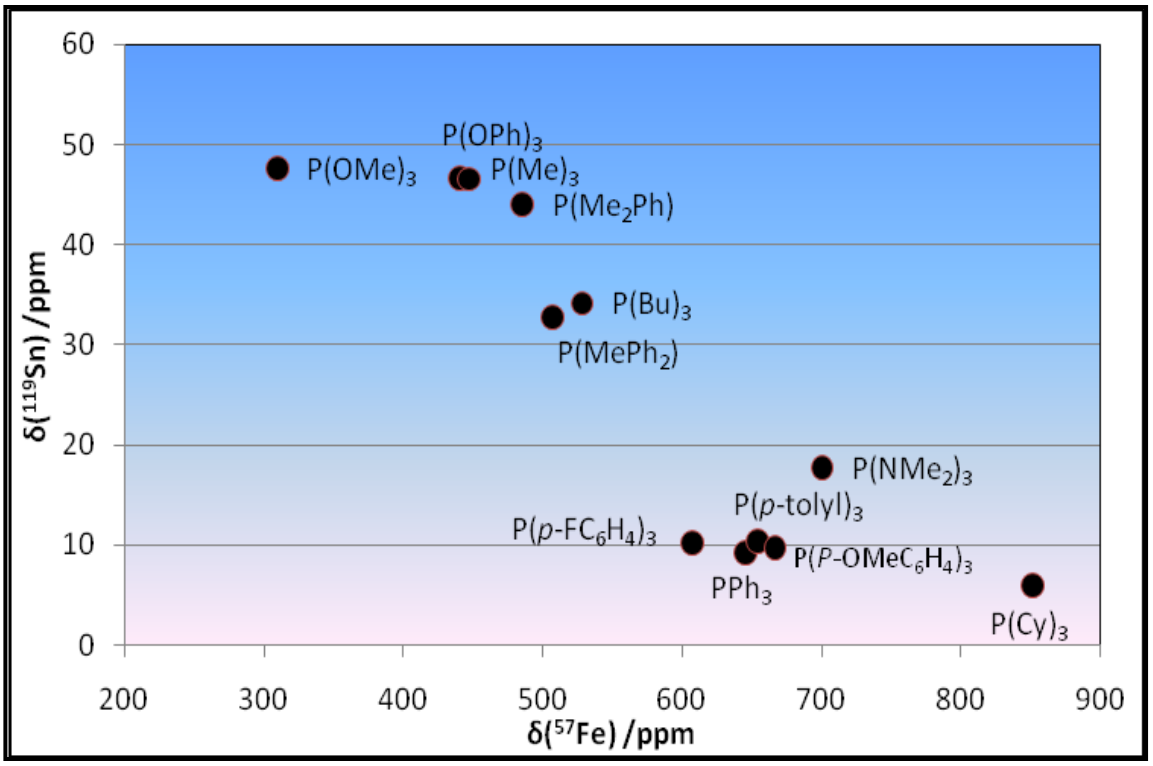


Figure 5.7a A plot of δ(^{57}Fe) vs. δ(^{119}Sn) chemical shifts in ppm (r^2 = -0.893, *p*-value = 0.0000923).

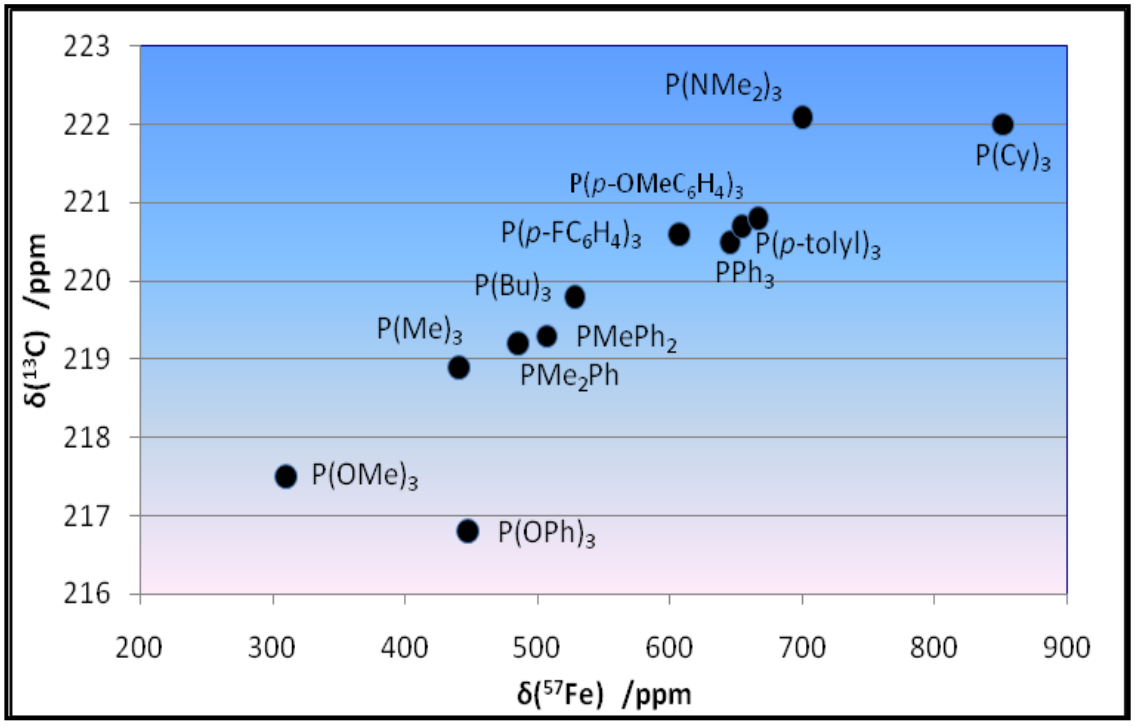


Figure 5.7b A plot of δ(^{57}Fe) vs. δ(^{13}C) (CO) chemical shifts in ppm (r^2 = 0.905, *p*-value = 0.0000509)

Figure 5.8a shows a rather poor negative correlation between the ^{57}Fe chemical shift and ν_{CO} (electronic property) upon changing the substituents on the phosphorus atom. There seems to be no coherent electronic influence on the relationship between δ(^{57}Fe) and ν_{CO} as shown in **Figure 5.8a**. It appears that a particular pattern develops for phosphine ligands with similar cone angle which suggests a competition between steric and electronic properties. There appears to be no comprehensive NMR study on the influence on the metal centre of the electronic property as a result of phosphine ligands with differing steric properties. Both the Hammett substituent constant and the Taft parameter have been derived from variables (substituents on the phosphorus atom) with nearly similar steric properties and thereby provide a significant insight into the electronic influence. **Figures 5.8b** and **c** show an interesting correlation between Tolman's steric property and the chemical shift of ^{57}Fe and ^{119}Sn where opposite trends are observed. A poor correlation has been observed (not shown) for $J_{(Fe\text{-}P)}$ (Hz) vs. ν_{CO} (cm^{-1}) and $J_{(Sn\text{-}P)}$ (Hz) vs. ν_{CO} (cm^{-1}).

The ^{57}Fe chemical shift exhibits a positive linear relationship with ligand steric parameter (r^2 = 0.973) with the iron nucleus becoming more deshielded as larger groups on the phosphorus are introduced (**Figure 5.8c**). Similar correlations have been observed for δ(^{187}Os) [41] in complexes of the type [(p-cymene)Os(Cl)$_2$PR$_3$] (r^2 = 0.97) and ^{57}Fe [27] in complexes of the type [CpFe(CO)(L)(COMe)] (r^2 = 0.941). The fact that L = CO fits the correlation very well in complexes of the type [CpFe(CO)(L)(COMe)] [27] even though the chemical and electronic properties are different from that of PR$_3$ suggest a very strong steric influence on the ^{57}Fe chemical shift. The correlation trends of the ligands that have the same size of cone angle (mainly *para*-substituted ligands, **Figures 5.8c, 5.9a** and **5.9b**) show clearly the influence of the electronic parameter in the absence of the steric property influence. Therefore it can generally be expected that in the absence of a steric influence, which seems to predominate in influencing the metal chemical shift, the δ(^{57}Fe) will respond accordingly to the electronic changes as result of changing substituents on the ligand (**Figure 5.8a**).

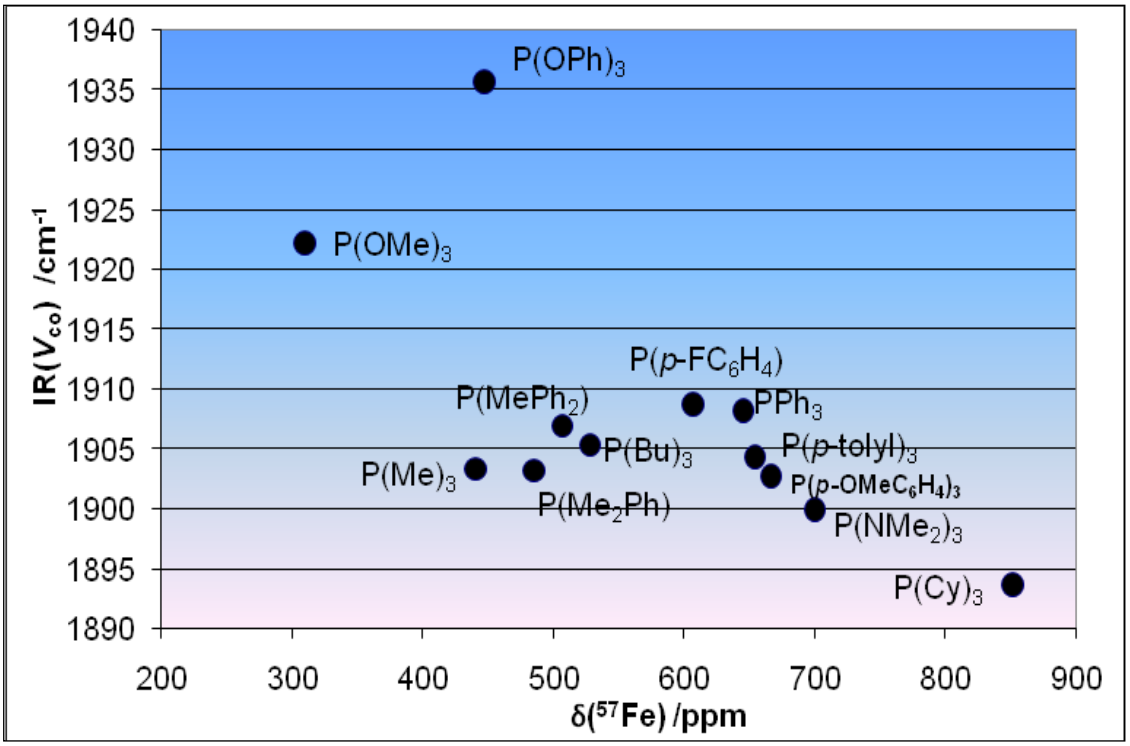


Figure 5.8a A plot of δ(^{57}Fe) (ppm) vs. IR (experimental ν_{CO}) in cm^{-1}

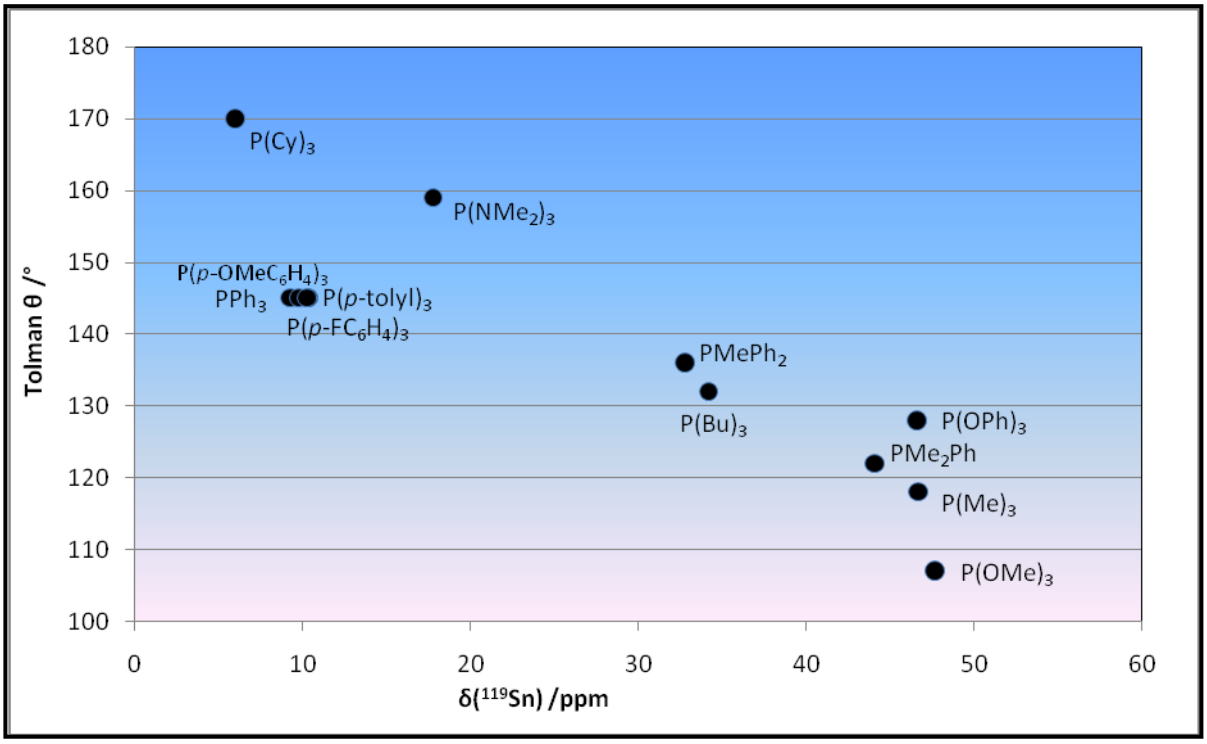


Figure 5.8b A plot of δ(^{119}Sn) (ppm) vs. Tolman cone angle (^{0}) (r^2 = -0.870, p-value = 0.000231).

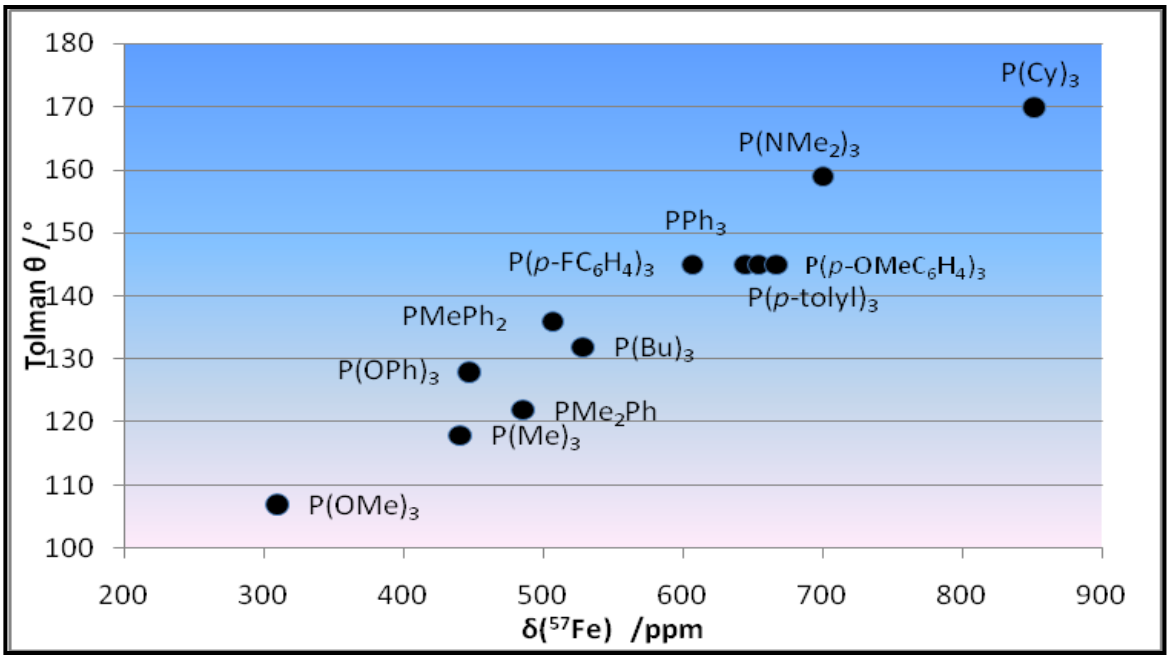


Figure 5.8c A plot of δ(^{57}Fe) (ppm) vs Tolman's Cone angle (θ) (r^2 = 0.973, *p*-value = 0.0000730)

5.5.2 Correlation between of NMR parameters and X-ray structural properties

The hetero-bimetallic complexes under study showed very interesting chemical and structural correlations in which a convincing relationship between solution and solid state properties exists. A very interesting correlation between the structural (Fe-P bond length) and solution state properties (δ(^{57}Fe) in solution) exists (r^2 = 0.913) which brings us closer to understanding the chemical properties of these types of complexes in both solid and solution states (**Figure 5.9a and b**). Such correlations have been observed by Leitner and co-workers in complexes of the type [Rh(acac^F)($R_2P(CH_2)_nPR_2$)] where acac = fluorinated acac, n = 2, R = ^{i}Pr, CH_3, Cy and Ph [42]. Plots of the correlation of δ(^{57}Fe) with other measurable NMR properties as with other structural parameters were also linear but of lower significance such as P-Fe-Sn bond angle and δ(^{57}Fe) (r^2 = 0.866) (**Figure 5.8b**). It is difficult to make a determination as to which structural parameter (between Fe-P and P-Fe-Sn) is most closely related to δ(^{57}Fe). Several fair negative correlations have also been established in this work such as between the Fe-P bond length and $J_{(Fe\text{-}P)}$ (r^2 = -0.778), between δ(^{57}Fe) and $^2J_{(119Sn\text{-}P)}$ (r^2 = -0.778) and between the Fe-CO bond length and ^{13}CO chemical shift (r^2 = -0.721), similarly found for Rh-CO [43]. A similar trend but

more poorly correlated relationship (**Figure 5.9b**) between Fe-Sn bond length and δ(^{57}Fe) has been established as for the Fe-P bond length and δ(^{57}Fe) (**Figure 5.9a**)

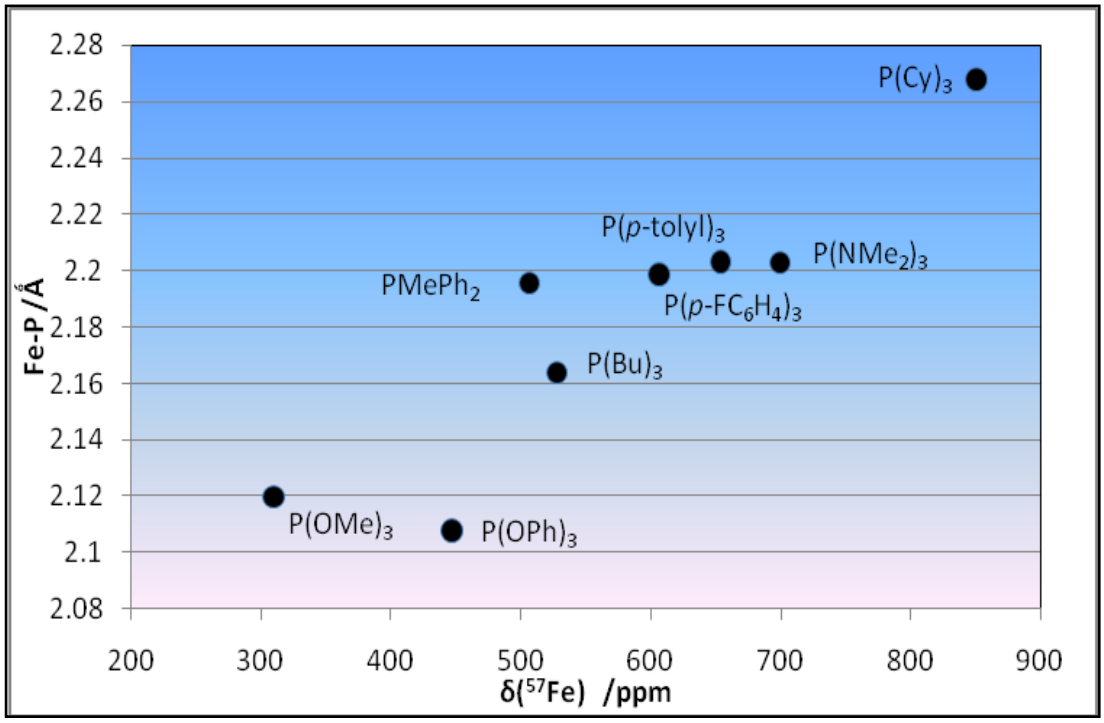


Figure 5.9a. A plot of Fe-P bond length (Å) vs. δ(^{57}Fe) (ppm) (r^2 = 0.913, *p*-value = 0.00152).

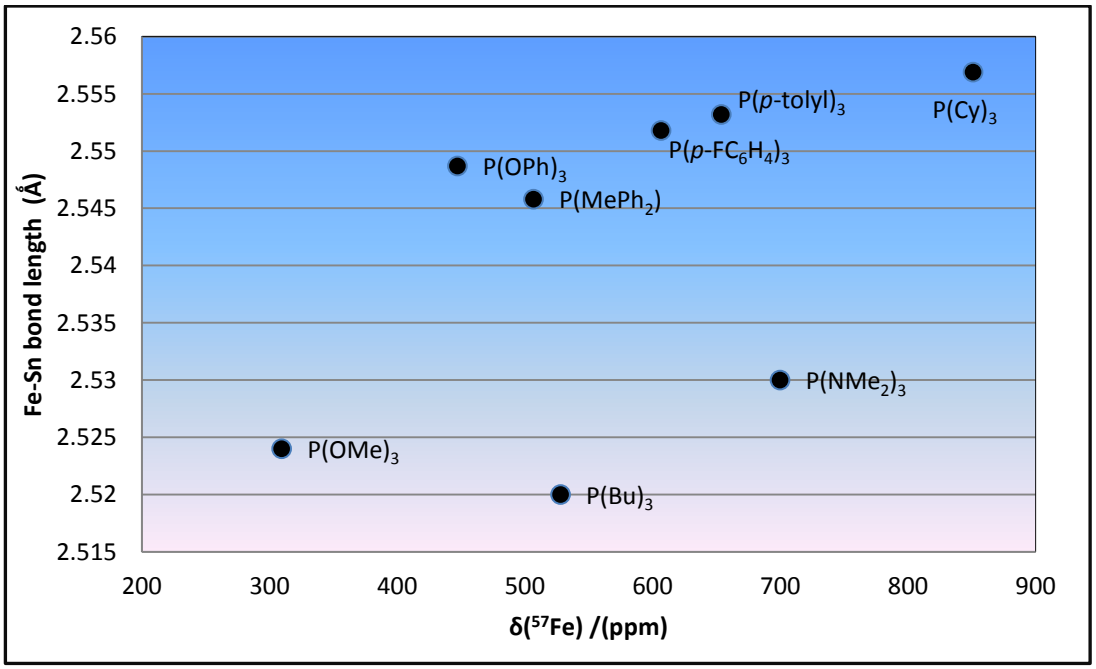
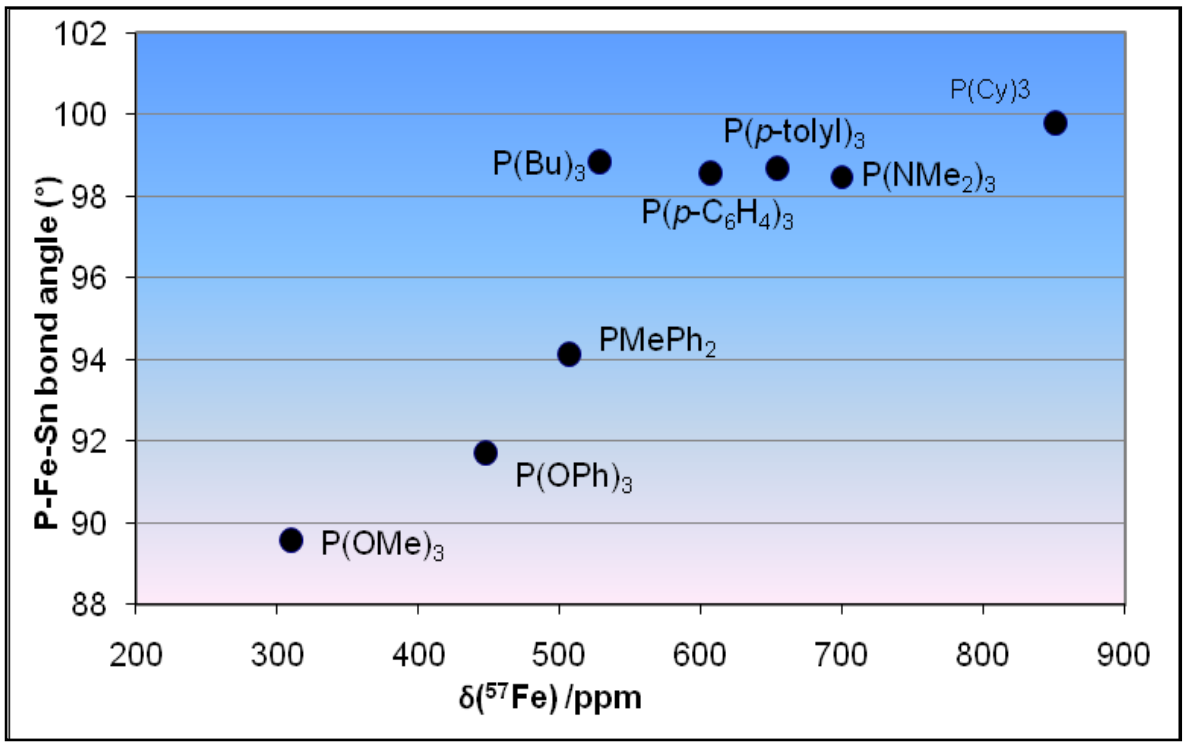


Figure 5.9b A plot of Fe-Sn bond length (Å) vs. δ(^{57}Fe) (ppm)



Figures 5.9c A plot Sn-Fe-P bond angle (°) against δ(^{57}Fe) (ppm) (r^2 = 0.866, *p*-value = 0.00543)

5.6 Conclusions

A systematic study of new complexes of the type [CpFe(CO)(PR_3)($SnPh_3$)] was undertaken in which multinuclear NMR spectroscopic (solution state) results were correlated with X-ray parameters (solid state) to determine the existence of any significant relationship between them. A fairly clear relationship between NMR and X-ray parameters has been established whereby the ^{57}Fe chemical shifts increase as the Fe-P bond lengths increase and as the Sn-Fe-P bond angles increases. A similar relationship between ^{57}Fe chemical shifts and Tolman's parameters exists whereby δ(^{57}Fe) increases as the steric property (cone angle) increases and decreases with increasing IR strectching frequency (ν_{CO}). It is interesting to note that the steric parameter seems to have a greater influence on the ^{57}Fe chemical shift than the electronic parameter. The ^{57}Fe chemical shift is very sensitive to the changes in the substituents on the phosphorus ligand and therefore renders it a useful probe into the structure and reactivity of cyclopentadienyl complexes.

References

1. (a) M.S. Holt, W.L. Wilson and J.H. Nelson, *Chem. Rev*., 89 (1989) 11; (b) E.H Brooks and

2. (a) N. Wheatly and P. Kalck, *Chem. Rev*., 99 (1999) 3379; (b) J. Beckmann, K. Jurschat, U. Kaltenbrunner, S. Rabe, M. Schürmann, D. Dakternieks A. Duthie and D. Müller, *Organometallics*, 19 (2000) 4887; (c) P. McArdle, L. O'Neill and D. Cunningham, *Inorg. Chim. Acta*, 291 (1999) 252; (d) H. Braunschweig, H. Bera, B. Geibel, R. Dörfler, D. Götz, F. Seeler, T. Kupfer and K. Radacki, *Eur. J. Inorg. Chem*., (2007) 3416 ; (e) M.F. Lippart and R.S. Rowe, *Coord. Chem. Rev*., 100 (1990) 267.

3. (a) A. Volger and H. Kunkely. *Coord. Chem. Review*, 230 (2000) 243; (b) V. Ritleng and M.J. Chetcuti, *Chem. Rev*., 107 (2007) 797.

4. G. Mavel, *Annu. Rep. NMR Spectrosc*. 5B (1973) 1

5. H.G. Schuster-Woldad, F. Basolo, *J. Am. Chem. Soc*., 88 (1966) 1657

6. C.A Tolman, *Chem. Rev*., 77 (1977) 313

7. (a) D. White and N.J. Coville, *Adv. Organomet. Chem*., 36 (1994) 95; (b) T.L. Brown and K. Lee, *J. Coord. Chem. Rev*., 128 (1993) 89; (c) E.C. Alyea, S.A. Dias, G. Ferguson and R. Restivo, *J. Inorg. Chem*., 16 (1977) 2329; (d) D.M.P. Mingos and T.E. Muller, *J. Organomet. Chem*., 500 (1995) 251; (e) I.A. Guzei and M. Wendt, *Dalton Trans*., (2006) 3991.

8. R.D. Gorsich, *J. Am. Chem. Soc*., 84 (1962) 2486

9. (a) M. Akita, T. Oku, M. Tanaka and Y. Moro-oka, *Organometallics*, 10 (1991) 3080; (b) L. Carlton, W.E. Lindsell and P.N. Preston, *J. Chem. Soc. Dalton Trans*., (1982) 1483; (c) P.M. Treichel and D.A. Komar, *J. Organomet. Chem*., 206 (1981) 77; (d) F.W.B. Einstein and R. Restivo, *Inorg. Chim. Acta*, 5 (1971) 501; (e) W.R. Cullen, J.R. Sam and J.A.J. Thomson, *Inorg. Chem*., 10 (1971) 843; (f) R. Ugo, S. Cenini and F. Bonati, *Inorg. Chim. Acta*, (1967) 541

10. L. Párkányi, K.H. Pannel and C. Hernandez, *J. Organomet. Chem*., 347 (1988) 295.

11. A. Bax, R.H. Grffey and B.L. Hawkins, *J. Magn. Reson*., 55 (1983) 301.

12. *Bruker SHELXTL, Version 5.1 (Includes XS, XL, XP, XSHELL)*, Bruker AXS Inc., Madison Wisconsin, 1999.

13. G.M. Sheldrich, *SADABS*, University of Göttingen: Göttingen, Germany, 1996.

14. *Bruker SHELXTL, Version 5.1 (Includes XS, XL, XP, XSHELL)*, Bruker AXS Inc., Madison Wisconsin, 1999.

15. (a) A.L. Spek, *J. Appl. Crystallogr*., 36 (2003) 7; (b) A.L. Spek, *Acta Crystallogr., Sect*. A, 46 (1990) C34.

16. T.S. Piper and G. Wilkinson, *J. Inorg. Nucl. Chem*., 3 (1956) 104.

17. M.O. Albers and N.J. Coville, *Coord. Chem. Rev*., 53 (1984) 227.

18. (a) P. Chini, G. Longoni and V.G. Albano, *Adv. Organomet. Chem*., 14 (1976) 285, (b) R.B. King, C.C. Frazier, R.M. Hanes and A.D. King, *J. Am. Chem. Soc*., 100 (1979) 479, (c) E.L. Meutterties and J. Stein, *Chem. Rev*., 79 (1979) 479.

19. (a) C.J. Benezra, *J. Am. Chem. Soc*., 95 (1973) 6890; (b) L. Evelyn, L.D. Hall, P.R. Steiner and D.H. Stokes, *Org. Magn. Reson*., 5 (1973) 141.

20. D.W. White and J.G. Verkade, *J. Magn. Reson*., 3 (1970) 111.

21. D.C.H Bigg, R. Spratt and B.J. Walker, *Tetrahedron Lett*., (1970) 107.

22. B.E. Maryanoff, A.T. McPhail and R.D. Hutchins, *J. Am. Chem. Soc*., 103 (1981) 4432

23. J.J. Verkade and L.D. Quin, *in Phosphorus-31 NMR Spectroscopy in Stereochemical Analysis, Organic Compounds and Metal Complexes*, Vol. 8; W.G. Bentrude and W.N. Setzer, VHS Publishers, Florida, 1987, Chapter 11.

24. (a) J.G. Verkade, *Coord. Chem. Rev*., 9 (1972) 1; (b) T.G. Appleton, H.C. Clark and L.E. Manzer, *Coord. Chem. Rev*., 10 (1973) 335.

25. L. Carlton, *Annu. Rep. NMR Spectrosc*., 63 (2008) 49.

26. L. Carlton, A. Emdin, A. Lemmerer and M.A. Fernandes, *Magn. Reson. Chem*., 46 (2008) S56

27. E.J.M. Meier, W. Kózmiński, A. Linden, P. Lustenberger and W. von Philipsborn, *Organometallics*, 15 (1996) 2469

28. A.N. Nesmeynov, Y.A. Chapvoskii, L.I. Denisovich, B.V. Lokshin and I.V. Polovyanyuk, *Proc. Acad. Sci. USSR: Chem*., 174 (1967) 576.

29. (a) P. von Philipsborn, *Chem. Soc. Rev*., 28 (1999) 95; (b) T. Jenny, W. von Philipsborn, J. Kronnenbitter and A. Schwenk, *J. Organomet. Chem*., 205 (1981) 211; (c) R. Benn, In *Transition Metal NMR*, P.S. Pregosin, Ed., Elsevier, Amsterdam, (1991) 103

30. (a) G. Davenport, S.R. Hall, W. Dreissig, *Xtal 3.2 Reference Manual*, Universities of Western Australia, Geneva and Maryland, 1992; (b) C.K. Johnson, *ORTEP*, *Report ORNL-3794*; Oak Ridge National Laboratory, Oak Ridge, TN, 1970.

31. E. Keller, *SCHAKAL-92*. Universität Freiburg, 1992.

32. (a) B.Y. Ho and J.J. Zuckerman, *J. Organomet. Chem*., 49 (1973) 1; (b) M.I. Bruce, *Comprehensive Orgametallic Chemistry*; G. Wilkenson, F.W. Stone F.G. Stone, Eds., Pergamon, Oxford, Vol. 9 (1982) p 1209.

33. (a) W.A.G. Graham, *Inorg. Chem*., 7 (1968) 315; (b) W. Jetz, P.B. Simons, J.A.J Thompson W.A.G. Graham, *Inorg. Chem*., 5 (1966) 2217.

34. (a) H.P. Weber and R.F. Bryan, *Acta. Cryst*., 22 (1967) 822; (b) R.F. Bryan, *J. Chem. Soc. (A)* (1967) 192.

35. J.A. Zubieta and J.J. Zuckerman, *Progress In Inorganic Chemistry*, S.J. Volzy, Ed., Interscience, New York, (1978) p 251.

36. E.D. Schemplex, *Inorg. Chem*., 11 (1967) 2012.

37. W. Leitner, M. Bühl, R. Fornika, C. Six, W. Baumann, E. Dinjus, M. Kessler, C. Krüger, A. Rufińska, *Organometallics*, 18 (1999) 1196.

38. P.B. Graham, M.D. Rausch, K. Täshler, W.von Philipsborn, *Organometallics*, 10 (1991) 3049.

39. M.C. Read, J. Glaser, I. Persson, M. Sandström, *J. Chem. Soc*., *Dalton Trans*., (1994) 3243.

40. W. von Philipsborn, *Pure Appl. Chem*. 58 (1986)

41. A.G. Bell, W. W. Kózmiński, A. Linden, and W. von Philipsborn, *Orgagnometallics,* 15 (1996) 3124.

42. (a) W. Leitner, M. Bühl, R. Fornika, C. Six, W. Baumann, E. Dinjus, M. Kessler, C. Krüger and A. Rufínska, *Organometallics*, 18 (1999) 1196; (b) K. Angermund, W. Baumann, E. Dinjus, R. Fornika, H. Görls, M. Kessler, C. Krüger, W. Leitner and F. Lutz, *Chem. Eur. J*., 3 (1977) 313.

43. G.J.J. Steyn, A. Roodt, I. Poleteava and Y.S. Varshavsky, *J. Organomet*. 536 (1997) 197.

CHAPTER 6

Synthesis, NMR and X-Ray Crystallographic Studies of Iron(II) Cyclopentadienyl *bis*-Phosphine and *bis*-Phosphite Complexes

6.1 Introduction

Hetero-bimetallic complexes of the type [$CpFe(CO)(PR_3)(SnPh_3)$] containing phosphine and phosphite ligand have been synthesized and discussed in Chapter 5. Substitution of both CO ligands from the starting [$CpFe(CO)_2SnPh_3$] by the phosphine or phoshite ligand is expected to change the chemistry of the disubstituted complex due to the presence of two pi-acceptor or sigma donor ligands or a combination of both. Organometallic compounds bearing phosphine or phosphite ligands have been synthesized and studied for a variety of reasons. For example; (i) increased catalytic potency by compounds such as Wilkinson's catalyst, Grubb's catalysts and their derivatives [1], (i) increased stability of many organometallic complexes for the purposes of characterization and ease of control, (ii) in the design of organometallic compounds for industrial application [2], etc. However increased stability in most cases reduces chemical reactivity. Alternatively, the chemistry of [$CpFe(PR_3)_2SnPh_3$)] complexes could be altered by functionalization of the Cp ligand, known to be versatile, robust and tunable without cleaving the Cp-M bond. The success of phosphine or phosphite introduction into organometallic compounds bearing a Cp-M framework is varied with respect to steric hindrance, a factor which has been comprehensively quantified by Tolman's equation [3]. The successful continued use of Tolman's electronic and steric properties as a predictive measure of chemical reactivity is in most cases due to their possible correlation with physicochemical properties of ligands involved.

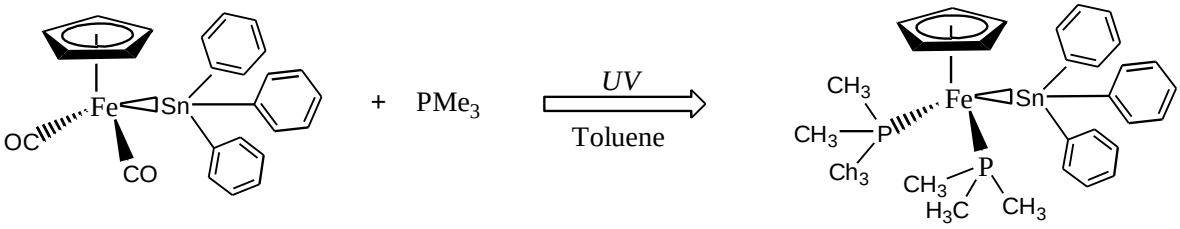
Attention is here focused on the representative disubstituted (and decarbonylated) hetero-bimetallic complexes of the type [$CpFe(PR_3)_2SnPh_3$)] which are structurally similar to the monocarbonylated complexes. In this Chapter, phosphine (trimethylphosphine and dimethylphenylphosphine) and phosphite (trimethylphosphite and triphenylphosphite) ligands

which exhibit a relatively small steric hindrance as measured by the size of their cone angles will be used to demonstrate disubstitution of CO ligands from the starting complex [$CpFe(CO)_2(SnPh_3)$] by a photochemical method. Four bis- phosphine and phosphite tin-iron complexes were synthesized and their single crystal structures determined. A variety of complexes bearing a P-Fe-Sn bond connection have been synthesized before [4], but there is little if any structural comparison among these complexes. Single crystal structures are presented to provide an insight into the nature of the Fe-Sn bond and other structural features around iron with respect to the tin and phosphorus atom(s) and their influence on the Cp-Iron bond distances.

6.2 Experimental: Preparation of disubstituted hetero-bimetallic complexes of iron and tin, [$Fe(Cp)(PR_3)_2(SnPh_3)$]

Materials for the synthesis of compounds **14** - **17** were as for compounds **10**, **11**, **12** and **13** in Chapter 5, section 5.2. Similarly, NMR spectroscopic and X-ray crystallographic experimental details are as in Chapter 5, section 5.2. Synthesis and characterisation of the starting compound **1** was described by Gorsich [5], and compounds **14** - **17** were prepared by a method similar to that of Treichel and Komar [6]. Compounds (**14** - **17**) were prepared using the same procedure as for compound **2** in Chapter 5. All operations and manipulations were performed under an inert atmosphere of nitrogen or argon. The ^{31}P, ^{57}Fe and ^{119}Sn chemical shifts and selected coupling interactions are provided in **Table 6.2.**

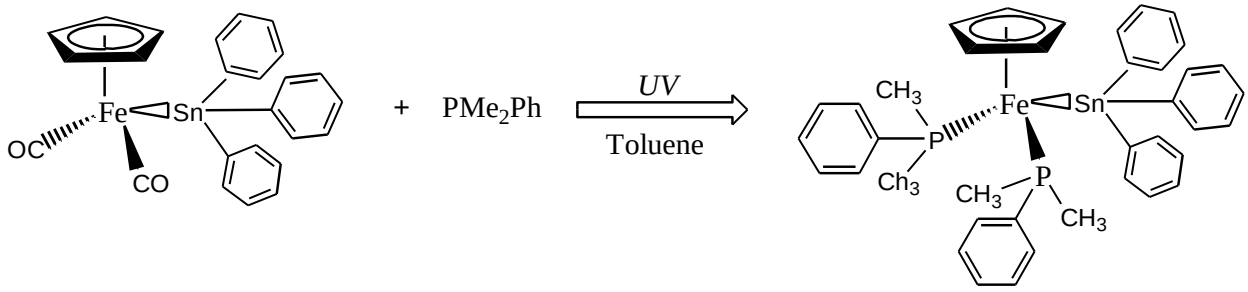
6.2.1 Preparation of [$Fe(PMe_3)_2(SnPh_3)$] …… (14)



A pale yellow solution of [$Fe(Cp)(CO)_2(SnPh_3)$] (**1**) (50 mg ~ 0.10 mmol) and an excess of triemethyl phosphine (10 drops) in toluene (10 ml) was prepared at room temperature in a Schlenk tube and irradiated overnight (15 hrs) using a UV light source, accompanied by constant stirring. The solvent was then removed *in vacuo* from the resulting yellow solution and the

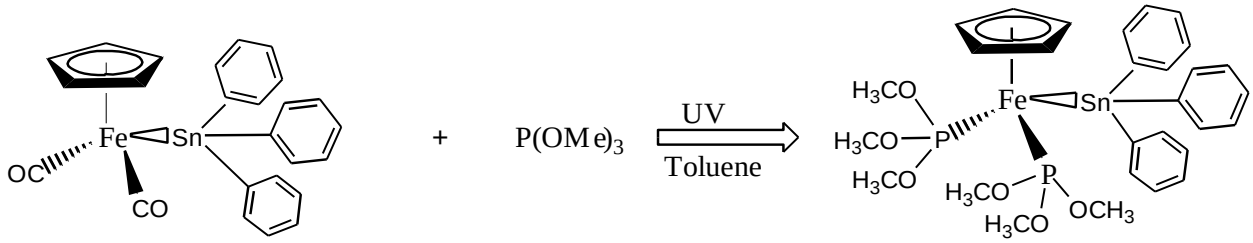
product extracted with CH_2Cl_2 (3 ml). The solvent was again removed *in vacuo* leaving behind a red precipitate which was then recrystallized from toluene. The crystals were then washed with n-hexane. The red-orange crystalline solid gave a yield of 46 mg (74%). NMR spectra were recorded from a solution in $CDCl_3$ at 300 K. ^{1}H NMR ($\delta_{(ppm)}$): 7.52 (m, 6H, $SnPh_3$); 7.18 (m, 9H, Ph_3); 4.09 (s, 5H, Cp); 1.30 (s, 18H, Me_3). ^{13}C NMR ($\delta_{(ppm)}$): 151.64 (s, *ipso*, 3C, Ph_3); 137.66 (s, *meta*, 6C, Ph_3, d, satellite, $^3J_{(Sn-C)}$ = 31 Hz) 127.30 (s, *ortho*, Ph_3, d, satellite, $^2J_{(Sn-C)}$ = 26 Hz), 126.20 (s, *para*, 3C, Ph_3), 74.08(s, 5C, Cp) 25.23 (d, 6C, Me_3, $^1J_{(P-C)}$ = 25 Hz).

6.2.2 Preparation of $[Fe(Cp)(PMe_2Ph)_2(SnPh_3)]$ …… (15)



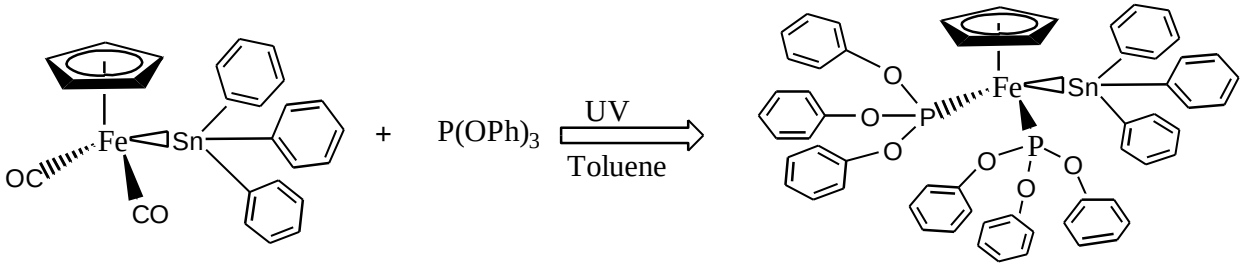
A pale yellow solution of $[Fe(Cp)(CO)_2(SnPh_3)]$ (**1**) (50 mg ~ 0.10 mmol) and an excess of dimethylphenyl phosphine (10 drops) in toluene (10 ml) was prepared at room temperature in a Schlenk tube and irradiated with UV light overnight (ca. 16 hrs) with constant stirring. The solvent was removed *in vacuo* from the deep red-orange solution and the product extracted with CH_2Cl_2 (3 ml). The resulting deep-orange solution was concentrated before addition of hexane (ca. 1 ml) to give red-orange crystals. The crystals were then washed with hexane (2 x 1 ml) to give a yield of 67.8% (51 mg). NMR spectra were recorded from a solution in $CDCl_3$ at 300 K. ^{1}H NMR ($\delta_{(ppm)}$): 7.44 (m, 5H, $Sn\underline{Ph}_3$, $PMe_2\underline{Ph}$) 7.23 (m, 20H, $Sn\underline{Ph}_3$, $PMe_2\underline{Ph}$); 4.02 (d, 5H, Cp, $^3J_{(P-H)}$ = 1.7 Hz); 1.7 (d, 12H, $P\underline{Me}_2Ph$, $^2J_{(P-H)}$ = 6.5 Hz), 1.40 (t, 12H, $P\underline{Me}_2Ph$, $^2J_{(P-H)}$ = 6.5 Hz). ^{13}C NMR ($\delta_{(ppm)}$): 151.41 (s, *ipso*, 3C, $Sn\underline{Ph}_3$); 145.40 (s, ipso, 2C, PMe_2Ph, d, satellite, $^1J_{(P-C)}$ = 15 Hz); 137.78 (s, ortho, 6C, $SnPh_3$, d, satellite, $^2J_{(Sn-C)}$ = 31 Hz), 129.46 (s, ortho, 4C, PMe_2Ph, d, satellite, $^2J_{(P-C)}$ = 4.6 Hz); 128.11(s, meta, 4C, PMe_2Ph, d, satellite, $^3J_{(P-C)}$ = 3.8 Hz), 128.07 (s, para, 2C, PMe_2Ph); 127.39 (s, meta, 6C, $SnPh_3$, d, satellite, $^3J_{(P-C)}$ = 27 Hz); 126.35 (s, para, 3C, $SnPh_3$); 75.02 (s, 5C, Cp); 24.63 (t, 4C, Me, $^1J_{(P-C)}$ = 14 Hz), 22.88 (t, 4C, Me, $^1J_{(P-C)}$ = 14 Hz).

6.2.3 Preparation of $[Fe(Cp)\{P(OMe)_3\}_2(SnPh_3)]$ …… (16)



A pale yellow solution mixture of $[Fe(Cp)(CO)_2(SnPh_3)]$ (**1**) (50mg, ca. 0.1mmol) and a two-fold excess of trimethyl phophite (10 drops) in toluene (10 ml) was prepared at room temperature in a Schlenk tube and irradiated with UV light source overnight (ca. 18 hrs) with constant stirring. An IR spectrum obtained from the solution showed no CO bands. A colour change from light yellow to light orange was observed. The solvent was removed *in vacuo* and the product extracted with dichloromethane (2 ml) and concentrated to ca. 1 ml before addition of hexane (1 ml) to effect crystallisation at -5 ^{0}C overnight. A bright yellow-orange micro-crystalline powder was obtained and was washed with hexane (1 ml x 2) and dried under a steady flow of nitrogen to give yield of 63 mg (87% yield). NMR spectra were recorded from a solution in $CDCl_3$ at 300 K. ^{1}H NMR ($\delta_{(ppm)}$): 7.61 (m, 6H, $SnPh_3$); 7.18 (m, 9H, $Sn\underline{Ph}_3$); 4.37 (s, 5H, Cp); 3.40 (d, 18H, Me, $^3J_{(P-H)}$ = 5.2 Hz). ^{13}C NMR ($\delta_{(ppm)}$): 151.4 (s, ipso, 3C, $SnPh_3$); 137.80 (s, ortho, 6C, Ph_3, d, satellite, $^2J_{(Sn-C)}$ = 31 Hz); 126.72 (s, meta, 6C, $SnPh_3$, d, satellite, $^3J_{(Sn-C)}$ = 32 Hz); 125.96 (s, para, 3C, $SnPh_3$,); 75.73 (s, 5C, Cp); 51.93 (d, 6C, OMe, $^2J_{(Sn-C)}$ = 8 Hz).

6.2.4 Preparation of $[Fe(Cp)\{P(OPh_3)\}_2(SnPh_3)]$ ……. (17)



A pale yellow solution mixture of $[Fe(CO)_2Cp)(SnPh_3)]$ (**1**) (50mg, 0.1mmol) and a 100 % excess of triphenylphosphite (~ 10 drops) in toluene (10 ml) was prepared at room temperature in a Schlenk tube and irradiated with UV light overnight with constant stirring. Before the solvent was removed an IR measurement was done to determine the extent of the reaction and no $\nu_{(CO)}$ bands were visible. After about 20 hrs of reaction, the solvent was removed *in vacuo* from the resulting dark orange solution and the product extracted with dichloromethane (2 ml). The solution was concentrated to ca. 1 ml before drop-wise addition of hexane (0.5 ml) to effect crystallisation. A fine orange powder obtained and washed with hexane (1 ml x 2) to give a yield of 70 mg (32%). NMR spectra were recorded from a solution in $CDCl_3$ at 300 K. ^{1}H NMR ($\delta_{(ppm)}$) : 7.61 (m, 6H, $SnPh_3$); 7.19 (m, 9H, OPh, $SnPh_3$); 7.01 (m, 18H, OPh, $SnPh_3$); 6.6 (m, 12H, OPh). 4.31 (s, 5H, Cp); ^{13}C NMR ($\delta_{(ppm)}$): 152.7 (s, ipso, 6C, OPh, d, satellite, $^2J_{(P-C)}$ = 6.9 Hz); 149.78 (s, ipso, 3C, $SnPh_3$); 138.16 (s, *ortho*, 6C, SnPh, d, satellite, $^2J_{(P-C)}$ = 31 Hz); 129.13 (s, *ortho*, 12C, OPh); 127.31 (s, *meta*, 6C, $SnPh_3$, d, satellite, $^3J_{(Sn-C)}$ = 34 Hz); 126.58 (s, 3C, *para*, $SnPh_3$); 123.71(s, *para*, 6C, OPh); 121.39 (s, *meta*, 12C, OPh); 76.68 (s, 5C, Cp).

6.3 X-ray crystallography

The crystals of compound **15** and **16** were prepared by addition of counter solvent (n-hexane) to a concentrated solution in CH_2Cl_2 (ranging from 0.5 to 1 ml) and left in the freezer (~ -15 ^{0}C) overnight. The crystals were then washed with a minimum amount of cold n-hexane (< 1 ml). On the other hand, the X-ray quality crystals of compound **14** were obtained from a concentrated solution of toluene at low temperature (~ -5 ºC). The single crystal X-ray diffraction analysis was performed as described in Chapter 5 and the refinement data for compounds **14**, **15** and **16** are

provided here below in **Table 6.1**. The orange micro-crystalline lumps of compound **17** lost crystalline features at once after washing with n-hexane and drying under a steady flow of nitrogen gas.

Table 6.1. Crystal Refinement Data for compound **14**, **15** and **16**.

Parameter	Compound **14**	Compound **15**	Compound **16**
Molecular formula	C29 H38 Fe P2 Sn	C39 H42 Fe P2 Sn	C29 H38 Fe O6 P2 Sn
Formula weight	623.07	747.21	719.07
Temperature (K)	293(2)	293(2)	173(2) K
Wavelength (Å)	0.71073	0.71073	0.71073
Crystal system	Monoclinic	Triclinic	Monoclinic
Space group	P2(1)/c	P-1	Cc
Unit cell dimensions: a (Å) b (Å) c (Å) α (^{0}) β (^{0}) γ (^{0})	9.8568(4) 28.2810(13) 11.2686(5) 90 115.699(3) 90	10.8323(15) 11.5739(16) 13.826(2) 89.458(3) 80.744(3) 87.149(3)	10.8663(2) 17.5017(4) 16.3980(4) 90 97.2740(10) 90
Volume (Å^3)	2830.5(2)	1708.7(4)	3093.(12)
Z	4	2	4
Density (Calculated) (Mg/m^3)	1.462	1.452	1.544
Absorption coefficient (mm^{-1})	1.523	1.275	1.419
F(000)	1272	764	1464
Crystal size (mm^3)	0.50 x 0.17 x 0.06	0.44 x 0.27 x 0.16	0.33 x 0.19 x 0.19
Theta range for data collection (^{0})	2.13 to 27.00	1.49 to 27.00	2.22 to 27.99
Index ranges	-12,<=h<=10, -36<=k<=35 -14<=I<=13	-13<=h<=13 -10<=k<=14 -17<=I<=17	-14<=h<=13 -23<=k<=23 -21<=l<=21
Reflections collected	12656	11523	17543
Independent reflections	6107 [R(int) = 0.0420]	7416 [R(int) =0.0252	6663[R(int) = 0.0511
Completeness to theta = 27.00^0	98.6 %	99.4 %	99.8 %
Absorption corrections	Integration	Integration	Integration
Max. and min. transmissions	0.9390 and 0.7168	0.8533 and 0.6272	0.7743 and 0.6517
Refinement method	Full-matrix least-squares on F^2	Full-matrix least-squares on F^2	Full-matrix least-squares on F^2
Data / restraints / parameters	6107 / 0 / 304	7416 / 0 / 392	6663 / 2 / 352
Goodness-of-fit on F^2	0.981	1.018	1.031
Final R indices [I>2sigma(I)]	R1 = 0.0335, wR2 = 0.0677	R1 = 0.0283, wR2 = 0.0610	R1 = 0.0282 wR2 = 0.0601
R indices (all data)	R1 = 0571 wR2 = 0.0740	R1 = 0414, wR2 = 0.0655	R1 = 0.0333 wR2 = 0.0661

6.4 Results and discussion.

Heterobimetallic complexes of the type $[CpFe(PR_3)_2SnPh_3]$ (R = Me_3, Me_2Ph, $\{OMe\}_3$ and $\{OPh\}_3$) (**14** – **17**) were prepared photochemically, by substitution of the carbonyl ligands using more than a two-fold excess of phosphine or phosphite ligands, from the dicarbonylated starting complex $[CpFe(CO)_2SnPh_3]$ **1**, in toluene solution. As in the syntheses of monocarbonylated complexes of the type $[CpFe(CO)PR_3SnPh_3]$, complete decarbonylation was achieved overnight without any trace remaining of the starting material i.e. $[CpFe(CO)_2SnPh_3]$. The heterobimetallic complex $[CpFe(PMe_3)_2SnPh_3]$ has been previously prepared by Treichel and Komar [6] who achieved a complete decarbonylation of $[CpFe(CO)_2SnPh_3]$ by UV irradiation at 81 °C (at reflux) in acetonitrile solution. Phosphine complexes **14** and **15** were isolated as red-orange crystals and the phosphite complex as orange crystals in moderate to fairly good yields. The $^{31}P\{^1H\}$ NMR analysis of compound **14** and **15** show significant signs of decomposition over a long period (at least three days at room temperature) in dichloromethane solution.

The preparation of complexes **14** - **17** was a demonstration of a complete decarbonylation of dicarbonylated complex **1** (Chapter 5) by a modified photochemical method under mild conditions, hence the four representative compounds. It is anticipated that the size of the ligand as measured by its cone angle will be the determining factor in the success of complete decarbonylation as there was no isolation of disubsituted complexes where R = Cy (cone angle, θ = 170) or NMe_2 (θ = 159 ^{0}). Isolation of compound **17** (R_3 = $\{OPh\}_3$, θ = 128 ^{0}) represented a possible border line in our series beyond which complexes containing phosphine ligands with cone angle equal to or greater than 136 degrees could not be obtained using our reaction conditions. It can be reasonably expected that as the cone angle increases, the percentage *s* character in the phosphorus lone pair will consequently decrease [3]. It is important however to note that electronic and steric parameters are intimately related and difficult to separate. Phosphite ligands have generally smaller cone angles in comparison to phosphine ligands, a consequence of the flexible bond angle through the oxygen atom. However no crystals of **17** of suitable quality for X-ray structure determination were obtained. There were no signs of decomposition of the isolated materials (**14**, **15**, **16**, **17**) after several months of storage at < 5 °C

under of argon. Complexes **14** - **17** were also characterized by multinuclear (^{1}H, ^{13}C, ^{31}P, ^{57}Fe and ^{119}Sn) NMR spectroscopy (see experimental section 6.2 and **Table 6.2**).

6.4.1 NMR Spectroscopy

Table 6.2 NMR spectroscopic data for the complexes [CpFe(PR_3)$_2$SnPh$_3$]

	Ligand (PR_3)	Electronic Parameter (ν)	Cone angle (θ)	$\delta(^{1}H)$ (Cp)	$\delta(^{13}C)$ (Cp)	$\delta(^{31}P)$	$\delta(^{57}Fe)$	$\delta(^{119}Sn)$	$^{1}J_{(Fe-P)}$	$^{2}J_{(^{117}Sn-P)}$	$^{2}J_{(^{119}Sn-P)}$	Yields (%)
14	$P(Me)_3$	2064.1	118	4.09	74.08	26.71	870.8	21.21	57.7	499.2	522.1	74
15	PMe_2Ph	2064.3	122	4.02	75.02	35.71	967.4	4.30	58.7	484.2	506.7	68
16	$P(OMe)_3$	2079.5	107	4.37	75.73	184.96	646.2	26.15	99.0	632.0	665.4	87
17	$P(OPh)_3$	2085.3	128	4.31	76.68	161.9	601.6	18.23	108.7	597.9	625.6	32

The ^{1}H (Cp ring), ^{31}P (PR_3) and ^{57}Fe chemical shifts of the phosphine complexes (**14** – **15**) are clearly distinguished from those of phosphite complexes (**16** – **17**), thus reflecting the influence of the electron-donating and electron-withdrawing capacities on the respective chemical shifts by the substituent on the phosphorus atom. Both ^{1}H and ^{31}P chemical shifts of phosphite complexes occur at relatively higher frequencies in comparison to phosphine complexes [7]. However, this pattern is not clear for ^{13}C and ^{119}Sn chemicals shifts where no clear distinction is observed. The ^{57}Fe NMR chemical shift of phosphine complexes (**14** and **15**) are significantly higher than the phosphite complexes (**16** and **17**), a trend that is consistent with the previous observations in the monocarbonylated complexes of the type [CpFe(CO)(PR_3)SnPh$_3$] (See **Table 5.3**, Chapter 5). This trend relates to the fact that the phosphite ligands are generally stronger π-accepters and have greater influence on ΔE on the metal. Despite the small number of compounds in this study, it can be concluded that the steric properties of these ligands contribute more significantly to the influence on ^{57}Fe chemical shifts than the electronic factor (**Table 6.2**). This observation is contrary to the trend established in the monocarbonylated complexes **2** – **13** (Chapter 5). It is important though to bear in mind that steric and electronic effects are intimately related and difficult to separate in any pure way [3]. The $^{1}J_{(Fe-P)}$ increases as the electronic parameter increases whereas there is no clear trend for $^{2}J_{(Sn-P)}$. The change in $^{1}J_{(Fe-P)}$ will be mainly influenced by the π-acceptor ability of the ligand and percentage *s* character of the Fe-P bond.

A characteristic feature of the disubstituted complexes **14** – **17** with respect to δ(^{119}Sn{^{1}H}) is that the ^{119}Sn couples to two equivalent phosphorus nuclei resulting in a triplet multiplicity. The $^{1}J_{(Fe\text{-}P)}$ for phosphine compounds **14** and **15** averages at 58 Hz lower than for the phosphite compounds **16** and **17** at 104 Hz. A similar trend is also observed for $^{2}J_{(^{119}Sn\text{-}P)}$ (491 Hz and 614 Hz for phosphine and phosphite complexes respectively) as for $^{2}J_{(^{117}Sn\text{-}P)}$ [8]. It is interesting to note a directly propotional correlation between ^{31}P chemical shift and $^{1}J_{(Fe\text{-}P)}$ or $^{2}J_{(Sn\text{-}P),}$ whereas the opposite is observed with ^{57}Fe chemical shift. An account of factors influencing transition metal NMR chemical shifts [9] is geven in detail in Chapter 2 (section 2.6.3). Figure **6.1** shows an NMR spectrum of ^{57}Fe-^{31}P{1H} with both internal projection and separately recorded spectrum for ^{31}P.

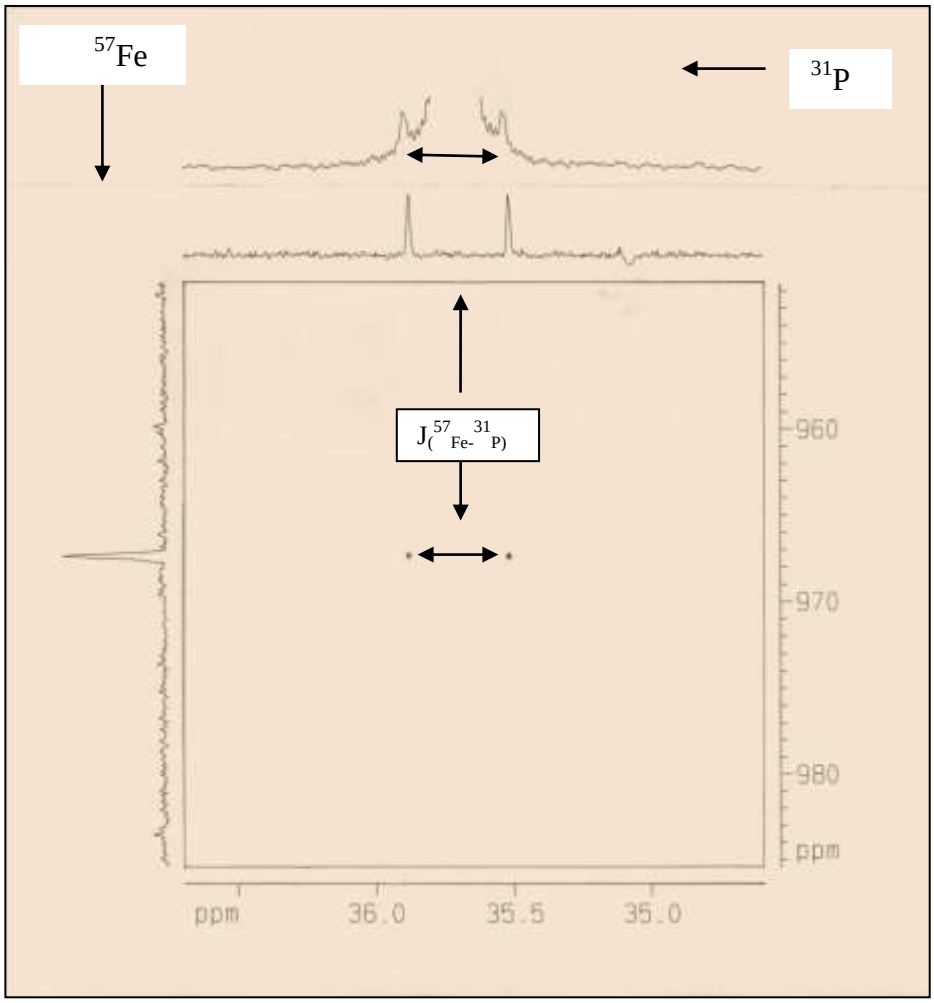


Figure 6.1 ^{57}Fe NMR spectrum of [CpFe(PMe_2Ph)$_2$($SnPh_3$)] **15** in CDCl3 at 300 K (^{31}P axis shows the 1D ^{31}P{1H} spectrum separately obtained (top) and the internal projection (bottom)).

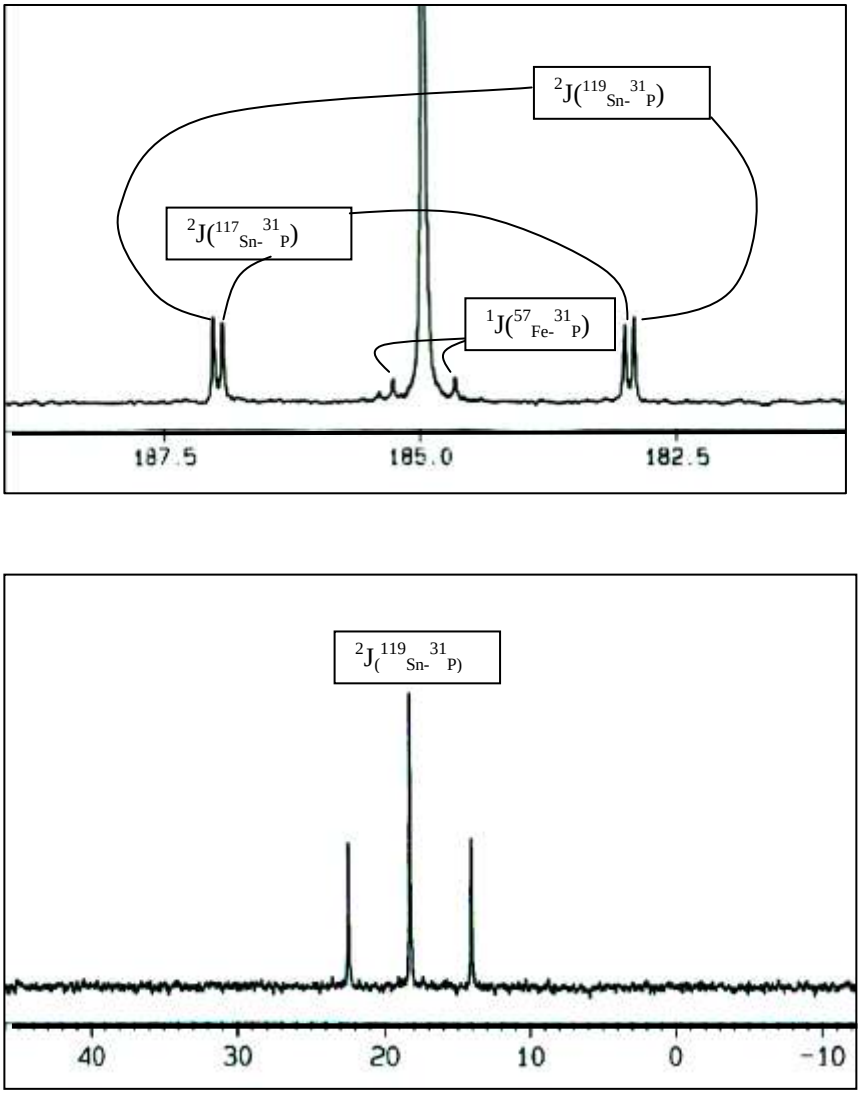


Figure 6.2 ^{31}P NMR spectrum of $[CpFe\{P(OMe)_3\}_2(SnPh_3)]$ **16** (top) and ^{119}Sn NMR spectrum of $[CpFe\{P(OPh)_3\}_2(SnPh_3)]$ **17** (bottom)

Figures 6.2 illustrate the kind of spin interaction from which the geometry and electronic information about the molecular structure of the disubstituted complexes of the type $[CpFe\{P(R)_3\}_2(SnPh_3)]$ could be derived.

6.4.2 X-ray crystallographic study

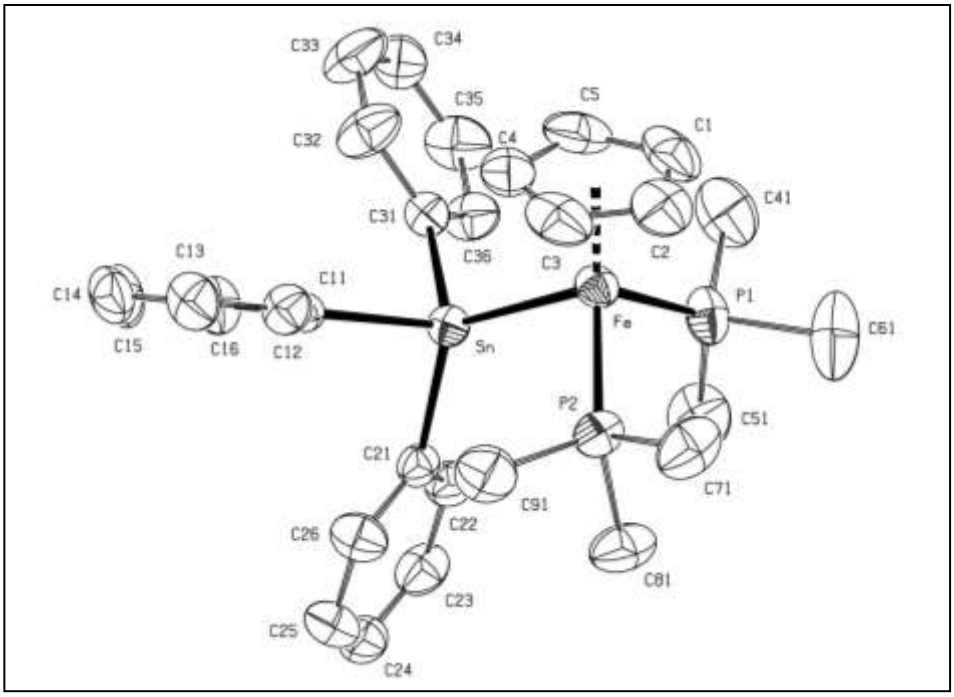
Compounds **14** and **16** crystallize into monoclinic crystal systems in P2(1)/c and Cc space groups respectively whilst **15** crystallizes into a triclinic system in the P-1 space group as in the

monocarbonylated complex [CpFe(CO)(PMe_2Ph)$SnPh_3$]. Complexes **14**, **15** and **16** assume a three legged "piano stool" geometry with the cyclopentadiene ring lying above the Fe atom and P_1, P_2 and Sn atoms forming the legs or put in simple terms as distorted octahedral (or tetrahedral) depending on the description of the π-bonding linkage to the cyclopentadienyl ring. The angle subtended at the iron atom by the covalently bonded atoms for **15** averages 95.47(6) ^{0} with the P_1-Fe-P_2 bond angle being the highest 97.68(4) ^{0}, **14** averages 95.34(3) ^{0} with P_1-Fe-Sn being the highest at 96.87(2) ^{0} and **16** averaging 91.89(3) ^{o} with P_1-Fe-P_2 the highest at 95.66(4) ^{o} (**Table 6.3**). The above calculations assume the averaged Fe-C(cp) bond length in which a single line is subtended from the iron atom to the centroid of the cyclopendienyl (cp) ring. The centroid of the ring is determined from the average-sum of the bond lengths between the iron and all the carbons atoms of the cp ring. The Fe-C(cp) bond length distribution for compound **14** can be grouped into two averages of 2.090 Å and 2.112(5) Å which may not necessarily suggest that the cyclopentadienyl ligand is bonded in an $^3\eta$ manner because of their small difference. But if a single line is drawn from the Iron atom to the centroid of the ring as may be the case for complexes **15** and **16** which have Fe-C(cp) bond averages of 2.084(6) Å and 2.08792) Å respectively, an approximate tetrahedral arrangement results.

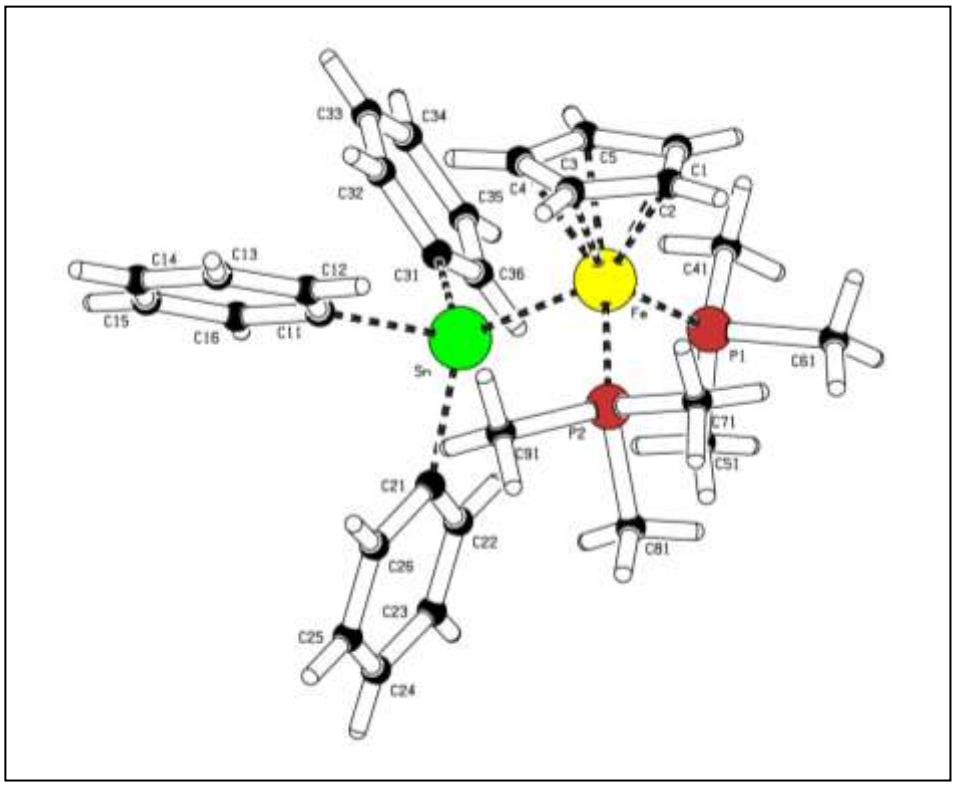
Figures 6.3, 6.4 and 6.5 show the overall stereochemistry and atomic numbering scheme, and selected bond lengths and angles are given in **Tables 6.3**. The ease of access to a disubstituted triphenylphosphite complex (ligand cone angle of 128 °) compared to a triphenylphosphine compound (ligand cone angle of 145 °) seems to be sterically dependent and is likely to be supported by the flexibility of P–O–C bond angle (i.e by adapting to the geometry that minimizes the size of the cone angle). This phenomenon was indeed demonstrated by Ernst and co-workers who showed that the $P(OMe)_3$ ligand can adopt a configuration where all three methyl groups are not bent back away from the metal center [10] (minimum steric hindrance) and more recently by Coville and co-workers [11] who have shown complexes containing $(alkoxy)_3P$ ligands to exhibit conformational flexibility with crystallographically determined cone angles significantly greater than values reported by Tolman [3] (high steric hindrance). Darensbourg and co-workers have studied the steric impact in complexes of the type $M(CO)_4[P(OPh)_3]_2$ (M = Mo and W) which demonstrate flexibility around the $P(OPh)_3$ ligand [12].

Table 6.3 Selected bond lengths (Å) and angles (deg) for compounds [CpFe(PMe_3)$_2$$SnPh_3$] (**14**), [CpFe($PMe_2Ph$)$_2$$SnPh_3$] (**15**) and [CpFe{$P(OMe)_3$}$_2$$SnPh_3$] (**16**).

Bond lengths (Å)	**14**	**15**	**Bond lengths (Å)**	**16**
Sn-C(31)	2.208(2)	2.186(3)	**Sn-C(31)**	2.184(7)
Sn-C(21)	2.200(2)	2.203(3)	**Sn-C(21)**	2.190(7)
Sn-C(11)	2.198(2)	2.204(3)	**Sn-C(11)**	2.175(2)
Sn-Fe	2.5715(5)	2.5446(5)	**Sn-Fe**	2.529(0)
Fe-C(1)	2.086(2)	2.079(4)	**Fe-C(1)**	2.094(0)
Fe-C(2)	2.090(2)	2.091(4)	**Fe-C(2)**	2.088(3)
Fe-C(3)	2.106(2)	2.080(4)	**Fe-C(3)**	2.091(1)
Fe-C(4)	2.118(2)	2.090(4)	**Fe-C(4)**	2.074(3)
Fe-C(5)	2.094(2)	2.083(4)	**Fe-C(5)**	2.088(1)
Fe-P(1)	2.1842(7)	2.1844(10)	**Fe-P(1)**	2.103(7)
Fe-P(2)	2.2098(7)	2.1840(10)	**Fe-P(2)**	2.115(0)
P(1)-C(51)	1.842(3)	1.828(4)	**P-O(01)**	1.626(1)
P(1)-C(41)	1.839(3)	1.836(4)	**P-O(02)**	1.604(9)
P(1)-C(61)	1.861(3)	1.840(4)	**P-O(03)**	1.594(9)
P(2)-C(81)	1.845(3)	1.829(3)	**P-O(04)**	1.609(2)
P(2)-C(91)	1.827(3)	1.833(4)	**P-O(05)**	1.604(0)
P(2)-C(71)	1.836(2)	1.836(3)	**P-O(06)**	1.620(0)
Bond angles (°)	**14**	**15**	**Bond angles (º)**	**16**
C(31)-Sn-Fe	112.54(7)	112.40(8)	**C(31)-Sn-Fe**	115.98(10)
C(21)-Sn-Fe	126.89(7)	127.53(7)	**C(21)-Sn-Fe**	108.84(9)
C(11)-Sn-Fe	116.29(7)	115.41(8)	**C(11)-Sn-Fe**	126.96(9)
P(2)-Fe-P(1)	94.93(3)	97.68(4)	**P2-Fe-P1**	95.66(4)
P(2)-Fe-Sn	96.87(2)	94.09(3)	**P2-Fe-Sn**	89.75(3)
P(1)-Fe-Sn	94.23(2)	94.66(3)	**P1-Fe-Sn**	89.27(3)
C(51)-P(1)-Fe	120.62(9)	124.28(13)	**Fe-P4-O(01)**	120.41
C(41)-P(1)-Fe	114.90(10)	114.53(14)	**Fe-P4-O(02)**	117.01
C(61)-P(1)-Fe	118.74(9)	115.38(14)	**Fe-P4-O(03)**	116.71
C(81)-P(2)-Fe	118.53(9)	122.40(13)	**Fe-P7-O(04)**	112.42
C(91)-P(2)-Fe	121.08(9)	117.42(13)	**Fe-P7-O(05)**	118.46
C(71)-P(2)-Fe	113.74(8)	114.73(14)	**Fe-P7-O(06)**	121.69

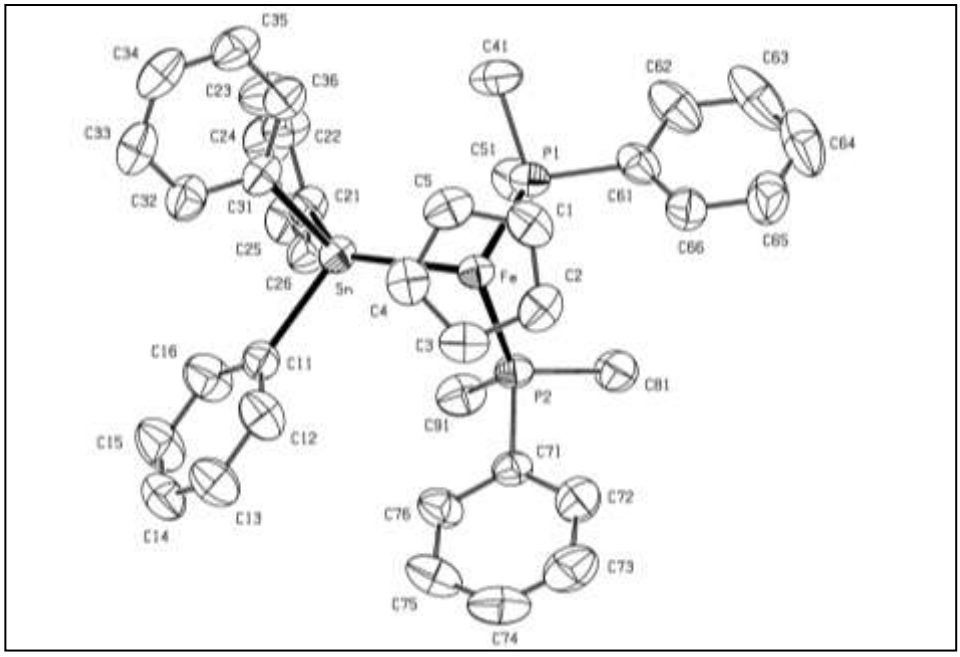


A

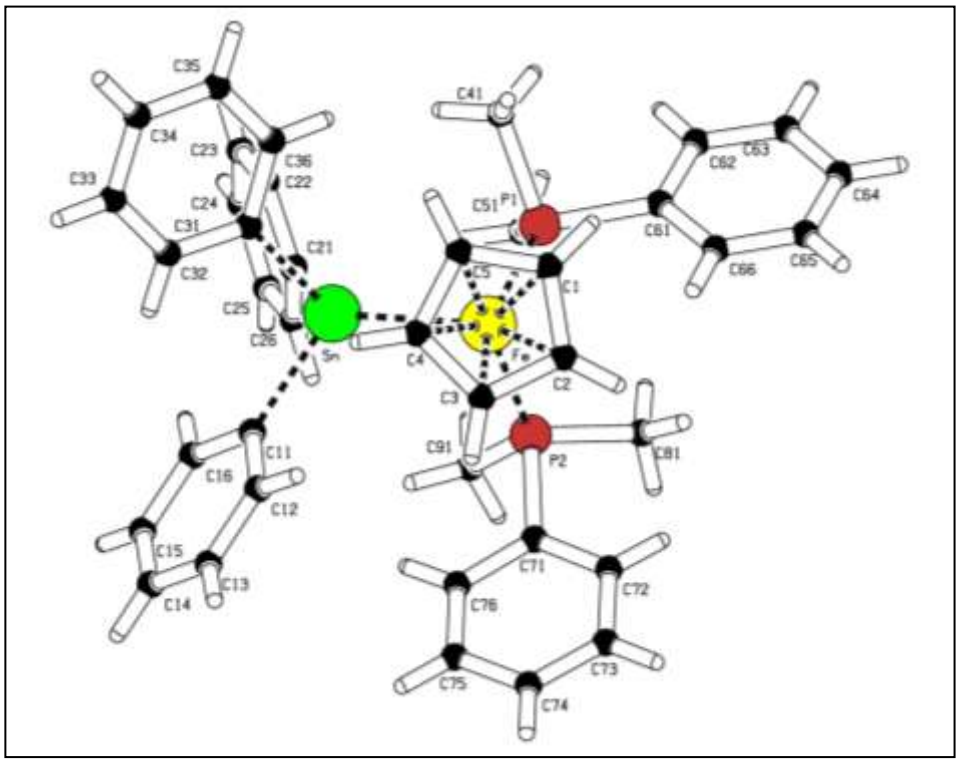


B

Figure 6.3 (A) ORTEP drawing of [CpFe(PMe_3)$_2$$SnPh_3$] **14** showing thermal ellipsoids at the 50% probability level and (B) SCHAKAL stereoview for clarity

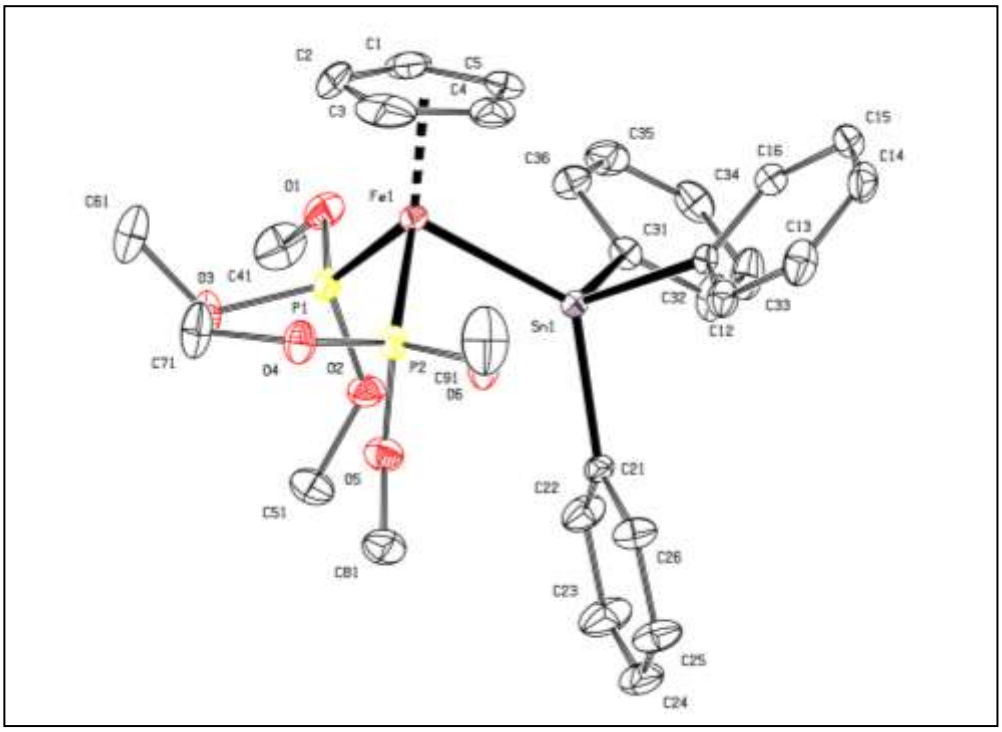


A

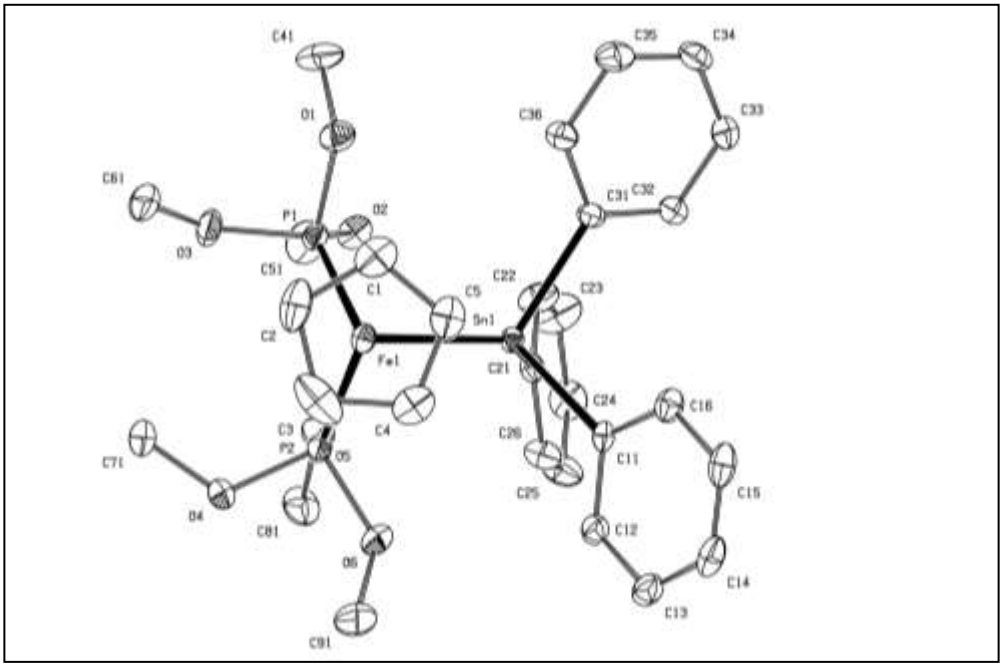


B

Figure 6.4 (A) ORTEP drawing of [CpFe(PMe_2Ph)$_2$$SnPh_3$] **<u>15</u>** showing thermal ellipsoids at the 50% probability level and (B) SCHAKAL stereoview for clarity.



(A)



(B)

Figure 6.5 (A) ORTEP drawing of [CpFe{P(OMe)$_3$}$_2$SnPh$_3$] **16** showing thermal ellipsoids at the 50% probability level and (B) SCHAKAL stereoview for clarity.

6.4.2.1 The Iron-Tin bond interactions.

As noted by Graham and co-workers [13], it has been customary to interpret bond-shortening relative to single bond character as indicative of multiple bond character. The average Fe-Sn bond lengths in **15**, **14** and **16** are 2.5446(5) Å, 2.5715(5) Å and 2.5288(5) Å respectively and are not short enough to suggest double bond character. These Fe-Sn bond lengths are similar to those of complexes of the type [CpFe(CO)(PR_3)$SnPh_3$] (**2** - **13**) which ranged between 2.5196(9) Å to 2.5569(9) Å and also similar to the dicarbonyl complex [CpFe($CO)_2SnPh_3$] (2.536(3) Å) [14] . The Fe-Sn bond lengths are significantly larger among the dicarbonylated [CpFe($CO)_2SnPh_3$], monocarbonylated [CpFe(CO)(PR_3)$SnPh_3$] and the decarbonylated [CpFe($PR_3)_2SnPh_3$] complexes containing -$SnPh_3$ in comparison to the Fe-Sn bond length averages from complexes of the type [CpFe($CO)_2SnX_3$] (X = Cl or Br) which average 2.466(2) Å [14,15] where a different conformation about the Fe-Sn bond has been found.

6.4.2.2. The triphenyltin group.

The tin atom has an approximate tetrahedral geometry consisting of three-triphenyl groups and a fourth position occupied by the iron atom. The Sn-C (phenyl ring carbons) bond length average 2.19(8) Å which is slightly larger than the average 2.18 Å observed for the tetramethyltin and trimethyltin halides [5] and falls within the average lengths found in other tin compounds as summarized by Schempler [16]. The inter C-Sn-C bond angles for **14**, **15** and **16** average 98.77(5) ^{0}, 98.89(11) ^{0} and 100.57(8) ^{o} respectively and are significantly shorter than the normal tetrahedral value of 109.5 ^{0}. The average Fe-Sn-C bond angles of 117.93(10) ^{0} for **14** and 118.06(14) ^{0} for **15** are similar to the values reported for compounds of the type [CpFe($CO)_2(SnX_3)$] [14,15] (where X = Cl, Br, or Ph). Cullen and co-workers [17] have suggested that an imbalance in the *p*-orbital charge density at the tin atom would result in the distortion from tetrahedral environment (thus implying an increased s-character for the Fe-Sn bond) [18]. This distortion may also be partly due to the different substituents attached to the tin atom. It is worth noting that among the Fe-Sn-C bond angles for both **14** and **15**, there exists a single large bond angle of 126.89(7) ^{0} for **14** and 127.53(7) ^{0} for **15** compared to the other smaller Fe-Sn-C bond angles averaging 114.42(2) ^{0} for **14** and 113.91(3) ^{0} for **15.** This

inconsistency can be assumed to be as a result of methyl hydrogens of PMe_3 for **14** and PMe_2Ph for **15** which are orientated axially opposite to the Cp ring carbons and closer in space to the Sn atom. It is interesting to note that among C-Sn-Fe bond angles for compound **16** the same trend is observed where the smallest angle differs from the largest by at least 18^0.

6.4.2.3 The Cyclopentadienyl ring.

The average C-C bond lengths in the ring are 1.407(4) Å for **14,** 1.399(5) Å for **15** and 1.402(0) Å for **16** which are slightly larger than the corresponding mean value of 1.396(14) Å for $[CpFe(CO)_2SnPh_3]$. The ring is planar and therefore the maximum displacement of an atom from the plane is expected to be in the range of 0.03 Å as in complexes of the type $[CpFe(CO)(PR_3)SnPh_3]$ (see Chapter 5, section 5.4.2). The Fe-C(Cp) bond length averages between 2.086(2) and 2.118(2) which is within the range of both complexes of the type $[CpFe(CO)(PR_3)SnPh_3]$ (PR_3 = phosphine or phosphite ligands) and $[CpFe(CO)_2SnPh_3]$. Similarly, the iron atom is found to be 1.71(5) Å as expected from the centroid of cyclopentadienyl as found for the complex **[**$CpFe(CO)_2SnPh_3$] [14].

6.5 Conclusions

Disubstituted (decarbonylated) complexes of the type $[CpFe(PR_3)_2SnPh_3]$ were obtained by photochemical irradiation using UV light source under mild conditions and fully characterized by multinuclear NMR spectroscopy and single crystal diffraction methods. Despite a limited number of compounds synthesized (only four), the NMR spectroscopic results are consistent with the trend already established in the previous work (Chapter 5) i.e. that the ^{57}Fe chemical shift increases as Tolman's cone angle increases and is very sensitive to changes in the substituents on the phosphorus ligands. The $^1J_{(Fe\text{-}P)}$ seems to increase as Tolman's electronic property increases. The opposite is observed for $\delta(^{57}Fe)$ which decreases with increasing Tolman's electronic parameter. However, it seems that the electronic property of the phosphorus substituent has a greater influence on the ^{57}Fe chemical shifts than the steric factor as observed in the previous work in Chapter 5. X-ray crystallographic data are consistent with their monosubstituted analoques in which a 'piano stool' or 'tripod' framework is evident.

References

1. (a) R.H. Crabtree, *Top Organomet. Chem*., 34 (2011) 1; (b) F.A. Cotton and G. Wilkinson *in Advanced Inorganic Chemistry, A Comprehensive Text*, John Wiley and Sons, New York, 4th Ed., (1980) 87.

2. (a) E. Fiset and J.-F Morin, *Polymer*, 50 (2009) 1369; (b) G.D. Wilson, M.M. Caruso, N.T. Reimer, S.R. White, N.R. Sottos and J.S. Moore, *Chem. Materials*, 20 (2008) 3288; (c) M. Gandelman, K.M. Naing, B. Rybtchinski, E. Poverenov, Y. Ben-David, N. Ashkenazi, R.M. Gauvin and D. Milstein, *J. Am. Chem. Soc*., 127 (2005) 15265; (d) A. Deiters and S.F. Martin, *Chem. Rev*., 104 (2004) 2199; (e) C.E. Carraher Jr., C.U. Pittman Jr., *in Macromolecules Containing Metal and Metal-Like Elements, Biomedical Applications*, A. S. Abdel-El-Aziz, J. E. Sheats and M. Zeidin, , John Wiley, New York, Volume 3 (2004) 1.

3. C.A. Tolman, *Chem Rev*., 77 (1977) 313.

4. (a) B. Rouida, M. Pankowski, W. Chodkeiwics and G. Jaouen, *J. Organomet. Chem*., 342 (1988) C10-C12; (b) F.W.B. Einstein and R. Restivo, *Inorg. Chim. Acta*, 5 (1971) 501; (c) P.M. Treichel and D.A. Komar, *J. Organomet. Chem*., 206 (1981) 77; (d) B. O'Owyer and A. R. Manning, *Inorg. Chim. Acta*, 38 (1980) 103; (e) H. Nakazawa, Y. Yamaguchi, K. Kawamura and K. Miyoshi, *Organometallics*, 16 (1997) 4626.

5. R.D. Gorsich, *J. Am. Chem. Soc*., 84 (1962) 2486.

6. P.M. Treichel and D.A. Komar, *J. Organomet. Chem*., 206 (1981) 77.

7. (a) J.G. Verkade, *Coord. Chem. Rev*., 9 (1972) 1; (b) T.G. Appleton, H.C. Clark and L.E. Manzer, *Coord. Chem. Rev*., 10 (1973) 335.

8. R.G. Kidd and R.J. Goodfellow, in: *NMR and the Periodic Table*, R.K. Harris and B.E. Mann, eds., Academic Press, London, (1978).

9. (a) C.J. Jameson and J. Mason, in: *Multinuclear NMR*, J. Mason, ed., Plenum Press, New York, 1987; (b) L. Carlton, *Annu. Rep. NMR Spectrosc*., 63 (2008) 49.

10. (a) L. Stahl and R.D. Ernst, *J. Am. Chem. Soc*., 109 (1987) 5673; (b) L. Stahl, W. Trakarnpruk, J.W. Freeman, A.M. Arif and R.D. Ernst, *Inorg. Chem*., 34 (1995) 1810.

11. (a) J.M. Smith, N.J. Coville, L.M. Cook and J.C.A. Boeyens, *Organometallics*, 19 (2000) 5273; (b) J.M. Smith and N.J. Coville, *J. Organometallics*, 20 (2001) 1210.

12. D.J. Darensbourg, J.R. Andreatta, S.M. Stranahan and J.H. Reibenspies, *Organometallics*, 26 (2007) 6832.

13. W.A. Graham, W. Jetz, P.B. Simons and J.A.J. Thomson, *Inorg. Chem*., 5 (1966) 2217.

14. R. F. Bryan, *J. Chem. Soc*. (A) (1967) 192.

15. R.F. Bryan, P.T. Greene, G.A. Melson and P.F. Stokely, *Chem. Comm*., (1966) 722.

16. E.D. Schempler, *Inorg. Chem*., 11 (1967) 2012

17. W.R. Cullen, J.R. Sam and J.A.J. Thomson, *Inorg. Chem*., 10 (1971) 843

18. (a) H.A. Bent, *J. Inorg. Nuclear Chem*., 19 (1961) 43; (b) H.A. Bent, *Chem. Rev*., 61 (1961) 275.

CHAPTER 7

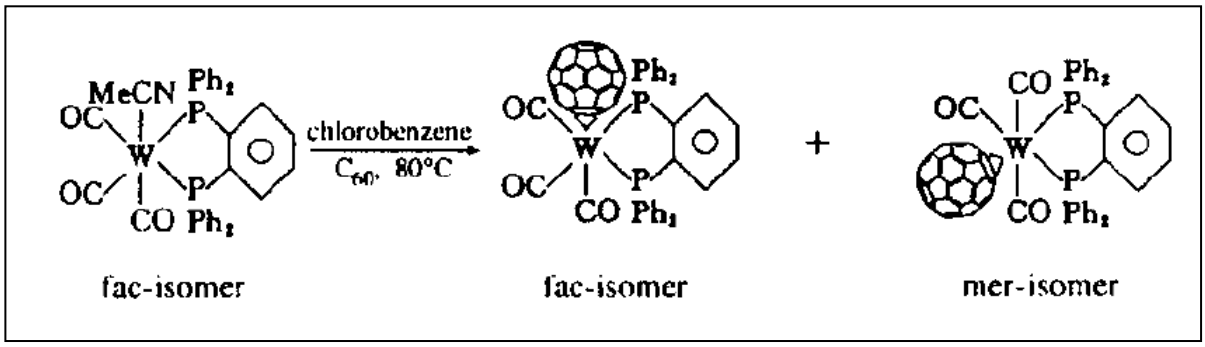
Synthesis and Characterization of Tetracarbonyl Tungsten Complexes: $[W(CO)_4(NCMe)(PR_3)]$

7.1 Introduction

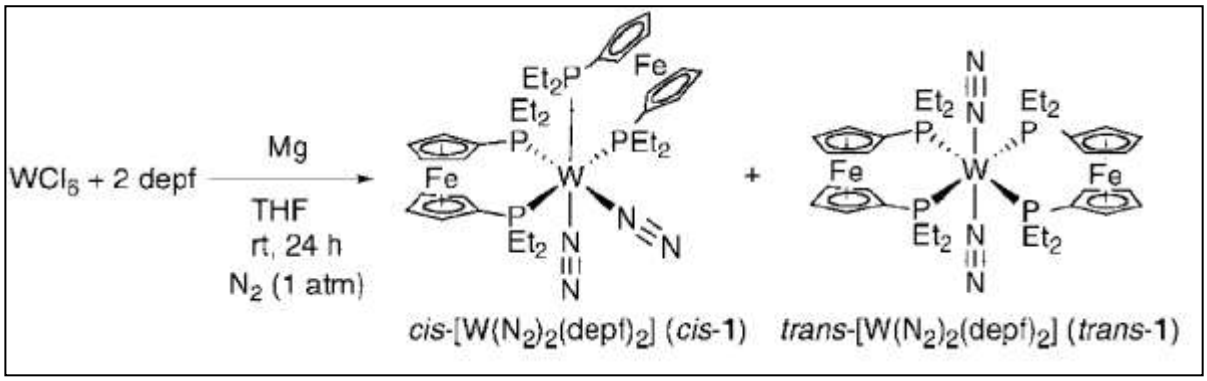
Synthesis of organometallic complexes of the type $[W(CO)_4(L)(PR_3)]$ where PR_3 is a tertiary phosphine or phosphite and L is a labile ligand such as nitrile N-donor group have been reported as far back as 1961 [1]. Among the N-donor group compounds are acetonitrile complexes where the labile acetonitrile group can be replaced easily by other ligands [2]. These compounds have since been prepared as precursors for a variety of tungsten complexes from octahedral [3] to seven coordinate (through oxidative addition reactions) [4] organometallic compounds with varying oxidation states i.e. $[WCl(SnCl_3)(CO)_3(NCR)_2]$ (R = Me, Et, *n*-Bu and Ph) and $\{[WH(CO)_3(NCMe)(PPh_3)_2]$-$[SnCl_5.MeOH]\}$. The six coordinate complex, $[W(CO)_5(NCMe)]$ has been found to transform vinylthiirane and a series of methyl-substituted vinylthiiranes into a series of 3,6-dihydro-1,2-dithiin compounds [5]. This process is significant in the cleavage of carbon-sulfur bonds in which the cyclic thioethers are central to the process relating to the hydrodesulfurization of petroleum feedstocks [6].

Our interest in the synthesis of the six coordinate tungsten(0) organometallic compounds of the type $[W(CO)_5PR_3]$ arises for a number of reasons and the most common among them is steric influence by the phosphorus donor groups such as phosphines and phosphites [7] in the synthesis of bridged heterobimetallic complexes of tungsten and platinum (Chapter 8) or rhodium (Chapter 9). Synthesis of this type of complex from $W(CO)_6$ has been achieved through a number of preparative procedures such as refluxing in high boiling solvent (e.g. diglyme) [8] and

photochemically by replacing carbonyl groups to give mono- and disubstituted derivatives [9]. The $[W(CO)_5PR_3]$ complexes are isolated in high yield as stable, non-volatile monomeric compounds. The synthesis of $[W(CO)_5PR_3]$ let to a flurry of reports of tungsten(0) complexes, among them are compounds of the general formula $[W(CO)_{6-n}(AR_3)_n]$ where AR_3 is a trialkyl or tertiary phosphine, phosphite, arsine or stibine [8], complexes containing two different donor ligands $[W(CO)_4(PR_3)(PR'_3)]$ [3b,10,11] and the first fullerene complex containing a diphenylphosphinobenzene (dppb) ligand, [*fac/mer*-$W(CO)_3$(dppb)(η^2-C_{60})] via a displacement reaction of [*fac*-$W(CO)_3$(MeCN)(dppb)] [3c] (Scheme 7.1). Recently, there has been major interest in the preparation and reactivity of transition metal dinitrogen complexes [12] such as tungsten-dinitrogen complexes bearing ferrocenyldiphosphines [13] (Scheme 7.2). These complexes offer an opportunity of acting as a bridging metallo-ligand.



Scheme 7.1 Reaction of [*fac*-$W(CO)_3$(MeCN)(dppb)] complex with C_{60} (from ref. [3c])



Scheme 7.2 Novel reaction of a six coordinate tungsten(VI) compound with a diphosphino complex. (from ref. [13])

Our aim in this particular piece of work is to synthesize a number of six coordinate tungsten(0) complexes of the type $[W(CO)_5(PR_3)]$ and $[W(CO)_4(PR_3)(NCMe)]$ where PR_3 is *para*-tolylphosphine, $[P(p\text{-}MeC_6C_4)_3]$, *para*-methoxyphenylphosphine $[P(p\text{-}OMeC_6H_4)_3]$, *para*-fluorophenylphosphine $[P(p\text{-}FC_6H_4)_3]$, *para*-trifluorophenylphosphine $[P(p\text{-}CF_3C_6H_4)_3]$ and dimethylaminophosphine $[P(NMe_2)_3]$. Trimethylamine-oxide as decarbonylating agent (the mechanism was discussed in Chapter 1, Section 1.5) is applied to promote the substitution of the carbonyl by a labile acetonitrile ligand. Herein, we report the synthesis of complexes of the type $[W(CO)_4(NCMe)(PR_3)]$ which can be used as metallo-ligands in the synthesis of bridged heterobimetallic complexes of tungsten and platinum or rhodium.

7.2 Experimental: Synthesis, NMR and X-ray characterization of $[W(CO)_5(PR_3)]$

Tungsten hexacarbonyl ($W(CO)_6$), phosphines (PR_3, R = *p*-tolyl, *p*-$OMeC_6H_4$, *p*-$CF_3C_6H_4$, *p*-FC_6H_4, and NMe_2; R_3 = $MePh_2$ and $Ph_2C_6F_5$) and trimethylamine oxide (Me_3NO) were purchased from various suppliers and used without further purification. Diglyme (2-methoxyethyl ether) was distilled from sodium and acetonitrile, benzene, hexane and THF were purified according to the procedures in Chapter 3. Complexes of the type $[W(CO)_5(PR_3)]$ **18** - **22** were prepared by the method of Magee and co-workers [8a]. All operations were performed under an atmosphere of argon.

7.2.1 Preparation of $[W(CO)_5PPh_3]$ …… (18)

A solution of $W(CO)_6$ (1.000 g ~ 2.842 mmol) and PPh_3 (747 mg ~ 2.849 mmol) in diglyme (20 ml) was charged into a Schlenk tube and brought to a boiling (~ 165 ºC) temperature. The sublimed $W(CO)_6$ was occasionally returned back into the solution before the Schlenk tube was resealed to reflux overnight. After approximately 14 hrs of refluxing, the solution was cooled to room temperature and the greenish precipitate filtered leaving behind a clear yellow-green solution. The solution was left in a freezer for three days after which light yellow crystals were collected, washed with cold ethanol (5 ml x 2) and dried under reduced pressure giving a quantitative yield of 1.811 g (99%). NMR spectra were recorded from a solution in C_6D_6 at 300

K. ^{1}H NMR ($\delta_{(ppm)}$): 7.51 (m, 15H, PPh_3); ^{13}C NMR ($\delta_{(ppm)}$): 199.15 (d, 1C, CO, $^{2}J_{P-C}$ = 22 Hz), 197.26 (d, 4C, CO, $^{2}J_{P-C}$ = 6.9 Hz, dd, satellite, $^{1}J_{(W-C)}$ = 126 Hz), 135.25 (d, 3C, PPh_3, $^{1}J_{P-C}$ = 41 Hz), 132.99 (d, 6C, PPh_3, $^{2}J_{P-C}$ = 12 Hz), 130.33 (d, 3C, PPh_3, $^{4}J_{P-C}$ = 2.3 Hz), 128.63 (d, 6C, PPh_3, $^{3}J_{P-C}$ = 10 Hz).^{31}P NMR ($\delta_{(ppm)}$): 21.30 (s, ^{31}P, PPh_3, satellite, d, $^{1}J_{W-P}$ = 243 Hz). IR (compressed solid), $\nu_{(CO)}$ = 2071(s), 1985(m), 1893(vs) cm^{-1}.

7.2.2 Preparation of $[W(CO)_5P(p\text{-tolyl})_3]$……. (19)

A solution of $W(CO)_6$ (676 mg ~ 1.921 mmol) and P(*p*-tolyl)$_3$ (585 mg ~ 1.921 mmol) in diglyme (10 ml) was refluxed overnight in a sealed Schlenk tube. The solution was cooled and a resulting brownish precipitate was filtered leaving behind pale yellow solution which was left undisturbed at room temperature for 4 days. Pale yellow crystalline lumps were obtained and were washed with cold ethanol (3 ml x 3) and dried under reduced pressure giving a yield of 917 mg (76%). NMR spectra were recorded from a solution in C_6D_6 at 300 K. ^{1}H NMR ($\delta_{(ppm)}$): 7.45 (m, 6H, P(*p*-$CH_3C_6\underline{H}_4)_3$), 6.85 (m, 6H, P(*p*-$CH_3C_6\underline{H}_4)_3$), 1.94 (s, 9H, P(*p*-$C\underline{H}_3C_6H_4)_3$). ^{13}C NMR ($\delta_{(ppm)}$): 199.59 (d, 1C, CO, $^{2}J_{P-C}$ = 21 Hz), 198.04 (d, 4C, CO, $^{2}J_{P-C}$ = 6.9 Hz), 140.64 (d, 3C, P(*p*-$CH_3\underline{C}_6H_4)_3$, $^{4}J_{P-C}$ = 1.5 Hz), 133.26 (d, 6C, P(*p*-$CH_3\underline{C}_6H_4)_3$, $^{2}J_{P-C}$ = 12 Hz), 132.80 (d, 3C, P(*p*-$CH_3\underline{C}_6H_4)_3$, $^{1}J_{P-C}$ = 42 Hz), 129,60 (d, 6C, P(*p*-$CH_3\underline{C}_6H_4)_3$, $^{3}J_{P-C}$ = 11 Hz), 20.97 (s, 3C, P(p-$\underline{C}H_3C_6H_4$). ^{31}P NMR ($\delta_{(ppm)}$): 18.70 (s, P(*p*-$CH_3C_6H_4)_3$, satellite, d, $^{1}J_{W-P}$ = 242 Hz). IR (compressed solid), $\nu_{(CO)}$ = 2068(s), 1986(m), 1912(vs), 1895(vs) cm^{-1}.

7.2.3 Preparation of $[W(CO)_5P(p\text{-}OMeC_6H_4)_3]$ ……..…… (20)

A solution of $W(CO)_6$ (500 mg ~ 1.420 mmol) and P(*p*-$OMeC_6H_4)_3$ (501 mg ~ 1.420 mmol) in diglyme (10 ml) was refluxed for 8 hrs in a sealed Schlenk tube. The solution was allowed to cool to room temperature after which a small brownish precipitate was filtered off leaving behind a clear pale yellow solution. The solution was left at room temperature for four (4) days and no crystals formed. n-Hexane (1 ml) was added and still no crystals formed after several days. After about a month of slow evaporation, an off-white crystalline precipitate was then collected and washed with cold ethanol (3 ml x 3) giving a yield of 489 mg (51%). NMR spectra were recorded from a solution in $CDCl_3$ at 300 K. ^{1}H NMR ($\delta_{(ppm)}$): 7.34 (m, 6H, P(*p*-$OMeC_6\underline{H}_4)$),

6.94 (m, 6H, *p*-OMeC$_6$H$_4$), 3.83 (s, 9H, P(*p*-OMeC$_6$H$_4$)). ^{13}C NMR ($\delta_{(ppm)}$); 199.54 (d, 1C, CO, $^2J_{P-C}$ = 28 Hz), 197.53 (d, 4C, CO, $^2J_{P-C}$ = 9.0 Hz), 161.0 (d, 3C, P(*p*-OMeC$_6$H$_4$), $^4J_{P-C}$ = 2.0 Hz), 134.40 (d, 6C, P(*p*-OMeC$_6$H$_4$), $^2J_{P-C}$ = 18 Hz), 127.07 (d, 3C, P(*p*-OMeC$_6$H$_4$), $^1J_{P-C}$ = 61 Hz), 114.06 (d, 6C, P(*p*-OMeC$_6$H$_4$), $^3J_{P-C}$ = 14 Hz), 55.30 (s, 3C, P(*p*-OMeC$_6$H$_4$). ^{31}P NMR ($\delta_{(ppm)}$): 22.72 (s, 1P, P(*p*-OMeC$_6$H$_4$), satellite, d, $^1J_{W-P}$ = 244 Hz). IR (compressed solid), $\nu_{(CO)}$ = 2066(s), 1982(m), 1894(vs) cm^{-1}.

7.2.4 Preparation of [W(CO)$_5$P(*p*-FC$_6$H$_4$)$_3$] …… (21)

A mixture of W(CO)$_6$ (500 mg ~ 1.420 mmol) and P(*p*-FC$_6$H$_4$)$_3$ (449 mg ~ 1.420 mmol) in diglyme (6 ml) was refluxed for 8 hrs in a sealed Schlenk tube. The clear pale yellow solution was filtered to remove a blackish fine powdered precipitate and the filtrate was left undisturbed at room temperature for four (4) days during which no crystals formed. n-Hexane (1 ml) and diethyl ether (1 ml) were added drop-wise and again left undisturbed at room temperature for almost four (months) after which pale yellow crystals formed. Pale yellow crystalline flakes were washed with cold ethanol (3 ml) giving a yield of 590 mg (62%). NMR spectra were recorded from a solution in CD_2Cl_2 at 300 K. 1H NMR ($\delta_{(ppm)}$): 7.44 (m, 6H, P(*p*-FC$_6$H$_4$)$_3$, 7.18 (m, 6H, P(*p*-FC$_6$H$_4$)$_3$).^{13}C NMR ($\delta_{(ppm)}$): 198.50 (d, 1C, CO, $^2J_{P-C}$ = 22 Hz), 196.92 (d, 3C, CO, $^2J_{P-C}$ = 6.9 Hz), 164.00 (dd, 3C, P(*p*-FC$_6$H$_4$)$_3$, $^1J_{P-C}$ = 25 Hz, $^5J_{F-C}$ = 2.3 Hz), 134.91 (dd, 6C, P(*p*-FC$_6$H$_4$)$_3$, $^2J_{P-C}$ = 14 Hz, $^3J_{F-C}$ = 8.4 Hz), 130.89 (dd, 3C, P(*p*-FC$_6$H$_4$)$_3$, $^4J_{P-C}$ = 3.1 Hz, $^1J_{F-C}$ = 43 Hz), 116.9 (dd, 6C, P(*p*-FC$_6$H$_4$)$_3$, $^3J_{P-C}$ = 11 Hz, $^2J_{F-C}$ = 21.5 Hz). ^{31}P NMR ($\delta_{(ppm)}$): 21.24 (s, 1P, P(*p*-FC$_6$H$_4$)$_3$, satellite, d, $^1J_{W-P}$ = 247 Hz). IR (compressed solid), $\nu_{(CO)}$ = 2072(s), 2014(m), 1985(sh), 1892(vs) cm^{-1}.

7.2.5 Preparation of [W(CO)$_5$P(*p*-CF$_3$C$_6$H$_4$)$_3$] …….. (22)

A mixture of W(CO)$_5$ (838 mg ~ 2.381 mmol) and P(*p*-CF$_3$C$_6$H$_4$)$_3$ (1110 mg ~ 2.881 mmol) in diglyme (10 ml) and THF (10 ml) was refluxed for 14 hrs in a sealed Schlenk tube. Once stirring was stopped, the light yellow solution was cooled to room temperature before the solvent was removed *in vacuo*. The off-white crystalline precipitate started forming after about 10% of the solvent volume was removed. After the complete solvent removal, the off-white precipitate was then washed with cold ethanol (5 ml x 2) and dried under vacuum giving a yield of 983 mg

(53%). NMR spectra were recorded from a solution in $CDCl_3$ at 300 K. ^1H NMR ($\delta_{(ppm)}$): 7.76 (m, 6H, P(*p*-$CF_3C_6H_4)_3$, 7.58 (m, 6H, P(*p*-$CF_3C_6H_4)_3$. ^{13}C NMR ($\delta_{(ppm)}$): 197.58 (d, 3C, CO, $^2J_{(P-C)}$ = 24 Hz), 196.32 (d, 4C, CO, $^2J_{(P-C)}$ = 6.9 Hz), 138.31 (d, 3C, P(*p*-$CF_3C_6H_4)_3$, $^1J_{(P-C)}$ = 39 Hz), 133.22 (d, 6C, P(*p*-$CF_3C_6H_4)_3$, $^2J_{(P-C)}$ = 13 Hz), 133.05 (dd, 3C, P(*p*-$CF_3C_6H_4)_3$, $^2J_{(F-C)}$ = 133 Hz, $^4J_{(P-C)}$ = 1.9 Hz), 125.98 (m. 6C, P(*p*-$CF_3C_6H_4)_3$), 123.34 (q, 3C, P(*p*-$CF_3C_6H_4)_3$, $^1J_{(F-C)}$ = 272 Hz), 71.25 (d, 3C, P(*p*-$CF_3C_6H_4)_3$, $^1J_{(F-C)}$ = 139 Hz). ^{31}P NMR ($\delta_{(ppm)}$): 24.25 (s, $P(NMe_2)_3$, satellite, d, $^1J_{(W-P)}$ = 248 Hz). IR (compressed solid), $\nu_{(CO)}$ = 2076(s), 1987(m), 1923(vs), 1907(sh) cm^{-1}.

7.2.6 Preparation of $[W(CO)_5P(NMe_2)_3]$ …… (23.1)

A mixture of $W(CO)_6$ (500 mg ~ 1.420 mmol) and $P(NMe_2)_3$ (231 mg ~ 1.420 mmol) in diglyme (10 ml) was refluxed overnight in a sealed Schlenk tube. After ca. 24 hrs, the solution was cooled to room temperature and left undisturbed for one day in which time relatively large yellow crystals were collected and washed with cold ethanol (5 ml) giving a yield of 626 mg (91%). NMR spectra were recorded from a solution in $CDCl_3$ at 300 K. ^1H NMR ($\delta_{(ppm)}$): 2.63 (d, 18H, $P(N\underline{Me}_2)_3$, $^3J_{(P-H)}$ = 10.3 Hz). ^{13}C NMR ($\delta_{(ppm)}$): 199.38 (d, 1C, CO, $^2J_{(P-C)}$ = 28 Hz), 197.77 (dt, 4C, CO, $^1J_{(W-C)}$ = 126 Hz, $^2J_{(P-C)}$ = 8.9 Hz), 38.33 (d, 6C, $P(NMe_2)_3$, $^2J_{(P-C)}$ = 6.4 Hz). ^{31}P NMR ($\delta_{(ppm)}$): 127.47 (s, 1P, satellite, d, $^1J_{(W-P)}$ = 313 Hz). IR (compressed solid), $\nu_{(CO)}$ = 2067(s), 1981(s), 1939(sh), 1872(vs) cm^{-1}.

7.2.7 Preparation of $[W(CO)_5P(MePh_2)]$ …… (23.2)

A mixture of $W(CO)_6$ (560 g ~ 4.00 mmol) and $P(MePh_2)$ (920 mg ~ 4.595 mmol) in diglyme (20 ml) was refluxed overnight in a sealed Schlenk tube. After ca. 24 hrs, the solution was cooled to room temperature and left undisturbed for three days in which time no crystals were formed. The resultant solution was centrifuged to remove greyish precipitate after which the solvent was removed under vacuum leaving behind a light yellow liquid (1.920 g ; 92%). NMR spectra were recorded from a solution in C_6D_6 at 300 K. ^1H NMR ($\delta_{(ppm)}$): 7.24 (m, 4H, $Me\underline{Ph}_2$), 7.00 (M, 6H, $MePh_2$), 1.69 (d, 3H, $^2J_{(P-H)}$ = 6.8 Hz, $\underline{Me}Ph_2$). ^{13}C NMR ($\delta_{(ppm)}$): 199.65 (d, 1C, CO, $^2J_{(P-C)}$ = 20 Hz), 197.45 (d, 4C, CO, $^2J_{(P-C)}$ = 7.24, dd, satellite, $^1J_{(W-P)}$ = 126 Hz), 137.15 (d, 2C, $^1J_{(P-C)}$ = 42 Hz, $Me\underline{Ph}_2$), 131.37 (d, 4C, $^2J_{(P-C)}$ = 12 Hz, $Me\underline{Ph}_2$), 130.25 (d, 2C, $^4J_{(P-C)}$ = 2.2 Hz), $Me\underline{Ph}_2$), 128.85 (d,

4C, $^{3}J_{(P-C)}$ = 9.8 Hz, Me<u>Ph</u>$_2$,), 20.40 (d, 1C, $^{1}J_{(P-C)}$ = 29 Hz, <u>Me</u>Ph$_2$). ^{31}P NMR ($\delta_{(ppm)}$): -3.40 (s, <u>P</u>MePh$_2$, satellite, d, $^{1}J_{(W-P)}$ = 237 Hz). IR (liquid), $\nu_{(CO)}$ = 2069(s), 1928(sh), 1887(vs) cm^{-1}.

7.2.8 Preparation of [W(CO)$_5$P(Ph$_2$C$_6$F$_5$)]……..…….....(<u>23.3</u>)

A solution of W(CO)$_6$ (350 mg ~ 0.994 mmol) and PPh$_2$C$_6$F$_5$ (352 mg ~ 0.999 mmol) in diglyme (12 ml) was refluxed overnight in a sealed Schlenk tube. The solution was the cooled to room temperature and left undisturbed for three days (no crystals formed). The solvent was then removed under reduced pressure leaving behind greenish-yellow liquid (576 mg, 85.7%). NMR spectra were recorded from a solution in C$_6$D$_6$ at 300 K. ^{1}H NMR ($\delta_{(ppm)}$): 7.03 (m, 4H, Ph$_2$), 6.71 (m, 6H, Ph$_2$). ^{13}C NMR ($\delta_{(ppm)}$): 198.32 (d, 1C, <u>C</u>O, $^{2}J_{(P-C)}$ = 25 Hz), 196.78 (d, 4C, <u>C</u>O, $^{2}J_{(P-C)}$ = 7.2 Hz), dd, satellite, $^{1}J_{(W-P)}$ = 126 Hz), 146.32 (d, 2C, C$_6$F$_5$, $^{1}J_{(F-C)}$ = 250 Hz), 142.78 (d, 1C, C$_6$F$_5$, $^{1}J_{(F-C)}$ = 259 Hz), 138.24 (d, 2C, C$_6$F$_5$, $^{1}J_{(F-C)}$ = 260 Hz), 133.70 (d, 2C, Ph$_2$, $^{1}J_{(P-C)}$ = 42 Hz), 133.25 (d, 1C, C$_6$F$_5$, $^{1}J_{(F-C)}$ = 22 Hz), 132.40 (d, 4C, Ph$_2$, $^{2}J_{(P-C)}$ = 15 Hz), 131.13 (d, 2C, Ph$_2$, $^{4}J_{(P-C)}$ = 1.8 Hz), 129.00 (d, 4C, Ph$_2$, $^{3}J_{(P-C)}$ = 11 Hz). ^{31}P NMR ($\delta_{(ppm)}$): 10.60 (s, PPh$_2$C$_6$F$_5$, d, satellite, $^{1}J_{(W-P)}$ = 250 Hz).

7.3 Experimental: Synthesis, NMR and X-ray characterization of [W(CO)$_4$(NCMe)(PR$_3$)].

Complexes of the type [W(CO)$_4$(NCMe)(PR$_3$)] **<u>24</u>** - **<u>29</u>** (where PR$_3$ is as in 7.1) were prepared by the method of Adams and Perrin [5] with slight modification described by Carlton and co-workers [3b]. An average excess (5%) of decarbonylating agent (Me$_3$NO) was introduced in the synthesis of tetracarbonyl tungsten complexes.

7.3.1 Preparation of [W(CO)$_4$(NCMe)(PPh$_3$)] …….....(<u>24</u>)

A solution of Me$_3$NO (180 mg ~ 2.396 mmol) in acetonitrile (5 ml) was added drop-wise from a dropping funnel into a warm solution (75 ºC) of [W(CO)$_5$PPh$_3$] (1.270 g ~ 2.166 mmol) in acetonitrile (8 ml) over a period of one minute. The colour of the reaction mixture changed dramatically from pale yellow to bright yellow upon introduction of the first few drops of Me$_3$NO. The solution was further stirred for 40 min at 75 ºC in a sealed Schlenk tube. The bright yellow solution was cooled to room temperature after which the solvent (acetonitrile) and Me$_3$N

were evaporated under a gentle flow of argon leaving behind a yellow crystalline material giving a yield of 1.135 g (87%). NMR spectra were recorded from a solution in C_6D_6 at 300 K. ^{1}H NMR ($\delta_{(ppm)}$): 7.51 (m, 15H, PPh_3), 1.79 (s, 3H, NCMe). ^{13}C NMR ($\delta_{(ppm)}$): 206.79 (d, 1C, CO, $^2J_{P-C}$ = 4.6 Hz), 206.59 (d, 1C, CO, $^2J_{P-C}$ = 31 Hz), 203.09 (d, 2C, CO, $^2J_{P-C}$ = 6.9 Hz), 135 (d, 3C, PPh_3, $^1J_{P-C}$ = 37 Hz), 133.88 (d, 6C, PPh_3, $^2J_{P-C}$ = 12 Hz), 129.80 (d, 3C, PPh_3, $^4J_{P-C}$ = 1.6 Hz), 128.56 (d, 6C, PPh_3, $^3J_{P-C}$ = 9.2 Hz), 122.20 (s, 1C, N<u>C</u>Me), 3.00 (s, 1C, NC<u>Me</u>). ^{31}P NMR ($\delta_{(ppm)}$): 30.51 (s, 1P, PPh_3, satellite, d, $^1J_{(W-P)}$ = 242 Hz).

7.3.2 Preparation of $[W(CO)_4(NCMe)\{P(p\text{-tolyl})_3\}]$ ……..… (<u>25</u>)

Compound **<u>25</u>** was prepared following a similar procedure to **<u>24</u>**. A solution of Me_3NO (25 mg ~ 0.334 mmol) in acetonitrile (3 ml) was added drop-wise into a warm solution (77 ºC) of $[W(CO)_5P(p\text{-tolyl})_3]$ (200 mg ~ 0.318 mmol) in acetonitrile (5 ml) over a period of a approximately a minute. A colour change was observed upon addition of the first few drops from pale yellow to bright yellow. The reaction mixture was further stirred for 40 minutes in sealed Schlenk tube. The solution was cooled to room temperature before the solvent was evaporated under a gentle flow of argon leaving behind bright yellow crystalline material. The bright yellow crystals were washed with cold ethanol (3 ml) and dried under reduced pressure giving a yield of 176 mg (86%). NMR spectra were recorded from a solution in CD_2Cl_2 at 300 K. ^{1}H NMR ($\delta_{(ppm)}$): 7.34 (m, 6H, *p*-$CH_3C_6\underline{H}_4$), 7.20 (m, 6H, *p*-$CH_3C_6\underline{H}_4$), 2.35 (s, 9H, *p*-$C\underline{H}_3C_6H_4$), 1.72 (s, 3H, NC<u>Me</u>). ^{13}C NMR ($\delta_{(ppm)}$): 207.19 (d, 1C, CO, $^2J_{P-C}$ = 5.2 Hz), 206.58 (d, 1C, CO, $^2J_{P-C}$ = 31.0 Hz), 202.38 (d, 2C, CO, $^2J_{P-C}$ = 6.9 Hz), 133.94 (d, 6C, *p*-$CH_3\underline{C}_6H_4$, $^2J_{P-C}$ = 12 Hz), 131.74 (d, 3C, *p*-$CH_3\underline{C}_6H_4$, $^3J_{P-C}$ = 32 Hz), 129.33 (d, 6C, *p*-$CH_3\underline{C}_6H_4$, $^4J_{P-C}$ = 9.2 Hz), 122.51 (s, 1C, N<u>C</u>Me), 20.96 (s, 3C, *p*-$\underline{C}H_3C_6H_4$), 1.00 (s, 1C, NC<u>Me</u>). ^{31}P NMR ($\delta_{(ppm)}$): 26.83 (s, 1P, P(*p*-$CH_3C_6H_4)_3$, satellite, d, $^1J_{(W-P)}$ = 237 Hz). IR (compressed solid), $\nu_{(CO)}$ = 2012(s), 1892(s), 1867(vs), 1833(vs) cm^{-1}.

7.3.3 Preparation of $[W(CO)_4(NCMe)\{P(p\text{-}OMeC_6H_4)_3\}]$ ……(<u>26</u>)

To a warm (55 ºC) solution of $[W(CO)_5P(p\text{-}OMeC_6H_4)_3]$ (200 mg ~ 0.295 mmol) in acetonitrile (3 ml) was added Me_3NO (7 mg ~ 0.311 mmol) in acetonitrile (2 ml) drop-wise over a period of one minute. The colour changed instantly upon addition of the solution of Me_3NO from pale yellow to bright yellow. The solution was stirred for a further 10 minutes at 55 ºC after which the

solution was cooled to room temperature. The solvent was removed under a stream of argon leaving behind a bright yellow micro-crystalline powder (162 mg ~ 81%). NMR spectra were recorded from a solution in benzene at 300 K. 1H NMR (C_6D_6, $\delta_{(ppm)}$): 7.64 (m, 6H, P(*p*-$OMeC_6\underline{H}_4)_3$), 6.66 (m, 6H, P(*p*-$OMeC_6\underline{H}_4)_3$), 3.18 (s, 9H, P(*p*-$O\underline{Me}C_6H_4)_3$), 0.26 (s, 3H, $NC\underline{Me}$). ^{13}C NMR ($\delta_{(ppm)}$): 207.64 (d, 1C, CO, $^2J_{(P-C)}$ = 5.3 Hz), 207.1 (d, 1C, CO, $^2J_{(P-C)}$ = 31 Hz), 203.5 (d, 2C, CO, $^2J_{(P-C)}$ = 7.4 Hz), 161.18 (d, 3C, P(*p*-$OMe\underline{C}_6H_4)_3$, $^4J_{(P-C)}$ = 1.6 Hz), 135.41 (d, 6C, P(*p*-$OMeC_6H_4)_3$, $^2J_{(P-C)}$ = 13 Hz), 127.15 (d, 3C, P(*p*-$OMeC_6H_4)_3$, $^1J_{(P-C)}$ = 10 Hz), 122.28 (s, 1C, $N\underline{C}Me$), 114.22 (d, 6C, P(*p*-$OMeC_6H_4)_3$, $^3J_{(P-C)}$ = 10 Hz), 54.81 (s, 3C, P(*p*-$O\underline{Me}C_6H_4)_3$), 1.13 (s, 1C, $NC\underline{Me}$). ^{31}P NMR (CD_2Cl_2, $\delta_{(ppm)}$): 24.66 (s, $\underline{P}$(*p*-$OMeC_6H_4)_3$, satellite, d, $^1J_{(W-P)}$ = 240 Hz). IR (compressed solid), $\nu_{(CO)}$ = 2014(s), 1908(s), 1872(vs), 1844(vs) cm^{-1}.

7.3.4 Preparation of $[W(CO)_4(NCMe)\{P(p\text{-}FC_6H_4)_3\}]$ …….. (27)

A solution of Me_3NO (21 mg ~ 0.292 mmol) in acetonitrile (2 ml) was added drop-wise into a warm (55 ºC) solution of $[W(CO)_5P(p\text{-}FC_6H_4)_3]$ (167.9 mg ~ 0.262 mmol) in acetonitrile (3 ml) over a period of a minute. The colour of the solution changed from pale yellow to yellow-green after about two minutes of stirring at 55 ºC in a sealed Schlenk tube. Stirring was continued for a further 10 min after which the solution was cooled and the solvent evaporated under a stream of argon leaving behind yellow-green crystals with a yield of 176 mg (92%). NMR spectra were recorded from a solution in CD_2Cl_2 at 300 K. ^{1}H NMR ($\delta_{(ppm)}$): 7.47 (m, 6H, P(*p*-$FC_6H_4)_3$), 7.15 (m, 6H, P(*p*-$FC_6H_4)_3$). ^{13}C NMR in C_6D_6 solution ($\delta_{(ppm)}$): 206.34 (d, 1C, CO, $^2J_{(P-C)}$ = 18 Hz), 202,72 (d, 2C, CO, $^2J_{(P-C)}$ = 6.6 Hz), 166.31 (d, 3C, P(*p*-$F\underline{C}_6H_4)_3$, $^4J_{(F-C)}$ = 93 Hz), 135.19 (m, 6C, P(*p*-$F\underline{C}_6H_4)_3$), 139.98 (m, 3C, P(*p*-$FC_6H_4)_3$), 122.29 (1C, $N\underline{C}Me$), 115.93 (m, 6C, P(*p*-$FC_6H_4)_3$), 0.89 (1C, $NC\underline{Me}$). ^{31}P NMR ($\delta_{(ppm)}$): 27.53 (s, 1P, P(*p*-FC_6H_4), satellite, d, $^1J_{(W-P)}$ = 244 Hz). IR (compressed solid), $\nu_{(CO)}$ = 2017(m), 1887(vs), 1849(vs) cm^{-1}.

7.3.5 Preparation of $[W(CO)_4(NCMe)\{P(p\text{-}CF_3C_6H_4)_3\}]$ …….. (28)

To a solution of $[W(CO)_5P(p\text{-}CF_3C_6H_4)_3]$ (228 mg ~ 0.288 mmol) in acetonitrile (3 ml) was added a solution of Me_3NO (22 mg ~ 0.293 mmol) in acetonitrile (2 ml) drop wise over a period of a minute. There was an instant colour change upon addition of Me_3NO solution from pale yellow to bright yellow. The reaction mixture was further stirred for 10 minutes at 55 ºC after

which it was cooled to room temperature. The solvent was removed under a gentle stream of argon leaving behind bright yellow crystals (213 mg ~ 92%). NMR spectra were recorded from a solution in CD_2Cl_2 at 300 K. ^{1}H NMR ($\delta_{(ppm)}$): 7.80 (m, 6H, P(*p*-$CF_3C_6H_4)_3$ 7.71 (m, 6H, P(*p*-$CF_3C_6H_4)_3$, 1.89 (s, 3H, NC<u>Me</u>). ^{13}C NMR ($\delta_{(ppm)}$): 205.35 (d, 1C, CO, $^2J_{(P-C)}$ = 5.0 Hz), 204.44 (d, 4C, CO, $^1J_{(P-C)}$ = 33 Hz), 200.93 (d, 1C, <u>C</u>O, $^2J_{P-C}$ = 6.90 Hz),137.93 (d, 3C, *p*-$CF_3C_6H_4$, $^1J_{(P-C)}$ = 36 Hz), 133.48 (d, 6C, *p*-CF_3<u>C</u>$_6H_4$, $^2J_{(P-C)}$ = 12 Hz), 131.74 (d, 3C, *p*-CF_3CH_3<u>C</u>$_6H_4$, $^2J_{(F-C)}$ = 33 Hz), 125.25 (m, 6C, *p*-CF_3<u>C</u>$_6H_4$), 122.51 (s, 1C, N<u>C</u>Me), 3.56 (s, 1C, NC<u>Me</u>). ^{31}P NMR ($\delta_{(ppm)}$): 24.25 (s, 1P, P(*p*-$CF_3C_6H_4$), satellite, d, $^1J_{(W-P)}$ = 249 Hz). IR (compressed solid), $\nu_{(CO)}$ = 2022(s), 1900(vs), 1842(vs) cm^{-1}.

7.3.6 Preparation of $[W(CO)_4(NCMe)\{P(NMe_2)_3\}]$ ……. (<u>29</u>)

A solution of Me_3NO (82 mg ~ 1.091 mmol) in acetonitrile (2 ml) was added drop-wise to a warm (65 ºC) solution of $[W(CO)_5P(NMe_2)_3]$ (520 mg ~ 1.067 mmol) in acetonitrile (3 ml) over a period of a minute. There was an instant colour change upon addition of the Me_3NO solution from pale yellow to bright yellow. The mixture was stirred for a further 5 min at 65 ºC before cooling to room temperature and evaporating the solvent under a gentle stream of argon to give bright yellow crystals (yield 529 mg, 99%). NMR spectra were recorded from a solution in C_6D_6 at 300 K. ^{1}H NMR ($\delta_{(ppm)}$): 2.50 (d, 18H, $P(NMe_2)_3$, $^3J_{(P-H)}$ = 10.1 Hz). ^{13}C NMR ($\delta_{(ppm)}$): 206.34 (d, 1C, CO, $^2J_{(P-C)}$ = 5.6 Hz) 206.12 (d, 1C, CO, $^2J_{(P-C)}$ = 39 Hz), 203.29 (d, 2C, CO, $^2J_{(P-C)}$ = 9.0 Hz), 123.0 (s, 1C, NCMe), 38.30 (d, 6C, $P(N$<u>Me</u>$_2)_3$, $^2J_{(P-C)}$ = 7.7 Hz), 1.19 (s, 1C, NCMe). ^{31}P NMR ($\delta_{(ppm)}$): 132.16 (s, $P(NMe_2)_3$, satellite, d, $^1J_{(W-P)}$ = 307 Hz). IR (compressed solid), $\nu_{(CO)}$ = 2071(s), 2017(s), 1986, 1872(vs), 1832(vs) cm^{-1}.

7.3.7 Preparation of $[W(CO)_4(NCMe)\{P(MePh_2)\}]$ …….. (<u>30</u>)

A solution containing excess amount of Me_3NO (300 mg ~ 3.978 mmol) in acetonitrile (5 ml) was added drop-wise to a solution of $[W(CO)_5P(MePh_2)]$ (~ 1.800 g ~ 3.434 mmol) in acetonitrile (5 ml) over a period of two minutes at room temperature. The light yellow colour changed to bright yellow after 30 minutes of reaction at room temperature. The solution was warmed to ca. 60 ^{0}C and stirred at the same temperature for 5 minutes. The reaction mixture was cooled to room temperature after which the solvent was removed by evaporating the solvent

under a gentle stream of argon and dried overnight under reduced pressure to give brownish-yellow liquid (yield 1.650 g, 89%). NMR spectra were recorded from a solution in C_6D_6 at 300 K. ^{1}H NMR ($\delta_{(ppm)}$): 7.60 (m, 2H, Ph), 7.05 (m. 8H, Ph), 1.93 (d, 3H, $^2J_{(P-H)}$ = 6 Hz). ^{13}C NMR ($\delta_{(ppm)}$): 207.09 (d, 1CO, $^2J_{(P-C)}$ = 30 Hz, satellite, dd, $^1J_{(W-C)}$ = 154 Hz, $^2J_{(P-C)}$ = 30 Hz), 206.77 (d, 1CO, $^2J_{(P-C)}$ = 5 Hz, satellite, dd, $^1J_{(W-C)}$ = 158 Hz, $^2J_{(P-C)}$ = 5 Hz), 202.90 (d, 2CO, $^2J_{(P-C)}$ = 7 Hz, satellite, dd, $^1J_{(W-C)}$ = 130 Hz, $^2J_{(P-C)}$ = 7 Hz), 136.88 (d, 2C, Ph, $^1J_{(P-C)}$ = 37 Hz), 132.28 (m, 4C, Ph), 131.39 (m, 2C, Ph), 128.63 (m, 4C, Ph), 19.45 (d, 1C, Me, $^1J_{(P-C)}$ = 27 Hz). ^{31}P NMR ($\delta_{(ppm)}$): 6.79 (s, PMePh$_2$, satellite, d, $^1J_{(W-P)}$ = 237 Hz). IR (liquid), $\nu_{(CO)}$ = 2069(s), 2013(s), 1870(vs), 1832(vs) cm^{-1}.

7.3.8 Preparation of [W(CO)$_4$(NCMe){P(Ph$_2$C$_6$F$_5$)}] …….. (31)

To a light yellow solution of [W(CO)$_5$(PPh$_2$C$_6$F$_5$)] (400 mg ~ 0.591 mmol) in acetonitrile (2 ml) at room temperature was added 5% excess of Me$_3$NO (45.7 mg ~ 0.608 mmol) at once. The colour changed immediately to bright yellow. The solution was then stirred for a period of 10 min at ~56 ^{0}C. The solvent was evaporated under gentle stream flow of argon. There was no indication of formation of crystals during the evaporation process. The product was washed with ethanol (10 ml) and then dried under reduced pressured leaving behind a bright yellow powder (450 mg, 84%). NMR spectra were recorded from a solution in C_6D_6 at 300 K. ^{1}H NMR ($\delta_{(ppm)}$): 7.59 (m, 4H, Ph$_2$), 7.03 (m, 6H, Ph$_2$). ^{13}C NMR ($\delta_{(ppm)}$): 205.53 (d, 1CO, $^1J_{(P-C)}$ = 20 Hz), 205.37 (d, 1CO, $^1J_{(P-C)}$ = 10 Hz), 201.94 (d, 2CO, $^1J_{(P-C)}$ = 6.3 Hz), 146.39 (d, 2C, C_6F_5, $^1J_{(F-C)}$ = 252 Hz), 142.20 (d, 1C, C_6F_5, $^1J_{(F-C)}$ = 255 Hz), 138.08 (d, 2C, C_6F_5, $^1J_{(F-C)}$ = 248 Hz), 133.35 (d, 1C, C_6F_5, $^1J_{(F-C)}$ = 49 Hz), 133.30 (4C, Ph$_2$, $^2J_{(P-C)}$ = 13 Hz), 130.76 (s, 2C, Ph$_2$), 128.80 (d, 4C, Ph$_2$, $^3J_{(P-C)}$ =10 Hz). ^{31}P NMR ($\delta_{(ppm)}$): 19.99 (s, PPh$_2$C$_6$F$_5$, satellite, d, $^1J_{(W-P)}$ = 251 Hz). IR (liquid), $\nu_{(CO)}$ = 1641 cm^{-1}.

7.4 Experimental: X-ray Crystallography

The crystals for crystallography for compound **19** were grown by slow evaporation of the solvent mixture of diglyme and n-hexane whereas **21** was obtained from diglyme and diethyl ether. The crystals of compound **19** and **22** were selected as representative structures for complexes of the

type $[W(CO)_5PR_3]$. The pale yellow micro-crystals were then analysed by single crystal X-ray diffraction as described in Chapter 3 and the refinement data are provided here below in **Table 7.1**.

Table 7.1 Crystal Refinement Data for compounds **19** and **22**

Parameter	$[W(CO)_5P(p\text{-tolyl})_3]$ **19**	$[W(CO)_5P(p\text{-}CF_3C_6H_4)_3]$ **22**
Molecular formula	C26 H21 O5 P W	C26 H12 F9 O5 P W
Formula weight	628.25	790.18
Temperature (K)	173(2)	173(2)
Wavelength (Å)	0.71073	0.71073
Crystal system	Triclinic	Orthorhombic
Space group	P-1	Pbca
Unit cell dimensions: a (Å)	10.8091(2)	11.6536(2)
b (Å)	15.1129(2)	17.52.86(3)
c (Å)	15.9199(3)	26.7063(4)
α (^{0})	105.8350	90
β (^{0})	94.3840	90
γ (^{0})	91.1840	90
Volume (Å^3)	2492.28(7)	5455.33(16)
Z	4	8
Density (Calculated) (Mg/m^3)	1.674	1.924
Absorption coefficient (mm^{-1})	4.732	4.391
F(000)	1224	3024
Crystal size (mm^3)	0.67 x 0.17 x 0.13	0.23 x 0.15 x 0.08
Theta range for data collection (^{0})	1.33 to 28.00	2.23 to 28.00
Index ranges	-14<=h<=14, -14<=k<=19 -21<=I<=21	-15<=h<=15 -23<=k<=23 -35<=I<=35
Reflections collected	40710	111466
Independent reflections	12036 [R(int) = 0.0469]	6595 [R(int) =0.01010]
Completeness to theta = 28.00^0	100.0 %	100.0 %
Absorption corrections	Integration	Semi-empirical from equivalents
Max. and min. transmissions	0.5782 and 0.1437	0.7202 and 0.4316
Refinement method	Full-matrix least-squares on F^2	Full-matrix least-squares on F^2
Data / restraints / parameters	12036 / 0 / 595	6595 / 0 / 379
Goodness-of-fit on F^2	0.925	1.025
Final R indices [I>2sigma(I)]	R1 = 0.0238, wR2 = 0.0444	R1 = 0.0331, wR2 = 0.0648
R indices (all data)	R1 = 0.0371 wR2 = 0.0467	R1 = 0.0612 wR2 = 0.0750

Table 7.2 Crystal refinement data for compound **24** – **29**.

Parameter	Compound **24**	Compound **25**	Compound **26**	Compound **27**	Compound **28**	Compound **29**
Molecular formula	C24H18NO4PW	C27H24NO4PW	C27H24NO7PW	C24H15F3NO4PW	C27H15F9NO4PW	C12H12N4O4PW
Formula weight	599.21	641.29	689.29	653.19	803.22	500.15
Temperature (K)	173(2)	173(2)	173(2)	173(2)	173(2)	173(2)
Wavelength (Å)	0.71073	0.71073	0.71073	0.71073	0.71073	0.71073
Crystal system	Triclinic	Triclinic	Triclinic	Triclinic	Monoclinic	Monoclinic
Space group	P-1	P-1	P-1	P-1	P2(1)/n	P2(1)/c
Unit cell dimensions:						
a (Å)	10.0328(3)	8.45820(10)	8.5096(2)	8.3234(10)	9.8311(2)	16.2528(3)
b (Å)	10.4805 (3)	8.97850(10)	9.1457(2)	8.7508(2)	16.0667(3)	7.26970(10)
c (Å)	11.2798(3)	17.4828(2)	18.0699(5)	16.7540(3)	18.1693(3)	16.5964(3)
α (^{0})	85.6460(10)	80.9650(10)	96.966(2)	77.0130(10)	90	90
β (^{0})	84.9510(10)	86.7650(10)	98.534(2)	83.9220(10)	91.9700(10)	112.7860(10)
γ (^{0})	75.5730(10)	84.5830(10)	101.151(2)	79.2410(10)	90	90
Volume (Å^3)	1142.41(6)	1304.18(3)	1349.09(6)	1165.58(4)	2868.21	1807.88(5)
Z	2	2	2	2	4	4
Density (Calculated) (Mg/m^3)	1.742	1.633	1.698	1.861	1.860	1.838
Absorption coefficient (mm^{-1})	5.155	4.522	4.398	5.079	4.176	6.498
F(000)	580	628	676	628	1544	968
Crystal size (mm^3)	0.47 x 0.21 x 0.13	0.43 x 0.20 x 0.09	0.19 x 0.17 x 0.04	0.31 x 0.14 x 0.06	0.42 x 0.18 x 0.18	0.45 x 0.34 x 0.22
Theta range for data collection (^{0})	1.82 to 28.00	1.18 to 28.00	1.15 to 25.00	2.42 to 28.00	1.69 to 28.00	1.36 to 28.00
Index ranges	-12<=h<=13 -13<=k<=13 -14<=l<=14	-11<=h<=11 -11<=k<=11 -23<=l<=23	-10<=h<=9 -10<=k<=10 -21<=l<=21	-10<=h<=10 -11<=k<=11 -22<=l<=22	-12<=h<=12 -21<=k<=21 -23<=l<=23	-21<=h<=21 -9<=k<=9 -21<=l<=21
Reflections collected	12504	23727	13414	27510	23387	36732
Independent reflections	5519[R(int)= 0.0206]	6292 [R(int) = 0.0290]	4743[R(int) = 0.0547]	5626 [R(int) =0.0272]	6906 [R(int) = 0.0335]	4353[R(int) = 0.0433]
Completeness to theta = 28.00^0	99.9 %	100 %	99.9	100.0	100.0	100.0
Absorption corrections	Integration	Semi-empirical from equivalents	None	Semi-empirical from equivalents	Semi-empirical from equivalents	Integration
Max. and min. transmissions	0.5538 and 0.1955	0.6864 and 0.2466	0.8440 and 0.4893	0.7503 and 0.3020	0.5203 and 0.2730	0.3290 and 0.1580
Data / restraints / parameters	5519 / 0 / 281	6292 / 0 / 308	4743 /13 / 334	5626 / 0 / 307	6906 / 0 / 389	4353 / 0 / 199
Goodness-of-fit on F^2	1.031	1.125	1.061	1.054	1.043	1.112
Final R indices [I>2sigma(I)]	R1 =0.0195, wR2=0.0429	R1 =0.0209, wR2=0.0515	R1=0.0369, wR2=0.0657	R1=0.0166, wR2=0.0407	R1=0.0305, wR2=0.0729	R1=0.0177, wR2=0.0418

R indices (all data)	R1 = 0.0224 wR2=0.0440	R1 =0.0255, wR2=0.0614	R1=0.0569, wR2=0.0880	R1 =0.0184, wR2=0.0413	R1=0.0419, wR2=0.0782	R1=0.0210, wR2=0.0425
Largest diff. peak and hole (e.Å^{-3})	0.809 and -0.526	1.114 and -0.559	0.751 and -0.965	1.046 and -0.504	1.287 and -0.782	0.982 and -0.778

All crystals were refined by full-matrix least-squares method on F^2

The crystals of compounds **24** to **29** were prepared by slow evaporation of the solvent (acetonitrile) under a stream of argon gas. The bright yellow crystals were then analysed by single crystal X-ray diffraction as described in Chapter 3 and the refinement data are provided below in **Table 7.2**.

7.5 Results and discussion: Complexes of the type $[W(CO)_5(PR_3)]$

Pentacarbonyl phosphine tungsten complexes of the type $[W(CO)_5PR_3]$ (where R = Ph, *p*-tolyl, *p*-$OMeC_6H_4$, *p*-FC_6H_4, *p*-$CF_3C_6H_4$ and NMe_2) were synthesized by the method of Magee and co-workers [8a] in yields varying from 51 to 99%. A molar equivalent reaction mixture of $[W(CO)_6]$ and the phosphine was refluxed for at least 8 hrs with occasional agitation to return the sublimed hexacarbonyl complex $[W(CO)_6]$ to solution. Addition of a low boiling ether e.g. THF helps in recycling the $[W(CO)_6]$ back into the solution. However this exercise (addition of either THF or ether) is accompanied by formation of a black precipitate, presumably the result of decomposition due to higher reflux temperature at 165 ºC. Generally, addition of excess phosphine resulted in the formation of a disubstitution product (results not included in this thesis). Compounds **18** and **19** crystallized upon leaving the solution at room temperature overnight. Compound **22** only crystallized by slow evaporation in diglyme solution at room temperature after more than three months. Compounds **20**, **21**, and **23** were crystallized for X-ray diffraction analysis by slow evaporation upon addition of small quantities of diethyl ether (Et_2O) in good yields (> 80%). The resultant pale yellow crystals were then washed with cold ethanol from which two (**19** and **22**) representative single crystal X-ray analyses were performed (**Table 7.1**).

7.5.1 NMR spectroscopy

The NMR spectroscopic data for pentacarbonyl phosphine complexes of tungsten are given in **Table 7.3**. Included in **Table 7.3** are the results of the achieved yields. As expected, the carbon nuclei of the phenyl ring show coupling to the phosphorus nucleus in the range of 1.5 Hz

(through four bonds) to 43 Hz (through a single bond). The distinctive coupling interaction between the *trans*- and the *cis*- positioned carbons of the carbonyl group with the phosphorus atom are also given in **Table 7.3.** Only compounds **20** and **23** show a significant deviation in terms of $^{2}J_{(P\text{-}CO)}$ from the pattern displayed by the other four complexes. Phosphorus chemical shift signals show a one bond coupling interaction with the tungsten nucleus in the range of 242 (**19**) to 313 (**23**) Hz. There is no significant difference in the phosphorus and tungsten chemical shifts in compounds **18** to **22** except for **23.1** which shows higher $\delta(^{31}P)$ and lower $\delta(^{183}W)$. The $^{31}P\text{-}^{183}W$ coupling interaction is measured from the satellite signals from $^{31}P\{^{1}H\}$ spectra.

Table 7.3 Selected NMR data for the complexes of the type $[W(CO)_5PR_3]$

Compound[a]	Ligand	$^{2}J_{(P\text{-}CO)}$ (Hz) (*trans*-) : (*cis*-)		^{31}P NMR (ppm)	$^{1}J_{(W\text{-}P)}$ (Hz)	^{183}W[e] NMR (ppm)	Yields (%)
18	PPh_3[b]	22	6.9	21.30	243	201	99
19	P(*p*-tolyl)$_3$[c]	21	6.9	18.70	242	198	76
20	P(*p*-$OMeC_6H_4$)$_3$[b]	28	9.0	22,72	244	202	51
21	P(*p*-FC_6H_4)$_3$[c]	22	6.9	21.24	247	206	62
22	P(*p*-$CF_3C_6H_4$)$_3$[b]	24	6.9	24.25	250	199	53
23.1	P(*p*-NMe_2)$_3$[b]	27	8.9	127.4	313	89	91
23.2	P($MePh_2$)[d]	20	7.2	-3.40	238	174	89
23.3	$PPh_2C_6F_5$	25	7.2	10.60	250	221	86

[a] Recorded from ~ 0.02 M solution at 300 K. [b] Recorded from CDCl3 solution. [c] Recorded from CD_2Cl_2/CH_2Cl_2 solution. [d] Recorded from a solution in C6D6. [e] Chemical shift in ppm relative to $\Xi(^{183}W)$ = 4.15 MHz in which the protons of TMS resonate at exactly 100 MHz. To convert to a scale relative to $W(CO)_6$ $\Xi(^{183}W)$ = 4.151888 MHz [14] subtract 455 ppm, to convert to a scale relative WF_6 $\Xi(^{183}W)$ = 4.161780 MHz [15] subtract 2831 ppm; to convert to a scale relative to WO_4^{2-} [14] subtract 3939 ppm.

7.5.2 X-ray crystallographic study

Single crystal structures of the representative compounds (**19** and **22**) were recorded in which an octahedral geometry about the tungsten is displayed (Figure 7.1 and 7.2). The averaged inter-atomic bond distances and inter-bond angles are listed in **Table 7.4**. Compound **19** crystallizes into two polymorphs which are clearly differentiated by their selected bond lengths and angles listed in **Table 7.4**. The observed W – P bond lengths for compound **22** and both **19A** and **19B**

are comparable to the literature values for complexes such as $[W(CO)_5P(Me_3)]$ [16]. The bond angle P-W-C1, where C1 (CO) is the carbon positioned *trans* to the phosphorus atom is similarly comparable to bond angles in compound **22** and both **19A** and **19B**.

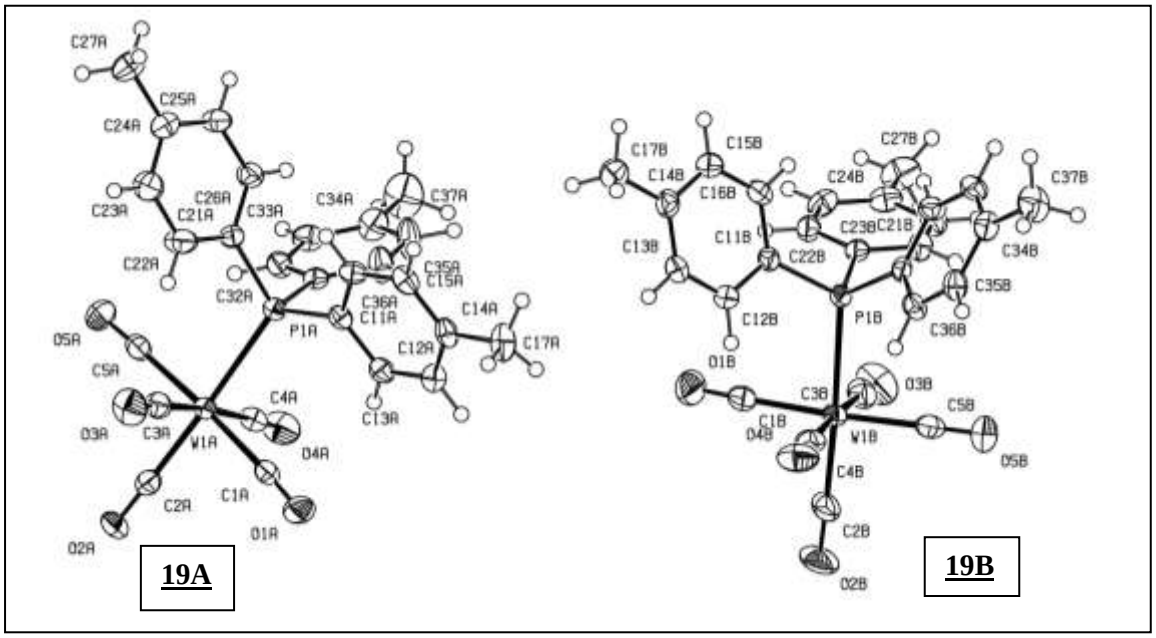


Figure 7.1 ORTEP diagrams of isomeric forms (**19A** and **19B**) showing thermal ellipsoids of complex **19** at 50% probability level.

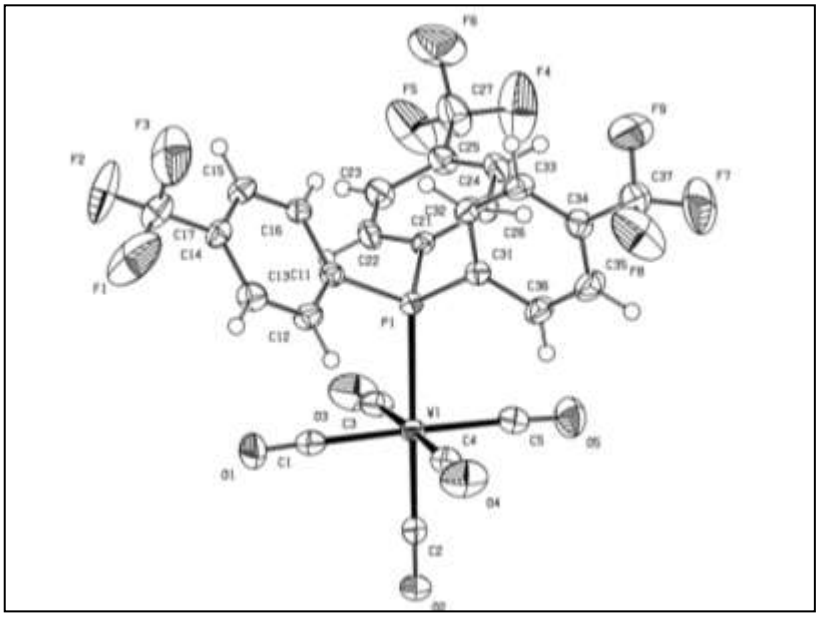


Figure 7.2 ORTEP diagram of showing thermal ellipsoids of complex **22** at 50% probability level.

Table 7.4 Selected bond lengths (Å) and angles (º) for compounds **19A**, **19B** and **22**.

	$[W(CO)_5P(p\text{-}CH_3C_6H_4)_3]$ (**19A**)	$[W(CO)_5P(p\text{-}CH_3C_6H_4)_3]$ (**19B**)	$[W(CO)_5P(p\text{-}CF_3C_6H_4)_3]$ (**22**)
Bond lengths (Å)			
W – P1	2.5522	2.5363	2.5254
W – C1	1.9941	1.9909	2.0010
W – C2	2.0154	2.0550	2.0470
W – C3	2.0308	2.0291	2.0285
W – C4	2.0530	2.0642	2.0361
W – C5	2.0402	2.0327	2.0419
Bond angles (º)			
P – W – C1	175.55	176.38	179.28
P – W – C2	88.08	89.79	90.58
P – W – C3	95.29	93.19	91.19
P – W – C4	87.57	91.44	91.57
P – W – C5	95.30	86.91	90.55

The orientation of the two crystal isomers or polymorphs of **19A** and **19B** indicates only two contacts by the hydrogen atoms of the methyl group on the *para*-tolyl ring. The carbonyl groups of the isomers are orientated *cis*- to each other, thus propagating lateral contacts through the methyl and phenyl hydrogen atoms. However, the packing pattern in a unit cell shows carbonyl groups showing different interactions with neighbouring molecules.

7.6 Results and discussion: Complexes of the type *cis*-$[W(CO)_4(PR_3)(NCMe)]$

Tertracarbonyltungsten phosphine complexes of the type *cis*-$[W(CO)_4(NCMe)(PR_3)]$ were prepared from $[W(CO)_5(PR_3)]$ (where R_3 = Ph_3, $\{p\text{-tolyl}\}_3$, $\{p\text{-}OMeC_6H_4\}_3$, $\{p\text{-}FC_6H_4\}_3$, $\{p\text{-}CF_3C_6H_4\}$ and $\{NMe_2\}_3$) in yields varying from 81% to 99%. Without exception, all complexes were obtained as bright yellow crystals of *cis*-$[W(CO)_4(NCMe)(PR_3)]$ and no trace of *trans*-

products were observed. Decarbonylation of $[W(CO)_5PR_3]$ was achieved using a method similar to that of Adam and Perrin [5]. On average a five percent (5%) excess of the stoichiometric amount of Me_3NO was uniformly applied in the syntheses of all complexes accompanied by stirring at temperatures varying between 55 and 65 ºC for a time period varying from 8 min to 15 min. Bright yellow crystals of complexes **24** to **29** were characterised by both NMR and single crystal X-Ray diffraction methods. The compound *cis*-$[W(CO)_4(NCMe)(PPh_3)]$ has been prepared previously by a photolytic method, the procedure described by Angelici and Malone [17].

7.6.1 NMR spectroscopic study of *cis*-$[W(CO)_4(NCMe)(PR_3)]$ complexes.

The NMR spectroscopic data for complexes **24** to **29** are listed in Table 7.5. The chemical shifts of the carbon of the carbonyls differ as a result of their geometric position relative to the phosphorus atom. The carbonyl carbon *trans* to the phosphorus atom is identified by a larger coupling interaction whereas the carbonyl carbon *trans* to the nitrogen experiences the least. An interesting phenomenon observed in this series of tungsten complexes is that the carbonyl group seems to be a stronger *trans* director than the phosphine or the acetonitrile ligands. There were no traces of *trans*-$[W(CO)_4(NCMe)(PR_3)]$ observed during the NMR analysis of these compounds. Since the steric parameter (size of the cone angle) of the phosphine ligands in complexes **24**, **25**, **26** and **27** is equal (145 º) with the exception of $P(NMe_2)$ (159 º), only the electronic parameter distinctive to each ligand will exert an influence in the chemical shift of the transition metal nucleus, i.e. tungsten. The formation of *trans*-$[W(CO)_4(PPh_3)(PR_3)]$ seems to be independent of the size of the PR_3 though the ratio of *cis*- to *trans*- decreased with increasing size of PR_3 as reported by Carlton [3b]. In our case *trans*- $[W(CO)_4(PPh_3)_2]$ and $[W(CO)_4P(NMe_2)_3]$ were isolated only when $W(CO)_6$ was treated with an excess of the phosphine ligand under the same reaction conditions as in the syntheses of *cis*-$[W(CO)_5(NCMe)(PR_3)]$. These disubstituted complexes were characterised by both NMR and X-ray diffraction confirming their existence in both solution and solid states. There is a significant change in the ^{183}W chemical shift arising from the differing electronic effects of phosphine liagnds having the same steric effect (equal cone angle size), ranging from 658 ppm (**25**, R = tolyl) to 667 ppm (**24**, R = Ph). The full ^{183}W chemical shift range is from 598 ppm (**29**, R = NMe_2) to 667 ppm (**24**, R = Ph). The rationale for transition metal chemical shift differences in

complexes of transition metals caused by changes in ligand properties (e.g. changes in the subsituents on the phosphorus atom) has been described in detail in Chapter 2.

Table 7.5 Selected NMR data for complexes of the type *cis*-[$W(CO)_4(NCMe)(PR_3)$] **24**, **25**, **26**, **27**, **28** and **29**.

Compound[a]	Ligand	$^2J_{(P-\underline{C}O)}$ (Hz)			$\delta(^{31}P)$ (ppm)	$^1J_{(W-P)}$ (Hz)	$\delta(^{183}W)$[d] (ppm)	Yield (%)
		CO *trans* to P atom	CO *trans* to N atom	CO *cis* to P atom				
24	PPh_3[b]	31	4.6	6.9	30.5	242	667	87
25	P(*p*-tolyl)$_3$[c]	31	5.2	6.9	26.8	237	658	86
26	P(*p*-$OMeC_6H_4)_3$[c]	31	5.3	7.4	24.7	240	661	81
27	P(*p*-$FC_6H_4)_3$[c]	18	5.2	7.0	27.5	244	666	92
28	P(*p*-$CF_3C_6H_4)_3$[c]	33	5.0	6.9	31.8	246	660	92
29	$P(NMe_2)_3$[b]	39	5.6	9.0	132.0	307	598	99
30	$P(MePh_2)$[b]	30	5.1	7.3	6.79	237	643	89
31	$P(Ph_2C_6F_5)$[b]	20	10	6.3	19.99	251	673	84

[a] Recorded from ~ 0.02 M solution at 300 K. [b] Recorded from C_6D_6 solution. [c] Recorded from CD_2Cl_2/CH_2Cl_2 solution. [d] Chemical shift in ppm relative to $W(CO)_6$, $\Xi(^{183}W)$ = 4.15 MHz in which the protons of TMS resonate at exactly 100 MHz.

7.6.2 X-Ray crystallographic studies

Bright yellow X-ray quality crystals of compounds **24** to **29** and **31** (crystal structures, refinement data and selected bond lengths and angles in Appendix A) obtained from acetonitrile solution by slow evaporation of solvent under a stream of argon. Selected bond lengths and angles are listed in **Table 7.6** and crystal structures shown in **Figures 7.3** to **7.8**. The crystal structures of *cis*-[$W(CO)_4(NCMe)(PR_3)$] show distorted octahedral geometry about the tungsten, where the *cis*- confirmation is in agreement with the results of solution NMR spectroscopy. The phenyl rings of **24**, **25**, **26**, **27**, **28** and **31** (**Figs 7.3** to **7.7**) are distributed in such way that one ring is orientated vertically relative to the metal centre, the second slightly axial whilst the third seems to be orientated parallel to the NCMe group. It is assumed that such orientation is enhanced by the π-π electron interaction of the aromatic ring and the triple bonded N≡C of

NCMe. However, a different situation arises when the phosphorus substituent is R = NMe_2, W-N-C (182.5 °) where the angle is bending away from NMe_2. Reports on a large variety of disubstituted complexes of the type *trans*-$[W(CO)_4(PR_3)_2]$ (R = Ph [3b]; R = NMe_2 (results not shown in this thesis)), *trans*-$[W(CO)_4(PPh_3)(PR_3)]$ [3b,10, 18, 19] (R = nBu, PMe, $MePh_2$, Me_2Ph, 4-$OMeC_6H_4$, 4-MeC_6H_4, 4-FC_6H_4, OEt, OMe and OPh) *trans*-$[W(CO)_4(PPh_3)(py)]$ [20] suggest that the size of ligands determines the orientation i.e *cis* or *trans*. Compound **29** (**Fig. 7.8**) also exhibits a *cis*- octahedral geometry and since there are no phenyl rings or other π-systems in the complex to interact with π-system in the NCMe ligand, there seems to be no significant orientation by phosphine ligand $\{P(NMe_2)_3\}$ with respect to the NCMe group. However $[W(CO)_4(NCMe)P(NMe_2)_3]$ **29** shows a clear tendency by the angle subtended by W-N-CMe to bend away from the methyl groups of the substituent on the phosphorus atom. The bond angle through W-N-CMe for compound **25** (173.83 º) (**Fig. 7.4**) and **26** (173.57 º) (**Fig. 7.5**) is smallest showing a stronger bending towards the phenyl ring in agreement with the view of π-π electron interaction between the aromatic ring and the triple bonded N≡C of NCMe.

Table 7.6 Selected bond lengths and angles for **24**, **25**, **26**, **27**, **28** and **29**.

	$P(Ph)_3$ **24**	$P(p\text{-tolyl})_3$ **25**	$P(p\text{-}OMeC_6H_4)_3$ **26**	$P(p\text{-}FC_6H_4)_3$ **27**	$P(p\text{-}CF_3C_6H_4)_3$ **28**	$P(NMe_2)_3$ **29**
Bond lengths (Å)						
W – P	2.540(1)	2.557(0)	2.554(2)	2.545(2)	2.519(7)	2.557(3)
W – N	2.173(8)	2.185(5)	2.208(6)	2.188(3)	2.184(1)	2.189(8)
W – C1	1.985(1)	1.985(7)	1.976(9)	1.980(7)	1.995(4)	1.963(2)
W – C2	1.971(5)	1.968(9)	1.940(10	1.963(9)	1.959(7)	1.979(4)
W – C3	2.035(1)	2.044(9)	2.055(8)	2.019(7)	2.019(5)	2.030(8)
W – C4	2.038(3)	2.021(3)	2.024(8)	2.043(8)	2.051(9)	2.036(3)
N – C10	1.132(5)	1.131(2)	1.120(1)	1.138(0)	1.130(1)	1.133(0)
Bond angles (º)						
P-W-N	86.97	82.87	83.12	84.72	88.40	92.14
P-W-C2	178.95	177.54	178.82	176.30	176.23	176.41
N-W-C2	177.22	179.23	178.83	178.78	175.71	176.22
C3-W-C4	177.57	177.43	173.04	175.16	175.36	176.45
W-N-C5	178.22	173.83	173.57	177.12	175.09	177.50

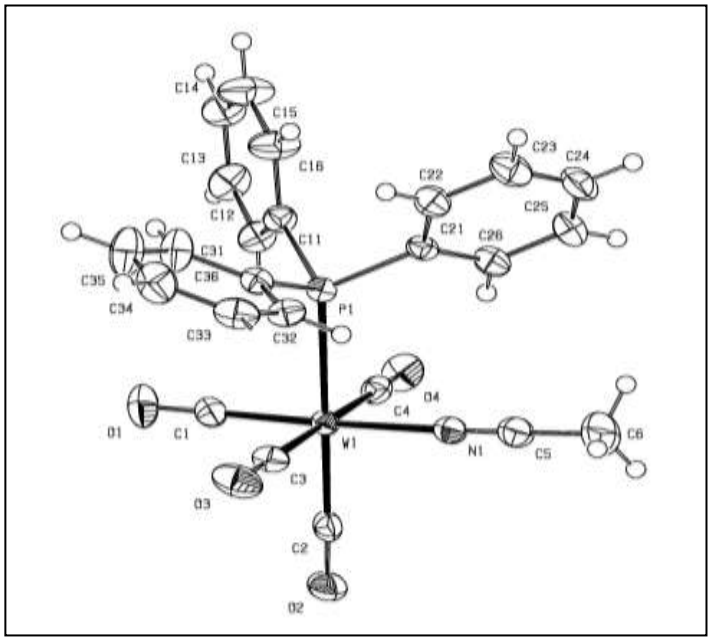


Figure 7.3 ORTEP diagram of $[W(CO)_4(NCMe)(PPh_3)]$ **<u>24</u>** showing thermal ellipsoids at 50% probability level.

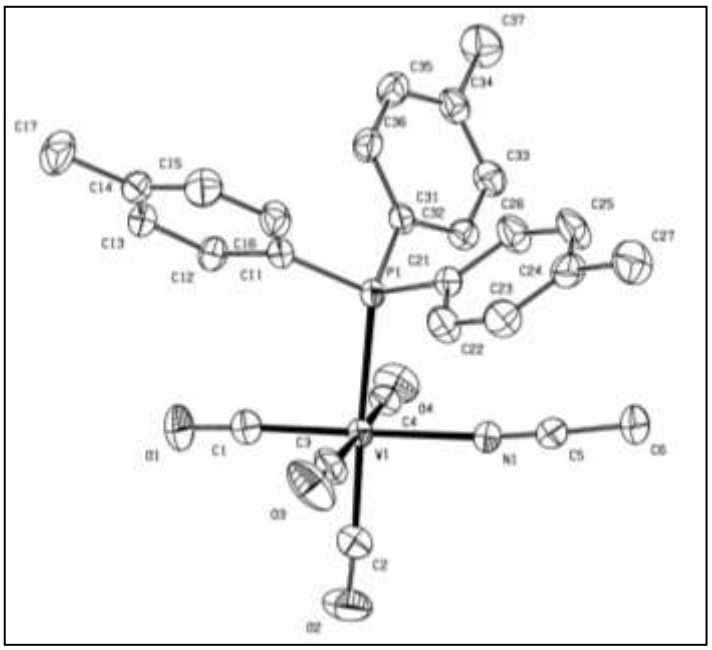


Figure 7.4 ORTEP diagram of $[W(CO)_4(NCMe)P(p\text{-}MeC_6H_4)_3]$ of **<u>25</u>** showing thermal ellipsoids at 50% probability level. Hydrogen atoms have been omitted for clarity.

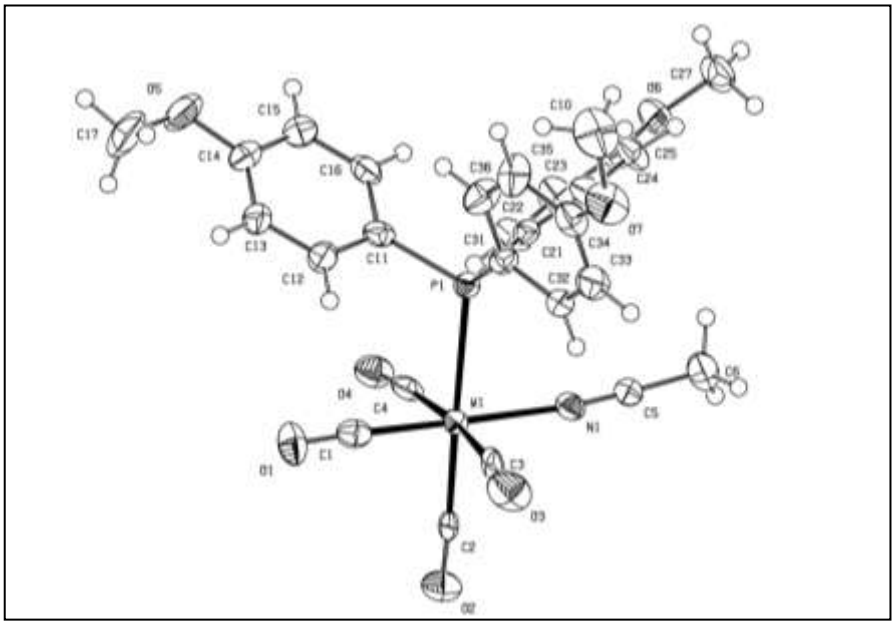


Figure 7.5 ORTEP diagram of $[W(CO)_4(NCMe)P(p\text{-}OMeC_6H_4)_3]$ **<u>26</u>** showing thermal ellipsoids at 50% probability level.

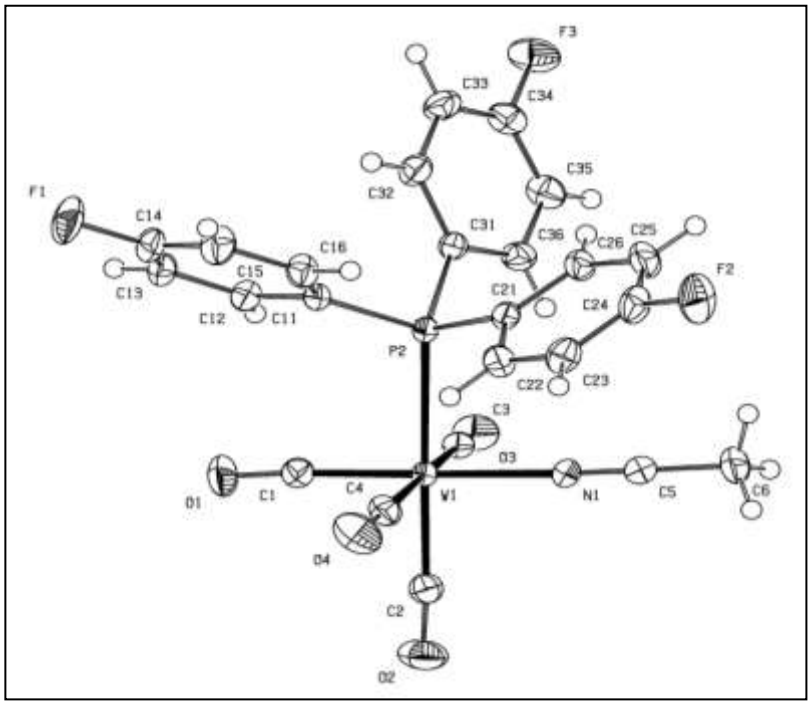


Figure 7.6 ORTEP diagram of $[W(CO)_4(NCMe)P(p\text{-}FC_6H_4)_3]$ **<u>27</u>** showing thermal ellipsoids at 50% probability level.

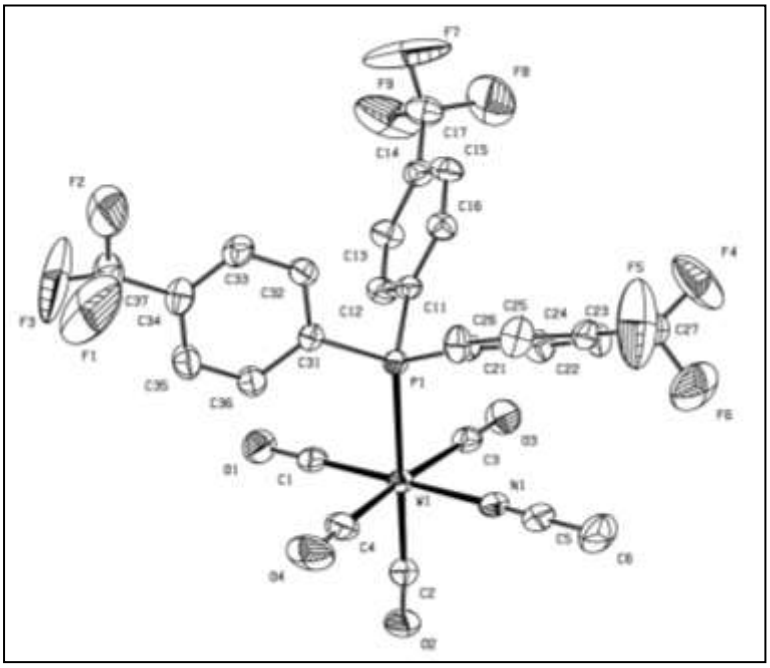


Figure 7.7 ORTEP diagram of $[W(CO)_4(NCMe)P(p\text{-}CF_3C_6H_4)_3]$ **28** showing thermal ellipsoids at 50% probability level. Hydrogen atoms have been omitted for clarity.

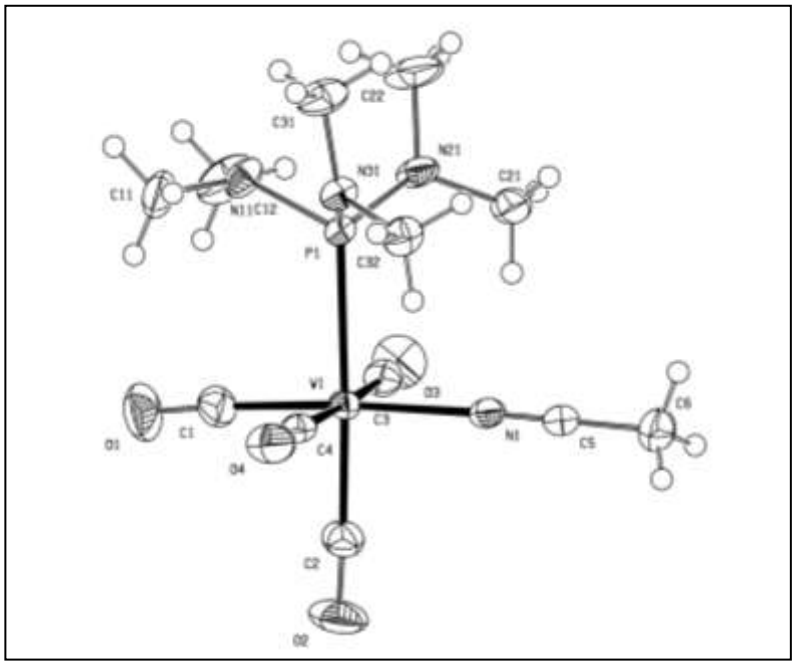


Figure 7.8 ORTEP diagram of $[W(CO)_4(NCMe)P(NMe_2)_3]$ **29** showing thermal ellipsoids at 50% probability level.

7.7 Conclusions

Tungsten phosphine complexes of the type $[W(CO)_5PR_3]$ where R is = Ph, *p*-tolyl, *p*-$OMeC_6H_4$, *p*-FC_6H_4, *p*-$CF_3C_6H_4$ and NMe_2 were synthesised by thermal methods in good yields. The Me_3NO-promoted decarbonylation of petacarbonyl tungsten complexes proceeds under mild conditions to form disubstituted complexes of the type $[W(CO)_4(NCMe)(PR_3)]$ also in good yields. Crystal structures of $[W(CO)_4(NCMe)(PR_3)]$ (where R = Ph, *p*-tolyl, *p*-$OMeC_6H_4$, *p*-FC_6H_4, *p*-$CF_3C_6H_4$ and NMe_2) were analysed and found to form *cis*- complexes where the CO ligand seems to be a stronger *trans*-director than the nitrogen of the NCMe.

References

1. D.P. Tate, W.R. Knipple and J.M. Augl, *Inorg. Chem*., 1 (1962) 433.

2. (a) P.K. Baker and A. Bury, *J. Organomet. Chem*., 359 (1989) 189; (b) P.K. Baker and J.A. Quinlan, *Inorg. Chim. Acta*., 162 (1989) 179; (c) D. Miguel, J.A. Pérez-Martinez, V. Riera and S. Garcia-Granda, *J. Organomet. Chem*., 463 (1993) 121; (d) M. Cano, M. Panizo, J.A. Campo, J. Tornero and N. Menéndez, *J. Organomet. Chem*., 463 (1993) 121.

3. (a) F. Alper, C Kayran and S. Özker, *J. Organomet. Chem*., 691 (2006) 2734; (b) L. Carlton, A. Emdin, A. Lemmerer and M.A. Fernandes, *Magn. Reson. Chem*., 46 (2008) S56; (c) Li-Cheng, Ying-Huai Zhu and Qing-Mei Hu, *Polyhedron*, 16 (1997) 2141.

4. (a) T. Szymańska-Buzar, T. Tadeusz and I. Czeluśniak, *Polyhedron*, 21 (2002) 1817; (b) T. Szymańska-Buzar and T. Glowiak, 17 (1998) 3419.

5. R.D. Adams and J.L. Perrin, *J. Am. Chem. Soc*., 121 (1999) 3984.

6. (a) R.J. Angelici, *Polyhedron*, 16 (1997) 3071; (b) C. Bianchini, J.A. Casares, A. Meli, V. Sernau, F Vizza and R.A. Sánchez-Delgado, *Polyhedron*, 16 (1997) 3099; (c) W.D. Jones, D.A. Vicic, R.M. Chin, J.H. Roache and A.W. Myers, *Polyhedron*, 16 (1997) 3115; (d) B.C. Wiegand and C.M. Friend, *Chem. Rev*., 92 (1992) 491; (e) R.J. Angelici, *J. Coord. Chem. Rev*., 105 (1990) 61; (f) U. Riaz, O.J. Curnow and M.D. Curtis, *J. Am. Chem. Soc*., 116 (1994) 4357; (h) W.D. Jones and R.M. Chin, *J. Am. Chem. Soc*., 116 (1994) 198; (i) C. Bianchini, A. Meli, M. Peruzzini, F. Vizza, S. Moneti, V. Herrera and R.A. Sáchez-Delgado, *J. Am. Chem. Soc*., 116 (1994) 4370; (j) J. Chen, R. Angelici, *J. Appl. Organomet. Chem*., 6 (1992) 479.

7. H. Daamen, A. Oskam and D.J. Stufkens, *Inorg. Chim. Acta*, 38 (1980) 71.

8. (a) T.A. Magee, C.N. Mathews, T.S. Wang and J.H. Wotiz, *J. Am. Chem. Soc*., 81 (1959) 2273; (b) *ibid*, *J. Am. Chem. Soc*., 83 (1961) 3200.

9. R. Mathieu, M. Lenzi and R. Poiblanc, *Inorg. Chem*., 9 (1970) 3020

10. W.A. Schenk and W. Buchner, *Inorg. Chim. Acta*, 70 (1983) 189; (b)

11. M.L. Boyles, D.A. Brown, D.A. Drake, C.K. Hostetler, C.K. Maves and J.A. Mosbo, *Inorg. Chem*., 24 (1985) 3126.

12. (a) M. Hidai and Y. Mizobe, *Chem. Rev*., 95 (1995) 1115; (b) S. Gambarotta, *J. Organomet. Chem*. 500 (1995) 117; (c) M.D. Fryzuk and S.A. Johnson, *Coord. Chem. Rev*., 200-202 (2000) 379; (d) B.A. MacKay and M.D. Fryzuk, *Chem. Rev*., 104 (2004) 385; (e) S. Gambarotta and J. Scott, *Angew. Chem. Int. Ed*., 43 (2004) 5298; (f) M. Hidai and Y. Mizobe, *Can. J. Chem*., 83 (2005) 358; (g) H.-J. Himmel and M. Reiher, *Angew.Chem. Int. Ed*., 45 (2006) 6264.

13. M. Yuki, Y. Mayike, Y. Nishibayashi, I. Wakiji and M. Hidai, *Organometallics*, 27 (2008) 3947.

14. R. Benn, C. Brevard, A. Rufińska, G. Schroth, *Organometallics*, 6 (1987) 838.

15. H.C.E. McFarlane, W. McFarlane, D.S. Rycroft, *J. Chem. Soc., Dalton Trans*., (1976) 1616.

16. F.A. Cotton and D.J. Darensbourg, *J. Am. Chem. Soc*., 20 (1981) 4440

17. R.J. Angelici and M.D. Malone, Inorg. Chem., 6 (1967) 1731.

18. T. Szymańska-Buzar, T. Glowiak and I. Czeluśniak, *Polyhedron*, 21 (2002) 1817.

19. D.J. Darensbourg, J.R. Andreatta, S.M. Stranahan and J.H. Reibenspies, *Organometallics*, 26 (2007) 6832.

20. L. Hirsivaana, M. Haukka and J. Puriainen, *Eur. J. Inorg. Chem*., (2001) 2255

CHAPTER 8

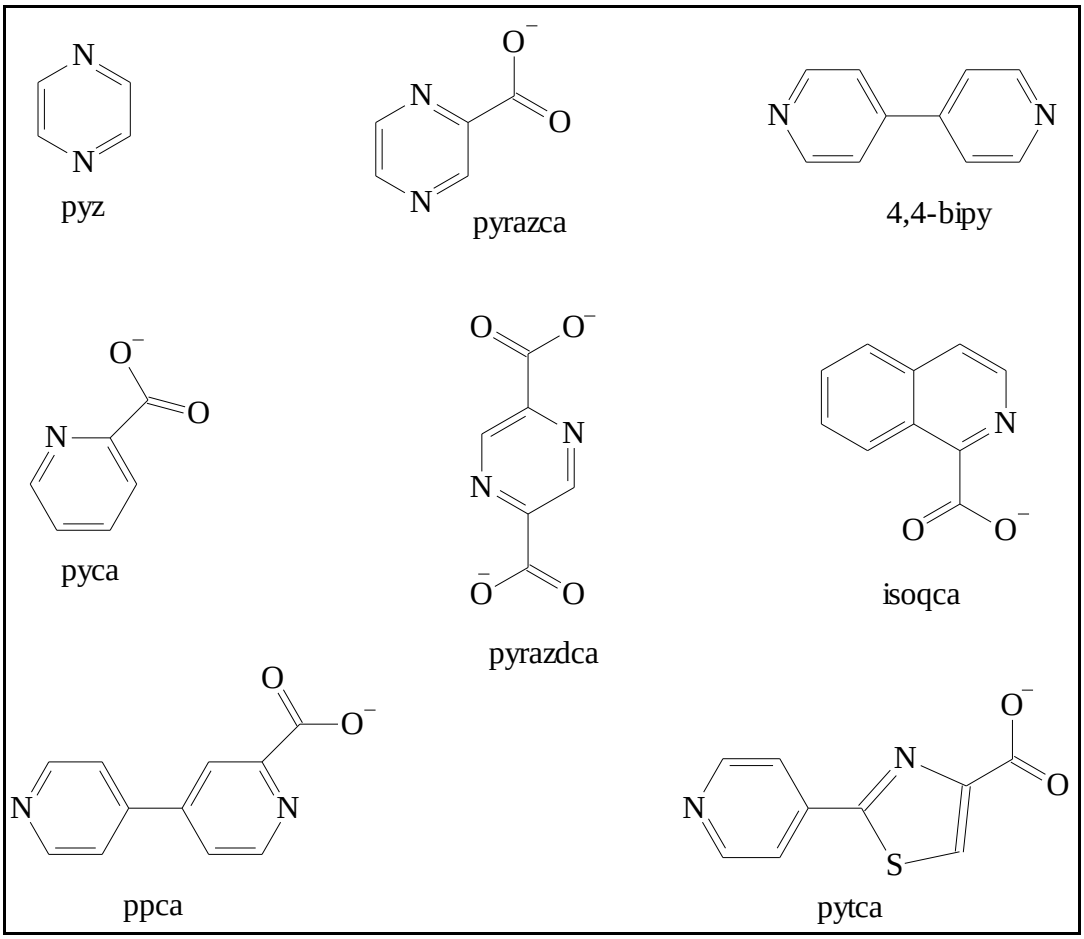
Synthesis, X-Ray and NMR Spectroscopic Studies of Bridged Bimetallic Complexes of Rhodium and Tungsten

8.1 Introduction

Organometallic complexes bearing ligands that display multiple coordination modes have found potential application in the areas of optoelectronic materials, magnetic materials, molecular storage, ion-exchange, size/shape-selective separations, catalysis and molecular switches [1]. The multiple functionality which results from multiple coordination modes leads to the formation of stable mixed-metal-containing building blocks of the structural form of infinitely repeating multi-dimensional units which exhibit complex channel-containing 3D structures. There are many such inorganic-organic framework materials where ligands with multiple coordination modes yield multi-valent hybrid materials and many interesting structures [2].

Pyridyl ligands that contain carboxylate groups such as pyridine-2-carboxylate (pyca) and pyrazine-2-carboxylate (pyrazca), and their substituted derivatives exhibit the ability to engage in several coordination modes simultaneously. This ability is made possible by characteristic coordination via the N-donor and/or carboxylate groups. Some of the common multifunctional ligands falling under this category that have proven to be useful in the synthesis of mono- and bi-metallic compounds are bipyridine (bipy), 4-(pyridin-4-yl)pyridine-2-carboxylate (ppca) [3], 2-(4-pyridyl)thiazole-4-carboxylate (pytca) (**Scheme 8.1 [2c, 2d, 2f, 4]**). Pyridyl ligands are perhaps the most extensively utilised group because of their versatility in the design of specific ligands with varied geometrical arrangements for the construction of a very large number of coordination polymers [5]. The carboxylic acid unit represents another prevalent functional

group which readily forms a chelating ligand in conjunction with an aromatic N-donor group such as pyridine, isoquinoline, etc. [6]. Pyrazine is an attractive bridging ligand due to the geometry and availability of the lone pair of electrons on the nitrogen as well as being aromatic. This aromaticity permits electronic communication between metals centres through optimal ligand and metal orbital overlap [7].

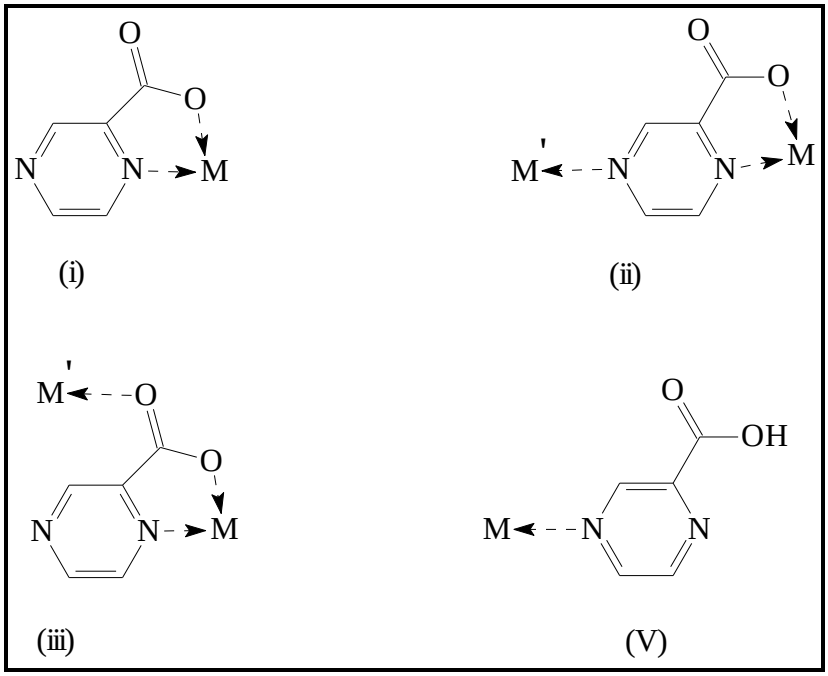


Scheme 8.1 Examples of bridging ligands containing a nitrogen atom. Legends: pyz = pyrazine, pyrazca = pyrazine-2-carboxylate, 4,4-bipy = bipyridine, pyca = pyridine-2-carboxylate, pyrazdca = 2,2-pyrazinedicarboxylate, isoqca = isoquinoline-1-carboxylate, ppca = 4-(pyridin-4-yl)pyridine-2-carboxylate and pytca = 2-(4-pyridyl)thiazole-4-carboxylate.

The 2-pyrazinecarboxylic acid (O_2CpyrazH) or 2-pyrazinecarboxylate (pyrazca) can be a terminal bidentate ligand in which case, it coordinates to the metal ion through an oxygen atom of the carboxylate group and the vicinal N atom or can also acts a bidentate/monodentate

bridging ligand in which case the second nitrogen atom can coordinate with another metal ion or through the other oxygen of the carboxylate group through what is called three-atom bridge link. In this particular link, two metals are linked through an oxygen-carbon-oxygen bridge (**Scheme 8.2**) while the single-atom bridge links two metals through an oxygen atom (not shown).

While the coordination site of pyrazca and ppca are mainly in a linear arrangement with respect to each other, in the case of pytca, the chelating nitrogen is no longer exactly opposite the terminal nitrogen, but rather oriented at an angle to it. This particular feature offers this ligand a special ability to function as a bent spacer [8].



Scheme 8.2 Examples of coordination modes of pyrazca: (i) bidentate terminal, (ii) bidentate/N-monodentate bridge, (iii) bidentate/O-monodentate bridge, (iv) N-monodentate terminal ligand (ref. [9])

It can therefore be anticipated that the bent orientation of the ligand's N-donor atoms and the presence of an additional Lewis base site in the form of sulphur-ring atom could promote construction of more diverse structures compared to those containing pyrazca or pyraz ligands. In this thesis, we explore the coordination and possible electronic communication capabilities between metal centres of complexes of the ligands pyrazine-2-carboxylate (pyrazca), pyrazine 2,

2'-pyrazinedicarboxylate (pyrazdca) and 2-(4-pyridyl)thiazole-4-carboxylate (pytca) containing rhodium and tungsten.

8.2 Experimental

All reactions were carried out under an atmosphere of argon at ambient temperature, unless specified otherwise. Solvents such as dichloromethane, THF, diethyl ether, acetonitrile and diethyl amine were distilled, purified and dried before use as described in Chapter 3. All starting materials were used as purchased from the suppliers without further purification. The rhodium complex $[RhH(PPh_3)_4]$ was prepared following a literature procedure [10], however the synthesis described herein follows the more recent, optimised method of Robinson and co-workers [11]. The compound $[(PPh_3)_2Rh(H)_2(pyrazca)]$ was prepared following the slightly modified method of Carlton [6a]. Tungsten complexes of the type $[W(CO)_4(NCMe)(PR_3)]$ were prepared as in Chapter 7 where R = Ph, *p*-tolyl, *p*-$OMeC_6H_4$, *p*-$CF_3C_6H_4$, *p*-FC_6H_4 and R_3 = $MePh_2$. A stock solution of MeOH/THF (1:1) was prepared once for all reactions between $[(PPh_3)_2Rh(H)_2(pyrazca)]$ and $[W(CO)_4(NCMe)(PR_3)]$ as it was for all NMR measurements of bridged rhodium-tungsten complexes from a stock solution of CD_3OD/THF (1:1). Stock solutions of MeOH/THF and CD_3OD/THF were preserved under an atmosphere of argon at all times.

8.2.1 Synthesis and characterization of $[RhH(PPh_3)_4]$ ……**40**

Hot solutions of rhodium trichloride trihydrate ($RhCl_3.3H_2O$) (0.26 g, 1.24 mmol) in ethanol (EtOH) (20 ml) and potassium hydroxide (KOH) (0.4 g) in EtOH (20 ml) were added rapidly in succession (first $RhCl_3.3H_2O$ followed by KOH and avoiding contact of the two solutions until mixed with the PPh_3 solution) to a vigorously stirred hot solution of PPh_3 (2.62 g, 10 mmol) in EtOH (80 ml). The mixture was left to stir at ≥ 90 ºC for ten minutes at reflux. A yellow suspension formed within a minute of $RhCl_3.3H_2O$ and KOH addition to the PPh_3 solution. The bright yellow precipitate was filtered whilst still warm and washed with EtOH (20 ml), water (20 ml), EtOH (20 ml) and finally with n-hexane (40 ml) and dried under vacuum to give a yield of 1.220 g (85%). The NMR spectra were recorded from a solution in CD_3OD. IR (compact material): $\nu_{(Rh-H)}$ 2157 cm^{-1}.

8.2.2 Synthesis and characterization of [$(PPh_3)Rh(H)_2$(pyrazca)]…….41

A mixture of [$RhH(PPh_3)_4$] **40** (347 mg, 0.301 mmol) and 2-pyrazinecarboxylic acid (38 mg, 0.306 mmol) in THF (8 ml) was warmed to 60 ºC and stirred at the same temperature for 5 min. An off-white to pale yellow precipitate formed almost immediately during the stirring and was separated by filtration from the deep red solution and washed with ether (3 ml x 4) giving a light yellow microcrystalline powder. The product was dried under vacuum giving a yield of 204 mg (52%). The NMR spectra were recorded from a solution in CD_3OD at 300 K. ^1H NMR ($\delta_{(ppm)}$): 8.65 (d, py, $^4J_{(H-H)}$ = 1 Hz), 7.76 (d, py, $^3J_{(H-H)}$ = 3 Hz), 7.56 (m, Ph), 7.37 (m, py), 7.25 (m, Ph), -15.15, (m, RhH), -20.35 (m, RhH). $^{31}P\{^1H\}$ NMR ($\delta_{(ppm)}$): 43.56 (d, P, $^1J_{(Rh-P)}$ = 118 Hz). IR (compact material): $\nu_{(Rh-H)}$ 2162, $\nu_{(C=O)}$ 1666 cm^{-1}.

8.2.2.1 Reaction of [$(PPh_3)Rh(H)_2$(pyrazca)] 41 with [$W(CO)_4(NCMe)(PPh_3)$] 24

A small scale reaction mixture of [$W(CO)_4(NCMe)(PPh_3)$] **24** (14 mg ~ 0.0233 mmol) and [$(PPh_3)Rh(H)_2$(pyrazca)] **41** (30 mg ~ 0.0234 mmol) in benzene (3 ml) was stirred at room temperature for a period of 3 min. Compound **41** remained undissolved in benzene at room temperature. The colour changed from yellow to violet within 3 min of mixing. The solution was then warmed to approximately 60 ^0C to dissolve compound **41** as well. The solution was stirred for a further 5 min at 60 ^0C during which the violet colour grew more intense. The solution was removed from the oil bath and left to cool to room temperature before being concentrated (by gently blowing argon over the solution) to about 1 ml after which few drops of n-hexane were added to induce crystallisation. Deep blue-grey material was collected and analysed by both ^{31}P and ^1H NMR from a solution in C_6D_6. The NMR results showed formation of oxidized tungsten and rhodium complexes.

8.2.3 Synthesis and characterization of [{$Rh(H)_2(PPh_3\}_2$(pyrazdca)]……..42

To a solution of $RhH(PPh_3)_4$] **40** (174 mg, 0.136 mmol) in THF (5ml) at room temperature was added a suspension of 2,2-pyrazinedicarboxylic acid (pyrazdca) (14 mg, 0.68 mmol) in THF (2 ml). The red-orange coloured solution of [$Rh(H)(PPh_3)_4$] in THF turned brown during drop-wise addition of pyrazdca. The solution was warmed to 50 ºC and stirred at this temperature for a further 20 min in a sealed Schlenk tube after which heating and stirring were stopped. The solution was

then allowed to cool to room temperature after which the solvent was removed *in vacuo* leaving behind a dark brown paste. The yellow-brown paste was washed several times with cold ether (3 ml x 5) to give a bright yellow powder 163 mg (48%). The NMR spectra were recorded from a solution in CD_3OD at 300 K. ^1H NMR ($\delta_{(ppm)}$): 8.09, 7.73 (s, pyrazH), 7.40 – 7.20 (m, Ph), -16.18 (m, RhH), -20.47 (m, RhH). $^{31}P\{^1H\}$ NMR ($\delta_{(ppm)}$) = 39.2 (d, $^1J_{(Rh-P)}$ = 117 Hz). Elemental analysis: calculated for $C_{78}H_{66}N_2O_4P_4Rh_2$: C, 65.74; H, 4.67: N, 1.97%. Found: C, 64.85; H, 5.39; N, 2.06. IR (compact material): $\nu_{(Rh-H)}$ 2068 Hz, $\nu_{(C=O)}$ 1645(br) cm^{-1}.

8.2.4 Synthesis and characterization of $[Rh(H)_2(pytca)(PPh_3)_2]$ ……**43**

To a red solution of $[Rh(H)_2(PPh_3)_4]$ **40** (532 mg, 0.416 mmol) in THF (5 ml) at room temperature was added a solution of 2-(4-pyridyl)thiazole-4-carboxylic acid (pytca) (86 mg, 0.417 mmol) in THF (5 ml). The solution of pytca in THF was added drop-wise over a period of just under a minute. The initial red colour suddenly changed to cream accompanied by the formation of a white precipitate within five minutes of stirring at ~ 57 ºC. Stirring was continued for a further 10 minutes in a sealed Schlenk tube at which point the paste became too thick to allow stirring. Heating was stopped and the cream paste allowed to cool to room temperature after which the precipitate was separated by centrifuge and washed with Et_2O (5 ml x 4) and dried under vacuum to give a yield of highly electrostatic white powder of 338 mg (84%). NMR spectra were recorded from a solution of CD_3OD /THF at 300K. ^1H NMR ($\delta_{(ppm)}$): 8.39 (d, pytca, $^3J_{(H-H)}$ = 6 Hz), 7.73 (s, pytcaH), 7.72 (d, pytca, $^3J_{(H-H)}$ = 6 Hz), 7.53 (m, Ph), 7.43 (m, Ph), 7.34 (m, Ph), -16.43 (m, RhH), -19.64 (m, RhH). $^{13}C\{^1H\}$ NMR ($\delta_{(ppm)}$): 167.98 (s, CO), 165.52 (s, pytca), 155.22 (s, pytca), 150.40 (s, pytca), 139.69 (s, pytca), 134.76 (m, *ortho*, Ph), 134.53 (d, Ph, $^1J_{(P-C)}$ = 23 Hz), 131.12 (s, *para*, Ph), 129.33 (m, *meta*, Ph), 127.52 (s, pytca), 123.38 (s, pytca). $^{31}P\{^1H\}$ NMR ($\delta_{(ppm)}$): 42.49 (dt, PPh3, $^1J_{(Rh-P)}$ = 119 Hz, $^2J_{(P-P)}$ = 11 Hz). Elemental analysis: Calculated for $C_{45}H_{37}N_2O_2P_2RhS$: C, 64.75; H, 4.47; N, 3.36%. Found: C, 63.78; H, 4.30; N, 3.36. IR (compact material) $\nu_{(Rh-H)}$ 2090, 2053 cm^{-1}; $\nu_{(C=O)}$ 1634(br) cm^{-1}.

8.2.5 Synthesis and characterization of $[(PPh_3)_2Rh(H)_2(pytca)W(CO)_4(PPh_3)]$ …**45**

A clear solution of $[(PPh_3)_2Rh(H)_2(pytca)]$ **43** (30 mg, 0.036 mmol) in THF/MeOH (3 ml, 1:1) at room was added drop-wise into a yellow solution of $[W(CO)_4(NCMe)(PPh_3)]$ **24** (22 mg, 0.036 mmol) in THF/MeOH (3 ml, 1:1) also at room temperature within 10 seconds. The solution was

then sealed in a Schlenk tube under argon and stirred at room temperature overnight. There was no immediate colour change. The colour changed from yellow to red-orange overnight. The solvent was removed by a gentle flow of argon gas over the sample leaving behind a red solid paste which was dried under vacuum to a yield of 35 mg (70%). A small amount of the sample was redissolved in MeOH/THF (1:1) and few drop of Et_2O were added to induce crystallization. No crystals formed at room temperature or at -5 ºC, but decomposed red powder was isolated. NMR spectra were recorded from a solution in CD_3OD /THF (1:1) at 300 K. ^1H NMR ($\delta_{(ppm)}$): 8.14 (d, pyridyl-H, $^3J_{(H-H)}$ = 7 Hz), 7.63 – 7.27 (m, pytca, Ph), -16.50 (m, RhH), -19.84 (m, RhH). $^{31}P\{^1H\}$ ($\delta_{(ppm)}$): 41.87 (d, RhP, $^1J_{(Rh-P)}$ = 119 Hz), 32.36 (s, WP, satellite, d, $^1J_{(W-P)}$ = 239 Hz). IR (compressed solid) $\nu_{(Rh-H)}$ 2070 cm^{-1}; $\nu_{(C\equiv O)}$ 2007, 1866, 1849 cm^{-1}; $\nu_{(C=O)}$, 1634(br) cm^{-1}.

8.2.6 Synthesis and characterization of $[(PPh_3)_2Rh(H)_2(pytca)\text{-}W(CO)_4P(tolyl)_3]$ ……**46**

A reaction mixture of $[(PPh_3)_2Rh(H)_2(pytca)]$ **43** (50 mg, 0.052 mmol) and $[W(CO)_4(NCMe)P(tolyl)_3]$ **25** (38 mg, 0.60 mmol) in THF/MeOH (6 ml,1:1) was stirred at room temperature overnight in a sealed Schlenk tube. The initial light orange solution turned red overnight accompanied by formation of a red precipitate which was isolated and washed with EtOH (3 ml) to give a red powder (15 mg). The mother liquor solution was left at room temperature for five days after which a red crystalline lump was collected and dried under a gentle stream of argon gas giving a combined yield of 43 mg (57%). NMR spectra were recorded from a solution in CD_3OD /THF at 300K. ^1H NMR ($\delta_{(ppm)}$): 8.18 (d, pyridyl-H, $^3J_{(H-H)}$ = 6 Hz), 7.71(s, 1H, thiazole-H), 7.46-7.23 (m, pytca, Ph), 7.13 (m, Ph), -16.54 (m, RhH), -19.71 (m, RhH). $^{31}P\{^1H\}$ ($\delta_{(ppm)}$): 41.80 (d, RhP, $^1J_{(Rh-P)}$ = 119 Hz), 29.19 (s, WP, satellite, d, $^1J_{(W-P)}$ = 239 Hz). Elemental analysis (crystalline lump): Calculated for $C_{70}H_{58}N_2O_6P_3SRhW$: C, 58.59; H, 4.07; N, 1.96%. Found: C, 58.88; H, 4.19; N, 1.96%. IR (compact material) $\nu_{(Rh-H)}$ 2076 cm^{-1}; $\nu_{(C\equiv O)}$ 2004, 1869, 1845 cm^{-1}; $\nu_{(C=O)}$ 1630 cm^{-1}.

8.2.7 Synthesis and characterization of $[(PPh_3)_2Rh(H)_2(pytca)\text{-}WCO)_4P(4\text{-}FC_6H_4)_3]$ …… **47**

A reaction mixture of $[W(CO)_4(NCMe)P(4\text{-}FC_6H_4)_3]$ **27** (45 mg, 0.070 mmol) and $[(PPh_3)_2Rh(H)_2(pytca)]$ **43** (58 mg, 0.069 mmol) in THF/MeOH (1:1, 4 ml) was stirred at room

temperature overnight in a sealed Schlenk tube. The colour changed from bright yellow to deep red overnight. The solvent was removed *in vacuo* leaving behind a red powder giving a yield of 96 mg (95%). The NMR spectra were recorded from a solution in CD_3OD /THF at 300 K. ^1H NMR ($\delta_{(ppm)}$): 8.16 (d, pyridyl-H, $^3J_{(H-H)}$ = 7 Hz), 7.71 (s, thiazole-H), 7.65 (m, pytca), 7.44 – 7.10 (m, Ph), -16.54 (m, RhH), -19.76 (m, RhH). $^{31}P\{^1H\}$ NMR ($\delta_{(ppm)}$); 42.01 (d, RhP, $^1J_{(Rh-P)}$ = 118 Hz), 29.23 (s, WP, satellite, d, $^1J_{(W-P)}$ = 239 Hz). IR (compact material) $\nu_{(Rh-H)}$ 2071 cm^{-1}, $\nu_{(C\equiv O)}$ 2009, 1870, 1869 cm^{-1}; $\nu_{(C=O)}$ 1632(br) cm^{-1}.

8.2.8 Synthesis and characterization of $[(PPh_3)_2Rh(H)_2(pytca)\text{-}WCO)_4P(4\text{-}CF_3C_6H_4)_3]$ ……**48**

A reaction mixture of $[(PPh_3)_2Rh(H)_2(pytca)]$ **43** (36 mg, 0.043 mmol) and $[W(CO)_4(NCMe)P(4\text{-}CF_3C_6H_4)_3]$ **28** (35 mg, 0.043 mmol) in THF/MeOH (1:1, 4 ml) was stirred overnight in a sealed Schlenk tube at room temperature. The colour changed overnight from light yellow to deep red. The solvent was removed *in vacuo* leaving behind a red solid lump composed of micro crystalline powder giving a yield of 62 mg (91%). The NMR spectra were recorded from a solution in CD_3OD /THF at 300 K. ^1H NMR ($\delta_{(ppm)}$): 8.34 (d, pyridyl-H, $^3J_{(H-H)}$ = 6 Hz), 7.60 – 7.32 (m, pytca, Ph), -16.46 (m, RhH), -19.68 (m, RhH). $^{31}P\{^1H\}$ NMR ($\delta_{(ppm)}$): 42.47 (d, RhP, $^1J_{(Rh-P)}$ = 118 Hz), 32.49 (s, WP, satellite, d, $^1J_{(W-P)}$ = 239 Hz). IR (compact material) $\nu_{(Rh-H)}$ 2071 cm^{-1}, $\nu_{(C\equiv O)}$ 2009, 1892, 1875 cm^{-1}; $\nu_{(C=O)}$ 1633 cm^{-1}.

8.2.9 Synthesis and characterization of $[(PPh_3)_2Rh(H)_2(pytca)\text{-}WCO)_4P(4\text{-}OMeC_6H_4)_3]$ ……**49**

A reaction mixture of $[(PPh_3)_2Rh(H)_2(pytca)]$ **43** (56 mg, 0.066 mmol) and $[W(CO)_4(NCMe)P(4\text{-}OMeC_6H_4)3]$ **26** (53 mg ~ 0.066 mmol) in THF/MeOH (1:1, 4 ml) was stirred overnight in a sealed Schlenk tube at room temperature. The colour changed overnight from light yellow to deep red. The solvent was removed in vacuo leaving behind a red solid lump composed of micro crystalline powder giving a yield of 91 mg (92%). NMR spectra were recorded from a solution in CD_3OD /THF at 300 K. ^1H NMR ($\delta_{(ppm)}$): 8.14 (d, pyridyl-H, $^3J_{(H-H)}$ = 6 Hz), 7.65 (m, pytca), 7.46-7.22 (m, Ph), 6.82 (m, Ph), -16.52 (m, RhH), -19.72 (m, RhH).

$^{31}P\{^{1}H\}$ NMR ($\delta_{(ppm)}$): 41.83 (d, RhP, $^{1}J_{(Rh-P)}$ = 118 Hz), 27.9 (s, WP, satellite, d, $^{1}J_{(W-P)}$ = 240 Hz). IR (compact material) $\nu_{(Rh-H)}$ 2069 cm^{-1}; $\nu_{(C\equiv O)}$ 2006, 1866, 1845 cm^{-1}; $\nu_{(C=O)}$ 1630(br) cm^{-1}.

8.2.10 Synthesis and characterization of $[(PPh_3)_2Rh(H)_2(pytca)\text{-}WCO)_4PMePh_2]$ ……**50**

A clear solution of $[(PPh_3)_2Rh(H)_2(pytca)]$ **43** (86 mg, 0.103 mmol) in THF/MeOH (4 ml, 1:1) was added drop-wise into a clear yellow solution of $[W(CO)_4(NCMe)P(MePh_2)]$ **30** (66 mg, 0.123 mmol) in THF/MeOH (6 ml, 1:1). The clear yellow solution changed to red-brown upon addition of $[(PPh_3)_2Rh(H)_2(pytca)]$ **43** after which it was sealed in a Schlenk tube and stirred overnight at room temperature. After ca. 24 hrs of stirring at room temperature, the colour changed to oxblood red. The resultant solution was centrifuged to remove a grey precipitate after which the solvent was removed under reduced pressure leaving behind a red crystalline powder (yield of 92 mg; 67%). NMR spectra were recorded from a solution in CD_3OD /THF at 300 K. ^{1}H NMR ($\delta_{(ppm)}$): 8.20 (d, pyridyl-H, $^{3}J_{(H-H)}$ = 6.7 Hz), 7.67 (s, 1H, thiazole-H), 7.60 (m, pytca), 7.48-7.29 (m, Ph), 2.37 (d, 3H, Me, $^{2}J_{(P-H)}$ = 7 Hz), -16.47 (m, 1H, RhH), -19.78 (m, 1H, RhH). $^{31}P\{^{1}H\}$ NMR ($\delta_{(ppm)}$): 42.13 (d, Rh<u>P</u>, $^{1}J_{(Rh-P)}$ = 119 Hz), 8.26 (s, W<u>P</u>, satellite, d, $^{1}J_{(W-P)}$ = 237 Hz). IR (compact material) $\nu_{(Rh-H)}$ 2069 cm^{-1}; $\nu_{(C\equiv O)}$ 2007, 1865, 1838; $\nu_{(C=O)}$1632, cm^{-1}.

8.2.11 Synthesis and characterization of $[(PPh_3)_2Rh(H)_2(pytca)\text{-}WCO)_4PPh_2C_6F_5]$ ……**50a**

A solution of $[W(CO)_4(NCMe)(PPh_2C_6F_5)]$ **31** (52 mg ~ 0.0719 mmol) and $[(PPh_2)Rh(H)_2(pytca)]$ **43** in (55.5 mg ~ 0.0665 mmol) in THF/MeOH (4 ml, 1:1) was stirred at room temperature overnight. The colour started changing within 5 min of reaction. The resultant deep red solution was centrifuged to remove a dark brown precipitate after which the solvent was removed *in vacuo* leaving behind ox-blood powder (52 mg, 53%). NMR spectra were recorded from a solution in CD_3OD /THF at 300 K. ^{1}H NMR ($\delta_{(ppm)}$): 8.16 (d, pyridyl-H, $^{3}J_{(H-H)}$ = 6.0 Hz), 7.67 (s, 1H, thiazole-H), 7.48-7.30 (m, pytca, P<u>Ph</u>$_2C_6F_5$), -16.47 (m, 1H, RhH), -19.70 (m, 1H, RhH). $^{31}P\{^{1}H\}$ NMR ($\delta_{(ppm)}$): 42.08 (d, Rh<u>P</u>, $^{1}J_{(Rh-P)}$ = 118 Hz), 25.2 (s, W<u>P</u>, satellite, d, $^{1}J_{(W-P)}$ = 240 Hz). IR (compact material) $\nu_{(Rh-H)}$ 2071 cm^{-1}; $\nu_{(C\equiv O)}$ = 1980, 1876 (br); $\nu_{(C=O)}$ 1640 cm^{-1}.

8.3 X-ray crystallography

Table 8.1 Crystal and structure refinement data for the compound $[(PPh_3)_2Rh(H)_2(pytca)W(CO)_4P(tolyl)_3]$ **46** co-crystallised with MeOH.

Compound	
Empirical formula	C71 H62 N2 O7 P3 Rh S W
Formula weight	1466.96
Temperature	173(2) K
Wavelength	0.71073 Å
Crystal system	Triclinic
Space group	P-1
Unit cell dimensions: a (Å) b (Å) c (Å) α (^{0}) β (^{0}) γ (^{0})	11.1746(3) 17.4074(4) 18.1475(5) 73.7060(10) 76.5220(10) 76.2200(10)
Volume	3238.01(15) $Å^3$
Z	2
Density (calculated)	1.505 Mg/m^3
Absorption coefficient	2.191 mm^{-1}
F(000)	1476
Crystal size	0.34 x 0.28 x 0.10 mm^3
Theta range for data collection	1.50 to 28.00°.
Index ranges	-14<=h<=14, -22<=k<=22, -23<=l<=23
Reflections collected	29487
Independent reflections	15578 [R(int) = 0.0682]
Completeness to theta = 28.00°	99.8 %
Absorption correction	Integration
Max. and min. transmission	0.8107 and 0.5229
Refinement method	Full-matrix least-squares on F^2
Data / restraints / parameters	15578 / 1 / 786
Goodness-of-fit on F^2	0.863
Final R indices [I>2sigma(I)]	R1 = 0.0407, wR2 = 0.0726
R indices (all data)	R1 = 0.0741, wR2 = 0.0812
Largest diff. peak and hole	1.767 and -0.778 $e.Å^{-3}$

Intensity data were collected on a Bruker APEX II CCD area detector diffractometer with graphite monochromated Mo K_α radiation (50 kV, 30 mA) using the APEX 2 [12] data collection software. The collection method involved ω-scans of width 0.5° and 512 x 512 bit data frames. Data reduction was carried out using the program *SAINT+* [13] and face indexed absorption corrections were made using the program *XPREP* [13]. The crystal structure was solved by direct methods using *SHELXTL* [14]. Non-hydrogen atoms were first refined isotropically followed by anisotropic refinement by full matrix least-squares calculations based on F^2 using *SHELXTL*. Hydrogen atoms were first located in the difference map then positioned geometrically and allowed to ride on their respective parent atoms. Diagrams for publication material were generated using SHELXTL, PLATON [15] and ORTEP-3 [16].

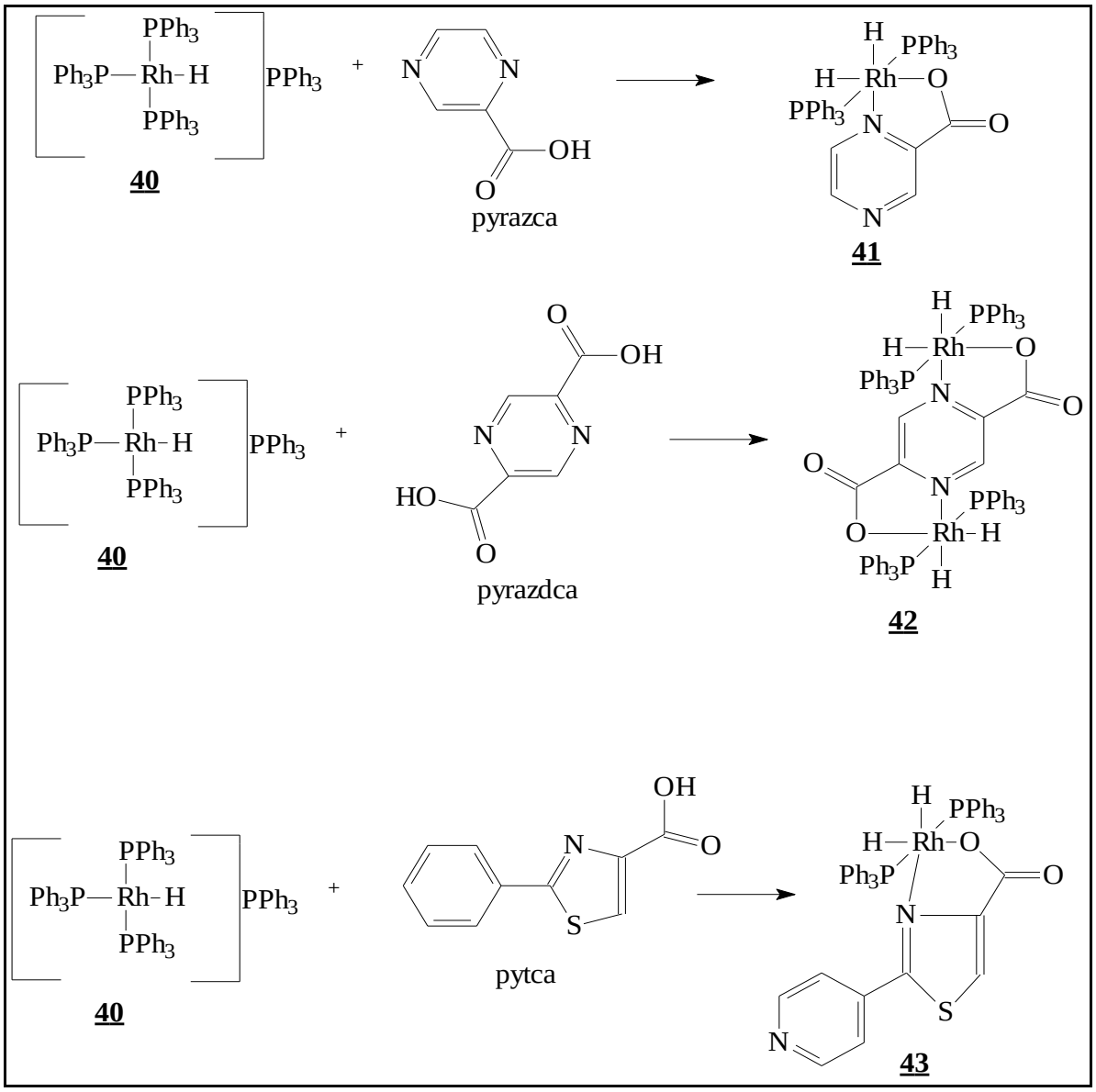
8.4 Results and discussion

8.4.1 Reaction of rhodium(III)hydride 41 with tungsten phosphine complex 24

The reaction of the rhodium(I)hydride complex **40** with pyrazinecarboxylic acid (pyrazca) at room temperature gives the dihydrido complex **41** in a moderate yield as air-stable pale yellow crystals (**scheme 8.3**). The attempted reaction of $[Rh(H)_2(pyrazca)(PPh_3)_2]$ **41** with $[W(CO)_4(NCMe)(PPh_3)]$ **24** at room temperature to give $[(PPh_3)_2Rh(H)_2(pyrazca)$-$W(CO)_4(PPh_3)]$, gave a deep blue-grey microcrystalline powder after 6 hrs under inert atmosphere which was characterized by $^{31}P\{^1H\}$ NMR as oxidized tungsten and rhodium complexes. The results of NMR analysis by monitoring the chemical shift of ^1H showed the appearances of new multiplet hydride signals of possibly a proton *trans*- to the oxygen and two new multiplet signals due to the protons *trans*- to the nitrogen. Similarly, the $^{31}P\{^1H\}$ NMR showed the appearance of new phosphorus-tungsten and phosphorus-rhodium bonded signals over the reaction period. The results observed at low temperatures (-30 ºC) were the same as for higher temperatures, however at much slower rate, as observed for by ^1H and $^{31}P\{^1H\}$ NMR analysis in a sealed tube NMR under argon. Results from this reaction suggest a very sensitive product or intermediate in which case the carboxylate becomes a possible source of oxygen (rigorous exclusion of oxygen from the solvent was successfully dealt with by a small scale freeze-thaw procedure in the sealed NMR tube).

8.4.2 Reaction of rhodium(I)hydride 40 with pyrazinedicarboxylic (pyrazdca).

The reaction of two molar equivalents of $[Rh(H)(PPh_3)_4]$ **40** with pyrazinedicarboxylic (pyrazdca) at room temperature gives a bright yellow powder of the rhodium(III)dihydro complex $[\{Rh(H)_2(PPh_3\}_2(pyrazdca)]$ **42** in good yield (**Scheme 8.3**).



Scheme 8.3 Schematic representation of different synthetic routes leading to carboxylate rhodium(III)dihydrido complexes.

Compounds **41**, **42** and **43** were characterised by multinuclear NMR analysis. The ^{31}P and ^{1}H NMR chemical shift analysis of **42** shows a symmetrical geometry about the pyrazine ring in which a perfect signal overlap exists. As with the synthesis of **41**, the reaction of rhodium(I)phosphine compounds with a carboxylic acid containing a nitrogen donor atom proceed by oxidative addition to give rhodium(III) compounds. This reaction process is accompanied by change in the coordination number of the rhodium atom from four to six.

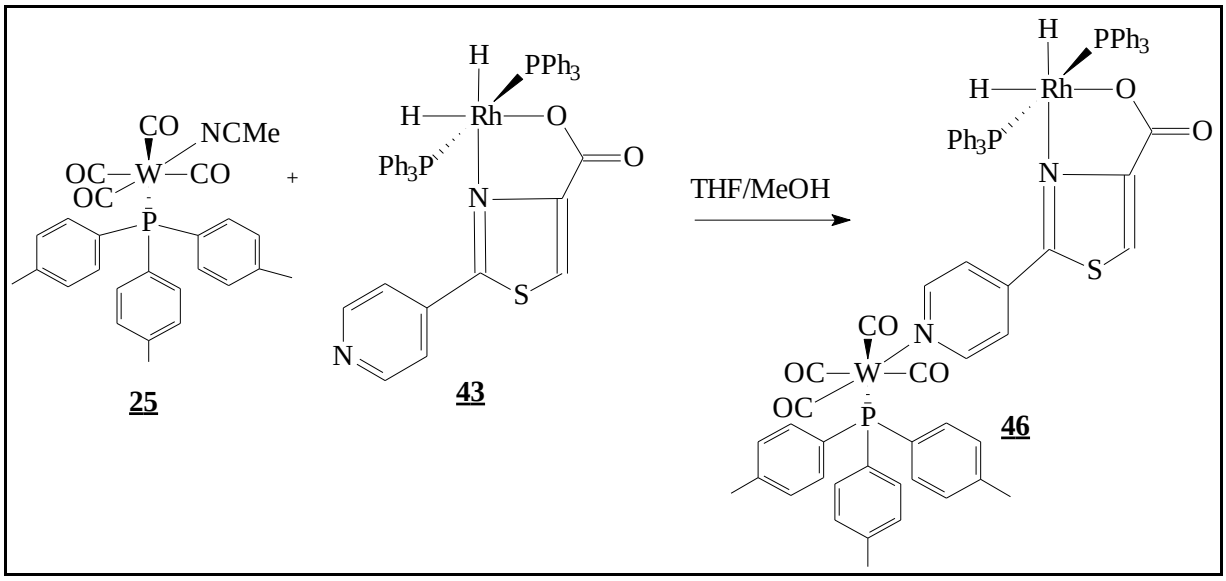
8.4.3 Reaction of rhodium(I)hydride 40 with 2-(4-pyridyl)thiazole-4-carboxylate (pytca)

The reaction of $[Rh(H)(PPh_3)_4]$ **40** with 2-(4-pyridyl)thiazole-4-carboxylate (pytca) in a THF/MeOH (1:1) mixture at room temperature gives a dihydro complex $[(PPh_3)_2Rh(H)_2(pytca)]$ **43** in good yields as an air stable white powder. Compound **43** does not dissolve in either chloroform or dichloromethane but does so readily in MeOH where it remains stable for over 6 months at temperatures below -10 ^{0}C. The ^{1}H NMR spectrum shows two multiplets at low fields indicating the two multiplet signals for the hydrides (which should theoretically resolve into ddt spin interaction). The multiplets result from spin coupling to each other, rhodium and two symmetrical phosphorus atoms. The multiplet at -16.43 ppm is assigned to the proton *trans*- to nitrogen of the thiazole ring and the other at -19.64 ppm to proton *trans*- to the carboxylate group. The hydrides are assumed to be in the same plane as the carboxylate oxygen and the thiazole nitrogen. The higher chemical shift signal (doublet) in the ^{1}H NMR spectrum is assigned to the hydrogens positioned *ortho* to the nitrogen of the pyridyl ring and remaining hydrogens of the same ring splitting into a doublets as well, appearing at the same chemical shift position as for the hydrogen of the thiazole ring. The $^{31}P\{1H\}$ spectrum consists of a single doublet confirming the axially positioned phosphorus atoms *trans* to each other (**Fig. 8.3**)

8.4.4 Reaction of $[Rh(H)_2(PPh_3)_2(pytca)]$ 43 with $[W(CO)_4(NCMe)PR_3]$ complexes

The reaction of $[Rh(H)_2(PPh_3)_2(pytca)]$ **43** with $[(W(CO)_4(NCMe)(PR_3)]$ (R = Ph, *p*-tolyl, *p*-$OMeC_6H_4$, *p*-$CF_3C_6H_4$, *p*-FC_6H_4 and NMe_2) in THF/MeOH solution mixture (1:1) for at-least 6 hrs at room temperature gives $[(PPh_3)_2Rh(H)_2(pytca)\text{-}W(CO)_4(PR_3)]$ as an orange-red microcrystalline powder in fair yields (**Scheme 8.4**). The progress of the reaction for compound $[(PPh_3)_2Rh(H)_2(pytca)\text{-}W(CO)_4(PPh_3)]$ **45** was monitored by $^{31}P\{^{1}H\}$ and ^{1}H NMR (**Figures 8.1 – 8.3**) which was accompanied by a colour change from yellow to deep red solution. The NMR

spectra in **Figures 8.1-3** show the progress of the reaction in the synthesis of $[(PPh_3)_2Rh(H)_2(pytca)W(CO)_4(PPh_3)]$ **45** at time zero, after 2 hrs, 6 hrs and overnight.



Scheme 8.4 Representative reaction scheme for the synthesis of the complex of the type $[(PPh_3)_2Rh(H)_2(pytca)W(CO)_4P(tolyl)_3]$ **46**

The higher chemical shift signal (doublet) signal (8.3 ppm) in the ^1H NMR spectrum of complex $[(PPh_3)_2Rh(H)_2(pytca)\text{-}W(CO)_4PPh_3]$ **45** disappeared at the same rate as the appearance of a new signal (at 8.1 ppm) upon coordination to the tungsten complex which clearly indicates the shielding influence of the tungsten group. There is a small change (~ 0.21 ppm) in the ^1H chemical shift of the pyridyl hydrogen as a result of W-N bond formation. As might be expected, the ^1H NMR chemical shift of the hydrides indicates no change as a result of tungsten-nitrogen (pyridyl) bond formation (**Fig. 8.1**). The reaction seems to be complete overnight, as there is no trace of starting material. However, observations from reactions performed under reduced pressure in a sealed NMR tube show that as soon after 70% conversion of the reagents into the expected products is achieved, several new products starts to form accompanied by disappearance of the hydride NMR signals. This process seems to be facilitated by the presence of electronegative substituents on the phosphorus (W-P) atom by making it an even better π-acceptor. Since the reactions are conducted in an oxygen free environment, it is assumed that the solvents, i.e. MeOH or THF are likely participants in the formation of the new products.

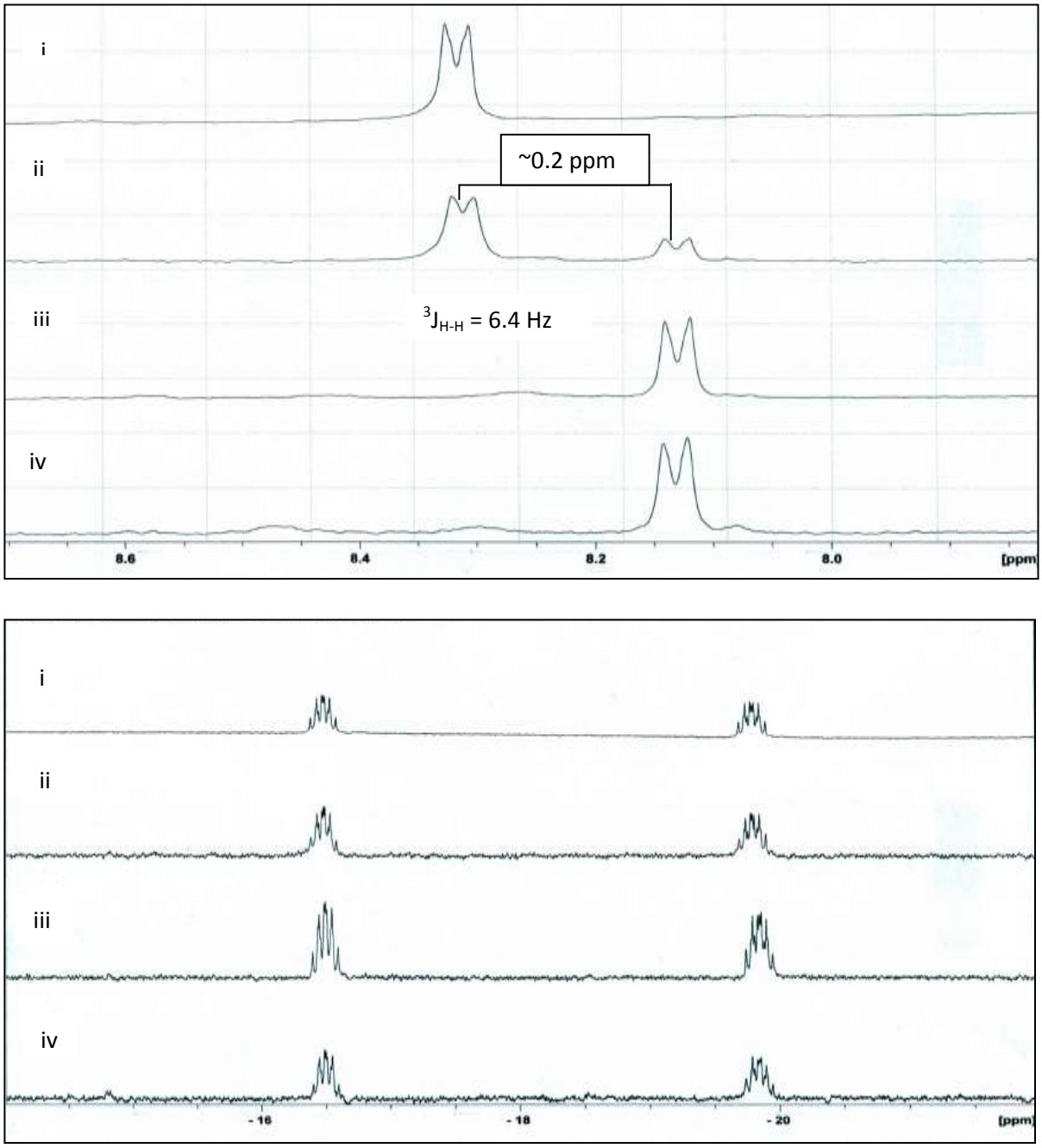


Figure 8.1 Progress of reaction as monitored by ^{1}H NMR between rhodium(III)dihydro complex $[Rh(H)_2(PPh_3)_2(pytca)]$ **43** and tungsten phosphine complex $[W(CO)_4(NCMe)(PPh_3)]$ **24** in the synthesis of complex $[(PPh_3)_2Rh(H)_2(pytca)W(CO)_4(PPh_3)]$ **45** at: (i) time zero, (ii) 2 hrs, (iii) 6 hrs, (iv) overnight in CD_3OD/THF (1:1) mixture at room temperature. The top spectrum shows the higher chemical shift pyridyl hydrogen and bottom spectrum shows lower chemical shift region for hydrides.

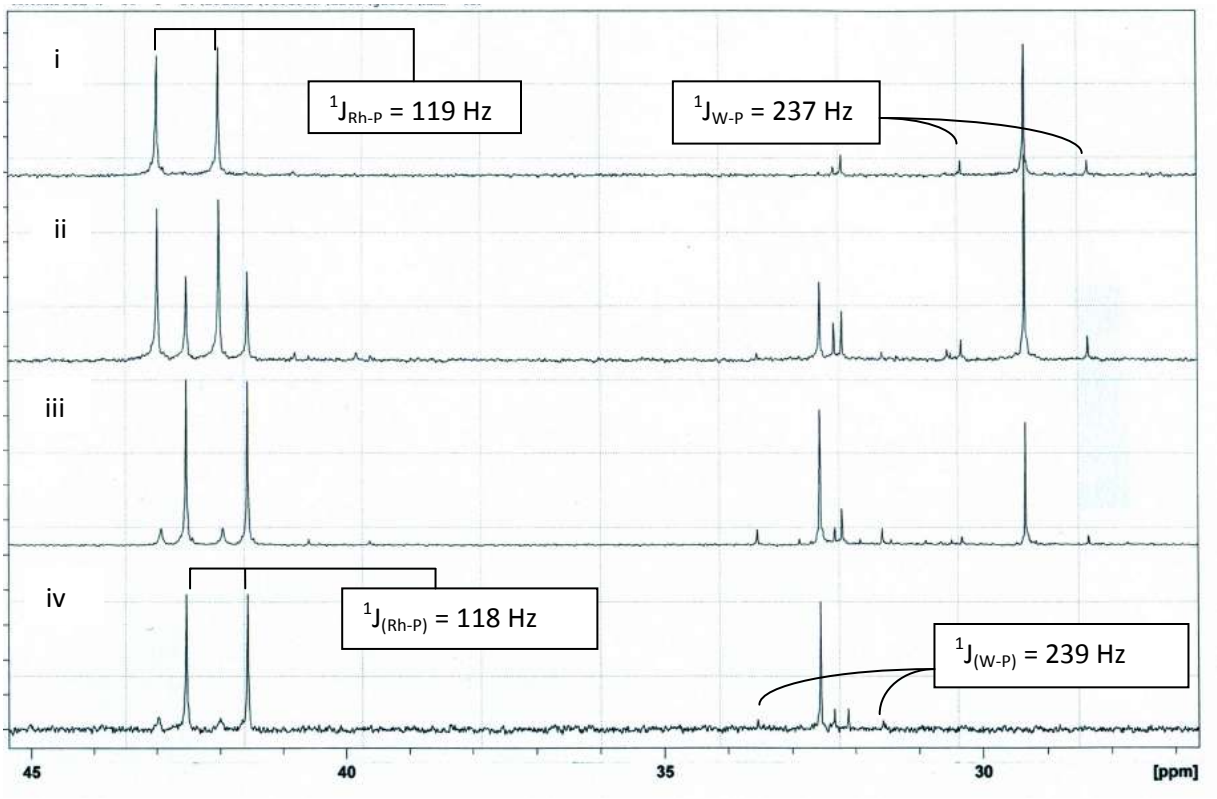


Figure 8.2 $^{31}P\{^1H\}$ NMR spectra of the reaction between rhodium(III) complex $[Rh(H)_2(PPh_3)_2(pytca)]$ **43** and tungsten phosphine complex $[W(CO)_4(NCMe)(PPh_3)]$ **24**; (i) time zero, (ii) 2 hrs, (iii) 6 hrs, (iv) overnight in CD_3OD/THF (1:1) mixture at room temperature.

The interesting observation from this reaction as indicated by $^{31}P\{^1H\}$(**Fig. 8.2**) and the higher chemical shift region of ^1H NMR (**Fig. 8.1**) spectra is that no intermediate product seems to form in the process of forming the final product. It is worthy to note that whilst the symmetrically positioned phosphorus atoms bonded to the rhodium are experiencing a shielding effect reflected by the $^{31}P\{^1H\}$ chemical shift change to lower chemical shift, the phosphorus bonded to tungsten is experiencing a slight deshielding effect due to coordination to the pyridyl ring (**Fig. 8.2**). In this particular case, there exists a possibility of a local magnetic field generated by the ring current contributing to a more deshielding region around the tungsten atom, which seems to account for the deshielding effect experienced by the phosphorus atom (W-P). A chemical shift change of 3.2 ppm by the symmetrically positioned phosphorus atoms bonded to rhodium is observed for compound **45** after coordination with tungsten complex. A possible electronic communication through the tungsten and rhodium atoms as reflected by the slight $^{31}P\{^1H\}$ NMR

chemical shift change of about 0.5 ppm by the Rh-P can be rationalised by the effective conjugation system through the aromatic pyridyl through to the thiazole ring and eventually through the two metal centres. Complexes of the type $[(PPh_3)_2Rh(H)_2(pytca)\text{-}W(CO)_4(PR_3)]$ seem to be generally unstable in toluene solution as indicated by ^1H NMR with the appearance of new pair of multiplet signals due to the hydrides (spectrum not shown).

8.5 NMR spectroscopy of the complexes of the type $[(PPh_3)_2Rh(H)_2(pytca)\text{-}W(CO)_4(PR_3)]$

Table 8.2 Selected NMR chemical shifts of ^{15}N, ^{31}P, ^{103}Rh and ^{183}W, and the significant coupling constants for compounds **41** – **50** recorded at 300 K in CD_3OD/THF solution.

Compound	$\delta(^{15}N)$ (Rh-N) (ppm)	$\delta(^{15}N)$ (W-N) (ppm)	$\delta(^{31}P)$ (W-P) (ppm)	$\delta(^{31}P)$ (Rh-P) (ppm)	$\delta(^{183}W)$ (ppm)	$\delta(^{103}Rh)$ (ppm)	$^1J_{(W\text{-}P)}$ (Hz)	$^1J_{(Rh\text{-}P)}$ (Hz)
41				**43.56**		**506**		**118**
42				**38.07**		**626**		**117**
43	**-106**	**-68**		**42.49**		**508**		**119**
45 (PPh_3)	**-105**	**-125**	**32.37**	**41.87**	**984**	**503**	**239**	**120**
46 $P(tolyl)_3$	**-105**	**-125**	**29.19**	**41.80**	**991**	**510**	**239**	**118**
47 $P(4\text{-}FC_6H_4)_3$	**-106**	**-125**	**29.40**	**42.00**	**986**	**501**	**239**	**118**
48 $P(4\text{-}CF_3C_5H_4)_3$	**-107**	**-125**	**34.19**	**41.73**	**994**	**509**	**239**	**118**
49 $P(4\text{-}OMeC_6H_4)_3$	**-107**	**-125**	**27.90**	**41.83**	**987**	**502**	**240**	**118**
50 $P(MePh_2)$	**-106**	**-125**	**8.26**	**42.13**	**988**	**506**	**239**	**119**
50a $P(Ph_2C_6F_5)$	**-106**	**-125**	**25.20**	**42.08**	**992**	**503**	**240**	**119**

The ^{15}N NMR spectrum of $[Rh(H)_2(PPh_3)(pytca)]$ **43** (**Fig. 8.3**) shows clearly two types of nitrogen atoms; nitrogen coordinated to the rhodium atom appearing at -106 ppm and the pyridyl nitrogen appearing at -68 ppm. There is an average chemical shift change of 57 ppm by the pyridyl nitrogen upon coordination with tungsten phosphine complexes (**Fig. 8.4**). However the change in the chemical shift of the thiazole nitrogen is insignificant possibly due to diminished electronic influence through the connecting bonds (**Figs. 8.3 and 8.4**). A significant change in the ^{31}P chemical shift of the W-P of approximately 3 ppm with respect to the starting tungsten

complex has been noticed for all the coordinated complexes of the type $[(PPh_3)_2Rh(H)_2(pytca)\text{-}W(CO)_4(PR_3)]$. This ^{31}P chemical shift is accompanied by a very small change of just under 2 Hz in the coupling interaction between the tungsten and the phosphorus atom (**Table 8.2**).

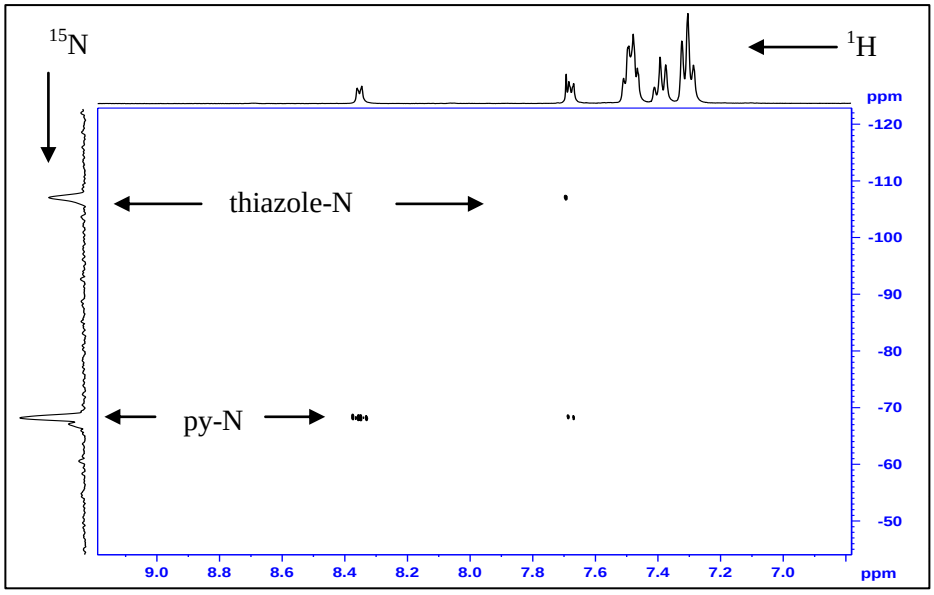


Figure 8.3 ^{15}N-^{1}H NMR spectrum of $[(PPh_3)_2Rh(H)_2(pytca)]$ **43** before coordination in CD_3OD/THF solution at 300 K.

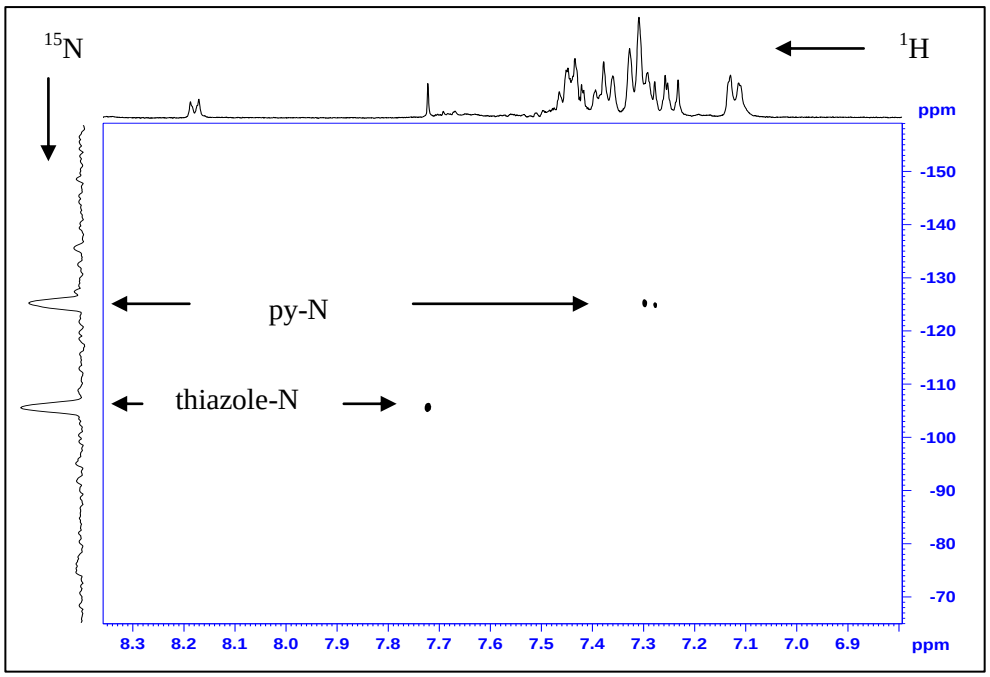


Figure 8.4 ^{15}N-^{1}H NMR spectrum of $[(PPh_3)_2Rh(H)_2(pytca)\text{-}W(CO)_4P(tolyl)_3]$ **46** in CD_3OD/THF solution at 300 K.

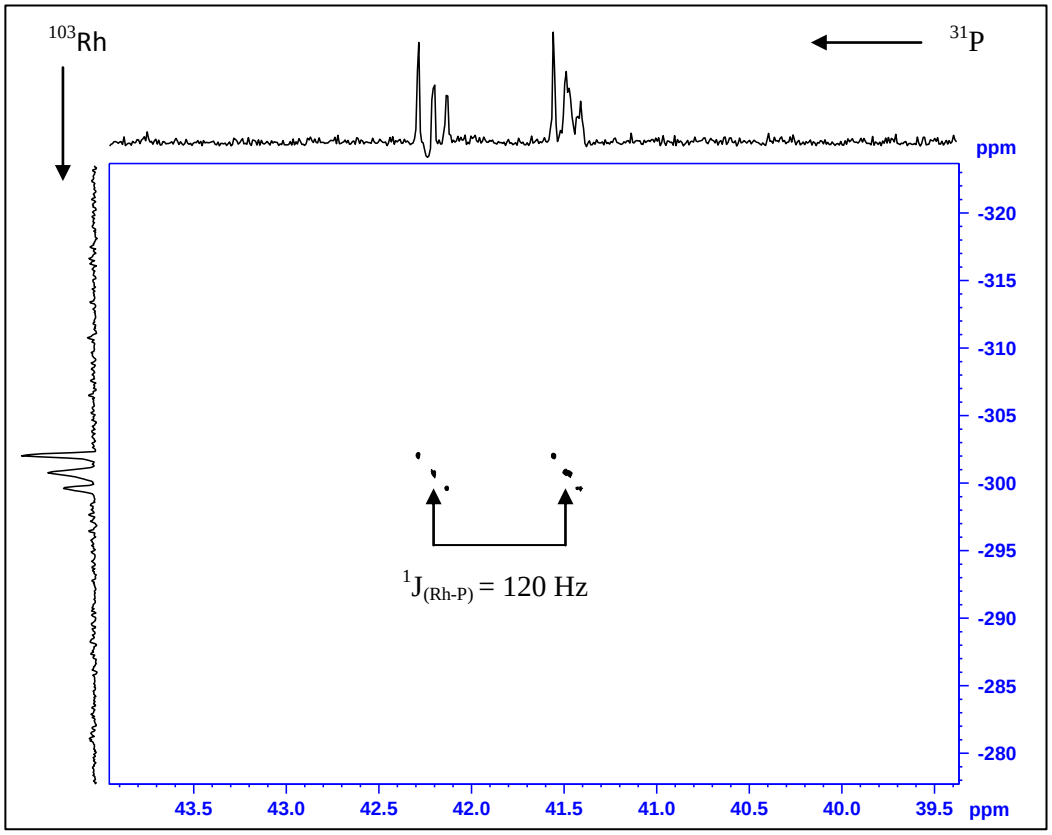


Figure 8.5 A representative NMR spectrum of ^{103}Rh-^{31}P{^{1}H} of the complexes of the type [$(PPh_3)_2Rh(H)_2$(pytca)-$W(CO)_4PR_3$] (**45**, R = Ph) in (CD_3OD/THF at 300 K, f2 (Y-axis) projection represents ^{103}Rh and f1(X-axis) ^{31}P NMR scales

The chemical shift of ^{103}Rh remains generally unchanged after coordination of [$(PPh_3)_2Rh(H)_2$(pytca)] with [$W(CO)_4(PR_3)$(NCMe)]. However the ^{183}W chemical shift shows a significant change from lower to higher chemical shift (**Tables 7.5** and **8.2**) ranging from the lowest of 293 ppm for **47** to the highest of 333 ppm for compound **46**. The ^{183}W chemical shift is not reflecting a proportional response with respect to the σ-donor or π-acceptor ability of the *para*-substituent on the phosphine ligand where $\delta(M) \alpha 1/\Delta E$ (this relationship has been described in detail in Chapter 2).

Figure 8.5 shows a representative spectrum with an indirectly detected rhodium signal indicating spin-coupling interaction with the hydrides resulting into a triplet splitting in both internal dimensions. The presence of this spin-spin interaction helps in determination of the proximity of

the neighbouring atoms, which in this case is ^{1}H-^{103}Rh-^{31}P spin system. **Figure 8.6** seeks to illustrate the extent to which the spectral chemical shift width of the transition metal nucleus was increased (within the capacity of the transmitter and the probe) before being reduced progressively to determine the accurate reading. (The spectral width of 2000 ppm does not represent the maximum possible range).

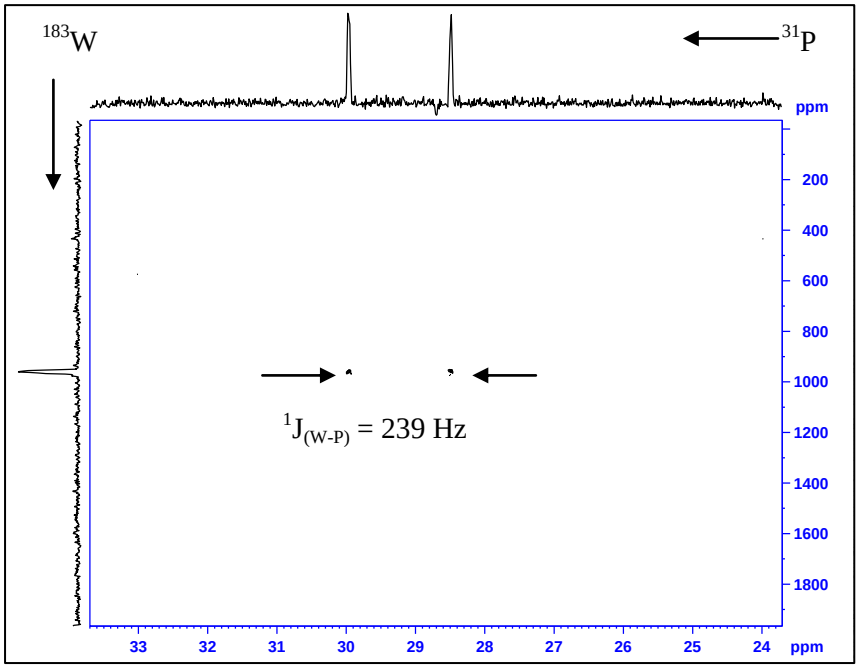


Figure 8.6 ^{183}W-$^{31}P\{^{1}H\}$ spectrum of $[(PPh_3)_2Rh(H)_2(pytca)$-$W(CO)_4P(4$-$FC_6H_4)_3]$ **47** from a solution of CD_3OD/THF at 300 K (the ^{31}P axis shows the internal projections and ^{183}W axis shows an extended spectral width covering a range of 2000 ppm).

8.6 NMR data correlations

Figure 8.7 shows a startling similarity in terms of chemical shift sensitivity by the two transition metals despite the number of connecting bonds and differing magnetic properties. It is interesting to note that the range of chemical shift change in the two metal centres is almost the same, i.e 10 ppm for ^{183}W and 9 ppm for ^{103}Rh. The similarity in the chemical shift changes can be regarded as unexpected because the change in $\delta(^{103}Rh)$ in response to variation of the phosphine on tungsten is as large as the change in $\delta(^{183}W)$ even though the rhodium is positioned much further away from this phosphine.

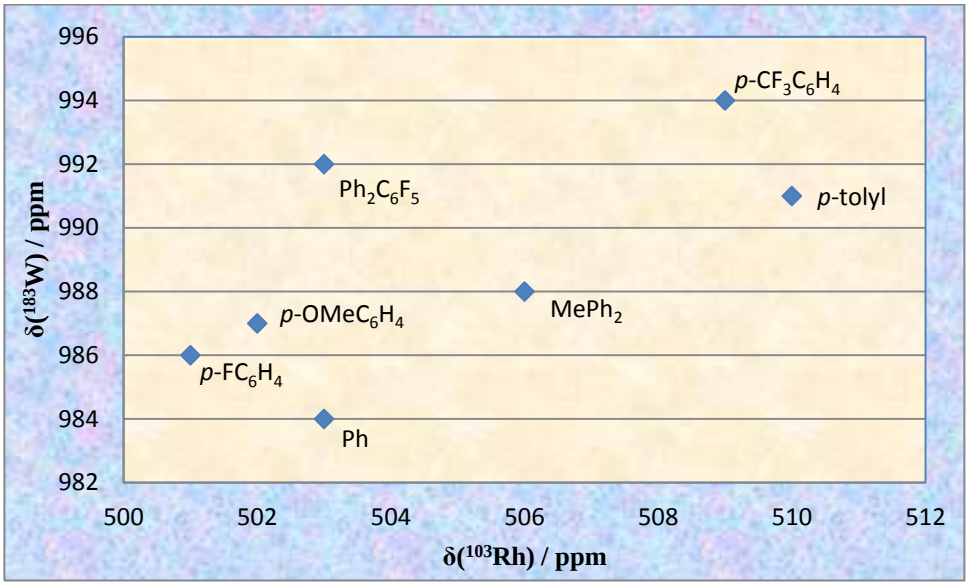


Figure 8.7 A plot $\delta(^{183}W)$ against $\delta(^{103}Rh)$ NMR data for complexes of the type $[(PPh_3)_2Rh(H)_2(pytca)\text{-}W(CO)_4(PR_3)]$.

The electronic changes on the rhodium metal as reflected by the change in the chemical shift would be significant given the number of bonds (13) connecting the metal and the substituent on the phosphine ligand, i.e. Rh - N =C – C = C – C = N – W – P – C = C – C = C – R. Since the molecule is not linear according to the representative crystal structure (**Figure 8.9**), the influence of the substituent on the tungsten-bonded phosphorus is likely to be smaller. The molecular structure shows a clear conjugation system at least between the two metal centres which theoretically should enhance electronic interaction. Pyridyl nitrogen and phosphine coordinate to the tungsten through lone pair electrons. Depending on the overall electronic effect of the phosphine ligand as influenced by the *para*-substituent, the extent of π-acceptor or σ-donor ability on the nitrogen should in theory facilitate electron delocalization through the conjugate system. In other reported work, similar studies on electronic communication through metal centres bridged by organic linkers has been established to be dependent on the mode of interaction as either M-C or M-N in which case the latter was established to limit effective electron delocalization between metal centres [17]. However, these studies on electronic communication between the terminal redox groups of organometallic complexes with terminal metal centres bridged by linear or non-linear, conjugated or non-conjugated linkers mode use of electrochemical methods such as cyclic voltammetry and potential energy diagrams [18].

A number of scenarios were investigated to establish any possible external influences including the possibility of induced solvent magnetic susceptibility change, the presence of water in solution and the state of solution (old or freshly prepared sample). A possible magnetic susceptibility effect was investigated by changing the percentage composition of deuterated solvent mixture i.e varying the ratio of THF : MeOD. Drops of de-ionised water were added to determine any possible effect of moisture in a freshly prepared 1:1 ratio of THF and MeOD. Reasons for adding water included its possible influence on a hydrogen bonding network involving the dinuclear complex and the solvent. Such hydrogen bonded interactions might be influenced by phosphine substituent and influence the metal chemical shift. No significant chemical shift changes were observed. One of the possible reasons for this unusual behaviour could that there is a strong through space interaction between the two metal centres supported by the geometry of the molecule (which merits future investigation). Representative X-ray crystal structure analysis of the complexes of the type $[(PPh_3)_2Rh(H)_2(pytca)\text{-}W(CO)_4(PR_3)]$ suggest at least one possible π-π interaction (To be discussed in the next section).

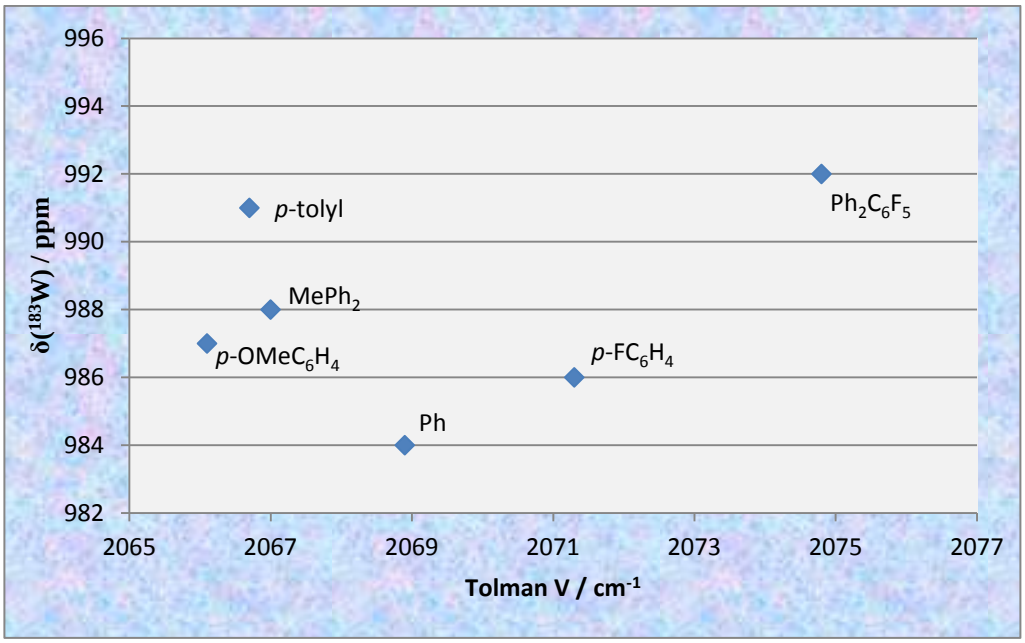


Figure 8.8A A plot $\delta(^{183}W)$ against Tolman electronic parameter for complexes of the type of $[(PPh_3)_2Rh(H)_2(pytca)\text{-}W(CO)_4(PR_3)]$.

Figures 8.8A and 8.8B show interesting relationships between $^{183}W/^{103}Rh$ chemical shifts and Tolman's electronic parameters in response to the change in the *para*-positioned substituent of

the phosphine ligand within the coordination sphere of tungsten. This figures show different responses as exhibited by both chemical shifts of ^{183}W and ^{103}Rh with respect to the changing electronic properties of the substituent on the phosphine ligand. The trend in order of increasing electron withdrawing strength of the phosphine ligand in our series (Tolman's electronic parameter) is as follows: P(*p*-$OCH_3C_6H_4)_3$ < P(*p*-tolyl)$_3$ < $PMePh_2$ < (PPh_3) < P(*p*-$FC_6H_4)_3$ ($PPh_2C_6F_5$) is not included in Tolman's data but is likely to the most strongly electron-withdrawing) and yet the chemical shift changes for both ^{183}W and ^{103}Rh (**Figures 8.8A** and **8.8B**) are not consistent with the trend.

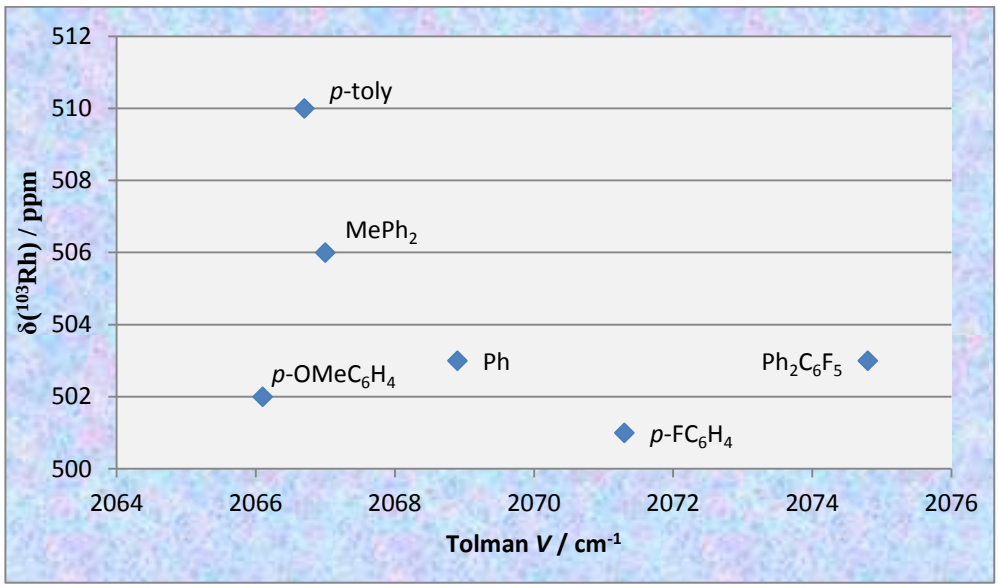


Figure 8.8B A plot δ(^{103}Rh) against Tolman electronic parameter for complexes of the type of [(PPh_3)$_2$Rh(H)$_2$(pytca)-W(CO)$_4$(PR_3)].

It is clear that the pattern that has developed from these poor correlations is not consistent with electronic properties (σ-donor or π-acceptor abilities) of the substituents. This behaviour suggests a number of possible interactions including among others through space interaction. Even more surprising is the pattern observed from **Fig. 8.8A** where despite the proximity of the substituent on the phosphorus ligand bonded to the tungsten, there is no clear relationship between the values of Tolman v_{co} for the substituent and δ(^{183}W). There is an insignificant correlation between the chemical shift of both tungsten and rhodium with the Hammett constant (result not shown). Similarly there is no significant correlation between the NMR data parameters such as δ($^{31}P_{(W)}$) vs δ($^{31}P_{(Rh)}$) and $^{1}J_{(W-P)}$ vs $^{1}J_{(Rh-P)}$ (results not shown).

8.7 X-ray crystallography

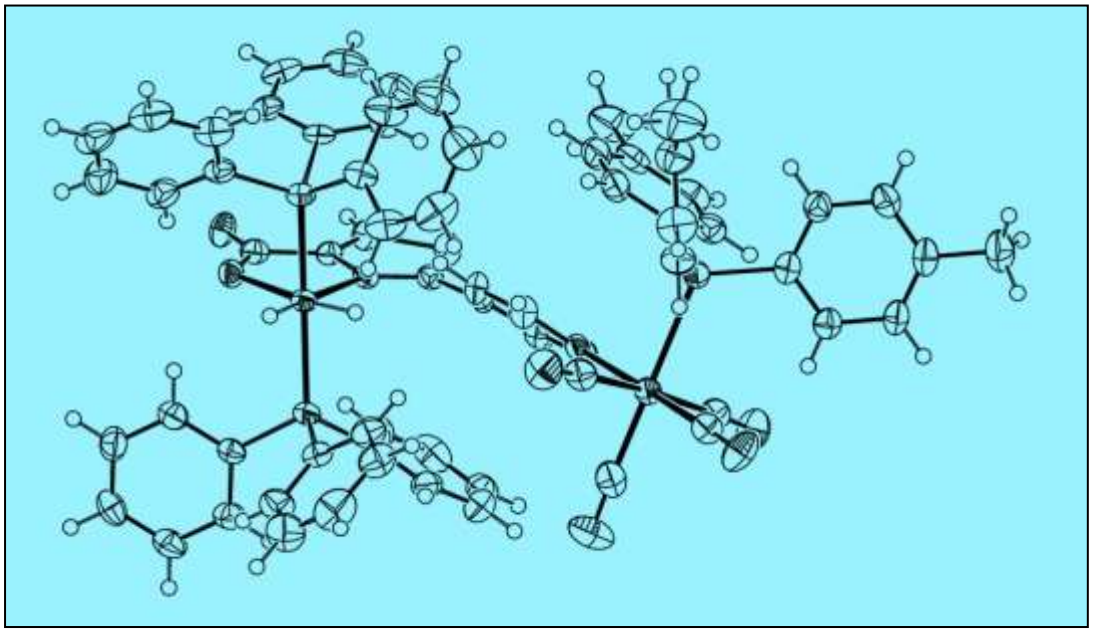


Figure 8.9 ORTEP drawing of $[(PPh_3)_2Rh(H)_2(pytca)\text{-}W(CO)_4P(tolyl)_3]$ **46** showing thermal ellipsoids at the 50% probability level. Hydrides are inserted geometrically. Co-crystallized MeOH is omitted.

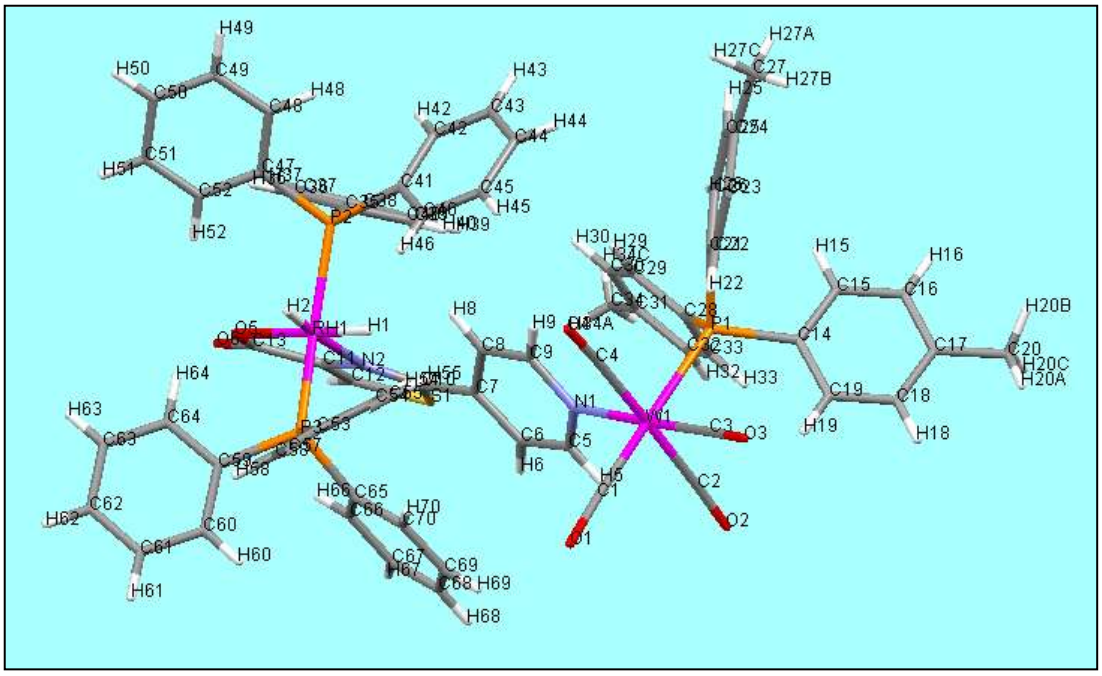


Figure 8.10 MERCURY generated capped sticks diagram with atom labeling for clarity for $[(PPh_3)_2Rh(H)_2(pytca)\text{-}W(CO)_4P(tolyl)_3]$ **46** [19]. Co-crystallized MeOH is omitted.

X-ray quality crystals of $[(PPh_3)_2Rh(H)_2(pytca)\text{-}W(CO)_4P(tolyl)_3]$ **46** were grown from a solution in MeOH by slow evaporation of the solvent over 4 days at room temperature. The X-ray structure shows co-crystallized methanol (not shown for clarity purpose). The X-ray structure of compound **46** is shown in **Figs. 8.9** and **8.10**, and the selected bond lengths and angles are listed in **Table 8.3**. The crystal structure of **46** shows that 2-(4-pyridyl)thiazole-4-carboxylate (pytca) coordinates to the rhodium(I) complex in a bidentate fashion using one carboxylate oxygen atom O(5) and the adjacent nitrogen N(2). The carboxylate-nitrogen coordination to the rhodium atom is orientated in the same plane as the hydride atoms (**Fig. 8.11**) whilst the phosphine ligands are positioned axially which compares well with other transition metal complexes with octahedral geometry coordinated through nitrogen- and oxygen- containing groups [20].

The rhodium atom Rh(1) bonds to nitrogen N(5) and oxygen O(2) with bond lengths of 2.221(3) Å and 2.189(3) Å respectively. The bond angles N(2)-Rh-H(2) and O(5)-Rh-H(1) are both significantly lower than 180° and the H(1)-Rh-H(2) is significantly lower than 90^0 (76(2)). The geometric sizes (defined by cone angle) of the axially positioned PPh_3 ligands on the rhodium atom make them twist slightly out of the plane accounting for the P(3)-Rh-P(2) bond angle being smaller than 180^0. It is also interesting to observe that the pyridyl ring is also twisted in such a way that it aligns itself with phenyl rings of the PPh_3 and $P(tolyl)_3$. This is assumed to be occurring through π-π-π interaction of the phenyl rings and a second π-π interaction between a phenyl and a thiazole rings **(Figure 8.11**). The bond lengths of Rh-H(1) and Rh-H(2) of 1.41(3) Å and 1.42(3) Å respectively are significantly shorter than in a similar systems where a rhodium atom is similarly coordinated to nitrogen and oxygen at the same time [21]. However the accuracy of this comparison is dependent and qualified by how the protons were determined and finally positioned within the crystal structure. The Rh-P bonds lengths are similar in $[(PPh_3)_2Rh(H)_2(pytca)\text{-}W(CO)_4P(tolyl)_3]$ **46**.

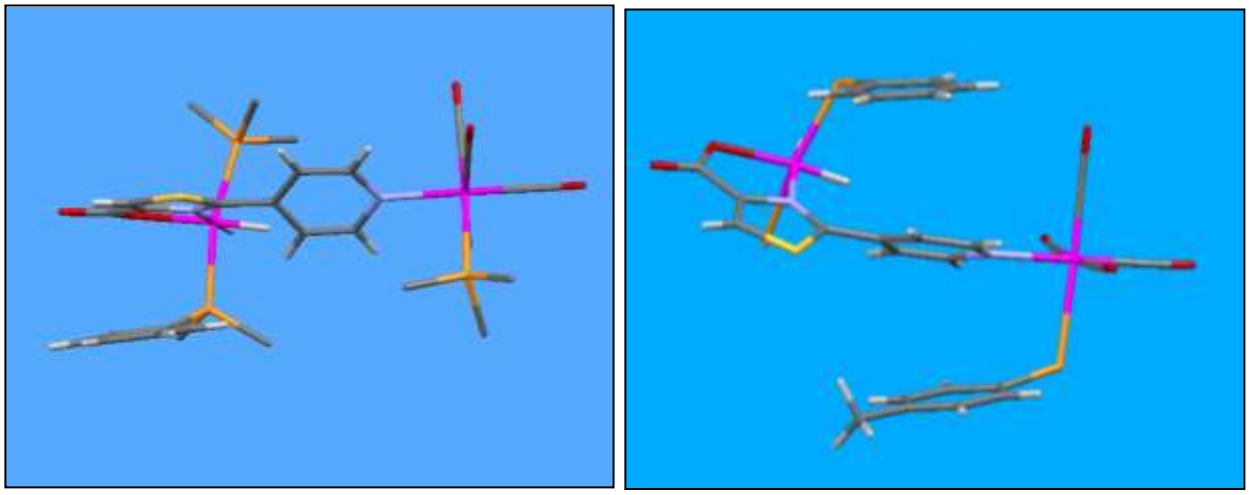


Figure 8.11 Simplified MERCURY generated capped sticks showing possible π-π stacking (between a phenyl and thiazole rings) and *π-π-π* stacking among three phenyl rings of $[(PPh_3)_2Rh(H)_2(pytca)\text{-}W(CO)_4P(tolyl)_3]$ **46**.

The geometry around the tungsten atom in **46** resembles closely that of complexes of the type $[W(CO)_4(NCMe)(PR_3)]$ (Chapter 7) in that the nitrogen of the pyridyl coordinates to the metal centre *trans* to one of the carbonyl ligands. The carbonyl ligand is in our case a stronger *trans*-director than the nitrogen, thus suggesting that the substituent on the phosphorus atom (i.e. *p*-$P(tolyl)_3$ group) is exerting minimum steric hindrance. Therefore, it can be assumed that the *cis* orientation along P(1)-W-N(1) is stabilised by the strong *trans* directing capacity of the carbonyl ligand and is also supported by the π-π-π interaction of the three phenyl rings (**Fig. 8.10**). The bond angles C(3)-W-N(1) (177.63(15) º) and P(1)-W-C(1) (174.99(14) º) show a slightly smaller steric hindrance because of their higher values though significantly less than the ideal 180°. The nitrogen-tungsten bond length, W-N(1) of 2.254(3) Å is slightly longer than the precursor $[W(CO)_4(NCMe)P(tolyl)_3]$ **25** (Chapter 7) whereas W-P(1) compares very well.

Table 8.3 Selected bond length (Å) and angles (deg) for $[(PPh_3)_2Rh(H)_2(pytca)\text{-}W(CO)_4P(tolyl)_3]$ **46**.

Bond lengths (Å)		Bond angles (°)	
C(1) – W(1)	1.176(6)	C(1) – W(1) – N(1)	90.34(16)
C(2) – W(1)	2.022(5)	C(2) – W(1) – N(1)	91.96(15)
C(3) – W(1)	1.975(5)	C(3) – W(1) – N(1)	177.63(15)
C(4) – W(1)	2.045(5)	C(4) – W(1) – N(1)	90.99(15)
C(7) – C(10)	1.463(5)	C(1) – W(1) – P(1)	174.99(14)
C(14) – P(1)	1.831(4)	N(1) –W(1) – P(1)	86.15(9)
C(21) – P(1)	1.833(4)	C(12) – S(1) – C(10)	89.8(2)
C(28) – P(1)	1.829(4)	N(2) – Rh(1) – O(5)	75.70(11)
N(1) – W(1)	2.254(3)	N(2) – Rh(1) – P(3)	98.77(9)
N(2) – Rh(1)	2.189(3)	O(5) – Rh(1) – P(3)	102.21(8)
O(5) – Rh(1)	2.221(3)	N(2) – Rh(1) – P(2)	95.85(9)
P(1) – W(1)	2.5469(11)	N(2) – Rh(1) – H(1)	98.3(16)
P(2) – Rh(1)	2.3002(11)	O(5) – Rh(1) – H(1)	173.1(17)
P(3) – Rh(1)	2.2815(11)	N(2) – Rh(1) – H(2)	174.2(16)
Rh(1) – H(1)	1.41(3)	O(5) – Rh(1) – H(2)	109.9(16)
Rh(1) – H(2)	1.42(3)	H(1) – Rh(1) – H(2)	76(2)
		C(10) – N(2) – Rh(1)	137.2(3)
		C(11) – N(2) – Rh(1)	112.9(3)
		C(13) – O(5) – Rh(1)	117.2(3)
		P(3) – Rh(1) – P(2)	162.18(4)

8.8 Conclusions

$[RhH(PPh_3)_4]$ reacts oxidatively with mono- and dicarboxylic acids of pyrazine and pyridyl-thiazole carboxylic acid ligands under mild conditions to form octahedral Rh(III)dihydride complexes of the type $[(PPh_3)_2Rh(H)_2(pyrazca)]$, $[\{(PPh_3)_2Rh(H)_2\}_2(pyracdca)]$ and $[(PPh_3)_2Rh(H)_2(pytca)]$ in good yields. A further reaction of $[(PPh_3)_2Rh(H)_2(pytca)]$ with tungsten phosphine complexes of the type $[W(CO)_4(NCMe)(PR_3)]$, also under mild conditions results in the formation of the coordinated complex $[(PPh_3)_2Rh(H)_2(pytca)\text{-}W(CO)_4(PR_3)]$ in fairly good yields. A plot of $\delta(^{183}W)$ against $\delta(^{103}Rh)$ suggest a fair correlation as a result of the changes in the *para*-substituents on the tungsten phosphine ligand even though Rh is far from the phosphine substituent on the tungsten. The chemical shift changes in $\delta(^{103}Rh)$ are as large as changes in the $\delta(^{183}W)$ on variation of phosphine substituent. There is a distinct similarity between $\delta(^{183}W)$ and $\delta(^{103}Rh)$ in response to the Tolman's electronic influence by the *para*-substituent on the tungsten phosphine ligand but no correlation between either δ(183W) or δ(103Rh) and Tolman's electronic parameter ν_{CO}. Measurements to rule out the possibility of a hydrogen bonding network and changes in solvent magnetic susceptibility were made and no significant changes in the metal chemical shift were observed. However this phenomenon merits further investigation given the possibility of a through space interaction supported by the geometry of the molecule. The X-ray structure of the bridged metal complex shows an interesting phenomenon whereby a π-π-π interaction through one of the rhodium bonded PPh_2 rings, pyridyl and one of the tungsten $P(tolyl)_3$ rings, and a second π-π interaction involving phenyl (Rh-PPh) and thiazole rings are evident. Studies to investigate such a through space interaction are difficult in a solution medium.

8.6 References

[1]. (a) B.F. Hoskins and R. Robson, *J. Am. Chem. Soc*., 111 (1989) 5962; (b) C. Janaik, *Coord. Chem. Rev*., 250 (2006) 66; (c) S. Kitagawa, R. Kitaur and S. Noro, *Angew. Chem. Int. Ed*., 43 (2004) 2334.

[2]. (a) Y.-H. Lui, Y.-L. Lu, H.-C. Wu, J.-C. Wang, K.-L. Lu, *Inorg. Chem*. 41 (2002) 2592; (b) B. Zhao, P. Cheng, X.Y. Cheng, C. Cheng, W.Shi, D.Z. Liao, S.P. Yan, Z.H. Jiang, *J. Am. Chem. Soc*., 126 (2004) 3012; (c) S.K. Ghosh, G. Savitha, P.K. Bharadwaj, *Inorg. Chem*., 43 (2004) 5495; (d) M. Kurmoo, C. Estournès, Y. Oka, H. Kumagai, K. Inoue, *Inorg. Chem*., 44 (2005) 217; (e) X.J. Li, R. Cao, Y.Q. Sun, W.H. Bi, X. Li, Y.Q. Wang, Eur. *J. Inorg. Chem*. (2005) 321; (f) S. -I. Noro, H. Miyasaka, S. Kitagawa, T. Wada, T. Okubo, M. Yamashita, T. Mitani, *Inorg. Chem*., 44 (2005) 133.

3. (a) D.M. Ciurtin, Y.-B. Dong, M.D. Smith, T.Barcaly and H.-C. zur Loye, *Inorg. Chem*., 40 (2001) 2825; (b) D.M. Ciurtin, N.G. Pschire, M.D. Smith, U.H.F. Bungz and H.-C. zur Loye, *Chem. Mater*., (2001) 2743; (c) N.G. Pschire, D.M. Smith, D.M. Ciurtin, U.H.F. Bunz and H.-C. Zur Loye, *Angew. Chem., Int. Ed*., 41 (2002) 583; (d) S.A. Barnett and N.R. Champness, *Coord. Chem. Rev*., 246 (2003) 145.

4. (a) R.W. Matthews and R.A. Walton, *Inorg. Chem*., 10 (1971) 1433; (b) C.J. Oconnor and E. Sinn, *Inorg. Chem*., 20 (1981) 545; (c) Y.-C. Liang, M.-C. Hong, J.-C. Liu and R. Cao, *Inorg. Chim. Acta*, 328 (2002) 152; (d) J. Leciejewicz, H. Ptasiewicz-Bak, T. Premkumar and S. Govindarajan, *J. Coord. Chem*., 57 (2004); (e) C.L. Chen, A.M. Goforth, M.D. Smith, C.Y. Su and H.-C. zur Loye, *Angew. Chem., Int. Ed*., 44 (2005) 6673.

5. (a) N.G. Pschirer, D.M. Ciurtin, M.D. Smith, U.H.F. Bunz, and H.C. zur Loye, *Angew. Chem. Int. Ed*., 41 (2002) 583; (b) Y.B. Dong, G.X. Jin, M.D. Smith, R.Q. Huang, B. Tang and H.C. zur

Loye, *Inorg. Chem*., 41 (2002) 4909; (c) S. Shotwell, H.L. Ricks, J.G.M. Morton, M. Laskoski, J. Fiscus, M.D. Smith, K.D. Shimizu, H.C. zur Loye and U.H.F. Bunz, *J. Organomet. Chem*., 671 (2003) 43; (d) Y.B. Dong, X. Zhao, B. Tang, H.Y. Wang, R.Q. Huang, M.D. Smith and H.C. zur Loye, *Chem. Commun*., (2004) 220; (e) Y.B. Dong, X. Zhao, R. Huang, M.D. Smith and H.C. zur Loye, *Inorg. Chem*., 43 (2004) 5603; (f) Y.B. Dong, G.X. Jin, X. Zhao, B. Tang, R Q. Haung, M.D. Smith, K.E. Stitzer and H.C. zur Loye, *Organometallics*, 23 (2004) 1604; (g) C.L. Chen, A.M. Goforth, M.D. Smith, R.C. Layland and H.C. zur Loye, *Inorg. Chem*., 44 (2005) 8762.

6. L. Carlton, M.-P. Belcuig and G. Patrick, *Polyhedron*, 11 (1992) 1501; (b) L. Carlton and J.J. Molapisi, *J. Organomet. Chem*., 609 (2000) 60; (c) O.M. Yaghi. M.O'Keeffe, N.W. Ockwig, H.K. Chae, M. Eddaoudi and J. Kim, *Nature* (2003) 775; (d) G. Fan, G. Xie, S. Chen, S. Gao and Q. Shi, *J. Organomet. Chem*., 59 (2006) 791; (e) C.-L. Chem, J.M. Ellsworth, A.M. Goforth, M.D. Smith, C.-Y. Su and H.-C. zur Loye, *Dalton Trans*., (2006) 5278; (f) J.M. Ellsworth and H.-C. zur Loye, *Dalton Trans*., (2008) 5835; (g) J.M. Ellsworth, Z.M. Khaliq, M.D. Smith and H.-C. zur Loye, *Solid State Sciences*, 10 (2008) 825.

7. C. (a) Creutz and H. Taube, *J. Am. Chem. Soc*., 91 (1969) 3988; (b) P.W. Carrek, M. Goldstei, E.M. Mcparti and W.D. Unsworth, *J. Chem. Soc*., (1971) 1644; (c) J.K. Beattie, N.S. Hush and P.R. Taylor, *Inorg. Chem*., 15 (1976) 992; (d) R.W. Callahan, F.R. Keene, T.J. Meyer and D.J. Salmon, *J. Am. Chem. Soc*., 99 (1977) 1064; (e) T.J. Meyer, *Acc. Chem. Res*., 11 (1978) 94; (f) J.A. Baumann, D.J. Salmon, S.T. Wilson and T.J. Meyer, *Inorg. Chem*., 18 (1979) 2472.

8. J. Ellsworth, C.-J. Su, Z. Khaliq, R. Hipp, A.M. Goforth, M.D. Smith and H.-C zur Loye, *J. Mol. Struct*., 796 (2006) 86; .

9. A. Cuevas, C. Kremer, M. Hummert, H. Schumann, F. Lloret, M. Julve and J. Faus, *Dalton. Trans*., (2007) 342.

10. N. Ahmad, J.J. Levison, S.D. Robinson and M.F. Uttley, *Inorg*. Synth., 15 (1974) 45.

11. N. Ahmad, J.J. Levison, S.D. Robinson and M.F. Uttley, *Inorganic Syntheses*, 28 (1990) 81.

12. Bruker. *APEX2. Version 2.0-1. Bruker AXS Inc*., Madison, Wisconsin, USA, (2005).

13. Bruker. *SAINT-NT. Version 6.0. (includes XPREP and SADABS) Bruker AXS Inc*., Madison, Wisconsin, USA, (2005).

14. *Bruker SHELXTL, Version 5.1 (Includes XS, XL, XP, XSHELL)*, Bruker AXS Inc., Madison Wisconsin, (1999).

15. (a) A.L. Spek, *J. Appl. Crystallogr*., 36 (2003) 7; (b) A.L. Spek, *Acta Crystallogr*., *Sect*. A, 46 (1990) C34.

16. L.J. Farrugia,. *J. Appl. Cryst*., **30** (1997) 565

17. J.-L. Zuo, E. Herdtweck, F.F. de Biani, A.M. Santos and F.E. Kühn, *New. J. Chem*., 26 (2002) 889.

18. P.F.H. Schwab, M.D. Levin and J. Michl, *Chem. Rev*., 99 (1999) 1863.

19. MERCURY software version 2.4

20. (a) A.C. Cooper, J.C. Huffman and K.G. Caulton, *Inorg. Chim. Acta*, 270 (1998) 261; (b) R. Acharyya, F. Basuli, R.-Z. Wang, T.C.W. Mak and S. Bhattacharya, *Inorg. Chem*., 43 (2004) 704

21. M.B. Ezhova, B.O. Patrick, K.P. Sereviratne, B.R. James, F.J. Waller and M.E. Ford, *Inorg. Chem*., 44 (2005) 1482

CHAPTER 9

Synthesis and Characterization of Bridged Trimetallic Complexes of Platinum and Tungsten

9.1 Introduction

Platinum Group Metals (PGM) have many industrial applications such as in electronics, in automobile emission control devices, as catalysts in the manufacture of silicon rubber, in fuel cells, as a component in medical implants, in the treatment of certain types of cancer (such as testicular cancer though with some severe side effects) and in jewellery [1]. A review on the industrial application of platinum as a catalyst has appeared in the literature many years ago [2]. The most common oxidation states of platinum are +2 and +4 where tetra-coordinate Pt(II) compounds tend to adopt 16-electron square planar geometry.

The chemistry of metal alkynyl complexes has been of much interest for some time and the first comprehensive literature review by Nast in 1982 stimulated a huge interest in this topic [3]. Several reviews with the theme of the chemistry of platinum alkynyl compounds dealing specifically with their structural diversity [4], chemical reactivity [5] and their increasing potential application in Materials Science [6] have since appeared in the literature. The interest in the chemistry of alkynyl linkers stems from their favourable electronic and structural features, their ability to interact with metal centres via $p\pi$-$d\pi$ interactions which can be modulated by the introduction of aromatic conjugated spacers or variation of metal centres and for the preparation of carbon rich oligomeric and polymeric materials [7]. These compounds continue to find use as non-linear optical materials, in electrical conductivity, in liquid crystal engineering [6a,6d,6c,8] and recently for their photochemical and photophysical properties with promising applications in light emitting diodes, optical sensors and molecular devices [9]. There is growing interest in the synthesis of heterometallic complexes with acetylide-functionalised oligopyridine ligands involving *d* metal centres [10] (**Figure 9.1**).

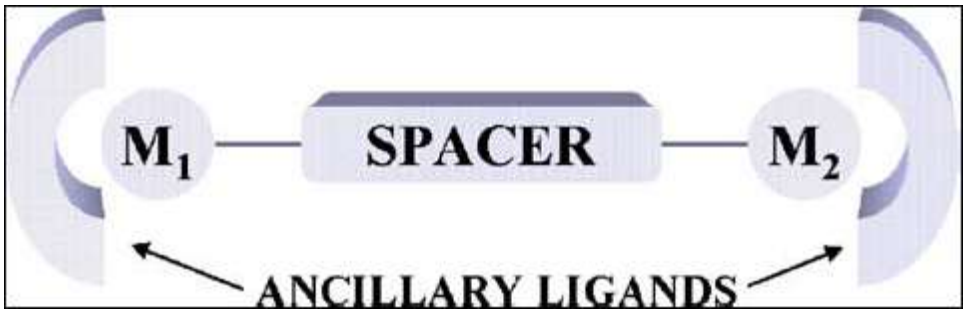


Figure 9.1 Representation of a heterobimetallic complex bridged by unsaturated hydrocarbon link : M_1 and M_2 are linked by a bridging ligand (ref. [10d]).

Alkynylplatinum(II) complexes have been prepared by a variety of methods such as alkynyl transfer from Grignard, organolithium and organosodium reagents [11] or from less reactive metals such as tin, mercury and gold [12]. A commonly used base-promoted method based on the famous Sonogashira coupling reaction [13] (mechanism described in Chapter 1, section 1.3.2) seems to be reliable considering the number of publications in the literature both in organic and organometallic fields [10a,11,14]. The preparation of alkynylplatinum(II) complexes proceeds from dichloroplatinum(II)L_2 (L = dppe or dppp) which can be synthesised by a variety of procedures using platinum(II) compounds [15]. Among the commonly used procedures in the preparation of these complexes is the use of (diphosphine)platinum(II)dichloride following the method of Slack and Baird [16] from K_2PtCl_4 (*caution*: *allergen*- not used in our synthesis) or from (1,5-cyclooctadiene)dichloroplatinum(II), [(cod)$PtCl_2$] following the procedure of Hackett and Whitesides [15d].

Platinum(II) complexes containing ethynylpyridine linkages have been synthesized as building blocks for supramolecular self-assembly structures in both two- and three-dimensional units [17]. Other transition metal complexes containing ethynylpyridine as ligand include those of Au [18], Pd [17d], Ru and Re [19]. Ethynylpyridine bridged complexes containing platinum and tungsten form the basis of our attention because of their potential as building blocks for molecular rods and molecular self assembly structures such as neutral molecular squares. There is however a lack of literature information on bridged neutral molecular assembly units containing transition metals from group six and ten. The aim of the work discussed in the chapter is to synthesize new trimetallic complexes bridged by carbon-rich conjugated-organic linkers and to investigate

evidence of metal-metal interactions by NMR spectroscopy. These complexes also offer interesting challenges for multinuclear NMR analysis.

9.2 Experimetal

All reactions were carried out under an atmosphere of argon at ambient temperature, unless specified otherwise. Solvents such as dichloromethane, THF, diethyl ether, methanol, acetonitrile and diethylamine were dried and purified by distillation before use following the methods described in Chapter 3 or used as purchased. Dichloro(1,5-cyclooctadiene)platinum(II), [(cod)$PtCl_2$], dppp (bis-(diphenylphosphino)propane), copper iodide (CuI), 4-ethynylpyridine hydrogenchloride and magnesium sulphate ($MgSO_4$) were used as purchased without further purification. An average of 10 mg of each product in CD_2Cl_2/CH_2Cl_2 (0.6 ml) was used for NMR analysis for all the complexes in this study with the exception of compound **54** where for one measurement, 95 mg (0.05 mmol) dissolved in C_6D_6 (0.7 ml) was used for a ^{31}P-$^{15}N\{^1H\}$ experiment. NMR data for ^{15}N, ^{31}P, ^{183}W and ^{195}Pt chemical shifts are presented in **Table 9.1**.

9.2.1 Preparation of [(dppp)$PtCl_2$] ……..(51)

*bis-(*Diphenylphosphino)propaneplatinum(II)dichloride [(dppp)$PtCl_2$] **51** was prepared following a modified procedure of Hackett and Whitesides [15d]. A clear solution of bis(diphenylphosphinopropane) (dppp) (800 mg, 1.940 mmol) in CH_2Cl_2 (10 ml) was added drop-wise to a partially dissolved stirred solution of [(cod)$PtCl_2$] (717 mg, 1.916 mmol) in CH_2Cl_2 (30 ml) at room temperature over a period of 2 minutes. The cloudy solution became clearer as more dppp solution was added and suddenly turned cloudy with a white precipitate forming after approximately 5 min. of gentle stirring. The thick white suspension was stirred for a further 4 hrs after which stirring was stopped and the white precipitate filtered and washed with cold CH_2Cl_2 (5 ml x 3). The white precipitate was washed with dilute HCl (10 ml x 2) and dried *in vacuo* giving a bright white powder with a yield of 1295 mg (99%). NMR spectra were recorded from a solution in $CDCl_3$ at 300 K. ^1H NMR ($\delta_{(ppm)}$): 7.76 (m, 8H, PPh_2), 7.40 (m, 12H, PPh_2), 2.49 (m, 4H, PCH_2), 2.04 (m, 2H, CH_2). $^{13}C\{^1H\}$ NMR ($\delta_{(ppm)}$): 133.42 (d, Ph, $^3J_{(P-C)}$ = 5 Hz), 131.26 (s, Ph), 128.35 (tt, Ph, $^3J_{(Pt-C)}$ = 65 Hz, $^2J_{(P-C)}$ = 6 Hz), 25.17 (dd, PCH_2, $^1J_{(P-C)}$ = 22 Hz, 18.63 (s, CH_2). $^{31}P\{^1H\}$ NMR ($\delta_{(ppm)}$): -4.9 (s, 2P, PPh_2, satellite, d, $^1J_{(Pt-P)}$ = 3408 Hz).

9.2.2 Preparation of [Pt(dppp)(4-ethynylpyridine)$_2$] ……..(52)

The dialkynylplatinum(II) complex (**52**) was prepared following a modified procedure of Anderson and co-workers [1717g]. 4-Ethynylpyridine hydrochloride (180 mg, 1.290 mmol) was slowly dissolved in MeOH (10 ml) resulting in a green solution into which Na_2CO_3 (150 mg ~ 1.289 mmol) was added at once. The solution was sealed and stirred overnight after which the green colour had changed to slightly brownish-green. Stirring was stopped and the green solution containing 4-ethynylpyridine free of hydrogen chloride was transferred into a partially dissolved solution of [(dppp)$PtCl_2$] (374 mg, 0.551 mmol) in THF (2 ml) and Et_2NH (8 ml) at 0º C. The solution was stirred for 10 min. before CuI (15 mg, 0.0787 mmol) was added at once. There was a noticeable colour change of the greenish solution to yellow-green and finally a consistent yellowish-brown within 20 min. of CuI addition at 0º C. The mixture was stirred for a further 2h30 min after which the solvent was removed *in vacuo*. The light brown solid precipitate was redissolved in CH_2Cl_2 (10 ml) and washed with water (2 x 5 ml). The solution was dried with $MgSO_4$ and filtered under reduced pressure by the aspiration method. The solvent was again removed *in vacuo* from the light brown solution leaving behind yellowish-brown crystalline flakes giving a yield of 310 mg (70%). NMR spectra were recorded from a solution in CD_2Cl_2/CH_2Cl_2 at 300 K. ^{1}H NMR ($\delta_{(ppm)}$): 8.51 (br, 4H, C_5H_4N), 7.77 (m, 8H, PPh_2), 7.45 (m, 12H, PPh_2), 6.67 (br, 4H, C_5H_4N), 2.54 (m, 4H, PCH_2) and 2.07 (m, 2H, CH_2). $^{13}C\{^1H\}$ NMR ($\delta_{(ppm)}$): 148.41 (s, 4C, py; satellite, d, $^5J_{(Pt\text{-}C)}$ = 174 Hz, Pt-C≡C-py), 135.65 (m, 4C, PPh_2), 133.45 (s, Ph, satellite, d, 8C, $^2J_{(P\text{-}C)}$ = 10 Hz, PPh_2, satellite, d, $^3J_{(Pt\text{-}C)}$ = 168 Hz), 130.84 (s, 4C, Pt-C≡C-py; satellite, d, $^5J_{(Pt\text{-}C)}$ = 152 Hz), 130.23 (s, *ipso*, py), 128.40 (s, d, satellite, d, 8C, $^3J_{(P\text{-}C)}$ = 11 Hz, PPh_2; satellite, d, $^4J_{(Pt\text{-}C)}$ = 159 Hz), 125.72 (d, 4C, PPh_2, $^4J_{(Pt\text{-}C)}$ = 165 Hz), 112.18 (dd, 2C, $^1J_{(Pt\text{-}C)}$ = 145 Hz, $^2J_{(P\text{-}C)}$ = 25 Hz, Pt-C≡C), 108.07 (dd, 2C, $^2J_{(Pt\text{-}C)}$ = 35 Hz, $^3J_{(P\text{-}C)}$ = 17 Hz, Pt-C≡C), 25.73 (m, PCH_2), 19.99 (s, CH_2). $^{31}P\{^1H\}$ ($\delta_{(ppm)}$): -6.2 (s, 2P, PPh_2, satellite, d, $^1J_{(Pt\text{-}P)}$ = 2191 Hz). IR (compressed solid): $\nu_{(C\equiv C)}$ = 2117 cm^{-1}.

9.3 Synthesis of trimetallic complexes of the type [(dppp)Pt{(4-C≡CC$_5$H$_4$N)W(CO)$_4$PR$_3$}$_2$].

Synthesis of complexes of the type [W(CO)$_4$(CH$_3$CN)(PR$_3$)] (where R = Ph, *p*-tolyl, *p*-OMeC$_6$H$_4$, *p*-CF$_3$C$_6$H$_4$, *p*-FC$_6$H$_4$ and NMe$_2$) has been described in Chapter 7.

9.3.1 Preparation of [(dppp)Pt{(4-C≡CC$_5$H$_4$N)W(CO)$_4$(PPh$_3$)}$_2$] ……(54)

A yellow-orange solution of [(dppp)Pt(4-ethynylpyridine)$_2$] **52** (81 mg, 0.0997 mmol) and [W(CO)$_4$(CH$_3$CN)(PPh$_3$)] **24** (150 mg, 0.268 mmol) in THF (7 ml) in a sealed Schlenk tube was stirred in the dark overnight at room temperature. Stirring was stopped and the solvent removed *in vacuo* leaving behind shiny orange flakes giving a yield of 196 mg (99%) at 90% purity. Attempt to purify the product on a 25 cm column (internal diameter 6 mm) of neutral alumina using eluent mixture of Et$_2$O:Petroleum ether = 1:1 proved unsuccessful with only ~10% of original mixture being recovered. Crystallization of the compound by slow evaporation from solutions of THF-hexane, CH$_2$Cl$_2$-Et$_2$O, benzene-*n*-hexane mixtures was not successful either. NMR spectra were recorded from a solution in CD$_6$D$_6$ at 300 K. ^{1}H NMR (δ(ppm)): 7.93 (d, 4H, ^{3}J$_{(H-H)}$ = 6.5 Hz,), 7.71 – 6.89 (m, PPh$_2$, PPh$_3$), 6.02 (d, 4H, C$_5$H$_4$N, ^{2}J$_{(H-H)}$ = 6.6 Hz), 2.00 (m, 4H, PCH$_2$), 1.55 (m, 2H, CH$_2$). ^{13}C{^{1}H} (δ$_{(PPM)}$): 210.25 (d, 1CO, ^{2}J$_{(P-C)}$ = 4.1 Hz), 209.29 (d, 1CO, ^{2}J$_{(P-C)}$ = 33 Hz), 205.56 (d, 1CO, ^{2}J$_{(P-C)}$ = 7.0 Hz), 197.75 (d, 1CO, ^{2}J$_{(P-C)}$ = 7.0 Hz), 154.45, 136.23, 126.60 (s, C$_5$H$_4$N), 133.62, 131.13, 129.86, 128.83 (m, PPh$_2$, PPh$_3$), 121.95 (dd, Pt-C≡C, ^{2}J$_{(Pt-C)}$ = 145 Hz, ^{3}J$_{(P-C)}$ = 23 Hz), 107.39 (dt, Pt-C≡C, ^{1}J$_{(Pt-C)}$ = 303 Hz, ^{2}J$_{(P-C)}$ = 18 Hz), 25.46 (m, PCH$_2$), 19.77 (s, CH$_2$). ^{31}P{^{1}H} (δ$_{(ppm)}$): 31.41 (s, WP; satellite, d, ^{1}J$_{(W-P)}$ = 238 Hz), -6.31 (s, 2P, PtP; satellite, d, ^{1}J$_{(Pt-P)}$ = 2178 Hz). IR (compressed solid): $\nu_{(C\equiv C)}$ = 2116 cm^{-1}; $\nu_{(CO)}$ = 2007, 1864, 1829 cm^{-1}.

9.3.2 Preparation of [(dppp)Pt{(4-C≡CC$_5$H$_4$N)W(CO)$_4$P(*p*-tolyl)$_3$}$_2$]…….(55)

A yellow-orange solution of [(dppp)Pt(4-ethynylpyridine)$_2$] **52** (30 mg ~ 0.0369 mmol) and [W(CO)$_4$(CH$_3$CN){P(*p*-tolyl)$_3$}] **25** (48 mg ~ 0.0748 mmol) in THF (3 ml) in a sealed Schlenk tube was stirred at room temperature overnight during which time the colour of the solution changed to deep orange. The solvent was removed and the product dried *in vacuo* leaving behind brown crystalline flakes giving a yield of 60 mg (81%). NMR spectra were recorded from a

solution in CD_2Cl_2/CH_2Cl_2 at 300 K. ^1H NMR ($\delta_{(ppm)}$): 7.94 (d, 4H, C_5H_4N, $^3J_{(H-H)}$ = 6.7 Hz), 7.66, 7.39, 7.81, 7.06 (m, PPh_2, P(tolyl)$_3$), 6.13 (d, 4H, C_5H_4N, $^3J_{(H-H)}$ = 6.6 Hz), 2.55 (m, 4H, PCH_2), 2.26 (s, 18H, CH_3), 2.03 (m, 2H, CH2). $^{31}P\{^1H\}$ ($\delta_{(ppm)}$): 28.24 (s, WP; satellite, d, $^1J_{(W-P)}$ = 236 Hz), -6.38 (s, 2P, PtP; satellite, d, $J_{(Pt-P)}$ = 2186 Hz). IR (compressed solid): $\nu_{(C\equiv C)}$ = 2116 cm^{-1}; $\nu_{(CO)}$ = 2006, 1868, 1835 cm^{-1}.

9.3.3 Preparation of [(dppp)Pt{(4-C≡CC_5H_4N)W(CO)$_4$P(*p*-OMeC_6H_4)$_3$}$_2$].. (**56**)

A yellow solution of [(dppp)Pt(4-ethynylpyridine)$_2$] **52** (31 mg, 0.0381 mmol) and [W(CO)$_4$(CH_3CN)P(4-OMeC_6H_4)$_3$] **26** (55 mg, 85 mmol) in THF (3 ml) in a sealed Schlenk tube was stirred at room temperature. The colour of the solution changed overnight to brown-yellow from which the solvent was removed and the product dried *in vacuo* leaving behind orange-brown crystalline flakes giving a yield of 66 mg (82%). NMR spectra were recorded from a solution in CD_2Cl_2/CH_2Cl_2 at 300 K. ^1H NMR ($\delta_{(ppm)}$): 7.96 (m, 4H, C_5H_4N), 7.96, 7.66, 7.39, 7.20, 6.79 (m, PPh_2, P(4-OMeC_6H4)$_3$), 6.16 (m, 4H, C_5H_4N), 3.73 (m, OMe), 2.55 (m, PCH_2), 2.10 (m, CH_2). $^{31}P\{^1H\}$ ($\delta_{(ppm)}$): 25.76 (s, WP; satellite, d, $^1J_{(W-P)}$ = 239 Hz), -6.67 (s, 2P, PtP; satellite, d, $^1J_{(Pt-P)}$ = 2183). IR (compressed solid): $\nu_{(C\equiv C)}$ = 2117 cm^{-1}; $\nu_{(CO)}$ = 2005, 1865, 1830 cm^{-1}.

9.3.4 Preparation [(dppp)Pt{(4-C≡CC_5H_4N)W(CO)$_4$P(*p*-FC_6H_4)$_3$}$_2$]…….(**57**)

A reaction mixture of [(dppp)Pt(4-ethynylpyridine)$_2$] **52** (30 mg, 0.0369 mmol) and [W(CO)$_4$(CH_3CN)P(4-FC_6H_4)$_3$] **27** (51 mg, 0.0780 mmol) in THF (3 ml) was stirred in a sealed Schlenk tube at room temperature overnight. The colour changed overnight from yellow-orange to orange-brown. The solvent was removed and the product dried *in vacuo* leaving behind shining orange flakes giving a yield of 73 mg (97%). NMR spectra were recorded from a solution in CD_2Cl_2/CH_2Cl_2 at 300 K. ^1H NMR ($\delta_{(ppm)}$): 7.98 (d, 4H, C_5H_4N, $^3J_{(H-H)}$ = 6.6 Hz), 7.65, 7.44, 7.28, 7.16, 7.00 (m, PPh_2, P(4-$CF_3C_6H_4$)$_3$), 6.20 (d, 4H, C_5H_4N, $^3J_{(H-H)}$ = 6.6 Hz), 2.55 (m, 4H, PCH_2), 2.07 (m, 2H, CH_2). $^{31}P\{^1H\}$ NMR ($\delta_{(ppm)}$): 28.51 (s, WP; satellite, d, $^1J_{(W-P)}$ = 134 Hz), -6.58 (s, 2P, PtP; satellite, d, $^1J_{(Pt-P)}$ = 2189 Hz). IR (compressed solid): $\nu_{(C\equiv C)}$ = 2112 cm^{-1}; $\nu_{(CO)}$ = 2008, 1871, 1840 cm^{-1}.

9.3.5 Preparation of [(dppp)Pt{(4-C≡CC_5H_4N)W$(CO)_4$P(*p*-$CF_3C_6H_4)_3$}$_2$]….(**58**)

A reaction mixture of [(dppp)Pt(4-ethynylpyridine)$_2$] **52** (30 mg, 0.0369 mmol) and [W$(CO)_4(CH_3CN)$P(4-$CF_3C_6H_4)_3$] **28** (60 mg ~ 0.0747 mmol) in THF (3 ml) at room temperature was stirred overnight in a sealed Schlenk tube. The yellow orange solution changed overnight to yellowish-brown. The solvent was removed by a gentle stream of argon and the product dried *in vacuo* leaving foamy orange crystalline flakes giving a yield of 64 mg (74%). NMR spectra were recorded from a solution in CD_2Cl_2/CH_2Cl_2 at 300 K. ^{1}H NMR ($\delta_{(ppm)}$): 8.40 (m, 4H, C_5H_4N), 7.75 – 7.37 (m, PPh_2, P(4-$CF_3C_6H_4)_3$), 6.20 (m, 4H, C_5H_4N), 2.56 (m, PCH_2, 2.05 (m, CH_2). ^{31}P{^{1}H} ($\delta_{(ppm)}$): 32.06 (s, WP; satellite, d, $^1J_{(W-P)}$ = 246 Hz), -6.42 (s, 2P, PtP; satellite, d, $^1J_{(Pt-P)}$ = 2185 Hz). IR (compressed solid): $\nu_{(C\equiv C)}$ = 2117 cm^{-1}; $\nu_{(CO)}$ = 2021, 1904 (sh), 1882, 1848 cm^{-1}.

9.3.6 Preparation [(dppp)Pt{(4-C≡CC_5H_4N)W$(CO)_4$P$(NMe_2)_3$}$_2$]……..(**59**)

A reaction solution mixture of [(dppp)Pt(4-ethynylpyridine)$_2$] **52** (50 mg, 0.062 mmol) and [W(CO)4(CH_3CN)P$(NMe_2)_3$] **29** (65 mg, 0.130 mmol) in THF (3 ml) was stirred in a sealed Schlenk tube overnight. There was no significant colour change from the original yellowish-brown solution overnight. The solvent was removed and the product dried *in vacuo* leaving behind brown flakes giving a yield of 68 mg (50%). NMR spectra were recorded from a solution in CD_2Cl_2/CH_2Cl_2 at 300 K. ^{1}H NMR ($\delta_{(ppm)}$): 8.40 (m, 4H, C5H_4N), 7.75 (m, 8H, PPh_2), 7.45 (m, 12H, PPh_2), 6.50 (m, 4H, C_5H_4N), 2.65 (d, 36H, NMe_2, $^3J_{(P-H)}$ = 9.3 Hz), 2.63 (m, 6H, PCH_2, CH_2). ^{31}P{^{1}H} NMR ($\delta_{(ppm)}$): 135.2 (s, WP; satellite, d, $^1J_{(W-P)}$ = 135 Hz), -6.4 (s, 2P, PtP; satellite, d, $^1J_{(Pt-P)}$ = 2235 Hz). IR (compressed solid): $\nu_{(C\equiv C)}$ = 2116 cm^{-1}; $\nu_{(CO)}$ = 2002, 1854, 1826 cm^{-1}.

9.4 Results and discussion: Alkynyl-bridged complexes of platinum and tungsten

Discussion of the synthesis and characterization of monometallic tungsten complexes of the type $[W(CO)_4(CH_3CN)PR_3]$ has been covered in Chapter 7 (see reaction steps (i) and (ii) in **Scheme 9.1**). Marcus and other researchers [20] have studied and theorized aspects of successful electron-transfer processes between two bridged metal centres. Techniques such as electrochemical cyclic voltammetry (CV), electron paramagnetic resonance (EPR), ^{57}Fe-Mössbauer spectroscopy (only suitable for Fe complexes), solid state NMR and IR spectroscopy, X-ray crystallography, and theoretical calculations have been applied in the study of electronic communication through two metal centres in addition to solution NMR spectroscopy [21]. It is anticipated that the two metal centres are likely to exhibit chemical differences due to their different oxidation states. The results of solution state NMR spectroscopy of heterotrimetallic complexes of the type $[(dppp)Pt\{(4\text{-}C{\equiv}CC_5H_4N)W(CO)_4(PR_3)\}_2]$, are presented and discussed.

9.4.1 Synthesis of ethynylplatinum(II) complex of the type $[(dppp)Pt\{4\text{-}C{\equiv}CC_5H_4N\}_2]$

Treatment of $[(cod)PtCl_2]$ with dppp in CH_2Cl_2 solution at room temperature gives a quantitative yield of $[(dppp)PtCl_2]$ **51** (reaction step (iii) in scheme 9.1). The complex gives a single resonance in its $^{31}P\{^1H\}$ NMR spectrum with a $^1J_{(Pt\text{-}P)}$ coupling constant of 3408 Hz confirming a symmetrical square planar platinum(II) complex. The platinum(II) complex **51** is fairly stable at room temperature though not soluble in many organic solvents. A slightly modified procedure of Anderson and co-workers [17g] for the reaction of $[(dppp)PtCl_2]$ with 4-ethynylpyridine (reaction step (iv) in scheme 9.1) in the presence of a catalytic amount of CuI (10 mg) in THF/Et_2NH solution gave an angular unit $[(dppp)Pt\{4\text{-}C{\equiv}CC_5H_4N\}_2]$ **52** in a nearly quantitative yields. In the present study compound **52** has been fully characterized by NMR analysis and the results compare well with the literature [17g]. The complex exhibits a single resonance in its $^{31}P\{^1H\}$ NMR spectrum, with $J_{(Pt\text{-}P)}$ coupling of 2190 Hz which represents a significant decrease of 1218 Hz from that observed for compound **51**.

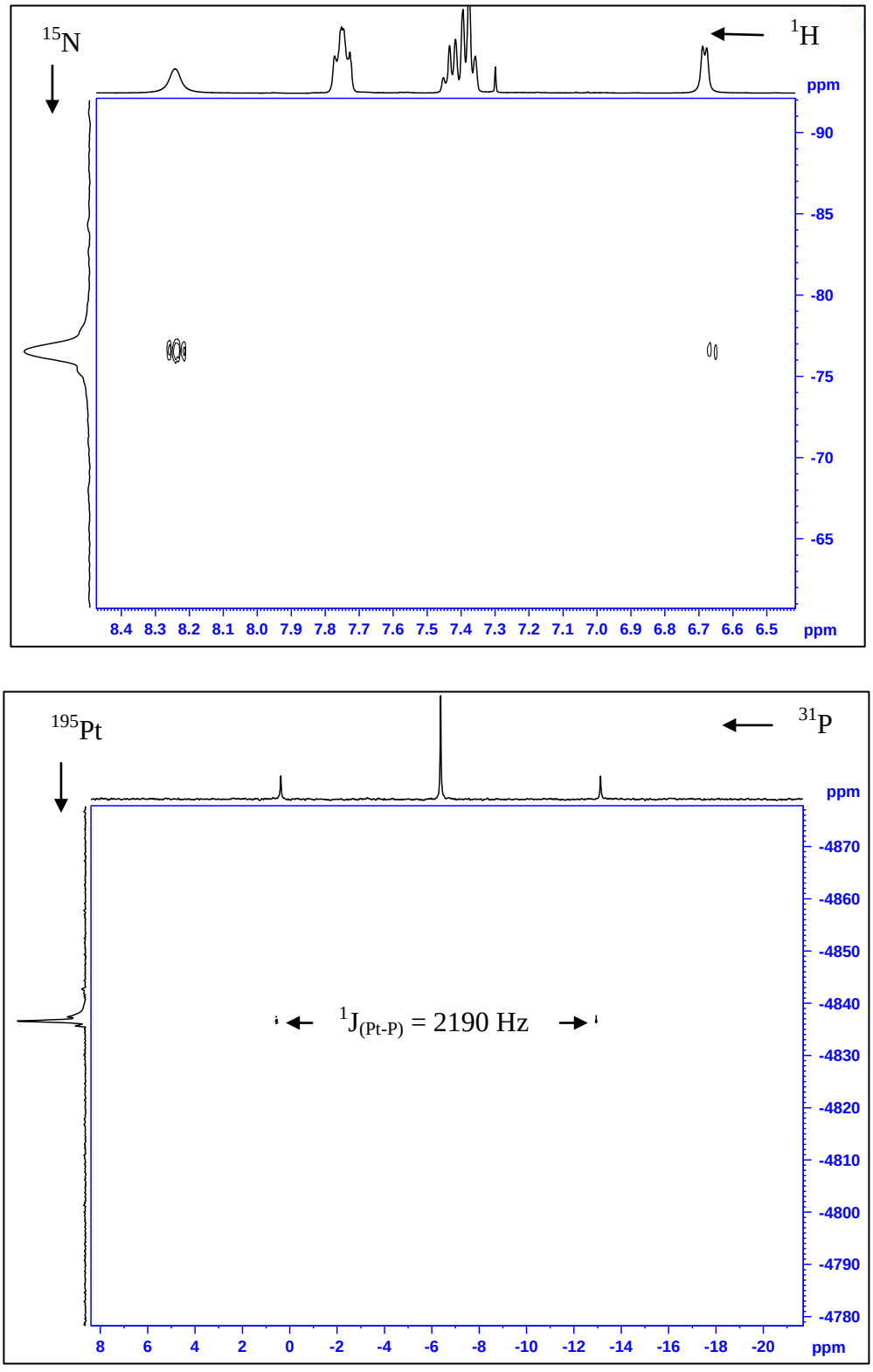
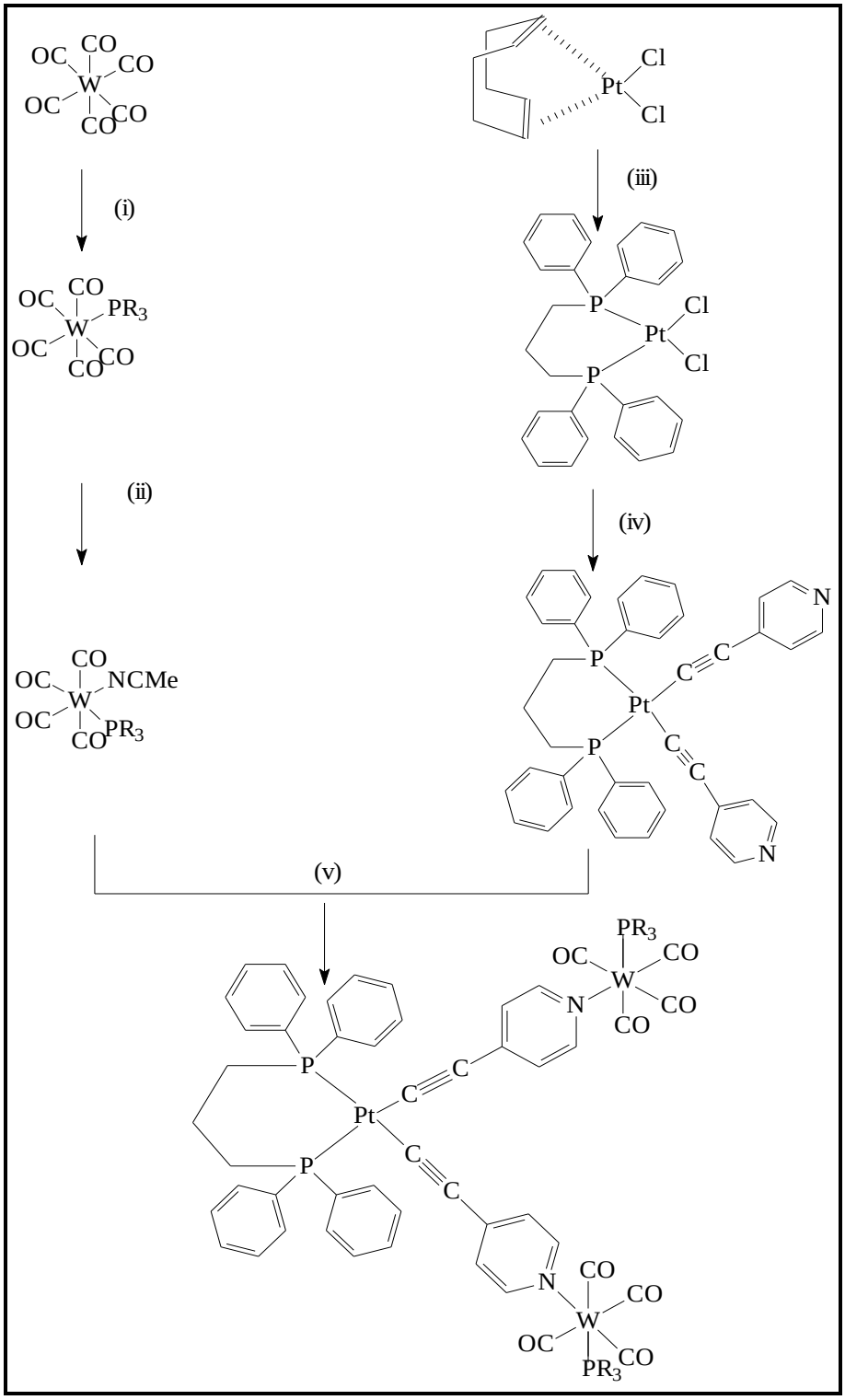


Figure 9.2 ^{15}N-^{1}H (top) and ^{195}Pt-$^{31}P\{^{1}H\}$ (bottom) NMR spectra of $[(dppp)Pt\{4\text{-}C{\equiv}CC_5H_4N\}_2]$ **52**



Scheme 9.1 A simplified synthetic route towards the formation of trimetallic complexes of the type [(dppp)Pt{4-C≡CC_6H_4N-W$(CO)_4PR_3$}$_2$]: (i) diglyme, PPh_3, Δ; (ii) Me_3NO, CH_3CN; (iii) dppp; (iv) CuI, Et_2NH; (v) THF

9.4.2 Synthesis of ethynylpyridineplatinum(II) complexes of the type [(dppp)Pt{(4-C≡CC$_5$H$_4$N)W(CO)$_4$PR$_3$}$_2$]

The tungsten phosphine complexes [W(CO)$_4$(CH$_3$CN)(PR$_3$)] contain the labile ligand CH$_3$CN which can be replaced by better electron donators such as the nitrogen of a pyridine. This strategy has been applied extensively in the synthesis of *cis* and *trans* isomers of [W(CO)$_4$(PPh$_3$)(PR$_3$)] (PR$_3$ = phosphine and phosphite) [22] and in the construction of neutral molecular squares [23]. The compound [(dppp)Pt{C≡CC$_5$H$_4$N}$_2$] **52** is treated with a 30% excess of the monometallic tungsten phosphine complex in THF at room temperature (step (v) in **scheme 9.1**) overnight. There is no clear colour change upon addition of the tungsten phosphine complex. Complexes **54** to **59** are isolated at 60 to 95% purity brownish-orange flakes which upon washing with cold diethylether change into orange powder. Attempts to purify these compounds on a short neutral alumina column were not successful as less than 10 % of impure product was collected. Attempts to grow crystals of these compounds for X-ray diffraction analysis were not successful either. The trimetallic complexes of the type [(dppp)Pt{4-C≡CC$_5$H$_4$N-W(CO)$_4$PR$_3$}$_2$] were confirmed by multinuclear NMR analysis and the data are shown in **Table 9.1- 9.2**.

9.4.3 NMR spectroscopic characterization of [(dppp)Pt{(4-C≡CC$_5$H$_4$N)W(CO)$_4$PPh$_3$}$_2$] 54

In the absence of structural confirmation of the successful coupling of tungsten and the alkynylplatinum complexes via the N-donor, NMR spectroscopy was the only viable option given the number of spin half nuclei in the proposed compound. A solution of compound **54** (15 mg, 0.008 mmol) in C$_6$D$_6$ (0.6 ml) at room temperature was analysed by ^{1}H, ^{31}P{^{1}H} and ^{15}N-^{1}H NMR experiments and another solution containing the same compound **54** (95 mg, 0.05 mmol) in C$_6$D$_6$ (0.7 ml) was analysed by ^{1}H, ^{13}C{^{1}H}, ^{31}P{^{1}H}, ^{15}N-^{1}H, ^{13}C-^{1}H (HSQC, COLOC), ^{31}P-^{15}N{^{1}H}, ^{183}W-^{31}P{^{1}H} and ^{195}Pt-^{31}P{^{1}H} measurement, also at room temperature (**Figures**. **9.2 – 9.4**). The significance of ^{31}P-^{15}N{^{1}H} NMR experiment which proved beyond doubt the nitrogen is bonded to tungsten is discussed in detail on page 252. The chemical shifts of symmetrically positioned pyridyl protons indicated by the two doublet signals showing H-H coupling exhibited insignificant change from those of the compound **54**. There is a noticeable decrease in the chemical shift position of ^{15}N from -76.49 to -143 ppm indicative of nitrogen coordination to the transition metal [24].

Table 9.1 Selected ^{31}P coupling constants for monometallic tungsten and ethynylpyridine-bridged trimetallic platinum-tungsten complexes.

$[W(CO)_4(CH_3CN)(PR_3)]$		$[(dppp)Pt\{(4\text{-}C{\equiv}CC_5H_4N)W(CO)_4PR_3\}_2]$			Ligand $P(R)_3$
	$J_{(W\text{-}P)}$ (Hz)		$J_{(Pt\text{-}P)}$ (Hz)	$J_{(W\text{-}P)}$ (Hz)	R
24	242	**54**	2178	238	Ph
25	237	**55**	2185	236	*p*-$CH_3C_6H_4$
26	240	**56**	2183	239	*p*-$OMeC_6H_4$
27	244	**57**	2188	246	*p*-FC_6H_4
28	246	**58**	2185	246	*p*-$CF_3C_6H_4$
29	307	**59**	2235	315	NMe_2
$[(dppp)PtCl_2]$ **51**			3408	-	-
$[(dppp)Pt\{4\text{-}C{\equiv}CC_5H_4N\}_2]$ **52**			2190	-	-

Table 9.2 Selected NMR data for monometallic tungsten and ethynylpyridine-bridged trimetallic platinum-tungsten complexes.

$[W(CO)_4(CH_3CN)(PR_3)]$			$[(dppp)Pt\{4\text{-}C{\equiv}CC_5H_4N\text{-}W(CO)_4PR_3\}_2]$					
	$\delta(^{183}W)$ (ppm)	$\delta(^{31}P)$ (ppm)		$\delta(^{15}N)$ (ppm)	$\delta(^{31}P)$ (Pt-P) (ppm)	$\delta(^{31}P)$ (W-P) (ppm)	$\delta(^{183}W)^a$ (ppm)	$\delta(^{195}Pt)^b$ (ppm)
24[c]	667	30.2	**54**	-143	-6.1	30.1	970	-4824
25[c]	658	26.8	**55**	-144	-6.4	28.2	969	-4825
26[c]	661	24.7	**56**	-143	-6.5	26.0	968	-4822
27[c]	666	27.5	**57**	-144	-6.7	32.2	971	-4826
28[c]	660	31.8	**58**	-147	-6.5	32.4	970	-4827
29[c]	598	132.0	**59**	-143	-6.4	135.2	910	-4821
$[(dppp)PtCl_2]$ **51**[d]				-	-4.98	-	-	-4506
$[(dppp)Pt\{4\text{-}C{\equiv}CC_5H_4N\}_2]$ **52**[c]				-76	-6.26	-	-	-4837

[a] Described in **Table 7.3**, [b] Chemical shift relative to $\delta(^{195}Pt) = 0.00$ ppm from a solution Na_2PtCl_6 (0.220 M) in D2O at 300 K in the field in which the protons of TMS resonate at 400 MHz, [c] Recorded from a solution in CD_2Cl_2/CH_2Cl_2. [d] Recorded from a solution in $CDCl_3$,.

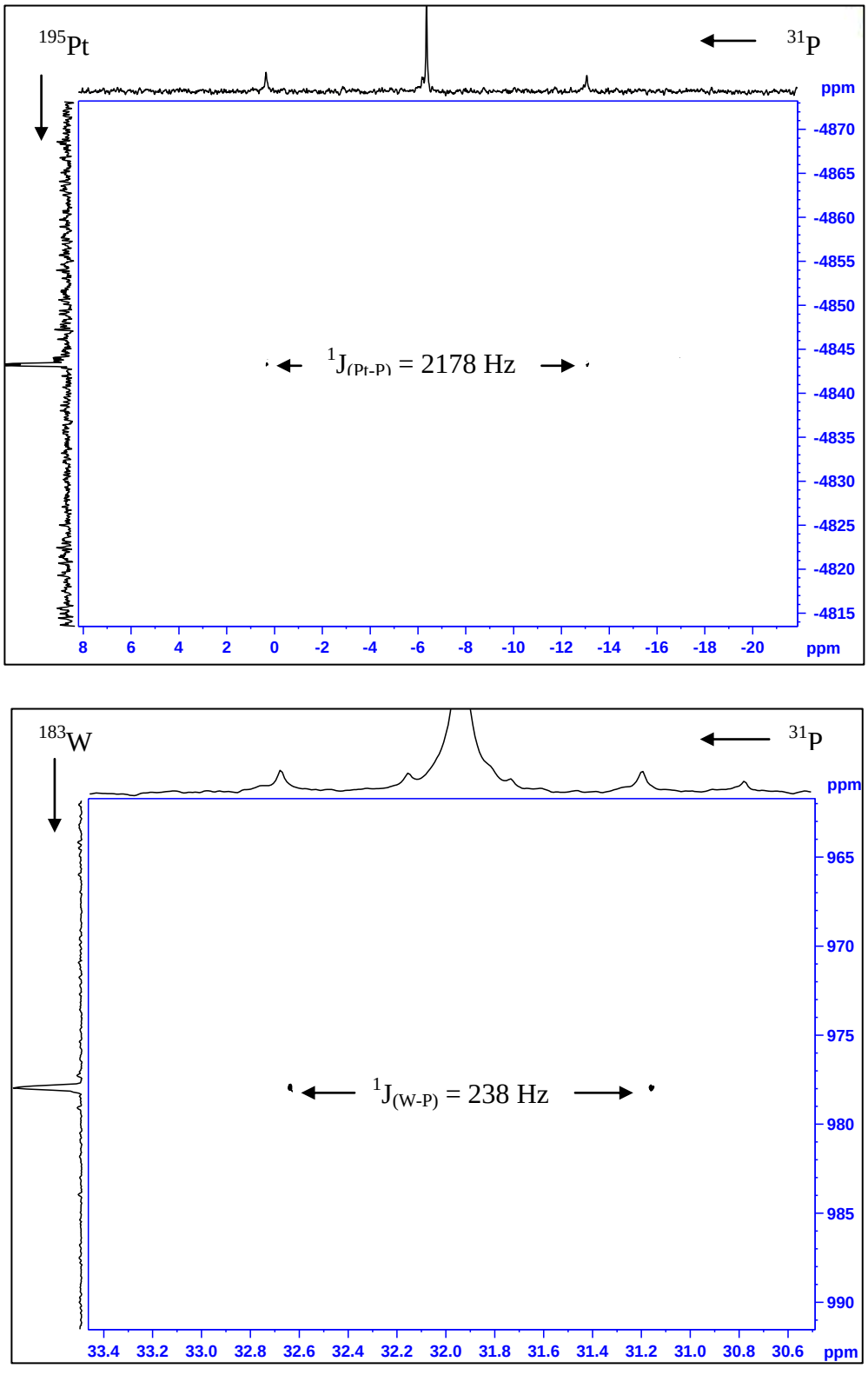
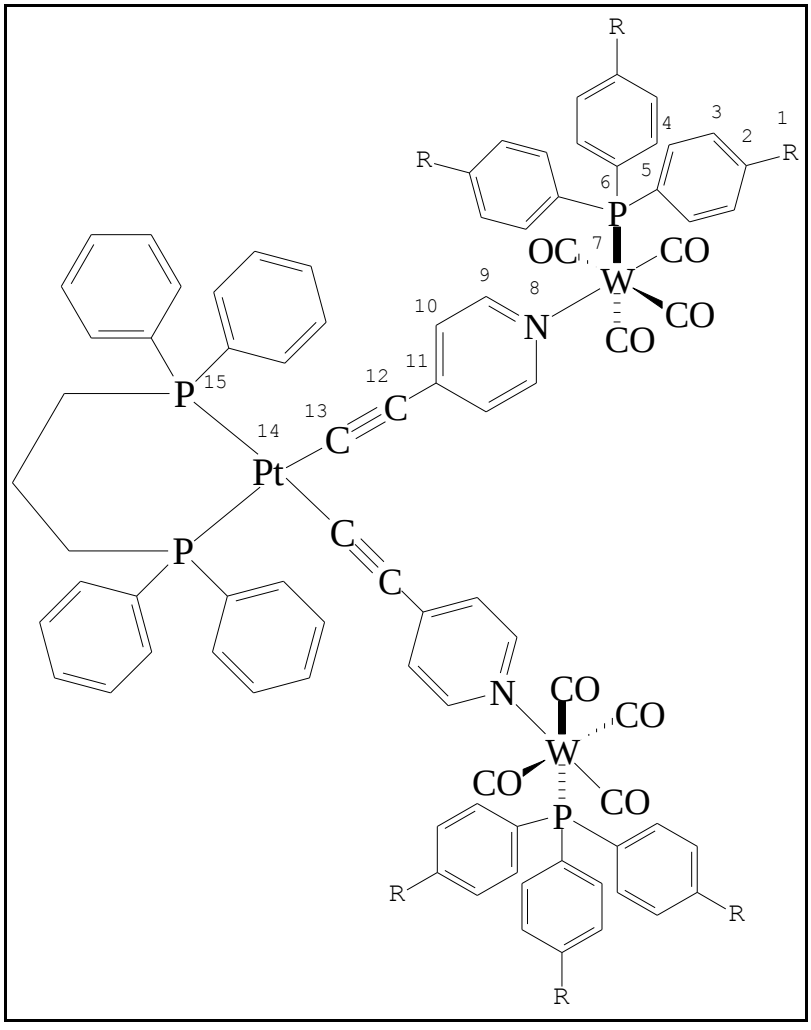


Figure 9.3 NMR spectra of ^{195}Pt-$^{31}P\{^{1}H\}$ (top) and ^{183}W-$^{31}P\{^{1}H\}$ (bottom) for $[(dppp)Pt\{(4\text{-}C{\equiv}CC_5H_4N)W(CO)_4PPh_3\}_2]$ **54**

Complexes of the type [(dppp)Pt{(C≡CC$_5$H$_4$N)W(CO)$_4$PR$_3$}$_2$] show an insignificant change in the ^{31}P chemical shift for platinum-phosphorus bonded nuclei whereas on average, there is approximately 2 ppm change for tungsten-phosphorus bonded nuclei relative to the starting materials (**Table 9.2**). Therefore only the phosphorus in the proximity of the nitrogen coordinating site shows a subtle change as reflected by the ^{31}P chemical shift. **Figure 9.3** shows NMR spectra of ^{195}Pt-^{31}P{^{1}H} and ^{183}W-^{31}P{^{1}H} whereby significant chemical shift changes were observed indicating formation of a new complex. There is a clear change in the ^{195}Pt chemical shift averaging at 12.16 ppm before and after coordination of the pyridine to the tungsten (**Table 9.2**). This subtle change in the chemical shift indicates a long-range interaction through the two metal centres.



Scheme 9.2 Proposed molecular structure of [(dppp)Pt{(4-C≡CC$_5$H$_4$N)W(CO)$_4$PR$_3$}$_2$] (R = H) **54**

The important bond connection crucial to the confirmation of compound **54** as representative compound of the trimetallic W---Pt---W series (assuming a complete symmetrical system along the platinum atom) is Pt-C(13)-C(12)-C(11)-C(10)-C(9)-N-W. This connection is followed from platinum to the ungsten metal centre. The compound [(dppp)Pt{C≡CC_5H_4N}$_2$] **52** had already been confirmed by the consistent NMR data with the literature and the structural X-ray results [17g]. Confirmation of the robustness of the Pt-C(13) bond of **54** upon N-W coordination is provided by the observation of $^{1}J_{(Pt-C)}$ and $^{2}J_{(P-C)}$. The ^{13}C chemical signal at 107.39 ppm splits into a triplet (coupling to ^{31}P, $^{2}J_{(P-C)}$ = 18 Hz) and has ^{195}Pt satellites ($^{1}J_{(Pt-C)}$ = 303 Hz). The signal from carbon C(12) splits into a doublet of doublets with spin interaction to both ^{195}Pt and ^{31}P ($^{2}J_{(Pt-C)}$ and $^{3}J_{(P-C)}$ respectively).

In order to confirm the presence of the ethynylpyridine group a long-range ^{15}N-^{1}H correlation experiment was recorded which showed a clear ^{15}N-^{1}H correlation signal with ^{15}N chemical shift at -143 ppm (**Figure 9.3**).

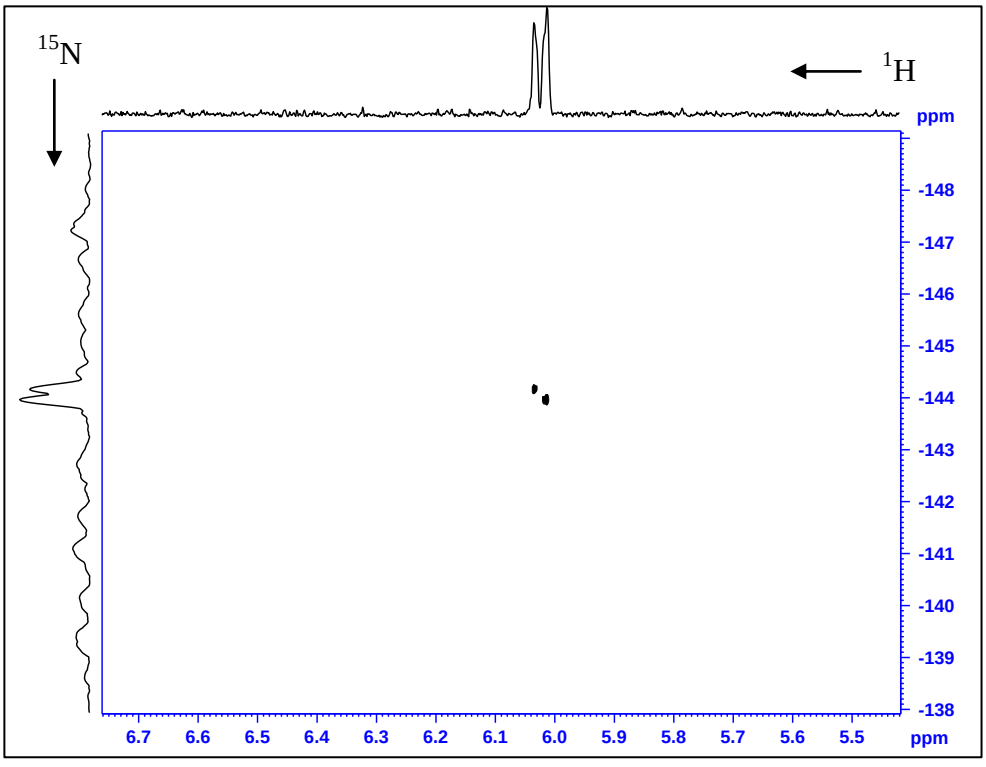


Figure 9.4 Long-range ^{15}N-^{1}H correlated NMR spectrum of *meta*-positioned proton of the pyridyl group of compound [(dppp)Pt{(4-C≡CC_5H_4N)W$(CO)_4PPh_3$}$_2$] **54**.

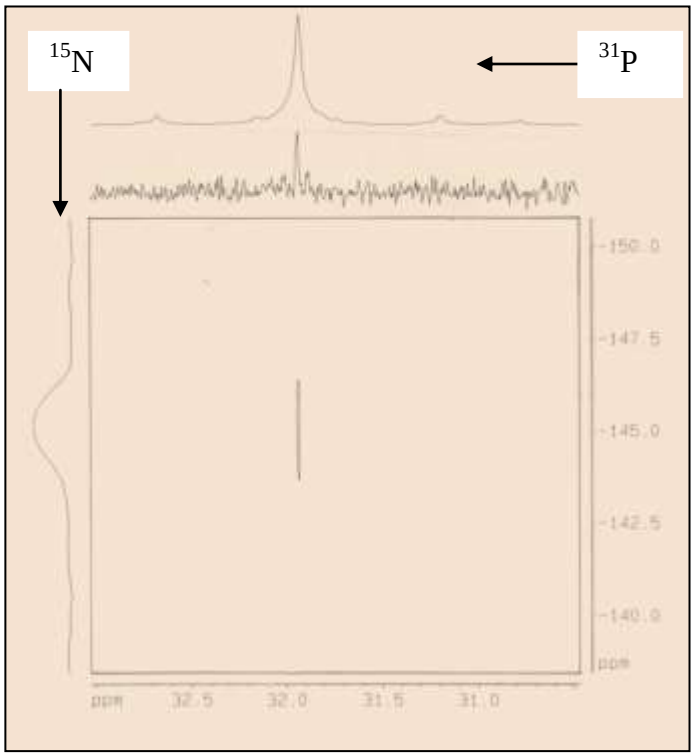


Figure 9.5 Correlated ^{31}P-^{15}N{^{1}H} NMR spectrum for compound **54**. Upper ^{31}P projection shows a separately recorded ^{31}P{^{1}H} spectrum and lower trace shows internal ^{31}P projection.

A crucial step in the confirmation of the successful coordination of the nitrogen of the pyridyl group to tungsten upon substitution of the labile CH_3CN is the existence of the N-W bond. This connection was to be confirmed by a ^{31}P-^{15}N{^{1}H} NMR experiment. Unfortunately, ^{183}W and ^{15}N isotopes are both low in natural abundance and have values of γ that are too low relative to the proton, to be able to observe any significant spin coupling between them in a relatively short period. Therefore the $^{2}J_{(P\text{-}N)}$ coupling interaction provided the only plausible alternative in establishing the W-N bond connection. The ^{31}P nucleus which has high natural abundance and a relatively higher γ value (relative to both ^{183}W and ^{15}N nuclei), could be used as a probe. Because of the slightly lower γ value relative to proton, larger quantities (95 mg in C_6D_6 (0.7 ml)) and longer recording times for the long-range ^{31}P-^{15}N{^{1}H} NMR experiment were necessary. **Figure 9.5** shows the results of the experiment recorded over four days at room temperature and clearly indicating W-N bond formation because of the corresponding ^{15}N signal at -143 ppm which is consistent with the long range ^{1}H-^{15}N NMR correlation results (based on the correlation results of the *meta* positioned proton to the nitrogen of the pyridyl group) shown in **Figure 9.4**.

The $^{13}C\{^{1}H\}$ spectrum (not shown) of **54** shows a clear ^{31}P-^{13}C spin coupling interaction which confirms a *cis*- N – W – P geometry. The deduction is based on the presence of one *trans*-coupling interaction between phosphorus and carbon showing a $^{2}J_{(P-C)}$ = 33 Hz. The assumption is that if there was a *trans*- N – W – P geometry in the system, then all of the ^{31}P-^{13}CO couplings would be of the order of 8 Hz or less. The $^{2}J_{(P-C)}$ coupling values of the *cis*- coordinated carbons to phosphorus vary from 4.1 to 7.0 Hz, with one of the *cis*-coordinated CO showing the least interaction and the most deshielded at 210.42 ppm (*trans*-CO-W-N). There is a small ^{13}C chemical shift change of 2.79 ppm from 206.58 to 209.37 ppm by the carbon *trans*- to the phosphorus atom relative to the corresponding starting tungsten complex $[W(CO)_4(CH_3CN)(PR_3)]$.

The *cis* geometry of complexes of the type $[W(CO)_4(PPh_3)(py^*)]$ (py* = 4-substituted pyridine) have been established by X-ray crystallographic and NMR study [25]. This geometry is seen for the monometallic complexes of the type $[W(CO)_4(CH_3CN)(PR_3)]$, where cis- N – W – P was confirmed by X-ray diffraction results (Chapter 7).

9.5 Correlation between NMR data and electronic parameters.

Correlations between NMR data and solution $\nu_{(C\equiv O)}$, or Tolmans' electronic parameters as well as Hammett substituent constants as a result of the *para*-substituent on the phosphine ligand are discussed. The *para*-substituent on the tungsten phosphine complex is separated by 13 bonds from the platinum metal (assuming a completely symmetrical system on the platinum metal centre). Five (PPh_3, P{tolyl}$_3$, P{4-OMeC$_6$H$_4$}$_3$, P{4-FC$_6$H$_4$} and P{4-CF$_3$C$_6$H$_4$}$_3$) of the six phosphine ligands on the tungsten metal share the same value of Tolman cone angle of 145 º except $P(NMe_2)_3$ which has a value of 157º which is 12º more sterically hindered. It is clear from NMR data correlations with electronic parameters as well as Hammett constant that $P(NMe_2)_3$ exerts a different influence on the system in relation to the *para*-substituted ligands (**Figs. 9.6 – 9.8**). It is also noted from **Figure 9.6** that the larger effect by $P(NMe_2)_3$ on the $\delta(^{183}W)$ relative to $\delta(^{195}Pt)$ is mainly due to the electronic rather than the steric property (a result of nitrogen instead of carbon being bonded to phosphorus.. It can be concluded that the change in the chemical shift of ^{195}Pt is due to the electronic influence emanating from the *para*-substituent on the *cis*-positioned phosphine of the tungsten metal centre. Considering that the para-substituent on the

phosphine of the tungsten metal centre is separated from the platinum by 13 bonds, a maximum change of about 7 ppm in $\delta(^{195}Pt)$ compared to approximately 3 ppm for ^{183}W (excluding $P(NMe_2)_3$ ligand) is significant and also illustrates the sensitivity of $\delta(^{195}Pt)$ as a good NMR spectroscopic probe. **Figure 9.6** shows a comparative influence of the para-subsituent on the phosphine in both the metal centres.

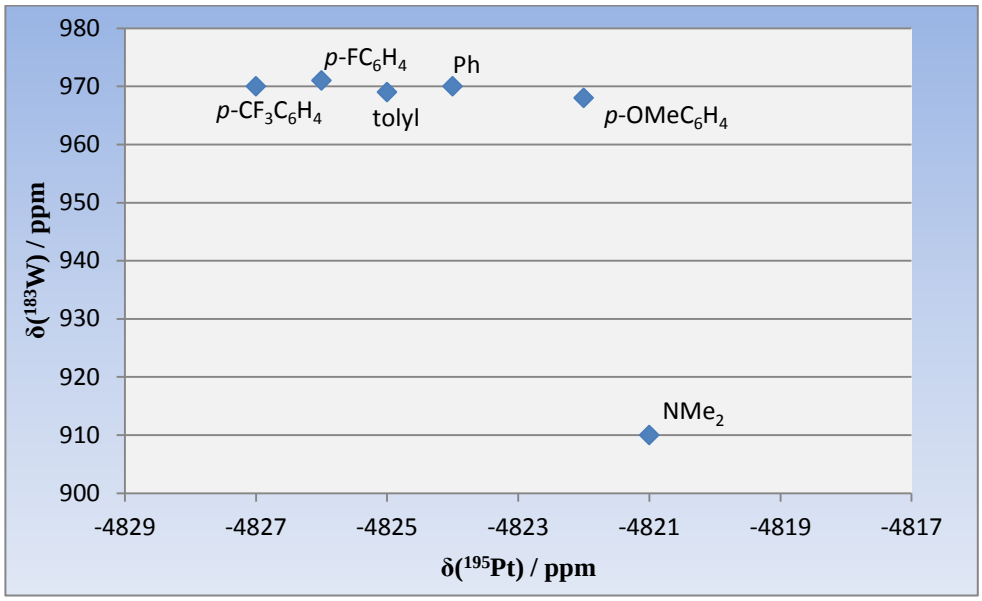


Figure 9.6 A plot $\delta(^{195}Pt)$ against $\delta(^{183}W)$ for PR_3 in the complexes of the type $[(dppp)Pt\{(4\text{-}C{\equiv}CC_5H_4N)W(CO)_4PR_3\}_2]$.

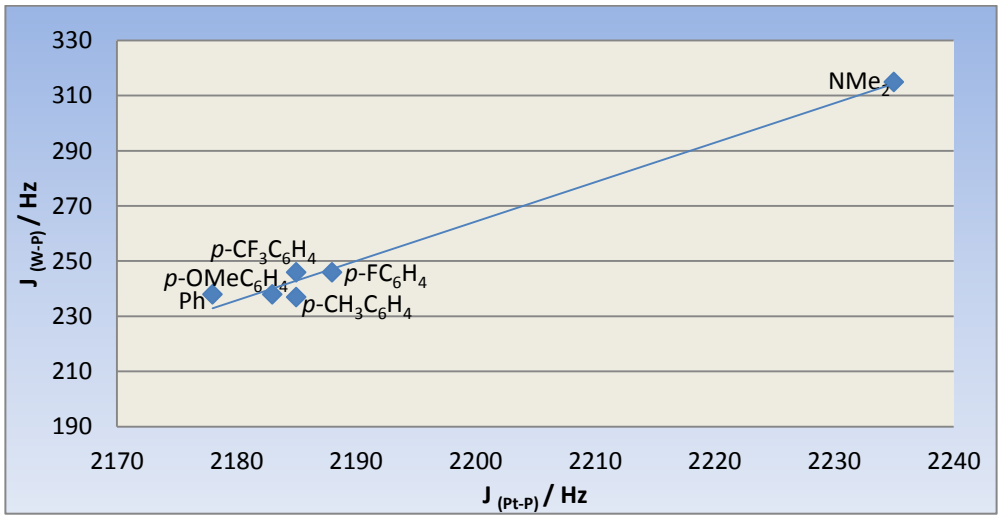


Figure 9.7 A plot $^1J_{(Pt\text{-}P)}$ against $^1J_{(W\text{-}P)}$ for PR_3 in the complexes of the type $[(dppp)Pt\{(4\text{-}C{\equiv}CC_5H_4N)W(CO)_4PR_3\}_2]$.

Figures 9.8 and 9.9 illustrate the influence of the electronic property of the *para*-substituted phosphine on the character of the M-P bond and the chemical shift of both δ(^{195}Pt) and δ(^{183}W). As observed before (Chapter 7), the electronic influence of the *para*-substituent of the phosphine ligand is reflected more coherently by the change in δ(^{183}W) than δ(^{195}Pt) because of the number bonds separating them (where δ(M) α 1/ΔE, M = ^{195}Pt or ^{183}W, discussed in Chapter 2).

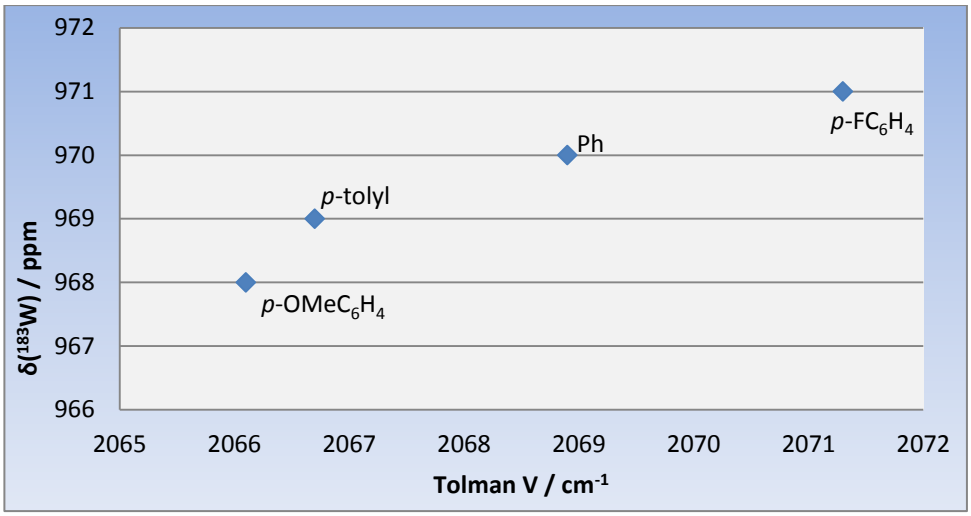


Figure 9.8 A plot δ(^{183}W) against the Tolman electronic parameter for PR_3 in complexes of the type [(dppp)Pt{(4-C≡CC_5H_4N)W$(CO)_4PR_3$}$_2$] (PR_3=$P(NMe_2)_3$ excluded for clarity).

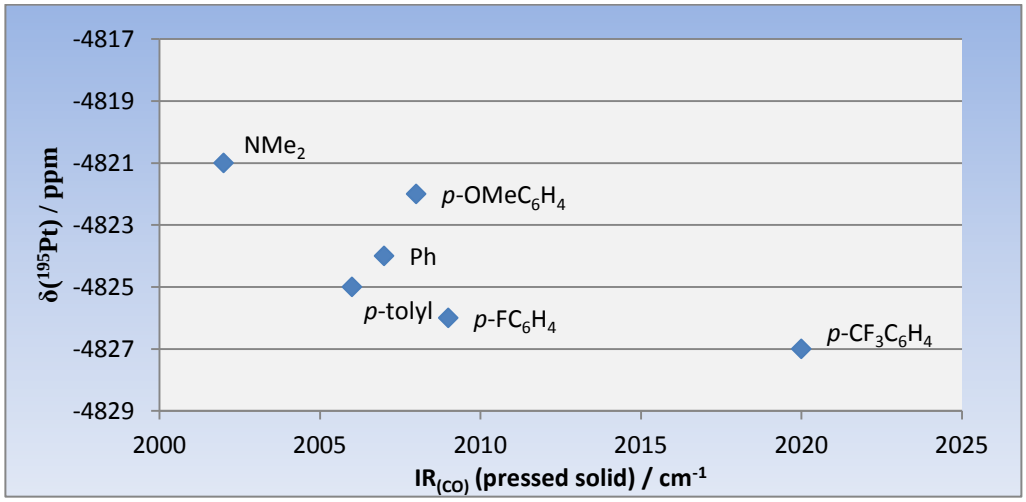


Figure 9.9 A plot δ(^{195}Pt) against $IR_{(CO)}$(pressed solid) electronic parameter for PR_3 in complexes of the type [(dppp)Pt{(4-C≡CC_5H_4N)W$(CO)_4PR_3$}$_2$].

There is a fair correlation between $\delta(^{195}Pt)$ and the electronic property of the phosphine *para*-substituent (**Figure 9.9**). However, trend in **Figures 9.8 and 9.9** seems to suggest a reverse effect experienced by the two transition metals as a result of changing *para*-substituted phosphine.

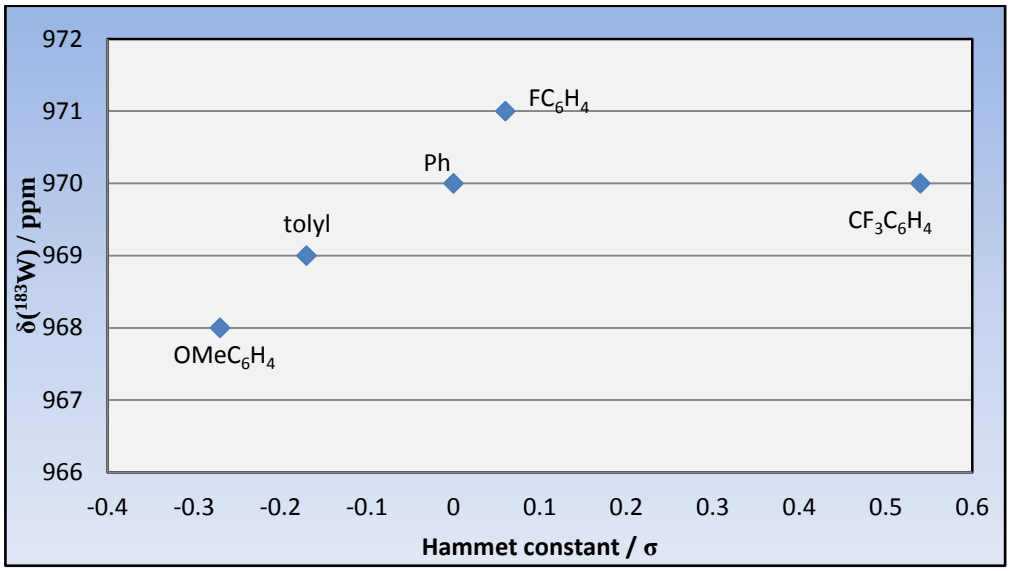


Figure 9.10 A plot $\delta(^{183}W)$ against Hammett constants for PR_3 in complexes of the type $[(dppp)Pt\{(4\text{-}C{\equiv}CC_5H_4N)W(CO)_4PR_3\}_2]$ ($PR_3 = P(NMe_2)_3$ excluded for clarity)

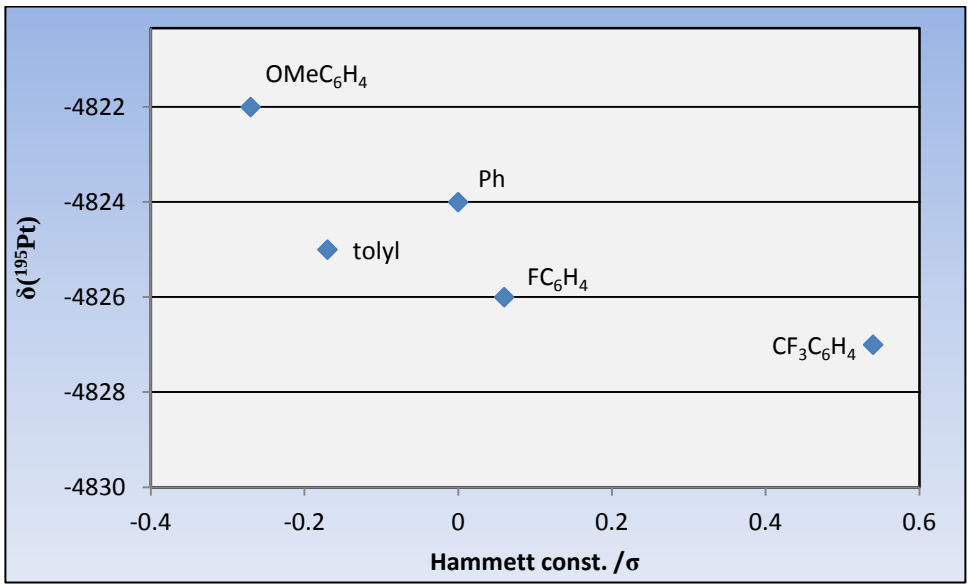


Figure 9.11 A plot $\delta(^{195}Pt)$ against Hammett constants for PR_3 in complexes of the type $[(dppp)Pt\{(4\text{-}C{\equiv}CC_5H_4N)W(CO)_4PR_3\}_2]$

The influence of the $P(NMe_3)_3$ ligand is significantly different from the *para*-substituted phosphine ligands due to a larger difference in electronic (though showing a significantly diminished influence at the Pt atom) and steric properties. There appears to be a meaningful correlation (**Figure 9.10**) between $\delta(^{193}W)$ and the Hammett constants, not counting $PPh_2(C_6F_5)$ (despite a chemical shift range of only 3 ppm for ^{183}W among the *para*-substituted phosphine ligands). There is a moderate correlation between $\delta(^{195}Pt)$ and Hammett constants values for the substituent on the phosphine phenyl groups. This correlation (Hammett σ against $\delta(^{195}Pt)$) suggest an electronic interaction over thirteen bonds. The correlation between $\delta(^{15}N)$ and $\delta(^{183}W)$ follows the same trend as for **Figure 9.6** where $P(p\text{-}CF_3C_6H_4)_3$ seems to show a similar steric hindrance (no records of Tolman's steric and electronic parameters for $4\text{-}CF_3C_6H_4$ found in the literature) as for the other *para*-substituted phosphine ligands (plot not shown). There is no significant correlation between $\delta(^{15}N)$ and $\delta(^{195}Pt)$ (plot not shown).

9.6 Conclusions

Ethynylpyridine-bridged trimetallic complexes containing platinum and tungsten have been synthesized under mild conditions in moderately good yields. These trimetallic complexes were characterised by multinuclear NMR spectroscopy (i.e. ^{1}H, ^{13}C, ^{15}N, ^{31}P, ^{183}W and ^{195}Pt) in which evidence for an electronic communication through the two metal centres was presented. Analysis of the NMR data (^{195}Pt, ^{31}P, ^{15}N and ^{1}H chemical shifts) in particular, provides evidence for a plane of symmetry along the platinum atom and dppp ligand which makes the two tungsten atoms identical. There seems to be a fair but negative correlation between $\delta(^{195}Pt)$ and $\delta(^{183}W)$ (not counting $P(NMe_2)_3$ related NMR data). There is a good correlation between $\delta(^{183}W)$ and Tolman's ν_{co} as a result of the electronic influence by phosphine substituents. The correlation between $\delta(^{195}Pt)$ and ν_{co} (experimental) suggests a fair but a negative relationship. There is moderate correlation between $\delta(^{195}Pt)$ and Hammett σ and, a relatively good correlation between $\delta(^{183}W)$ and Hammett constant. These correlations (between $\delta(^{195}Pt)$ against Tolman's electronic and Hammett σ) provide evidence for electronic communication through the two metal centres. A further study of the influence of phosphine ligands on complexes of the type $[(dppp)Pt\{(4\text{-}C{\equiv}CC_5H_4N)W(CO)_4PR_3\}_2]$ by employing ligands which differ significantly in both electronic and steric properties might be useful.

References

1. *http:/en.wikipedia.org/wiki/Platinum*, Dated 02-02-2011

2. F.G. Ciapetta and D.N. Wallace, *Catal. Rev*. 5 (1971) 67.

3. R. Nast, *Coord. Chem. Rev*., 47 (1982) 89.

4. (a) H. Lang, K. Köhler and S. Blau, *Coord. Chem. Rev*., 143 (1995) 113; (b) J. Forniés and E. Lalinde, *J. Chem. Soc., Dalton Trans*., (1996) 2587; (c) H. Lang, D.S.A. George and G. Rheiwald, *Coord. Chem. Rev*., 206-207 (2000) 101; (d) D. Michel, P. Mingos, R. Vilar and D. Rais, *J. Organomet. Chem*., 641 (2002) 126; (e) P. Mathur, S. Chatterjee and V.D. Avasare, *Adv. Organomet. Chem*., 55 (2008) 201; (f) M.I. Bruce, *Chem. Rev*., 91 (1991) 197.

5. (a) W. Beck, B. Niemer and M. Wieser, *Angew. Chem., Int. Ed. Engl*., 32 (1993) 923; (b) S. Lotz. P.H. van Rooyen and R. Meyer, *Adv. Organomet. Chem*., 37 (1995) 219 ; (c) U. Rosenthal, P. Arnt, W. Baumann, V.V. Burlakov and A. Spannenberg, *J. Organomet. Chem*., 670 (2003) 84; (d) M.I. Bruce, *Coord. Chem. Rev*., 248 (2004) 1603; (e) J.P. Selegue, *Coord. Chem. Rev*., 248 (2004) 1543; (f) V. Cardierno, M.P. Gamasa and J. Gimeno, *Coord. Chem. Rev*., 248 (2004) 1627; (g) H. Werner, *Coord. Chem. Rev*., 248 (2004) 1693; (h) G. Jia, *Coord. Chem. Rev*., 251 (2007) 2167.

6. (a) N.J. Long and C.K. Williams, *Angew. Chem., Int. Ed*. 42 (2003) 2586; (b) S. Szafert and J.A. Gladysz, *Chem. Rev*., 103 (2003) 4175; (c) V. Rosenthal, *Angew. Chem., Int. Ed*. 42 (2003) 1794; (d) M.I. Bruce and P.J. Low, *Adv. Organomet. Chem*., 50 (2004) 179; (e) S. Szafert and J.A. Gladysz, *Coord. Chem. Rev*., 106 (2006) PR1; (f) M. Akita and T. Koike, *Dalton Trans*., (2008) 3523.

7. J.R. Berenguer, E. Lalinde and M.T. Moreno, *Coord. Chem. Rev*., 254 (2010) 832.

8. (a) P. Nguyen, P. Gómez-Elipe and I. Manners, *Chem. Rev*., 99 (1999) 1515; (b) C.E. Powel amd M.G. Humphrey, *Coord. Chem. Rev*., 248 (2004) 725; (c) E.E. Silverman, T. Cardolaccia, X. Zhao, K.Y. Kim, K.H. Glusac and K.S. Schanze, *Coord. Chem. Rev*., 249 (2005) 1491; (d) W.Y. Wong, *Coord. Chem. Rev*., 251 (2007) 2400.

9. (a) V.W.W. Yam, W.Y. Lo, C.H. Lam, W.K.M. Fung, K.M.C. Wong, V.C.Y. Lau and N. Zhu, *Coord. Chem. Rev*., 245 (2003) 39; (b) V.W.W. Yam, *J. Organomet. Chem*., 689 (2004) 1393; (c) F.N. Castellano, I.E. Pomestchenko, E. Shikhova, F. Hua, M.L. Muro and N. Rajapakse, *Coord. Chem. Rev*., 250 (2006) 1819; (d) W.Y. Wong, *Dalton Trans*. (2007) 4495; (e) Z.N. Chen, N. Zhao, Y. Fan and J. Ni, *Coord. Chem. Rev*., 253 (2009) 1.

10. R. (a) Zeissel, M. Hissler, A. El-ghayoury and A. Harriman, *Coord. Chem. Rev*., 178 -180 (1998) 1251; (b) A. Ceccon, S. Santi, L. Orian and A. Michl, *Coord. Chem. Rev*., 248 (2004) 683; (c) Z.N. Chen, Y. Fan and J. Ni, *Dalton Trans*. (2008) 573; (d) P. Aquirre-Etcheverry and D. O'Hare, *Chem. Rev*., 110 (2010) 4839.

11. (a) M.I. Bruce, D.A. Harbourne, F. Waugh and F.G.A. Stone, *J. Chem Soc*., (1968) 356; (b) I. Collamati and A. Furlani, *J. Organomet. Chem*., 17 (1969) 209; (c) R.A. Bell, M.H. Chisholm, D.A. Couch and L.A. Rankel, *Inorg. Chem*., 16 (1977) 677.

12. (a) C.J. Cardin, D. Cardin and M.F. Lappert, *J. Chem. Soc. Dalton Trans*., (1977) 767; (b) R.J. Cross and J. Gemmill, *J. Chem. Soc. Dalton Trans*., (1984) 199 and 205; (c) R.J. Cross and M.F. Davidson, *J. Chem. Soc. Dalton Trans*., (1986) 411

13. K. Sonogashira, T. Yatake, Y. Tosuo, S. Takahashi and N. Hagihara, *J. Chem. Soc., Chem Comm*., (1977) 291.

14. (a) J.F. Almeida and A. Pidcock, *J. Organomet. Chem*., 209 (1981) 415; (b) A. Furlani, S. Licoccia and M.V. Russo, *J. Chem. Soc. Dalton Trans*., (1984) 2197; (c) R.J. Cross, and M.F.

Davidson, *Inorg. Chim. Acta*, 97 (1985) L35; (d) G.K. Anderson and G.J. Lumetta, *J. Organomet. Chem*., 295 (1985) 257; (e) R.J. Cross and M.F. Davidson, *J. Chem. Soc. Dalton Trans*., (1986) ; (f) R. Chinchilla and C. Nájera, *Chem. Rev*., 107 (2007) 874.

15. (a) A.D. Westland, *J. Chem. Soc*., (1965) 3060; (b) T.G. Appelton, M.A. Bennet and I.B. Tomkins, *J. Chem. Soc. Dalton Trans*., (1976) 439; (c) D.A. Slack and M.C. Baird, Inorga. Chim. Acta, 24 (1977) 277; (d) M. Hackett and G.M. Whitesides, *J. Am. Chem. Soc*., 110 (1988) 1449; (e) K. Yasufuku, H. Hoda and H. Yamazaki, in *Inorganic Syntheses*, Ed. H.D. Kaesz, Vol. 26, John Wiley and Sons, New York (1989), 369.

16. M.A. Andrews, G.L. Gould, W.T. Klooster, K.S. Koenig and E.J. Voss, *Inorg. Chem*., 35 (1996) 87.

17. (a) P.J. Stang and J.A. Whiteford, *Organometallics*, 113 (1994) 3776; (b) J.A. Whiteford, C.V. Lu and P.J. Stang, *J. Am. Chem. Soc*., 119 (1997) 2524; (c) J.A. Whiteford, P.J. Stang and S.D. Huang, *Inorg. Chem*., 37 (1998) 5595; (d) C. Müller, J.A. Whiteford and P.J. Stang, *J. Am. Chem. Soc*., 120 (1998) 9827; (e) P.F.H. Schwab, M.D. Levin and J. Michl, *Chem. Rev*., 99 (1999) 1863; (f) G.F. Swiegers and T.J. Malefetse, *Coord. Chem. Rev*., 225 (2002) 91; (g) Y.K. Kryschenko, S.R. Seidel, A.M. Arif and P.J. Stang, *J. Am. Chem. Soc*., 125 (2003) 5193; (h) M. Janka, G.K. Anderson and N.P. Rath, *Organometallics*, 23 (2004) 4382.

18. M. Ferrer, A. Gutiérrez, L. Rodríguez, O. Rossel, J.C. Lima, M. Font-Bardia and X. Solans, *Eur. J. Inorg. Chem*., (2008) 2899.

19. F.E. Kühn, J. Zuo, F.F. de Biani, A.M. Santos, Y. Zhang, J. Zhao, A. Sandulache and E. Herdtweck, *New. J. Chem*., 28 (2004) 43.

20. (a) R.A. Marcus, *J. Chem. Phys*., 24 (1956) 966; (b) R.A. Marcus, *J. Chem. Phys*., 43 (1965) 679; (c) R.A. Marcus, *J. Electroanal. Chem*., 438 (1997) 251; (d) P.J. Low, R.L. Roberts, R.L.

Cordiner and F. Hartl, *J. Solid State Electrochem*., 9 (2005) 717; (e) S. Santi, L. Orian, C. Durante, E.Z. Bencze, A. Bisello, A. Donoli, A. Ceccon, F. Benetollo and L. Crociani, *Chem, Eur. J*., 13 (2007) 7933.

21. A. Ceccon, S. santi, L. Orian and A. Bisello, *Coord. Chem. Rev*., 248 (2004) 683

22. L. Carlton, A. Emdin, A. Lemmerer and M.A. Fernandes, *Magn. Reson. Chem*., 46 (2008) S56.

23. J. Manna, C.J. Kuehl, J. A. Whiteford, P.J.Stang, D.C. Muddiman, C.D. Hofstadler and R. D. Smith, *J. Am. Chem. Soc*., 119 (1997) 11611.

24. J. Mason, *Chem. Rev*., 87 (1987) 1299.

25. L. Carlton, M.A. Fernandes and L.V. Mokoena, Paper in preparation

CHAPTER 10

Attempted Synthesis of Ethynyl and Diynyl Bridged Trimetallic Complexes

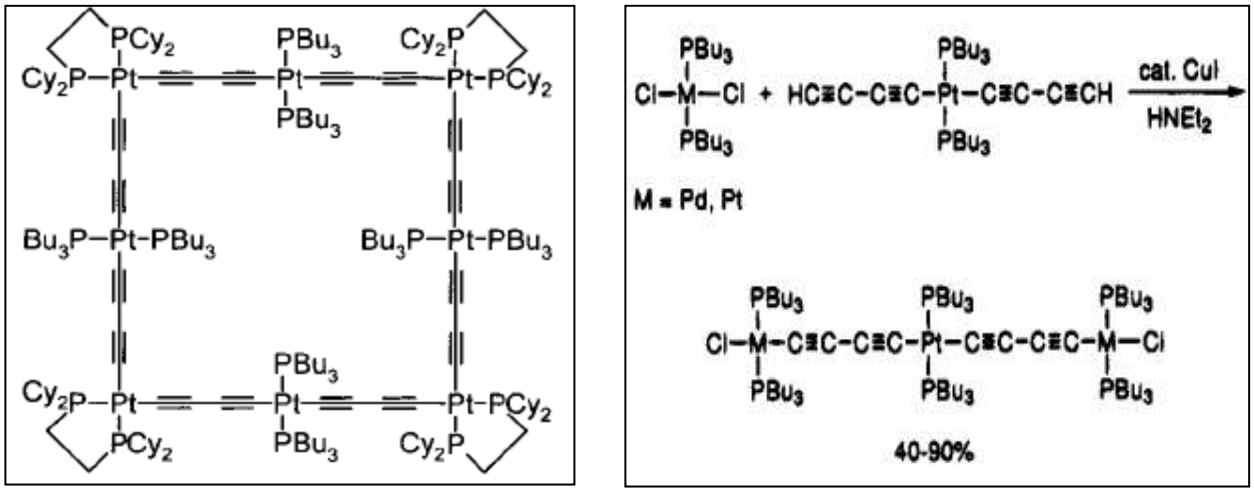
10.1 Introduction to trimetallic complexes linked by $(-C\equiv C-)_n$ chain

There is a growing interest in the chemistry of heteromultimetallic compounds that are bridged by π-conjugated organic fragments because of their potential application in the design of metal-containing rigid rod materials such as one-dimensional molecular wires (electrical conducting wires), nanoscale devices, organometallic polymers non-linear optical, and liquid crystalline materials and as potential catalytic precursors [1]. In heterobimetallic complexes, metals have a potential to modify the properties of their neighbours by means of cooperative effects. Recently, interest in this type of complex has been stimulated by potential use for their photochemical and photophysical behaviour with promising application in light emitting diodes and optical sensors.

The interest in the alkynyl metal complexes in particular, stems from their rich diversity and potential application in materials science as already mentioned. The most interesting features of these systems are their favourable electronic and structural properties, and their ability to interact with metal centres via $p\pi$-$d\pi$ overlap which makes them versatile building blocks in the preparation of carbon-rich oligomeric and polymeric materials having unique properties [2]. Alkynyl-containing ligands have been used in the preparation of a series of self-assembled polygons, ranging from triangles to octagons [3].

In the majority of the examples reported to date, the products are charged. It is desirable to synthesize multi-nuclear aggregates that are neutral and to offer possible advantages by acting as hosts for electron-deficient guests and as potential catalytic precursors. In addition they also offer advantages as being readily soluble in many common organic solvents in contrast to their

charged counterparts. **Figure 10.1** shows an example of a neutral platinum macrocycle bridged by dialkynyl linkers. There is a large body of literature data on the preparation of bi-, tri- and multi-nuclear aggregates or cluster complexes which are described in comprehensive reviews [1g,h,i,4].



(A) **(B)**

Figure 10.1 (A) Typical neutral molecular square composed of bis(phosphine)platinum corner units [5]; and (B) linear propagation of heterometallic molecular wire with diynyl linkers [6].

To our knowledge, there are no reports on the syntheses of platinum molecular squares with dppe as corner units bridged by only $(–C\equiv C-)_n$ linkers to other transition metals such as rhodium, tungsten, mercury and iridium. The scope of our research in this work was to synthesize bridged neutral heteropolynuclear platinum-rhodium, platinum-mercury and platinum-tungsten complexes containing acetylyne linkers of the type $(-C\equiv C-)_n$ (where n = 1 or 2). The research would follow established methods of syntheses accompanied by comprehensive multinuclear NMR analysis of transition metals such as ^{103}Rh, ^{183}W, ^{195}Pt and ^{199}Hg with an aim of establishing any electronic communication between the metal centres. The inclusion of iridium is based on similar structural and coordination properties to those of rhodium.

10.2 Experimental

All reactions were carried out under an atmosphere of argon at ambient temperature, unless specified otherwise. High quality solvents such as dichloromethane, THF, diethyl ether, absolute ethanol, methanol, acetonitrile and diethylamine were distilled, purified and dried before use as described in Chapter 3 or used as purchased. Compounds [(cod)$PtCl_2$], dppe, copper iodide (CuI), ethynytrimethylsilane ($HC{\equiv}CSiMe_3$) and $MgSO_4$ were used as purchased from suppliers without further purification. Higher grade xyly-isocyanide (2,6-dimethyl)phenyl isocyanide (XNC), triphenylphosphine (PPh_3) and $RhCl_3.3H_2O$ were used as purchased without any purification. Carbonylhydridotris(triphenylphosphine)rhodium(I) [$Rh(H)(CO)(PPh_3)_3$] and tetrakis(triphenylphosphine)rhodiun(I)hydride [$Rh(H)(PPh_3)_4$] were prepared following the method of Robinson and co-workers [7], and carbonylchlorobis(triphenylphosphine)rhodium(I) [$Rh(Cl)(CO)(PPh_3)_2$] following the method of Wilkinson and co-workers [8]. An average of 10 mg in CD_2Cl_2/CH_2Cl_2 (0.6 ml) was used for NMR analysis for all the complexes in this study unless specified otherwise.

10.2.1 Preparation of [$Hg(C{\equiv}CSiMe_3)_2$] ……60

A milky suspension of excess $Me_3SiC{\equiv}CH$ (1 ml, 7.07 mmol) in Et_3N (20 ml), THF (2 ml) and a catalytic amount of CuI (15 mg) was stirred at room temperature for 30 minutes accompanied by a colour change to a milky-yellow suspension. The milky-yellow suspension was transferred in small portions into a suspension of $HgCl_2$ (1 g, 3.68 mmol) in THF (5 ml) over a period of a minute. A greyish precipitate formed within a minute of contact. The solution was then stirred in a sealed Schlenk tube at room temperature overnight. The grey precipitate was separated from a yellow-orange solution and the solvent removed *in vacuo*. The resulting orange paste was redissolved in n-hexane (3 ml) and washed with H_2O (5 ml), and dried over $MgSO_4$. The solvent was removed under a gentle stream of argon leaving behind a white crystalline material giving a yield of 810 mg (56%). NMR spectra were recorded from a solution in $CDCl_3$ at 300 K. ^1H NMR ($\delta_{(ppm)}$): 0.30 (s, CH_3). $^{13}C\{^1H\}$ NMR ($\delta_{(ppm)}$): 139.48 (s, Hg-$\underline{C}{\equiv}$C-), 113.36 (s, Hg-C$\equiv\underline{C}$-), 0.28 (s, Me_3, d, satellite, $^1J_{(Si\text{-}C)}$ = 56 Hz.

10.2.2 Preparation of [(dppe)$PtCl_2$] ……**61**

The compound [(dppe)$PtCl_2$] **61** was prepared by a modified procedure of Hackett and Whitesides [9]. A clear solution of bis-(diphenylphosphinoethane) (dppe) (1.23 g, 3.00 mmol) in CH_2Cl_2 (15 ml) was added drop-wise to a milky suspension of [(cod)$PtCl_2$] (1.00 g, 2.67 mmol) in CH_2Cl_2 (20 ml) over a period of four minutes. The milky solution cleared as more dppe was added. Half-way through the addition of dppe solution (~ 7.5 ml), the clear solution suddenly turned into a milky suspension again and remained the same after a night of stirring at room temperature. The solvent was removed *in vacuo* after which the white precipitate was washed with Et_2O (20 ml) leaving behind a white powder to give a yield of 1.77 g (99%). NMR spectra were recorded from a solution in $CDCl_3$ at 300 K. 1H NMR ($\delta_{(ppm)}$): 7.89 (m, Ph), 7.50 (m, Ph), 2.40 (m, CH_2). $^{31}P\{^1H\}$ NMR ($\delta_{(ppm)}$): 41.80 (s, 2P; d, satellite, $^1J_{(Pt\text{-}P)}$ = 3622 Hz).

10.2.3 Preparation of *trans*- [$(PPh_3)_2Pt(C{\equiv}CSiMe_3)_2$] …….. **62**

The compound *trans*-[$(PPh_3)_2Pt(C{\equiv}CSiMe_3)_2$] **62** was prepared by the method of Gladysz and co-workers [10]. A Schlenk tube was charged with *trans*-$(PPh_3)_2PtCl_2$ (250 mg, 0.315 mmol) in Et_2NH (20 ml) and a catalytic amount of CuI (20 mg, 0.1 mmol) into which excess $HC{\equiv}CSiMe_3$ (0.4 ml ~ 3.25 mmol) was added. The tube was sealed and the reaction mixture was then stirred at ~ 70 ºC for 30 minutes during which time the colour changed from a yellow to a milky suspension. Heating was stopped after 30 minutes and the solution was allowed to stir at room temperature overnight. The solvent volume was reduced *in vacuo* to approximately a quarter of the original volume. The resultant solution was taken up in small quantities into the solvent mixture CH_2Cl_2/H_2O (4 ml/2 ml) after which the organic layer was separated and dried with $MgSO_4$. The solvent was then removed *in vacuo*. The whitish powder was washed with H_2O (3 ml x 3) and cold EtOH (3 ml) and lastly with Et_2O (5 ml). The resultant cream white powder was dried under vacuum giving a yield of 283 mg (76%). NMR spectra were recorded from a solution in CDCl3 at room temperature. ^1H NMR ($\delta_{(ppm)}$): 7.79, 7.35 (m, Ph), -0.45 (s, Me_3). $^{13}C\{^1H\}$ NMR ($\delta_{(ppm)}$): 134.72 (d, Ph, $^2J_{(C\text{-}P)}$ = 6 Hz), 131.20 (d, Ph, $^2J_{(P\text{-}C)}$ = 32 Hz), 129.45 (s, Ph), 126.97 (d, Ph, $^3J_{(P\text{-}C)}$ = 6 Hz), 117.80, 58.21 (s, C≡C-Si), 0.6 (s, $SiCH_3$). $^{31}P\{^1H\}$ NMR ($\delta_{(ppm)}$): 17.31(s, 2P; d, satellite, $^1J_{(Pt\text{-}P)}$ = 2692 Hz.

10.2.4 Preparation of [(dppe)Pt(C≡CC≡CH)$_2$] ……..63

Compound **63** was prepared by a modified procedure of Anderson and co-workers [1e]. A solution containing KOH (9.0 g, 160 mmol), H_2O (25 ml) and DMSO (6 ml) was heated to 70 ºC for 45 minutes in a three necked flask equipped with a condenser and a dropping funnel (fitted just before 1.4-dichloro-2-butyne (5 ml, 50 mmol) was added). A connecting tube filled with pre-dried $CaCl_2$ was connected between the condenser and a Schlenk tube containing a solution of [(dppe)$PtCl_2$] **61** (983 mg, 1.479 mmol) in THF (20 ml), Et_2NH (10 ml) and a catalytic amount of CuI (35 mg) at 0 ºC. A dropping funnel was connected and charged with 1.4-dichloro-2-butyne (5 ml) and added drop-wise over a period of 1 hour 15 minutes (1.15 h) while keeping the temperature of the three necked flask at 70 ºC and the Schlenk at 0 ºC. A white milky solution in the Schlenk tube gradually turned bright yellow within 20 minutes of HC≡C─C≡CH gas being channelled through the connecting tube at a rate of one bubble per second. The reaction mixture in the Schlenk tube was brought to room temperature after 30 minutes of complete addition of dichlorobutyne (i.e. 1.15 h) and stirred for a further 3 hrs after which the solvent was removed *in vacuo*. The resulting yellow powder was then washed with water (4 x 10 ml), methanol (3 x 10 ml) and ether (3 x 5 ml). The light yellow powder was re-dissolved in CH_2Cl_2 (10 ml) and filtered under a reduced pressure. The resulting yellow solution was evaporated under a gentle stream of argon gas and dried *in vacuo* leaving behind a bright yellow crystalline powder giving a yield of 920 mg (90%). NMR spectra were recorded from a solution in CD_2Cl_2 at 300 K. ^{1}H NMR ($\delta_{(ppm)}$): 7.78 (m, Ph), 7.48 (m, Ph), 2.39 (m, PCH_2), 1.84 (t, CH, $^6J_{(Pt\text{-}H)}$ = 64 Hz). $^{13}C\{^1H\}$ NMR ($\delta_{(ppm)}$): 133.34 (m, Ph), 131 (s, Ph), 129.00 (m, Ph), 128.33 (m, Ph), 97.8 (m, α-C), 93.06 (m, β-C), 71.68 (s, γ-C), 61.83 (s, C≡C-H), 27.96 (m, CH_2). $^{31}P\{^1H\}$ NMR ($\delta_{(ppm)}$): 42.06 (s, 2P; d, satellite, $^1J_{(Pt\text{-}P)}$ = 2296 Hz).

10.2.5 Preparation of [Rh(H)(CO)(PPh_3)$_3$] ……64

A solution of [$RhCl_3.3H_2O$] (260 mg), 1.24 mmol) in EtOH (20 ml) was added to a vigorously stirred, boiling solution of PPh_3 (2.64 g, 10 mmol) in EtOH (100 ml). After a delay of about 15 seconds, aqueous formaldehyde (10 ml, 40% w/v solution) and a solution of KOH (800 mg, 14 25 mmol) in hot EtOH (20 ml) were added rapidly and successively to the vigorously stirred, boiling reaction mixture. The reaction mixture was heated in a sealed Schlenk tube for a further 10 min and filtered while still warm. The bright yellow, microcrystalline product was filtered and

washed with EtOH (20 ml), H_2O (20 ml), EtOH (20 ml) and *n*-hexane (10 ml) and dried *in vacuo* leaving behind a bright yellow powder giving a yield of 810 mg (99%). NMR spectra were recorded from a solution in $CDCl_3$ at room temperature. ^1H NMR (δ(ppm)): -9.7 (s, RhH). $^{31}P\{^1H\}$ NMR ($\delta_{(ppm)}$): 41.24 (d, Rh-P, $^1J_{(Rh-P)}$ = 155 Hz).

10.2.6 Preparation of [Rh(Cl)(CO)(PPh$_3$)$_2$] ……65

A solution of $RhCl_3.3H_2O$ (500 mg, 2.89 mmol) in hot EtOH (20 ml) was slowly added to a rapidly stirred, boiling solution of a two-fold excess of PPh_3 (2 g, 7.62 mmol) in EtOH (100 ml). The solution remained turbid for a minute and half with stirring at 86 ºC. A formaldehyde solution (20 ml, 37 %) was added to cause the red solution to change to pale yellow in about a minute. A yellow microcrystalline precipitate was isolated by filtration while the solution was still warm, and washed with EtOH (20 ml x 2) and Et_2O (30 ml). The yellow product was dried *in vacuo* giving a yield of 1.25 g (63%). NMR spectra were recorded from a solution in $CDCl_3$ at 300 K. ^1H NMR ($\delta_{(ppm)}$): 7.72, 7.38 (m, Ph). $^{13}C\{^1H\}$ NMR ($\delta_{(ppm)}$): 134.74 (d, Ph, $^2J_{(P-C)}$ = 6.4 Hz), 132.94 (d, Ph, $^1J_{(P-C)}$ = 23 Hz), 130.10 (s, Ph), 128.13 (d, Ph, $^3J_{(P-C)}$ = 5 Hz). $^{31}P\{^1H\}$ NMR ($\delta_{(ppm)}$): 28.45 (d, PPh, $^1J_{(Rh-P)}$ = 127 Hz).

10.2.7 Attempted preparation of [Hg{C≡C-Rh(PPh$_3$)$_2$(XNC)}$_2$] …….. 66

To a custom made Schlenk-type tube containing a solution of $Hg(C{\equiv}CSiMe_3)_2$ (35 mg ~ 0.0889 mmol) in toluene (18 ml) was added excess $(Bu_4N)F$ (0.5 ml) drop-wise during which the solution turned milky immediately. The solution was left to stir at room temperature for 20 min after which H_2O (1 ml) was added drop-wise and allowed to stir for a further five minutes. A second custom made Schlenk-type tube connected to the first one via a glass tube was charged with $[Rh(H)(PPh_3)_4]$ **40** (205 mg ~ 0.178 mmol). The system was freeze-thaw dried three times and, while keeping the H_2O frozen, the liquefied solution was transferred through a connecting tube into the Schlenk tube containing $[Rh(H)(PPh_3)_4]$ **40** during which time gas was evolved. The reaction mixture was stirred for 30 minutes after which the system was purged with argon and excess isocyanide (XNC = xylyl-isocyanide or (2.6-dimethyl)phenyl isocyanide) (26 mg) was added at once as quickly as possible while stirring was continued for a further 10 minutes. The orange-brown solution cleared immediately and the solvent removed *in vacuo*. NMR spectra of the crude and the isolated material were recorded from a solution in toluene-d_8 at room

temperature. The NMR interpretation of ^{1}H and ^{31}P spectra indicated mainly the presence of starting materials.

10.2.8 Attempted preparation of *trans*-[$(PPh_3)_2Pt\{C\equiv C\text{-}Rh(PPh_3)_2(XNC)\}_2$] ……..……..67

The reaction was carried out the same way as for experiment 10.2.7. A solution of *trans*-[$(PPh_3)_2Pt\{C\equiv CSiMe_3\}_2$] (50 mg, 0.0551 mmol) in toluene (20 ml), $(Bu_4N)F$ (0.5 ml) and H_2O (1 ml) was stirred for 20 min at room temperature (no colour change up to this stage) before being transferred through a connecting tube into a Schlenk tube containing [$Rh(H)(PPh_3)_4$] **40** (127 mg, 0.110 mmol) during which time the colour changed to red. Isocyanide was added at once and reaction was allowed to stir for a further 5 minutes after which the solvent was removed leaving behind a reddish paste. The NMR spectra of the product were recorded from a solution in $CDCl_3$ at 300 K. NMR analysis of the isolated product indicated the presence of the starting materials only.

10.2.9.1 1st Attempted preparation of *trans*-[$(PPh_3)_2Pt\{C\equiv C\text{-}Rh(CO)(PPh_3)_2\}_2$]…..….68

The experimental setup was as for experiment 10.2.7. Tertabutylammonium-flouride, $(Bu_4N)F$ (0.5 ml) was added drop-wise into a clear solution of *trans*-[$(PPh_3)_2Pt\{C\equiv CSiMe_3\}_2$] (50 mg ~ 0.0551 mmol) in toluene (15 ml) and stirred at room temperature for 30 minutes. H_2O (20 drops) were added and the solution was allowed to stir for a further 5 min. The solution was freeze dried three times before the toluene solution was decanted into an attached Schlenk tube containing [$Rh(H)(CO)(PPh_3)_3$] (101 mg ~ 0.154 mmol). The solution was stirred for a further five 5 minutes after which an aliquot was analysed for the progress of the reaction by $^{31}P\{^{1}H\}$ NMR. The solution was then left to stir for another 48 hrs after which the solvent was removed leaving behind an orange powder (137 mg). The NMR spectra of the isolated product were recorded from a solution in $CDCl_3$ at 300 K. ^{1}H and ^{31}P NMR analysis did not indicate formation of expected or new products suggesting that no reaction took place because of the signals indicative of starting materials.

10.2.9.2 2nd Attempted preparation of *trans*-[$(PPh_3)_2Pt\{C\equiv C\text{-}Rh(CO)(PPh_3)_2\}_2$] ..…..69

The experimental procedure was similar to that of **10.2.7.** A clear solution of *trans*-[$(PPh_3)_2Pt\{C\equiv CSiMe_3\}_2$] (50 mg, 0.0551 mmol) in Toluene (5 ml), $(Bu_4N)F$ (0.5 ml) and H_2O

(1 ml) was stirred for 30 min at room temperature before being decanted through a connecting tube into Schlenk tube containing [Rh(Cl)(CO)(PPh_3)$_2$] **65** (76 mg, 0.110 mmol) and a catalytic amount of CuI (10 mg) in Et_3N/THF (6 ml of 1:1). There was no significant colour change. The reaction mixture was allowed to stir at room temperature for two days after which the solvent was removed *in vacuo*. NMR spectra were recorded from a solution in CD_2Cl_2/CH_2Cl_2 at 300 K and the results were that of starting materials (no reaction took place).

10.2.9.3 3rd Attempted preparation of *trans*-[(PPh_3)$_2$Pt{C≡C-Rh(CO)(PPh_3)$_2$}$_2$] ……70

The experimental procedure was similar to that reported by Lui and co-workers [11] in which a solution *trans*-[(PPh_3)$_2$Pt{C≡C$SiMe_3$}$_2$] (50 mg, 0.0551 mmol) and K_2CO_3 (8 mg, 0.0579 mmol) in a mixture of MeOH (3 ml) and Et_2O (3 ml) was stirred at room temperature overnight. Before [Rh(H)(CO)(PPh_3)$_3$] **64** was added, a small volume of the resultant solution was filtered and the solution concentrated by evaporation under a gentle flow of argon gas. The pale white precipitate was characterised as the starting material, *trans*-[(PPh_3)$_2$Pt{C≡C$SiMe_3$}$_2$].

10.2.10.1 1st Attempted preparation of [Hg{C≡C-Rh(CO)(PPh_3)$_2$}$_2$] ……..71

The experimental procedure is similar to 10.2.7. A solution of (Bu_4N)F in THF (1 ml) was added drop-wise into a clear colourless solution of [Hg(C≡C$SiMe_3$)$_2$] **60** (30 mg, 0.0757 mmol) in toluene (10 ml). The reaction mixture was allowed to stir for 20 minutes during which time the colour changed to light orange. Water (10 drops) was added to the orange coloured solution with no colour change and left to stir for a further five minutes. The solution was decanted into a Schlenk-type tube containing a solution of [Rh(H)PPh_3)$_4$] **40** (205 mg ~ 0. 0.223 mmol) in THF via a connecting tube. Carbon monoxide (CO) was bubbled at a rate of a bubble per second for 4.30 h. The orange solution became slightly yellowish after 30 minutes of bubbling. The reaction was stopped after 4 hrs of constant stirring and the solvent removed *in vacuo* leaving behind yellow powder (starting materials). No reaction took place.

10.2.10.2 2nd Attempted Preparation of [Hg{(C≡C-Rh(CO)(PPh_3)$_2$}$_2$] ……72

The experimental procedure was similar to that reported by Lui and co-workers [11]. A solution of [Hg(C≡C$SiMe_3$)$_2$] **60** (50 mg, 0.126 mmol) and K_2CO_3 (18 mg, 0.140 mmol) in THF (3 ml) and MeOH (3 ml) was stirred at room temperature for overnight. There was no significant colour

change from the initial solution. A solution of [Rh(H)(CO)(PPh_3)$_3$] **64** (115 mg, 0.126 mmol) in THF (3 ml) was added drop-wise to a clear colourless solution under a minute and after which it was sealed and stirred for overnight at room temperature. A small volume of the orange solution was concentrated under reduced pressure and the precipitate were characterised as that of the starting material. The bulk of solution was further stirred at room temperature for 48 hrs and still only starting materials were isolated.

10.2.11.1 1st Attempted preparation of [(dppe)Pt{C≡CC≡C-Rh(CO)(PPh_3)$_2$}$_2$] 73

A solution of [(dppe)Pt(C≡CC≡CH)$_2$] **63** (33 mg ~ 0.0477 mmol) in THF (3 ml) and Et_3N (8 ml) was added drop-wise into a suspension of [Rh(H)(CO)(PPh_3)$_3$] **64** (65 mg ~ 0.099 mmol) THF (3 ml) and stirred in a sealed Schlenk tube for three days. There was no indication of gas evolution during the addition. The solution was monitored for any colour change in the first hour, after 4 hrs, 14 hrs and every 24 hrs thereafter. There was no significant colour change from the initial yellow-orange suspension. The solvent was removed *in vacuo* leaving behind orange powder. A sample of crude material was secured from which the NMR spectra were recorded from a solution in $CDCl_3$ at 300 K. No reaction took place (mixture of starting material).

10.2.11.2 2nd Attempted preparation of [(dppe)Pt{C≡CC≡C-Rh(CO)(PPh_3)$_2$}$_2$] …..74

To a solution of [(dppe)Pt(C≡CC≡CH)$_2$] **63** (35 mg, 0.0506 mmol) and a catalytic amount of CuI (10 mg) in THF (4 ml) and Et_2NH (10 ml) was added drop-wise a solution of [Rh(Cl)(CO)(PPh_3)$_2$] **65** (70 mg, 0.101 mmol) in THF (4 ml). The colour of the solution changed from orange to bright yellow within approximately two minutes of mixing. The reaction was sealed in a Schlenk tube and left to stir in the dark for 1 hour during which time a precipitate formed. The bright yellow precipitate was isolated and washed with EtOH (10 ml) followed by Et_2O (10 ml) and dried under vacuum giving a yield of 54 mg. A small amount (20 mg) was redissolved in CH_2Cl_2 and run through a short column of celite using petroleum ether and acetone (1:1) as eluent. An orange-brown powder material was isolated. NMR spectra were recorded from solution in CD_2Cl_2/CH_2Cl_2 at 213 and 300 K. The $^{31}P\{^1H\}$ NMR spectrum showed no indication of starting materials or formation of expected product but an unknown product. The reaction procedure was repeated but the solution was left to stir in the dark

overnight. The resultant reddish brown material was analysed by $^{31}P\{^{1}H\}$ and ^{1}H NMR, and no indication of the expected product was found.

10.2.12 Attempted preparation of [(dppe)Pt{C≡CC≡C-Ir(CO)(PPh$_3$)$_2$}$_2$] 75

The experimental procedure was as for **72**. A solution of [(dppe)Pt(C≡CC≡CH)$_2$] **63** (90 mg, 0.130 mmol) and catalytic amount of CuI (10 mg) in THF (2 ml) and Et_2NH (2 ml) was added to a solution of [Ir(Cl)(CO)(PPh$_3$)$_2$] (200 mg, 0.256 mmol) in THF (2 ml). The reaction was sealed and left to stir in the dark for 3 hrs hour after which the solvent was removed *in vacuo* leaving behind a yellow-orange powder. NMR spectra were recorded from a solution in CD_2Cl_2/CH_2Cl_2 at 213 and 300 K. The $^{31}P\{^{1}H\}$ NMR spectrum showed no indication of starting materials or formation of new product.

10.2.13a Attempted preparation of [(dppe)Pt{C≡CC≡C-Rh(XNC)(PPh$_3$)$_2$}$_2$] ……..76

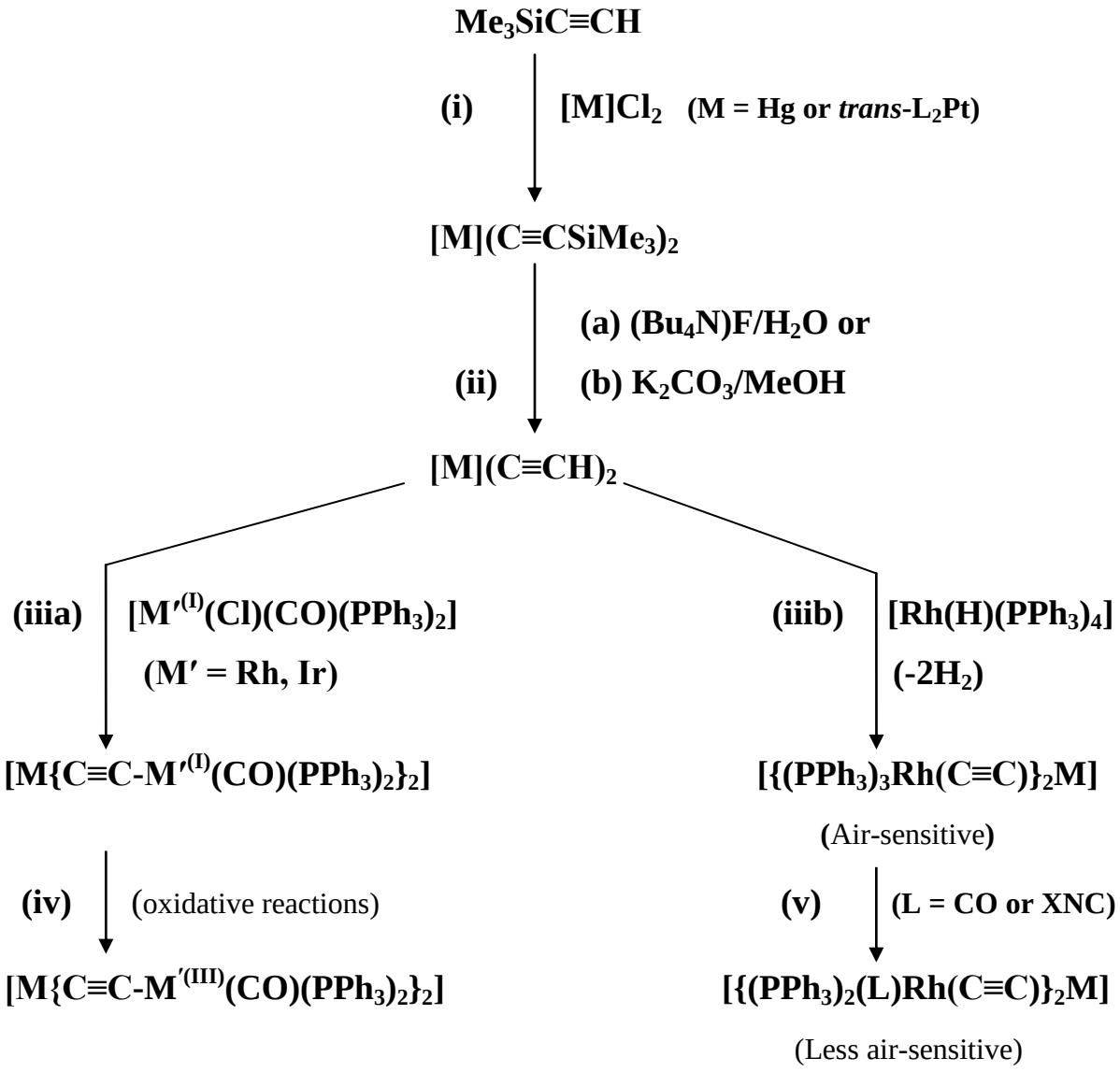
A reaction mixture of [(dppe)Pt(C≡CC≡CH)$_2$] **63** (5 mg ~ 0.007 mmol) and [Rh(H)(PPh$_3$)$_4$] **40** (18.5 mg ~ 0.014 mmol) in tolune-d8 (0.8 ml) was prepared in a sealed NMR tube under reduced pressure and monitored for possible formation of the product by ^{31}P and ^{1}H NMR at 213 and 300 K. An excess amount of XNC (2 mg) was added as quickly as possible after opening the NMR tube and analysed for ^{31}P and ^{1}H NMR again. The colour changed from orange to red-orange within a period of 8 min. However the interpretation of ^{31}P and ^{1}H NMR spectra of the isolated product indicated a possible array of Wilkinson's catalyst derivatives and no presence of expected product. The reaction procedure was repeated in CH_2Cl_2 solvent at room and lower temperatures, and was discovered that the [Rh(H)(PPh$_3$)$_4$] **40** decomposes rapidly in chlorinated solvents.

10.2.13b Attempted preparation of [(dppe)Pt{C≡CC≡C-Rh(CO)(PPh$_3$)$_2$}$_2$] ……....76

A reaction mixture of [(dppe)Pt(C≡CC≡CH)$_2$] **63** (44 mg ~ 0.064 mmol) and [Rh(H)(PPh$_3$)$_4$] **40** (164 mg ~ 0.128 mmol) in THF (4 ml) and Et_3N (2 ml) in a three-necked round bottom flask fitted with glass gas bubbler was stirred at room temperature for about 20 min. There was no immediate colour change observed. CO gas was introduced at rate of a bubble per second for 1.5 hr. The colour of the reaction mixture remained the same throughout CO addition. The NMR interpretation of ^{195}Pt, ^{103}Rh, ^{31}P and ^{1}H spectra of the isolated material did not indicate the presence of the expected product but unknown compound.

10.3 Results and discussion

Preparations of ethynyl-bridged trimetallic complexes of M_1-[C≡C]$_n$-Hg-[C≡C]$_n$-M_2 and M_1-[C≡C]$_n$-Pt-[C≡C]$_n$-M_2 (where n = 1; M_1 = M_2 = Rh or Ir) were intended to proceed using the established synthetic methods as applied elsewhere in the literature as shown in scheme 10.1.



Scheme 10.1 Reaction scheme for the proposed synthesis of ethynyl-bridged heterotrimetallic complexes (L_2 = PPh_3). (i) THF/Et_2NH, CuI [12]; (ii) $(Bu_4N)F$ and H_2O [13] or K_2CO_3 and MeOH [10a,14]; (iiia) THF/Et_2NH, CuI, [12], (iiib) –$2H_2$ [15], (iv) Oxidative additions [16], (v) –PPh_3 [15].

10.3.1 Synthesis of ethynyl compounds of platinum and mercury: Scheme 10.1, step (i)

Alkynyl compounds containing platinum and mercury have been prepared by a variety of methods some of which were discussed in Chapter 9.3 [10]. In this part of the work, a copper-catalysed Sonogashira reaction seems to proceed smoothly. Thus, as illustrated in **scheme 10.1**, treatment of a THF suspension of *trans*-[$(PPh_3)_2PtCl_2$] or $HgCl_2$ with an excess amount of [$HC{\equiv}CSiMe_3$] in the presence of a catalytic amount of CuI and basic solvent such as diethylamine followed by purification afforded the desired products in good yields (**Scheme 10.2**).

$$Me_3SiC{\equiv}CH + CuI \xrightarrow{THF/Et_2NH} Me_3SiC{\equiv}CCu + HI \quad \text{.....(10.1)}$$

$$Me_3SiC{\equiv}CCu + HgCl_2 \xrightarrow{HI} CuI + HCl + Hg(C{\equiv}CSiMe_3)_2 \ \underline{60} \text{.....(10.2)}$$

$$Me_3SiC{\equiv}CH + (L_2)PtCl_2 \xrightarrow{(i)} [(L_2)Pt\{C{\equiv}CSiMe_3\}_2] \ \underline{62} \text{ .....(10.3)}$$

$$[(dppe)PtCl_2] + HC{\equiv}CC{\equiv}CH \xrightarrow{(i)} [(dppe)Pt(C{\equiv}CC{\equiv}CH)_2] \ \underline{63} \text{.....(10.4)}$$

Scheme 10.2 Syntheses of platinum and mercury alkynyl complexes; (i) CuI, Et_2NH and THF [12].

The proposed mechanism (Eq. 10.1 and 10.2) by which CuI in the presence of a basic solvent facilitates the reaction has been illustrated in Chapter 1.3.2. It is assumed that the reaction proceeds by metalation of the alkyne in which the acidic proton is first abstracted by the basic solvent followed by the introduction of the chlorinated transition metal complex followed by the regeneration of the catalyst. A similar approach was applied in the syntheses of compounds **62**, **63** and the alkynyl mercury compound **60**. Compound [$(dppe)PtCl_2$] **61** as a precursor for compound [$dppe)Pt(C{\equiv}CC{\equiv}CH)_2$] **63** was prepared by the established method of Hackett and Whitesides [9] in which a labile cyclooctadiene ligand is replaced by a chelating or monodentate phosphine ligand in quantitative yields.

10.3.2 Synthesis of rhodium(I) complexes

Hydrido phosphine complexes of rhodium(I) of the type $[Rh(H)(PPh_3)_4]$ **40** and $[Rh(H)(CO)(PPh_3)_3]$ **64** were synthesized by the established method of Robinson and co-workers [7] in high yields, and $[Rh(Cl)(CO)(PPh_3)_2]$ **65** by the method of Wilkinson and co-workers [8]. The compound $[Rh(H)(CO)(PPh_3)_3]$ **64** has been prepared by other methods such as the reduction of hydrazine in ethanolic suspension [17] and by the reaction of $[Rh(Cl)(CO)(PPh_3)_2]$ with sodium tetrahydroborate or triethylamine and hydrogen in ethanol [18]. The reaction scheme 10.5 involves the use KOH in the place of tetrahydroborate [19] in the presence of excess phosphine. In the preparation of tetrakis(triphenylphosphine)rhodium(I)hydride, $[Rh(H)(PPh_3)_4]$ **40** (described in Chapter 8.2) and as for $[Rh(H)(CO)(PPh_3)_3]$ **64**, the presence of excess triphenylphosphine helps to stabilize the complex in solution (**Scheme 10.3**).

$$RhCl_3.3H_2O + 4PPh_3 \xrightarrow{KOH} [Rh(H)(PPh_3)_4]\ \mathbf{40} \quad \text{.....(10.0)}$$

$$RhCl_3.3H_2O + 3PPh_3 \xrightarrow{KOH,\ HCHO} [Rh(H)(CO)(PPh_3)_3]\ \mathbf{64} \quad \text{.....(10.5)}$$

$$RhCl_3.3H_2O + 2PPh_3 \xrightarrow{HCHO} [Rh(Cl)(CO)(PPh_3)_2]\ \mathbf{65} \quad \text{.....(10.6)}$$

Scheme 10.3 Preparation of rhodium(I)phosphine complexes

The complex *trans*-$[Rh(Cl)(CO)(PPh_3)_2]$ **65** has been prepared by other methods utilizing alternative carbon monoxide sources [20]. Rhodium(III) chloride and PPh_3 in hot ethanol solution in the presence KOH as reducing agent and formaldehyde as a source of carbon monoxide afford **65** in high yields (Eq. 10.6).

10.3.3 Attempted desilylation of ethynyl-bridged trimetallic complexes: Scheme 10.1; step (ii)

Alkynyl compounds containing trimethylsilyl such as *trans*-$[(PPh_3)_2Pt(C{\equiv}CSiMe_3)_2]$ and $Hg(C{\equiv}CSiMe_3)_2$ were successfully isolated and characterised. A proposed *in situ* reaction scheme for the desilylation or deprotection of $Hg(C{\equiv}CSiMe_3)_2$ is shown in **Scheme 10.4** (a similar scheme was proposed for the platinum analogue). ***N.B***. Isolation of $[Hg(C{\equiv}CH)_2]$ as a

pure compound was never attempted as it is generally regarded as potentially explosive or unstable.

$$[Hg(C{\equiv}CSiMe_3)_2] + (Bu_4N)F \longrightarrow Hg(C{\equiv}C^{-}.Bu_4N^{+})_2 + 2FSiMe_3 \quad \text{.....(10.7)}$$

$$Hg(C{\equiv}C^{-}.Bu_4N^{+})_2 + H_2O \longrightarrow Hg(C{\equiv}CH)_2 + 2Bu_4N^{+}.OH^{-} \quad \text{.....(10.8)}$$

Scheme 10.4 Proposed reaction scheme for desilylation of the mercury complex

Scheme 10.4 shows the proposed reaction mechanism for the preparation of the protonated ethynyl precursor which is required for reaction with Rh(I) complexes for the purpose of forming trimetallic complexes containing mercury and rhodium or platinum and rhodium. The rationale for the approach in the attempted synthesis is based on the reported success of the desilylation process as proposed in **Eq. 10.7 and 10.8** which involves the desilylation of the alkyne by tetrabutylammnium fluoride (TBAF) in the presence of small amount of H_2O, where $SiMe_3$ is known to react with fluoride [10,11,13]. At this stage desilylation was to be followed by the protonation (the protons coming from water) before the introduction of CuI (for Sonagashira coupling). The assumption at this stage was that the alkyne mercury complex is deprotonated to react with $[Rh(CO)(PPh_3)_2]^+$ or $[Ir(CO)(PPh_3)_2]^+$ following successes elsewhere [21]. The use of TBAF as desilylation agent has been successfully applied in many transition metal complexes containing alkynyl ($\{-C{\equiv}C-\}_n$, n = 2 or more) groups [13]. There are reported cases where potassium fluoride KF has also been used in the place of TBAF [13d] with lower yields. However, detailed analysis of the isolated products indicated that no reaction took place with respect to **Eq**. **10.7** and **10.11** i.e. the desilylation step. Potassium carbonate (K_2CO_3 in MeOH) was tried without success despite reported successes elsewhere [22]. Elevated temperatures and longer reaction times have been tried in the desilylation or deprotection stage with poor yields [13g]. The only major difference between the reported successful applications of these desilylation agents in which transition metals are bridged by alkynyl $(-C{\equiv}C-)_n$ groups (n = 2 or more) is that in our case n = 1.

Alternatively, the reaction of rhodium hydride compounds with alkynyl compounds (dependent on the success of step (ii)) in **scheme 10.1** was to proceed spontaneously as reported by Carlton and co-workers [15] but for obvious reasons this step could not be reached.

10.3.4 Attempted synthesis of butadiynyl-bridged complexes of platinum and rhodium or iridium.

Attempted syntheses of diynyl-bridged trimetallic complexes of platinum and rhodium or iridium used an approach based on Sonogashira type, CuI-catalyzed reactions in basic medium. The attempted procedure followed the method of Bruce and co-workers [23] where physical properties such as colour change and the texture of the resultant product appears to indicate successful conversion. However the isolated product failed to give interpretable NMR spectra (no significant improvement was observed on lowering the temperature). Attempts to purify the isolated product on a short column were limited by poor solubility and signs of decomposition in most organic solvents. An interesting observation from the $^{31}P\{^{1}H\}$ NMR spectrum of the isolated product from **Eqs. 10.14** and **10.15 (Scheme 10.5)** was that it showed no new signal(s) other than an insignificant signal of the starting material and oxidized phosphines. These results suggested possible fluxional systems (possible broadening of signals), hence the low temperature measurements. There were no indications of resolved signals at low temperatures (close to -60 ^{o}C) for either Pt-P nor Rh-P or Ir-P. The solubility of the isolated product is poor in chlorinated solvents whereas signs of decomposition in toluene-d_8 are evident because of rapid colour change upon solvation.

An attempted synthetic procedure as proposed in **Scheme 10.5** (**Egs. 10.16** and **10.17)** follows a successful reaction elsewhere [15] where RC≡CH reacts with $[M(H)(PPh_3)_4]$ (R = Ph and M = Rh) to give an air sensitive product which upon introduction of CO or XNC ligand is converted to a less air sensitive product. The reaction procedure was repeated by varying the solvents (THF, toluene and CH_2Cl_2) at different temperatures (213 – 300 K) and also under vacuum (sealed NMR tube). Attempts to crystallise the isolated material at room and lower (freezer) temperatures, and by slow evaporation were not successful. NMR interpretation (^{31}P, ^{103}Rh and ^{195}Pt) of the products from both **Eqs.10.16 and 10.17** did not indicate the presence of any expected compound but mainly multiple side products. An interesting observation from this result is that there was no significant ^{195}Pt NMR signal i.e. of the resultant product or the starting material.

$$[(dppe)Pt(C{\equiv}CC{\equiv}CH)_2] + 2[Rh(Cl)(CO)(PPh_3)_2] \xrightarrow{(i)} [(dppe)Pt\{C{\equiv}CC{\equiv}C\text{-}Rh(CO)(PPh_3)_2\}_2] \quad \text{.....(10.14)}$$

$$[(dppe)Pt(C{\equiv}CC{\equiv}CH)_2] + 2[Ir(Cl)(CO)(PPh_3)_2] \xrightarrow{(i)} [(dppe)Pt\{C{\equiv}CC{\equiv}C\text{-}Ir(CO)(PPh_3)_2\}_2] \quad \text{.....(10.15)}$$

$$[(dppe)Pt(C{\equiv}CC{\equiv}CH)_2] + 2[Rh(H)(PPh_3)_4] \xrightarrow{(ii)} [(dppe)Pt\{C{\equiv}CC{\equiv}C\text{-}Rh(PPh_3)_3\}_2] \quad \text{.....(10.16)}$$

$$[(dppe)Pt\{C{\equiv}CC{\equiv}C\text{-}Rh(PPh_3)_3\}_2] + L \xrightarrow{(iii)} [(dppe)Pt\{C{\equiv}CC{\equiv}C\text{-}Rh(PPh_3)_2(L)\}_2] \quad \text{.....(10.17)}$$

Scheme 10.5 Proposed reaction of platinum-diynyl complexes with rhodium(I) and iridium(I) phosphine complexes (i) Cat. CuI, Et_2NH/Et_3N and THF [12]; (ii) $-H_2$ [15]; (iii) ligand exchange, L = CO or XNC [15].

10.4 Conclusions

The reaction of platinum(II) and mercury(II) compounds following Sonagashira coupling with ethynyltrimethysilane at low temperatures, produced alkynyl complexes in good yields. However, deprotection or desilylation was not successful despite reported successes in the literature using TBAF, KF and K_2CO_3 in MeOH at room to higher temperatures. The reaction of L_2PtCl_2 (L = dppe) complex with butadiyne (produced *in situ*) following a modified literature method produced $[L_2Pt(C{\equiv}CC{\equiv}CH)_2]$ in good yields. Reaction of $[L_2Pt(C{\equiv}CC{\equiv}CH_2)_2]$ with $Rh^{(I)}$ and $Ir^{(I)}$ complexes in THF, toluene or CH_2Cl_2 gave products that could not be fully characterised by NMR or showed the presence of other unknown products but no traces of the expected products.

References

1. (a) V. W.-W Yam, K.M.-C, S.H.-F Chong, V.C.-Y Lau, S.C.-F, L. Zhang, K.-K Cheung, *J. Organomet. Chem*., 670 (2003) 205; (b) N.J. Long, C.K. Williams, *Angew. Chem., Int. Ed*., 42 (2003) 2586; (c) V. Rosenthal, *Angew. Chem., Int. Ed*., 42 (2003) 1794; (d) S. Szafert, J.A. Gladysz, *Chem. Rev*., 103 (2003) 4175; (e) M. Janka, G.K. Anderson and N.P. Rath, *Organometallics*, 23 (2004) 4382; (f) M.I. Bruce and P.J. Low, *Adv. Organomet. Chem*., 50 (2004) 179; (g) C.E. Powel and M.G. Humphrey, *Coord. Chem. Rev*., 248 (2004) 725; (h) S. Szafert and J.A. Gladysz, *Chem. Rev*., 106 (2006) PR1; (i) W.Y. Wong, *Coord. Chem. Rev*., 251 (2007) 2400; (j) P. Aquirre-Etcheverry and D. O'Hare, *Chem. Rev*., 110 (2010) 4839.

2. J.R. Berenguer, E. Lalinde and M.T. Moreno, *Coord. Chem. Rev*., 254 (2010) 832.

3. H. Jiang and W. Lin, *J. Am. Chem. Soc*., 125 (2003) 8084.

4. (a) P.F.G. Schwab, M.D. Levin and J. Michl, *Chem. Rev*., 99 (1999) 1863; (b) V.W.W. Yam and K.K.W. Lo, *Chem. Soc. Rev*., 28 (1999) 323; (c) H. Lang, D.S.A. George and G. Rheinwald, *Coord. Chem. Rev*., 206-207 (2000) 101; (d) G.F. Swieger and T.J. Malefetse, *Chem. Rev*., 100 (2000) 3484; (e) G.F. Swieger and T,J. Malefetse, *Coord. Chem. Rev*., 225 (2002) 91; (f) V.W.W. Yam, W.Y. Lo, C.H. Lam, W.K.M. Fung, K.M.C. Wong, V.C.Y. Lau and N. Zhu, *Coord. Chem. Rev*., 245 (2003) 39; (g) T.C.W. Mak, X.L. Zhao, Q.M. Wang and G.C. Guo, *Coord. Chem. Rev*., 261 (2007) 2311; (h) W.Y. Wong, *Dalton Trans*, (2007) 4495; (i) Z.N. Chen, N. Zhao, Y.Fan and J. Ni, *Coord. Chem. Rev*., 253 (2009) 1.

5. B.J. Holliday and C.A. Markin, *Angew. Chem., Int. Ed*., 40 (2001) 2022.

6. W. Weng, T. Bartik, M. Brady, B. Bartik, J.A. Ramsden, A.M. Arif and J.A. Gladysz, *J. Am. Chem. Soc*., 117 (1995) 11922.

7. N.Ahmad, J.J. Levison and S.D. Robinson, *Inorganic Syntheses*, 28 (1990) 81.

8. D. Evans, J.A. Osborn and G. Wilkinson, *Inorganic Syntheses*, 28 (1990) 79

9. M. Hackett and G.M. Whitesides, *J. Am. Chem. Soc*., 110 (1988) 1449

10. (a) W. Weng, T. Bartik, M. Brady, B. Bartik, J.A. Ramsden, A.M. Arif and J.A. Gladysz, *J. Am. Chem. Soc*., 117 (1995) 11922; (b) T.B. Peters, Q. Zheng, J. Stahl, J.C. Bohling, A.M. Arif, F. Hampel and J.A. Gladysz, *J. Organomet. Chem*., 641 (2002) 58; (c) Q. Zheng, F. Hampel and J.A. Gladysz, *Organometallics*, 23 (2004) 5896.

11. L. Liu, W.-Y. Wong, Y.-W. Lam and W.-Y. Tam, *Inorg. Chim. Acta*, 360 (2007) 109.

12. (a) K. Sonogashira, T. Yatake, Y. Tohda, S. Takahashi and N. Hagihara, *J. Chem. Soc*. *Chem. Commun*., (1977) 291; (b) D. Villemin and E. Schigeko, *J. Organomet. Chem*., 246 (1988) C24.

13. (a) A. Wong, P.C.W. Kang, C.D. Tagge and D.R. Leon, *Organometallics*, 9 (1990) 1992; (b) Y. Sun, N.J. Taylor and A.J. Carty, *Organometallics*, 11 (1992) 4293; (c) J. Lewis, B. Lin and P.R. Raithby, *Transition Met. Chem*., 20 (1995) 569; (d) U.H.F. Bunz, *Angew. Chem. Int. Ed. Engl*., 35 (1996) 969; (f) M.N. Bakola-Christianopoulou and K.K. Apazidou, *Appl. Organometal. Chem*., 12 (1998) 818; (g) N. Panziera, P. Pertci, I. Fratoddi, A. La Groia and M.V. Russo, *J. Organomet. Chem*., 691 (2006) 2648; (h) H.P. Gupta, M.S. Kumar, S. Upreti and A.J. Elias, *Eur. J. Inorg. Chem*., (2006) 5022; (i) R. Packheiser, P. Ecorchard, T. Rüffer and H. Lang, *Chem. Eur. J*., 14 (2008) 4948.

14. G. Xu, C. Campana and T. Ren, *Inorg. Chem*., 41 (2002) 3521.

15. L. Carlton, L.V. Mokoena and M.A. Fernandes, *Inorg. Chem*.,47 (2008) 8696.

16. (a) S. Gatard, C.-H. Cheng, B.M. Foxman and O.V. Ozerov, *Organometallics*, 27 (2008) 6257; (b) C.R. Baar, H.A. Jenkins, J.J. Vittal, G.P.A. Yap and R.J. Puddephatt, *Organometallics*, 17 (1998) 2818.

17. S.S. Bath and L. Vaska, *J. Am. Chem. Soc*., 85 (1963) 3500.

18. P.S. Hallman, D. Evans, J.A. Osborn and G. Wilkinson, *Chem. Commun*., (1967) 305.

19. D.A. Evans, G. Yagupsky and G. Wilkinson, *J. Chem. Soc. A*., (1968) 2660.

20. (a) R.F. Heck, *J. Am. Chem. Soc*., 86 (1964) 2796; (b) J. Chatt and B.L. Shaw, *J. Chem. Soc*., (1966) 1437.

21. (a) K. Sonogashira, T. Yatake, Y. Tohda, S. Takahashi and N. Hagihara, *J.Chem. Soc*., *Chem. Comm*., (1977) 291; (b) D. Villemin and E. Schigeto, *J. Organomet. Chem*., 346 (1988) C24; R. Chinchilla and C. Nájera, *Chem. Rev*., 107 (2007) 874.

22. (a) G. Xu, C. Campana and T. Ren, *Inorg. Chem*., 41 (2002) 3521; (b) L. Liu, W.-Y. Wong, Y.-W. Lam and W.-Y. Tam, *Inorg. Chim. Acta*, 360 (2007) 109.

23. M.I. Bruce, B.C. Hall, P.J. Low, M.E. Smith, B.W. Skelton and A.H. White, *Inorg. Chim. Acta*, 300-302 (2000) 633.

CHAPTER 11

GENERAL CONCLUSIONS

In this thesis a significant number of new heterobi- and tri-metallic complexes with both directly bonded and bridged metal centres were synthesised and characterised by techniques such as IR, elemental analysis, NMR spectroscopy and single crystal X-ray diffraction. A tremendous development in the field of NMR spectroscopy has allowed us to investigate the effect of substituents within the inner coordination sphere of the selected transition metal complexes. For this purpose, a special NMR instrument configuration which can offer triple-resonance measurements for extremely insensitive nuclei was employed.

Monometallic adducts of $Ph_3SnCl.py^*$ and $Ph_3PbCl.py^*$ (py* = pyridine or para-substituted pyridine derivatives of dimethylamino, methoxy, methyl, phenyl, carboxaldehyde, bromo, benzoyl and acetyl) were studied as metallo-ligand precursors for the synthesis of heterobimetallic complexes of Fe - Sn. Adducts of $Ph_3PbCl.py$ and $Ph_3SnCl.py$ (py = pyridine) were studied for the effect of change in temperature by measuring the chemical shift of ^{207}Pb and ^{119}Sn between 183 and 313 K in CD_2Cl_2/CH_2Cl_2 solution. A significant change in the chemical shift of ^{297}Pb and ^{119}Sn as a result of change in the temperature was observed. The chemical shifts of ^{207}Pb and ^{119}Sn of $Ph_3PbCl.py^*$ and $Ph_3SnCl.py^*$ were measured at a determined temperature and correlated against the Hammett constant. A fair correlation agreement was observed. Representative single crystal structures of each of $Ph_3PbCl.py^*$ and $Ph_3SnCl.py^*$ series were analysed and were confirmed to have increased coordination number from four to five forming a *trans*-triorganobipyramidal geometry.

A significant number of new heterobimetallic complexes of the type $[(CpFe(CO)(PR_3)(SnPh_3)]$ (PR_3 = triphenylphosphine, trimethylphosphine, dimethylphenylphosphine, diphenylmethylphosphine, tris(*para*-fluorophenyl)phosphine, tris(*para*-tolyl)phosphine, tris(*para*-methoxyphenyl)phosphine, tributylphosphine, tricyclohexylphosphine, trimethylphosphite, triphenylphosphite and tris(dimethylamino)phosphine were synthesised by photochemical irradiation methods under mild conditions in relatively high yields. Eight of these

compounds were analysed by X-ray diffraction methods and the results correlated against the solution properties as measured by NMR spectroscopy. Heterobimetallic complexes of the type [CpFe(CO)(PR_3)($SnPh_3$)] form a '*piano stoo*l' type geometry in which the CO, PR_3 and $SnPh_3$ ligands form tripod legs with Cp at the apex. Correlation of the NMR (solution state) and X-ray (solid state) parameters i.e. $\delta(^{57}Fe)$ vs. Fe-P bond lengths, $\delta(^{57}Fe)$ vs. P-Fe-Sn bond angle (^{o}), etc. ranged from very good for $\delta(^{57}Fe)$ vs. steric property (Tolman cone angle θ) to fair for $\delta(^{57}Fe)$ vs. $\delta(^{31}P)$. It is observed from these trends that the steric parameter seems to have greater influence on the ^{57}Fe chemical shift than the electronic parameter (Tolman ν_{co}). A small number of disubstituted heterobimetallic complexes of [CpFe(PR_3)$_2$($SnPh_3$)] (PR_3 = trimethyphosphine, dimethylphenyphosphine, trimethylphosphite and triphenylphosphite) were synthesized under the same conditions as monocarbonylated compounds in good yields. These compounds were characterised principally by NMR spectroscopy and X-ray diffraction techniques. Despite a limited number of new compounds synthesized in this series, a clear pattern was observed whereby the electronic property of the ligands was found to have a major influence on the chemical shift of the transition metal nucleus (^{57}Fe). The observed trend agrees with the chemical properties of the ligands in which phosphites are better π-acceptors than phosphines.

A fair number of metallo-ligand precursors of the type [$W(CO)_4$(PR_3)(NCMe)] (R = phenyl, *p*-tolyl, *p*-methoxyphenyl, *p*-fluorophenyl, *p*-trifluoromethylphenyl and dimethylamino) were synthesized in good yields under mild conditions. This was achieved by using stoichiometric amounts of decarbonylating agent, Me_3NO. All complexes were characterised by, among other methods, NMR and X-ray spectroscopy. It was found that the phosphine ligand is always *cis*-orientated the to acetonitrile ligand confirming the stronger *trans*-directing capacity of CO ligand.

In an endeavour to extend our study of electronic communication through bridged metal – metal, bimetallic complexes of the type [(PPh_3)$_2$Rh(H)$_2$(pytca-$W(CO)_4$(PR_3)] (pytca = 2-(4-pyridyl)thiazole-4-carboxylate; PR_3 = triphenylphosphine, tris(*p*-fluorophenyl)phosphine, tris(*p*-methoxyphenyl)phosphine, tris(*p*-tolyl)phosphine, tris(*p*-trifluoromethylphenyl)phosphine, diphenylmethylphosphine, and (*p*-pentafluorophenyldipehnyl)phosphine) were synthesized under mild conditions in moderate yields. The new complexes were characterised principally by NMR and one by X-ray diffraction. A subtle change in the chemical shifts of both ^{183}W and ^{103}Rh

nuclei seems to suggest a uniform influence by, among other parameters, changes in the substituent on the phosphorus atom which is six bonds away from tungsten and thirteen bonds from rhodium atoms. We cannot rule out other complementary influences such as bulk solvent magnetic susceptibility, hydrogen bonding effects, ligand steric effects, π-π interactions, etc. Fair correlation agreements were found between ^{183}W vs. ^{103}Rh chemical shifts and a poor correlation between ^{183}W and ^{103}Rh with Tolman's electronic parameter for the 4-phenyl substituent on the phosphine bound to tungsten.

Ethynylpyridine-bridged trimetallic complexes of the type [(dppp)Pt{(C≡CC$_5$H$_4$N)W(CO)$_4$(PR$_3$)}$_2$] (R = where R = Ph, *p*-tolyl, *p*-OMeC$_6$H$_4$, *p*-CF$_3$C$_6$H$_4$, *p*-FC$_6$H$_4$ and NMe$_2$) were synthesized under mild conditions in moderately good yields. It was not possible to obtain crystals of X-ray quality of these compounds, however characterisation by multinuclear NMR spectroscopy involving the nuclei ^{1}H, ^{13}C, ^{15}N, ^{31}P, ^{183}W and ^{195}Pt confirmed unambiguously the formation of a bond between tungsten and nitrogen. There seems to be fair inverse correlation between δ(^{195}Pt) and δ(^{183}W) (more pronounced if the δ(^{195}Pt and ^{183}W) data due to P(NMe$_2$)$_3$ are not counted). The correlation between chemical shift of ^{183}W and Tolman's electronic parameter (ν_{co}) shows a positive influence whereas that of ^{195}Pt with ν_{co} (experimental) shows a negative correlation as a result of change of substituent on the PR$_3$ ligand. There exists a relatively good correlation between ^{183}W chemical shift and Hammett substituent constant for the *para*-phenyl substituent on the phosphine bonded to tungsten and a moderate correlation with δ(^{195}Pt). A significant observation in this series is the extent to which NMR spectroscopy is able to detect the electronic communication through the two metal centres (Pt----W) as a result of the influence of the phosphine substituents on the tungsten (6 bonds) and its influence on the platinum (separated by 13 bonds).

Platinum(II) and mercury(II) trimethylsilyl-protected alkynyl complexes of the type [M–(C≡CSiMe$_3$)$_2$] were synthesised under mild condition in good yields following the Sonagashira coupling procedure. Attempts to employ desilylation/deprotection procedures of these complexes and to eventually synthesize trimetallic complexes of the type [M-{C≡C-M'}$_2$] were not successful. Therefore, oxidative addition of the alkyne to rhodium and iridium could not take place. We have not been able as yet to characterise fully by NMR or X-ray spectroscopic techniques the products of the reaction between *trans*-Pt[C≡C-C≡CH]$_2$ and [M(Cl)(CO)(PPh$_3$)$_2$]

complexes following the literature method described in Chapter 10, section 10.3.4 . New ways of preparing complexes of the type [M-{C≡C-M'}$_2$] by other methods such as by using acetylene gas merit investigation.

Appendix A

Crystal structure and refinement data for $[W(CO)_4(NCMe)\{P(Ph_2C_6F_5)\}]$ 31

(Identification code 11m_rm2_0a)

Intensity data were collected on a Bruker APEX II CCD area detector diffractometer with graphite monochromated Mo K_α radiation (50kV, 30mA) using the APEX 2 (Bruker, 2005a) data collection software. The collection method involved ω-scans of width 0.5° and 512x512 bit data frames. Data reduction was carried out using the program *SAINT+* (Bruker, 2005b) and face indexed absorption corrections were made using *XPREP* (Bruker, 2005b).

The crystal structure was solved by direct methods using *SHELXTL* (Bruker, 1999). Non-hydrogen atoms were first refined isotropically followed by anisotropic refinement by full matrix least-squares calculations based on F^2 using *SHELXTL*. Hydrogen atoms were first located in the difference map then positioned geometrically and allowed to ride on their respective parent atoms. Diagrams and publication material were generated using SHELXTL, PLATON (Spek, 2003) and ORTEP-3 (Farrugia, 1997).

References

Bruker (2005a). APEX2. Version 2009.1-0. Bruker AXS Inc., Madison, Wisconsin, USA.

Bruker (2005b). SAINT+. Version 7.60A. (includes XPREP and SADABS) Bruker AXS Inc., Madison, Wisconsin, USA.

Bruker (1999). SHELXTL. Version 5.1. (includes XS, XL, XP, XSHELL) Bruker AXS Inc., Madison, Wisconsin, USA.

Farrugia, L. J. (1997). J. Appl. Cryst. **30**, 565

Spek, A. L. (2003). *J. Appl. Cryst.* **36**, 7-13.

Table A.1. Crystal data and structure refinement for $[W(CO)_4(NCMe)\{P(Ph_2C_6F_5)\}]$ **31**

Identification code	11m_rm2_0a	
Empirical formula	C24 H13 F5 N O4 P W	
Formula weight	689.17	
Temperature	173(2) K	
Wavelength	0.71073 Å	
Crystal system	Orthorhombic	
Space group	P2(1)2(1)2(1)	
Unit cell dimensions	a = 10.7531(3) Å	□= 90°.
	b = 13.2825(3) Å	□= 90°.
	c = 16.7488(4) Å	□ = 90°.
Volume	2392.20(10) $Å^3$	
Z	4	
Density (calculated)	1.914 Mg/m^3	
Absorption coefficient	4.966 mm^{-1}	
F(000)	1320	
Crystal size	0.37 x 0.18 x 0.07 mm^3	
Theta range for data collection	1.96 to 28.00°.	
Index ranges	-14<=h<=8, -17<=k<=15, -22<=l<=13	
Reflections collected	14971	
Independent reflections	5780 [R(int) = 0.0936]	
Completeness to theta = 28.00°	100.0 %	
Absorption correction	Integration	
Max. and min. transmission	0.7225 and 0.2609	
Refinement method	Full-matrix least-squares on F^2	
Data / restraints / parameters	5780 / 0 / 326	

Goodness-of-fit on F^2	0.980
Final R indices [I>2sigma(I)]	R1 = 0.0389, wR2 = 0.0816
R indices (all data)	R1 = 0.0502, wR2 = 0.0864
Absolute structure parameter	-0.022(9)
Largest diff. peak and hole	0.971 and -0.945 e.Å^{-3}

Table A.2. Bond lengths [Å] and angles [°] for 11m_rm2_0a.

C(1)-W(1)	1.974(7)
C(2)-W(1)	1.970(8)
C(3)-W(1)	2.031(8)
C(4)-W(1)	2.019(8)
C(5)-N(1)	1.135(8)
C(5)-C(6)	1.461(9)
C(11)-P(1)	1.833(6)
C(21)-P(1)	1.830(6)
C(31)-P(1)	1.840(7)
N(1)-W(1)	2.193(6)
P(1)-W(1)	2.5203(17)

N(1)-C(5)-C(6)	177.4(8)
C(5)-N(1)-W(1)	171.0(6)
C(2)-W(1)-C(1)	90.4(3)
C(2)-W(1)-C(4)	87.0(3)
C(1)-W(1)-C(4)	88.2(3)
C(2)-W(1)-C(3)	88.8(3)
C(1)-W(1)-C(3)	85.4(3)

C(4)-W(1)-C(3)	172.3(3)
C(2)-W(1)-N(1)	92.5(3)
C(1)-W(1)-N(1)	175.2(3)
C(4)-W(1)-N(1)	95.7(3)
C(3)-W(1)-N(1)	90.9(3)
C(2)-W(1)-P(1)	174.6(2)
C(1)-W(1)-P(1)	94.5(2)
C(4)-W(1)-P(1)	95.3(2)
C(3)-W(1)-P(1)	89.5(2)
N(1)-W(1)-P(1)	82.39(15)

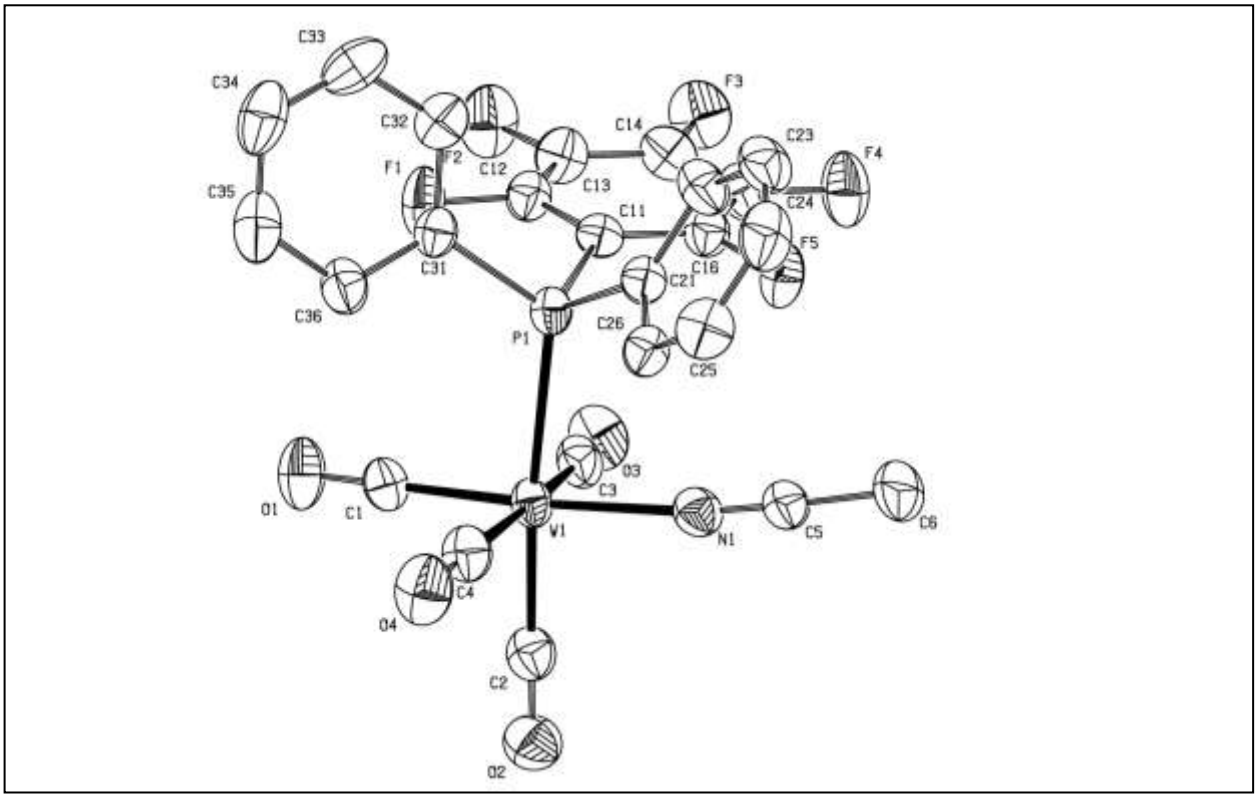


Figure A.1 ORTEP Diagrams (50% probability level):